

**PLASTIC YIELDING CHARACTERISTICS OF A ROD
UNDER SUCCESSIVELY APPLIED TORSION AND
TENSION LOADINGS.**

ABU RAYHAN MOHAMMAD ALI, M Sc Eng.

This thesis is submitted to Dublin City University as the fulfilment of the requirement
for the award of Degree of

Doctor of Philosophy

School of Mechanical and Manufacturing Engineering

Dublin City University

June 1995

Dedicated to my parents

DECLARATION

This is to certify that the material presented in this thesis is entirely my own work, except where specific references have been made to the works of others, and no part of this work has been submitted in support of an application for another degree or qualification to this or any other establishment

Signed



Abu Rayhan Mohammad Ali

June 1995

ID 91700566

ACKNOWLEDGEMENTS

I would like to thank to Professor M S J Hashmi for his supervision and guidance during this research work. Thanks are also expressed to Dr M El-Baradie for his helpful suggestions from time to time during my studies.

I would also like to thank to Professor S A Meguid of the University of Toronto for his constructive suggestions and helpful advice during his short visit to DCU. I highly appreciate the help of Dr L Looney for her comments on the initial draft of the thesis.

I would like to express my thanks to Mr Liam Domican and Mr Ian Hopper for their technical assistance at various stages of this work.

Finally, the patience and encouragement of my wife, Sharmin, and family deserve greater acknowledgement than words can express.

ABSTRACT

Plastic yielding characteristics of a rod under successively applied torsion and tension loadings

By

Abu Rayhan Mohammad Ali

This thesis is concerned with the elasto-plastic behaviour of circular rods under combined torsion-tension loading. Three aspects of the work were examined. In the first, an instrumented mechanical torque-tension machine was designed, built and commissioned to enable the application of biaxial loading under controlled conditions. The main features of the machine are (i) it can apply either simultaneous or individual loadings subject to a specific deformation history and (ii) it provides the time variations of the controlling and the controlled deformation parameters using the appropriate load cells and transducing elements. Whilst the machine was controlled by analogue signals, it was designed such that it could allow digital control of the different command signals. An analytical model to calculate the stiffness of the machine has been developed.

The second was wholly devoted to the experimental investigations where solid, copper and steel, circular rods were subjected to complex non-proportional biaxial loading paths. In these paths, elasto-plastic torsion followed by tension, keeping the angle of twist constant, and elasto-plastic tension followed by torsion, holding the corresponding axial displacement constant, were examined. Other loading paths, where the initial axial loads and the torques were maintained constant, and where the torque and the axial load were applied successively, were also studied. The experimental programme also considered the biaxial loading of thin-walled steel tubes. In the third, the experimental results were compared with two different analytical models from the literature. Numerical solutions were also obtained along the lines described in an available literature.

Experimentally, it has been observed that when the rod is initially subjected to a torque and then, keeping the angle of twist constant, to a gradually increasing axial load, the rod behaves as if its torque carrying ability becomes drastically reduced without in any way affecting its load carrying ability. Similarly, when the rod is initially subjected to an axial load and then, keeping the axial displacement constant, to a gradually increasing torque, the rod behaves as if its load carrying ability becomes drastically reduced without in any way affecting its torque

carrying ability. Such reductions in the load or torque capacity appear to be governed by the material plastic yield criterion.

During the successively applied loading, it has been observed that when the rod is initially subjected to an initial torque and then to a successively applied axial load and torque, keeping the axial displacement or the angle of twist constant in an alternate manner, the rod soon regains its axial load carrying capability irrespective of the initially applied torque. Similarly, during the multiple alterations of successively applied torque or axial load, it has been observed that at any stage for the axial load or torque, whichever was applied subsequently, the rod regains its carrying capability of the parameter involved. Experimental test results with fitted strain gauges show that, even when the angle of twist or axial displacement was held constant, the strain readings increase rapidly with the decrease of the initially applied torque or axial load at the confined zone where the plastic deformation begins. Elsewhere of the specimen the strain readings decrease.

The findings of this work have direct bearing on the relaxation of tightening torques or axial loads as experienced by critical engineering components, such as couplings, bolted joints and rotating shafts, which are subjected to similar type of biaxial loadings.

NOMENCLATURE

A	cross-sectional area
A_0, B_0	function defined in equation 4.36(a)
E	Young's modulus
F	axial load
F	normalised axial load (F/F_y)
G	modulus of rigidity
H'	slope of effective stress generalized plastic strain curve
I	second moment of inertia
J	polar moment of inertia
J_1	first invariant of strain
L	length
P	ratio of shear stress to yield shear
Q	ratio of axial stress to uniaxial yield stress
T	torque
T	normalised torque (T/T_y)
Y	yield stress in tension
a	radius of solid rod
c	radius of the elastic-plastic boundary
k	yield stress in shear
ℓ	length
n	strain hardening parameter
n'	safety factor in designing
u, v, w	displacements
k_f	stress concentration factor
R	outer radius of solid rod
\underline{r}	r/R
α	a constant
δ_{ij}	Kronecker delta
ν	Poisson's ratio
θ/ϕ	angle of twist
ρ	parameter characterizing state of plastic deformation
σ	axial stress

σ_{ij}	general stress tensor
σ'_{ij}	deviator stress tensor
$\bar{\sigma}$	effective stress
$\underline{\sigma}_m$	dimensionless volumetric stress
$\bar{\underline{\sigma}}$	dimensionless effective stress
$\underline{\sigma}_r, \underline{\sigma}_\theta, \underline{\sigma}_z, \underline{\sigma}_a, \underline{\tau}$	dimensionless stresses
$\underline{\sigma}'_r, \underline{\sigma}'_\theta, \underline{\sigma}'_z, \underline{\tau}$	dimensionless deviatoric stresses
τ	shear stress
ε	axial strain
$\underline{\varepsilon}$	normalised axial strain ($\varepsilon/\varepsilon_y$)
γ	shear strain
$\underline{\gamma}$	normalised shear strain (γ/γ_y)
$\underline{\varepsilon}_r, \underline{\varepsilon}_\theta, \underline{\varepsilon}_z, \underline{\varepsilon}_a$	modified strains
ε_{ij}	general strain tensor
$\bar{\varepsilon}^p$	generalized plastic strain
$\underline{\bar{\varepsilon}}^p$	modified generalized plastic strain
$e_r, e_\theta, e_z, \gamma$	deviator strains
$\underline{e}_r, \underline{e}_\theta, \underline{e}_z$	modified deviatoric strain
λ	proportionality factor in Lévy - Mises equation
η	= c/a
ξ	= r/a

superscripts

e	elastic component
'	deviatoric component
p	plastic component

subscripts

a	alternating component of the stress
e	elastic component
m	volumetric component
o	any arbitrary loading condition
p	plastic component

y	yield condition
x,y,z,xy,yz,zx	referred to cartesian co-ordinates
r,θ,rθ,θz,zr	referred to cartesian co-ordinates
1,2,3	principal components
me	mean components of the stress
en	endurance limit

LIST OF FIGURES

Chapter One	Page no.
Figure - 1.1 - The method of approach adopted in the present study	10
Chapter Three	
Figure - 3.1 - Schematic diagram of the machine (front view)	73
Figure - 3.2 - Schematic diagram of the machine (side view)	74
Figure - 3.3 - Schematic diagram of the main frame of the machine	75
Figure - 3.4 - Details of the bottom plate	76
Figure - 3.5 - Details of the drive shaft housing	77
Figure - 3.6 - Details of the top plate	78
Figure - 3.7 - Details of the ball screw	79
Figure - 3.8 - Details of the cross-head	80
Figure - 3.9 - The complete cross-head arrangement including the dowel pin load cell and other auxiliary components	81
Figure - 3.10 - Assembly drawing of the torque-tension shaft	82
Figure - 3.11 - Assembly drawing of the torsion shaft	83
Figure - 3.12 - Geometry of the specimen holder	84
Figure - 3.13 - Dimension of the gripper in detailed	85
Figure - 3.14 - Assembly drawing of the preloading unit	86
Figure - 3.15 - Schematic diagram of a Moog brushless drive system	87
Figure - 3.16 - Dimensions of motor-1	88
Figure - 3.17 - The characteristic curve of motor-1	89
Figure - 3.18 - Details of gearbox-1	90
Figure - 3.19 - Details of motor-2	91
Figure - 3.20 - The characteristic curve of motor-2	92
Figure - 3.21 - Various dimension of gearbox-2	93
Figure - 3.22 - The flow chart of the operating principle of the controllers	94
Figure - 3.23 - Various connections of the controller and the power supply unit	95
Figure - 3.24 - Circuit diagram among the controllers and motors	96
Figure - 3.25 - The schematic diagram of the control panel	97
Figure - 3.26 - The output characteristic curve of the angle measuring transducer	98
Figure - 3.27 - Details of the angle measuring transducer	99
Figure - 3.28 - The schematic diagram of the instrumentation	100
Figure - 3.29 - Force analysis diagram of the torque-tension machine (upper part)	101
Figure - 3.30 - Force analysis diagram of the torque-tension machine (lower part)	102

Chapter Four

Figure - 4 1	- Variations of the initially applied torque with the axial strain	127
Figure - 4 2	- Variations of the initially applied axial load with the shear strain	128
Figure - 4 3	- Variations of the initially applied torque for different strain hardening parameters	129
Figure - 4 4	- Variations of the initially applied axial load for different strain hardening parameters	130
Figure - 4 5	- Specimen subjected to a initial torque	131

Chapter Five

Figure - 5 1	- Calibration curve for the vertical speed of the cross-head	146
Figure - 5 2	- Calibration curve for the tensile loading of the specimen	147
Figure - 5 3	- Calibration curve for the angular speed of the specimen	148
Figure - 5 4	- Calibration curve for the torque applied to the specimen	149
Figure - 5 5(a)	- Torque versus angle of twist curve	150
Figure - 5 5(b)	- Axial load versus angle of twist curve	150
Figure - 5 5(c)	- Torque versus angle of twist curve when torque maintained constant	151
Figure - 5 6(a)	- Axial load versus axial displacement curve	151
Figure - 5 6(b)	- Torque versus axial displacement curve	152
Figure - 5 6(c)	- Torque versus axial load curve when load maintained constant	152
Figure - 5 7	- Geometry of the specimen	153
Figure - 5 8(a)	- Geometry of the uniform diameter specimen	154
Figure - 5 8(b)	- Position of the strain gauges in the uniform diameter specimen	154
Figure - 5 8(c)	- Geometry of the reduced section specimen	155
Figure - 5 8(d)	- Position of the strain gauges in the reduced section specimen	155
Figure - 5 9(a)	- Specially designed head to fit with the thin-walled tube	156
Figure - 5 9(b)	- The assembly drawing of the thin-walled tube	157
Figure - 5 10	- Different types of strain gauges used	158
Figure - 5 11	- Different stages of strain gauges preparation	159
Figure - 5 12(a)	- A typical full bridge connection between the strain gauges and the switch and balance unit	160
Figure - 5 12(b)	- Circuit diagram between the strain indicator and the balance unit	160
Figure - 5 13	- Axial strain versus time curve	161
Figure - 5 14	- Shear strain versus time curve	162

Chapter Six

Figure - 6 1	- Uniaxial tensile load versus axial strain curve (steel)	197
--------------	---	-----

Figure - 6 2	- Axial stress versus axial strain curve (steel)	197
Figure - 6 3	- Normalised axial stress versus normalised axial strain curve	198
Figure - 6 4	- Torque versus shear strain curve (steel)	199
Figure - 6 5	- Normalised torque versus normalised axial load curve for steel (angle of twist constant)	200
Figure - 6 6(a)	- Normalised axial strain versus normalised torque and load curve for steel (T = yield torque)	201
Figure - 6 6(b)	- Normalised axial strain versus normalised torque and load curve for steel (T = 75% of yield torque)	202
Figure - 6 6(c)	- Normalised axial strain versus normalised torque and load curve for steel (T = 50% of yield torque)	203
Figure - 6 7	- Normalised torque versus normalised axial load curve for copper (angle of twist constant)	204
Figure - 6 8(a)	- Normalised axial strain versus normalised torque and load curve for copper (T = yield torque)	205
Figure - 6 8(b)	- Normalised axial strain versus normalised torque and load curve for copper (T = 75% of yield torque)	206
Figure - 6 8(c)	- Normalised axial strain versus normalised torque and load curve for copper (T = 50% of yield torque)	207
Figure - 6 9	- Normalised axial strain versus normalised shear strain curve for steel (torque maintained constant)	208
Figure - 6 10	- Normalised axial load versus normalised torque curve for steel (axial displacement constant)	209
Figure - 6 11(a)	- Normalised shear strain versus normalised axial load and torque curve for steel (F = yield load)	210
Figure - 6 11(b)	- Normalised shear strain versus normalised axial load and torque curve for steel (F = 75% of yield load)	211
Figure - 6 11(c)	- Normalised shear strain versus normalised axial load and torque curve for steel (F = 50% of yield load)	212
Figure - 6 11(d)	- Normalised shear strain versus normalised axial load and torque curve for steel (F = 25% of yield load)	213
Figure - 6 12	- Normalised axial load versus normalised torque curve for copper (axial displacement constant)	214
Figure - 6 13(a)	- Normalised shear strain versus normalised axial load and torque curve for copper (F = yield load)	215
Figure - 6 13(b)	- Normalised shear strain versus normalised axial load and torque curve for copper (F = 75% of yield load)	216
Figure - 6 13(c)	- Normalised shear strain versus normalised axial load and torque curve for copper (F = 50% of yield load)	217
Figure - 6 13(d)	- Normalised shear strain versus normalised axial load and torque curve for copper (F = 25% of yield load)	218

Figure - 6 14	- Normalised axial strain versus normalised shear strain curve for steel (axial load maintained constant)	219
Figure - 6 15	- Determination of yield points due to combined loading for steel (angle of twist constant)	220
Figure - 6 16	- Determination of yield points due to combined loading for copper (angle of twist constant)	221
Figure - 6 17	- Determination of yield points due to combined loading for steel (axial displacement constant)	222
Figure - 6 18	- Determination of yield points due to combined loading for copper (angle of twist constant)	223
Figure - 6 19(a)	- Comparison of experimentally obtained yield stresses with those of Mises' and Tresca's for steel	224
Figure - 6 19(b)	- Comparison of experimentally obtained yield stresses with those of Mises' and Tresca's for copper	225
Figure - 6 20(a)	- Variations of torque and shear strain gauges' readings with axial strain (uniform diameter specimen)(specimen - 1)	226
Figure - 6 20(b)	- Variations of torque and shear strain gauges' readings with axial strain (uniform diameter specimen)(specimen - 2)	227
Figure - 6 20(c)	- Variations of torque and shear strain gauges' readings with axial strain (uniform diameter specimen)(specimen - 3)	228
Figure - 6 20(d)	- Variations of torque and shear strain gauges' readings with axial strain (uniform diameter specimen)(specimen - 4)	229
Figure - 6 21(a)	- Variations of torque and shear strain gauges' readings with axial strain (reduced section specimen)	230
Figure - 6 21(b)	- Variations of axial load and axial strain gauges' readings with shear strain (reduced section specimen)	231
Figure - 6 22(a)	- Variations of normalised torque and axial load with time for steel (initial T = 98% of yield torque)	232
Figure - 6 22(b)	- Variations of normalised torque and axial load with time for steel (initial T = 75% of yield torque)	233
Figure - 6 22(c)	- Variations of normalised torque and axial load with time for steel (initial T = 50% of yield torque)	234
Figure - 6 23(a)	- Variations of normalised torque and axial load with time for copper (initial T = yield torque)	235
Figure - 6 23(b)	- Variations of normalised torque and axial load with time for copper (initial T = 75% of yield torque)	236
Figure - 6 23(c)	- Variations of normalised torque and axial load with time for copper (initial T = 50% of yield torque)	237
Figure - 6 24(a)	- Variations of normalised axial load and torque with time for steel (initial F = yield load)	238
Figure - 6 24(b)	- Variations of normalised axial load and torque with time for steel (initial F = 75% of yield load)	239

Figure - 6 24(c)	- Variations of normalised axial load and torque with time for steel (initial F = 50% of yield load)	240
Figure - 6 24(d)	- Variations of normalised axial load and torque with time for copper (initial F = 25% of yield load)	241
Figure - 6 25(a)	- Variations of normalised axial load and torque with time for copper (initial F = yield load)	242
Figure - 6 25(b)	- Variations of normalised axial load and torque with time for copper (initial F = 75% of yield load)	243
Figure - 6 25(c)	- Variations of normalised axial load and torque with time for copper (initial F = 50% of yield load)	244
Figure - 6 25(d)	- Variations of normalised axial load and torque with time for copper (initial F = 25% of yield load)	245
Figure - 6 26	- Comparison of experimental results with Gaydon's theoretical model for steel (twist constant)(yield at 0.05% offset)	246
Figure - 6 27(a)	- Comparison of experimental results with Gaydon's theoretical model for steel (twist constant)(yield at 0.02% offset)	247
Figure - 6 27(b)	- Comparison of experimental results with Gaydon's theoretical model for steel (twist constant)(yield at proportional limit)	248
Figure - 6 28	- Comparison of experimental results with Brooks' model for steel (twist constant)	249
Figure - 6 29(a)	- Comparison of experimental results with Gaydon's theoretical model for copper (twist constant)(yield at 0.02% offset)	250
Figure - 6 29(b)	- Comparison of experimental results with Gaydon's theoretical model for copper (twist constant)(yield at proportional limit)	251
Figure - 6 30	- Comparison of experimental results with Gaydon's theoretical model for steel (axial displacement constant)	252
Figure - 6 31	- Comparison of experimental results with Gaydon's theoretical model for copper (axial displacement constant)	253
Figure - 6 32	- Comparison of experimental results with Brooks' theoretical model (twist constant)	254
Figure - 6 33	- Comparison of thin-walled tube's results with those of solid steel and copper (twist constant)	255
Figure - 6 34	- Comparison of thin-walled tube's results with those of solid steel and copper (axial displacement constant)	256
Figure - 6 35(a)	- Variations of the applied torque with the axial load for steel (torque applied first)	257
Figure - 6 35(b)	- Variations of the applied torque with the axial load for copper (torque applied first)	257
Figure - 6 35(c)	- Variations of the applied axial load with the torque for steel (load applied first)	258
Figure - 6 35(d)	- Variations of the applied axial load with the torque for copper (load applied first)	258

Figure - 6 36	- Subsequent ultimate yield locus for steel (torque applied first)	259
Figure - 6 37	- Subsequent ultimate yield locus for copper (torque applied first)	260
Figure - 6 38	- Subsequent ultimate yield locus for steel (load applied first)	261
Figure - 6 39	- Subsequent ultimate yield locus for copper (load applied first)	262
Figure - 6 40(a)	- Comparison of subsequent ultimate yield loci for two different loading paths (assuming fully strain-hardened)(steel)	263
Figure - 6 40(b)	- Comparison of subsequent ultimate yield loci for two different loading paths (assuming fully plastic torque)(steel)	264
Figure - 6 41(a)	- Comparison of subsequent ultimate yield loci for two different loading paths (assuming fully strain-hardened)(copper)	265
Figure - 6 41(b)	- Comparison of subsequent ultimate yield loci for two different loading paths (assuming fully plastic torque)(copper)	266

Appendix - A

Figure - A 1	- Dimensions of the left column	286
Figure - A 2	- Details of the back column	287
Figure - A 3	- Details of the base plate	288
Figure - A 4	- Position of the keyway in the left ballscrew	289
Figure - A 5	- Position of the keyway in the right ballscrew	290
Figure - A 6	- Dimensions of the guide rod	291
Figure - A 7	- Geometry of the steeped shaft	292
Figure - A 8	- Details of the thin plates	293
Figure - A 9	- Geometry of the top cover plate	294
Figure - A 10	- Details of the linear ball bearing	295
Figure - A 11	- Details of the torque-tension shaft	296
Figure - A 12	- Geometry of the torsion shaft	297
Figure - A 13	- Details of the bottom face of the torsion shaft	298
Figure - A 14	- Geometry of the square drive	299
Figure - A 15	- Geometry of the adjuster	300
Figure - A 16	- Geometry of the nut-1	301
Figure - A 17	- Details of the nut-2	302
Figure - A 18	- Schematic diagram of a Moog brushless servomotor	303
Figure - A 19	- Dimensions of the timing pulley	304
Figure - A 20	- Details of the timing belt	304
Figure - A 21	- Geometry of the base plate-1	305
Figure - A 22	- Details of the frame-1	306
Figure - A 23	- Details of the spur gears	307
Figure - A 24	- Geometry of the base plate-2	308

Figure - A 25	- Details of the frame-2	309
Figure - A 26	- Front connections of the controller	310
Figure - A 27	- Front connection of the power supply unit	311
Figure - A 28	- Details of the axial load cell	312
Figure - A 29	- Details of the torque load cell	313
Figure - A 30	- Details of the L V D T	314

Appendix - D

Figure - D 1	- Normalised axial stress versus axial strain curve of Eq - 4-6(a)	323
--------------	--	-----

Appendix - E

Figure - E 1	- Stress components at a point in loaded body	334
Figure - E 2	- Effect of loading path on plastic strain	334
Figure - E 3	- Idealized stress-strain curves	335
Figure - E 4	- Stress distributions for a non-strain-hardening and a strain hardening material	335
Figure - E 5	- Torque versus angle of twist/unit length curve	335

Appendix - F

Figure - F 1	- The uniaxial tensile load versus axial strain curve for copper	337
Figure - F 2	- Pure torque versus shear strain curve for copper	337
Figure - F 3	- The uniaxial tensile load versus axial strain curve for steel-2	338
Figure - F 4	- Pure torque versus shear strain curve for steel-2	338
Figure - F 5	- The uniaxial tensile load versus axial strain curve for thin-walled tube	339
Figure - F 6	- Pure torque versus shear strain curve for thin-walled tube	339

LIST OF PLATES

Chapter Three

Plate - 3 1	- Details of the torque-tension machine	103
Plate - 3 2	- Position of the specimen in the gripper	104
Plate - 3 3	- Position of the torque load cell	105
Plate - 3 4	- Photograph of the controllers, control panel and the external power supply units	106
Plate - 3 5	- Position of the angle measuring transducer	107
Plate - 3 6	- Position of the L V D T	108
Plate - 3 7	- Photograph of the data logging during the test programme	109

Chapter Five

Plate - 5 1	- Photograph of the digital strain indicator and the switch and balance unit	163
-------------	--	-----

LIST OF TABLES

Chapter Three

Table - 3 1	- The specifications of the torque-tension machine	26
Table - 3 2	- Details of the ball screw	29
Table - 3 3	- Functions of various pins on the X μ 7 connector	49
Table - 3 4	- Set-up limits of torque and speed in motor-1 and motor-2	51
Table - 3 5	- Connection of power connector X μ 4	53
Table - 3 6	- Specification of the taper roller bearings	63
Table - 3 7	- Specification of the cylindrical roller bearings	63

Chapter Six

Table - 6 1	- Mechanical properties of the steel (lot-1) and copper	168
-------------	---	-----

Appendix - F

Table - F 1	- Mechanical properties of the steel-2 and thin-walled tube	336
-------------	---	-----

CHAPTER ONE

INTRODUCTION AND JUSTIFICATION

1.1 JUSTIFICATION AND IMPORTANCE OF THE WORK

In metal forming processes, such as forging, extrusion, drawing, rolling etc , where very large plastic strains and deformations occur, elastic strains are usually neglected and the materials can be assumed to be perfectly plastic. On the other hand, where the plastic strains are of the same order of magnitude as the elastic strain, the problems are elasto-plastic problems. These types of problems are of prime importance to the structural and machine designer. With the great premium placed on the saving of weight in aircraft, missile, and space applications, designers can no longer use large factors of safety and designing must be done for maximum load to weight ratio, and this inevitably means designing into the plastic range.

In assessing the ultimate load carrying capacity of some structures, it is frequently necessary to consider the elasto-plastic behaviour of structures. These (ultimate loads) can be calculated from a knowledge of load-deformation relationships for the individual elements of which the structure is composed. Deformation in the elasto-plastic range is much more difficult to calculate than elastic deformations because relationships between the stresses and strains are non-linear and are dependent on the loading history. Furthermore, the stress distribution in most structural members loaded into the elasto-plastic range is also difficult to determine, because the shape of the elastic-plastic interface is itself related to the stress distribution and is therefore unknown until the complete solution is found. However, for a solid circular rod subjected to combined torque and tension, this restriction is removed since the shape of the interface must be annular to preserve axial symmetry.

Structural elements and machine components are usually designed so that material does not yield under the expected loading conditions. The magnitude of the stress, which causes the material to yield under uniaxial or combined loading, can be well predicted by using various theoretical "yielding criteria". Once the yielding has started, the material is said to be either in plastic or elastic - plastic condition depending on the type of material used. If a circular steel bar is subjected to combined axial load and torsion, yielding does not occur until the combined stress state reaches the critical value; i.e., the yield locus of that particular material. Upon reaching the yield locus, if further axial load and/or torque is applied, plastic flow starts in the material. The linear elastic torsion theory stipulates that the maximum shear stress occurs at the outer fibre of the material, accordingly for problems concerning the simultaneous application of axial load and torque, yielding takes place at the outer fibre of the specimen.

Upto the yield point, the combined loading effects can be well explained by various theoretical equations and by different yielding criteria. But the response of the material is difficult to explain, when the axial load or torque is applied beyond the combined yield stresses, holding one parameter, either torque or axial load, as constant. If the axial load is increased continuously to beyond the combined yield stress, holding the angle of twist constant for a certain pre-torque within the elastic range, the manner in which this axial load will effect the magnitude of the initially applied torque requires careful study. Similarly, when both the axial load and the torque are successively applied to a pre-torqued or pre-loaded specimen the response becomes very complex. As it is well known that the behaviour of the material is strongly dependent on the strain path in the plastic region, so that when a solid rod is subjected to the above mentioned types of loadings, it is difficult to predict the exact response of the material both theoretically and experimentally, where the latter needs detailed experimental facilities. However, most of the existing research works, concerning the elastic-plastic response of materials, have been conducted using thin-walled tubes for the sake of simplicity of analysis.

In this research programme, the detailed theoretical and experimental investigations regarding the response of a circular rod in the elastic-plastic range under combined tension and torsion have been carried out. To this end, a torque tension machine has been designed, manufactured and commissioned which facilitates both simultaneous and independent applications of torsional and tensile loads to the specimen.

1.2 INDUSTRIAL RELEVANCE OF THE WORK

Assembly applications can be segmented into two categories. One is the joint in which clamping force is being supplied by the fastener to prevent any movement to the mating part where performance and reliability are a function of the load. In the other category, the fastener is used as a pin or rivet. This type of joint is designed to allow motion in either of the two directions: one is a scissors type motion and the other is a flexing type application. Bolts and nuts, screws fall into the first category.

Fastening bolts are still the most frequently used method in joint technology. This is the case for many components used within the motor, aerospace, and machine tool industries. Designers are reducing the margin of safety which is built into a machine. This change is accountable specially to an aerospace industry which works to a safety factor of 1.1 as the maximum expected load [1]. This forces fastening systems into more acute performance ranges. Moreover, with fasteners and fastener assembly becoming a very expensive part of the end product, utilising the maximum capability of the system is a must. A company can no longer afford to use only 50% of the proof load of a bolt due to poor torque-tension control. Consequently, factors affecting the design and integrity of bolted joints are of considerable industrial interest.

Considerable investigations are still being carried out into bolted joints, specially into the quality of the tightening involved and into the bolt itself. Bolted joints still pose many

problems for engineers, since they involve complex parts working under severe and often limiting conditions. The financial penalties which result from their failure are disproportionate to their intrinsic cost, and this fact justifies the attention which must be paid to them. Recent investigations carried out into numerous failure cases have shown without doubt that such problems and/or incidents are largely due to the misappreciation of the proper response of fastener during tightening and the change it undergoes with additional external load or over tightening.

The design and assembly of bolted joints must assure that the joint remains tightly clamped and the fastener is capable of withstanding the static and dynamic loads that are applied. Service performance of a joint depends on many factors, such as the properties of the fastener and the structure being clamped, response of the bolt and joint under additional load, the tightening process and, not last but not least, on the type of lubrication used. In establishing the design capability of a bolted joint, some frequently asked questions are to be answered, such as

- (i) How tight should the bolt be and what assurance is there that the assembly process can consistently achieve this level of tightening ?
- (ii) What level of external load will cause the joint to open ?
- (iii) What load is felt by the bolt when the service stresses are applied to the fastened assembly ?
- (iv) What are the properties of the bolted joint under dynamic loads or fatigue conditions ?

With recent improvements in the control of fastener tightening and new knowledge of bolt and joint properties, these questions merit detailed attention in order to obtain the maximum performance at minimum cost [2]. Now it has been found that by tightening the bolt to the yield point, not only are higher clamping forces produced but more consistent clamp loads are obtained [3-5]. A bolted joint tightened with yield control to the bolt torque-tension yield

point can withstand very substantial external loads without deterioration. Typically, a concentric joint can have an external load equal to the proof load of the fastener applied [2]

The load felt by the bolt when the service stresses are applied depends not only on the tightening procedure but also on the friction condition of the fasteners. The traditional torque control method of tightening bolts has been shown to give very inconsistent levels of achieved clamp loads when a number of fasteners are tightened to the same torque [3]. The requirement of consistency in clamp load, coupled with the desirability of obtaining the highest clamp loads possible has led to the development of a new tightening system referred to as "Joint Control Tightening" [6], where the bolts are tightened to yield points for the reasons mentioned earlier.

It has been established that as the friction condition at the fastener threads and the underhead bearing surface changes, the proportion of the applied torque available to develop the clamp load also changes [7]. The higher the values of friction coefficient at these areas, the lower the values of resulted clamp loads in the bolts as now more of the applied torque is used to overcome the thread friction. So bolts are yield tightened to reduce the scatter of the resulted clamp load in bolts and to attain consistency in preload whereas bolts are lubricated to increase the clamp load in the joints. Higher preloads are necessary not only to maintain a tight joint, which is the primary objective of a joint assembly, but also to increase the fatigue resistance of the bolts. In a hard concentric joint, preload is the predominant factor governing fatigue. Whereas in an eccentrically loaded joint, the preload is the major factor controlling the additional bolt load. Moreover at higher preload, the additional load felt by the bolt due to the application of external load, is less than that at lower preload [2].

It has also been found that even after yield tightening the bolts, there is a reserve of strength between the as tightened tensile stress and its uniaxial yield strength [8]. That means, if further external tensile load is applied to a yield tightened bolt, it does not fail or reach its tensile yield

point instantly, but can withstand a certain amount of additional tensile load. During this period, i.e., when external loads are applied to the "torque-tension" yield tightened fasteners, all bolts behave elastically. As it is well known that during the tightening process a fastener is subjected to torsional as well as axial stress applied simultaneously. Subsequently, when the assembly or the joint is subjected to external load, the fastener is subjected to additional axial stress or axial and bending stress. In this case, where the external load in the joint results in additional axial load in the pre-loaded fastener, it is expected that the plastic yielding would take place at a total yield load which is less than that if there is no torsional stress present.

So it was felt necessary to carry out investigations to know how the external tensile load affects the magnitudes of the applied torque or how further application of the torque affects the magnitude of the resulted preload in a bolt in the elastic and plastic range. To avoid the complex relationships among the tightening torque, friction co-efficient and pre-load, which results in a bolt, as already discussed earlier, a simple circular rod (fastener like structure) has been used as a specimen.

This research programme has been undertaken to carry out detailed experimental investigations regarding the elastic-plastic response of a circular rod subjected to successively applied torsional and tensile stresses. During bolt tightening, as the main stresses developed are only the tensile and shear stresses, as such the present research investigation is a similar condition to bolt tightening. However, during the tightening process other stress components do arise due to the effects of the helix angle and the geometry of thread, the effect of these stresses are not being considered in the present study because of simple design of the specimen.

1.3 AIMS OF THE STUDY

The main objectives of the current work can be summarised as follows

- (i) To design, build and commission an instrumented mechanical torque-tension machine which is capable of applying biaxial loads, such as torque and tension, either simultaneously or independently under different controlled conditions
- (ii) To carry out a detailed experimental investigation to observe the elastic-plastic response of a pre-stressed rod (i.e., either torque or tension) when subjected to subsequently applied parameters (i.e., either axial load or torque) under different controlled and boundary conditions, and to enhance better understanding of the mechanics of such response
- (iii) To verify the experimental results obtained during the biaxial loading with theoretical models

In order to achieve the above mentioned objectives, the following method of approach has been adopted

1.4 METHOD OF APPROACH

The method of approach, shown schematically in figure 1, has been divided into three main sections. The first one was devoted to design, manufacture and commissioning of an instrumented mechanical torque-tension testing machine to enable the application of biaxial loading under controlled conditions. The second was wholly concerned with the experimental investigations where solid rods were subjected to complex non-proportional biaxial loading paths. In these paths, elasto-plastic torsion followed by tension, keeping angle of twist constant, and elasto-plastic tension followed by torsion, holding corresponding axial displacement constant, were examined. Other loading paths, where the initial axial loads and the torques were maintained constant, and where the torque and the axial load were applied successively, were also studied. The experimental programme also considered the biaxial

loading of thin-walled steel tubes. In the third, the experimental results were compared with two different analytical models, developed by Gaydon [18] and Brooks [20], respectively.

In building the machine, the main frame along with its necessary auxiliary components were designed and manufactured, proper drive and control systems were selected, and appropriate load cells and transducing elements were attached to it. The machine was then commissioned and calibrated. In the theoretical investigations, a numerical solution scheme was developed along the lines of Gaydon.

The experimental investigations under combined loading were carried out according to the following steps:

- (i) Initial torque of known level, within the elastic range of the material was applied, and then, axial load was gradually increased beyond the uniaxial yield load, holding the corresponding angle of twist constant.
- (ii) Procedure (i) was repeated except the applied initial torque, rather than angle of twist, was maintained constant.
- (iii) Initial axial load of known level, within the elastic range of the material, was applied and then, torque was gradually increased beyond the yield torque, keeping the initial axial displacement constant.
- (iv) Procedure (iii) was repeated except, in this case the initially applied axial load, rather than axial displacement, was maintained constant.
- (v) Initial torque of known level, within the elastic range, was applied and then, holding the corresponding angle of twist constant, axial load was gradually increased until the specimen yielded due to the combined loading. Subsequently, small increments of torque and axial load were successively applied beyond the combined yield point, holding the axial displacement or the angle of twist constant in an alternate manner.
- (vi) Initial axial load of known level, within the elastic range of the material, was applied and then, holding the corresponding axial displacement constant, torque was gradually increased.

until the specimen yielded due to the combined loading. Then, axial load and torque were successively applied beyond the combined yield point, holding the angle of twist or axial displacement constant in an alternate manner.

1.5 LAYOUT OF THESIS

This thesis has been divided into seven chapters. Following this introductory chapter, chapter two gives a critical review of the relevant literature. Chapter three is devoted to the design, manufacture and commissioning of the test rig. This chapter also contains the details of various drive, control and data acquisition systems used in this machine. Chapter four gives the analytical formulation of different theoretical models used to compare with the experimental results. It also contains an analytical model to calculate the stiffness of the torque-tension machine. Chapter five is devoted to the experimental procedures followed during the tests and, for the selection and design of the test specimen. This also contains the calibration results of the testing machine. Chapter six is devoted to the analysis of the results and discussion and, also for the comparison of the experimental results with the theoretical predictions. Chapter seven mentions the summary of the findings of the research and recommendation for future works.

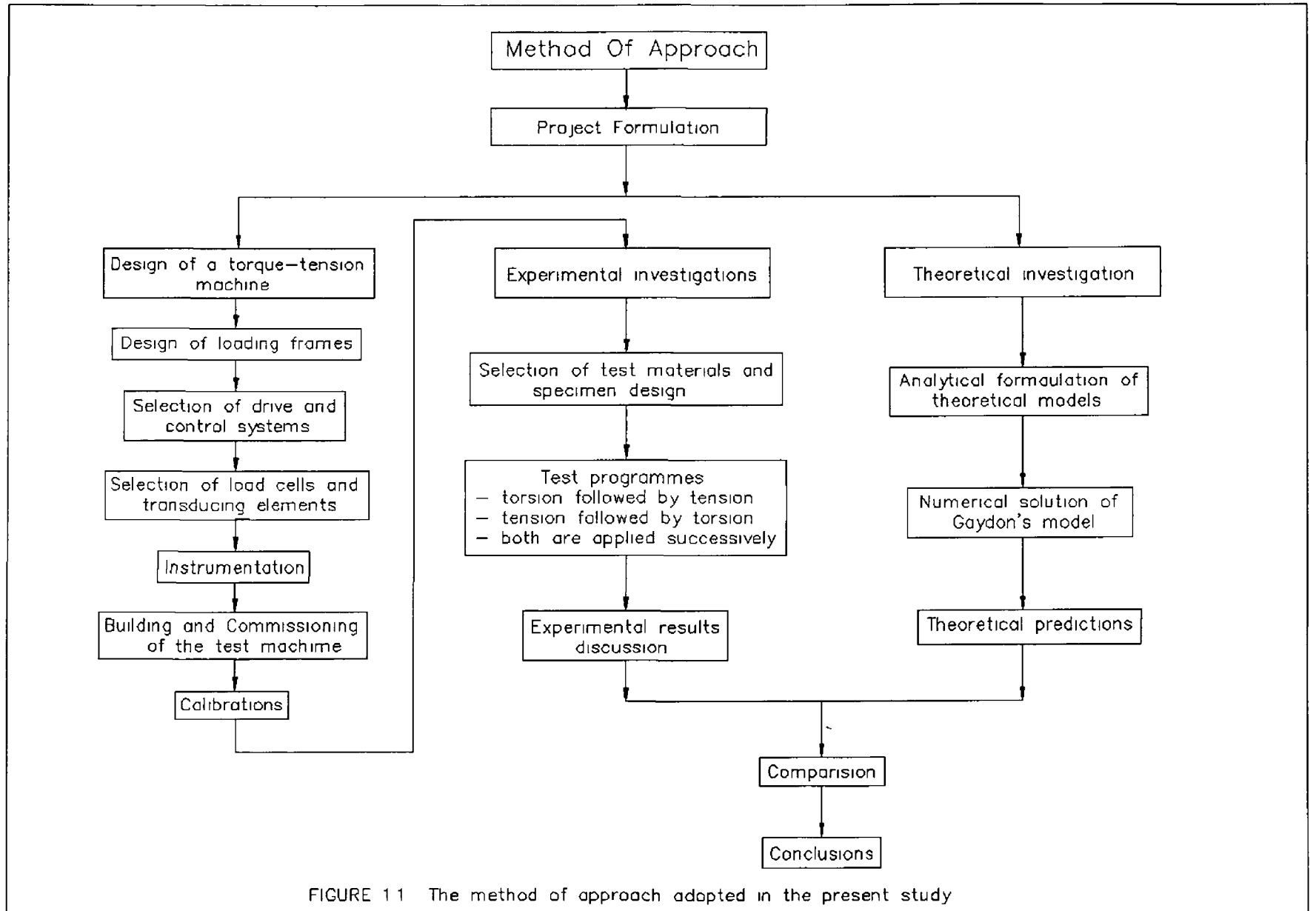


FIGURE 11 The method of approach adopted in the present study

CHAPTER TWO

LITERATURE REVIEW

2.1 INTRODUCTION

Most of the early experimental investigations under combined stresses and in the elastic-plastic or in the fully plastic region have been carried out either to verify different analytical and numerical solutions of the elastic-plastic or plastic stress-strain relationships, proposed by various investigators, or to verify different yield criteria. In most investigations, a thin walled tube has been used as the specimen for the sake of simplicity. However, as detailed experimental work under combined torsion and tension involves complex loading histories, and hence needs a proper testing machine, very few attempts have been made to conduct similar types of experimental work. This chapter provides critical review of the previous investigations related to the present work for both solid and thin walled specimens.

2.2 HISTORICAL PERSPECTIVE OF COMBINED LOADING IN THE ELASTO- PLASTIC REGION

The conditions under which various materials begin to deform plastically have been the subject of many experimental investigations during the last hundred years. Among these, investigations on various materials, which might be mentioned are, as outlined by Nadai [9], the tests with ductile metals, rock materials, marble and sandstone under combined stress, with zinc and steel, and concrete under combined stress. Tests on iron, copper, nickel, aluminium, lead, cadmium, mild steel, glass, brass and nickel-chrome-molybdenum steel were also reported in reference [9].

The most detailed experimental investigation under combined stresses in the elastic-plastic range have been carried out by Lode [10]. He tested thin-walled metal tubes of steel, copper and nickel, as outlined by Mendelson [76], under various combinations of longitudinal tension and internal pressure to verify different yield criteria. Lode devised a very sensitive method of differentiating between the Tresca and von Mises yield criteria by determining the effect of the intermediate principal stress on yielding. He introduced a parameter, called "Lode's stress parameter" to account for the influence of the intermediate stress in the von Mises criterion, which is the ratio of the difference between the intermediate stress and the average of the largest and smallest stresses to half the difference between the largest and smallest stresses. It was shown that the experimental results have better agreement with von Mises criterion than Tresca's.

In the following year, Lode also carried out same type of experiments, as outlined by Hill [11], to investigate the validity of the Levy-Mises strain-stress relations. An approximately constant ratio of axial and circumferential stresses was maintained in each test. It was found that the relation was valid to a first approximation, but despite appreciable scatter in the data due to anisotropy (i.e. in many instances Lode's strain parameter was not equal to -1 in simple tension, as it should be in an isotropic material from symmetry alone) in the drawn tubes, the results indicated a probable deviation from the Levy-Mises strain-stress relation.

K. Hohenemser [12] also carried out experimental investigations to verify the validity of the Reuss stress-strain equations. He used pre-strained mild steel, as outlined in [11], to secure a sharp yield point and reduce the rate of hardening to a value small compared with the elastic modulus. A cylindrical tube was twisted to obtain an approximately uniform distribution of stress at the point of yielding and then holding the angle of twist constant, the tube was extended longitudinally. Though one of the biaxial loading paths followed during the present experimental investigation was similar to the above mentioned path, the idea of performing the test was completely different. In the present case attempt was made to observe elastic-

plastic response of a pre-stressed solid rod when subjected to different parameter, such as torque or tension, whereas Hohenemser's experiment was performed to verify the validity of the Reuss stress-strain equations. However, no conclusion was found regarding the Hohenemser's experiment from any published paper. Later on, Morrison and Shepherd [14] carried out similar experiments to verify the validity of Reuss-Prandtl equations.

Taylor and Quinney [13] used aluminium, copper, and mild steel tubings, which were very nearly isotropic and stressed them in combined tension and torsion, primarily to verify different yield criteria. Thin walled tubes were first loaded in tension into the plastic range then partially unloaded and twisted until some further plastic flow occurred. The axial load was held constant while the torque was increased, so that stress ratios were not constant. The torque-twist or torque-extension diagrams were extrapolated back to zero twist or zero extension to establish approximately, but fairly accurate, the torque at which plastic flow recommenced. The degree of anisotropy was kept within allowable limits by observations of the change in internal volume of the tubes during pure tension. By first straining each specimen in tension, they were able to pre-strain the material by any desired amount and also to detect anisotropy in the material. Although Taylor and Quinney ignored the possibility of an elastic increment of strain during plastic flow, they also found the same results regarding the von-Mises yield criteria and concluded that the deviation from the von-Mises criterion was real and could not be explained on the basis of experimental accuracy or isotropy.

Morrison and Shepherd [14] subjected thin hollow tubes to tension and torsion to follow a complex path of stress to compare the experimentally found strain paths with those calculated by Prandtl-Reuss and Hencky stress-strain relations. Here plastic and elastic strains were comparable. The material used was 5 percent nickel steel and 11 percent silicon-aluminium alloy. They applied first tension, then holding the tensile stress constant, applied torsion, followed by further tension and torsion to obtain various strain paths. The measured

variations of length and twist were in substantial agreement with the predictions of the Reuss equations

Siebel [15] overstrained a thin tube by simultaneous action of bending and twisting couples. He tested the validity of the Reuss stress-strain relations when the stresses and the strains were not uniformly distributed. The test results were found to be predicted very accurately by the theory. To investigate the rapidity of approach to the plastic-rigid yield point values, Hill *et al* [16] used alloy steel bars of circular cross section which were strained in combined torsion and bending. In each test, the ratio of bending and twisting moments was held constant. In order to eliminate machining stresses, as far as possible, all the specimens were subjected to a stress relief anneal after machining. They compared their experimental results with the calculated yield point of the bar and obtained upper and lower bound solutions. The results showed that the plastic-rigid yield points may be used in design calculations.

Prager and Hodge [17] and Gaydon [18] developed analytical expressions for the stress distributions and deformations of solid circular bars subjected to combined tension and torsion in the elastic-plastic range. In both cases the analysis was restricted to a material with a specific Poisson's ratio ($=\frac{1}{2}$), i.e., they did not take the effect of elastic compressibility. The latter author considered various combinations of twist and extension. The Reuss equations were used throughout and these were integrated, for different cases, to give the shear stress and tension in the plastic range. However, during the present study a numerical solution for Gaydon's analytical model has been developed, which within the author's knowledge has not been performed by any other investigator.

Brooks *et al* [19-20] examined analytically and numerically the behaviour of a circular bar subjected to combined axial load and torque in the elasto-plastic range. In reference [20], Ramberg-Osgood curves were used to describe the material behaviour, and the analysis was based on the Prandtl-Reuss incremental stress-strain laws and the von Mises yield criterion.

Brooks [20] obtained numerical results for both proportional and non-proportional loading combinations. Elastic compressibility was taken into consideration which was shown negligible for all practical purposes.

Naghdi *et al* [21] conducted experimental investigation with tubular specimen, made of 24 S-T4 aluminium alloy, which were subjected to combined action of tension and torsion with variable loading paths. The loading was such that tension alone was followed by torsion and permitted the determination of the initial shear modulus when twist began. These tests were performed to determine the initial anisotropy of the material tested. The experimental results were discussed in the light of incremental-strain theories of plasticity.

In problems involving both elastic and plastic deformation, the plastic strain rates may vary with position and time by several orders of magnitude even for constant total deformation rates. For certain metals and alloys, such large variations in plastic strain rate cause significant changes of flow stress. Meguid *et al* [22-24] carried out a number of investigations, both theoretically and experimentally, under combined torque and tension for rate dependent material. Thin walled circular tubes of both elastic-perfectly plastic and work hardening materials were used in their works. In reference [23], bilinear deformation paths of twist at a constant rate followed by extension at different rates were examined to evaluate the plastic flow of the material under abruptly-changing deformation paths and strain-rates. Experimental results were compared with the existing strain-rate dependent theory. The experimental results indicated that there exist appreciable differences between the von-Mises equivalent stress versus equivalent plastic strain curves for the different bilinear paths investigated. These differences were attributed to the strain-rate sensitivity of the particular material. However, almost in all their experimental works they have considered only one non-proportional biaxial loading path, i.e., torsion followed by tension keeping angle of twist constant. They did not consider any other non-proportional loadings as has been considered in the present study. Furthermore, they tested thin-walled tube not the solid rod.

McMeeking [25] discussed the kinematics and stress analysis of the tension-torsion test of a thin-walled tube at finite strain. He formulated the relationships between increments of tension and torque and increments of extension and twist for an elastic-plastic material at finite plastic strain for the most common constitutive assumption. He evaluated the validity of the Prandtl-Reuss equations for different ranges of plastic strains (i.e., when plastic strains are very large and when they are comparable with the elastic strains).

Investigations on the springback of plastically deformed material under combined torsion and tension have been carried out by Narayanawamy *et al* [26]. Rectangular bars of two different materials have been used as the specimens. These specimens were standard ASTM E-8 specimens with 2 inch gauge length. Their experiments were of two types. In the first set of experiments, the bars were initially pulled at different level of axial strains in the plastic region, and then, were twisted for different angles of twist. At the end, both load and torque were removed simultaneously and angular springback of the material was recorded. The other type of experiment was of opposite nature, i.e., pre-torqued specimen was loaded by tension. They mainly investigated angular springback. They concluded that the springback was analytically predictable and experimentally found that the twist followed by pull produced smaller angular springback upon release of torque and force than that produced deformation in the reverse order.

Based on the kinematic hardening theory, Wei Jiang [27-28] conducted analytical investigations regarding the elastic-plastic response of thin-walled tubes subjected to combined axial load and torsion. Exact closed-form solutions were obtained for linear loading paths. Stress-strain relationships, together with the corresponding movements of the yield centre, were discussed for both monotonic and variable loadings. The response of the tube under non-proportional loading was shown to be path-dependent. Authors of reference [29] carried out similar type of investigations as mentioned above, where thin-walled tubes were subjected to axial load and internal pressure, instead of torsional load.

Experimental investigations under combined stresses have also been carried out to obtain the initial and the subsequent yield loci for different materials under different loading conditions. Though the main concern of the present research was not on the development of the subsequent yield loci, a few relevant works regarding the above mentioned topic have been presented here to give a much broader idea on the effect of combined stresses in the elasto-plastic range. Typical investigations, on the initial and the subsequent yield loci, conducted by Naghdi [30], McComb [31], Ivey [32], Mair and Pugh [33], Phillips and his co-workers [34-38], Tang [39], Bertsch and Findley [40], Marjanovic and Szczepinski [41], Shiratori *et al* [42-44], Moreton *et al* [45], Rees [46-49] and Yeh [50-51], might be mentioned.

Experimental work investigating the subsequent yield surface was initiated by Naghdi, Essengburg and Koff [30]. In their experiments, tubular specimens made of 2024-T4 aluminum were initially pre-stressed in shear, and the shapes of subsequent yield surfaces were determined in the first and fourth quadrant of a two-dimensional stress space. All yield surfaces corresponding to different pre-stress points were convex and elongated in the direction of the pre-stress. Also observed are the Bauschinger effect and a lack of cross effect. The lack of cross effect was also observed by McComb [31] who investigated the subsequent yield surface for the specimens of 2024-T4 aluminum.

Ivey [32] subjected a tubular specimen of 2024-T4 aluminum to combined tension and shear with pre-straining in shear direction. His results show considerable modification in shape of the subsequent yield surface due to strain hardening. A definite shrinkage of the size of the yield surface was noticed. Curvature near the pre-straining point was also found to increase. A general translation of the yield surface in the direction of pre-straining was evident.

Mair and Pugh [33] conducted a number of interesting tension-torsion tests on thin-walled copper tubes, where the specimens were pre-strained in tension, partially unloaded, and then strained in torsion. Yield was defined by the Lode extrapolation technique. The subsequent

yield surfaces were consistent with isotropic hardening accompanied by relatively slight distortion Bertsch and Findley [40] conducted extremely accurate tests on thin-walled tubes of 6061-T6 aluminum Seven subsequent yield surfaces with the same specimen were obtained when yielding was defined by small offset strain

Phillips and co-workers in numerous papers [34-38] also reported that the subsequent yield surfaces were convex and that cross effect was weak They subjected the specimens of aluminium 1100-0 to pre-stressing in tension, in torsion, and in combined tension and torsion Translation of the subsequent yield surface in the direction of pre-stressing was observed Further, the yield surface changes its size in the direction of pre-stressing and becomes smaller when moved away from the origin, but larger when directed towards the origin

Thin walled tubular specimen of annealed medium carbon steel was tested by Meguid *et al* [52] where the specimen was subjected to combined torque and tension to obtain the initial yield locus of the specimen Here they obtained almost the entire positive quadrant of the initial yield locus from a single run without unloading or reloading (neutral loading) Particular attention was given to the effect of the axial strain-rate on the shape of these initial yield loci

Rees and others [46-49] have conducted extensive investigations, both experimentally and theoretically, on the development of the yield locus considering biaxial loading cases Moreton *et al* [45] conducted experimental investigation where tubular specimens were subjected to combinations of internal pressure, axial load and torsion Their experimental results were compared theoretically by the author of reference [49]

Han and Yeh [51] have determined experimentally the initial and subsequent yield surfaces of annealed AISI type 304 stainless steel in the axial-torsional stress space Three loading paths

pure axial path, pure torsional path, and proportional axial-torsional path were investigated. Each path included loading, unloading, and reloading state.

2.3 REVIEW WORK ON BOLTED JOINTS

It has already been mentioned that during bolt tightening the main stresses developed are combined tensile and shear stresses and hence some previous works regarding the response of fasteners and their joints under load are presented in this section.

Most theoretical and experimental investigations within this area have been conducted for the purpose of improving the performance and reliability of the fasteners and their joints. Historically, Archimedes in 250 B.C. developed and recorded the first spiral screw and used it for lifting irrigation water. However, it was not until the middle of the 15th century that threaded fasteners were used for assembly [53]. It was the advent of the industrial revolution, however, that nuts and bolts became commonplace as fasteners. Many inventions of the time relied extensively on threaded fasteners. Among them were James Watt's steam engine, James Hargreave's spinning jenny and Eli Whitney's cotton gin [54-55]. Most of the early investigations regarding the fasteners were devoted to the development of uniform and standard threads, such as Whitworth thread, Sellers thread or ISO thread, which are now extensively being used as standard thread.

Over the past two decades, the demands for assurance of quality and reliability in engineering structures or components have steadily increased. To improve these, in mechanically fastened assemblies, detailed analysis of bolts and bolted joint has been carried out by many investigators. Fasteners' weight as well as the weight of components may be reduced by any of the following ways: by choice of material [56], subjecting the fastener to high design stresses, i.e., minimise fastener size [57], and by reducing the material content of the bolt's

head as investigated by Landtl [58] Extensive developments have taken place in the design of the fastener itself with the rolling of threads after heat treatment [59]

Gardiner [1] investigated the various factors that effect the torque-tension relationships of fasteners during the tightening process He mentioned that the torque-tension relationship was affected by tangible (physical item) and intangible variables (assembly method) Tangible factors were, plating conditions of the threads and bearing surfaces, hardness of the components, resilience of mating material, grade and class of fit, and lubrication Intangible factors were, operation performance, method of assembly and tool driving speed He tightened the fasteners using zinc plated and cadmium plated nut and found that the torque needed to reach a similar load was almost twice as much for the zinc plated hardware than for the cadmium plated one

A dynamically loaded joint fails in most cases either by fatigue or by rotation loosening of the fasteners Even the fatigue failure is often initiated by partial loosening Junker [60] investigated the self-loosening of pre-loaded bolted connections when subjected to vibration He applied various desired levels of vibration, which closely simulated the actual conditions, in a pre-loaded joint by means of a vibration machine Whilst Goodiner and Sweeney [61] as well as Sauer *et al* [62] tested only axial dynamically loaded connections, Junker generated transverse forces and displacement as well as combinations of transverse and axial force He has proposed special locking features to resist vibration It was found that the dynamic transverse forces were more undesirable than dynamic axial forces Axial forces cause relative movements through expansion of the nut thread, whereas, transverse forces cause relative movements through rocking action of the screw in the internal thread or rocking motions of the nut on the external thread

The primary objective of tightening a fastener is to develop sufficient clamping load to form and maintain as essentially solid joint even when working loads are applied Since the resulted

preload in the bolt not only depends on the friction but also on the methods of tightening processes, a number of investigations have been carried out to select the proper tightening process for a desired preload

Boys and Wallace [6] have introduced a new tightening control system, called "joint control system", where bolts are tightened to yield irrespective of the total torque required and lubrication conditions. The system operates by sensing the gradient of the torque-rotation characteristics and detects the yield point of the fasteners. It does not require pre-set control of torque or rotation angle as required by other tightening control processes such as "torque control" or "angle control" process. Their results showed that the system has increased bolt clamping loads and reduced their scatter very significantly. Finkelston and Wallace [3] also investigated detailed analysis of the bolted joint about the working loads imposed on the joint and the stresses felt by the bolt.

Sorel and other [63] have introduced a new method for measuring the value of the resulted preload more accurately during bolt tightening. The tightening tension can be measured by an ultrasonic impulse method using echographs with a time basic. They have shown that inaccuracy in the tightening measurement was less than $\pm 5\%$ if the tested bolts have met some simple geometrical criteria.

A test programme was designed and executed by Becker and others [64] to study the accuracy and precision of a bolt torquing system which tightens the bolts to their torque-tension yield point. The test programme compared bolt preload values to both the axial yield point and to the rotation torque applied to the bolt head. The test programme also included measuring the permanent elongation of the bolt to verify the performance. Results showed that parts of this test programme can be used to verify the accuracy and precision of the bolt torquing system in the manufacturing environment.

In reference [65], the authors investigated the plastic region tightening method applied to the cylinder bolts in developing the new 2.0 litre and 2.2 litre diesel engines. The bolts were tightened by "angle controlled tightening method" to bring the bolts' load into the plastic region. They used bolts with different shank diameters and with different tensile strength. The test results indicated that the plastic region tightening method made it possible to raise the minimum bolt load by 50% and reduce the bolt load variation to about one half as compared with the torque controlled method. Frictional effect was also largely eliminated. They proposed that, although the bolt's fatigue strength decreased as the plastic lengthening progressed, thread rolling after heat-treatment and well-finished thread root radius made it possible to provide satisfactory fatigue strength in the plastic region.

Maruyama and Nakagawa [66] carried out experimental studies on the behaviour of the bolted joints in elastic and plastic region separately. Firstly, the direct tension test of the bolt under uniaxial load was carried out. Secondly, the bolted joint was tightened in elastic or plastic region and then axial load was applied to that tightened joint after screwing the joint to a material testing machine. In another similar test, at first the bolt was tightened to a certain torque and then the torque in the threaded portion was reduced to zero, by untightening the bolt by a few degrees. Axial load was then applied to that pre-tightened bolted joint. The results showed that threaded part torque has little influence on the axial tension-elongation curve, and that the curve under external loading rapidly approached the curve of the single bolt regardless of whether or not the torsional stresses were eliminated by joint springback or backward rotation before the external load was applied. It was also found that the joint can withstand higher working loads when bolts were tightened into the plastic region.

Newnhan *et al* [8] also drew similar conclusions regarding the influence of torque on the uniaxial tensile strength of bolt. Here bolts were tightened to torque-tension yield point only and external load was applied by a hydraulic cylinder.

Chapman and others [2] investigated the static and dynamic strength of bolted joint tightening the bolts to their yield points by using "joint control tightening system" Firstly, the bolts were tightened to their torque-tension yield points and then holding the angle of twist constant, external tensile load was applied gradually until the bolts failed by their uniaxial tensile load They made similar conclusions regarding the static loading of the bolts, as found by the investigators in reference [66] Moreover, they also found that all bolts behaved elastically when external loads were applied to the joints even when the fasteners were tightened to their yield points Results about dynamic tests showed that fatigue strength increased with the preload and high fatigue bolts gave an improvement over standard fasteners at all preloads

Hagiwara *et al* [67] and other investigators [68,69] conducted almost the same type of investigations regarding the behaviour of the bolted connection tightened into the plastic region with various types of clamp joint Investigators referenced in [68] and [69] also investigated experimentally the influence of clamping force on the fatigue strength of bolts

Nakagome *et al* [68] also studied the influence of the thickness of the clamped parts taking force ratio (axial force developed in the bolt body/external load) into account It was found that when bolt was clamped in the plastic region, the fatigue limit of the bolted connection was improved and the variations of the clamping force, axial load and force ratio were hardly recognised They also concluded that force ratio decreased as the thickness of the clamped part increased

Monaghan and Duff [7] and Monaghan [70] investigated the effects of external loading and lubrication on a yield tightened joint It was found experimentally that lubrication conditions dramatically affected the magnitude of the maximum clamp load achieved on the joint and the torque distribution of the fasteners

Hariri [71] carried out experimental investigations on bolted joints where bolts were initially pre-torqued in the elastic range by means of an electronic hand torque wrench and then external tensile loads were applied holding angle of twist constant. Tensile load was applied with the help of a hand hydraulic pump. He noticed that the torque started decreasing when the combined stresses in the bolt bodies reached the yield stress in tension. However, because of limited testing facilities in his set-up, and as he used shear strain gauge to monitor the decrease of torque during the plastic deformation, it was not possible to explain the physical mechanism by which the torsional stress disappeared and its associated energy dissipated. It was also not possible to maintain a specific torque or axial load or axial displacement constant for different biaxial loadings of the bolted joints.

Tsuji and Maruyama [72-74] have investigated the behaviour of the bolted joints tightened into the plastic region. In reference [72], they have proposed a new estimation method for the interaction curve of the threaded portion based on the flow theory, instead of the traditional one based on the local yield condition. Experimental results [73] revealed that the new method is superior to the traditional one.

CHAPTER THREE

DESIGN, MANUFACTURE AND COMMISSIONING OF THE TEST RIG

3.1 INTRODUCTION

As part of this research work an instrumented torque-tension machine was designed, manufactured and commissioned. This machine enables the application of biaxial loads under controlled conditions. It can apply both torque and tension either simultaneously or independently to specimens of various cross-section. Suitable drive and control systems were selected for the machine. Appropriate load cells and transducing elements were attached to it to allow the necessary data acquisition, by which parameters such as axial load, torque, axial displacement and angle of twist, were monitored during tests. The machine was designed in such a way that it can be used for multiple purposes, as is explained later. Except for the lead screw and guide rods all the machined parts were manufactured in DCU.

Most existing torque-tension rigs, designed by various authors or industries [23,53,70,72,75], have mainly been used to apply necessary torque to fasteners and then to measure the resulting pre-load. The authors referenced in [53,70] have used a torque-tension rig where, after applying necessary torque to the fastener, it was possible to measure the resulting under head and thread torque. Investigators in references [8,66,71] used similar types of combined testing rigs with which it was possible to apply a tensile load to a previously tightened fastener. In these cases they have used either a universal testing machine or a hydraulic hand pump to apply the axial load, whereas an electronic hand wrench was used to apply the required torque. However, none of these rigs were able to maintain simultaneously torque/angle of twist and tensile load/axial displacement constant.

The present torque tension machine was designed to carry a maximum tensile load of 100kN and a torque of 200Nm. Its overall length, width and height are 84cm, 100cm and 196cm respectively. Total weight is slightly more than one tonne. It stands vertically on four steel columns and is operated by two servo controllers. Figures 3.1 and 3.2 show the schematic diagrams of the rig and table 3.1 gives the specifications of the machine in detail, (see also plate 3.1). Stiffness of the machine is approximately 41.7 kN/mm.

Table - 3.1 The specifications of the torque-tension machine

	Axis 1 (for tension)	Axis 2 (for torsion)
Capacity	100kN	200Nm
Force rating	100kN upto 48mm/min	200Nm upto 30°/sec
Load range (using analogue command)	3kN to 100kN	2Nm to 200Nm
Cross-head speed range	0.56mm to 48mm/min	
Drive shaft's rotational speed range		0.15° to 30°/sec
Crosshead alignment	0.5mm throughout full travel (no load condition)	
Crosshead travel	460cm	
Testing space	420cm	

This versatile machine has the following significant features

- 1) Within its maximum limits, the machine is able to apply any desired level of axial load and torque
- 2) It can apply different levels of axial load and torque both simultaneously and independently
- 3) It can maintain various parameters constant, such as torque or angle of twist, axial load or displacement

- 4) It is capable of maintaining different strain rates for both types of loadings
- 5) Both fastener and fastener like structures may be used as specimens
- 6) Specimen of various cross-section, and length upto 420cm can be used
- 7) Continuous data acquisition from load cells and transducers is possible
- 8) The machine is controllable with either analogue or digital (from a P C) signals
- 9) With a slight modification in its set-up, it could be used as a torque-compression machine
- 10) All parts and components can be easily dismantled to make any changes if necessary
- 11) As the entire machine rests on six level pads, it can be moved easily from one place to another

3.2 DESIGN OF THE TEST RIG

3.2.1 MAIN STRUCTURE AND ITS AUXILIARY COMPONENTS

The main frame of the machine consists of four vertical columns and three horizontal plates, namely, the top plate, middle plate (drive shaft housing) and bottom plate. These parts are made of machinable 0.5% carbon steel of 540 N/mm² tensile strength. The horizontal plates were inserted into slotted grooves machined in the columns, and screwed using by M16x20 socket head cap screws. These components were assembled together using screws rather than by welding to attain more accurate alignment of various horizontals and vertical components, and also for easy dismantling. Figure 3.3 shows the main frame, and figures A.1 and A.2 of appendix A show detailed drawings of the columns. There are no differences between the back and front columns except that more holes were drilled in the back columns to fix the motor's frame to the main structure of the machine.

The bottom plate holds the torsion shaft with the help of a pair of cylindrical roller bearings. The lower end of each ball screw rests in this plate by a pair of taper roller bearing. Details of the bottom plate are shown in figure 3.4.

The drive shaft housing holds the torque-tension shaft and the lower end of each guide rod. A pair of taper roller bearings was used to fix this shaft in the housing. Details of the housing are shown in figure 3.5. The top plate holds the other ends of the ball screws and guide rods. This plate contains a specially designed feature (details of which is given under the heading "preloading unit") for applying the necessary pre-load to the bearings which are fitted with the ball screws. It has also provisions for fixing necessary auxiliary components (i.e., gripper and/or holder) so that simple compression tests could be carried out by placing specimens in between this plate and the movable cross head. Figure 3.6 shows the dimensions of the top plate in detail.

The entire machine, along with its drive systems, rests on two base plates which sit on six levelling pads. The base plates were screwed to the four columns using a set of M5x1.5 socket head cap screws. Details of the base plate are shown in figure A.3 of appendix A.

3.2.2 MOVING PARTS AND RELATED COMPONENTS

(i) BALL SCREW

Two induction hardened ball screws, 1454mm long, 50mm in diameter and 10mm pitch thread were used to drive the cross head and apply the necessary axial load to the specimen. The material of the ball screws is carbon steel, with an average carbon content of 0.45% and average manganese content of 0.60%. This steel conforms to Swedish and German standards SS 1672 and DIN Ck 45. It is equivalent to steel type 3 in the ISO/R 638/I-1968 and ISO/R 683/XII-1971 international recommendations. Both screws were purchased from "PGM Ireland Ltd", model number PG-050-10. Details specification regarding the screws are given in table 3.2.

The 140mm long nut of each ball screw was screwed into the cross-head so that it (cross head) attains a linear vertical motion whenever the ball screws rotate. These screws

experience only compressive forces. The top and bottom ends of each ball screw were attached to the top and bottom horizontal plates respectively, by a set of taper roller bearings. A specially designed feature was made at the top ends of each ball screw, fitted into the top plate, to apply necessary pre-load to the above mentioned taper roller bearings. Over the unthreaded portion of each screw one steel timing pulley of 10mm pitch and 127.32 PCD has been keyed to drive (them ball screws) using timing belts. Details of the ball screw are shown in figure 3.7. Figures A.4 and A.5 (in appendix A) show the positions of the key way in the unthreaded portion of the ball screws.

Table - 3.2 Details of the ball screw

Pitch circle diameter	52.17 mm
Lead	10
Ball diameter	6.35 mm
Dynamic rating	4331 daN
Static rating	10041 daN
Nut spring rating	1954 N/ μ m
Hardness	180-225 (HB)
Yield point	370 N/mm ²
Tensile strength	620-760 N/mm ²
Hardness after induction hardening	57-63 (HRC)
Diameter tolerance	h8
Straightness	0.2 (mm/m)

(ii) GUIDE ROD

Two steel shafts, 1040mm long and 50mm in diameter, were chosen as guide rods. When torque is applied to the test specimen through the torque-tension shaft, the cross head, and hence the ball screws, also experience the same torque from the resulting twisting moment. Thus the guide rods were used to prevent the ball screws from experiencing the bending forces which develop due to this twisting moment. The guide rods were designed in such a

way that they can withstand the resulting bending moments and thus the ball screws experience only axial load during the simultaneous application of torque and tension

The top and bottom ends of each guide rod were fitted into the slots provided in the top and bottom plate of the machine respectively. The end faces of the rods were screwed into these plates to assure rigidity of the machine. Details of the guide rods are shown in figure A 6

The average chemical composition of these induction hardened steel shafts is as follows: C 0.58-0.62%, Mn 0.55-0.70%, P(max) 0.025%, Cr(max) 0.25%, Al 0.020-0.055%, Cu(max) 0.30% and Si 0.15-0.35%. The material specification and the tensile strength of these rods are DIN 50048-2.8 and 600-770 N/mm² respectively. The surface and the core hardness of these induction hardened shafts are 60 HRC and 200 HB respectively. Both rods were purchased from "Star ball retainer Co. of Ireland Ltd."

(iii) CROSS-HEAD

A steel block of UHB11 material was chosen as a movable cross head to apply the required axial load to the specimen. The length, width and height of the block are 60cm, 15.6cm and 15cm respectively. The standard specification of its material is AISI 1148. Its yield strength is 280 N/mm² and hardness 200 HB. Details of the cross-head are shown in figure 3.8

This cross head can attain linear vertical motion by means of a pair of ball screws, as detailed earlier. Although the cross head applies only the axial load to the specimen, it also experiences a twisting moment due to the application of torque. On each side of the cross head, one linear "super ball bushing" type bearing was attached to help slide the cross-head over the guide rods. A large groove was machined along the centre portion of this block to hold the following components:

The Stepped Shaft

This heat-treated high strength steel shaft was designed to carry the tensile as well as torsional load applied to the specimen. Two flat faces were machined at the top end of the shaft to prevent it from rotating when it experiences torque. However, these faces do not impose any restriction in movement of the shaft along the vertical direction. Because of this particular shape, the load cell for measuring the axial load does not experience any torque during application of torque to the specimen. This shaft also helps transmit the applied axial load to the load cell. The top stepped end of the shaft was inserted into the centre slot of the cross head, whereas the bottom end was keyed to one of the specimen holder. Near the bottom end, a 12mm diameter hole was drilled to insert a key and to attach it to the specimen holder. Details of the shaft are shown in figure A 7 and the complete cross-head arrangement, including the dowel pin (described below), load cell and other auxiliary components, is shown in figure 3 9.

Dowel Pin

Two induction hardened, heat treated, steel dowel pins were used in between the flat faces of the stepped shaft and the inner faces of the movable cross head to help reduce the friction between these mating surfaces. Because of the introduction of these pins, the flat faces of the stepped shaft and the inner faces of the cross head encounter line contacts with the dowel pins, instead of surface contact, and this helps increase the load measuring sensitivity of the axial load cell. This arrangement is specially effective when the stepped shaft experiences combined loading, i.e., both torque and tension. The diameter and the length of these pins are 12mm and 73mm respectively. The tensile yield strength of the material is 1520 N/mm². The position of these pins are shown in figure 3 9.

Load Cell For Axial Load

A donut shaped, 30,000 lbf (133.5 kN) capacity, compression type load cell was chosen to measure the axial load applied to the specimen. This load cell, along with the stepped shaft

and thin plates, was placed into the slot provided in the cross-head. Details information regarding the load cell is given in section 3.5. It was purchased from "RDP Electronics Ltd."

Heat-Treated Thin Plates

The axial load cell, sandwiched between two heat-treated circular steel plates, was inserted over the stepped shaft. Because of the large fillet radius of the stepped shaft, one of the plates whose thickness is 6.6mm, was placed at the top of the load cell so that its (plate's) larger corner radius helped the shaft sit properly with the load cell. The other 6mm thickness plate was placed beneath the load cell to help prevent the penetration of the harder edges of the axial load cell into the comparatively softer (not heat-treated) body of the cross head. After positioning the thin plates and the axial load cell over the stepped shaft, the entire assembly was placed into the groove of the cross-head provided for them. Details of these plates are shown in figure A.8.

Top Cover Plate

This is a heat treated rectangular steel block, which rests on the top of the cross head to hold the stepped shaft, the thin plates and the load cell firmly into their respective slots and thus helps restrain their vertical movement. A set of socket head cap screws was used to attach it to the cross-head. Details of the cover plate are shown in figure A.9.

This cover plate was designed with multiple purposes in mind. A shallow cylindrical slot was made in "face-1", whereas a deep 76.2mm in diameter hole was drilled in "face-2" to insert the axial load cell for recording the axial load during a compression test. The shallow cylindrical slot helps retain the stepped shaft firmly in its proper position. For the existing set-up of the machine, i.e., for applying tensile load and torque, "face-1" of the block is kept facing downward and placed in the appropriate slot of the cross head. For the torque-compression test, "face-2" would be kept facing downward on the cross head. However, for the torque-compression set-up, the "torque-tension" shaft needs to be modified.

(iv) SUPER BALL BUSHING

One pair of linear ball bearings was used in this machine. These bearings were attached to the movable cross head to help it slide over the guide rods, and to transmit the twisting moment to these rods. Each bearing was screwed to the cross head using a set of M16 socket head cap screws. Both bearings are adjustable so that different levels of interference between the inner diameter of the bearings and the outer diameter of the guide rods can be maintained, i.e., these bearings are suitable for a wider range of tolerance of shaft. These were purchased from "Star ball retainer Co. of Ireland Ltd." Details of the bearings are shown in figure A 10. The position of these bearings in the cross-head are shown in figure 3 1.

(v) SHAFTS

Three heat treated steel shafts were used in this machine for various purposes. These are as follows

Stepped Shaft

A Detailed description regarding this shaft has already been given in section 3 2 2 (iii)

Torque-Tension Shaft

This is a heat-treated steel shaft which was fitted into the drive shaft housing by a pair of taper roller bearings, mounted back to back. This shaft transmits not only torque, but also the axial load applied to the specimen. Two taper roller bearings of 45mm and 40mm in diameter were inserted over the 45mm and 40mm diameter sections of the shaft respectively. The 55mm diameter section of the shaft serves as the required shoulder for the larger bearing. Details of the shaft are shown in figure A 11. The assembly drawing of this shaft, along with the taper roller bearings and other accessories, is shown in figure 3 10.

At the bottom end of this shaft, a square extended portion, whose cross section and height are 19mm x19mm and 22mm respectively, was provided. This inserts into one end of the square drive to help transmit the necessary torque to the specimen. Near the top end of the shaft, a 12mm diameter hole was drilled for insertion of a key, which fixes it (the shaft) to the holder. A portion of the shaft was threaded so that with the help of a "preload nut", a necessary preload could be applied to the fitted taper roller bearings. A 6mm wide and 3.7mm deep slot was cut along the threaded portion of the shaft to help slide a "lock nut" along the slot and to lock the "preload nut", after applying the necessary pre-load to the bearings. The sharp edge of this "lock nut" was fitted into a 1.5mm radial groove.

Torsion Shaft

This is also a heat-treated steel shaft which was fitted into the bottom horizontal plate by a pair of cylindrical roller bearing. This shaft is able to rotate freely about its vertical axis and helps to transmit torque from the lower portion of the machine to the upper portions. Details of the shaft are shown in figure A 12.

This torsion shaft receives the required input torque from a pair of spur gears, one of which is fitted near its bottom end. In turn, the spur gears receive their input torque from the "motor-gear assembly unit-2". The shaft transmits torque to the torque load cell, fitted at the top of the shaft. Through the torque load cell, torque is transmitted to the square drive, to the torque-tension shaft, and eventually to the specimen through a holder and gripper. An assembly drawing of this shaft, along with all the necessary components attached to it, is shown in figure 3.11.

A similar square block, as used at the bottom end of the torque-tension shaft, was also machined at the top end of the torsion shaft. This square end was designed to allow insertion of this end into the lower portion of the torque load cell. The diameter of the middle section of this shaft was made comparatively large to serve as the required shoulder for the bearings.

At the lower end of the shaft, a keyway was made for assembling gear-1 with it. At the bottom face, along the vertical axis of the shaft, a 64mm diameter and 10mm deep hole was drilled to insert the free end of the angle measuring transducer's shaft into it. A 3mm diameter hole was tapped normal to the axis of the 64mm diameter hole, to allow a screw for holding the angle measuring transducer's shaft firmly to the torsion shaft. Details of the bottom face of the torsion shaft are shown in figure A 13.

(vi) SPECIMEN HOLDING DEVICES

Holder

Two heat treated steel holders, as shown in figure 3 12, were used to fix the specimen in the machine, and to transmit the necessary loads. Both holders were made of the same material and are symmetric in shape. These have been designed to withstand combined torque and tensile loads applied simultaneously. At one end of these holders, whose diameter is 127mm, a gripper was attached to hold the machined head of the specimen. Here eight equally spaced, 12mm diameter, holes were drilled for eight socket head cap screws to fix the holders to the grippers. At the other end, a 31.75mm inner diameter, 72.5mm long hole was drilled to insert the bottom end of the stepped shaft into one holder and the top end of the torque-tension shaft into the other one (details are shown in figure 3 1). These holders were attached to the above mentioned shafts by two, 12mm diameter, hardened and heat-treated dowel pins. A photograph of these holders, together with the grippers and the specimen, is shown plate 3 2.

Gripper

Two heat-treated, circular shaped, steel grippers were used in this machine to hold the machined heads of the specimens. Both grippers are made of same material and are symmetric in shape. These grippers were specially designed to fix bolt like specimens. Details regarding

the specimen are given in chapter five. Figure 3.13 shows the dimensions of the gripper in detail.

To accommodate the head of the specimen, a 20mm x 20mm square and 12mm deep slot was machined at the centre of each gripper. To set the specimen in these grippers, firstly the head of the specimen is moved along the 20mm wide and 8mm deep rectangular slot and then positioned at the centre of the slot. A 4mm high extended surface was machined into one side of the slot so that when the specimen head is positioned into the slot, the centre of the gripper exactly coincides with the centre of the specimen. Eight, 12mm diameter, equally spaced holes were tapped, on 95mm PCD, to attach the grippers to the holders. Here eight socket head cap screws were used.

To fix the specimens in the machine, as mentioned above, a similar gripping arrangement (i.e., square slot) could have been used in the holders as well. Instead, slots were machined in the grippers, so that on changing of the shape of the specimen-head, only the grippers would need to be modified. These are easier to machine and less expensive than holders.

(vii) SQUARE DRIVE

A steel block of square cross-section was used to make the necessary attachment between the top end of the torque load cell and the bottom end of the torque-tension shaft for transmitting the torque from the lower portion of the machine to the upper portion. This drive facilitates easy dismantling of the torque load cell for recalibration. Details of the square drive are shown in figure A.14, see also plate 3.3.

The square drive consists of two separate parts, part-1 and part-2, which are assembled together using four M12 socket head cap screws. In each part, a 19mm wide and 9.5mm deep slot was cut along the vertical axis to insert the square ends of the torque-tension shaft and

the torque load cell into the top and bottom slots of this drive respectively. In part-1, four 12mm diameter clearance holes, and in part-2, four 12mm diameter tapped holes were drilled for assembling these parts using screws. The square drive experiences only the torque applied to the specimen.

(viii) PRELOADING UNIT

These preloading units were designed to apply a necessary preload to the taper roller bearings fitted at both ends of the ball screws. One preloading unit was necessary for each ball screw. Each unit rests at the top end of one ball screw and sits inside the top horizontal plate. The unit consists of three parts. An assembly drawing of these parts is shown in figure 3.14.

Adjuster

This is a cylindrical component whose outside diameter and height are 180mm and 40mm respectively. It was attached to the top surface of the top plate by six M12 socket head cap screws. Its internal thread fits it to the external thread of nut-1 and thus, helps to tighten nut-1 for applying the necessary pre-load. Details of the adjuster are shown in figure A.15.

Nut-1

It is a specially designed steel nut, which has two different sections, a top and a bottom section. The top is an externally threaded section, whose pitch and major diameter are 2mm and 90mm respectively, whereas the bottom is a cylindrical section, 79mm in diameter, which has a lip at the very bottom edge. It was designed to exert the necessary pre-load to the outer ring of the taper roller bearing with the help of its 7mm wide and 6mm deep lip. The external thread of this nut meshes properly with the same pitched internal thread of the adjuster.

The bottom section of the nut was designed in such a way that a clearance gap exists in between the outer diameter of this section of the nut and the inner diameter of the 80mm

diameter hole, drilled in the top horizontal plate. A clearance gap also exists in between the end face of the nut and the top face of the taper roller bearing, which is maintained using a larger lip height. Two 10mm diameter and 10mm deep clearance holes were drilled on the top face to insert the circular ends of a spanner for tightening the nut. Details of the nut are shown in figure A 16.

Nut-2

It is also an externally threaded circular shaped steel part, which was designed to hold the position of nut-1 and prevent it from loosening under load, i.e., a lock nut. After applying the necessary pre-load to the bearings with the help of nut-1, nut-2 is then tightened into the threaded portion of the adjuster to lock nut-1. Nut-2 has the same thread pitch as that of nut-1. Two 10mm diameter and 10mm deep holes were drilled on 40mm PCD, to help insert the socket of a spanner for tightening it. Figure A 17 shows the schematic diagram of nut-2 in detail.

3.3 DRIVE SYSTEM

The torque-tension machine is operated by two separate drive systems. Two "Moog" brushless servo motors of different torque capacity and two "Carl Bockwoldt" helical gear boxes of different speed ratio were selected as drive systems. Drive system-1 provides the necessary axial load, whereas drive system-2 provides the necessary torque applied to the specimen. The "Moog" brushless motors and "Carl Bockwoldt" gear boxes are made in Germany and were purchased from Devitt Technologies Ltd, Ireland. Figure 3 15 shows the schematic diagram of a "Moog" brushless drive system.

3.3.1 DRIVE SYSTEM-1

Drive system-1, which is used to apply the necessary axial load, consists of the following parts:

LARGER MOTOR-GEAR ASSEMBLY (MGA UNIT-1)

The overall length (motor + gear box) of the MGA unit-1 is 649mm including the 106mm long output shaft of the gear box. The unit rests vertically on frame-1 positioned upside down. The flange of the gear box was bolted to base plate-1, which was in turn bolted to frame-1. The base plate, along with the entire assembly unit, can be moved a few millimetres horizontally, along the slots provided, for maintenance of proper belt tension. All motors and gear boxes were assembled at the DCU workshop.

Motor-1

A "Moog" D315-L15 type brushless AC servo motor was used in drive system-1. The size of the motor is 135mm x 135mm and its length is 253.5mm, including its 50mm long shaft. This 50mm long and 22mm diameter shaft was inserted into the slot provided at the back of the gear box-1 to assemble the motor with the gear box. Figure A 18 shows the schematic diagram of a Moog brushless servomotor and figure 3 16 shows the dimensions of motor-1.

The motor has a continuous stall torque capacity of 8.1Nm and nominal speed of 3000rpm. Its continuous stall current is 12.3 amp. The characteristic curve of this motor is shown in figure 3 17. This motor is an electronically commutated three phases electric motor with permanent magnet excitation. It has the following significant features:

- i) Optimised electromagnetic design
- ii) High energy magnets of low inertia rotor
- iii) Three phase windings on stator with thermistor protection
- iv) Sinusoidal back emf for improved low speed performance and higher efficiency
- v) Reliable integral brushless resolver for position feed back
- vi) Light weight aluminium housing for maximum heat transfer
- vii) Pre-loaded sealed bearings pre-lubricated with high temperature grease for extended life

- viii) Reliable brushless design, no mechanical commutator
- ix) Static load holding brake

This motor supplies the necessary torque which is eventually converted into the required axial force via the gear box, timing pulleys, timing belt, ball screws and cross-head

Gearbox-1

A German made, "Carl Bockwoldt", three-stage, CB59-NF80 type, helical gear box was assembled vertically with Motor-1 to form the MGA unit-1. The length of the gear box is 476mm, including its 50mm diameter and 110mm long shaft. Approximate weight of the gear box is 96 kg. Its gear ratio is 295:8, and maximum permissible output torque at rated power (at service factor 1) is 1200Nm. Its maximum permissible input speed is 4000rpm. The 250mm diameter flange of the gear box was attached to base plate-1 by four M12 bolts. Figure 3.18 shows the dimensions of the gear box in detail.

(ii) TIMING PULLEYS AND BELTS

To transmit power from the MGA unit-1 to the ball screws, two pairs of similar steel timing pulleys, and one pair of polyurethane "Bando" timing belts were chosen. The pitch and width of these pulleys and belts are 10mm and 16mm respectively. All the pulleys and the belts were purchased from "Hinchlief precision components Ltd. England".

Timing pulleys are made of standard steel with steel flanges. The outside diameter, the pitch diameter and the number of teeth of each pulley are 125.45mm, 127.32mm and 40 respectively. The supplied 15mm diameter centre holes of the pulleys were enlarged to 50mm to fit them over the shaft of gear box-1. Two pulleys were keyed to the shaft of gear box-1, and one pulley to each ball screw. After keying them into their respective positions, all the pulleys were also screwed with the help of long screw provided at their centre. The positions

of the pulleys in gear box-1 and in the ball screws are shown in figures 3.1 and 3.2. Figure A.19 shows the dimension of the pulley in detail. The part number of these pulleys according to HPC (C11) catalogue is 40PT-10-21.

One pair of polyurethane "Bando" type timing belts was used in conjunction with the timing pulleys to transmit power from gear box-1 to the ball screws. The power transmission capacity of these belts is approximately 30kW, whereas their power transmission efficiency is nearly 98%, with no slip or back-lash. These belts are oil resistance. Their speed can be increased up to 80m/s and, their pitch length and number of teeth are 1210mm and 121 respectively. Each belt was fitted over one pair of pulleys. The part number of these belts according to HPC (C11) catalogue is BT-10-1210. Details of the belt are shown in figure A.20.

(iii) FRAME AND BASE PLATE FOR MGA UNIT-1

Base plate-1

A 430mm x 305mm x 20mm steel plate was used as base plate-1 to attach the MGA unit-1 with its frame. Four 13mm diameter clearance holes, on 215mm PCD, were drilled to fasten it to the flange of gear box-1. Four M12 hexagonal bolts were used for this purpose. At the centre, a 60mm diameter hole was drilled to accommodate the shaft of the gear box. A 182mm diameter and 5mm deep slot was machined at the top face of the plate to help set the extended edge of the flange properly with it. Six 46mm long and 16mm wide through slots were made, three at each end of the plate, to bolt the base plate-1 to the frame. These slots also provide the sliding facility of the plate, horizontally on its frame, for maintaining proper belt tension. Details of the base plate-1 are shown in figure A.21.

Frame-1

This box section frame was designed to assemble MGA unit-1 with the main structure of the machine. It is made of square structural steel tubings of size 50mm x 50mm x 6mm. Figure

A 22 shows three views of this frame. All the square tubings, which are in contact with the main structure of the machine, were connected with bolts so that entire frame can be disassembled easily from the main body of the machine.

3.3.2 DRIVE SYSTEM-2

This drive system provides the necessary torque applied to the specimen. It consists of following components:

(i) SMALLER MOTOR-GEAR ASSEMBLY (MGA UNIT-2)

The overall length (motor + gear box) of this motor-gear assembly is 477mm including its 67mm long output shaft of the gear box. The entire unit rests vertically on frame-2 with the shaft of the gear box facing downward. The flange of the gear box was bolted to its base plate which in turn was bolted to frame-2. The base plate, along with the entire assembly unit, can be moved a few millimetres horizontally to help adjust the proper meshing of the spur gears.

Motor-2

This is also a "Moog" brushless A C servo motor but of type "D413-L10", whose cross section is 105mm x 105mm and length is 214mm, includes its 40mm long shaft. This motor was assembled with gear box-2 to form the MGA unit-2. Details of the motor are shown in figure 3 19.

The motor has a continuous stall torque capacity of 2.7 Nm and nominal speed of 4900 rpm. Its continuous stall current capacity is 6.7 ampere. The characteristic curve of this motor is shown in figure 3 20. It has the same significant features as those of motor-2, as mentioned earlier. This motor applies torque to the specimen through gear box-2.

Gearbox-2

This is also a German made, "Carl Bockwoldt", three-stage, helical gear box but of type "CB29-NF-63" This gear box was assembled with motor-2 to form the MGA unit-2 Torque from motor-2 is amplified by this gear box and is eventually transmitted to the specimen via a pair of spur gears and a number of auxiliary parts The torque transmitted by this gear box remains pure torque and is eventually applied to the specimen Its gear ratio is 150.7 and maximum permissible output torque, at rated power and at service factor 1, is 300Nm Its maximum permissible input speed is 4000rpm Figure 3.21 shows the various dimensions of the gear box in detail

(ii) SPUR GEAR

A pair of steel spur gears (gear-1 and gear-2) of MOD 3.0 and PCD 282mm was used to transmit torque from gear box-2 to the torsion shaft of the machine Their speed ratio is 1 i.e., both gears have 94 teeth and same PCD These case hardened gears are made of steel "En36" (B S 655M13) Their maximum load carrying capacity is 83hp at 1000rpm the position of these gears in the machine are shown in figure 3.2

Gear-2 was keyed with the shaft of gear box-2, whereas gear-1 was keyed with the torsion shaft Torque from MGA unit-2 is transmitted to the torsion shaft via this pair of gears and, from there, to the square drive and then to the torque-tension shaft, and eventually to the specimen through holder and gripper The 30mm diameter hole of gear-1 was enlarged to 44mm to fit over the torsion shaft of the machine Both gears were purchased from "HPC Ltd" and their part no according to "HPC" (C11) catalogue is "XG3-94" Details of these gears are shown in figure A.23

(iii) FRAME AND BASE PLATE FOR MGA-2

Base plate-2

A steel plate of 295mm x 220mm x 16mm was used as base plate-2 to attach MGA unit-2 with its frame. Four 9mm diameter clearance holes, on 130mm PCD, were drilled to help fasten the flange of gearbox-2. Four M8 hexagonal bolts were used for this purpose. At the centre of the plate, a 40mm diameter through hole was drilled to accommodate the shaft of gearbox-2. A 112mm diameter and 5mm deep slot was machined at the top face of the plate to help set the extended edge of the flange. Six 21mm long and 16mm wide slots, three at each end of the plate, were made to insert bolts for assembling base plate-2 to its frame. The entire MGA unit-2, along with the base plate, can move a total distance of 5mm (± 2.5 mm from the middle point of the slot) horizontally, to facilitate proper engagement of the spur gears. Details of this base plate are shown in figure A 24.

Frame-2

This box section type frame was designed to assemble MGA unit-2 to the main structure of the machine. The same structural steel tubings were used to build this frame as were used in case of frame-1. Figure A 25 shows different views of this frame in detail.

3.4 CONTROL SYSTEM

Two identical "Moog T161-003" brushless motor controllers, along with a power supply, were chosen to control the various input/output parameters and different modes of operation of the machine. The "Moog" controllers are made in Ireland and were purchased from "DTL". One controller (controller-1) operates the larger motor-gear assembly and controls the different levels of axial load and linear movement of the cross head, whereas the other one (controller-2) drives the smaller motor-gear assembly and controls different levels of torque and rotational speed assigned to the specimen. All these commands can be applied by analogue signals or by means of a digital link from a computer (RS-232).

These controllers control the communication of "Moog" brushless servomotors. These are high performance servo controllers designed for the highest specification motion control application. They are controlled by a 16 bit microprocessor, and provide full velocity servo loop closure with subordinate motor current control. Each controller has a continuous current rating of 15amp at 50°C ambient temperature and can provide a continuous torque of 13.9Nm. The peak current rating is 30amp. Approximate weight and dimensions of each controller are 2.4kg and 60.96mm x 226.9mm x 262.9mm respectively. The "T161" can close a position control loop around the motor shaft mounted resolver. They provide full system protection against overload and output short circuit. System errors are monitored and signalled. Figure 3.22 shows the flow chart of the operating principle of these controllers.

Each controller was tuned by the supplier to match its corresponding driving motor using a "MCO" module. One module for each controller was used, and inserted inside the control panel. Control of torque commands by controller-1, means the control of axial load applied to the specimen, whereas controller-2 control the torque applied to the specimen. However, the following significant features are available in each controller. Each controller

- i) can control the level of torque and velocity of the motors individually, and thus help to control the axial load/torque and vertical/rotational motion of the machine
- ii) can hold the position of the motors' shafts constant (i.e., can hold the angle of twist and/or axial displacement of the specimen constant)
- iii) can change the direction of motion of the motors

Besides these controls, many other input/output commands are also available on each controller such as, clockwise and counter clockwise limit switch inputs, motor torque output signals, motor hardware enable/disable inputs, etc. All these input/output signals are available through a number of connectors/ports, situated at the back panel of each controller. A list of the connectors, along with the additional features of the controller, are given in appendix B.

Power connector X μ 6, shown in figure 3 23, supplies power to the motors Pin 4, 5, 6 and 7 are used for this purpose The I/O connector X μ 5 facilitates the reading of various input/output parameters of the motors The input signal ($\pm 10V$) of the controllers is supplied to pin 19 At the front of the controllers, there are three status leds to diagnose whether different system and input limits are satisfactory or not Port X6, shown in figure A 26, can be used to control various input/output command signals by means of a handheld terminal, or a digital link from a computer (RS 232, RS 485) A special "extended function card" was inserted into the spare slot of each controller to control a number of input/output commands using analogue voltage (0- 10V) For the present set-up of the machine, velocity and torque commands are applied as analogue commands and the run or the hold mode and the forward or the reverse speed control modes are selected by means of a number of digital input logic signals

Axes enable input voltage of each controller is 15VDC Enabling of the system is only allowed after relay "power supply O K " is closed A 19inch rack was used to mount both controllers and the power supply

3.4.1 CONTROLLER-1

As mentioned earlier, two identical servo controllers were used to control the drive systems Controller-1 was used to control motor-1, and hence, MGA unit-1 Different levels of output torque from motor-1 are eventually converted to axial load via gearbox-1, pulley, belt, ball screw and movable cross head Rotational speed of the motor is converted to linear vertical motion of the cross-head Control of torque and rotational speed (velocity) of motor-1, by controller-1, means control of axial load, applied to the specimen, and the vertical linear movement of the cross head Clock-wise rotation of the motor causes the cross-head to move in an upward direction (i e , apply tensile load) and counter clock-wise rotation causes it to move in a downward direction (i e , apply compressive load)

3.4.2 CONTROLLER-2

Like controller-1, this controller can also control all input/output commands. Controller-2 controls motor-2 which was assembled with drive system-2. Different levels of output torque from this motor are eventually transmitted to the specimen, as pure torque, via its corresponding gearbox. Thus control of torque and velocity of motor-2 means the control of torque and the rotational speed transmitted to the specimen. The control of clock-wise and counter clock-wise rotation of motor-2 means the control of counter clock-wise and clock wise rotation of the specimen respectively.

3.4.3 EXTENDED FUNCTIONS CARD (EF CARD)

A special "extended functions card" was inserted into the spare slot of each controller to control a number of input/output signals by analogue command (0-10V), and also to select different modes of operation by means of a number of single digital input signals. Input/output commands available on these cards are applied through connector X μ 7. These cards were supplied by "DTL".

With the help of this "EF Card", controllers are able to set the motors either in run or hold mode by applying single digital input signals of zero or 5V respectively. In the hold mode, motors' shafts maintain a fixed angular position irrespective of the applied torque or velocity, i.e., when the hold mode switch is activated, the specimen maintains either a fixed angle of twist or a fixed axial displacement. In the run mode, motors are in their actual operating condition where different levels of torque and axial loads can be applied to the specimen at different speed.

In run mode, independent control of velocity and torque of the motors is possible by two independent potentiometer inputs. Both inputs can be varied by applying 0-10V analogue commands. A number of external power supply units, one pair for each controller, were used.

to apply the necessary voltages for controlling the velocity and torque commands of each motor. Specific velocities (rotational motion for torque application and linear vertical motion for axial load application) of motors are selected by varying 0-10V analogue inputs and then, keeping these speeds constant, different levels of torque and/or axial loads are applied to the specimen.

In run mode, the responses of drives (motors) under torque and velocity commands are as follows. If the velocity command is zero then the drive remains stationary irrespective of torque limit value. As the velocity command is increased the drive accelerates to that value as long as the torque load on the drive is less than the torque setting limit. When the torque limit setting is less than the torque (i.e., torsional/axial load) required to break the specimen, the velocity will decelerate to zero and the drive holds motor's torque (i.e., torsional/axial load) constant. If the torque limit is then increased above the torque required to break the specimen, then the drive will accelerate back to the initial velocity setting and continue to run. If the torque limit setting is initially set at a value greater than the torque (torque/axial force) required to break the specimen then the drive maintains the selected velocity setting, breaks the specimen as it goes.

These "EF Card" also provide the facility of changing the direction of motion of the drives. Drives can be set either in forward (clockwise) or in reverse (anti-clockwise) mode by selecting either zero or 5V digital inputs, respectively. The function of various pins on Xμ7 connector are given below in tabulated form.

Table - 3.3 Functions of various pins on the X μ 7 connector

Connector X μ 7, 9-way D-type, male	
Pin 1	Not connected
Pin 2	Position sensor feedback, 0-20V
Pin 3	Forward/Reverse select input, 0/5V
Pin 4	Velocity command input, 0-10V
Pin 5	Not connected
Pin 6	Run/Hold mode select input, 0/5V
Pin 7	Torque command input, 0-10V
Pin 8	Output command, -10 - + 10V
Pin 9	Not connected

Pin 4 and 7 of each X μ 7 connector are used to apply different levels of voltages (0-10V) for controlling the velocity and torque commands of the motor, respectively Pin 6 is used to select either run or hold mode, whereas pin 3 is used to select either forward or reverse motion of the motors Pin 8 supplies a -10V- +10V output to each controller as a command input The output of the external position sensor can be feed back to controller-2 via pin 2 This particular provision could be used only when the various input/output commands are controlled by a personnel computer, through port X6 of the controller This feed back system would allow the position sensor to make a closed loop with the motor and the controller, and thus help to record a more accurate value of the angular twist

3 4 4 INTERFACE CONNECTOR

At the front panel of each controller there is a connector X6, which is used for interfacing the controllers with a P C as an alternate to analogue control The controllers were manufactured to interface with a computer via an RS 232 serial link

To initialise the commissioning of the drive systems and to set the limits of different input/output parameters, such as motor's maximum torque limit, motor's maximum speed limit, etc , a handheld terminal called "Oyster Terminal" was used This "64-PTR-25" type

terminal with a RS 232 serial link was connected to the interface connector, X6, for the initial set-up of the controllers

This terminal has a built-in software (EPROMS) package. For many commands, like the set-up of working limits, information regarding the conditions of motors, such as the position of shafts of motors (in degree), various optional and different mode commands are available on this terminal (in a programmed form). As has already been mentioned, for the present set-up of the machine, the analogue commands, along with a number of single digital input signals, were used for controlling the drive systems, this handheld terminal was only used for setting the maximum torque and speed limits of the motors. However, for the present set-up (i.e., to control the machine by analogue commands), the commissioning of the machine was accomplished according to the procedure mentioned later on. A summary of the commands available in the software is given in appendix C. This terminal was supplied by "DTL" for the initial set-up of the controllers.

3.4.5 SET-UP LIMITS IN THE CONTROLLERS

For the present set-up, all the input commands are applied by analogue commands. It has already been mentioned that the torque and velocity commands of each motor can be independently controlled. The "Moog" control systems work in the following way. Different level of the motor's torque/speed, from zero to maximum available limits, can be obtained by varying a 0 to 10V analogue command. If any value, in between zero and its maximum available limit, is set as the peak torque or speed, then that peak torque or speed can be attained by applying the corresponding analogue voltage to the controller. Further application of voltage would not increase the motor's torque or speed but maintain it constant. This is explained in more detail in the following paragraph.

In case of motor-2, the maximum available torque limit is 2.7Nm. However, for the present set-up, the peak torque of this motor was set equal to 1.90Nm, so this value can be attained by applying an analogue voltage, nearly equal to 7.0V ($10 \times 1.9/2.7$). Any voltage above that value would not cause an increase in the motor's output torque. Thus, for the present setting of motor-2, different levels of torque in between zero and its maximum set-up limit can be obtained by varying between 0 and 7V analogue voltage. The following limits were set in motor-1 and motor-2:

Table - 3.4 Set-up limits of torque and speed in motor-1 and motor-2

Motor	max. torque limit	max. speed limit
Motor-1	2.367Nm	3000rpm
Motor-2	1.90Nm	1500rpm

3.4.6 POWER SUPPLY UNIT

One "Moog" motor-controller power supply unit, type 160-003, was chosen to supply the main power to both controllers as well as to both motors. This single phase power supply unit has a continuous power supply capacity of 1.5kW. Nominal input voltage is 230VAC, 44...66Hz. Its approximate weight and dimensions are 1.9kg and 60.96mm x 226.90mm x 262.90mm respectively. This power supply has sufficient capacity to supply power to upto six controllers. It has an integrated bleed resistor to dissipate excess motor energy during motor regeneration and therefore avoids an unacceptable increase in the D.C. voltage.

At the front panel of the power supply, as shown in figure A.27, there are seven status leds to warn whether power supply and various connections are satisfactory or not. At the backpanel, there are several input/output connectors including A.C. power connector (X3), External bleed resistor connector(X4), power supply signal and I/O connector (X5), serial interface connector (X6), D.C. bus connector (X7) and fan connector (X9). Details of these connections are given in appendix B.

In the "low voltage power and status connector" X5, there are a number of centralised power supplies such as +15VDC-2A line, -15VDC-2A line, +5VDC-7.5A line, etc., to supply power to other external devices if necessary. The +15VDC-2A line (pin 9) was utilised to power the hardware of the motors. The +5VDC line (pin 8) was used for digital input signals, and connected to the extended function cards for selecting various modes of operation.

3.4.7 CONNECTIONS

Besides the built-in connections in each device the following additional connections were made to the power supply, both motors and controllers.

Power Supply

The main 220VAC input is fed into the power supply via its backplane connector X3. Various outputs from the backplane connector X5 were set-up for the following purposes. The +5VDC output from pin 8 and digital ground connection from pin 12 are used as single digital input signals to select different modes of operation of the motors, such as, run or hold mode, forward or reverse mode, etc. From each of these pins, four parallel lines were drawn, two for each controller, and connected to four "two way" switches to supply either 5 or zero voltage to pin 3 and 6 of each X_μ7 connector. The +15VDC from pin 9 is used to make the motor's hardware "enable" by two "one way" on/off switches. Enabling of the motors means shafts are able to turn freely with or without load, i.e., commissioning of the motor. An analogue ground connection from pin 11 was used as the negative terminals of the four external power supply units. A circuit diagram, including the power supply, controllers and motors, is shown in figure 3.24.

Controllers

Both controllers have the same type of connections with the motors and power supply unit "160-003". Power connector X_μ4 of each controller was connected with the "8 pole power mating connector" of the motor. Connections are made as follows:

Table - 3 5 Connections of power connector X μ 4

Pin no	Input reference	Wire colour
4	PE	Green/Yellow
5	W	Brown
6	V	Blue
7	U	Black

Again "resolver connector" X μ 6 of each controller was connected with the "12 pole signal mating connector" of the motors, whose wiring was made according to the connection given in appendix B

Extended Functions Card

It has already been mentioned that for each controller one "EF card" was used Input/output commands available by these cards are applied by a "9-way D-type" male connector, called X μ 7, one for each controller XA7 represents the connector for controller-1 and XB7 that for controller-2 The term " μ " was used in general Both extended function cards have similar connections with the other devices, i e , with the motor, power supply etc

Pin 3 and 6 of each X μ 7 connector were connected to four "two way" switches, one switch for each pin, so that each (pin) receives either a 5V or zero voltage, from pin 8 or 12 of X5 connector of the power supply respectively This sets the motors in different modes of operation Pin 4 and 7 were connected with the positive terminals of the external power supply units to provide (0-10VDC) analogue voltage and to control the velocity and torque commands of the motors, respectively Pin 8 of each X μ 7 connector was connected with pin 19 of each X μ 5 connector Pin 8 supplies -10V- +10V output to each controller as the input command The output of the external position sensor can be feed back to controller-2 by

interfacing the position sensor via pin 2. Pins 1, 5 and 9 are not connected. Details of the connection are shown in figure 3.24.

Control Panel

A number of switches were attached to a 23cm x 17cm switch board through which all the necessary analogue, as well as single digital signals were applied to the controllers. This control panel served the following functions:

- i) Helps start the commissioning of the motor
- ii) Helps provide the necessary analogue commands (0-10V) for controlling the torque and velocity commands
- iii) Helps set the motor in different modes of operation

The schematic diagram of the control panel is shown in figure 3.25. Switches on the right half portion of the panel are used to control the different parameters of controller-1. The two-way switch, switch-1 is used to select either run or hold mode whereas, switch-2 to select either the upward or downward motion of the cross head. Switches 7 and 8 are used to apply different level of analogue voltage (0-10V) for controlling the applied axial load and vertical movement of the cross-head respectively. The "activate switch" switch-5, sets the controller either in "enable" or in "disable" condition.

Similarly switches on the left half portion of the control panel are used for controlling different command signals of controller-2. Here switch 3 is used to select the run or hold mode whereas, switch 4 to select the clockwise or counter clockwise rotation of the specimen. Switches 9 and 10 are used to apply the necessary analogue commands (0-10V) for controlling the applied torque and rotational motion of the specimen. The switch 6 sets controller-2 either in "enable" or in "disable" condition. A photograph of the controller unit, along with the control panel and the external power supply units, is shown in plate 3.4.

3 4 8 COMMISSIONING THE MACHINE

The following procedures are followed to activate each drive system of the machine

- i) The activate switch is put "ON" to set the controller in "enable" condition. At this time, the run/hold switch is to be kept on hold mode. Before plug-in the main cable of the power supply, the activate switch should be on the "OFF" side.
- ii) Different levels of analogue voltages can be applied to set the desired loads (axial and/or torsional load) and strain rate (linear and/or rotational).
- iii) The run/hold mode switch should be put on run mode, to start the test.
- iv) To cease the operation temporarily, or to hold the angle of twist/axial displacement constant during the load application, the run/hold mode switch should be put on hold mode.
- v) To deenergize the controller's functions completely, the activate switch should be put "OFF" to set the controller in "disable" condition.

By following the above procedure, both drive systems can be controlled either simultaneously or individually.

3.5 DATA ACQUISITION SYSTEM

Both controllers are able to monitor the output torque (i.e. motor's current) as well as the angular position of the motor-shafts, via the shafts mounted resolver feed back (while using a P C). However, in the present set-up, a number of external sensors were attached in the vicinity of the specimen to minimise the uncertainty involved in the transmission of various mating parts in between the motors and the specimen. Outputs from these devices are read by individual "RDP" amplifiers. The following devices were used for data acquisition from the machine.

AXIAL LOAD CELL

A donut shaped, 30,000 lbf (133.5kN) capacity, compression type load cell was used to measure the axial load applied to the specimen. Bonded foil type strain gauges are used in this load cell. Its maximum full scale non linearity is $\pm 0.5\%$ and maximum excitation voltage is 10.0VDC. Factory calibrated output is 2.8945mv per voltage excitation, i.e., for full scale deflection, output is 28.945mv. So for 10VDC excitation, response of this load cell is 0.216816mv/kN. As it was factory calibrated, no further calibration was considered necessary. Figure A.28 shows the dimensions of the load cell in detail. This load cell was purchased from "RDP Electronics Ltd", has frame size C, and model no "BL-915".

This load cell was inserted over the lower-portion of the stepped shaft and placed in between thin steel plates, as described earlier. The entire assembly, i.e., the axial load cell, along with the stepped shaft and the thin plates, was then positioned into the groove provided in the cross-head. The assembly drawing of these components is shown in figure 3.9. A clearance gap was maintained in between the inner diameter of the load cell and the outer diameter of the stepped shaft for easy disassembling and safety of the load cell. Because of this arrangement the load cell experiences an equivalent compressive load whenever the specimen is subjected to a tensile load.

Connection And Data Acquisition

The four coloured cables of the load cell represent the following connection

RED	(+) Excitation
BLACK	(-) Excitation
GREEN	(-) Output
WHITE	(+) Output

These cables were exited from the movable cross head through a 10mm wide slot. A RDP amplifier, type E308, was used to read output from the load cell. It was connected with the RDP amplifier as follows. The red and black cables of the load cell were connected with the "Ex +" and "Ex -" terminals of the rear panel of connector PL3 respectively. The excitation voltage was set equal to 10V by varying excitation potentiometer (RV1-rear panel) and with the help of excitation check switch (SW1-6, rear panel). The green and white cables were connected with the "Sig +" and "Sig -" terminals of connector PL3 respectively. As the output was in millivolt, input level switch (SW2- rear panel) was set to "mv" side.

To get a digital display of the output on the front screen of the amplifier, the following procedure was followed. As the full scale output of the load cell is 28 945mv for 10V excitation, an exact 28 945mv input voltage was applied to the terminals "Sig +" and "Sig -" of the amplifier, with the help of an external variable resistant potentiometer and a power supply. Then the digital number in the front screen of the amplifier was set equal to 133.5 by adjusting the "gain control" switch of the front panel. Before applying this 28 945mv to terminals "Sig +" and "Sig -", the digital number of the screen was set equal to zero with the help of "zero setting switch". Analogue output from the amplifier was fed into a chart/X-Y recorder by adjusting the gain with the help of "analogue output potentiometer" (RV2, rear panel).

TORQUE LOAD CELL

A "Norbar" rotary type torque transducer of 500Nm capacity was used to measure the torque applied to the specimen. It was purchased from "Norbar torque tools Ltd", with model number "50139/ETS". Details of this load cell are shown in figure A 29. It is a strain gauged torsion bar which is made from heat-treated alloy for maximum accuracy and stability. It has a full bridge arrangement for maximum signal output and temperature stability. It can measure both static and dynamic loads and can operate in both directions, i.e., clockwise and counter clockwise direction. The maximum non linearity of this unit is $\pm 0.1\%$. The normal operating

speed for the unit is up to 3000rpm but it can be used for short duration up to 9000rpm and it has an expected life cycle of 3000 hours

The maximum bridge excitation voltage of this load cell is 10V. It was calibrated by "Norbar tool Ltd" upto 200Nm full scale. Its output is 0.817mv/V excitation, so for 10V excitation, the full scale output is 8.17mv, i.e., 0.04084mv/Nm torque applied. This load cell has a centre shaft, which rotates freely within its housing. The housing needs very low torque to hold it in a fixed position. The top male part and the bottom female part of the load cell were inserted into the bottom end of the square drive and into the top square end of the torsion shaft respectively. Assembly drawings of the torque load cell, together with the square drive and the torsion shaft, are shown in figures 3.1 & 3.2

Connection And Data Acquisition

As the load cell was factory calibrated, no further calibration was considered necessary. To read the output from the transducer, a similar RDP amplifier, as used with the axial load cell, was used. This amplifier also supplied the necessary excitation voltage to the load cell. Various pins of the load cell were connected with the amplifier as follows

Pin no	Connection to
F	Excitation +ve
D	Excitation -ve
A	Signal +
B	Signal -

The same procedure was adopted during the calibration of the RDP amplifier as was followed in case of the axial load cell. Here 8.17mv input voltage was applied to the terminals "Sig +" and "Sig -" with the help of an external variable resistant potentiometer and, the amplifier's

front screen was adjusted to number 800, so the ratio of the torque obtained from the amplifier to the actual torque applied to the specimen was 4 (800/200)

ANGULAR POSITION TRANSDUCER

A D C/D C angular position transducer was chosen to measure the resulted angle of twist of the specimen. This transducer was purchased from "Penny & Giles Position Sensors Ltd ", model number "3810/300". It is basically a transformer in which the output is governed by the angular position of the input shaft in relation to the transducer body. The output is electrically isolated from the input. The required input is a stabilised 10VDC from a source impedance of less than 1 ohm. The D C output is converted to an A C waveform by an integral oscillator and then fed to the transformer primary winding. The output from the secondary winding is converted to D C by an integral demodulator and filter.

This transducer can rotate 360 degrees mechanical angle continuously. Its effective electrical angle is 300 degrees, i.e., its output is linear over these 300 degrees. Output sensitivity is 33mv per degree rotation of its shaft. The output characteristic curve of the load cell is shown in figure 3.26. The residual voltage is maximum at zero degree arc and its value is 50mv, i.e., output voltage is linear from 50mv upto 995mv ($33\text{mv/deg} \times 300\text{deg} + 50\text{mv} = 995\text{mv}$). Output increases for clockwise rotation of the shaft. The maximum non linearity is $\pm 0.5\%$ of full scale.

Set-Up Procedure

Details of the transducer are shown in figure 3.27. The 36.58mm (1.440 inch) diameter flange of this transducer was attached to a 240mm long, 80mm wide and 2mm thick aluminium plate using four M4 screws. The ends of this plate were bolted against the steel angles, attached to the main columns of the machine. The position of the transducer is shown in figures 3.1 and 3.2. The free end of the transducer's shaft was inserted into a 6.4mm diameter hole provided

at the bottom end of the torsion shaft and screwed into it using a M3 screw so that the transducer's shaft experiences the same twist as the torsion shaft. A photograph of the set-up of the transducer is shown in plate 3.5

Data Acquisition

The performance specification of this factory calibrated position sensor is true only for a $10.00 \pm 1\text{mVDC}$ input with a $10\text{k}\Omega \pm 0.2\%$ load impedance on the output. So to get the calibrated output for different angular positions of the shaft, a $10\text{k}\Omega$ resistance was connected across the positive and negative terminals of the output connections. The same type RDP amplifier as previously described was used to supply the excitation voltage (10VDC), and also to obtain the digital output. Analogue output from the back panel of the amplifier was also fed to a chart/X-Y recorder. Various coloured pins of the load cell were connected with the amplifier as follows:

Colour of pin	Connection to amplifier
Red	Excitation +ve
Black	Excitation -ve
Brown	Signal +
Blue	Signal -

Index Voltage

The index voltage marked on the transducer's body represents that voltage which corresponds to the exact middle position of its effective electrical angle. The index voltage of this transducer is 5.108V, i.e., when the output voltage of the transducer is 5.108, it represents exactly 150° rotation of the shaft from its 0° arc position. The shaft of this transducer was attached with the bottom end of the torsion shaft in such a way that whenever the specimen was positioned into the machine for an actual test, the indent groove on the shaft was kept

almost aligned with the red spot on the case, to get the precise middle range of the effective electrical angle

L.V.D.T.

In order to measure the total deformation of the specimen along the axial direction, a Mitutoyo digimatic indicator of 50mm stroke length capacity was used, model no "543-425E" Figure A 30 shows the details of the L V D T , see also plate 3 6 However during the present experimental investigations, this L V D T was not used, as the axial strain of the specimen was measured more directly using axial strain gauges

DATA LOGGING

The output signals produced by the load cells and the angular measuring transducer were amplified and then read by three separate digital transducer indicators These were purchased from RDP Electronics Ltd , UK Analogue outputs from these indicators were fed into a chart and/or a X-Y recorders, which were purchased from "Lab Tech Eup Ireland" Output signals from the strain gauges were read by a digital strain indicator, together with a switch and balance unit Analogue outputs from this strain indicator were also fed into the chart/X-Y recorder The digital indicator and the "switch and the balance unit" were purchased from "Measurements group UK Ltd " Figure 3 28 shows the schematic diagram of the data logging, see also plate 3 7

Four external power supply units were used to provide the necessary voltage to the extended function card Each controller needed two units, one for torque and another for velocity control

3.6 BEARINGS

Three pairs of taper roller bearings and one pair of cylindrical roller bearing were used in this torque-tension machine. These were purchased from "FAG Ireland Ltd". Taper roller bearings have conical rollers guided by a back face rib on the cone. These bearings are capable of taking high radial as well as axial load in one direction. In cylindrical roller bearings, the cylindrical rollers are in linear contact with the race ways. They have high radial load capacity.

At the top and bottom end of each ball screw, one pair of 35mm and 40mm diameter taper roller bearings were attached respectively. Each pair of bearing was mounted according to a "front to front" arrangement. This type of arrangement makes mounting easier when interference is expected for the inner ring. The "FAG" numbers of 35mm and 40mm in diameter taper roller bearings are 31307A and 31308A respectively. Necessary pre-load was applied to this pair of bearing with the help of nut-1 and nut-2, as detailed earlier.

Another pair of taper roller bearings was mounted on the torque-tension shaft. Here 40mm and 45mm diameter bearings were used and mounted according to a "back to back" arrangement. This type of arrangement was selected because of the short distance between the two bearings. The "FAG" bearing numbers of 40mm and 45mm diameter taper roller bearings are 30308A and 31309A respectively. Necessary pre-load to this pair of bearing was applied with the help of a locking nut and a hand spanner.

One pair of 40mm diameter cylindrical roller bearing was mounted over the torsion shaft to help transmit the torque from the spur gear to the specimen. This pair of bearing withstands radial load only. The "FAG" numbers of these bearings are NU208E TVP2. The following tables show the detailed specifications of different bearings used in the machine.

Table - 3 6 Specifications of The Taper roller bearings

FAG number	Load rating (kN)		d	D	B	C	T
	Static	Dyn					
31307A	65 5	57	35	80	21	15	22 75
31308A	85 0	72	40	90	23	17	25 25
30308A	104 0	86 5	40	90	23	20	25 25
31309A	110	91 5	45	100	25	18	27 25

Table - 3 7 Specification of The cylindrical roller bearing

FAG number	Load rating (kN)		d	D	B	E	F	H
	Static	Dyn						
NU208E TVP2	53 0	53 0	40	80	18	71 5	49 5	67 3

3.7 MATERIALS

Two different steel materials were used to manufacture the main frames and the various auxiliary components of the machine. Their industrial names are "UHB-11" and "Orvar Supreme Steel". Both types of materials were purchased from "Uddeholm Ltd, UK".

The UHB-11 is an easily machinable carbon steel whose standard specification is AISI 1148. Its typical compositions are, 0.50%C, 0.3%Si, 0.6%Mn and 0.04%S. Hardness of the steel is 200HB and Yield strength ($R_p 0.2$) is 280N/mm². This is a non heat-treatable steel except for special applications. The following parts were manufactured using this particular material: four main columns, drive shaft housing, top and bottom plate, movable cross head and base plates.

"ORVAR SUPREME" is a chromium-molybdenum-vanadium-alloyed steel whose standard specification is "Premium AISI H13, W-Nr 1 2344" Its typical analysis is as follows, 0.38%C, 1.0%Si, 0.4%Mn, 5.3%Cr, 1.3%Mo, and 0.9%V Its yield strength ($R_{p0.2}$) is 1520 N/mm² at room temperature The following parts were manufactured using this heat-treatable steel: stepped shaft, torque-tension shaft, torsion shaft, top cover plate, grippers, holders, square drive, thin plates, and all components of the pre-loading units

HEAT-TREATMENT

All the components manufactured from the "Orvar Supreme" steel were heat-treated according to the following procedure to obtain hardness of between 52-54 HRC

Preheating

1st preheat to 650 deg C

2nd preheat to 850 deg C

Soaking

Soaked (Austenized) at 1040 deg C for approx 40mins

Quenched to 50 deg C under 3 bar pressure of nitrogen

Tempering

Tempered twice at 200 deg C for two hours, cooling to room temperature each time

3.8 DESIGN EQUATIONS

STRESSES UNDER STATIC AND DYNAMIC CONDITION

Following equations, where appropriate, were used in designing various parts of the torque-tension machine. For a biaxial stress state induced by a normal stress σ and a shear stress τ on a particular plane, the design equation based on octahedral shear stress theory and for static loading, can be written as

$$\frac{1}{n} = \left[\left(\frac{\sigma}{Y} \right)^2 + \left(\frac{\tau}{\tau_y} \right)^2 \right]^{1/2}$$

where Y and τ_y are the yield stress in tension and in shear respectively, n is the design factor based on yield strength. For octahedral shear stress theory, $\tau_y = Y / \sqrt{3}$. For combined bending and uniform axial stresses, the normal stress σ can be expressed as

$$\sigma = \pm \frac{F}{A} \pm \frac{Mc}{I}$$

and due to the torque T , the resulting shear stress $\tau = Tc / J$, where J is the polar second moment of an area.

For varying normal and shear stresses on a plane at a point, the design equation, based on octahedral shear stress theory, is

$$\frac{1}{n} = \left[\left(\frac{\sigma_{me}}{Y} + k_f \frac{\sigma_a}{\sigma_{en}} \right)^2 + \left(\frac{\tau_{me}}{\tau_y} + k_{fs} \frac{\tau_a}{\tau_{en}} \right)^2 \right]^{1/2}$$

where σ_{me} and σ_a are the mean and the alternating component of the stress, σ_{en} is the endurance limit at critical location of machine element and k_f the stress concentration factor.

RIGIDITY

Rigidity is high stiffness and low deflection, in either or both the lateral and torsional directions. High rigidity is desirable because it produces a high natural frequency, maintains

gear contact, maintains uniform oil film in gears and bearings, and improves the performance accuracy of the machine

A torque produces an angular deflection. Generally angular rigidity is expressed as angular deflection per unit length of the shaft, i.e., degree/unit length. Angular rigidity in terms of torque, shear modulus of rigidity and polar moment of area is

$$\frac{\theta}{L} = \frac{180T}{\pi GJ} \quad (\text{deg /unit length})$$

where T is in inch-lb_f

Lateral loads produce lateral deflections which vary along the shaft depending on the type of loading and the geometric properties of the shaft. Lateral deflection can be calculated using either integration or area moment method as used in case of beams

TORQUE REQUIRED TO TURN THE BALL SCREW

Motion in a direction opposite to the direction of the applied load involves a torque T and an axial load F which are related by the equation

$$T = \frac{FD_p}{2} \tan(\rho + \lambda) + \frac{FD_c}{2} \mu_c$$

where μ_c = collar friction, D_p and D_c are the screw pitch and collar mean diameter respectively. The parameter ρ is a thread-friction parameter and λ is the lead angle.

BUCKLING FORMULA

Euler's design equation for slender column can be written as

$$\frac{F}{A} = \frac{\pi^2 E}{n (\zeta \ell / \kappa)^2}$$

where ζ is the end condition factor in buckling and ℓ / κ is the slenderness ratio. The Euler equation is applicable only when the ℓ / κ ratio is large, that is, when

$$\frac{\ell}{\kappa} > \frac{\pi}{\zeta} \left[\frac{2E}{Y} \right]^{\frac{1}{2}}$$

For smaller ℓ / κ ratios, the J B Johnson or parabolic formula should be used, which can be written as

$$\frac{F}{A} = \frac{Y}{n} \left[1 - \left(\frac{\zeta \ell}{2\pi\kappa} \right)^2 \frac{Y}{E} \right]$$

3.9 STIFFNESS OF THE MACHINE

In order to calculate the stiffness of the torque-tension machine an analytical model has been developed and presented in this section. For simplification of calculations the complex structure of the machine has been resolved into elements and represented as two dimensional beams as shown in figure 3 29(a). The mathematical model of the machine was studied using simple bending theory based on total strain energy principle. However, during modelling only the axial load and the resulting bending moments have been considered. The effect of twisting moment due to the applied torque has been excluded from this model. To simplify the model, various auxiliary parts, such as steeped shaft, holders, grippers etc, which are not involved in building the main structure of the machine, have also been excluded.

In developing the model, it was necessary to make the following assumptions

- (i) The beams are in 2D and are initially straight and unstressed
- (ii) The material of the beams is perfectly homogeneous
- (iii) The elastic limit is nowhere exceeded
- (iv) Neutral axis passes through the centroid of the cross-sections
- (v) The weight of the machine and friction forces are negligible
- (vi) The applied load is symmetrically static and shared equally by the front and the back columns of the machine

ANALYTICAL MODEL

Because of the symmetry of the torque-tension machine only half of it needs to be considered. Figure 3 29(b) shows the force analysis diagram for the upper portion of the machine, where load is transmitted through cross-head and lead screws. Considering frame "abfc" separately, as shown in figure 3 29(c), total vertical deflection at point "a" can be found using Castigliano's first theorem

$$\frac{\partial U_1}{\partial X} = \delta_a = \int_0^{L_1} \frac{M_{11}}{EI_1} \frac{\partial M_{11}}{\partial X} dS_1 + \int_0^{L_3} \frac{M_{33}}{EI_2} \frac{\partial M_{33}}{\partial X} dS_3 + \int_0^{L_2} \frac{M_{22}}{EI_2} \frac{\partial M_{22}}{\partial X} dS_2 \quad (i)$$

$$= \delta_1 + \delta_3 + \delta_2 \text{ (say)} \quad (ii)$$

- where
- U_1 - the total strain energy in the frame "abfc"
 - X - the half of the total applied axial load
 - L_1, L_2, L_3 - the total lengths of beams ab, bc and bf respectively
 - M_{11}, M_{22}, M_{33} - the bending moments at section 1-1, 2-2 and 3-3 of beams ab, bc and bf respectively
 - S_1, S_2, S_3 - the distances of points a, b and f from sections 1-1, 2-2 and 3-3 respectively
 - I_1, I_2 - the moment of inertia of the cross-section of beams ab and bc about their neutral axis, respectively. As beams bc and bf both are parts of lead screw, so $I_2 = I_3$
 - $\delta_1, \delta_3, \delta_2$ - the total vertical deflections resulted from the first, second and third terms of the Eq (i), respectively

But,

$$M_{11} = M_1 - XS_1$$

$$M_{33} = R_1 S_3 \quad (iii)$$

$$M_{22} = M_1 + R_1 L_3 + R_1 S_2 - XL_1 - FS_2$$

where, M_1 - the unknown redundancy bending moment at point a
 F - the unknown force at point a
 R_1 - the unknown reaction force at point f

Differentiating equations (iii) with respect to X and substituting the corresponding values in equation (i), becomes

$$\delta_1 = \frac{L_1^2}{EI_1} \left[\frac{XL_1}{3} - \frac{M_1}{2} \right] \quad (iv)$$

$$\delta_3 = 0 \quad (v)$$

$$\delta_2 = \frac{L_1 L_2}{2EI_2} \{ 2XL_1 + FL_2 - 2M_1 - R_1(2L_3 + L_2) \} \quad (vi)$$

The unknown values of R_1 , M_1 and F can be found from the relations

$$\frac{\partial U_1}{\partial R_1} = 0 \quad \text{and} \quad \frac{\partial U_1}{\partial M_1} = 0$$

But
$$\frac{\partial U_1}{\partial R_1} = \int_0^{L_1} \frac{M_{11}}{EI_1} \frac{\partial M_{11}}{\partial R_1} dS_1 + \int_0^{L_3} \frac{M_{33}}{EI_2} \frac{\partial M_{33}}{\partial R_1} dS_3 + \int_0^{L_2} \frac{M_{22}}{EI_2} \frac{\partial M_{22}}{\partial R_1} dS_2 \quad (vii)$$

$$= \delta + \delta' + \delta \quad (\text{say})$$

Differentiating equations (iii) with respect to R_1 and substituting the corresponding values in Eq (vii), gives

$$\delta = 0$$

$$\delta = \frac{R_1 L_3^3}{3EI_2}$$

$$\delta'' = \frac{1}{EI_2} \left\{ -XL_1 L_2 \left(L_3 + \frac{L_2}{2} \right) + M_1 L_2 \left(L_3 + \frac{L_2}{2} \right) + R_1 L_2 \left(L_3^2 + L_2 L_3 + \frac{L_2^2}{3} \right) - FL_2^2 \left(\frac{L_3}{2} + \frac{L_2}{3} \right) \right\}$$

But as $\delta + \delta' + \delta = 0$, so from the above equations,

$$R_1 = \frac{XL_1 L_2 Q}{Z} - \frac{M_1 L_2 Q}{Z} + \frac{FL_2^2 (L_3/2 + L_2/3)}{Z} \quad (viii)$$

where
$$Q = (L_3 + L_2/2) \quad (ix)$$

and
$$Z = L_3^3 / 3 + L_2 L_3^2 + L_2^2 L_3 + L_2^3 / 3 \quad (x)$$

Taking moment at point c, as $\sum M_c = 0$,

so
$$R_1(L_2 + L_3) + M_1 - XL_1 - FL_2 = 0 \quad (xi)$$

Again, according to the Castigliano's second theorem,
$$\frac{\partial U_1}{\partial M_1} = 0 \quad (xii)$$

which can be written as

$$\frac{\partial U_1}{\partial M_1} = \int_0^{L_1} \frac{M_{11}}{EI_1} \frac{\partial M_{11}}{\partial M_1} dS_1 + \int_0^{L_3} \frac{M_{33}}{EI_2} \frac{\partial M_{33}}{\partial M_1} dS_3 + \int_0^{L_2} \frac{M_{22}}{EI_2} \frac{\partial M_{22}}{\partial M_1} dS_2 \quad (xiii)$$

Using equations (iii) and (xii), and after simplification, Eq (xiii) provides

$$M_1(I_1 L_1 + I_2 L_2) - X \left(\frac{I_1 L_1^2}{2} + I_2 L_1 L_2 \right) + R_1 I_2 \left(L_2 L_3 + \frac{L_2^2}{2} \right) - F I_2 \frac{L_2^2}{2} = 0 \quad (xiv)$$

where, for simplification, $1/I_1$ and $1/I_2$ have been replaced by I_1 and I_2 respectively

Now substituting Eq (viii) into (xi), after simplification, becomes

$$F = M_1 D - XW \quad (xv)$$

where $D = B/C$ and $W = A/C$, in which,

$$A = \frac{L_1 L_2 Q (L_2 + L_3)}{Z} - L_1$$

$$B = \frac{L_2 Q (L_2 + L_3)}{Z} - 1$$

and
$$C = \frac{L_2^2 (3L_3 + 2L_2)(L_2 + L_3)}{6Z} - L_2$$

Now, substituting the values of R_1 , from Eq (viii), and F , from (xv), into Eq (xiv) gives

$$M_1 = X \frac{J}{K} \quad (xvi)$$

where

$$J = I_1 \frac{L_1^2}{2} + I_2 \left[\left(L_1 L_2 - \frac{WL_2^2}{2} \right) + \left(L_2 L_3 + \frac{L_2^2}{2} \right) \left\{ \frac{WL_2^2}{6Z} (3L_3 + 2L_2) - \frac{QL_1 L_2}{Z} \right\} \right]$$

and
$$K = I_1 L_1 + I_2 \left[\left(L_2 - \frac{DL_2^2}{2} \right) + \left(L_2 L_3 + \frac{L_2^2}{2} \right) \left\{ \frac{DL_2^2}{6Z} (3L_3 + 2L_2) - Q \frac{L_2}{Z} \right\} \right]$$

Thus knowing the values of M_1 , F and R_1 , from equations (xvi), (xv) and (viii) respectively, the values of δ_1 and δ_2 of equations (iv) and (vi) can be found

Figure 3 30(a) shows the free body diagram of the beam "de" Total vertical deflection at point c, due to transmitted axial load through lead screw, can be obtained as follows

$$\frac{\partial U_2}{\partial X} = \delta_c = \int_0^{L_5} \frac{M_{55}}{EI_5} \frac{\partial M_{55}}{\partial X} dS_5 + \int_0^{L_4} \frac{M_{44}}{EI_4} \frac{\partial M_{44}}{\partial X} dS_4 \quad (xvii)$$

where U_2 - the total strain energy in the beam "de"
 L_4, L_5 - the distances between the points c-e and c-d respectively
 M_{44}, M_{55} - the bending moments at section 4-4 and 5-5, respectively

The unknown redundancy moment M_3 can be obtained by taking moment at point d Thus $M_3 = XL_5$ As

$$M_{44} = M_3 = XL_5$$

and $M_{55} = M_3 - XS_5$

so equation (xvii) becomes

$$\delta_c = \frac{XL_5^2}{EI_4} \left[\frac{L_5}{3} + L_4 \right] \quad (xviii)$$

However, deflection of beam "dk" can be found considering it as a short compression block

Thus

$$\delta_d = \frac{XL_6}{EA_6} \quad (xix)$$

where L_6 and A_6 are the length and cross-section of the beam "dk"

Figure 3 30(b) shows the force analysis diagram for the lower portion of the machine, where the load is transmitted through drive shaft housing and vertical columns. The vertical displacement at point b can be found as follows

$$\begin{aligned} \frac{\partial U_3}{\partial X} = \delta_b &= \int_0^{L_7} \frac{M_{77}}{EI_7} \frac{\partial M_{77}}{\partial X} dS_7 + \int_0^{L_8} \frac{M_{88}}{EI_8} \frac{\partial M_{88}}{\partial X} dS_8 \\ &= \delta_7 + \delta_8 \text{ (say)} \end{aligned} \quad (xx)$$

As $M_2 = XL_7$ (taking moment at point m), $M_{77} = -M_2 + XS_7$, and $M_{88} = XL_7 - M_2 + F_2S_8$, so

$$\delta_7 = -\frac{XL_7^3}{6EI_7} \quad (xxi)$$

$$\delta_8 = \frac{F_2L_7L_8^2}{2EI_8} \quad (xxii)$$

The value of unknown redundancy force F_2 can be obtained from the relation

$$\frac{\partial U_3}{\partial M_2} = 0 \quad (xxiii)$$

So,

$$F_2 = X \frac{I_8}{I_7} \left(\frac{L_7}{L_8} \right)^2$$

Thus after knowing the values of δ_1 , δ_2 , δ_c , δ_d and δ_b , from equations (iv), (vi), (xviii), (xix) and (xx) respectively, the stiffness of the machine can be obtained for the design load

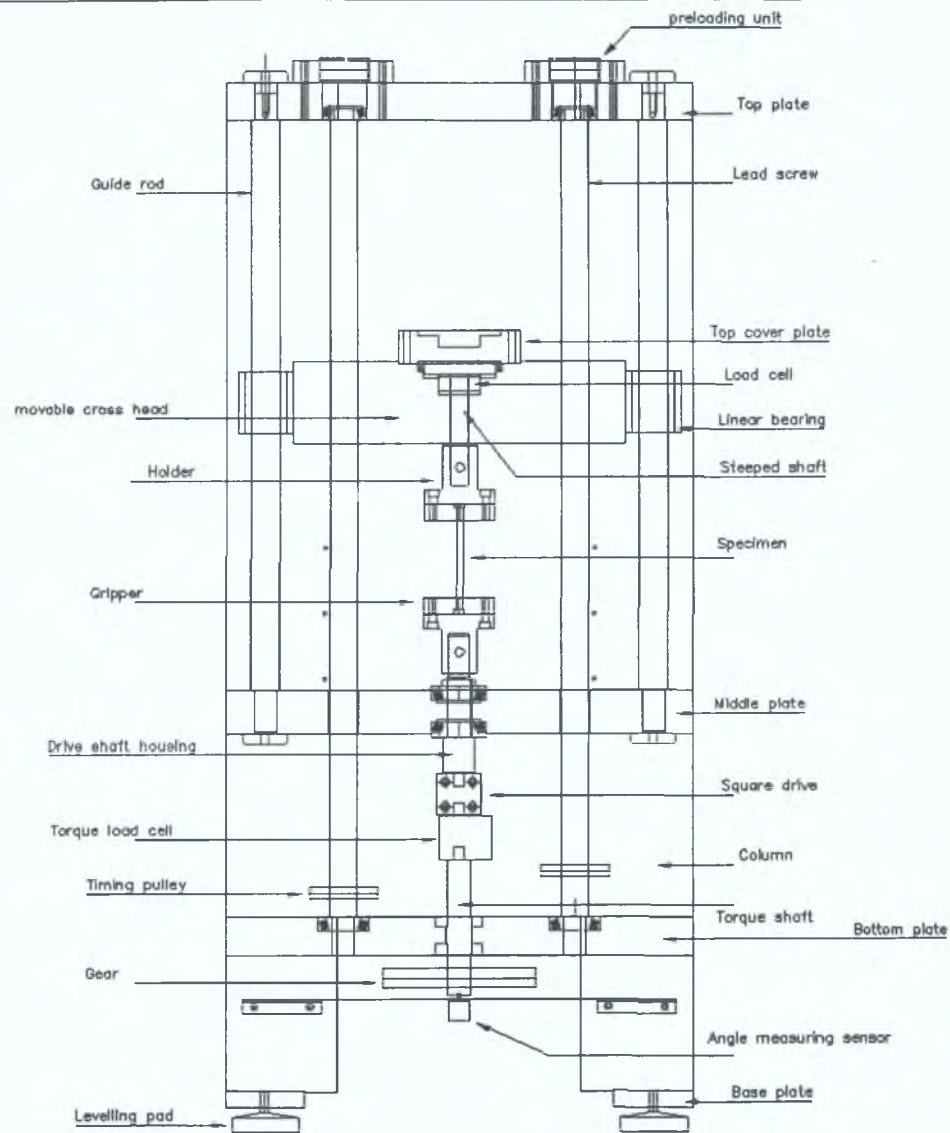


FIGURE – 3.1 Schematic diagram of the machine (Front view)
(Motors and frames are not shown in the figure)

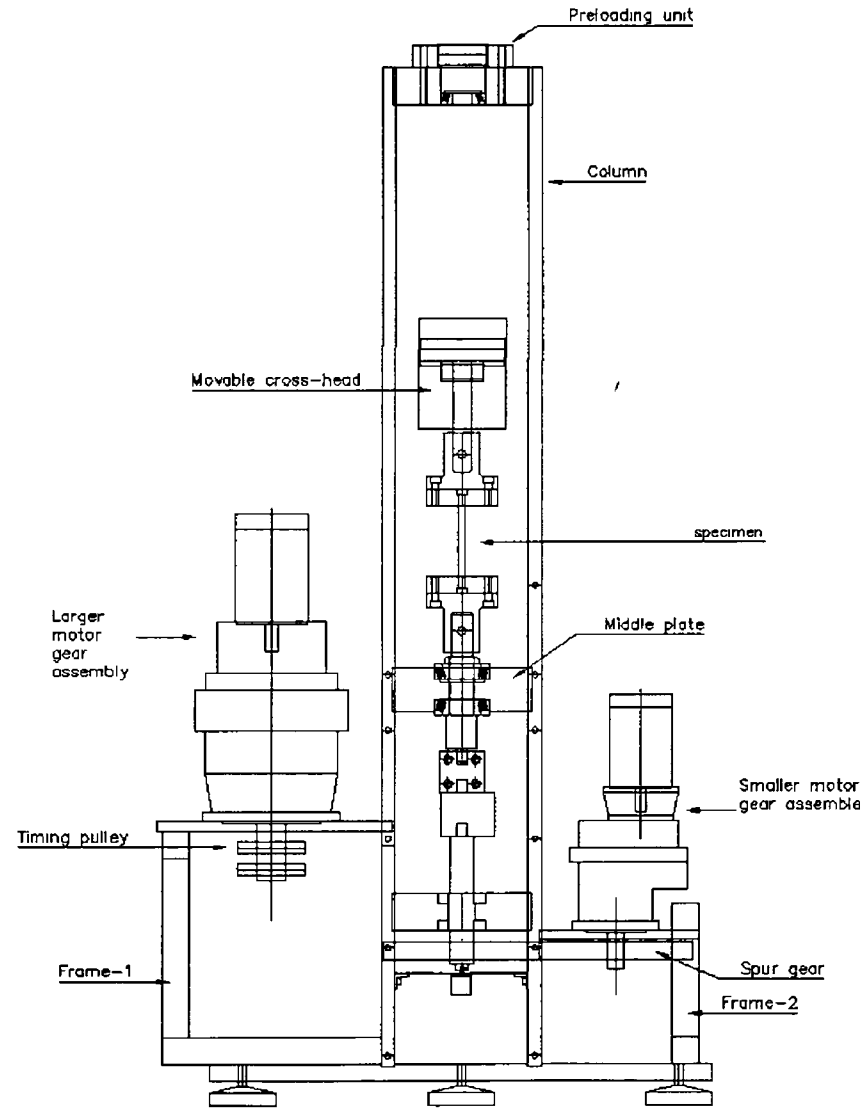


FIGURE - 32 Schematic diagram of the machine (Side view)
(Guide rods and ball screws are not shown in the figure)

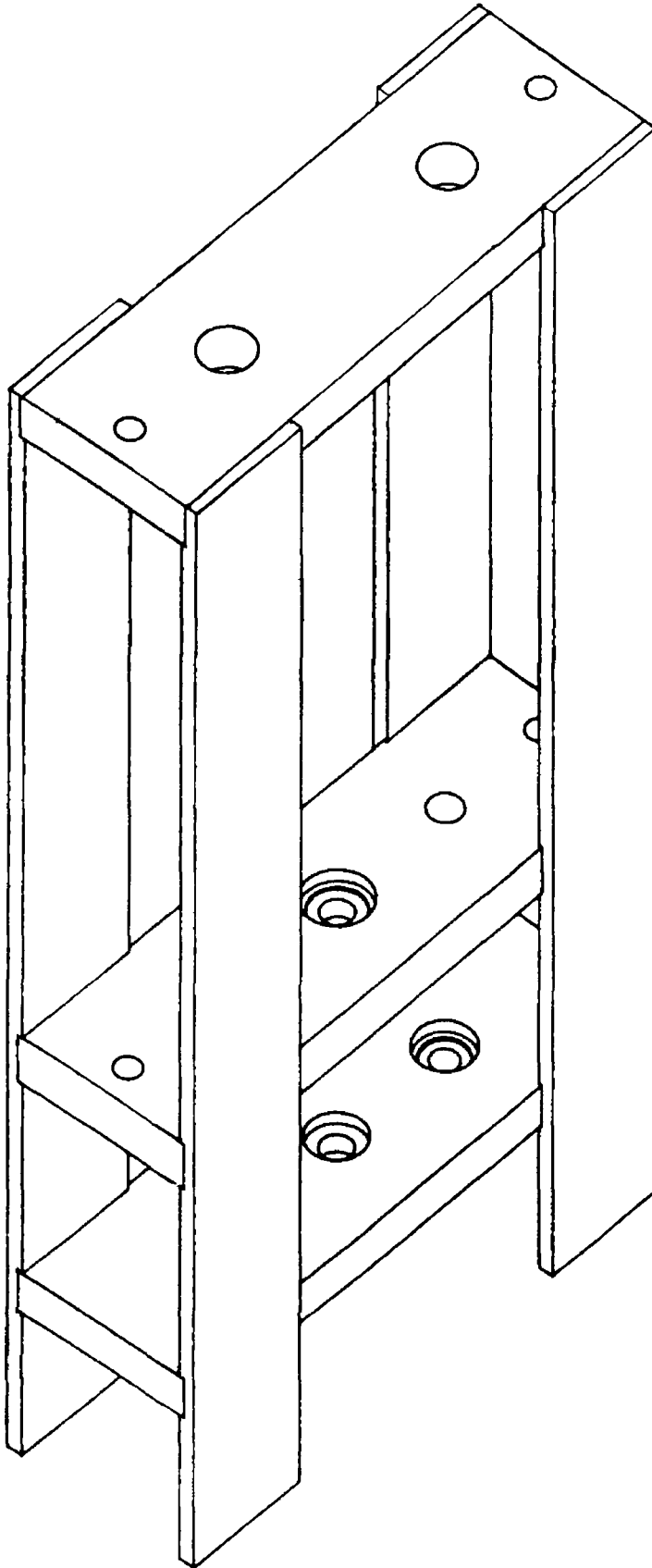


FIGURE - 3 3 The schematic diagram of the main frame of the torque-tension machine
(The bolts and the drilled holes are not shown in the figure)

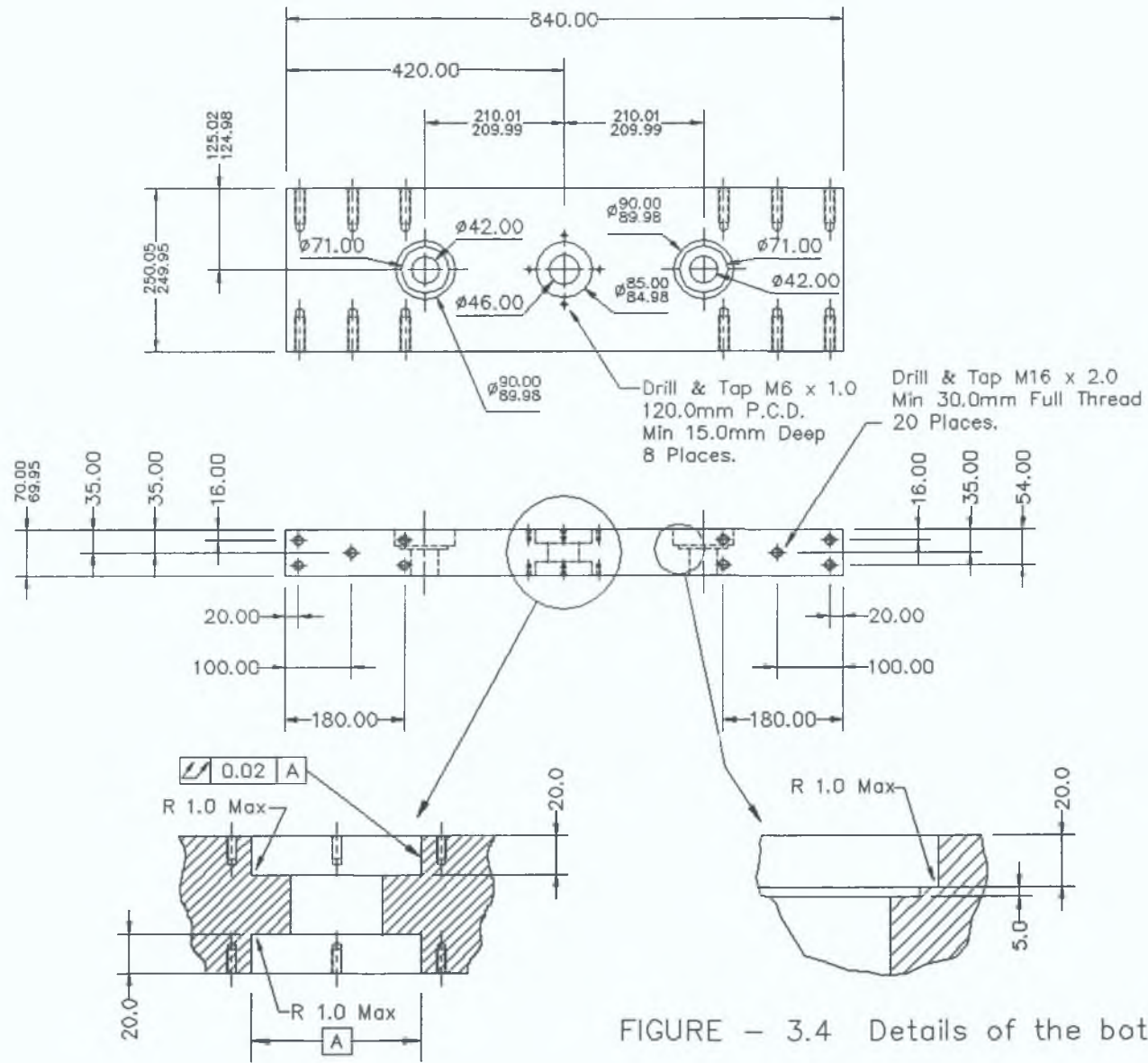


FIGURE - 3.4 Details of the bottom plate

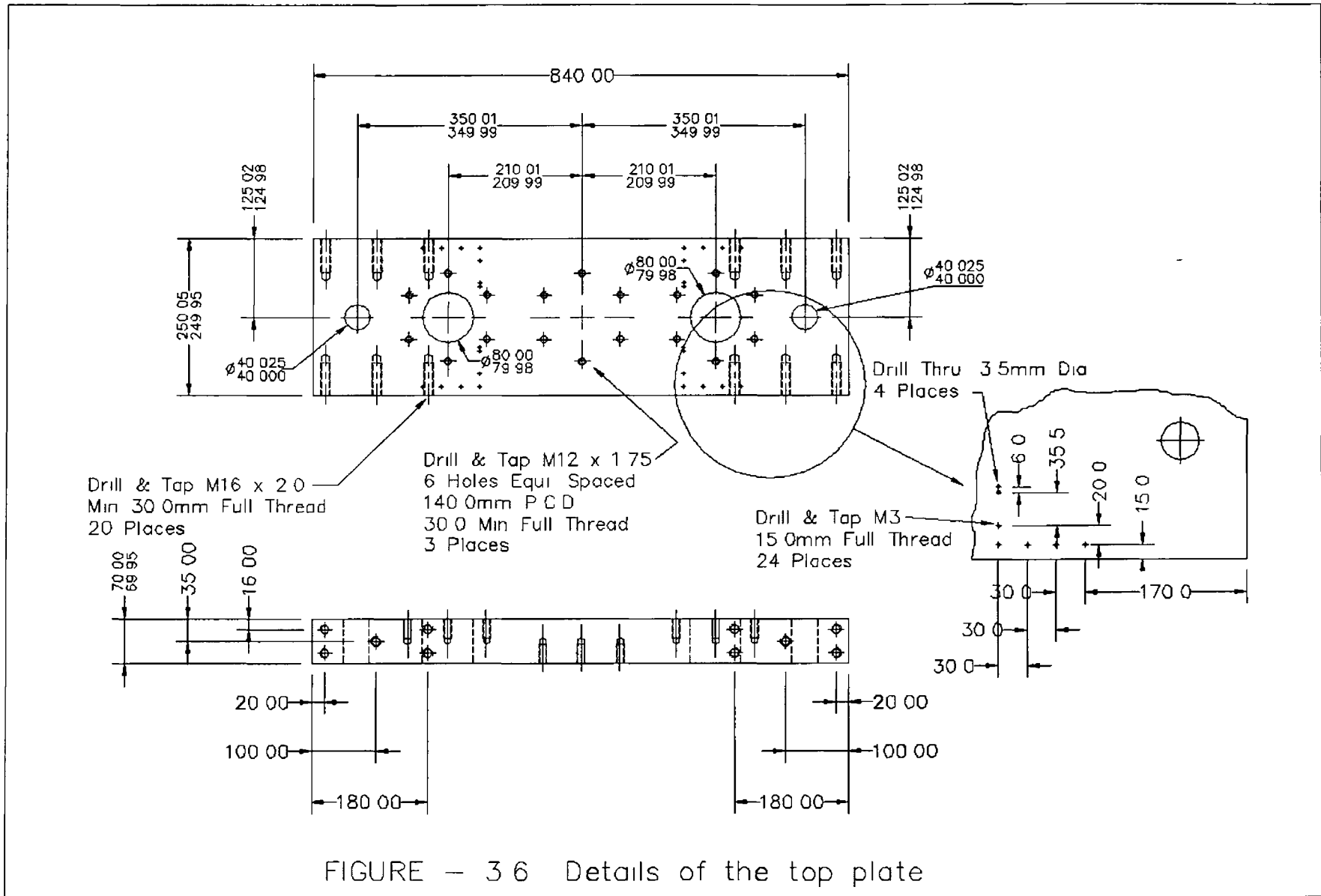


FIGURE - 3.6 Details of the top plate

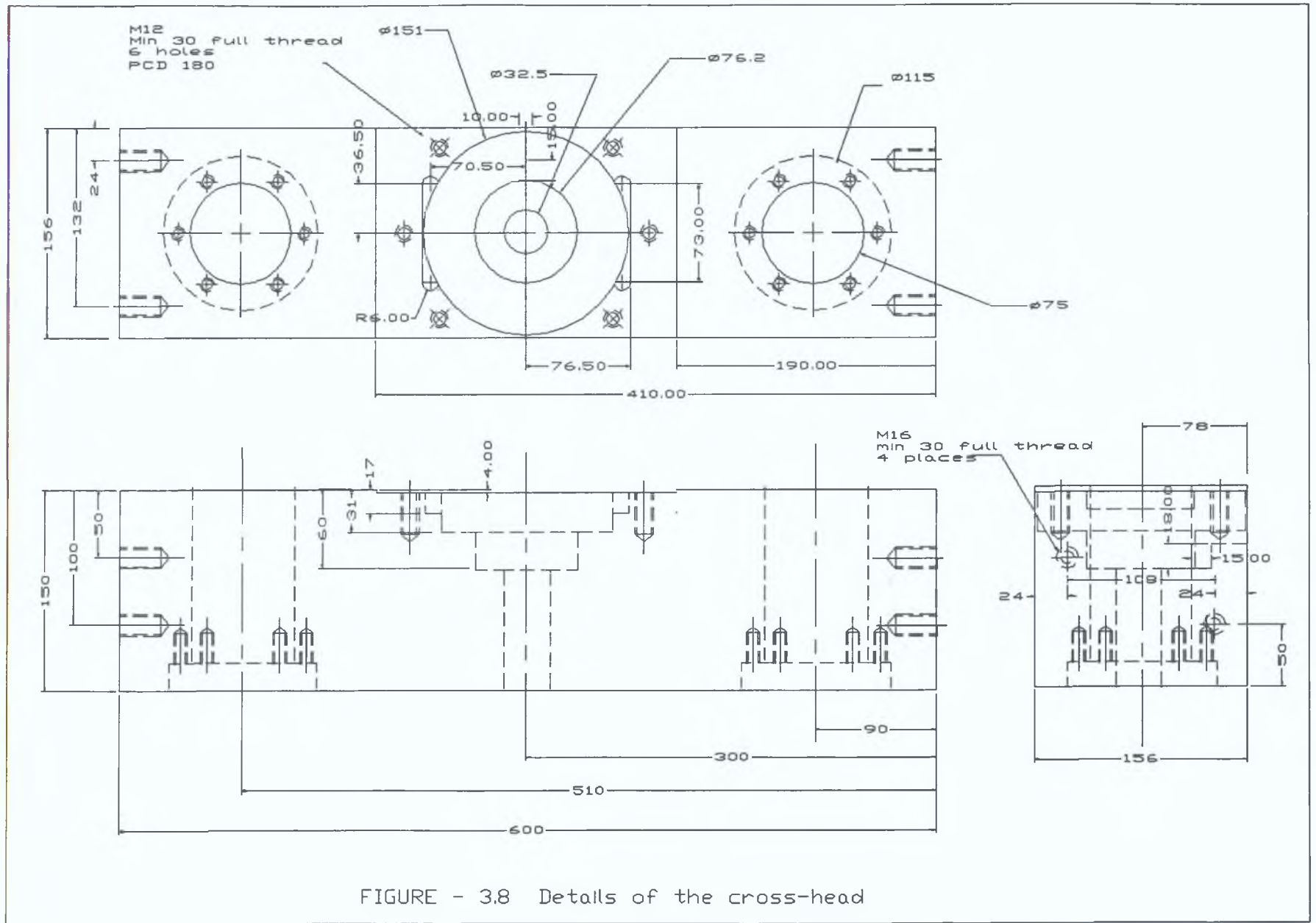


FIGURE - 3.8 Details of the cross-head

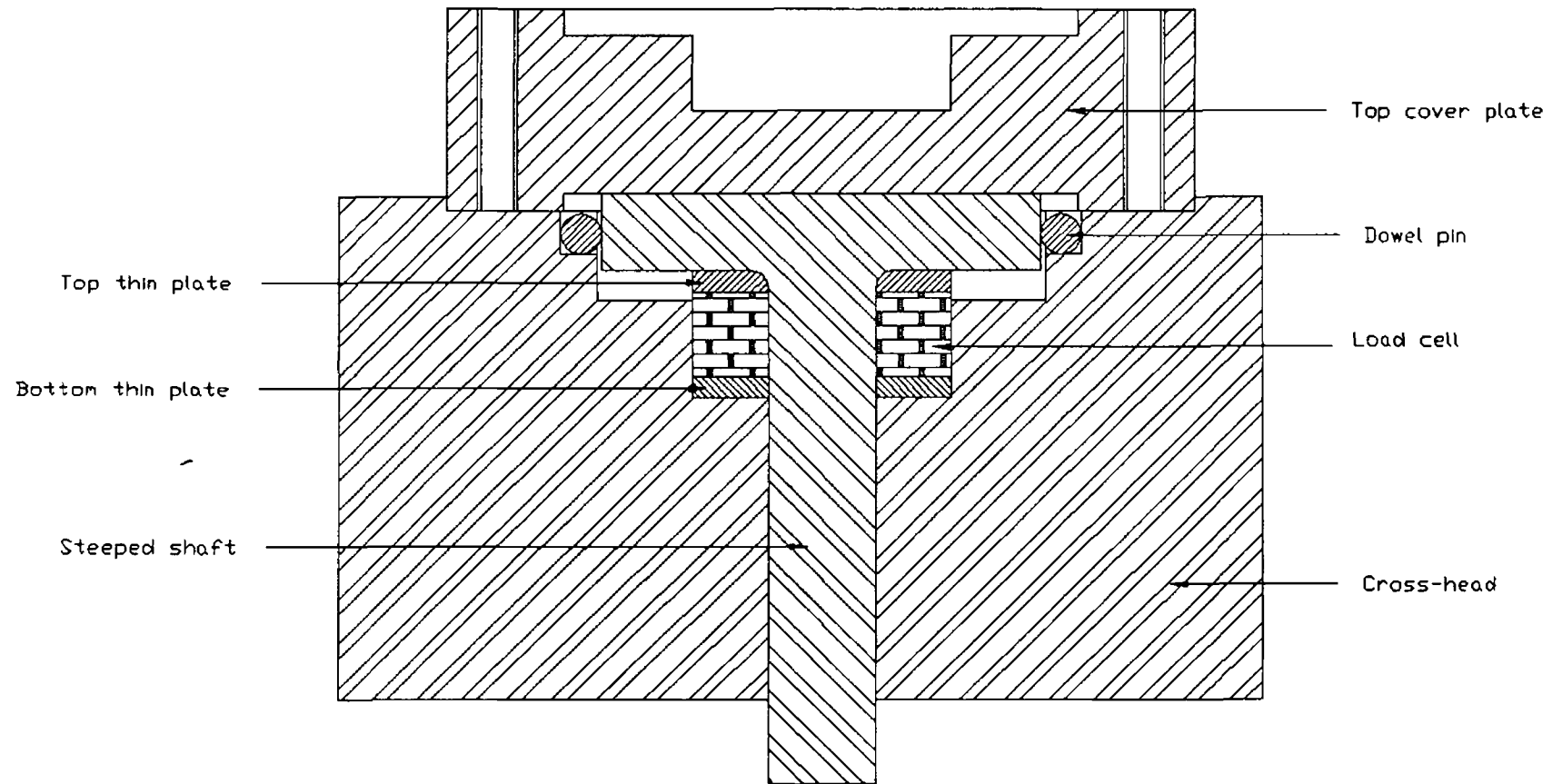


FIGURE - 39 The complete cross-head arrangement including the dowel pin, load cell and other auxiliary components

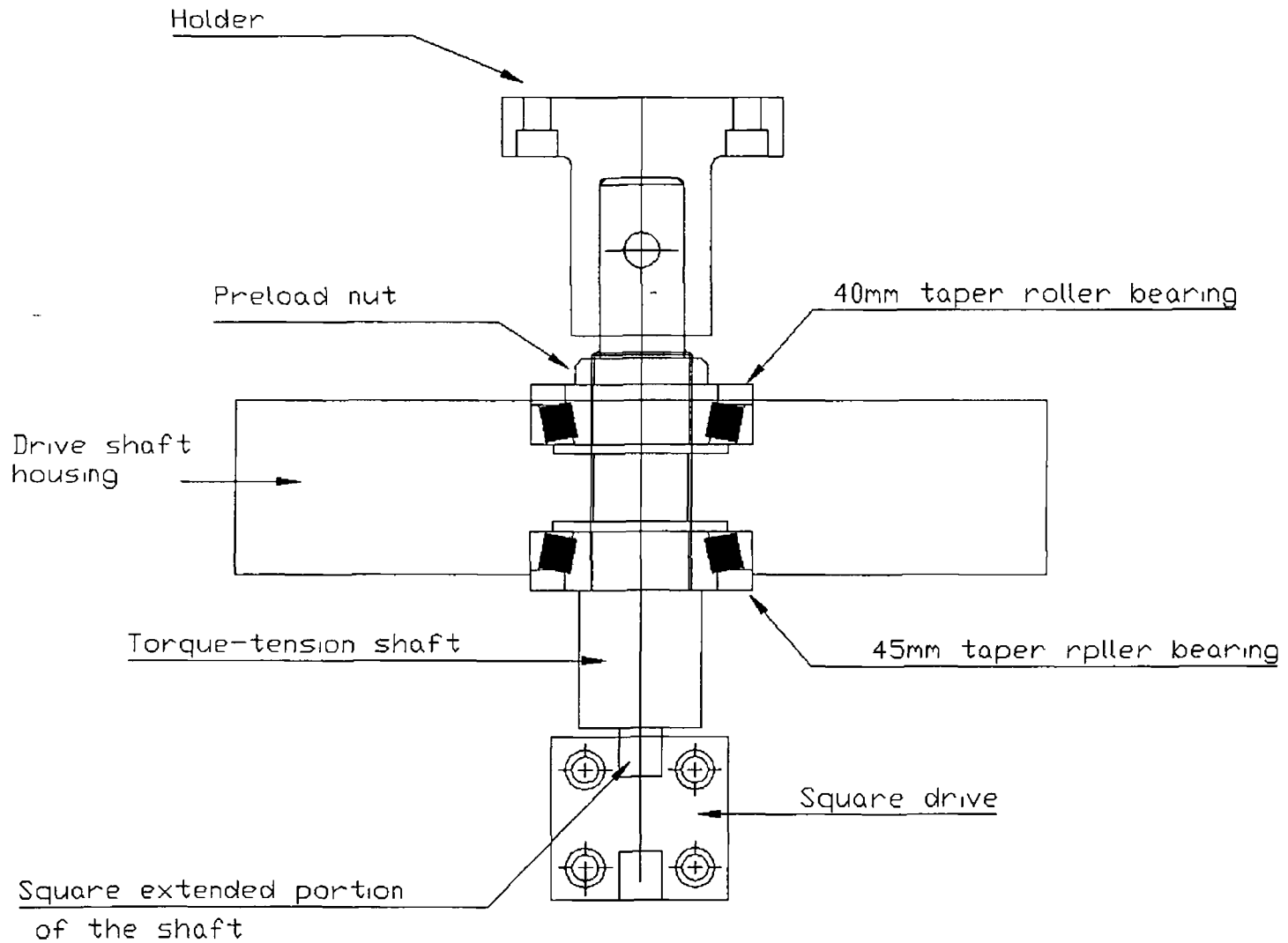


FIGURE - 3 10 Assembly drawing of the torque-tension shaft along with the taper roller bearings and other accessories

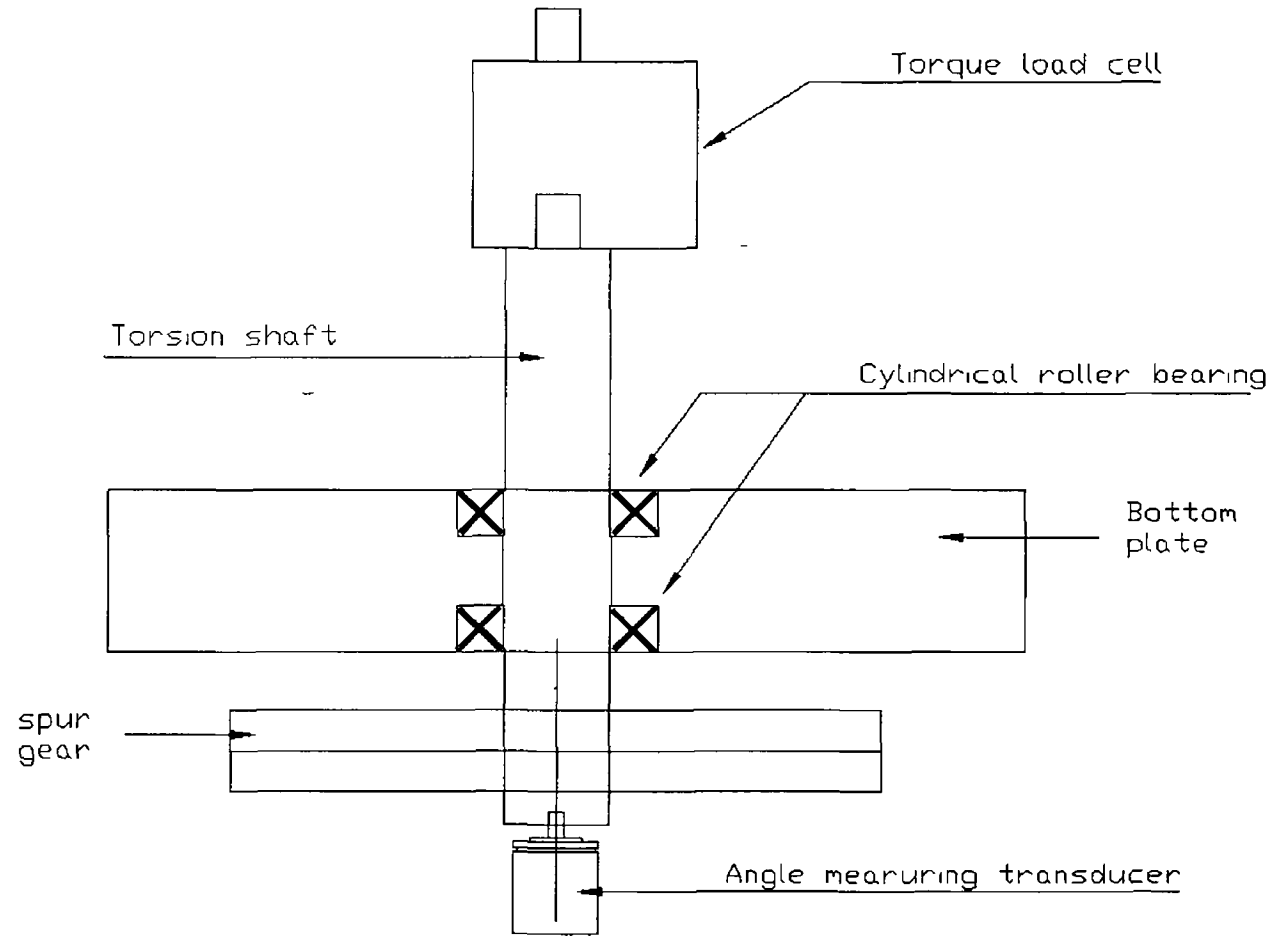


FIGURE - 311 Assembly drawing of the torsion shaft

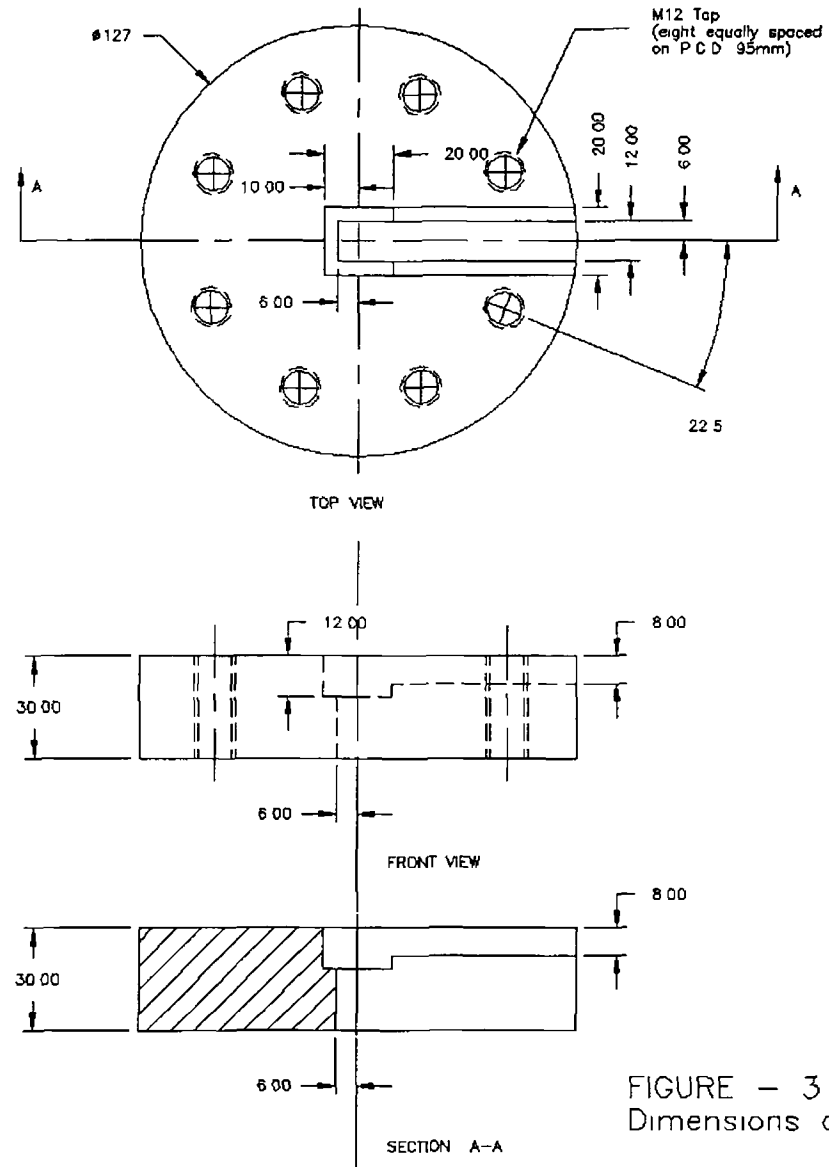


FIGURE - 3 13
Dimensions of the gripper in detailed

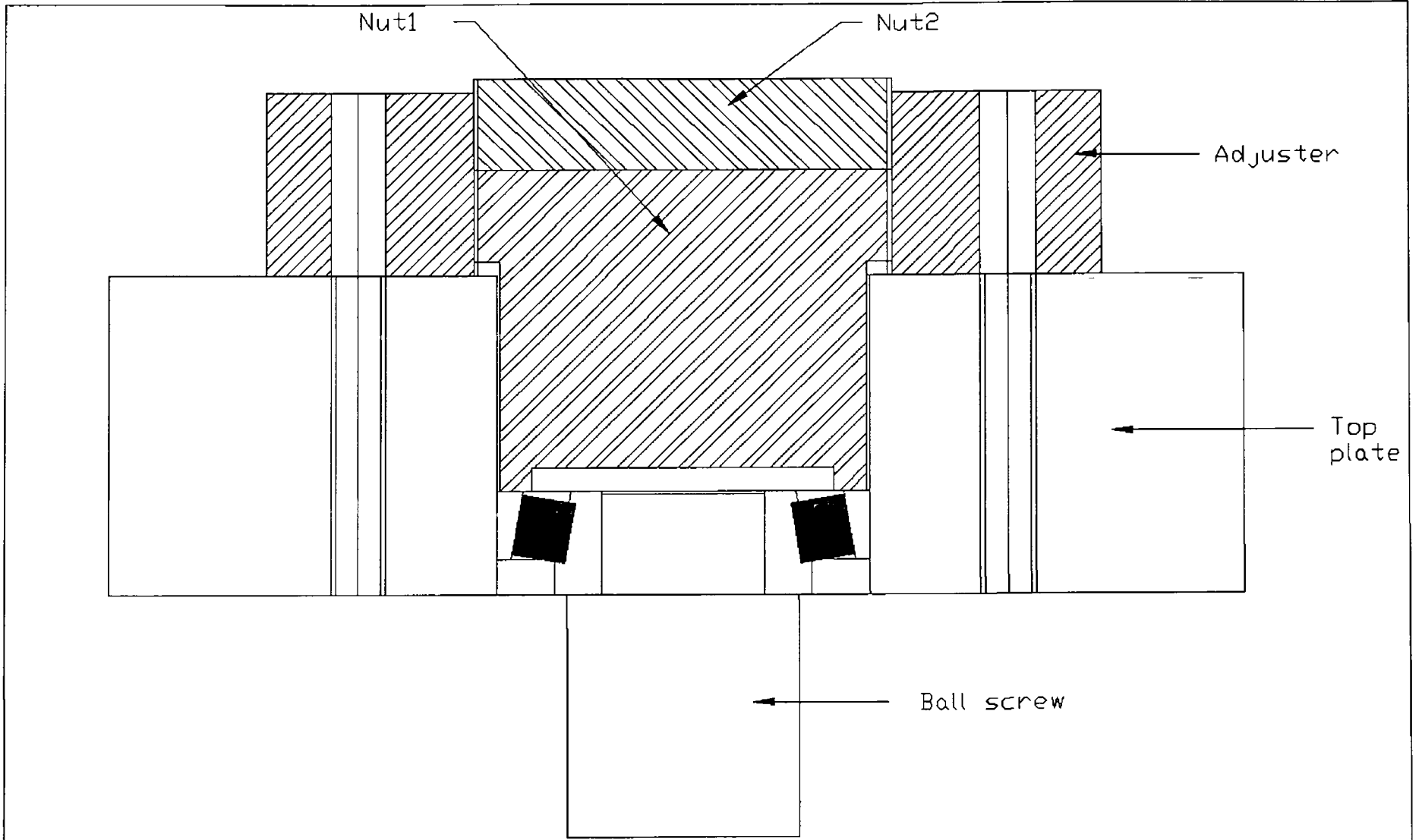


FIGURE - 314 Assembly drawing of the preloading unit

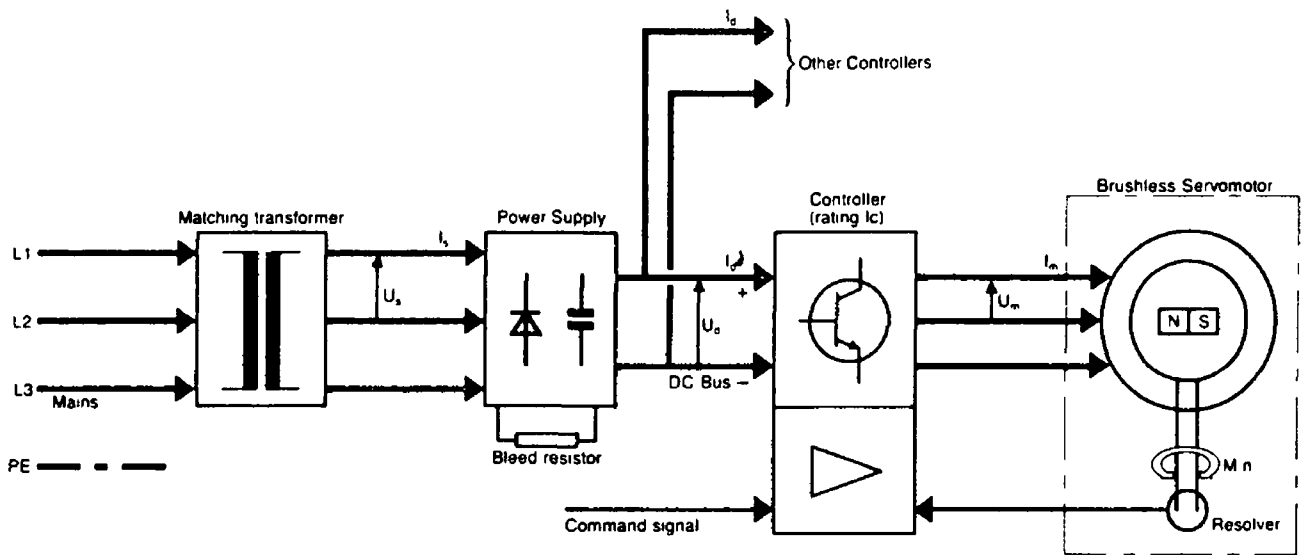
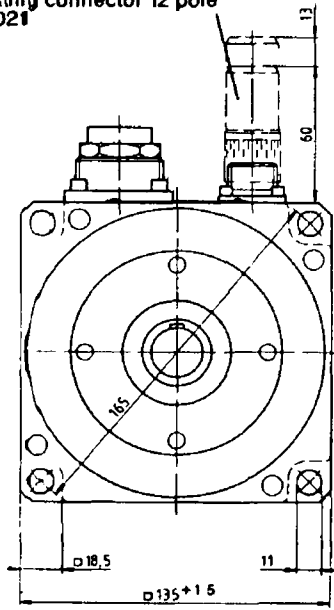


FIGURE - 3 15 The schematic diagram of a Moog brushless drive system

signal mating connector 12 pole
P/N A 63021



power mating connector 8 pole
P/N A 63002-001

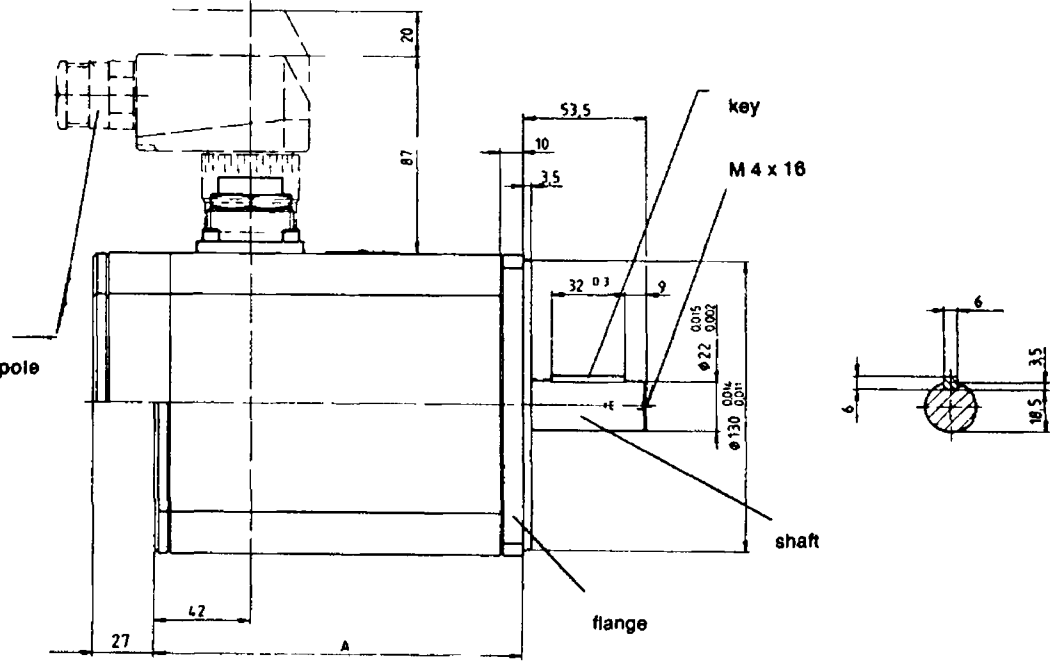


Figure - 3 16 Dimensions of motor-1

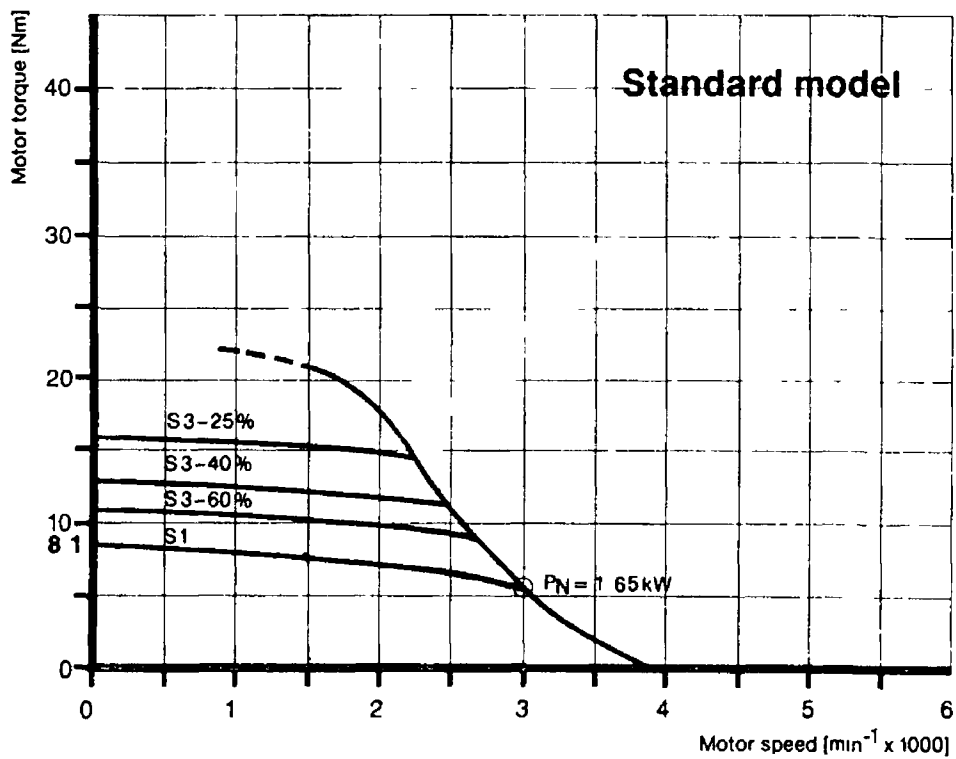


FIGURE - 3 17 The characteristic curve of motor-1

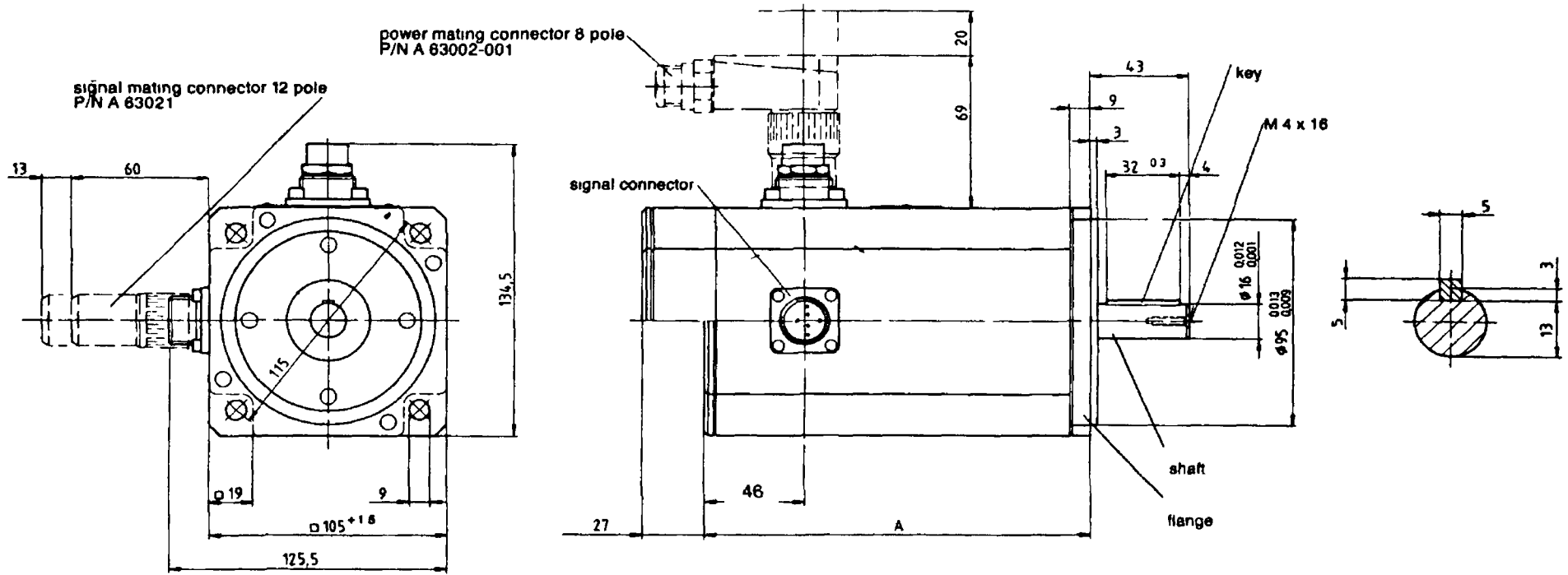


Figure - 3 19 Details of motor-2

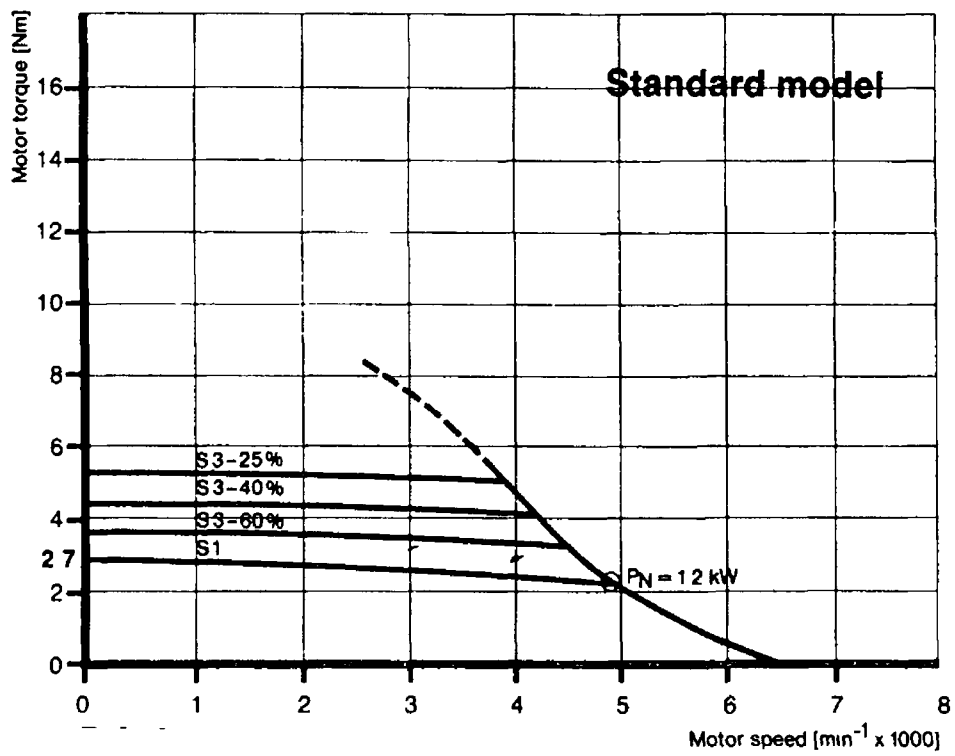
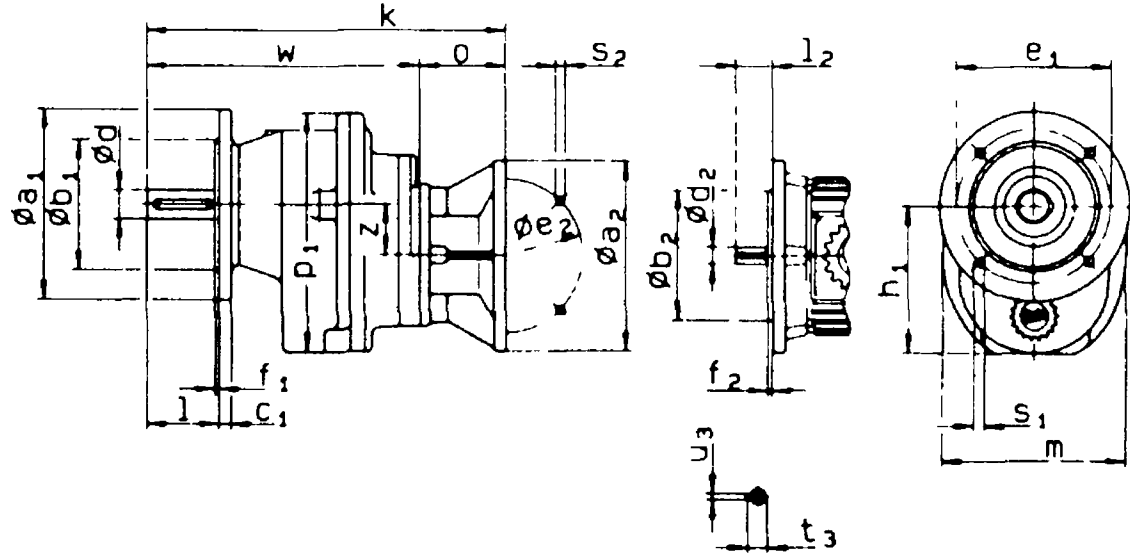


FIGURE - 3 20 The characteristic curve of motor-2

Flange Design



Ø	Ø	Ø			
a ₁	b ₁	c ₁	e ₁	f ₁	s ₁
160	110	10	130	35	4xØ 9

a	Ø a ₂	b	Ø b ₂	c	Ø d x l	Ø d ₂ x l ₂	e	Ø e ₂	f	f ₂	h	h ₁	i	k	m	n	o	p	p ₁	Ø s	s ₂	t	t ₃	u	u ₃	w	x	z	Zentrg Centg DIN 332/2
175	140	190	95	20	30 x 70	11 x 23	140	115	155	3	130	128	115	333	170	35	63	215	213	14	95	33	125	8	4	270	3	47	M 10

FIGURE - 3 21 Various dimensions of gearbox-2

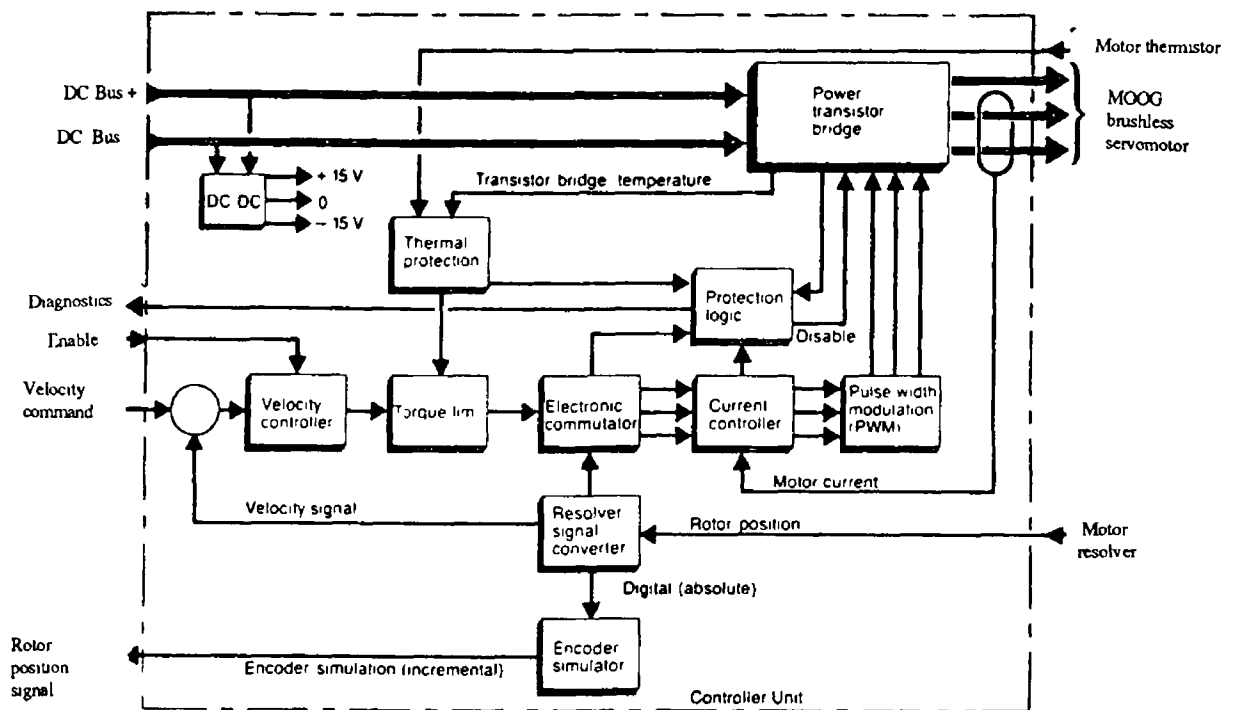


FIGURE - 3 22 The flow chart of the operation principle of the controllers

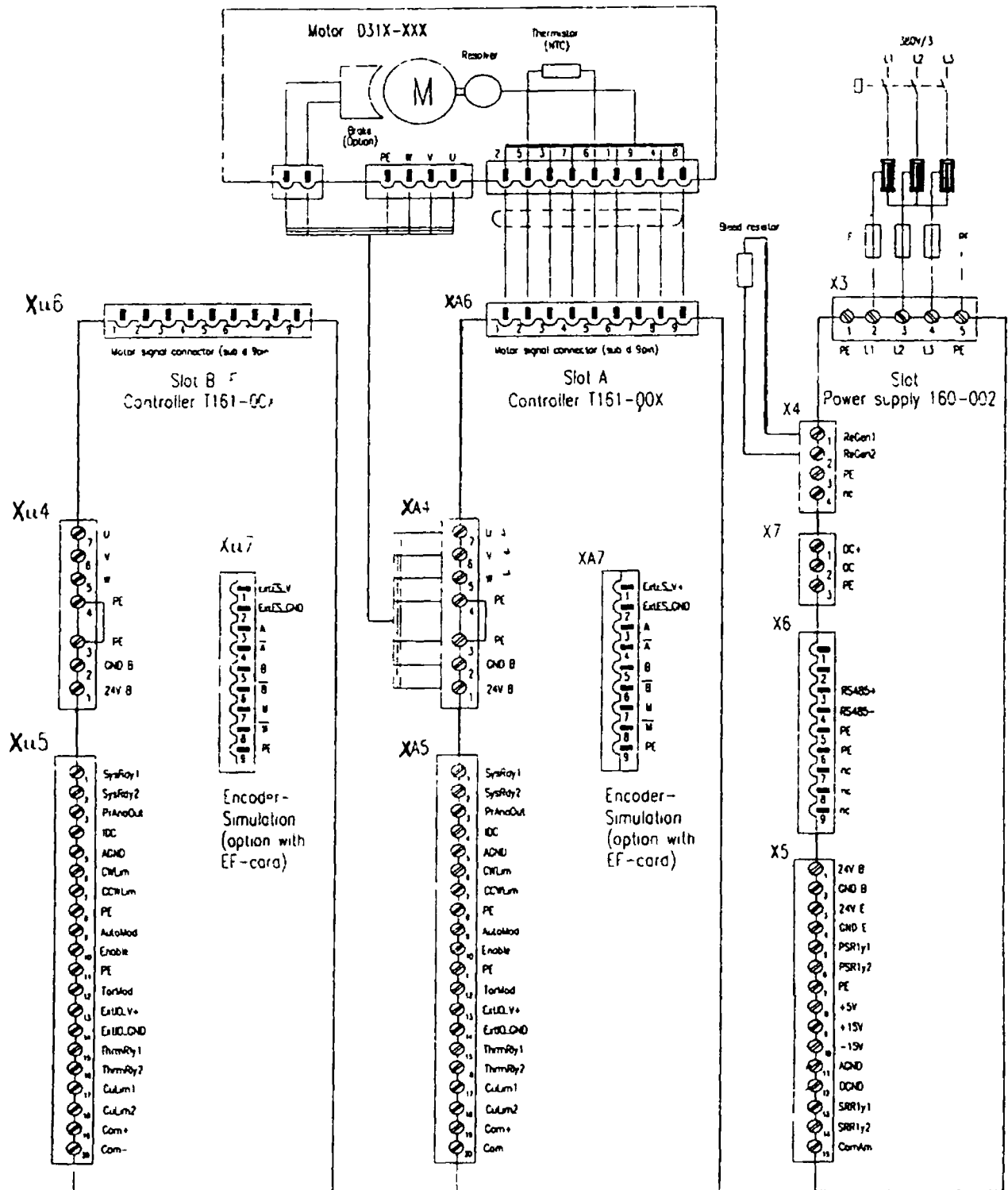


FIGURE - 3 23 Various connections of the controller and the power supply unit

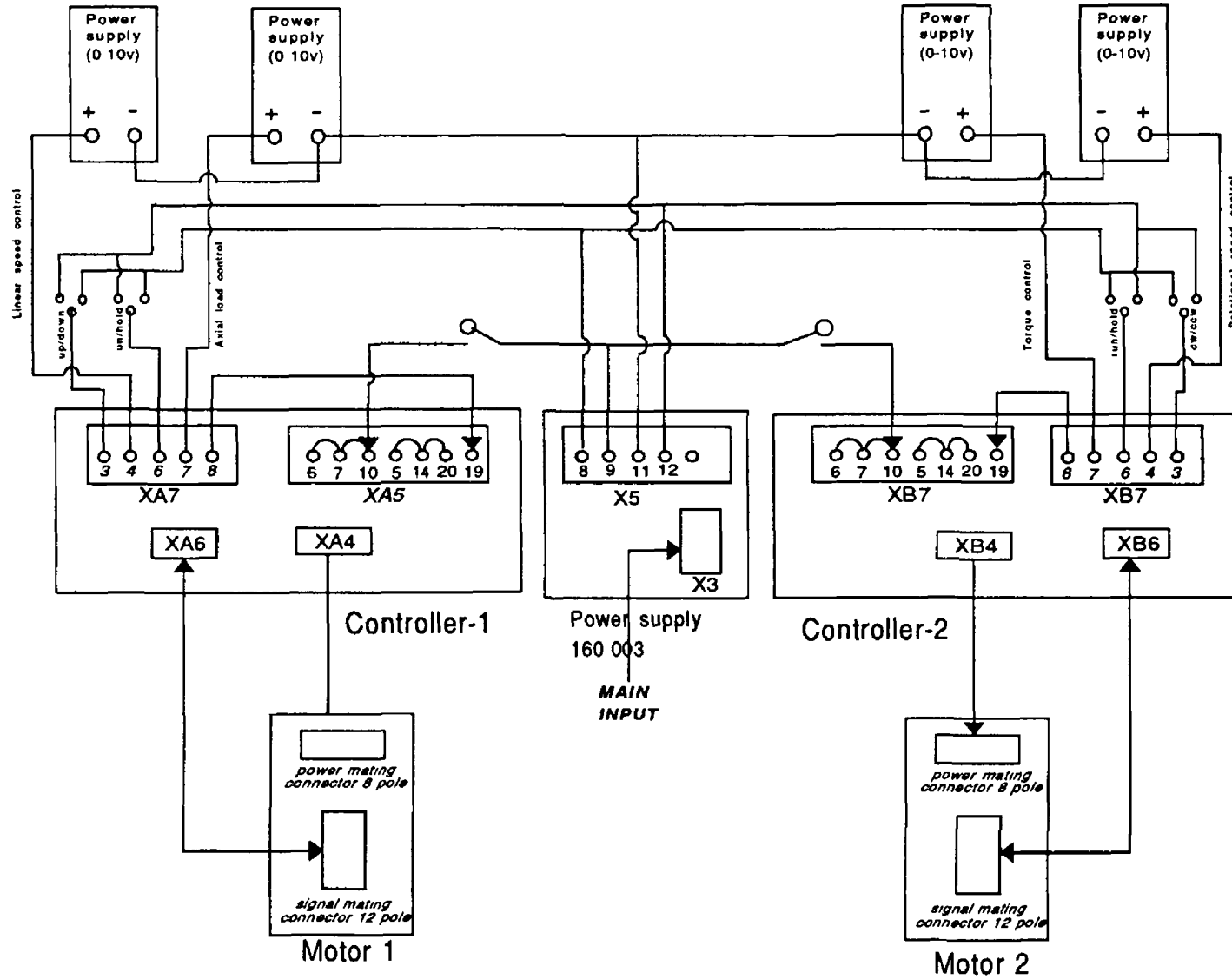


FIGURE - 3 24 Circuit diagram among the controllers and the motors

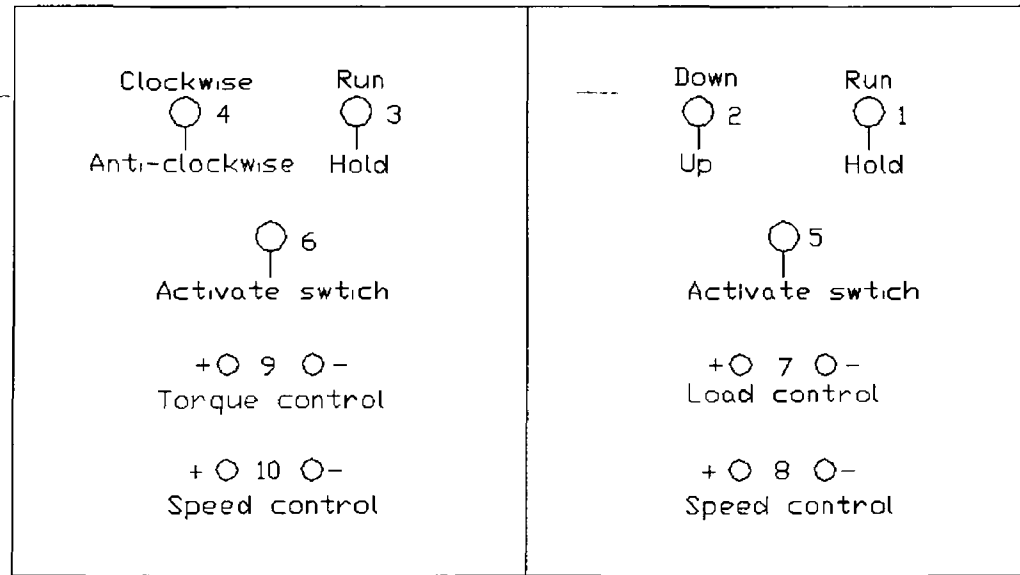


FIGURE - 325 The schematic diagram of the control panel

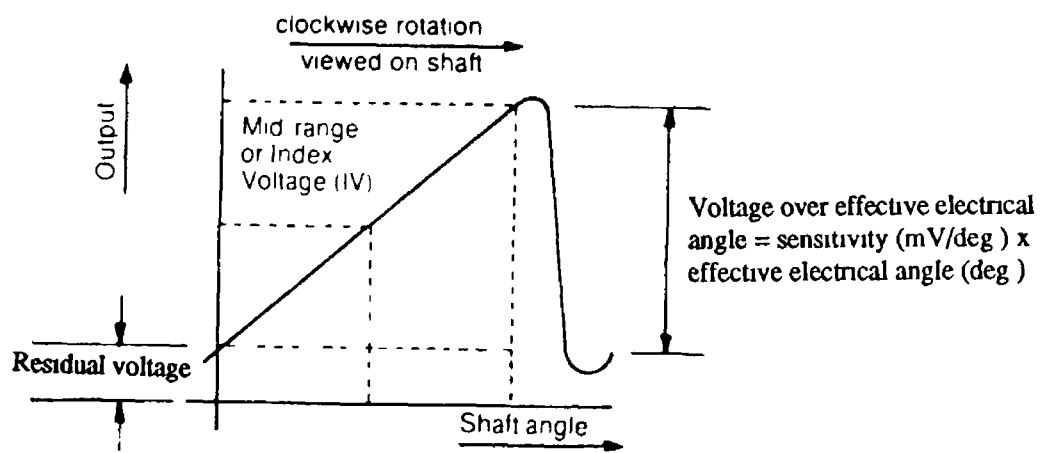


FIGURE - 3 26 The output charateristic curve of the angle measuring transducer

All dimensions are in millimetres (inches)

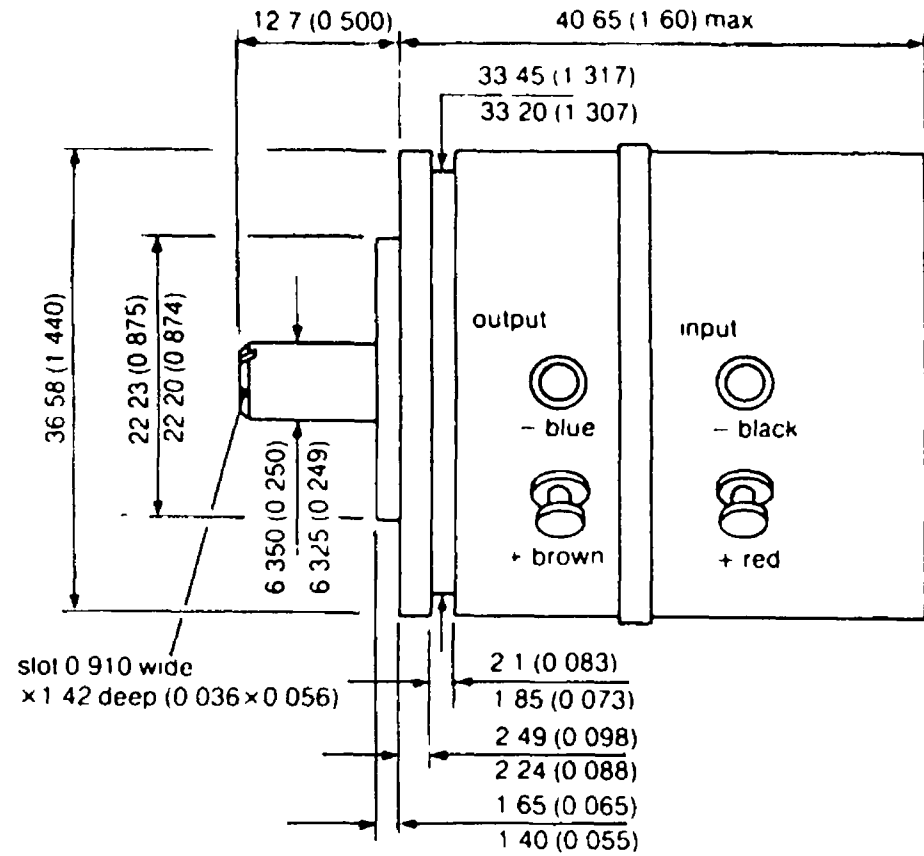
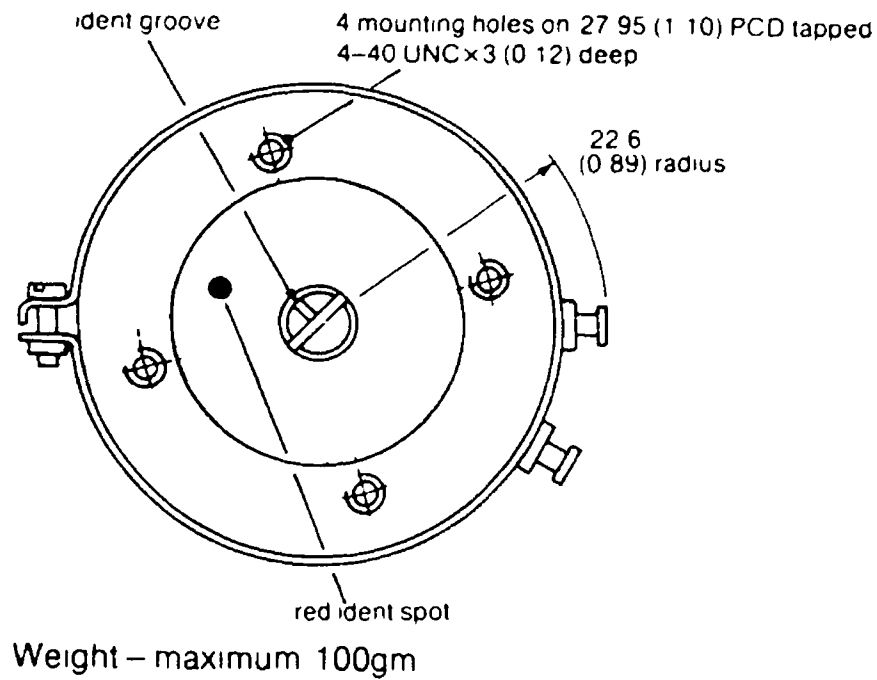


FIGURE - 3 27 Details of the angle measuring transducer

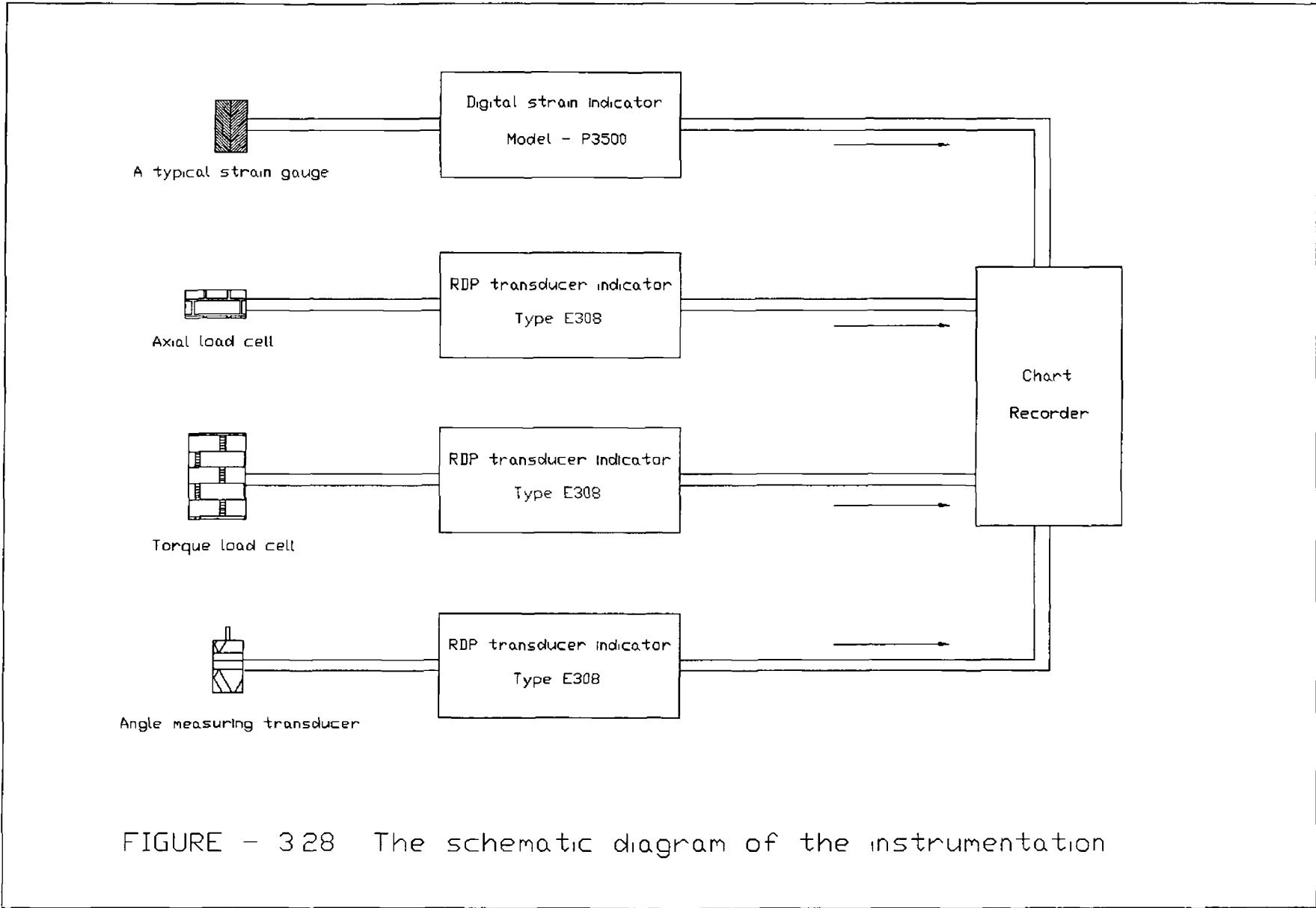


FIGURE - 328 The schematic diagram of the instrumentation

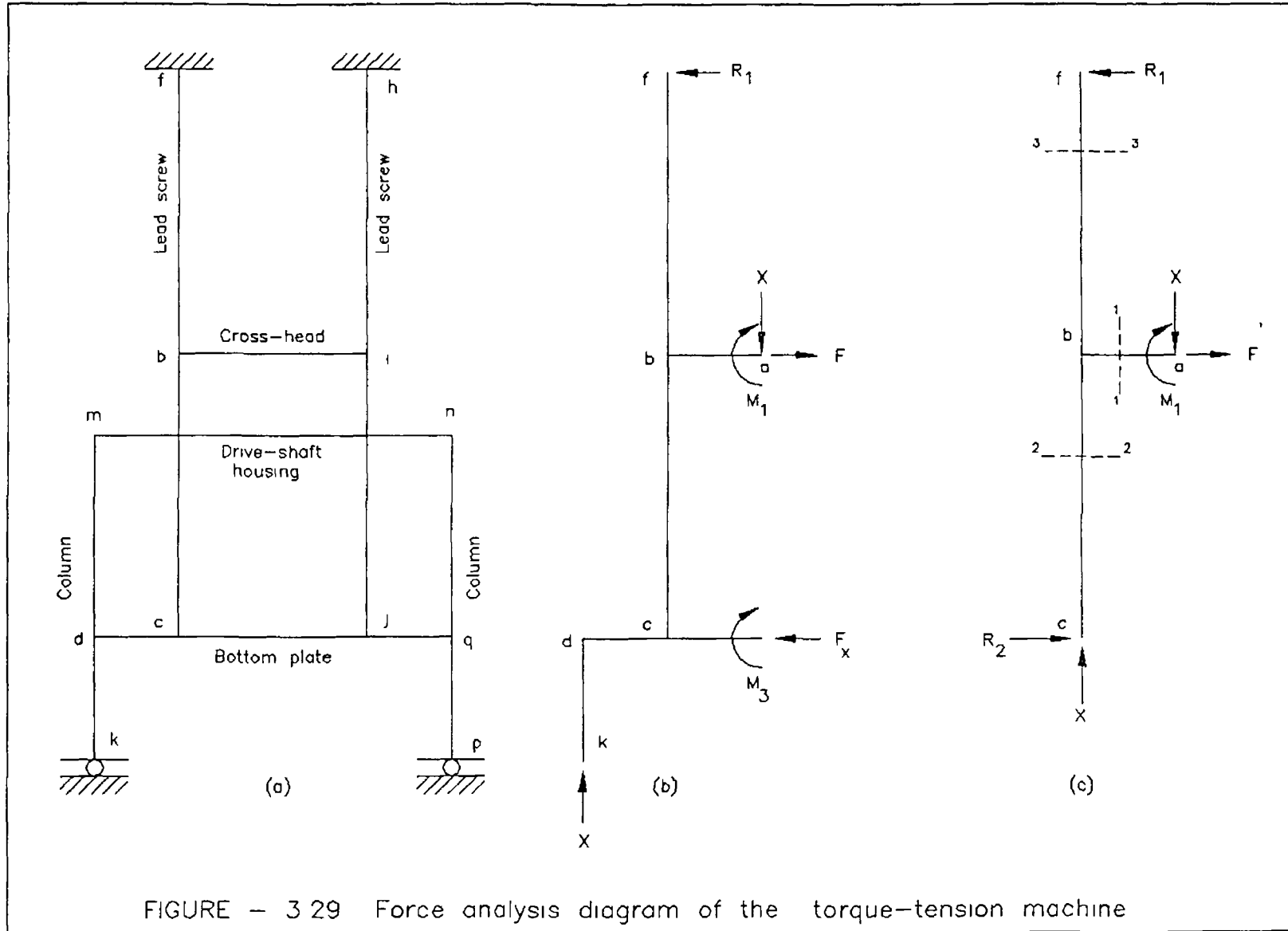


FIGURE - 3 29 Force analysis diagram of the torque-tension machine

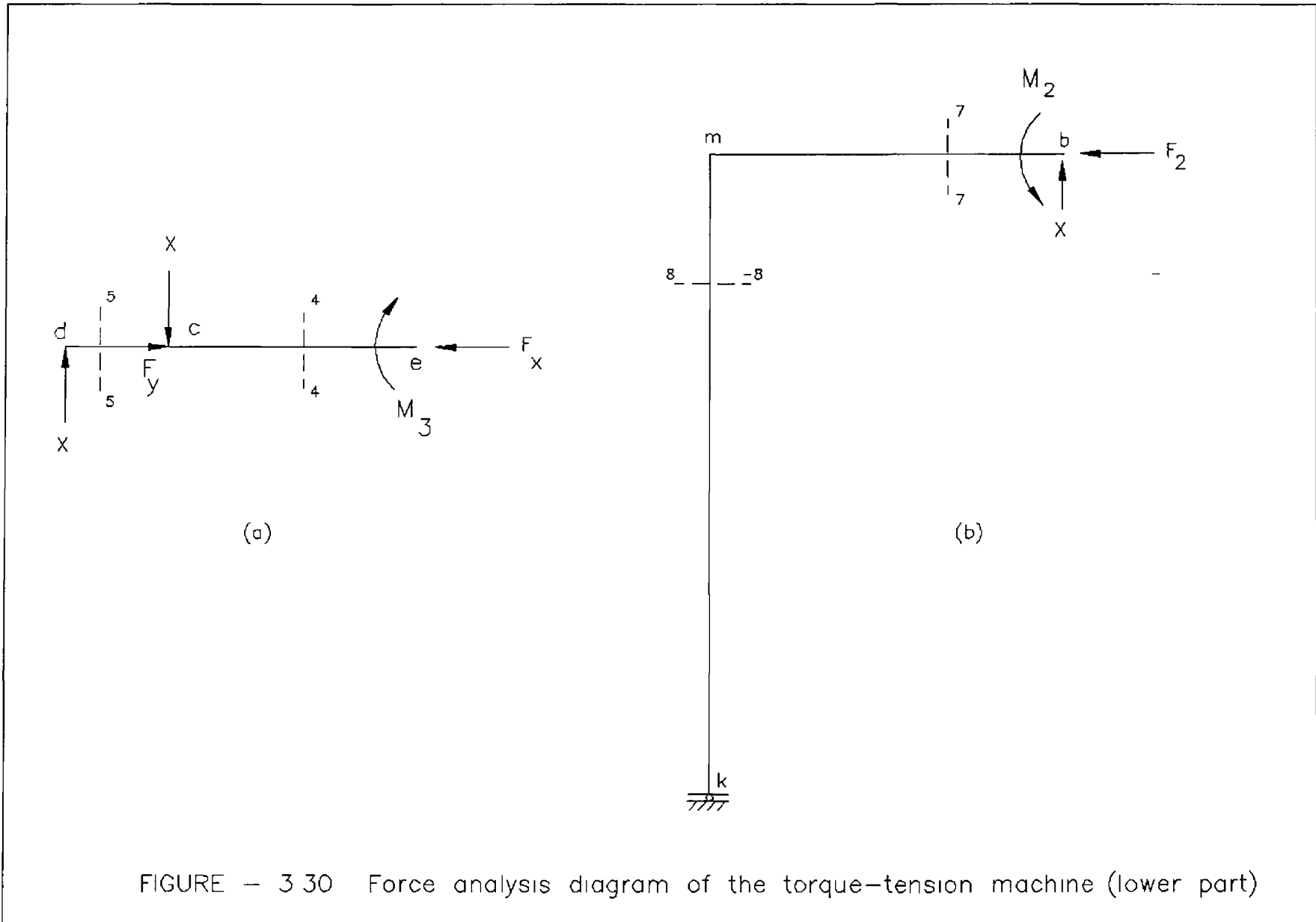


FIGURE — 3 30 Force analysis diagram of the torque-tension machine (lower part)

Preloading unit

Top plate

Cross-head

Drive shaft housing

Bottom plate

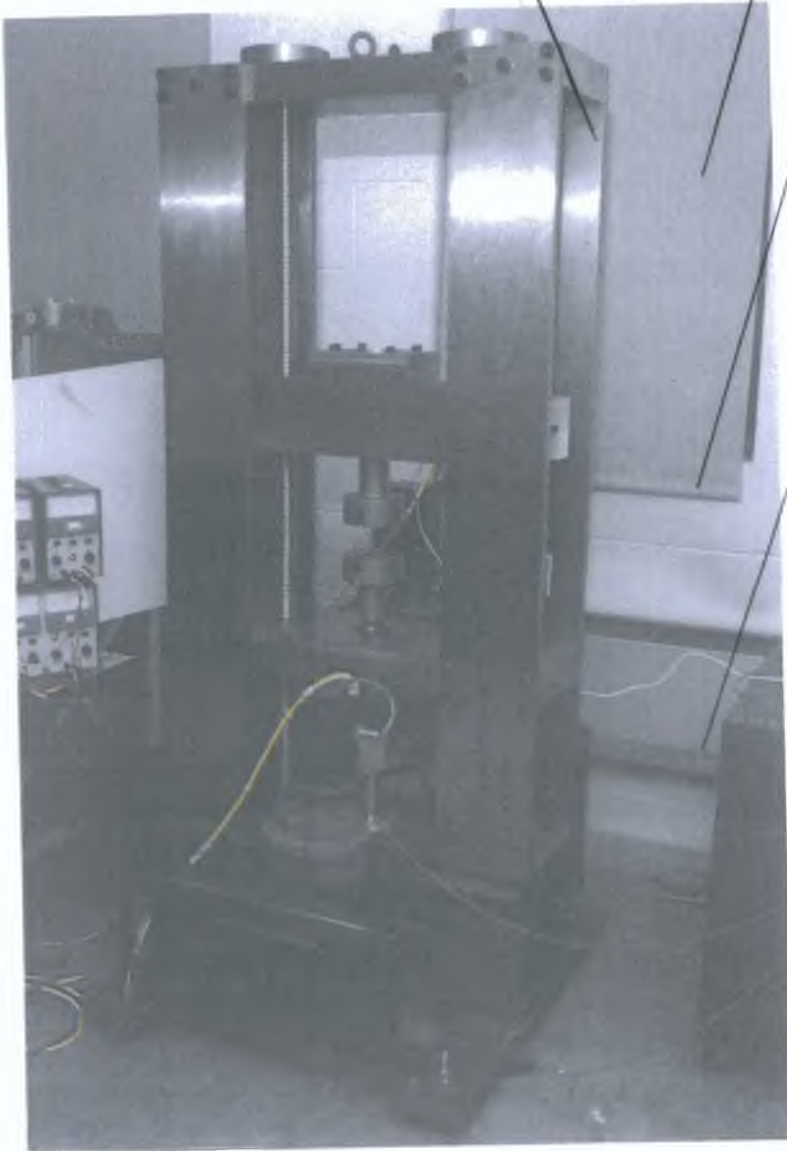


Plate 3.1 Details of the torque-tension machine

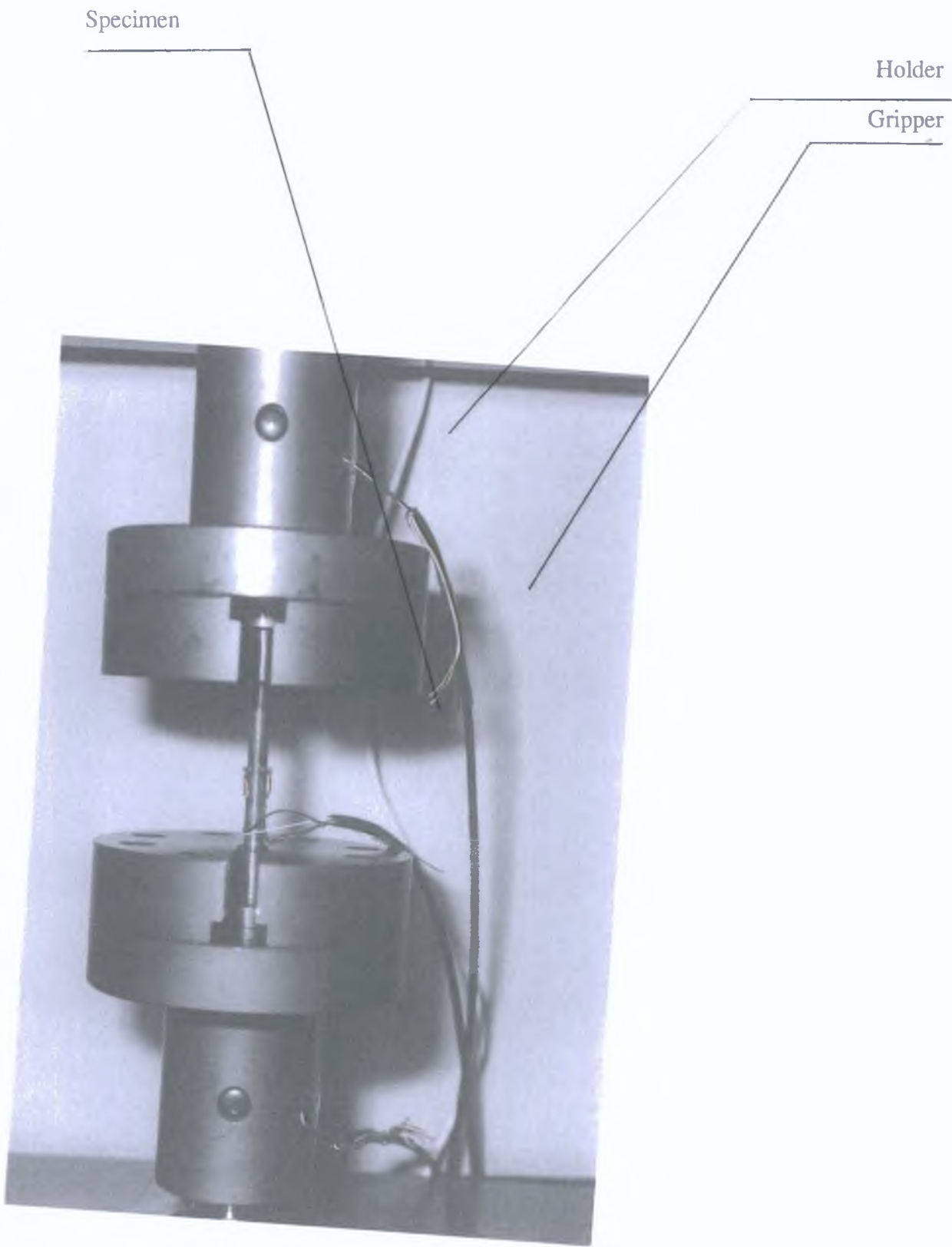


Plate 3.2 Position of the specimen in the gripper

Torque-tension shaft

Torsion shaft

Square drive

Torque load cell

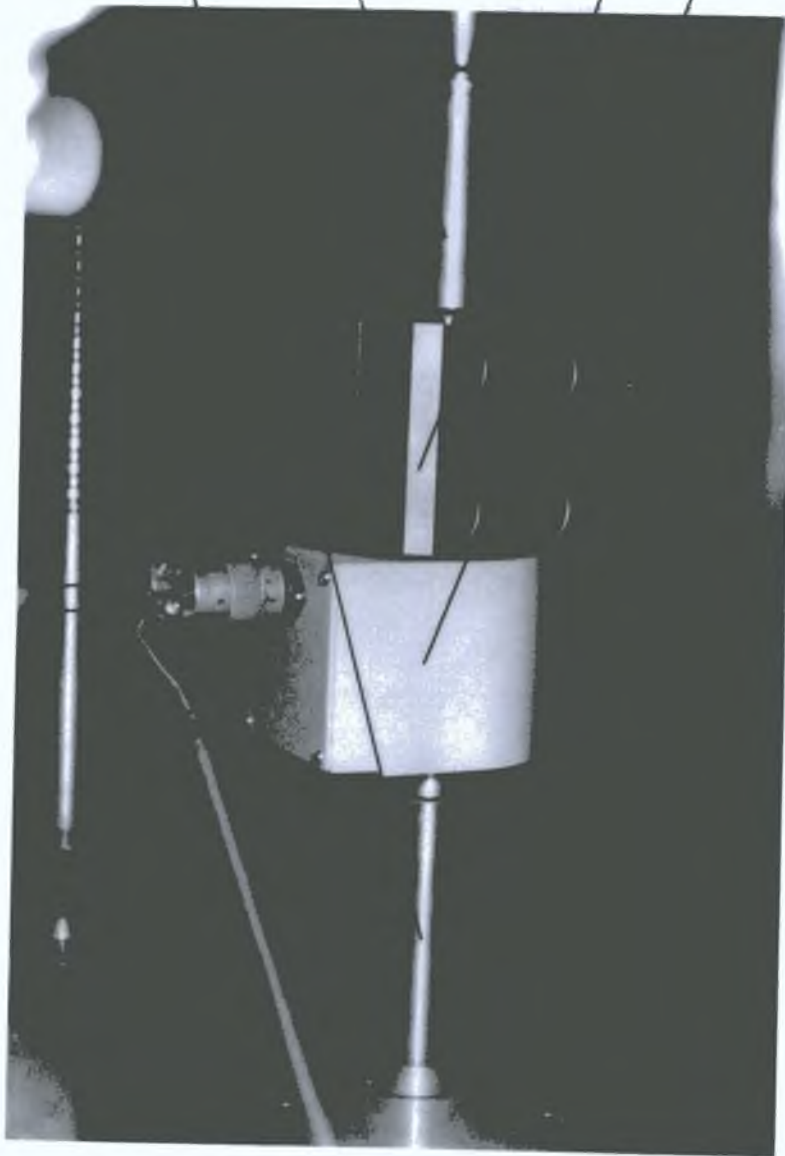


Plate 3.3 Position of the torque load cell

Controller-2

Controller-1

Power supply unit

Control panel

External power supply units

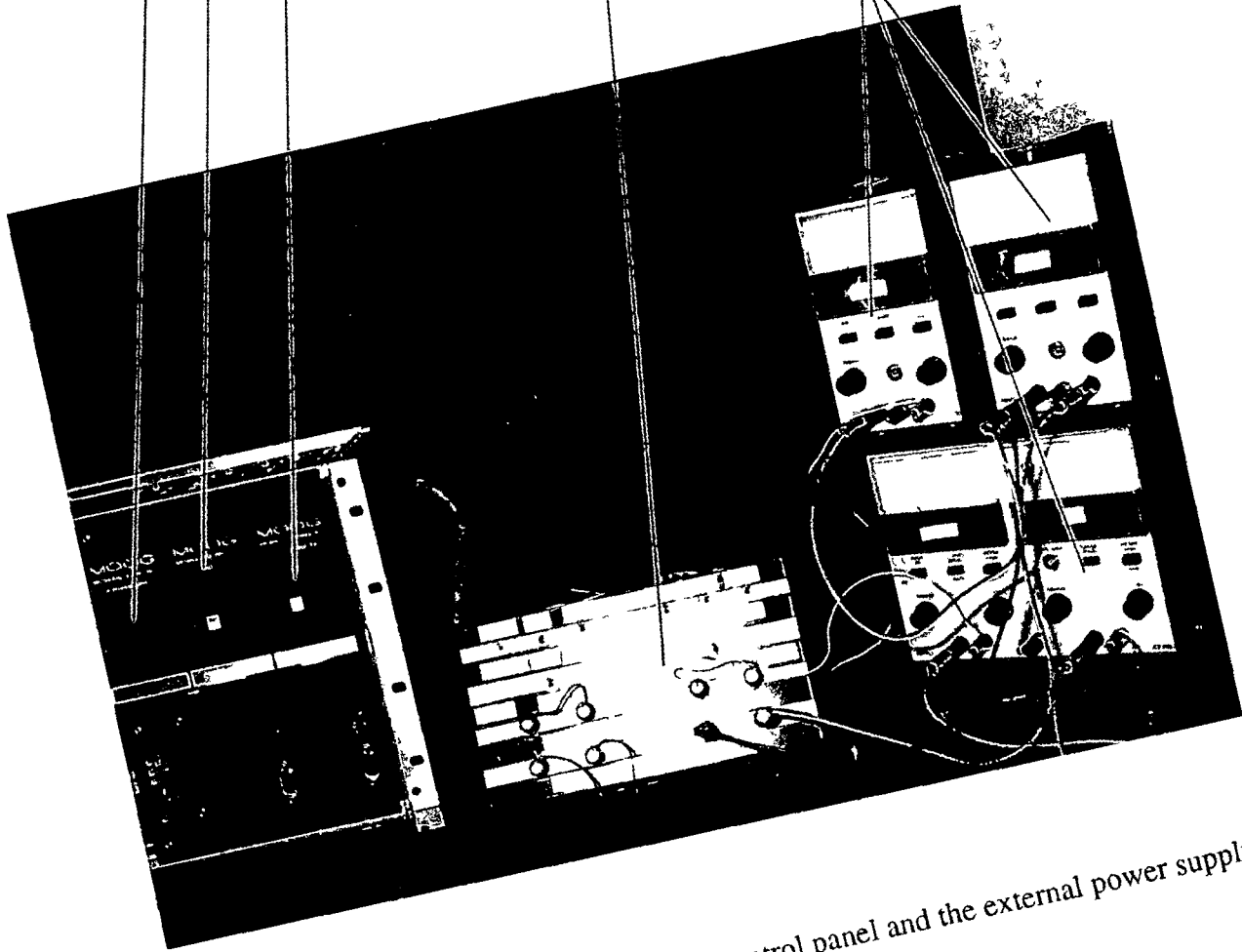


Plate 3 4 Photograph of the controllers, control panel and the external power supply units

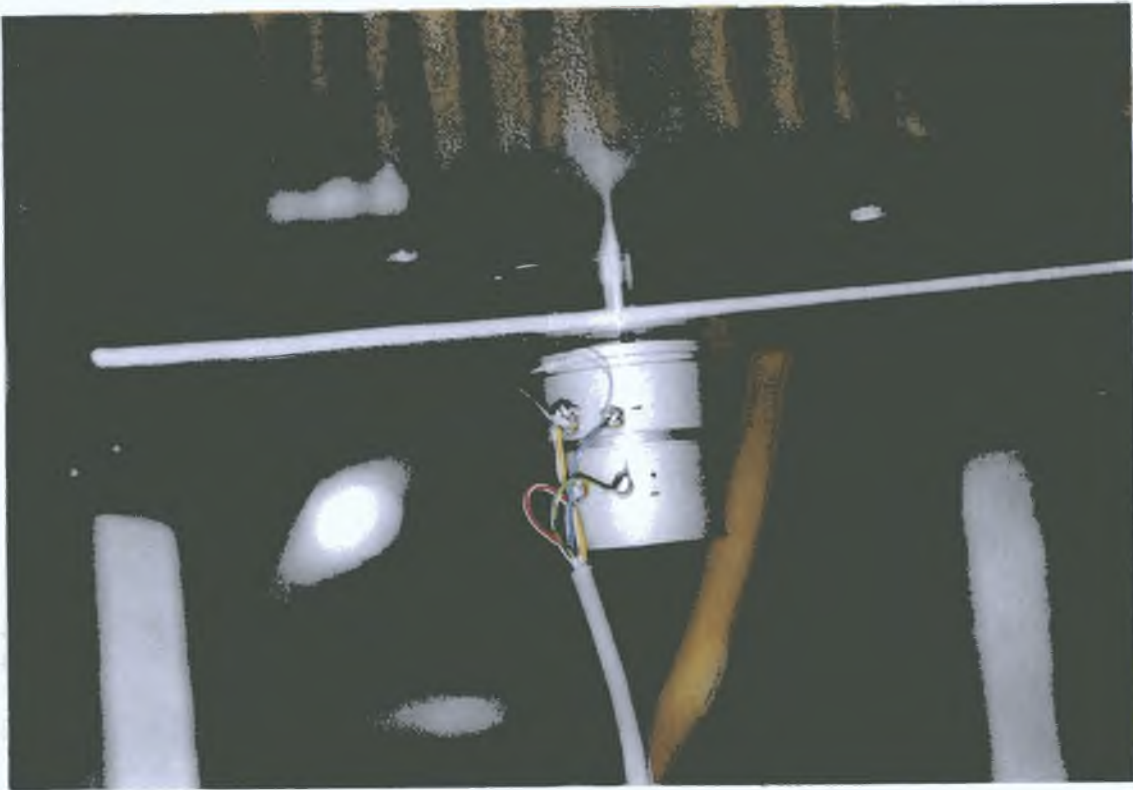


Plate 3.5 Position of the angle measuring transducer

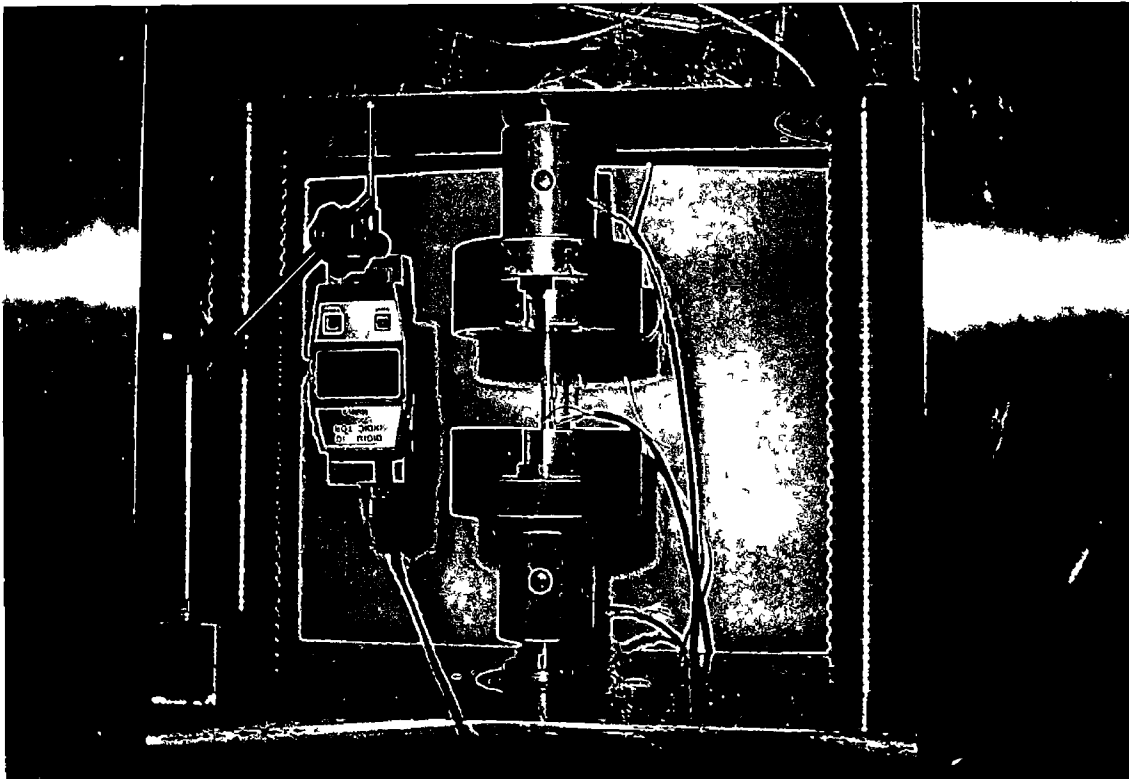


Plate 3 6 Position of the L V D T

RDP transducer indicator
for the torque load cell

RDP transducer indicator
for the axial load cell

Chart recorder

RDP transducer indicator
for the angle measuring
transducer

x-y recorder

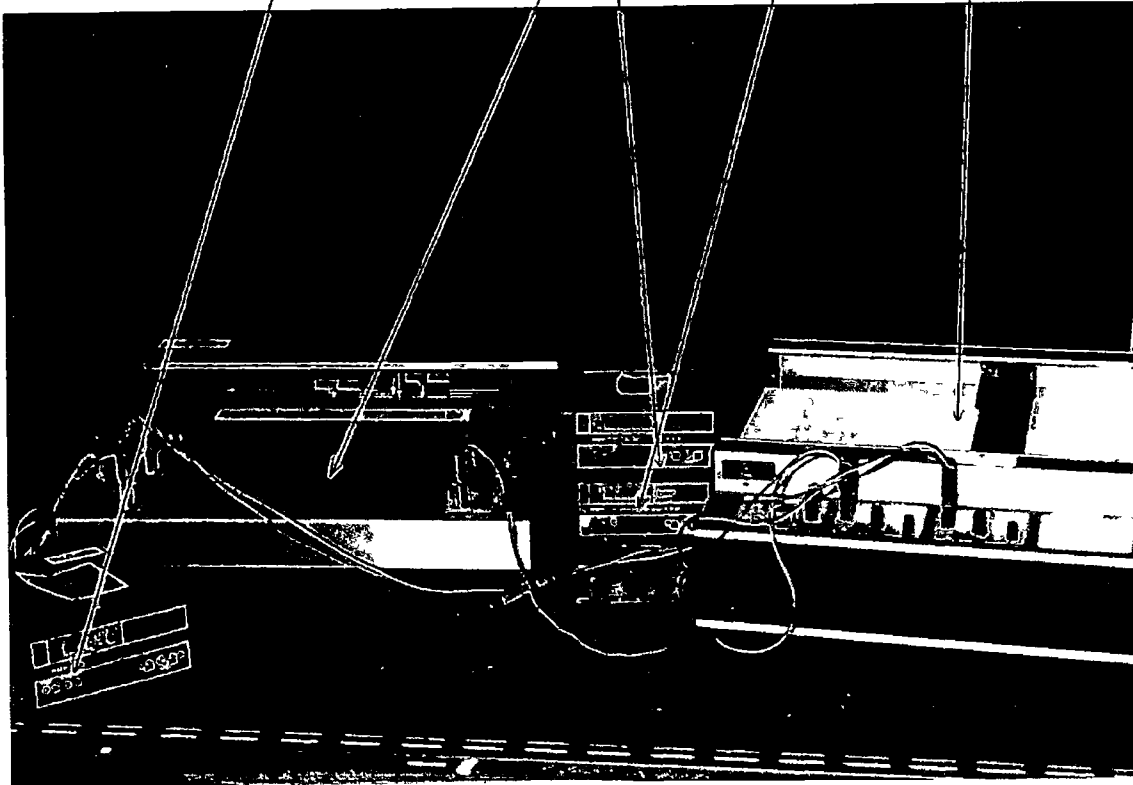


Plate 3 7 Photograph of the data logging during the test programme

CHAPTER 4

THEORETICAL INVESTIGATION

4.1 INTRODUCTION

This chapter contains the analytical formulation of two different theoretical models which are used to predict the variation of different quantities obtained during the biaxial loading programme, particularly when the solid rod is subjected to torsion followed by tension, keeping the angle of twist constant, and tension followed by torsion, keeping the axial displacement constant. To this end, and to get a better understanding of the behaviour of a rod under combined torque-tension loadings, a detailed description regarding the elasto-plastic stress-strain relations and yield criteria of material are given in appendix E. However, before outlining the above mentioned two theoretical models, a brief review of previous theoretical works under the combined torque-tension is given below.

4.2 REVIEW OF PREVIOUS THEORETICAL WORKS

A very few numbers of theoretical works regarding the biaxial (i.e., torque-tension) loading in the elasto-plastic region were conducted. Prager and Hodge [17] have first developed analytical expressions for the stress distributions and deformations of solid circular bars carrying combined torque and tension in the elasto-plastic range. Here they considered two different loading paths. In the first case the bar was subjected to an initial torque, equal to yield torque, and then to a gradually increasing axial strain, keeping the corresponding angle of twist constant. In the second case the bar was subjected to an initial load, equal to yield load, and then to an increasing shear strain, keeping the corresponding axial displacement constant. They restricted their analysis to a material with Poisson's ratio ν equal to $\frac{1}{2}$.

Gaydon [19] has developed more generalised analytical expressions for similar type of biaxial loadings of an elastic-perfectly plastic material. He examined a variety of different loading paths under combined torque and tension. Besides the above mentioned two loading paths (as considered by Prager), other paths where the ratios of load to torque and the relative rate of extension to rate of twist are constant were also considered by Gaydon. In his analytical expressions he kept provision so that different level of initial torque or axial load can be applied to the bar within the elasto-plastic range. Brooks *et al* [19-20] examined analytically and numerically the behaviour of a circular bar subjected to combined axial load and torque in the elasto-plastic range. Solid circular bars of both elastic-perfectly plastic and strain-hardening materials were used in their works. Elastic compressibility was taken into consideration. However, in the following sections the analytical models developed by Gaydon and Brooks *et al* are only discussed, as Gaydon's work is the extension of Prager's work.

4.3 GAYDON'S THEORETICAL ANALYSIS

Gaydon [18] has developed a number of theoretical models regarding the combined effects of torsion and tension in a solid circular cylinder for elastic-perfectly plastic material. The Reuss and von Mises equations have been used throughout the analysis. If a solid cylindrical bar is subjected to combined torque and tension, within the elastic limit, the longitudinal stress σ is constant over the cross section, and the shear stress τ is directly proportional to the radial distance r from the axis. It follows that yielding first occurs at $r = a$ when the stresses satisfy the von Mises yield criterion

$$\sigma^2 + 3\tau^2 = Y^2 \quad (4.1)$$

When the loading is continued into the plastic range, so that the radius of the elastic/plastic boundary is c , the stresses in the elastic region for an incompressible material, i.e., $\nu = 1/2$, are

$$\sigma = 3G\varepsilon \quad \tau = \frac{Gr\phi}{\ell} \quad 0 \leq r \leq c \quad (4.2)$$

In the plastic region ($c \leq r \leq a$), the Prandtl-Reuss stress-strain equations for cylindrical coordinates are (from Eqs E 20 and E 21)

$$d\epsilon = \frac{d\ell}{\ell} = \frac{d\sigma}{3G} + \frac{2}{3}\sigma d\lambda \quad (4.3)$$

$$d\gamma = \frac{rd\phi}{2\ell} = \frac{d\tau}{2G} + \tau d\lambda \quad (4.4)$$

4.3.1 TWIST HELD CONSTANT-INCREASING AXIAL LOAD

Suppose that a cylindrical bar of radius a is first twisted elastically and then extended into the elastic/plastic range by an increasing axial load. The angle of twist of the bar is held constant at a constant value θ_0 per unit length during the extension. Yielding begins at the outer radius when the longitudinal strain is ϵ_0 , the corresponding axial stress being $3G\epsilon_0$ for an incompressible material. Since the shear stress is $Ga\theta_0$ at $r = a$, the relationship between θ_0 and ϵ_0 is

$$a^2\theta_0^2 + 3\epsilon_0^2 = \frac{Y^2}{3G^2} \quad (4.5)$$

in view of the yield criterion (4.1). Subsequently, when the bar is plastic to a radius c , the stresses in the elastic zone corresponding to an axial strain ϵ are

$$\sigma = 3G\epsilon \quad \tau = Gr\theta_0 \quad 0 \leq r \leq c$$

Since the element at $r = c$ must be at the point of yielding, the radius to the elastic/plastic boundary is given by

$$c^2\theta_0^2 + 3\epsilon^2 = \frac{Y^2}{3G^2}$$

In the plastic region, the stresses must satisfy the yield criterion and the stress-strain equations 4.3 and 4.4. For the present case $d\gamma = 0$, as the angle of twist is kept constant. Elimination of $d\lambda$ using Eqs 4.3 and 4.4 and differentiation of Eq 4.1 and then substitution for $d\tau/\tau$ give

$$3Gd\epsilon = \frac{Y^2 d\sigma}{Y^2 - \sigma^2}$$

which is readily integrated to

$$\frac{3G}{Y} \varepsilon = \tanh^{-1}\left(\frac{\sigma}{Y}\right) + \text{const} \quad (c \leq r \leq a)$$

The constant of integration must be determined from the condition that

$$\sigma = 3G\varepsilon = \sqrt{Y^2 - 3G^2 r^2 \theta_0^2}$$

when an element at radius r first becomes plastic. Hence the tensile stress in the plastic region ($c \leq r \leq a$) is given by

$$\frac{\sigma}{Y} = \tanh\left(\frac{3G}{Y} \varepsilon - \sqrt{1 - \frac{3G^2}{Y^2} r^2 \theta_0^2} + \tanh^{-1} \sqrt{1 - \frac{3G^2}{Y^2} r^2 \theta_0^2}\right) \quad (4.6)$$

The shear stress in the plastic region follows from the above equation and from yield criterion 4.1, i.e., after determining the values of the tensile stresses by using the above equation, the corresponding shear stresses can be obtained from

$$\frac{\sqrt{3}\tau}{Y} = \sqrt{1 - \left(\frac{\sigma}{Y}\right)^2} \quad (4.7)$$

The variations of load and torque with extension can be calculated numerically by integrating Eqs 4.6 and 4.7, which will be discussed in detail in section 4.4.3. If the bar is initially twisted to an extent that makes it just plastic at $r = a$, then $Ga\theta_0 = Y/\sqrt{3}$ and $\varepsilon_0 = 0$. Substituting in 4.6, the stress distribution in the plastic region is obtained as

$$\frac{\sigma}{Y} = \tanh\left(\frac{3G}{Y} \varepsilon - \sqrt{1 - \frac{r^2}{a^2}} + \tanh^{-1} \sqrt{1 - \frac{r^2}{a^2}}\right) \quad (4.6a)$$

The bar becomes completely plastic when $\varepsilon = Y/3G$, giving $\sigma/Y = \tanh 1 \approx 0.762$ at $r = a$. If the extension is continued in the fully plastic range, Eq 4.6a holds over the entire cross-section of the bar. The stresses σ and τ at the boundary $r = a$ approach their asymptotic values Y and zero respectively as the strain increased. The approach is so rapid that σ is within 0.5 percent of Y when ε is only equal to Y/G . Plot of equation 4.6(a) in terms of σ/Y and $3G\varepsilon/Y$, for initial $Ga\theta_0 = Y/\sqrt{3}$ at $r = a$, is shown in figure D.1 of appendix D.

4.3.2 EXTENSION HELD CONSTANT-INCREASING TORQUE

Now suppose the bar is first extended to produce an axial strain ϵ_0 elastically, and then twisted by gradually increasing torque while the extension is held constant. The bar begins to yield at the outer radius again when the angle of twist per unit length is θ_0 , given by Eq 4.5. When the specific angle of twist per unit length θ is large enough to render the bar plastic to a radius c , the stresses in the elastic region are

$$\sigma = 3G\epsilon_0 \quad \tau = Gr\theta \quad 0 \leq r \leq c$$

Since the material at $r = c$ is at the point of yielding,

$$c^2\theta^2 + 3\epsilon_0^2 = \frac{Y^2}{3G^2}$$

For the present case, $d\epsilon = \theta$ and, setting $d\phi = l d\theta$ in the Prandtl-Reuss equations 4.3, 4.4 and eliminating $d\lambda$, it gives

$$Gr d\theta = \frac{Y^2 d\tau}{Y^2 - 3\tau^2}$$

in view of Eq 4.1. The integration of the above equation gives

$$\frac{\sqrt{3}G}{Y} r\theta = \tanh^{-1}\left(\frac{\sqrt{3}\tau}{Y}\right) + \text{const} \quad (c \leq r \leq a)$$

When an element first becomes plastic, its tensile stress is $\sigma_0 = 3G\epsilon_0$, the corresponding shear stress is given by

$$\sqrt{3}\tau = \sqrt{Y^2 - \sigma_0^2} = \sqrt{3}Gr\theta$$

The constant of integration follows from this initial condition, and the shear stress in the plastic region ($c \leq r \leq a$)

$$\frac{\sqrt{3}\tau}{Y} = \tanh\left(\frac{\sqrt{3}G}{Y} r\theta - \sqrt{1 - \frac{\sigma_0^2}{Y^2}} + \tanh^{-1}\sqrt{1 - \frac{\sigma_0^2}{Y^2}}\right) \quad (4.8)$$

The tensile stress in the plastic region then can be calculated by knowing the values of $\sqrt{3}\tau/Y$ from Eq 4.8 and from the yield criteria 4.1, i.e.,

$$\frac{\sigma}{Y} = \sqrt{1 - \left(\frac{\sqrt{3}\tau}{Y}\right)^2} \quad (4.9)$$

If the bar is initially extended just to the yield point before the torque is applied, $\sigma_0 = Y$ and $\theta_0 = 0$, the equations 4.8 and 4.9 reduce to

$$\frac{\sqrt{3}\tau}{Y} = \tanh\left(\frac{\sqrt{3}G}{Y} r\theta\right) \quad (4.8a)$$

$$\frac{\sigma}{Y} = \operatorname{sech}\left(\frac{\sqrt{3}G}{Y} r\theta\right) \quad (4.9a)$$

These expressions hold throughout the cross-section of the bar, which is now completely plastic. When $a\theta$ is equal to $\sqrt{3}Y/G$, the value of $\sqrt{3}\tau$ at $r = a$ is already within 0.5 percent of Y . The torque T and the axial load F are given by

$$\frac{\sqrt{3}T}{\pi a^3 Y} = 2 \int_0^1 \xi^2 \tanh\left(\frac{\sqrt{3}G}{Y} \xi a \theta\right) d\xi \quad (4.10a)$$

$$\frac{F}{\pi a^2 Y} = 2 \int_0^1 \xi \operatorname{sech}\left(\frac{\sqrt{3}G}{Y} \xi a \theta\right) d\xi \quad (4.10b)$$

where $\xi = r/a$

4.3.3 NUMERICAL SOLUTION OF GAYDON'S MODELS

To calculate the variations of load and torque numerically, for the above mentioned two cases, the following procedure was adopted

Angle Of Twist Constant - Axial Load Increases

To obtain the numerical values of torque with the axial strain, for different levels of initial torque, Eq 4.6 can be modified as

$$\frac{\sigma}{Y} = \tanh\left(\frac{\varepsilon}{\varepsilon_y} - \sqrt{1 - P^2 \xi^2} + \tanh^{-1} \sqrt{1 - P^2 \xi^2}\right) \quad (4.11)$$

where ε_y is the yield strain in tension, $P = \tau / \tau_y$ and $\xi = r/a$. The value of the shear stress τ is to be calculated at the outer surface of the cylinder where τ_y is the yield shear stress. Thus

different levels of initial torque, and hence different levels of initial shear stresses within the elastic and upto the yield point, can be set into the above equation by setting various values of P . Then to calculate the numerical values of σ/Y for a specific value of $\underline{\epsilon}$ ($= \epsilon/\epsilon_y$), Eq 4.11 is to be integrated over the entire cross-section of the bar. However, during the present investigation as variations of torque with the axial strains are to be plotted, the values of shear stresses can be calculated from Eq 4.7 by knowing different values of σ/Y from Eq 4.11. Thus numerical values of torque can be calculated by integrating Eq 4.7

$$\frac{\sqrt{3}T}{2\pi a^3 Y} = \int_0^1 \xi^2 \sqrt{1 - \left(\frac{\sigma}{Y}\right)^2} d\xi \quad (4.12)$$

The above equation can also be rewritten as

$$\frac{T}{T_y} = 4 \int_0^1 \xi^2 \sqrt{1 - \left(\frac{\sigma}{Y}\right)^2} d\xi \quad (4.13)$$

The above equation was numerically calculated using Simpson's rule for the increment of $\Delta\xi = 0.1$. However if the bar becomes plastic only upto η , where $\eta = c/a$, then the integration is to be performed over $\xi = \eta$ to 1.0 and, torque in the elastic core (i.e., for the range $\xi = 0$ to η) can be found from the elastic theory. Then the total torque becomes

$$\frac{T}{T_y} = \left(\frac{\tau_e}{\tau_y}\right) \eta^3 + 4 \int_{\xi=\eta}^{1.0} \xi^2 \left(\frac{\tau_p}{\tau_y}\right) d\xi \quad (4.14)$$

where τ_e is the maximum elastic shear stress at the layer $\xi = \eta$, which is a constant, and τ_p is the shear stress within the plastic region which varies along ξ . During the determination of the numerical values of torque, it was assumed, according to Sved and Brooks [19,20], that once the yielding starts at the outer fibre of the bar due to combined loading, the elastic-plastic boundary η moves inwards in such a way that $\Delta\underline{\epsilon} = -\Delta\eta$. However, for any values of initial shear stresses, and hence shear strains, within the elastic and upto the yield point, the values of corresponding axial strains for which yielding begins can be found from the yield criteria 4, which can be rewritten as

$$\left(\frac{\gamma}{\gamma_y}\right)^2 + \left(\frac{\epsilon}{\epsilon_y}\right)^2 = 1 \quad (4.1a)$$

When $\epsilon/\epsilon_y = 1.0$, Eq 4.13 is valid over the entire cross-section of the bar. Theoretical plots of Eq 4.14 for four different values of P , such as P equal to 1.0, 0.75, 0.5 and 0.25, are depicted in figure 4.1. A typical example of calculating the numerical value of torque with axial strain is given in appendix D.

Axial Displacement Constant- Torque Increases

To calculate the numerical values of the axial load with shear strain, for different levels of initial load, Eq 4.8 is rewritten as

$$\frac{\tau}{\tau_y} = \tanh\left(\frac{\gamma}{\gamma_y}\xi - \sqrt{1-Q^2} + \tanh^{-1}\sqrt{1-Q^2}\right) \quad (4.15)$$

where γ_y is the yield shear strain and $Q = \sigma/Y$. Thus different levels of initial load can be set into the above equation just changing the values of Q . However, during the present investigation as the variations of the axial load with the shear strain is required to plot, the values of the corresponding axial stresses can be found from Eq 4.9 after knowing the values of the shear stresses from Eq 4.15. Then numerical values of the axial load can be obtained integrating Eq 4.9

$$\frac{F}{F_y} = 2 \int_0^1 \xi \sqrt{1 - \left(\frac{\tau}{\tau_y}\right)^2} d\xi \quad (4.16)$$

Integration of the above equation was performed using Simpson's rule for the increment of $\Delta\xi = 0.1$. However, when the bar becomes plastic only upto η , then to obtain the axial load within the plastic region the integration is to be performed over $\xi = \eta$ to 1.0. Whereas axial load within the elastic core (i.e., for $\xi = 0$ to η) can be obtained from the elastic theory. Then total load can be calculated as

$$\frac{F}{F_y} = \left(\frac{\sigma_e}{Y}\right)\eta^2 + 2 \int_{\xi=\eta}^{1.0} \xi \left(\frac{\sigma_p}{Y}\right) d\xi \quad (4.17)$$

where σ_e is the elastic axial stress for the cross-section whose radius is η , which is a constant, and, σ_p is the axial stress within the plastic region which varies along ξ . However to calculate the numerical values of load, it was assumed, according to Sved and Brooks [19-20], that once the yielding starts at the outer fibre of the bar due to combined loading, the elastic-plastic boundary η moves inwards in such a way that $\Delta\gamma = -\Delta\eta$. For different levels of initial load, the values of the corresponding shear strains when yielding starts can be obtained from Eq 4.1a. Theoretical plots of Eq 4.17 for four different values of Q , $Q = 1.0, 0.75, 0.5$ and 0.25 , are shown in figure 4.2.

4.4 BROOKS' THEORETICAL ANALYSIS

Brooks [20] has developed analytical expressions to examine the behaviour of a circular cylinder subjected to combined axial load and torque in the elasto-plastic range. Ramberg-Osgood curves were used to describe the material behaviour, and the analysis was based on the Prandtl-Reuss incremental stress-strain laws and the von Mises yield criterion. He obtained numerical results for both proportional and non-proportional loading combinations. Elastic compressibility was taken into consideration which was shown negligible for all practical purposes.

Stress-Strain Relations In Uniaxial Tension

The uniaxial tensile stress σ and the corresponding strain ϵ for monotonically increasing loading can be accurately represented by Ramberg-Osgood empirical law

$$\epsilon = \frac{\sigma}{E} + \frac{3\sigma_1}{7E} \left(\frac{\sigma}{\sigma_1}\right)^n \quad (4.18)$$

in which σ_1 is the stress at a secant modulus of $0.7E$, and n is a strain-hardening parameter depending upon the material properties. From Eq 4.18 the elastic and plastic components of the axial strain are, respectively,

$$\varepsilon^e = \sigma / E \quad (4.18a)$$

$$\varepsilon^p = \frac{3\sigma_1}{7E} \left(\frac{\sigma}{\sigma_1} \right)^n \quad (4.18b)$$

Equilibrium And Compatibility Conditions

A cylindrical co-ordinate system (r, θ, z) is taken with the z axis coincident with the axis of the bar. The respective displacements are u, v and w . Since the bar is symmetrical about its longitudinal axis, the displacements, strains and stresses must be independent of variable θ . If it is further assumed that the section of the bar is uniform in the axial direction, and that cylindrical surface of the bar is free from forces, then the stress components are independent of z , while the tangential and axial displacements are linear functions of z . It follows that the strain components are

$$\begin{aligned} \varepsilon_r &= \frac{\partial u}{\partial r} & \varepsilon_\theta &= \frac{u}{r} & \varepsilon_z &= \frac{\partial w}{\partial z} \\ \gamma_{r\theta} &= \frac{\partial v}{\partial r} - \frac{v}{r} & \gamma_{\theta z} &= \frac{\partial v}{\partial z} & \gamma_{zr} &= \frac{\partial w}{\partial r} \end{aligned} \quad (4.19)$$

If the derivatives which vanish are omitted, the equilibrium equations reduce to

$$\frac{\partial \sigma_r}{\partial r} + \frac{1}{r}(\sigma_r - \sigma_\theta) = 0 \quad (4.19a)$$

$$\frac{\partial \tau_{r\theta}}{\partial r} + \frac{2}{r}\tau_{r\theta} = 0$$

$$\frac{\partial \tau_{zr}}{\partial r} + \frac{1}{r}\tau_{zr} = 0$$

Integration of the last two equations produces

$$\tau_{r\theta} = \frac{c_1}{r^2} \quad \tau_{zr} = \frac{c_2}{r}$$

where c_1 and c_2 are integration constants, both of which must be zero, since $\tau_{r\theta}$ and τ_{zr} are both zero on the outer boundary $\tau_{r\theta} = 0$ implies $\gamma_{r\theta} = 0$ so that the appropriate expression of Eq 4 19 gives

$$\frac{\partial v}{\partial r} - \frac{v}{r} = 0$$

which may be integrated in the following form by noting that v is a linear function of z ,

$$v = rzv(\rho) \quad (4 20)$$

In the above equation ρ is some parameter such as time characterising the state of plastic deformation Furthermore, since $\tau_{zr} = 0$ implies $\gamma_{zr} = 0$, it follows from the last expression in Eq 4 19 that w is independent of r The stress and strain deviators are defined as

$$\begin{aligned} \sigma_r &= \sigma_r - \sigma_m & \sigma_\theta &= \sigma_\theta - \sigma_m & \sigma_z &= \sigma_z - \sigma_m & \tau &= \tau_{\theta z} \\ e_r &= \varepsilon_r - \varepsilon_m & e_\theta &= \varepsilon_\theta - \varepsilon_m & e_z &= \varepsilon_z - \varepsilon_m & \gamma &= \gamma_{\theta z} / 2 \end{aligned} \quad (4 21)$$

in which

$$\sigma_m = \frac{1}{3}(\sigma_r + \sigma_\theta + \sigma_z) \quad \varepsilon_m = \frac{1}{3}(\varepsilon_r + \varepsilon_\theta + \varepsilon_z) \quad (4 22)$$

From equations 4 19, 4 21 and 4 22 it may be shown that

$$e_r = \frac{1}{3} \left(2 \frac{\partial u}{\partial r} - \frac{u}{r} - \frac{\partial w}{\partial z} \right) \quad e_\theta = \frac{1}{3} \left(2 \frac{u}{r} - \frac{\partial u}{\partial r} - \frac{\partial w}{\partial z} \right) \quad (4 23)$$

If these equations are differentiated with respect to r , the compatibility equation obtained by eliminating u and by noting that $\partial w / \partial r = 0$ is

$$\frac{\partial e_r}{\partial r} + 2 \frac{\partial e_\theta}{\partial r} = \frac{e_r - e_\theta}{r} \quad (4 24)$$

The only equilibrium equation remaining to be satisfied is Eq 4 19a, which, with the aid of Eqs 4 21, may be written in the form

$$\frac{\partial \sigma_r}{\partial r} + \frac{\partial \sigma_m}{\partial r} + \frac{1}{r}(\sigma_r - \sigma_\theta) = 0 \quad (4 25)$$

Stress-Strain Relationships

Here the Prandtl-Reuss incremental stress-strain laws are used in the plastic region and yielding is assumed to be in accordance with the von Mises criterion. For a material that strain hardens isotropically, these equations, which have already been mentioned earlier, may be summarised in tensor notation as

$$\frac{\partial e_{ij}}{\partial \rho} = \frac{1}{2G} \frac{\partial \sigma_{ij}}{\partial \rho} + \frac{3\sigma_{ij}}{2\bar{\sigma}H'} \frac{\partial \bar{\sigma}}{\partial \rho} \quad (4.26)$$

$$\epsilon_m = \frac{1-2\nu}{E} \sigma_m \quad (4.26a)$$

In these expressions, H' is equal to the slope of the equivalent stress $\bar{\sigma}$ - equivalent plastic strain $\bar{\epsilon}^P$ curve, where the equivalent stress $\bar{\sigma}$ is defined as

$$\bar{\sigma} = \sqrt{\frac{3}{2}(\sigma'_{ij}\sigma'_{ij})} \quad (4.27)$$

The equivalent plastic strain $\bar{\epsilon}^P$ is
$$\bar{\epsilon}^P = \int d\bar{\epsilon}^P = \int \frac{\partial \bar{\epsilon}^P}{\partial \rho} d\rho \quad (4.28)$$

For the uniaxial tension test, differentiation of equation 4.18b produces

$$\frac{d\epsilon^P}{d\sigma} = \frac{3n}{7E} \left(\frac{\sigma}{\sigma_1} \right)^{n-1}$$

and since $\bar{\sigma} = \sigma$ and $\bar{\epsilon}^P = \epsilon^P$ in this case, it follows that

$$\frac{d\bar{\epsilon}^P}{d\bar{\sigma}} = \frac{1}{H'} = \frac{3n}{7E} \left(\frac{\bar{\sigma}}{\sigma_1} \right)^{n-1} \quad (4.29)$$

Dimensionless Stresses And Strains

To simplify the analysis the stresses are converted to dimensionless components as follows

$$\begin{aligned} \underline{\sigma}_r &= \sigma_r / \sqrt{3}k, & \underline{\sigma}_\theta &= \sigma_\theta / \sqrt{3}k, & \underline{\sigma}_z &= \sigma_z / \sqrt{3}k, & \underline{\sigma} &= \sigma / \sqrt{3}k, & \underline{\tau} &= \tau / k \\ \underline{\sigma}'_r &= \sigma'_r / \sqrt{3}k, & \underline{\sigma}'_\theta &= \sigma'_\theta / \sqrt{3}k, & \underline{\sigma}'_z &= \sigma'_z / \sqrt{3}k, & \underline{\sigma}_m &= \sigma_m / \sqrt{3}k, & \underline{\bar{\sigma}} &= \bar{\sigma} / \sqrt{3}k \end{aligned} \quad (4.30)$$

Similarly, modified strain components are

$$\begin{aligned}\underline{\varepsilon}_r &= E\varepsilon_r / \sqrt{3}k, \quad \underline{\varepsilon}_\theta = E\varepsilon_\theta / \sqrt{3}k, \quad \underline{\varepsilon}_z = E\varepsilon_z / \sqrt{3}k, \quad \underline{\varepsilon} = E\varepsilon / \sqrt{3}k, \quad \underline{\gamma} = G\gamma_{\theta z} / k \\ \underline{e}_r &= Ee_r / \sqrt{3}k, \quad \underline{e}_\theta = Ee_\theta / \sqrt{3}k, \quad \underline{e}_z = Ee_z / \sqrt{3}k, \quad \underline{\varepsilon}_m = E\varepsilon_m / \sqrt{3}k, \quad \underline{\varepsilon}^p = E\varepsilon^p / \sqrt{3}k\end{aligned}\quad (4.31)$$

Equation 4.18 then reduces to the form

$$\underline{\varepsilon} = \underline{\sigma} + \alpha \underline{\sigma}^n \quad (4.32)$$

in which

$$\alpha = \frac{3}{7} \left(\frac{\sqrt{3}k}{\sigma_1} \right)^{n-1} \quad (4.33)$$

If the equations represented by 4.26 and 4.26a are combined with equations 4.29 and 4.33, the results, written in non-dimensional form, are

$$\begin{aligned}\frac{1}{(1+\nu)} \frac{\partial \underline{e}_r}{\partial \rho} &= \frac{\partial \underline{\sigma}_r}{\partial \rho} + \frac{3\alpha n \underline{\sigma}_r \underline{\sigma}^{(n-2)}}{2(1+\nu)} \frac{\partial \underline{\sigma}}{\partial \rho} \\ \frac{1}{(1+\nu)} \frac{\partial \underline{e}_\theta}{\partial \rho} &= \frac{\partial \underline{\sigma}_\theta}{\partial \rho} + \frac{3\alpha n \underline{\sigma}_\theta \underline{\sigma}^{(n-2)}}{2(1+\nu)} \frac{\partial \underline{\sigma}}{\partial \rho} \\ \frac{1}{(1+\nu)} \frac{\partial \underline{e}_z}{\partial \rho} &= \frac{\partial \underline{\sigma}_z}{\partial \rho} + \frac{3\alpha n \underline{\sigma}_z \underline{\sigma}^{(n-2)}}{2(1+\nu)} \frac{\partial \underline{\sigma}}{\partial \rho} \\ \frac{\partial \underline{\gamma}}{\partial \rho} &= \frac{\partial \underline{\tau}}{\partial \rho} + \frac{3\alpha n \underline{\tau} \underline{\sigma}^{(n-2)}}{2(1+\nu)} \frac{\partial \underline{\sigma}}{\partial \rho} \\ \underline{\varepsilon}_m &= (1-2\nu) \underline{\sigma}_m\end{aligned}\quad (4.34)$$

As $(\underline{e}_r + \underline{e}_\theta + \underline{e}_z) = (\underline{\sigma}_r + \underline{\sigma}_\theta + \underline{\sigma}_z) = 0$

so elimination of $\underline{\sigma}_z$ by means of the above expression permits the equivalent stress given by equation 4.27 to be written in the dimensionless form

$$\underline{\sigma} = \sqrt{3(\underline{\sigma}_r^2 + \underline{\sigma}_\theta^2 + \underline{\sigma}_r \underline{\sigma}_\theta) + \underline{\tau}^2} \quad (4.35)$$

Equation 4.35 may be combined with the fourth expression in group 4.34 to give

$$\frac{3\alpha n \underline{\sigma}^{(n-2)}}{2(1+\nu)} \frac{\partial \underline{\sigma}}{\partial \rho} = A_0 \left[\frac{\partial \underline{\sigma}_r}{\partial \rho} (2\underline{\sigma}_r + \underline{\sigma}_\theta) + \frac{\partial \underline{\sigma}_\theta}{\partial \rho} (2\underline{\sigma}_\theta + \underline{\sigma}_r) \right] + B_0 \frac{\partial \underline{\gamma}}{\partial \rho} \quad (4.36)$$

where

$$A_0 = [9\alpha n \bar{\sigma}^{(n-2)}] / [4\bar{\sigma}(1+\nu) + 6\alpha n \bar{\sigma}^{(n-2)} \bar{\tau}^2]$$

and

$$B_0 = [6\alpha n \bar{\sigma}^{(n-2)} \bar{\tau}] / [4\bar{\sigma}(1+\nu) + 6\alpha n \bar{\sigma}^{(n-2)} \bar{\tau}^2] \quad (4.36a)$$

Substituting Eq 4.36 into the first two equations in group 4.34 produces, after some rearrangement,

$$\frac{\partial \underline{e}_r}{\partial \rho} - \frac{\partial \underline{\sigma}_r}{\partial \rho} (1+\nu)(1+2A_0 \underline{\sigma}_r^2 + A_0 \underline{\sigma}_r \underline{\sigma}_\theta) - \frac{\partial \underline{\sigma}_\theta}{\partial \rho} (1+\nu)(A_0 \underline{\sigma}_r^2 + 2A_0 \underline{\sigma}_r \underline{\sigma}_\theta) = B_0(1+\nu) \underline{\sigma}_r \frac{\partial \gamma}{\partial \rho} \quad (4.37)$$

$$\frac{\partial \underline{e}_\theta}{\partial \rho} - \frac{\partial \underline{\sigma}_\theta}{\partial \rho} (1+\nu)(1+2A_0 \underline{\sigma}_\theta^2 + A_0 \underline{\sigma}_r \underline{\sigma}_\theta) - \frac{\partial \underline{\sigma}_r}{\partial \rho} (1+\nu)(A_0 \underline{\sigma}_r^2 + 2A_0 \underline{\sigma}_r \underline{\sigma}_\theta) = B_0(1+\nu) \underline{\sigma}_\theta \frac{\partial \gamma}{\partial \rho} \quad (4.38)$$

The equations required for the solution of the stress and strain deviators are equations 4.37 and 4.38 together with the compatibility equation 4.24 and the equilibrium condition 4.25. By putting $\underline{r} = r/R$, the compatibility equation may be expressed in non-dimensional form as

$$\frac{\partial \underline{e}_r}{\partial \underline{r}} + 2 \frac{\partial \underline{e}_\theta}{\partial \underline{r}} = \frac{\underline{e}_r - \underline{e}_\theta}{\underline{r}} \quad (4.39)$$

Similarly, substitution of equations 4.22 in 4.26a, and combining the result with equations 4.25 and 4.30 produces the non-dimensional form of the equilibrium equation as follows

$$\frac{\partial \underline{\sigma}_r}{\partial \underline{r}} + \frac{1}{(1-2\nu)} \frac{\partial \underline{e}_r}{\partial \underline{r}} + \frac{1}{(1-2\nu)} \frac{\partial \underline{e}_\theta}{\partial \underline{r}} = - \frac{\underline{\sigma}_r - \underline{\sigma}_\theta}{\underline{r}} \quad (4.40)$$

Expressions 4.37, 4.38, 4.39 and 4.40 form a set of quasi-linear hyperbolic differential equations of the first order which may be integrated in the $(\underline{r}-\rho)$ plane along the characteristics $\underline{r} = \text{constant}$ and $\rho = \text{constant}$ from known boundary conditions. As a solution in closed form is not possible, the integration is to be performed numerically by re-writing the equations in finite difference form. Details regarding the numerical solutions of the above mentioned equations are given in Brooks [20].

After determining the stress and strain deviators at any point, the conventional stresses and strains can be evaluated. From equations 4.21, 4.22, 4.30 and 4.31

$$\underline{\epsilon}_m = \underline{\epsilon}_z - \underline{e}_z = \underline{\epsilon}_z + \underline{e}_r + \underline{e}_\theta \quad (4.41)$$

Equations 4 30, 4 41 and the last of group 4 34, together give

$$\underline{\sigma}_r = \underline{\sigma}_r + \underline{\sigma}_m = \underline{\sigma}'_r + \frac{1}{(1-2\nu)}(\underline{\epsilon}_z + \underline{\epsilon}_r + \underline{\epsilon}_\theta) \quad (4 42)$$

The tangential stress $\underline{\sigma}_\theta$ can be found similarly Further, the axial stress becomes

$$\underline{\sigma}_z = \underline{\sigma}_z + \underline{\sigma}_m = -(\underline{\sigma}'_r + \underline{\sigma}'_\theta) + \frac{1}{(1-2\nu)}(\underline{\epsilon}_z + \underline{\epsilon}_r + \underline{\epsilon}_\theta) \quad (4 43)$$

The shearing stress $\underline{\tau}$ can be found from the fourth equation in group 4 34, into which equation 4 36 has been substituted Finally, the axial load and the torque acting on the section can be calculated by appropriate numerical integration of the axial and shearing stresses However during the present experimental investigations the theoretical curves given in reference [20] have been used for comparison with the experimental results Figure 4 3 shows the variations of the torque with the axial strain for different strain-hardening parameters, when the initially applied torque was equal to the yield torque and, figure 4 4 that of the axial load with the shear strain, when the initially applied load was equal to yield load In the first case, corresponding angle of twist was kept constant, whereas in the second case, corresponding axial displacement was held constant

4 5 THEORETICAL INVESTIGATION ON THE ELASTIC RECOVERY OF A INITIALLY TORQUED SPECIMEN

This section is devoted to carry out a theoretical investigation regarding the elastic response of a rod, fitted with strain gauges, when its initial torque carrying ability drastically becomes nil Suppose, a circular bar of diameter D_0 , with a reduced section of diameter d_0 , as shown in figure 4 5(a), is subjected to an initial torque T whose corresponding angle of twist is kept constant at its bottom edge "gh", i e , angular position of section "gh" is held constant During this theoretical investigation, it will be assumed that, in addition to the homogeneity of the material, all other assumptions applicable in the derivation of elastic torsion and angle of twist

formulas are also valid in this case. It will be further assumed that the effect of stress concentration due to the sharp edges at sections "cd" and "ef" may be neglected.

Due to the application of torque T , part-1 will experience a total angle of twist θ_1 , at section "cd", part-2 a further twist of θ_2 and part-3, an additional twist θ_3 , where

$$\theta_1 = \frac{Tl_1}{GJ_1} \quad (a)$$

$$\theta_2 = \frac{Tl_2}{GJ_2} \quad (b)$$

$$\theta_3 = \frac{Tl_3}{GJ_1} \quad (c)$$

Thus the total twist at section "cd" is θ_1 , at section "ef" is $(\theta_1 + \theta_2)$ and at "gh" is $(\theta_1 + \theta_2 + \theta_3)$. Now somehow, if the torque carrying ability of the reduced section "cdfe" becomes nil, and the angle of twist at section "gh" is held constant, the part-1 and part-3 of the bar will springback to their unstrained (untwisted) positions because of the elastic recovery of these sections. Then due to elastic recovery of part-1, cross-section "cd" of part-2 will experience a reverse angle of twist θ_1 and that of for part-3, cross-section "ef" will experience a forward twist θ_3 . Thus part-2, in addition to its own initial twist θ_2 , will experience an additional angle of twist equal to $(\theta_2 + \theta_3)$, i.e., a total twist of $(\theta_1 + \theta_2 + \theta_3)$. Thus it is seen from the above that when the torque carrying ability of part-2 of the bar starts decreasing, the angle of twist of part-2 will start increasing because of the elastic springback of parts 1 and 3.

Now if shear strain gauges are used, as shown in figure 4.5(b), to measure the strain readings due to an applied torque T , the corresponding readings of gauge 1, 2 and 3 will be γ_1 , γ_2 , and γ_3 respectively, where

$$\gamma_1 = \frac{D_o \theta_1}{2\Delta l}$$

$$\gamma_2 = \frac{d_o \theta_2}{2\Delta l}$$

$$\gamma_3 = \frac{D_o \theta_3}{2\Delta l}$$

Δl is the active gauge length and, θ_1 , θ_2 and θ_3 are the small angles produced by the strain gauges (for the gauge length Δl) Now again somehow, if the torque in section "cdfe" starts decreasing and after a certain time if it completely disappears, then due to the elastic recovery, γ_1 and γ_3 will also begin to decrease and eventually will become zero. But in case of γ_2 , initially shear strain will start increasing very rapidly because of additional effect of $(\theta_1 + \theta_3)$, whose magnitudes are much higher than those of $(\theta_1 + \theta_3)$ and ultimately become constant, when γ_1 and γ_3 will become zero. The above discussion implies that in a specimen of uniform cross-section even though the initially applied torque will be reduced when increasing axial load is applied, extreme care has to be taken in deciding the location of shear strain gauges and in using the readings from these gauges to determine the reduction in torque.

In a similar way it can be shown that in the case of a pre-loaded specimen, whose corresponding axial displacement is held constant, if, somehow, the axial load carrying ability of section "cdfe" becomes reduced, the axial strains from gauges 1 and 3 will be reduced to zero because of elastic recovery, whereas the strain from gauge 2 will initially increase very rapidly and eventually become constant. Thus similar conclusion can be drawn that extreme care has to be taken in deciding the location of axial strain gauges and in using the readings from these gauges to determine the reduction in axial load.

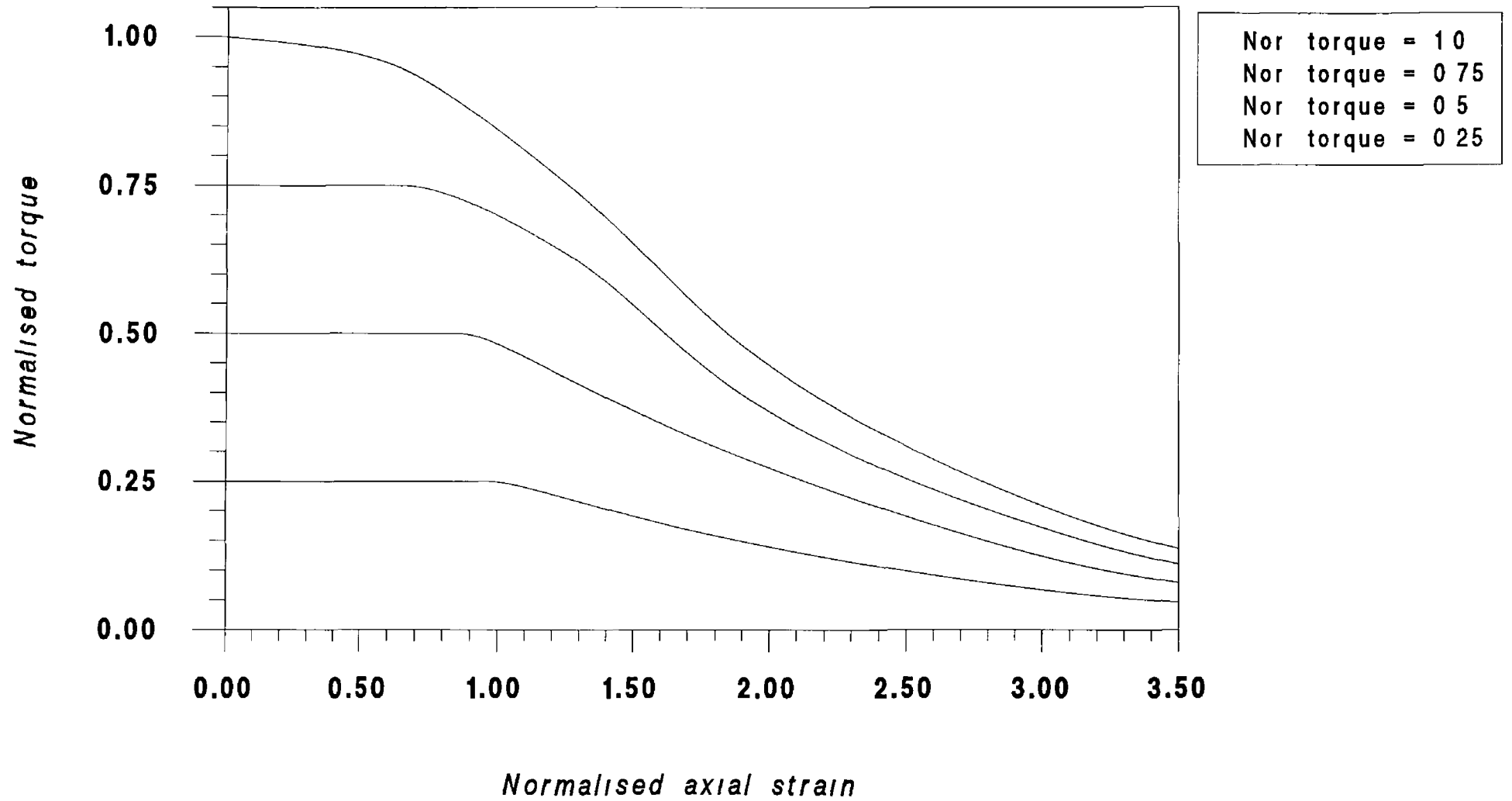


Figure 4.1 Variations of the initially applied torque with the axial strain

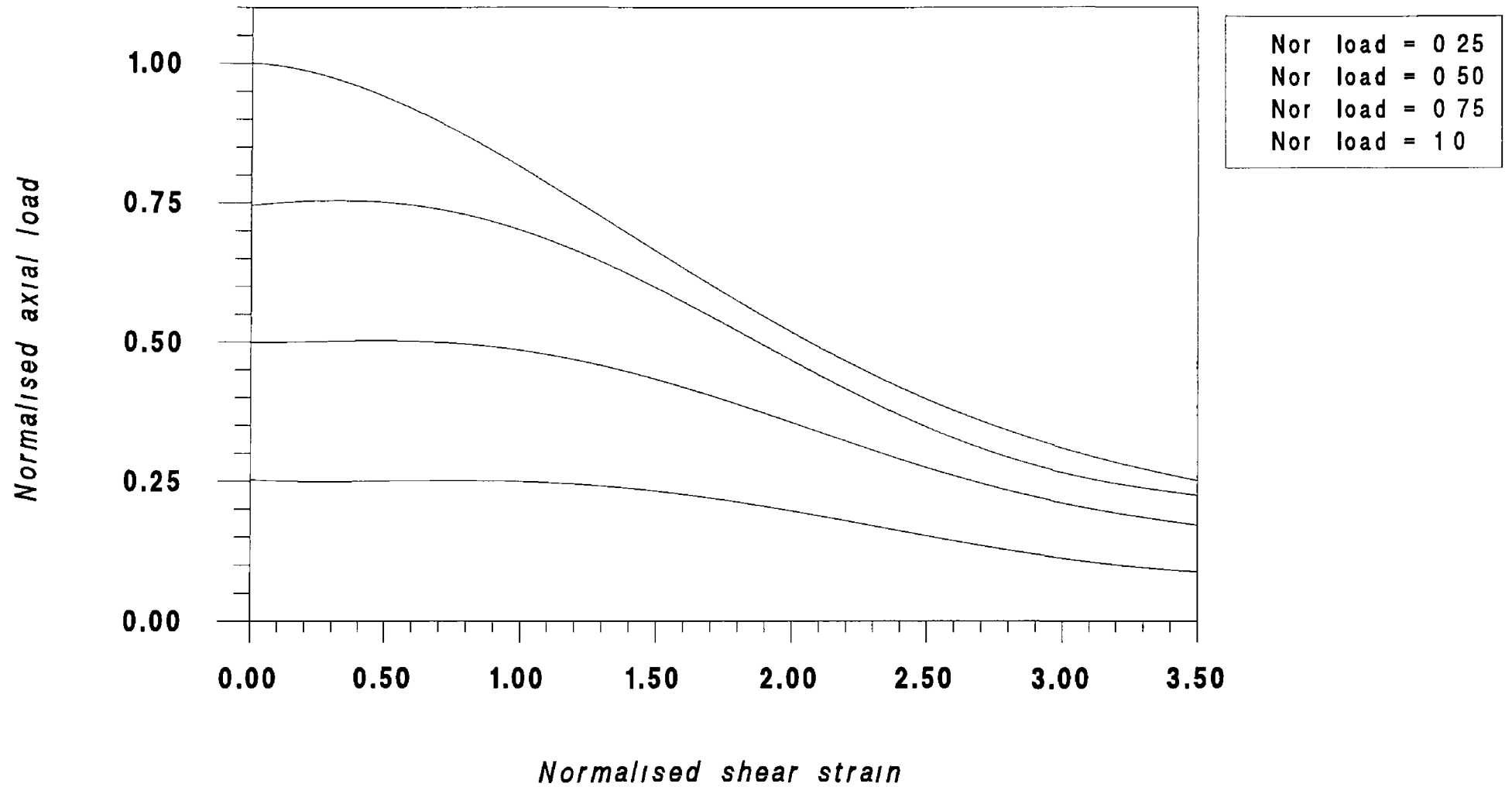


Figure 4.2 Variations of the initially applied axial load with the shear strain

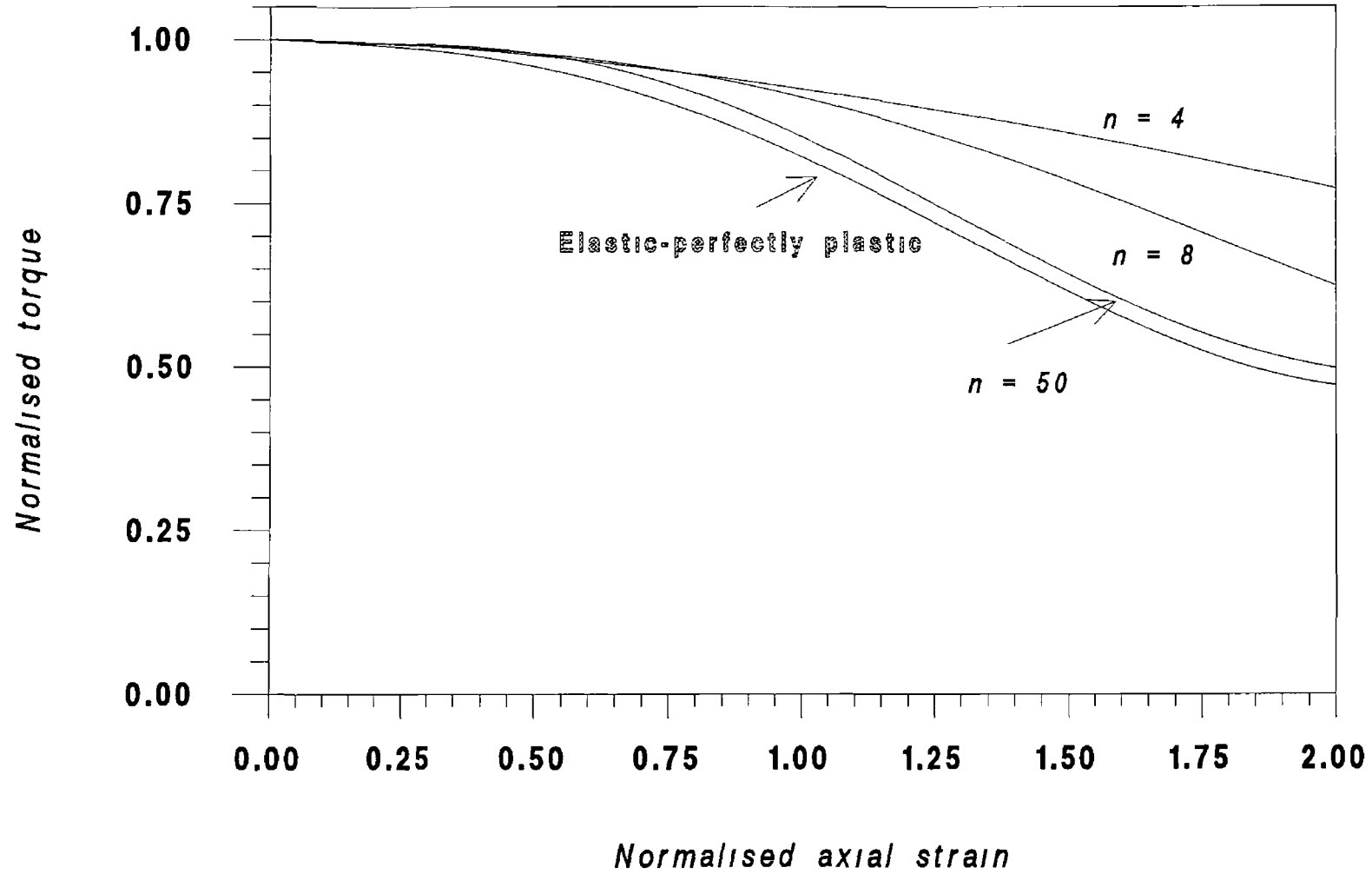


Figure 4.3 Variations of the initially applied torque for different strain-hardening parameters

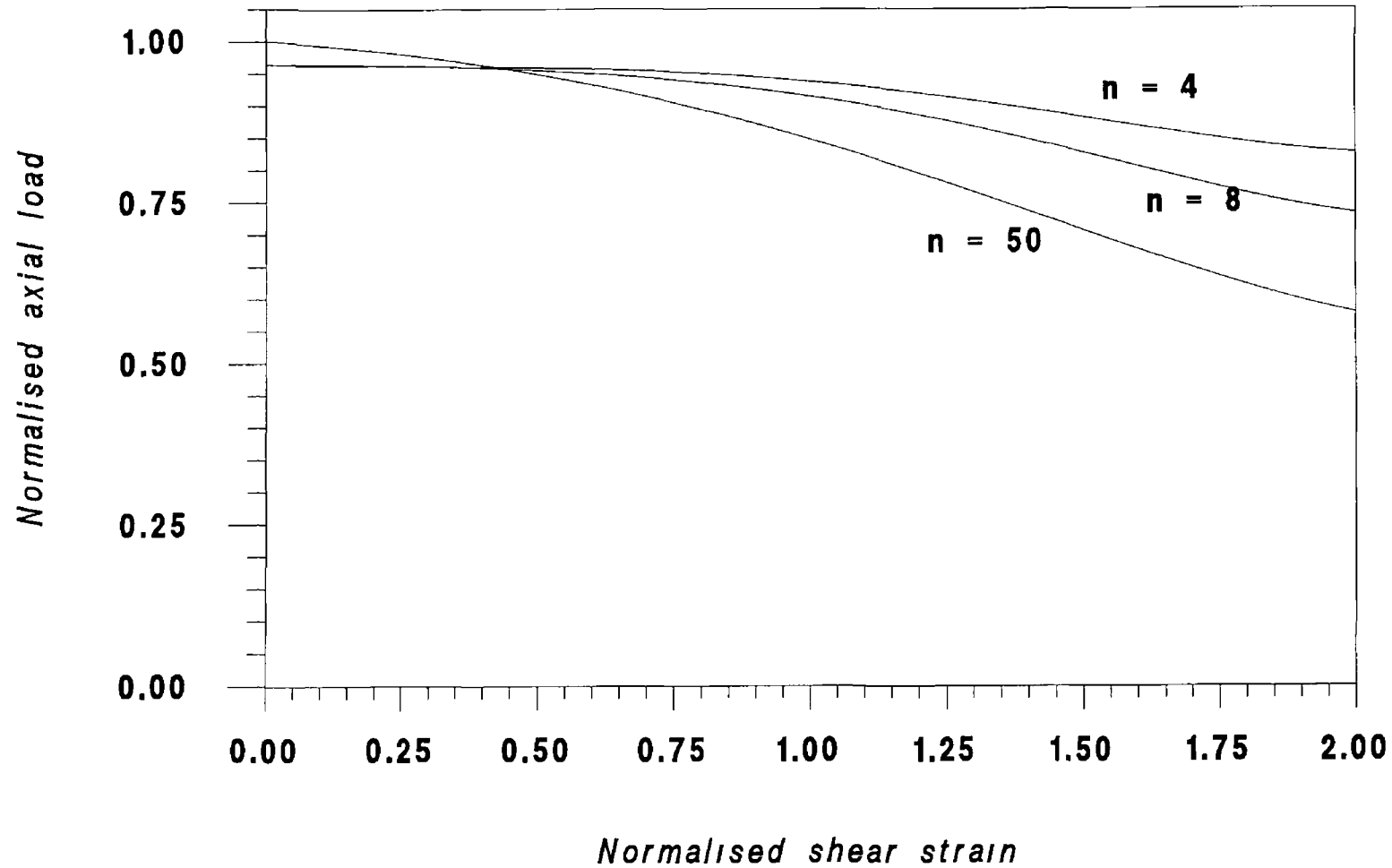


Figure 4.4 Variations of the initially applied axial load for different strain-hardening parameters

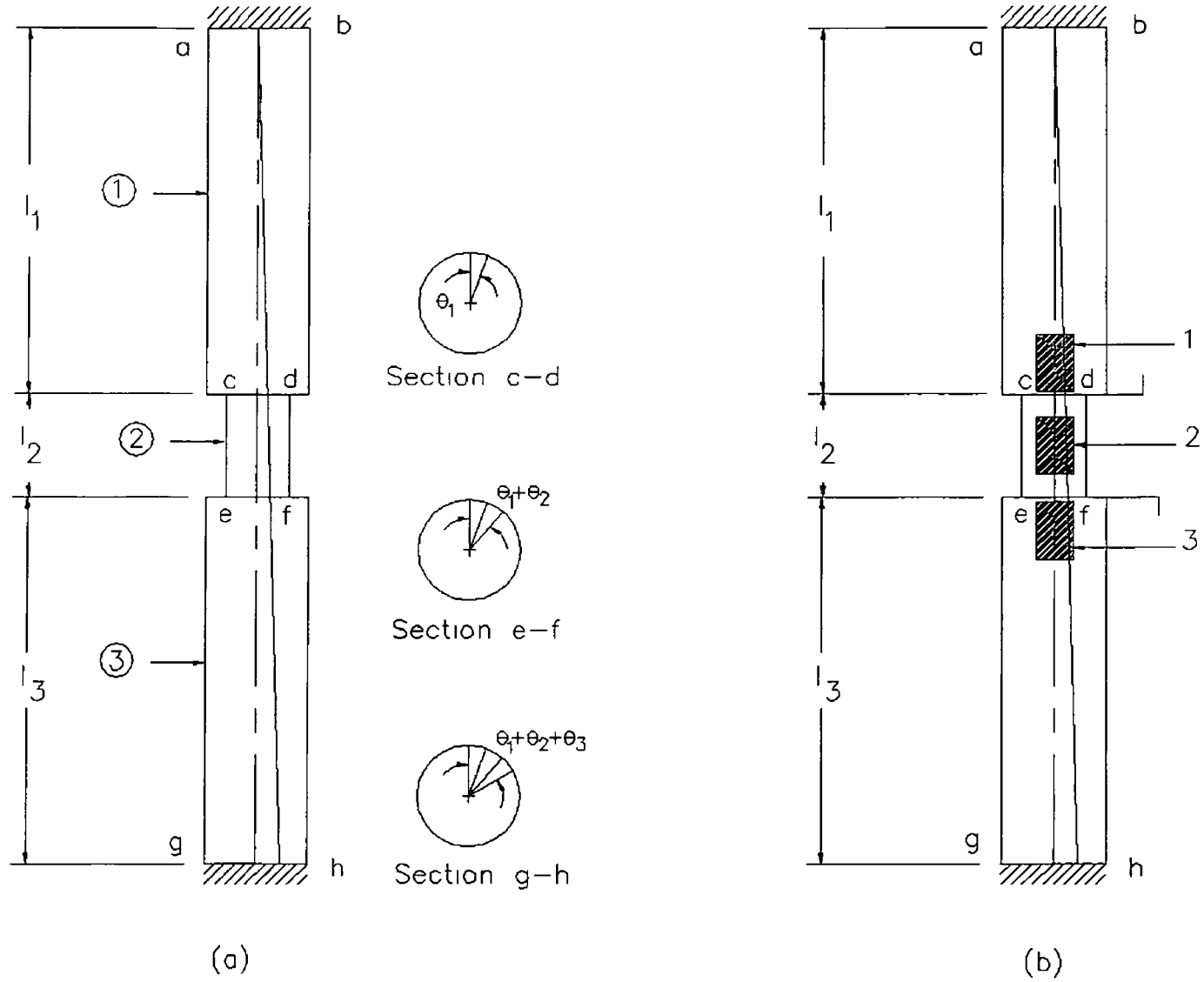


FIGURE - 4 5 Specimen subjected to initial torque

CHAPTER FIVE

EXPERIMENTAL PROCEDURE AND SELECTION OF SPECIMEN

5.1 INTRODUCTION

This chapter details the post-commissioning calibration of the test machine, the selection and preparation of the test specimens, and the experimental procedure

5.2 CALIBRATION OF THE TEST MACHINE

Two separate servo controllers were used in this machine to control different motor parameters. By controlling the torque and velocity commands of these controllers, it was possible to control the corresponding output torque and speed of each motor. Controller-1 was used to control the axis-1, i.e., to control the applied axial load and the vertical speed of the cross-head, whereas, controller-2 was used to control axis-2, i.e., to control the applied torque and the rotational motion of the specimen.

5.2.1 CALIBRATION OF AXIS-1

Different levels of analogue commands (0-10V) were applied to controller-1 as the torque and velocity commands to control the output torque and speed of motor-1. For axis-1, the control of the torque of the motor results in the control of the axial load applied to the specimen, whereas the control of the speed results in the control of the linear vertical motion of the cross-head. As both these commands can be independently applied, they were calibrated separately. During the calibration of axis-1, axis-2 remained inactive.

Calibration of Vertical Speed of The Cross-Head

This calibration was carried out to establish the relationship between the applied input analogue command (i.e., voltage), as a velocity command, and the resulting vertical linear motion of the cross-head

At first an LVDT was placed in between the grippers, and then different levels of voltage (0-10V) were applied to controller-1, through switch 8 of the control panel. This drove the cross-head at various speeds. The analogue commands were applied using an external power supply unit. Corresponding to each voltage, the vertical distance covered by the cross-head, over a certain interval of time was recorded. Figure 5.1 shows the resulting calibration curve for the case where the cross-head travelled in an upward direction. The figure shows a linear relation between the speed of the cross-head and the applied voltage which was obtained from a best fit of the test data. The calibration was performed without loading the machine, i.e., without fixing any specimen. During the calibration, output torque of motor-1 was always kept constant by applying a specific torque command (i.e., voltage) to controller-1.

Calibration of The Axial Load Applied To The Specimen

This calibration was carried out to find the relationship between the input analogue command (0-10V) applied to controller-1 as a torque command, and the actual axial load applied to the specimen, i.e., the output of the axial load cell. During calibration, the speed of the cross head was kept constant by applying a fixed velocity command (i.e., voltage) to controller-1.

To obtain an output from the axial load cell, the machine had to be loaded with a specimen. For this reason, a 12mm diameter, high strength steel specimen was attached to the grippers. Then different levels of analogue voltage (0-10V) were applied to controller-1, via switch 7 of the control panel, to apply different amounts of axial load to the specimen. The corresponding output from the axial load cell was recorded using a RDP transducer indicator. The specimen material was selected so that it could resist at least 100kN force before it failed in tension. As

the present set-up of the machine was arranged only for applying a tensile load, this calibration was done for tensile loading of the specimen only. The calibration curve is shown in figure 5.2 which shows a linear relation between the resulted axial load and the applied voltage. This curve was obtained from a best fit of the test data. The maximum non-linearity in the axial load for a given applied voltage was about 6.8%. It is worth noting that there was no increase in the axial load until the applied voltage was nearly equal to 775mV.

5.2.2 CALIBRATION OF AXIS-2

Different levels of analogue commands (0-10V) were applied to controller-2, as torque and velocity commands, to control the output torque and speed of motor-2. For axis 2, the control of torque of the motor results in control of the torque applied to the specimen, whereas control of speed results in control of the rotational motion of the specimen. As both commands can be controlled independently, they were calibrated separately. During the calibration of axis 2, axis 1 remained inactive.

Calibration of Rotational Motion of The Specimen

This calibration was necessary to establish the relationship between the input analogue command (i.e., voltage) applied to controller-2, as a velocity command, and the resulting rotational speed of the torque-tension shaft. The machine was not loaded during the calibration.

Different levels of voltage (0-10V) were applied to controller-2, through switch 10 of the control panel and the resulting rotational motion of the torque-tension shaft was recorded, over a certain interval of time. Rotation of the shaft, in degrees, was measured using the angle measuring transducer. Figure 5.3 shows the calibration curve established when the shaft rotated in a clock-wise direction. During calibration, the output torque of motor-2 was maintained constant by applying a specific torque command (i.e., voltage) to controller-2. The

figure shows a linear relation between the angular speed of the torque-tension shaft and the applied voltage which was obtained from a best fit of the test data

Calibration of The Torque Applied To The Specimen

This calibration was carried out to find the relationship between the applied input analogue command (0-10V), as a torque command, and the actual torque sensed by the specimen, i.e., the output of the torque load cell. During this calibration, the speed of the motor was maintained constant by applying a specific velocity command to the controller.

To cause an output from the torque load cell, the machine was loaded with a specimen. A 12mm diameter, high strength steel specimen was set into the machine, and then different levels of voltage were applied to controller-2. This applied different levels of torque to the specimen. The corresponding output, in units of Newton-Meter, from the torque load cell was recorded by a RDP transducer indicator. The specimen material was selected so that it could resist at least 200Nm torque before it failed. Figure 5.4 shows the calibration curve when the specimen was twisted in the clock-wise direction. The figure shows a linear relation between the developed torque and the applied voltage. The calibration curve was obtained from a best fit of the test data. The maximum non-linearity in the torque for a given applied voltage was about 4%. However, there was no increase in the torque until the applied voltage was nearly equal to 425mv.

5.2.3 PERFORMANCE CHARACTERISTICS OF THE MACHINE

To judge the performance characteristics of this torque-tension machine, a number of tests were carried out. To this end, a 150mm long, 11.5mm diameter steel specimen (En8), with machined heads, was set into the machine and the following tests were conducted. During the tests the linear speed of the cross-head was maintained at 1.45×10^{-2} mm/sec, whereas the angular velocity of the torque-tension shaft was 0.38°/sec.

(i) At first an initial torque of known value was applied to the specimen and then, holding its corresponding angle of twist constant, the tensile load was gradually increased upto a certain value so that the combined stress (according to the von Mises criteria) remained within the elastic limit of the material. The torque and the axial load were measured by the relevant load cells, and the angle of twist by the angle measuring transducer. All parameters were recorded by a X-Y recorder. Figure 5.5(a) shows the torque versus the angle of twist curve, whereas figure 5.5(b) shows the axial load versus the angle of twist curve. From the latter figure it is evident that the angle of twist was always maintained constant during the application of the axial load.

(ii) Procedure (i) was repeated except that the applied initial torque rather than angle of twist, was maintained constant, and then the tensile load was gradually increased upto a certain value so that the combined stress remained within the elastic limit of the material. Figure 5.5(c) shows the variation of the initially applied torque with the axial load, which reveals that the torque nearly remained constant during the application of load.

(iii) At first a known tensile load was applied to the specimen and then, holding its corresponding axial displacement constant, the torque was gradually increased so that the combined stress remained within the elastic limit of the material. Here the axial displacement was recorded using an LVDT. Figure 5.6(a) shows the axial load versus the displacement curve and figure 5.6(b) shows the effect of the applied torque on the axial displacement. From 5.6(b) it is evident that during the application of the torque, the axial displacement was successfully maintained constant.

(iv) Procedure (iii) was repeated except that in this case the initially applied axial load rather than the axial displacement was maintained constant, and then the torque was gradually applied. The variation of the axial load with the torque is shown in figure 5.6(c).

5.3 SPECIMEN SELECTION, DESIGN AND INSTRUMENTATION

5.3.1 TEST MATERIALS

The present study was conducted to examine the biaxial behaviour of two commonly used engineering materials, mild steel En8 (BS 970 & AISI 1040), and high conductivity oxygen free copper (BS 2874-C102). However, as the steels used were purchased from two different steel manufacturing companies, designated as steel-1 and steel-2, the mechanical properties of each lot of steel were determined separately. As lot-1 was used for most steel specimens, unless otherwise stated, the word "steel" has been used throughout the thesis to mean steel-1. The chemical composition (in percentages) of both steels was as follows, C 0.36-0.44, Mn 0.60-0.90, Si 0.10-0.40, S 0.05 and P 0.05, whereas that of copper, Cu 99.9, lead 0.005 and impurities 0.03. The uniaxial tensile and torsional characteristics of the steels and the copper are given in chapter six in detail. During the experimental investigations, all tests were conducted on as-received materials.

In the present experimental investigations thin-walled steel tubes were also tested under biaxial loading. Here, cold finished seamless pressure tubes (BS3602 part1, TC2 CFS 360), with 8mm outside and 6mm inside diameter, were used as the specimens. Their chemical composition (in percentages) was as follows, C 0.17, Si 0.35, Mn 0.40-0.80, S 0.045 and P 0.045.

5.3.2 SPECIMEN DESIGN

In order to avoid the complex relationships among the tightening torque, friction co-efficient and pre-load, which results in case of a bolt, a simple fastener-like structure (solid bar) was used as the test specimen. Except for the two extended end heads, the specimen had a circular cross-section throughout. Details of the specimen are shown in figure 5.7. The specimen was designed according to ASTM standardised form (ASTM E8) for a ductile-metal tension-test specimen.

To apply the tensile load and torque, either simultaneously or individually, the ends of the specimen were designed in such a way that when the torque was applied, the straight faces (face 1 and 11) prevented the specimen from rotation, and when the tensile loads were applied, the 7.8mm deep heads held the specimen in the slots of the grippers. For ease of manufacture, only two faces of each extended head were machined straight. The same specimen configuration was used for both material types. Throughout the experimental investigations, this particular shape was used for all the test specimens, unless otherwise stated.

Modified Solid Specimen

A number of biaxial tests were conducted using the modified version of the test specimen described above. Details of the modified specimens are shown in figure 5.8(a) and 5.8(c). Figure 5.8(a) shows the geometry of a uniform diameter specimen and figure 5.8(c) that of a reduced section specimen. At the centre of each reduced section specimen, a 17mm long, 8mm diameter section was machined on which shear strain gauges were attached.

Thin-Walled Specimen

The steel tube was pinned into a pair of specially designed features, shown in figure 5.9(a), to form the necessary heads of the specimen to fix it to the grippers. The assembly drawing of the tube, along with the specially designed heads, are shown in figure 5.9(b).

5.3.3 SPECIMEN INSTRUMENTATION

Three different types of strain gauges were used to measure the axial and shear strains of the loaded specimen. Details of the different type of strain gauges are shown in figure 5.10. All these gauges were purchased from the "Measurements Group UK Ltd". The strain gauge, type CEA-06-250UN-350, was used to measure the axial strain during the uniaxial loading of the specimen, whereas types, EA-06-125TM-120 and CEA-06-062UV-350, were used during combined loadings.

Strain Gauge Attachment

To obtain best results from a strain gauge, it is important to prepare the gauge and the surface of the specimen to which the gauge is to be attached. In order to prepare the specimen surface, an area larger than the installation was smoothed with fine grade emery paper (500 grit) to provide a sound bonding surface. Then the area was degreased with a solvent cleaner. For this purpose a "CSM-1" degreaser was used. Finally the specimen surface was neutralised with a "M-prep Neutraliser-5". Cotton wool was used for this operation.

After preparing the specimen surface, the desired location for the strain gauge was determined. A short length of adhesive tape was placed over the entire length of the gauge tabs. Then the gauge backing and the specimen surfaces were coated with a thin layer of "M-Bond 200" adhesive. The strain gauge was placed in its desired location and reasonable pressure was applied for about one minute to ensure that the assembly was firmly in place. Finally, the connecting wires were soldered to each strain gauge element. Figure 5.11 shows the different stages of strain gauge preparation.

Digital Strain Indicator

A digital strain indicator, model P-3500, along with a switch and balance unit, model SB-10, was used to read the strains of the loaded strain gauges. This digital strain indicator is a portable, battery-powered precision instrument for use with resistive strain gauges and transducers. It accepts full-, half-, or quarter-bridge inputs, and all required bridge completion components for 120-ohm and 350-ohm bridges are provided. It accepts gauge factors of 0.500 to 9.900, and gauge is settable to an accuracy of 0.001 by a front-panel ten-turn potentiometer. The instrument is capable of measuring up to $\pm 199990 \mu\epsilon$ (i.e. nearly 20% strain) in two ranges $\pm 19999 \mu\epsilon$ and $\pm 199990 \mu\epsilon$. Its accuracy is $\pm 0.05\%$ in both ranges for gauge factor greater than or equal to one. During the experiment, analogue output was taken from the front-panel BNC connector of this digital strain indicator to a chart or X-Y recorder. Plate 3.8 shows a photograph of the unit.

Switch And Balance Unit

In order to provide the bridge circuits of the strain gauges, a switch and balance unit was used. The unit is designed to provide a method of sequentially reading output of ten channels of strain gauge readings on a single strain indicator. Each channel can initially be balanced to zero output to greatly simplify data interpretation and reduction. In addition, any SB-10 can intermix quarter-, half- and full-bridge circuits, and offers full isolation for each individual circuit, thus preventing a defect in one input from having any effect on the other inputs. Its input bridge resistance varies from 50 to 10000 Ω . Direct readings can be obtained from the unit by switching to different channels. Figure 5.12(a) shows a typical full bridge connection between the strain gauges and the switch and the balance unit. The circuit diagram between the strain indicator and the balance unit is shown in figure 5.12(b).

5.4 PRELIMINARY TESTS

UNIAXIAL TENSILE TEST

Before a uniaxial tensile test was carried out, a pair of "CEA-06-250UN-350" uniaxial type, strain gauges was attached to the specimen. During the application of the load, only the "axis -1" was activated. After fixing the specimen into the machine, a small load was applied to it to eliminate all gaps and slackness. A small strain reading recorded by the strain indicator confirmed that the tensile loading had truly started. Then the load was gradually increased until the specimen failed in tension. The output from the axial load cell and the strain gauges were fed into a chart recorder which plotted the necessary figures. During the test, the specimen was extended quasi-statically at a constant strain rate of $1.6 \times 10^{-4} \text{ s}^{-1}$. The same procedure was followed for both types of materials.

PURE TORSION TEST

Initially a pair of "CEA-06-062UV-350" type strain gauges was attached to the specimen to measure the shear strain of the torqued specimen. After positioning the specimen into the

machine, a small torque was applied to it to eliminate all gaps and slackness in between the specimen heads and the grippers, and then the torque was gradually applied beyond the yield torque of the specimen. During the torque application the specimen was twisted at a nominal constant strain rate of $2.1 \times 10^{-4} \text{ s}^{-1}$. The output from the torque load cell and the strain gauges were recorded by a chart recorder.

DETERMINATION OF STRAIN RATES

During the application of the axial load, the cross-head travelled at a constant speed, so that it was possible to determine the axial strain rate of the specimen from the linear relationship between the axial strain and time, as recorded by the chart recorder. Figure 5.13 shows the relationship between the axial strain and the time elapsed during a uniaxial tension test of a steel specimen, for a particular cross-head speed. Similarly during the torque application, as the drive-shaft twisted at a constant angular speed, the shear strain rate of the specimen was obtained from the linear relationship between shear strain and time, as shown in figure 5.14.

5.5 TEST PROCEDURES FOR COMBINED LOADING

5.5.1 SPECIMEN SUBJECTED TO AN INITIAL TORQUE

Angle of Twist Held Constant

During this particular biaxial loading programme, a certain known torque was initially applied to the specimen, and then the corresponding angle of twist was held constant to observe the variation in the initially applied torque due to the gradual application of an axial load. During this test no strain gauges were needed as the resulting axial strain was calculated from the relationship between the axial strain rate and time.

After positioning the specimen into the grippers, small amounts of torque and axial load were applied to eliminate all gaps and slackness between the specimen heads and the mating surfaces of the grippers. Then a known torque within the elastic range of the material was

applied to the specimen by activating "drive-control system-2" Subsequently the "run/hold" mode switch, switch-3 of the control panel, was set to "hold" to keep the angle of twist constant It is worth noting that, when the switch-3 was changed from "run" to "hold" mode, there was a slight decrease (between 2-4%) in the initial value of the applied torque While keeping the angle of twist constant, an axial load was gradually applied via "drive-control system-1" and this was increased to beyond the uniaxial yield load of the specimen During this load application, the specimen was extended quasi-statically at a nominal constant strain rate of $1.6 \times 10^{-4} \text{ s}^{-1}$, whereas during the initial torque application, the specimen was twisted at constant shear strain rate of $2.1 \times 10^{-4} \text{ s}^{-1}$

All data were recorded simultaneously Output from the axial and the torque load cells were fed into a chart recorder The same test was repeated for different levels of initial torque (i.e., with different values of angle of twist) and for the following types of the specimens, solid steel and copper, and thin-walled steel specimens

Torque Maintained Constant

Before the specimen was set into the machine, a pair of "CEA-06-062UV-350" type shear strain gauges was attached to it Once set up, small amounts of torque and axial load were applied to eliminate the gaps and looseness between the joints Next a known torque, within the elastic range of the material, was applied to the specimen Furthermore, the applied initial torque, rather than the angle of twist, was maintained constant, i.e., switch-3 was always kept in "run" mode An axial load was then gradually applied, and increased beyond the uniaxial yield load of the specimen During the application of the axial load the specimen was extended at the same strain rate as previously, whereas during the torque application the specimen was twisted at a shear strain rate of $8.3 \times 10^{-3} \text{ s}^{-1}$

The output from the load cells and the strain indicator were fed into a chart recorder. The same test was repeated for different levels of initial torques. However, this particular test was conducted using only the solid steel specimens.

5.5.2 SPECIMEN SUBJECTED TO AN INITIAL AXIAL LOAD

Axial Displacement Held Constant

In this particular biaxial loading test, the tensile load was initially applied to the specimen, and then its corresponding axial displacement was kept constant to observe the variation in the applied load due to the application of a torque. No strain gauges were needed during this test as the resulting shear strain was calculated from the relationship between the shear strain rate and time.

After fixing the specimen into the grippers, a known tensile load within the elastic range was applied by "drive-control system-1". Then the "run/hold" mode switch, switch-1 of the control panel, was set to "hold" mode to restrain the axial displacement of the specimen. Switching from "run" to "hold" mode was associated with a slight decrease (between 2-4%) in the initial value of the axial load. Keeping the displacement constant, torque was gradually applied and increased beyond the yield torque of the specimen. During the test, the axial and the shear strain rates were maintained at $1.6 \times 10^{-4} \text{ s}^{-1}$ and $2.1 \times 10^{-4} \text{ s}^{-1}$ respectively.

The outputs from the different load cells were fed into a chart recorder. The above test was repeated for different levels of initial load for solid steel and the copper specimens and thin-walled steel tubes.

Axial Load Maintained Constant

Before these tests, a pair of EA-06-125TM-120 type axial strain gauges was attached with the specimen to measure the axial strain. Then the specimen was loaded biaxially in a similar

way as previously described, except that the initial axial load, rather than the axial displacement, was maintained constant. In this case, the "run/hold" mode switch, switch-1 was always kept in "run" mode to hold the axial load constant. During the application of the initial load, the specimen was extended at a nominal constant strain rate of $6.8 \times 10^{-3} \text{ s}^{-1}$, whereas, during the torque application, the shear strain rate was maintained at $2.1 \times 10^{-4} \text{ s}^{-1}$. This particular test was repeated for different levels of initial load, and for the solid steel specimens only.

5.5.3 BIAXIAL TESTS WITH THE MODIFIED SPECIMEN

A number of biaxial tests were carried out using modified version of the test specimen, i.e., uniform diameter and reduced section specimens. In case of the uniform diameter specimen three pairs of "CEA-06-062UV-350" type shear strain gauges were attached at three different locations, at the top, middle and bottom, of the specimen. The positions of the strain gauges 1, 2 and 3 are shown in figure 5.8(b). The specimen was subjected to an initial torque within the elastic range of the specimen, and then, to a gradually increasing axial load, and hence axial strain, whilst the angle of twist was kept constant. The variation in the initially applied torque measured by the torque load cell, together with the variation in three strain gauges' readings, were recorded simultaneously. During axial loading, the specimen was extended at a strain rate of $1.6 \times 10^{-4} \text{ s}^{-1}$. This particular test was repeated for four steel specimens.

Two biaxial tests were conducted using the reduced section steel specimens. In the first case, three pairs of "CEA-06-062UV-350" type shear strain gauges were attached to the specimen, as shown in 5.8(d). Then it was subjected to similar type of biaxial loadings as mentioned above. In the second case, three pairs of "CEA-06-250UN-350" type axial strain gauges were attached to a reduced section specimen and positioned in a similar way as detailed in figure 5.8(d). It was subjected to an initial axial load and the corresponding axial displacement was kept constant. The torque was gradually increased to far beyond the yield torque of the

specimen by twisting it at a nominal constant shear strain rate of $2.1 \times 10^{-4} \text{ s}^{-1}$. The readings from the axial and the torque cells, as well as from three strain gauges were fed simultaneously to a chart recorder.

5.5.4 TORQUE AND AXIAL LOAD APPLIED SUCCESSIVELY

During this biaxial loading programme both drive systems were operated. After positioning the specimen into the machine, a known initial torque, within the elastic range of the material was applied to the specimen. Then, holding the corresponding angle of twist constant, an axial load was gradually applied until the specimen yielded due to the combined loading. Subsequently, small increments of torque and axial load were applied successively beyond the combined yield point, holding the axial displacement or the angle of twist constant in an alternate manner. This test was repeated for different levels of initial torque. The outputs from the load cells were fed to a chart as well as into a X-Y recorder.

Similar biaxial tests, were carried out with different levels of axial load being applied first, and then, holding the corresponding displacement constant, the torque was gradually increased until the specimen yielded due to the combined loading. Both the axial load and the torque were applied successively beyond the combined yield point, keeping the axial displacement or the angle of twist constant in an alternate manner. These particular types of biaxial tests were conducted for both solid steel and the copper specimens. The steel specimens used were made from steel-2 material.

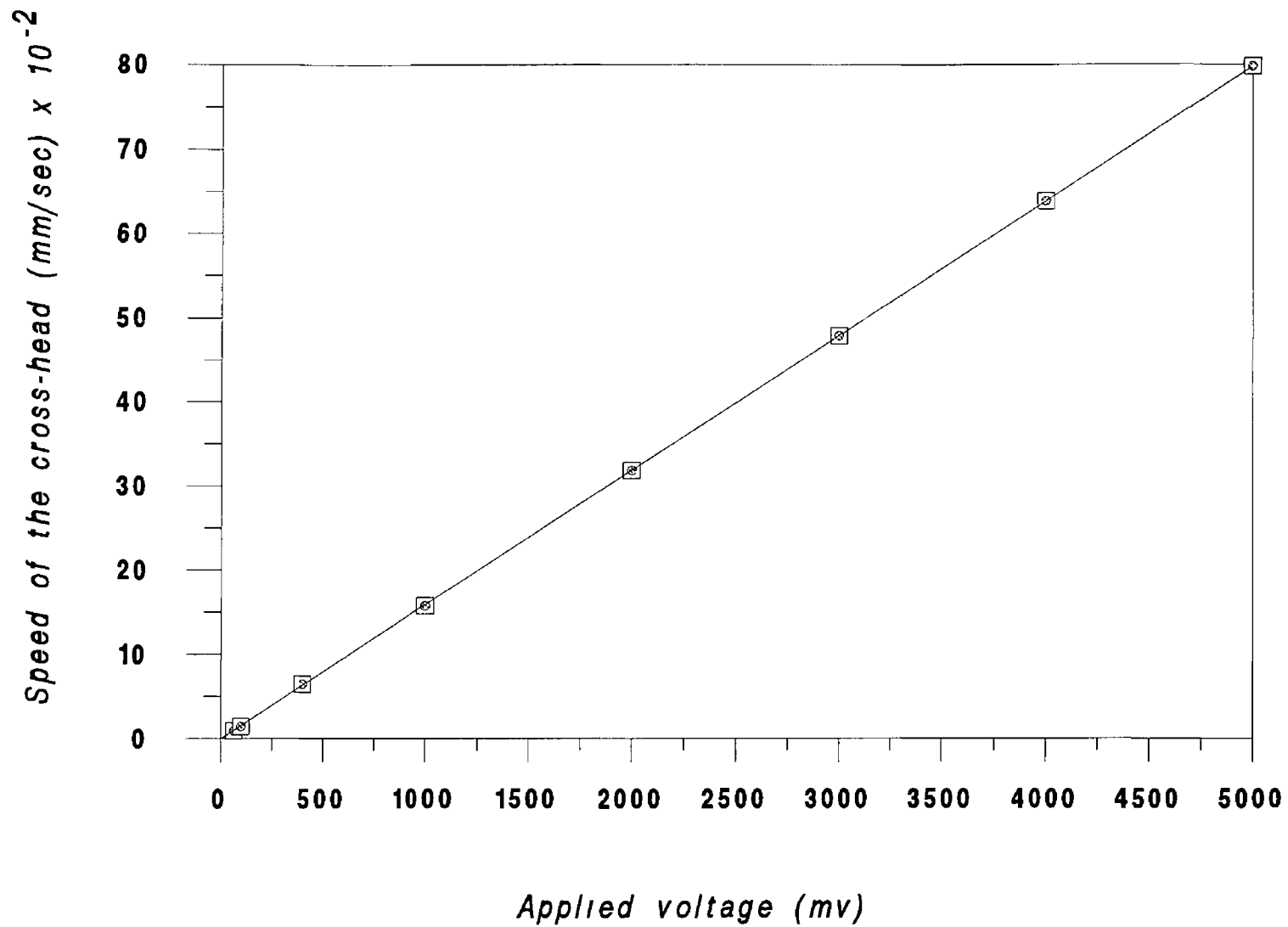


Figure 5.1 Calibration for the vertical speed of the cross-head

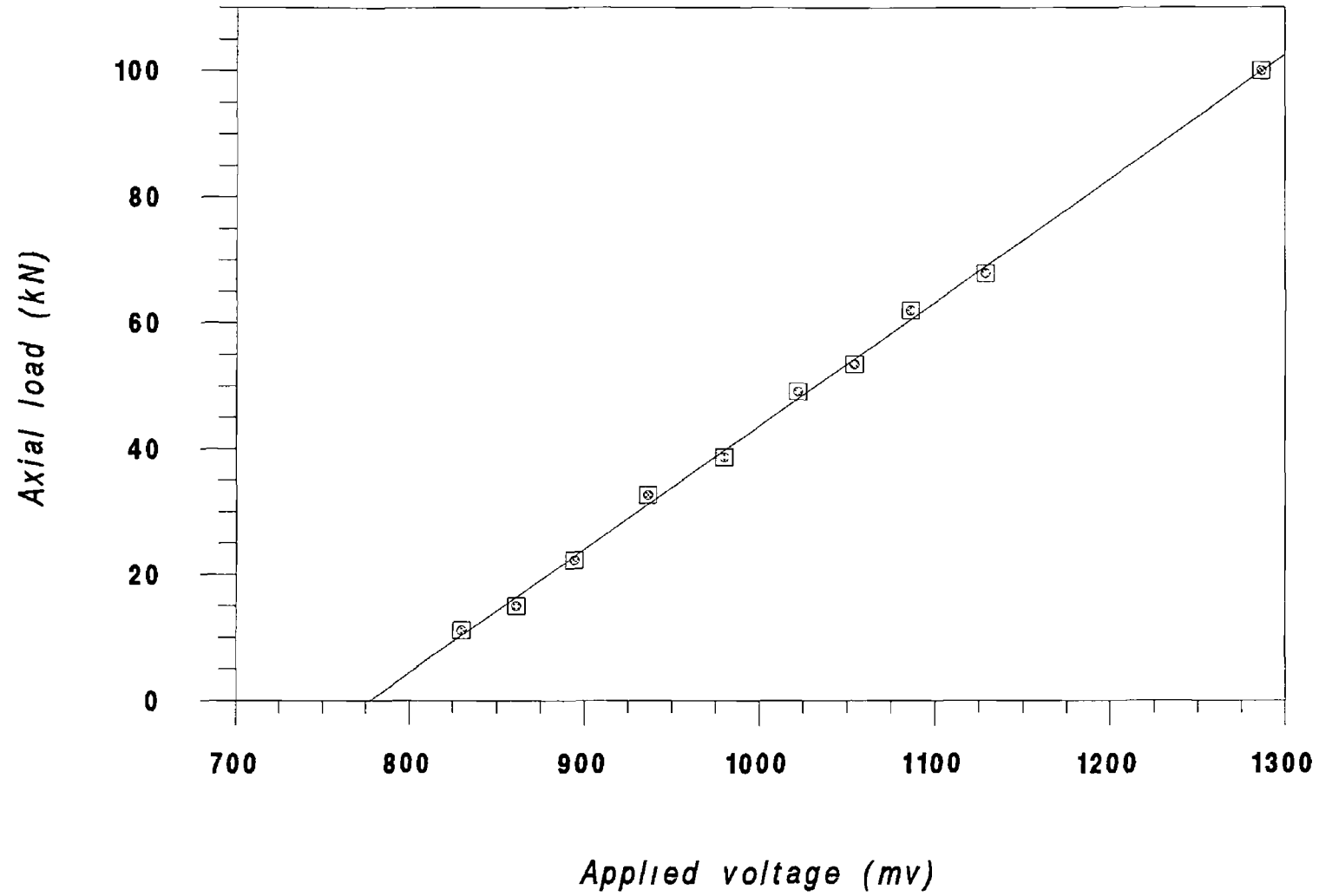


Figure 5.2 Calibration curve for the tensile loading of the specimen

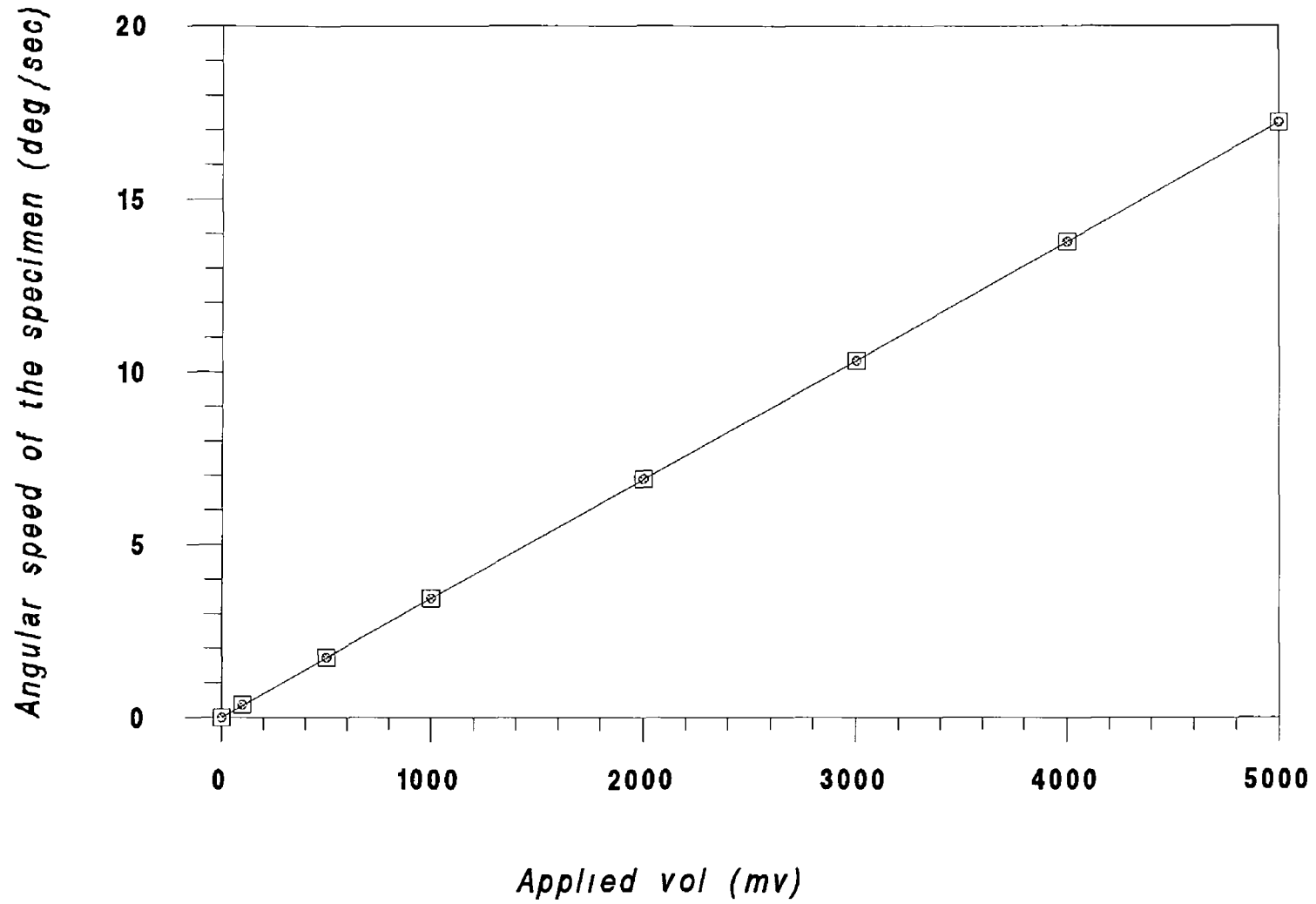


Figure 5.3 Calibration curve for the angular speed of the specimen

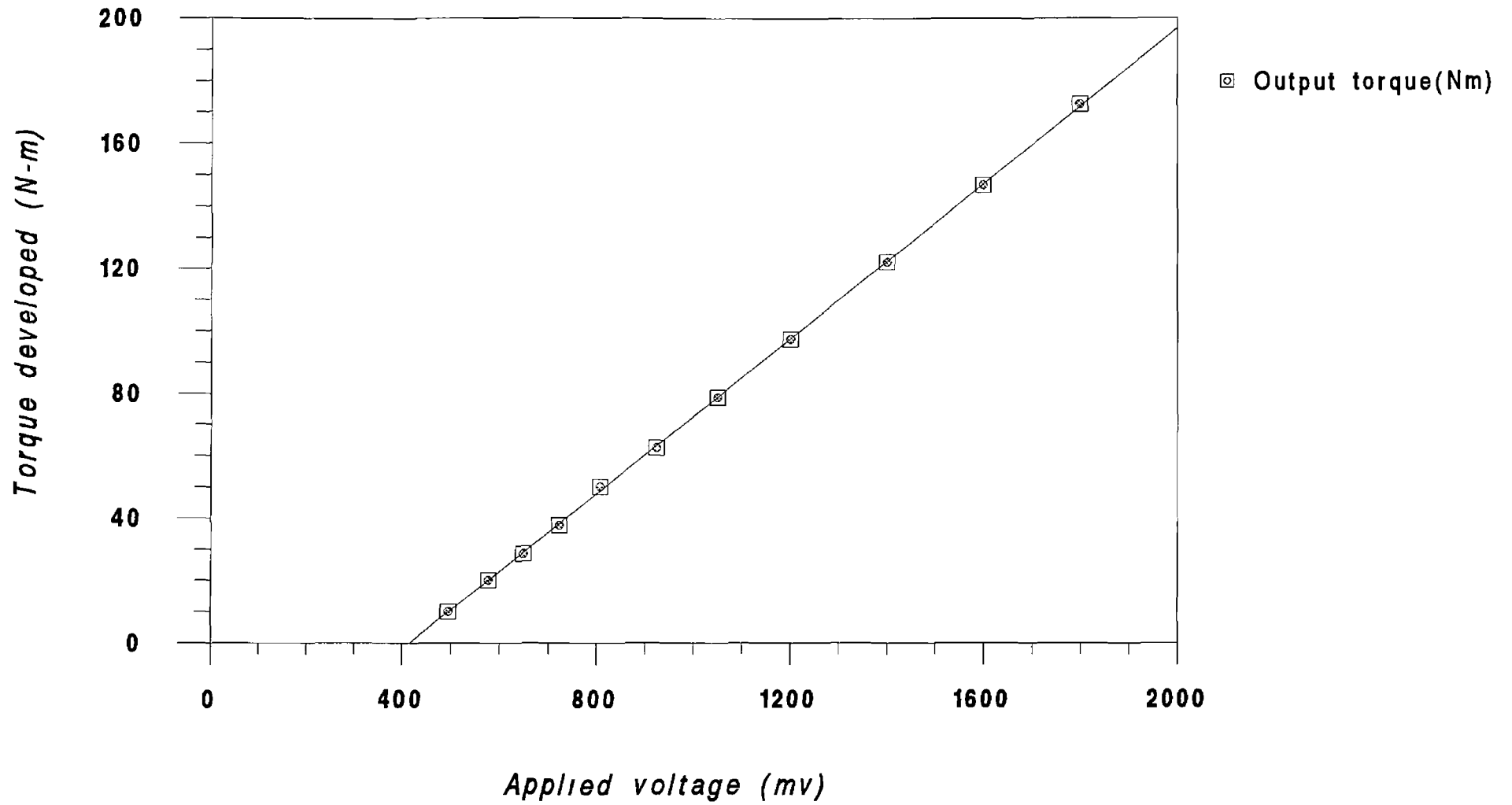


Figure 5.4 Calibration curve for the torque applied to the specimen

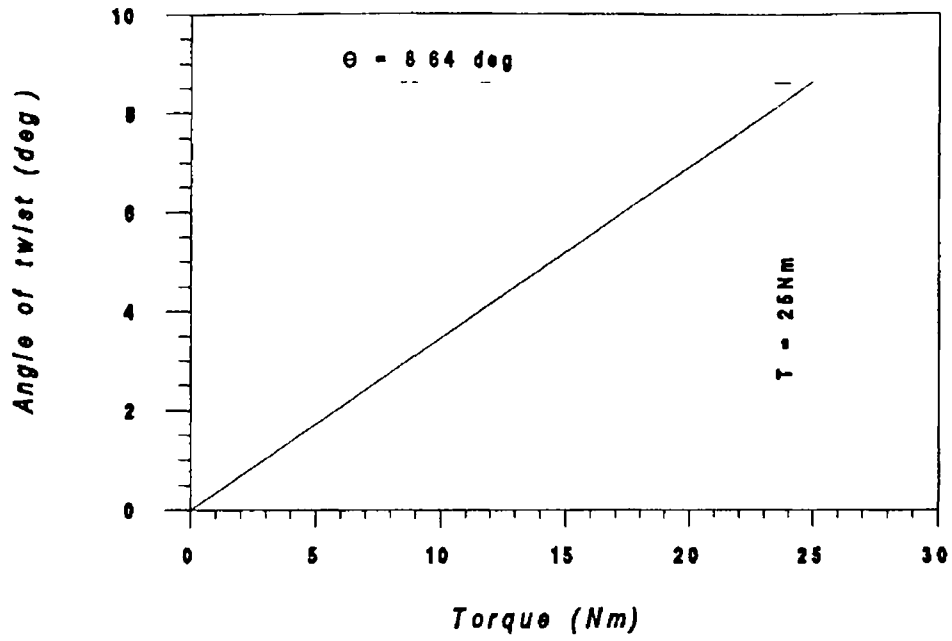


Figure 5.5(a) Torque versus angle of twist curve

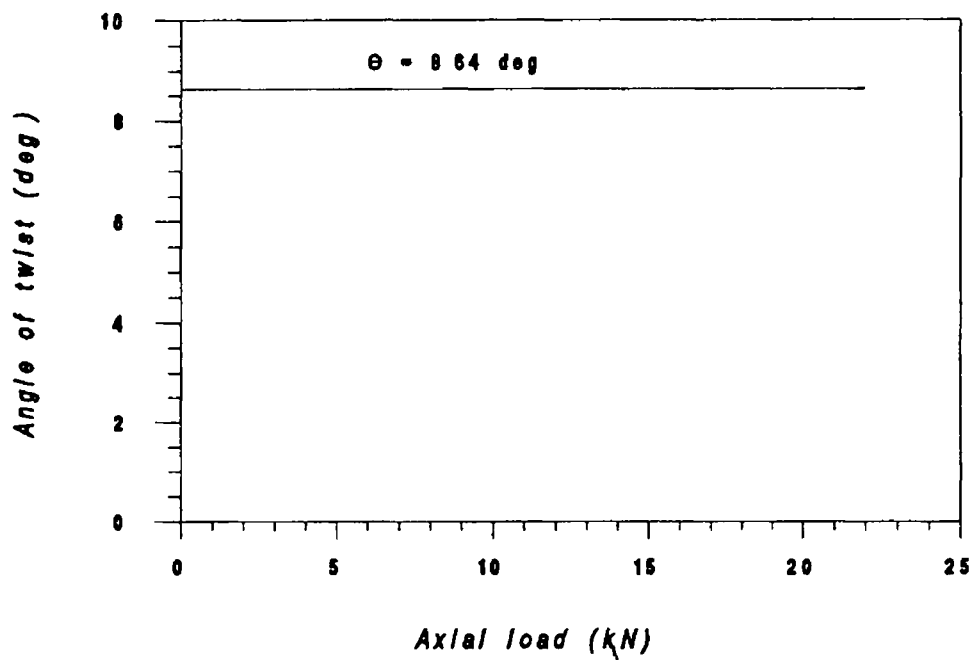


Figure 5.5(b) Axial load versus angle of twist curve

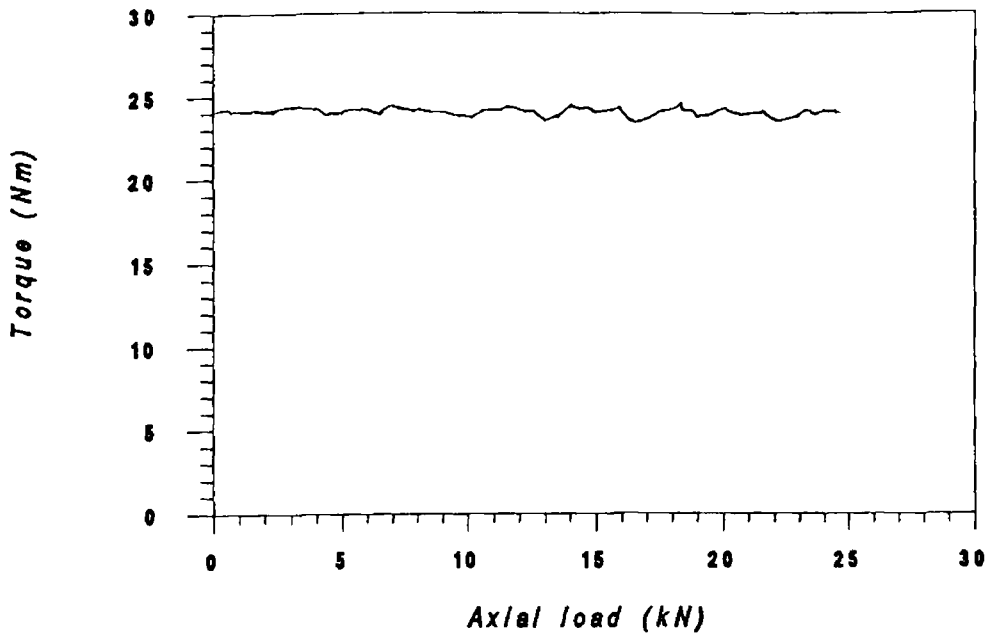


Figure 5 5(c) Torque versus axial load curve when torque maintained constant

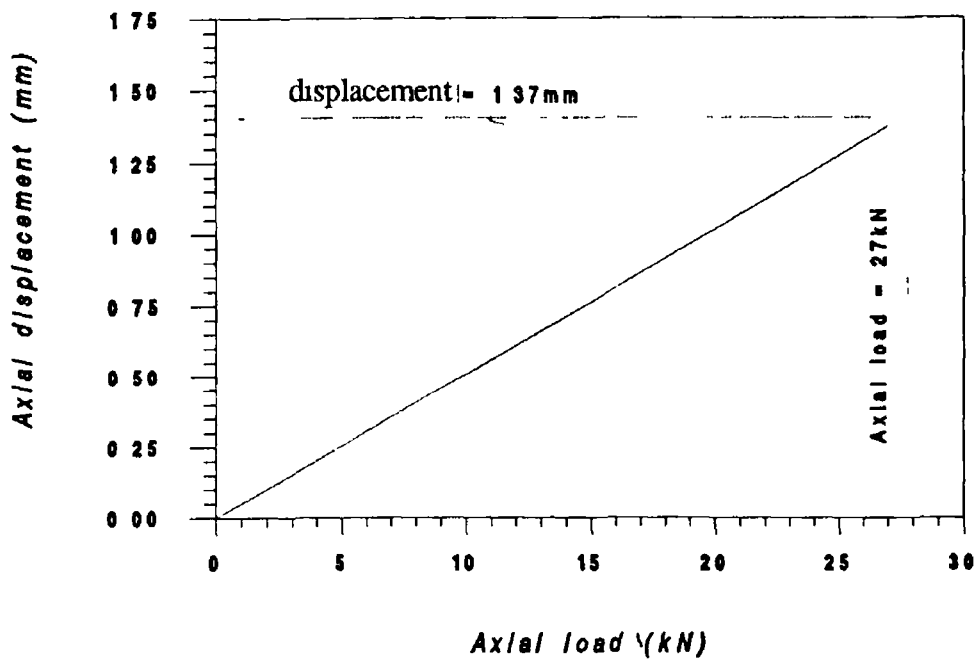


Figure 5 6(a) Axial load versus axial displacement curve

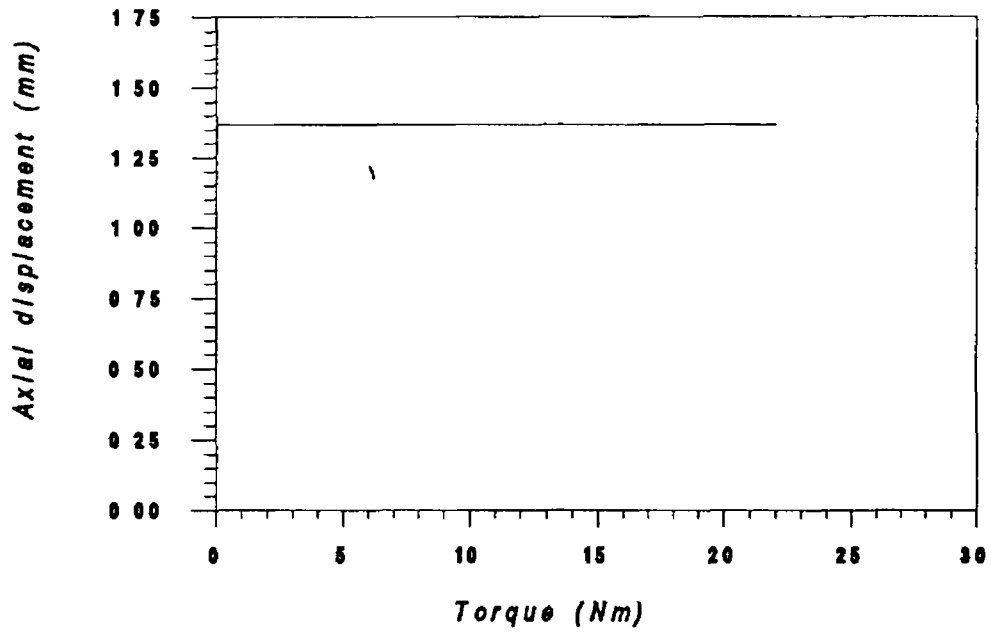


Figure 5 6(b) Torque verses axial displacement curve

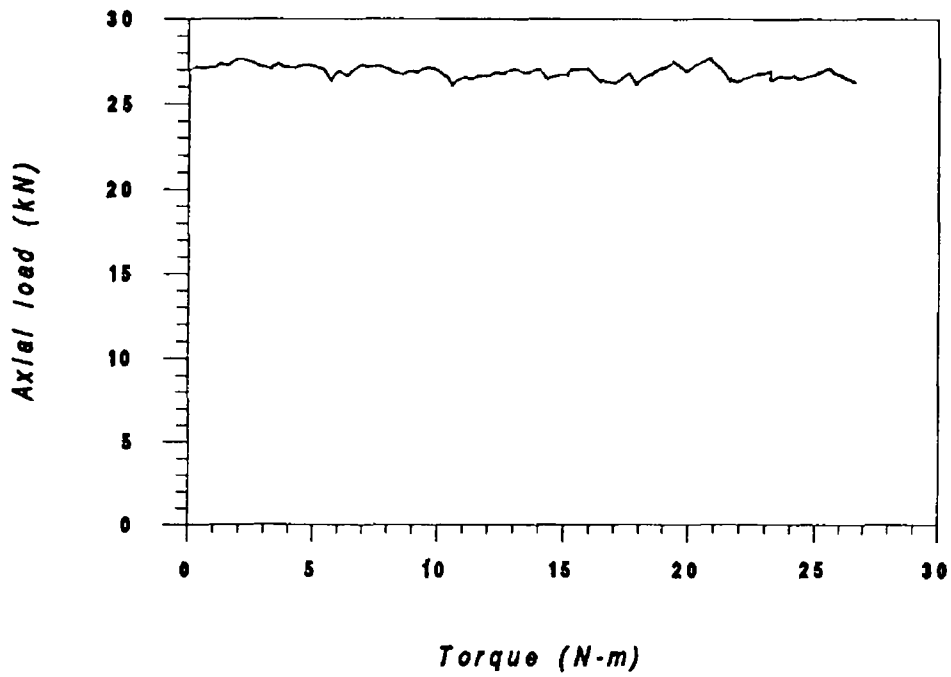


Figure 5 6(c) Torque versus axial load curve (load maintained constant)

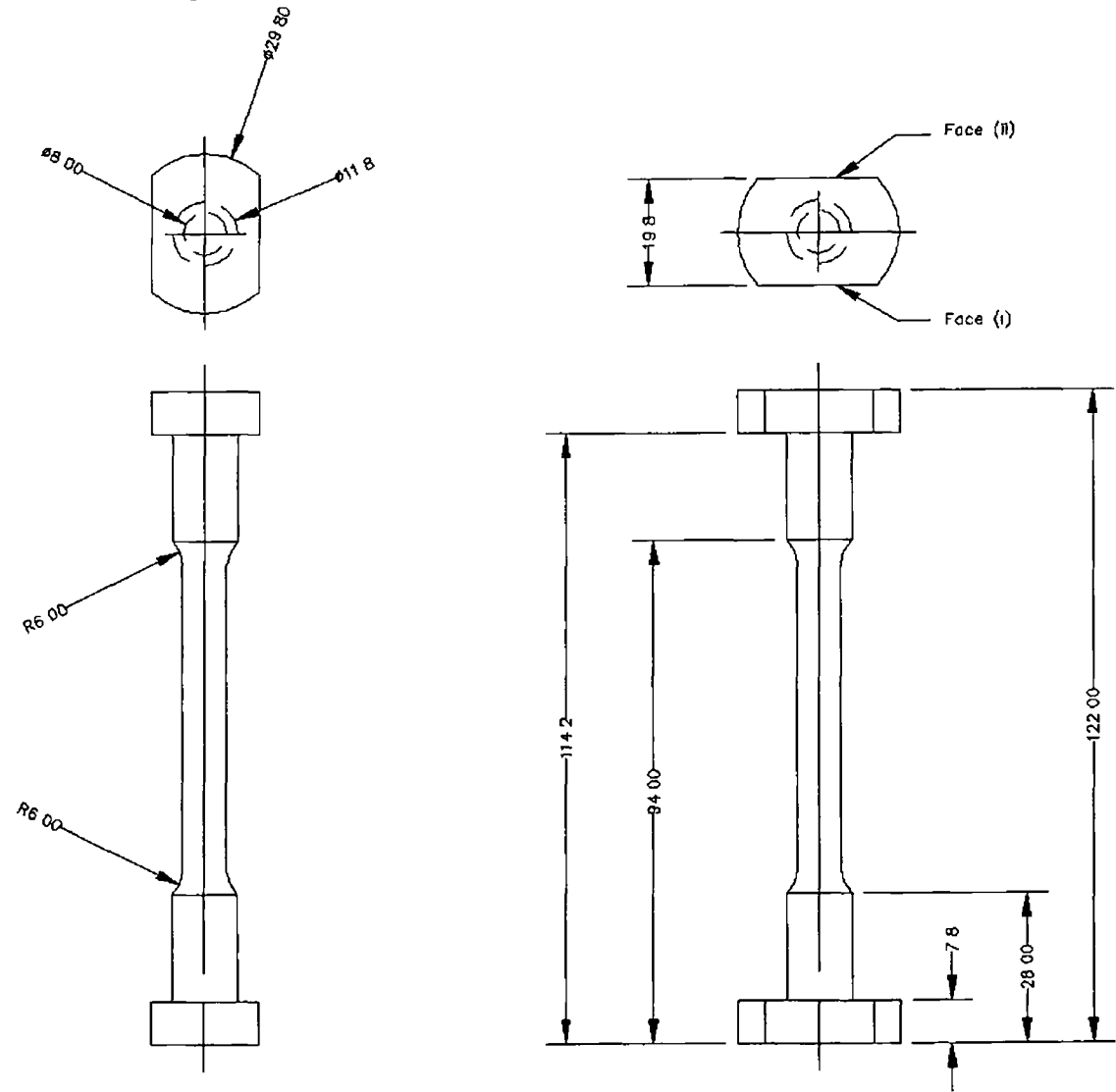


FIGURE 5.7 Geometry of the specimen

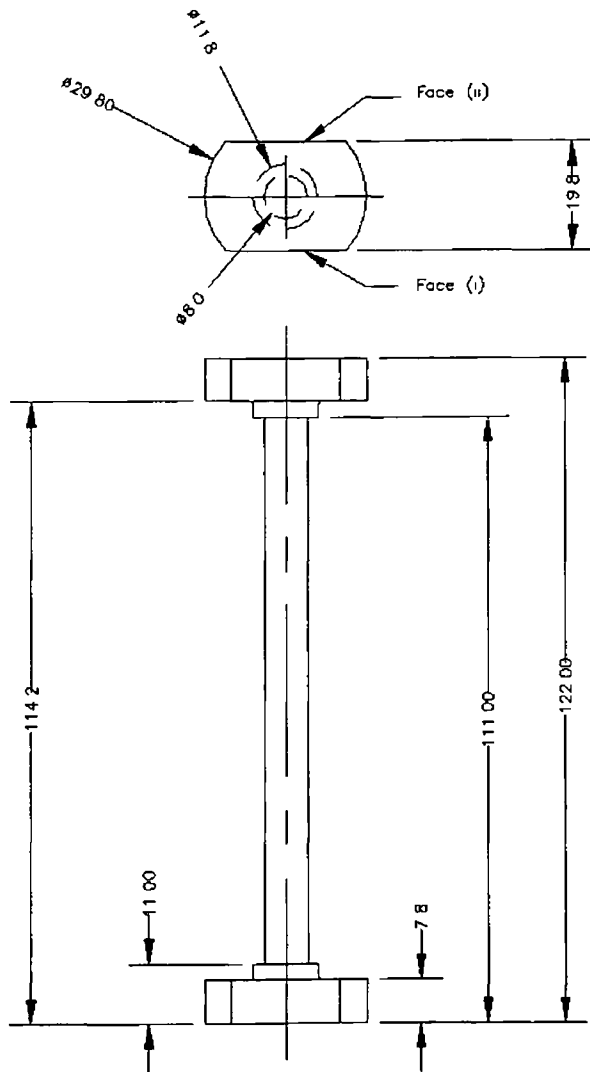


FIGURE 5.8(a) Geometry of the uniform diameter specimen

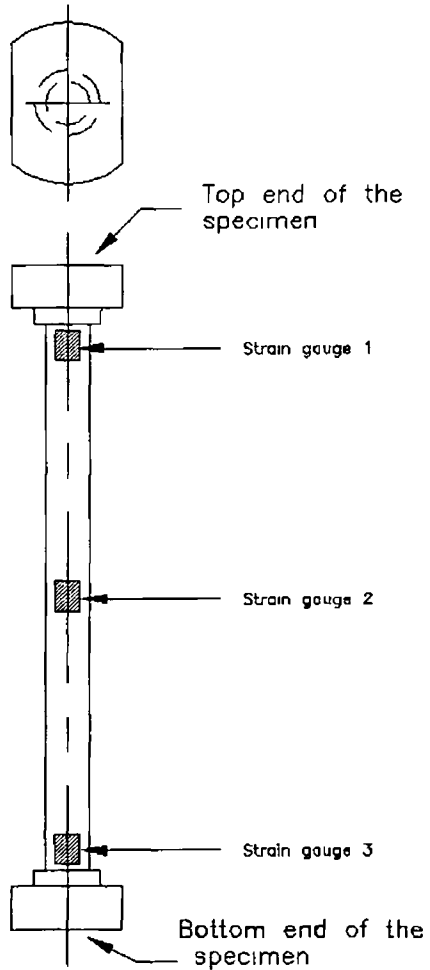


FIGURE 5 8(b) Position of the strain gauges in the uniform diameter specimen

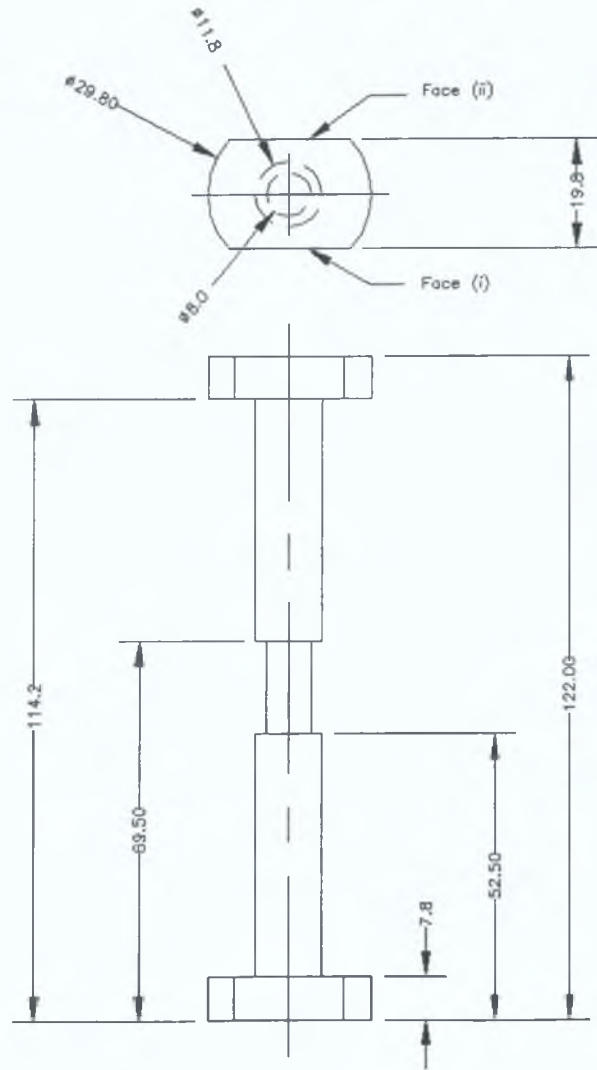


FIGURE 5.8(c) Geometry of the reduced section specimen

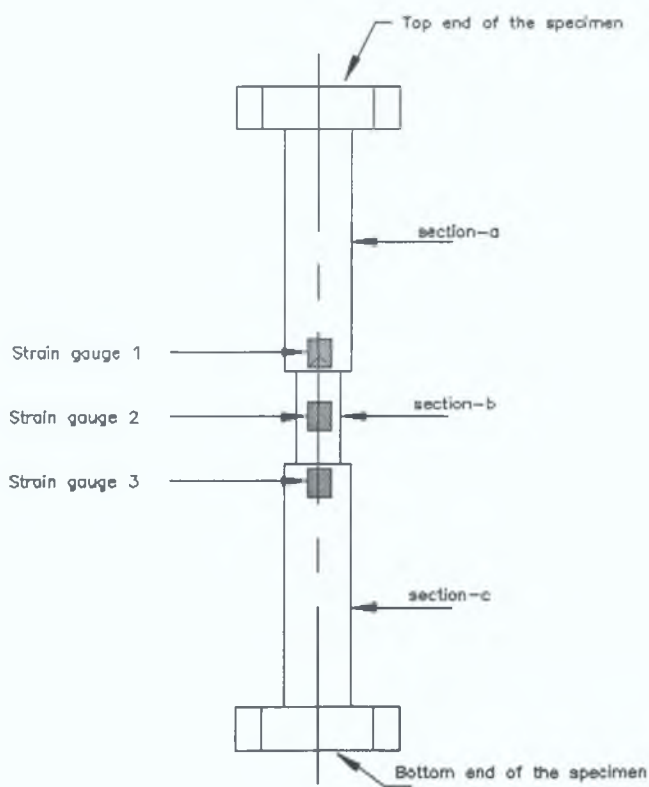


FIGURE 5.8(d) Position of the strain gauges in the reduced section specimen

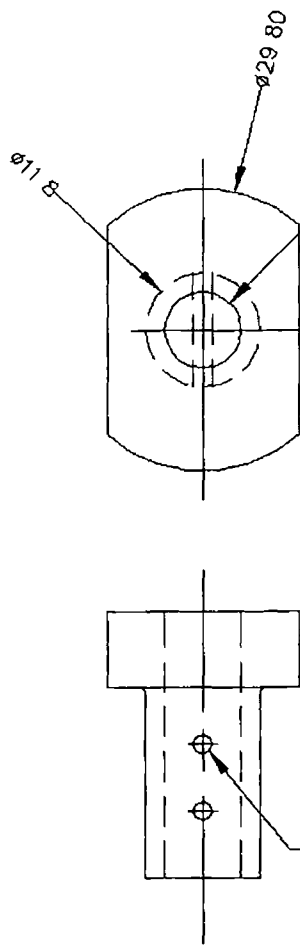
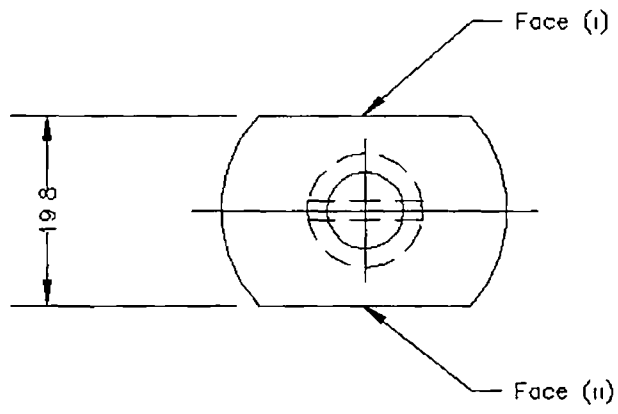
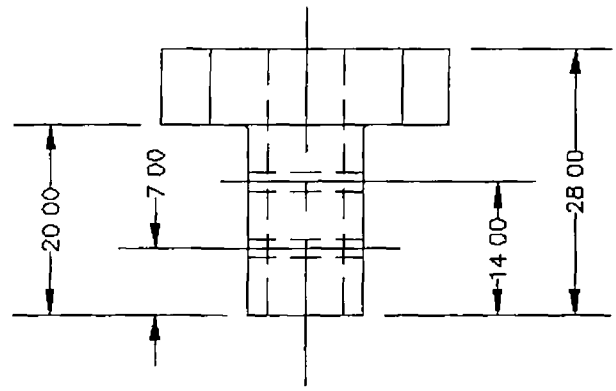


FIGURE - 5 9(a)

Ø8.00



- Ø2 two holes (h7)



Specially designed head to fit with the thin-walled tube

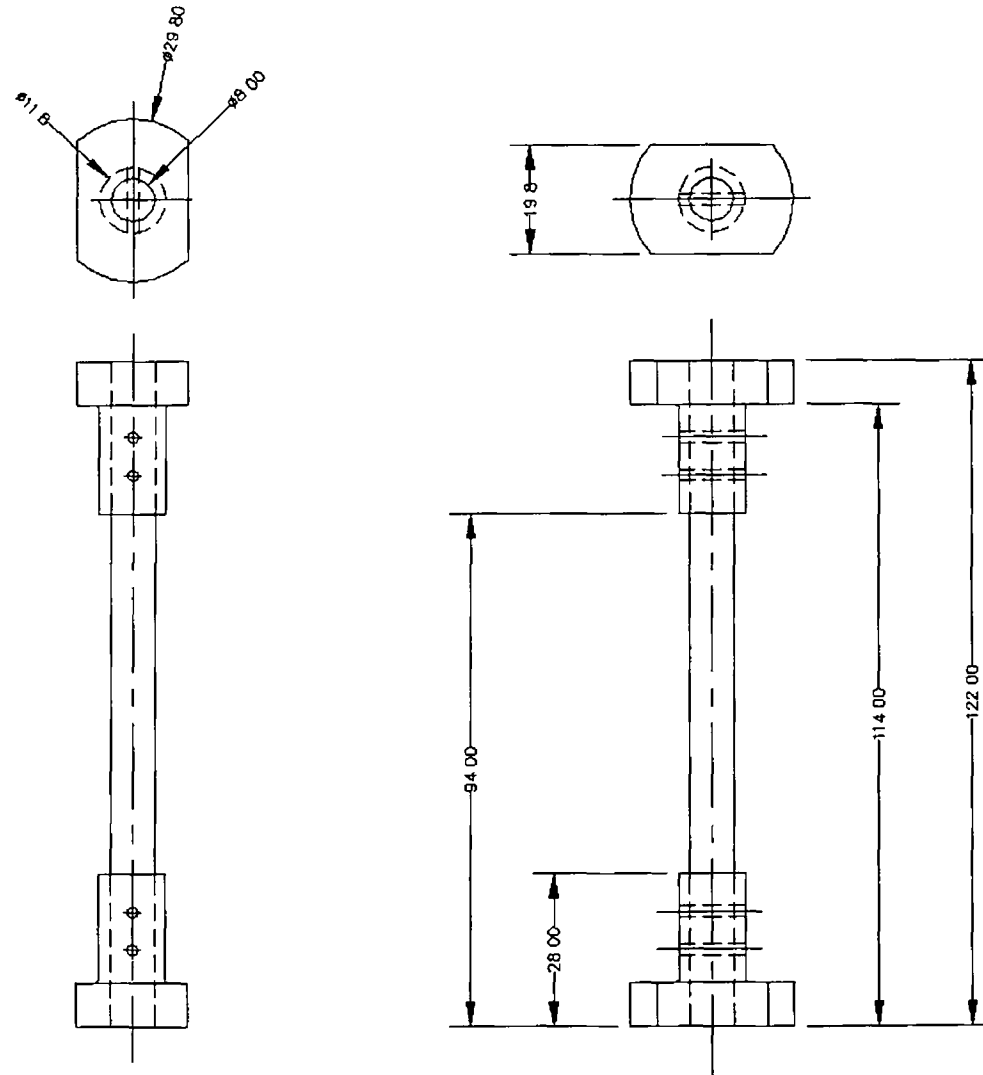


FIGURE - 5 9(b) The assembly drawing of the thin-walled tube



Strain gauge type CEA-06-250UN-350



Strian gauge type CEA-06-062UV-350



Strain gauge type EA-06-125TM-120

Figure 5 10 Different types of strain gauges used

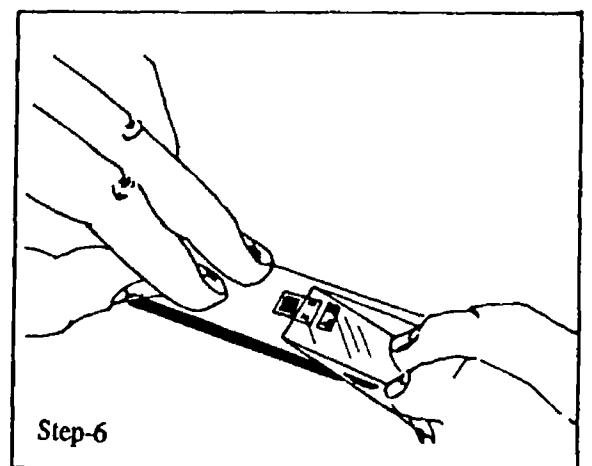
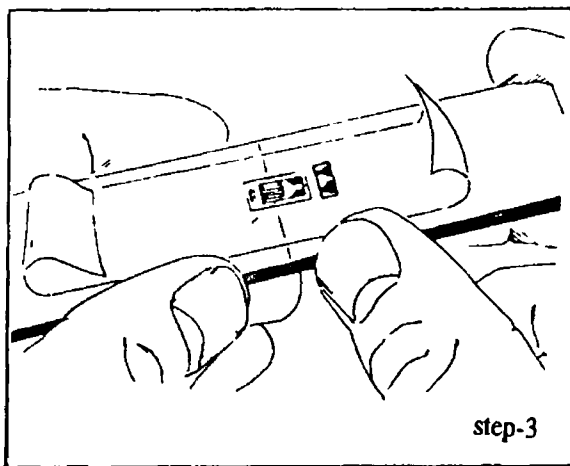
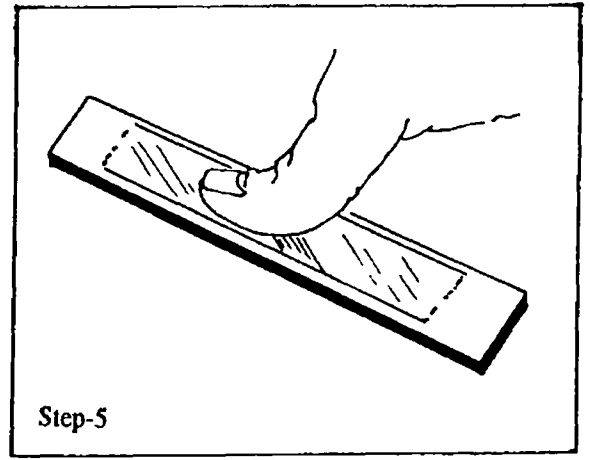
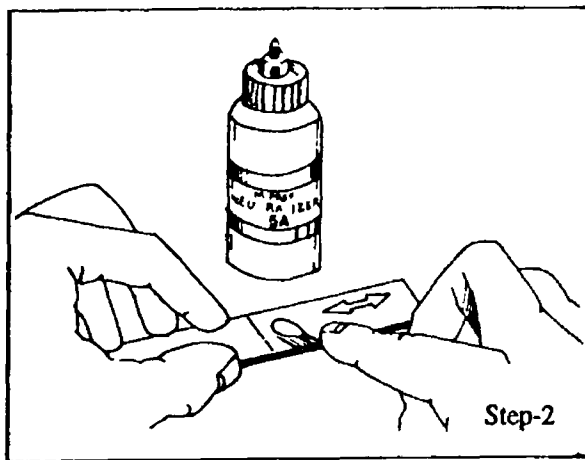
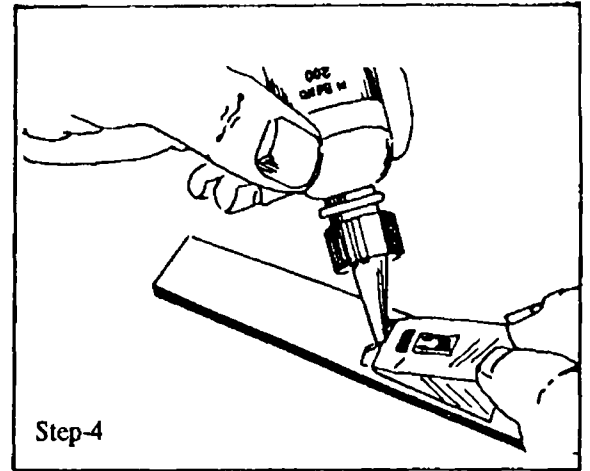
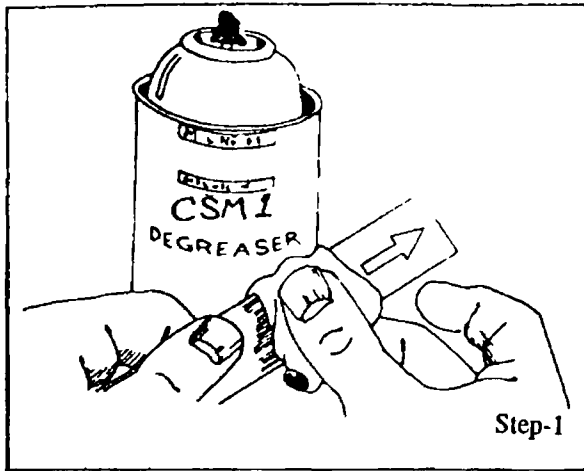


Figure 5 11 Different stages of strain gauge preparation

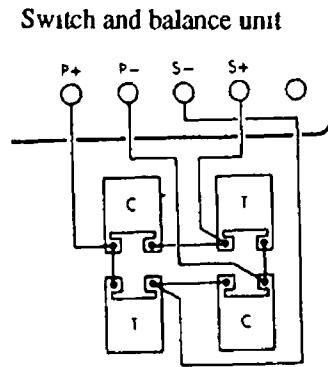


Figure 5 12(a) A typical full bridge connection between the strain gauges and the switch and balance unit

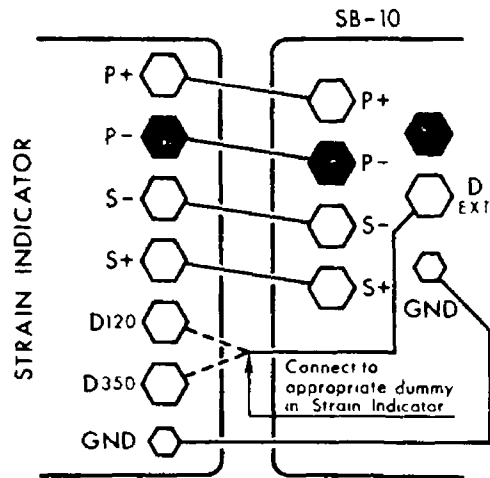


Figure 5 12(b) Circuit diagram between the strain indicator and the balance unit

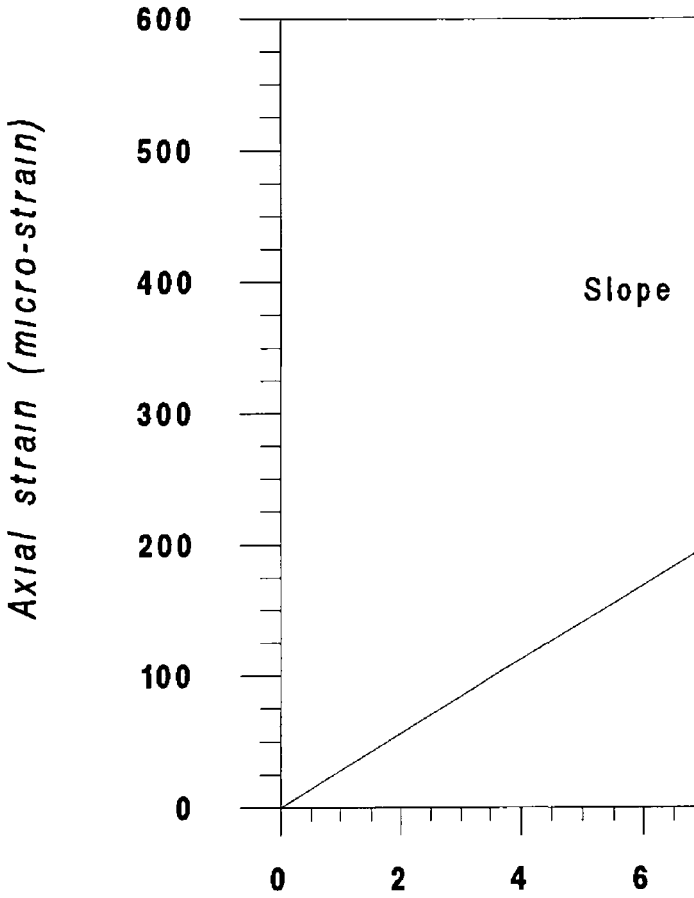
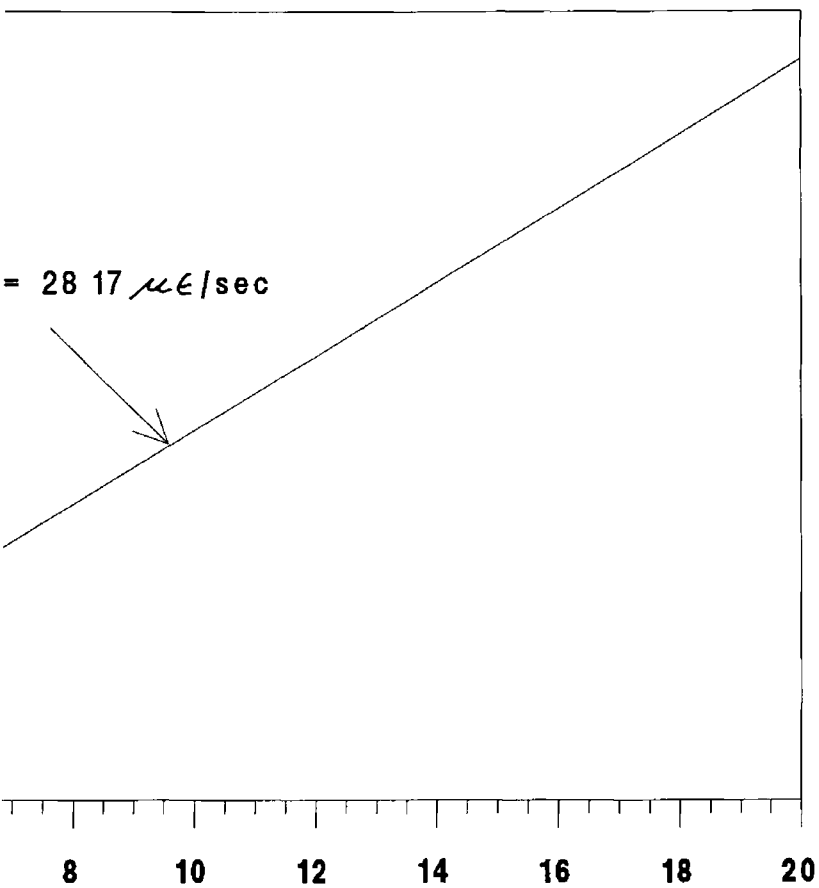


Figure 5.13 Axial



Time (sec)

strain versus time curve

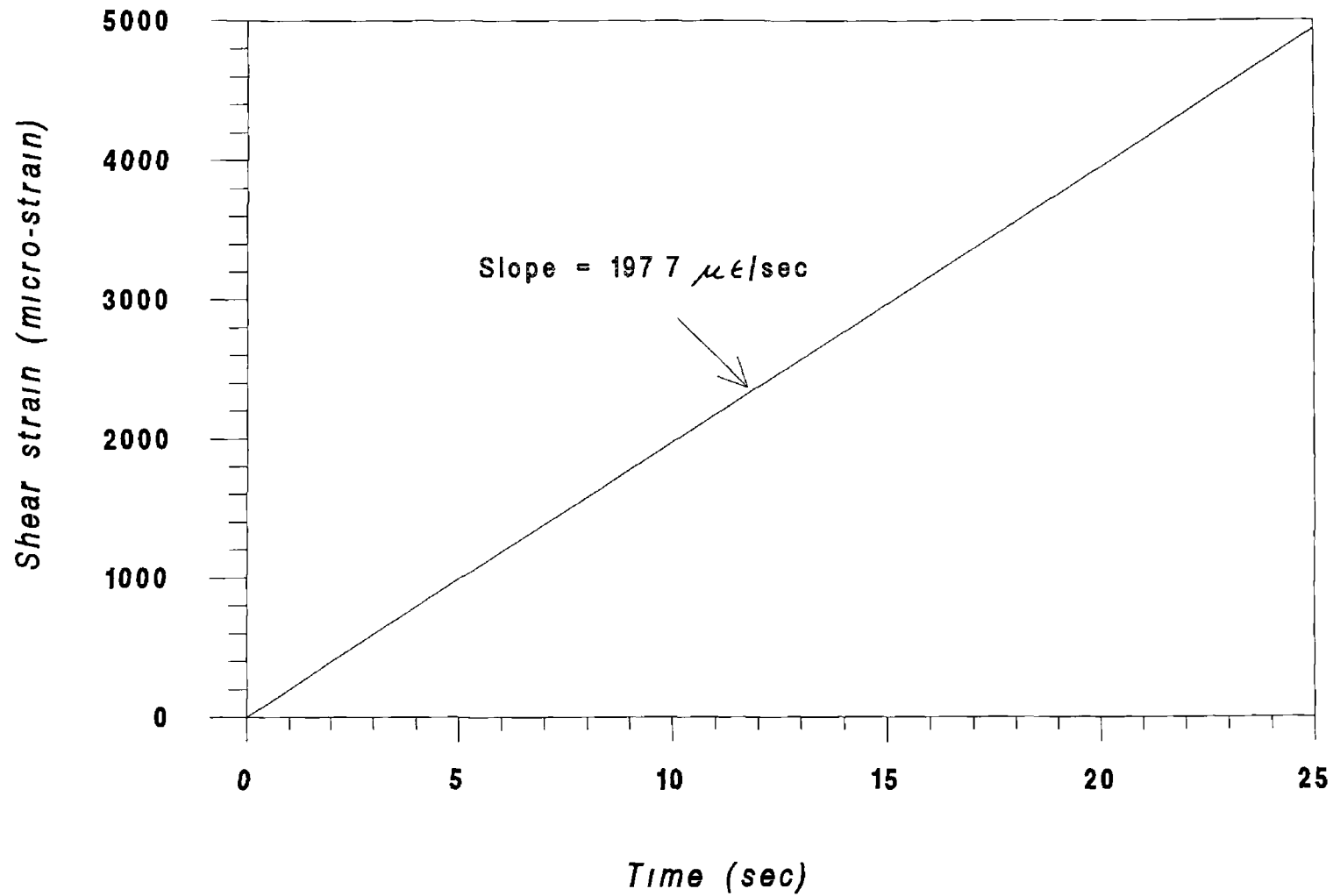


Figure 5.14 Shear strain versus the time curve

Digital strain indicator

Switch and balance unit

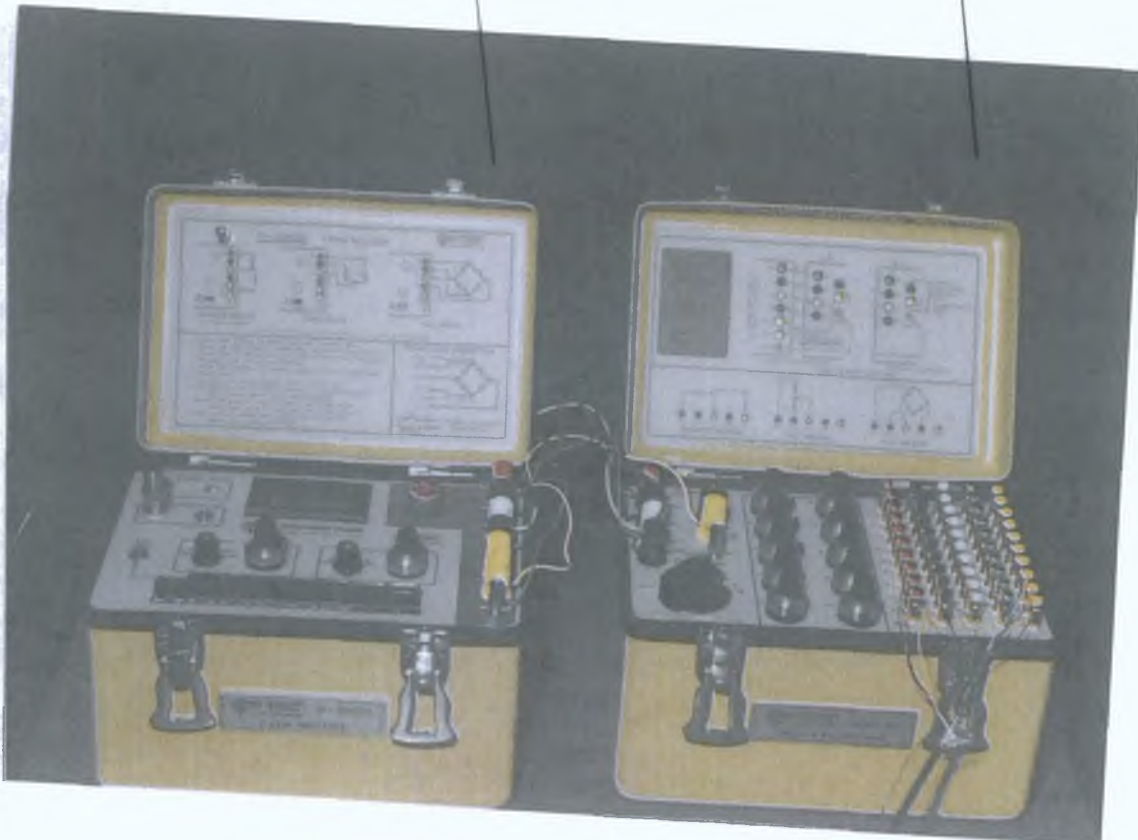


Plate 5.1 Photograph of the digital strain indicator and the switch and balance unit

CHAPTER SIX

ANALYSIS OF RESULTS AND DISCUSSION

6.1 INTRODUCTION

This chapter is devoted to the analysis and discussion of the experimental results carried out according to the procedures mentioned in section 5.5 of chapter five. The experimental investigation was aimed at (i) to observe the elastic-plastic response of a pre-stressed rod (i.e., either torque or tension) when subjected to subsequently applied parameters (i.e., either axial load or torque) under different controlled and boundary conditions, and (ii) to enhance better understanding of the mechanics of such response. To this end, a number of preliminary tests, such as uniaxial tensile and pure torsional tests, were conducted to determine the characteristics (i.e., uniaxial yield load and yield torque) of the material investigated. Subsequently, a number of biaxial loading tests were conducted details of which are given below. Six different types of biaxial loading paths were investigated as follows:

- (i) Initial torque of known level, within the elastic range of the material was applied, and then, axial load was gradually increased beyond the uniaxial yield load, holding the corresponding angle of twist constant.
- (ii) Procedure (i) was repeated except the applied initial torque, rather than angle of twist, was maintained constant.
- (iii) Initial axial load of known level, within the elastic range of the material, was applied and then, torque was gradually increased beyond the yield torque, keeping the initial axial displacement constant.
- (iv) Procedure (iii) was repeated except, in this case the initially applied axial load, rather than axial displacement, was maintained constant.

(v) Initial torque of known level, within the elastic range, was applied and then, holding the corresponding angle of twist constant, axial load was gradually increased until the specimen yielded due to the combined loading. Subsequently, small increments of torque and axial load were successively applied beyond the combined yield point, holding the axial displacement or the angle of twist constant in an alternate manner.

(vi) Initial axial load of known level, within the elastic range of the material, was applied and then, holding the corresponding axial displacement constant, torque was gradually increased until the specimen yielded due to the combined loading. Then, axial load and torque were successively applied beyond the combined yield point, holding the angle of twist or axial displacement constant in an alternate manner.

During the tensile loading the specimen was extended quasi-statically at a nominally constant axial strain rate of $1.6 \times 10^{-4} \text{ s}^{-1}$, while during the torque application the specimen was twisted at a constant shear strain rate of $2.1 \times 10^{-4} \text{ s}^{-1}$, unless otherwise stated. These controllable strain rates were set arbitrarily in such a way that they fall within the quasi-static range.

Furthermore, comparisons between the experimental and the theoretical results for loadings initially in torsion followed by tension, keeping the angle of twist constant, and in tension followed by torsion, holding the corresponding axial displacement constant, are also presented in this chapter. The experimental investigations were carried out to examine the biaxial behaviour of two commonly used engineering materials, mild steel (En8) and copper (BS-2874-C102). Thin-walled steel tubes were also considered during the investigation. It is worth noting that within the author's knowledge the biaxial loading programme for a solid rod undertaken during the present study has not been conducted by any other investigator, except what has been stated in the literature survey of this thesis as detailed in chapter two.

6.2 DEFINITION OF YIELD

Determination of the yield point is dependent on the definition of yielding used. From a theoretical point of view, the yield point can be defined as the point where permanent deformation begins to accumulate. However, experimentally it is difficult to determine this point. For this reason, researchers have drawn several conclusions from numerous investigations. The major discrepancies were caused by different materials used in the experiments and most importantly by the different definitions of yielding used in the investigation. The commonly used definitions are as follows: (i) Proportional limit method, where the yield point is defined as the point for which the relation between the stress and the strain is linear. This method is sensitive to the very earliest positive indication of yielding. (ii) Proof strain method, where the yield point is defined as the point for which a pre-determined amount of plastic strain is developed. Typically, a value of 0.2% strain offset is accepted. This method is widely used in most engineering applications. (iii) Lode extrapolation method [10], where the yield point is determined by backward extrapolation of stress-strain curve to intersect the elastic line, or to the line of zero plastic strain. This method requires an excessive amount of overstrain to define a yield point. During the present experimental investigations, the proportional limit and offset (for the steel investigated a value of 0.05% offset strain was considered) methods were used to define the yield stresses of the materials, as the differences between the yield and the ultimate stresses of the materials investigated were not large enough because of over hardening.

6.3 ELASTIC TESTS

UNIAXIAL TENSILE TESTS

To determine the necessary mechanical properties of both the steel and copper, uniaxial tensile tests were carried out on three separate specimens of each material investigated. The yield strength of the steel specimen was measured at 0.05% offset. The average yield load of the steel specimens was equal to 30.4kN and the standard deviation was 0.5312kN. This

deviation could be partly due to the non-homogeneity of the material and partly due to the difference in the tolerance of the diameters, which was ± 0.1 mm. Figure 6.1 shows the uniaxial tensile load versus engineering axial strain curve for the steel used in this investigation. The figure reveals that the specimen fractured nearly at 1.2% strain, which is very small compared to that of ordinary annealed mild steel. As the specimens tested were made from as-received material, the obtained yield load and therefore its corresponding yield stress was much higher than the manufacturer's supplied data because of over hardening of the material.

The nominal axial stress versus engineering axial strain curve for the steel is depicted in figure 6.2. Here the nominal stress has been plotted instead of the true stress because the specimen failed at very low strain. The yield stress calculated, for the corresponding yield load, was 605 N/mm² (MPa). The slope of the straight line from the origin to the proportional limit of a stress-strain diagram represents the modulus of elasticity. However, in the present study the modulus of elasticity was calculated from the straight line obtained during the unloading of the specimen to the stress free state. The average value of the modulus of elasticity for the steel was 212 GPa.

The uniaxial tensile test result for the copper specimen is shown in figure F.1 of appendix F, whereas the mechanical properties of the steel and copper are given in table 6.1. The normalised axial stress versus normalised axial strain curves for both materials are shown in figure 6.3. The figure also shows the comparison between the experimental stress-strain curves and those obtained theoretically, based on Ramberg-Osgood equation for different strain-hardening parameter (n), as detailed in chapter four (section-4.4). The figure reveals that because of the over hardening, both materials behaved almost like an elastic-perfectly plastic material.

Table - 6 1 Mechanical properties of the steel and copper

Materials	Modulus of Elasticity (GPa)	Modulus of Rigidity (GPa)	Tensile Yield Load (kN)	Yield Torque (Nm)	Tensile Yield Stress (MPa)	Shear Yield Stress (MPa)
STEEL (lot-1)	212	73	30 4	36 2	605	360
COPPER	115	49	12 5	15 1	249	150

PURE TORSION TESTS

Unlike the tension test, where the stress is uniformly distributed across the section of the specimen, in torsion test there is a stress gradient across the cross-section, and hence at the end of the elastic range yielding commences at the outer fibres first, while the core is still elastic. With continued twisting into the plastic range, more and more of the cross-section yields until the entire cross-section becomes plastic. The torque-shear strain diagram for the steel specimen is shown in figure 6 4. Unlike the tension test there is no fall off in the torque-shear strain curve, since necking does not occur and hence, strain-hardening occurs at a gradually decreasing rate as straining proceeds. For the steel specimens the yield torque was measured at the proportional limit whose value was equal to 36 2Nm and its corresponding yield shear stress was equal to 360MPa.

From the uniaxial tension test for the steel, the value of the tensile yield stress was equal to 605MPa, whereas for the same material its corresponding yield stress in shear was 360MPa. Thus the ratio of the yield stress in shear to the yield stress in tension for the steel was 0 59 and that of copper was 0 60. The torque versus shear strain curve for the copper is shown in figure F 2 of appendix F.

6.4 COMBINED LOADING OF SOLID BAR

6.4.1 TORSION FOLLOWED BY TENSION

Angle of Twist Held Constant

Of particular interest in the present study is the biaxial non-proportional loading of solid bars which were subjected to combined torsion and tension under different controlled conditions. In the first type of loading, the bar was first subjected to an initial torque and then, holding its corresponding angle of twist constant, the axial load was gradually increased beyond the uniaxial tensile load of the specimen. This procedure was repeated for four different initial normalised torque, $T(T/T_y)$ equal to 1.0, 0.75, 0.5 and 0.25.

With this type of loading it was possible to observe the nature of the variation of the initially applied normalised torque T with the subsequent application of the normalised axial load $F(F/F_y)$, as depicted in figure 6.5 for steel. The figure shows that for the quasi-static loading of the bar under investigation, the magnitude of the initially applied torque remains unchanged until the subsequently applied axial load causes the combined stress to reach the uniaxial yield stress of the material. As the axial load increases, the outer layers of the material begin to yield and the torque begins to decrease in a specific manner which is governed by the yield criteria. From figure 6.5 it is seen that when the initially applied torque is very close to the yield torque, i.e., $T = 1.0$, the torque starts to decrease as soon as the axial load is applied. Initially the torque decreases at a slower rate but as the axial load is further increased the torque decreases at a faster rate. When the axial load is increased nearly equal to the yield load, i.e., when $F = 1.0$, the normalised torque $T = 1.0$ decreases to about 0.72, thus resulting nearly 28% reduction in the initially applied torque.

However when the initially applied torque is nearly equal to 75% of the yield torque, i.e., $T = 0.75$, the applied torque remains unchanged until the normalised axial load F is increased to about 0.57 and in this case the normalised torque T decreases to about 0.64 when the applied load is increased to $F = 1.0$, which causes 14.6% reduction of the initial torque. For the case

when the initially applied torque is about 50% of the yield torque, the reduction of torque is very small at $F = 1.0$, and in this case the torque begins to decrease only when F is nearly equal to 0.93. However when the initial T is equal to 0.25, no reduction is observed in the torque with the increase of the axial load. During the present study, as the uniaxial yield load was defined at 0.05% offset, all the curves continued beyond the value $F = 1.0$, and moved towards the ultimate tensile strength of the specimen. From figure 6.5 it is evident that for all the cases, as discussed above, when the normalised axial load is nearly equal to 1.14, the specimens reach their uniaxial tensile strength and after that both the axial load and the torque start to decrease as necking starts.

From the above discussion it is clear that there is no reduction in the initially applied torque, and hence, no reduction in the corresponding shear stress as long as the combined stress does not reach a critical value. But when the combined stress in the bar becomes equal to a specific value, as dictated by the yield criteria, the material begins to demonstrate reduced capacity to carry the initially applied torque without in any way compromising the capacity to carry the axial stress. It is also evident from figure 6.5 that the higher the magnitudes of the initially applied torque, the greater is the rate of decrease of the torque carrying ability with the gradually applied axial load.

The data presented in figure 6.5 are replotted as normalised axial strain versus normalised torque and axial load curves as depicted in figures 6.6(a), 6.6(b) and 6.6(c) for different levels of initial torque, i.e., for T equal to 1.0, 0.75 and 0.5 respectively. These figures suggest that for the quasi-static extension of the bars due to the subsequently applied axial load, the initially applied torque carrying ability is reduced at a relatively slower rate than the rate of increase in the axial load. From these figures it is evident that though the specimens have yielded due to combined loading, well before the subsequently applied axial load causes yielding on its own, all the axial load curves follow the profile of the uniaxial tensile load curve. Thus from the above discussion it can be concluded that for this particular type of

biaxial loading and when the yielding commences, the sustaining ability of the material of different levels of initially applied torque becomes drastically reduced, with the increasing subsequently applied axial load, without in any way affecting its axial load carrying ability

Figures 6.6(a)-6.6(c) also show that, when the material yields due to combined loading, at first the initially applied torque decreases at a faster rate with the increase of the axial load. But as the axial load reaches nearly equal to its uniaxial tensile strength, whose corresponding normalised axial strain is about 1.65 (i.e., nearly 0.5% strain), the torque decreases relatively much slowly and soon the curves become flat. This is due to the fact that when the applied axial load becomes equal to its ultimate load, necking starts, and hence after that the axial load begins to decrease so that as the decrease in the axial load no longer satisfies the yield criteria, the torque soon stops decreasing and becomes constant. Thus the remaining torque carrying ability of the material is left unchanged.

However if the material were not over hardened and if it had not reached its ultimate strength for such a small value of the axial strain (only 0.5%), the reduction in the torque would have been much more than that in the present case, as it is known from the theory of plasticity that the behaviour of the material is strongly dependent on the strain path in the plastic region. It is worth noting that for the biaxial loading path investigated, the total reduction in the initially applied torque, before the torque curves become flat, is about 54%, 40% and 14% for the initial values of T equal to 1.0, 0.75 and 0.5 respectively.

For the same type of biaxial loadings, as discussed above, figure 6.7 represents the normalised torque versus normalised axial load curve and, figures 6.8(a), 6.8(b) and 6.8(c) show the normalised axial strain versus normalised torque and axial load curves for the copper specimens. All these figures show the similar trends like those obtained for the steel. From figure 6.7 it is seen that, for the initial $T = 1.0$, the torque reduces by nearly 34% when F is about 1.0. However, before the torque curves become flat, the total reduction in the initially

applied torque is 55%, 46.6% and 30% for the initial value of T equal to 1.0, 0.75 and 0.5 respectively

Torque Maintained Constant

The results for second case where the initial torque, rather than the angle of twist, was maintained constant when an increasing axial load was applied are depicted in figure 6.9 for the steel specimens. Here the normalised shear strain $\underline{\gamma} (\gamma/\gamma_y)$, instead of the angle of twist, is plotted against the normalised axial strain $\underline{\epsilon} (\epsilon/\epsilon_y)$. The results reveal that initially the engineering shear strain remains constant for a given initial torque. But as the axial load, and hence the axial strain, increases the outer layer begins to yield and, as the torque carrying ability reduces, to maintain the initially applied torque constant, the shear strain begins to increase rapidly. This procedure was repeated for four different initial torques, $T = 1.0, 0.75, 0.5$ and 0.25 . From the figure it is also evident that the higher the value of the initially applied torque, the greater is the rate of increase of the shear strain with the increase of the axial strain.

During the application of the initial torque, the shear strain rate was maintained arbitrarily at $8.3 \times 10^{-3} \text{ s}^{-1}$. Here the initially applied torque maintained constant and the axial load is gradually increased, so that when yielding starts to counter the reduced capability for carrying the torque a higher twisting rate (i.e., a higher shear strain) is maintained. This particular type of biaxial loading tests was only conducted for the steel specimen.

6.4.2 TENSION FOLLOWED BY TORSION

Axial Displacement Held Constant

In the third type of non-proportional loading, the specimen was first subjected to tension and then, keeping its corresponding axial displacement constant, the torque was gradually applied.

beyond the yield torque of the specimen at a nominal constant twist rate. This procedure was repeated for four different initial axial loads, $F = 0.97, 0.75, 0.5$ and 0.25 .

For this particular type of loading, the variations of the normalised axial load F and the normalised torque T for the steel are depicted in figure 6.10. This figure shows that with the gradual increase of the torque, the axial load remains unchanged until the outer layer of the rod begins to yield and the axial load carrying ability of the rod starts to decrease in a specific manner which is governed by the yield criterion. The figure also reveals that initially the axial load decreases slowly, but after $T = 1.0$, the axial load decreases rapidly as the load carrying capability is drastically reduced.

It is seen from the figure that when the initially applied axial load is nearly equal to its yield load, i.e., when $F = 0.97$, the axial load begins to decrease sharply with the increase of the torque. Here the axial load starts decreasing when the value of the normalised torque is about 0.16 and, when the torque is increased nearly equal to its yield torque, i.e., $T = 1.0$, the normalised axial load decreases to about 0.86 , thus causing nearly 11.3% reduction in the initial load. However when the initial axial load is about 75% of the yield load, i.e., $F = 0.75$, the axial load begins to decrease only when the normalised torque is increased to about 0.73 . And when $T = 1.0$, the axial load only decreases to about 0.72 which results only about 4% reduction in the initial load. For the other cases, where the initially applied loads are nearly equal to 50% and 25% of the yield load, the axial loads begin to decrease only when the normalised torque increases to about 0.83 and 1.35 respectively. However when T becomes equal to 1.4 , total reduction in the initial loads are nearly 30% , 24% and 20% , for the curves with initial value of F equal to $0.97, 0.75$ and 0.5 respectively. Furthermore, during this particular type of biaxial loading, as the yield torque was defined at the proportional limit, all the curves have exceeded the value $T = 1.0$ and moved towards the maximum torque the specimen can carry.

From the above discussion it is clear that when the combined stress in the bar under investigation becomes equal to a specific value, as dictated by the yield criteria, the material begins to yield and exhibits reduction in the ability to sustain the initially applied axial load, and hence in the corresponding normal stress. Furthermore, the above discussion also reveals that the percentage of reduction in the initially applied load due to the applied torque, is much lower than the percentage of reduction in the initially applied torque due to subsequently applied axial load. Figure 6.10 also reveals that the higher the values of the initially applied axial load, the greater the rate of decrease of these loads with the subsequently applied torque.

The data presented in figure 6.10 are replotted as normalised shear strain versus normalised axial load and torque curves and are depicted in figures 6.11(a)-6.11(d) for different initially applied axial loads. Figure 6.11(a) shows the variation of the initially applied normalised axial load and subsequently applied torque with the shear strain, when the initially applied axial load is nearly equal to yield load, i.e., $F = 0.97$. The figures 6.11(b), 6.11(c) and 6.11(d) show similar plots but with the initial load F equal to 0.75, 0.5 and 0.25 respectively. In similarity with the first type of loading, these figures reveal that for the subsequent quasi-static twisting of the bar, the increase in the torque and hence increase in the shear stress develops faster than the decrease in the axial load and the corresponding normal stress. It is also clear from these figures that even though the material yields due to the combined loading well before the subsequently applied torque reaches its yield torque, all the torque curves almost behave identically. Thus from the above discussion it can be concluded that for this particular type of biaxial loading and when the yielding begins, the axial load carrying ability of the material becomes considerably reduced, with the increasing torque, without in any way affecting its torque carrying ability.

However, unlike the first type of loading where the initially applied torque stopped decreasing when the applied axial load reached the uniaxial tensile strength of the rod, in the present

case, the initially applied axial load decreases continuously with the subsequently applied torque, at first rapidly and then slowly but almost at a constant rate. This is due to the fact that because of the combined loading the yielding commences in the outer fibres first, while the core remains still elastic. With continued twisting more and more of the cross-section yields and hence the plastic zone progresses towards the core of the bar investigated with more reduction in ability to sustain the initially applied axial load.

Figure 6.12 shows similar biaxial loading behaviour of the copper specimens, where the normalised axial load is plotted against the normalised torque. Figures 6.13(a), 6.13(b), 6.13(c) and 6.13(d) show the normalised shear strain versus normalised axial load and torque curves, for different initial axial load, F equal to 1.0, 0.75, 0.5 and 0.25 respectively. All the figures show the similar trend like those of steel specimens. However from figure 6.12 it is seen that, for the initial load $F = 1.0$ curve, the total reduction in the initially applied load is about 20% when the subsequently applied torque is nearly equal to its yield torque, i.e., when $T = 1.0$.

Axial Load Maintained constant

In the fourth case where the initially applied axial load, rather than the axial displacement, was maintained constant with the subsequently applied increasing torque is shown in figure 6.14 for the steel specimens. The results show that initially the engineering axial strain remains constant until the combined stress reaches the uniaxial yield stress of the material. Then, with further increase of the torque, and hence the shear strain, the axial strain starts to increase rapidly to maintain the initially applied load constant and compensate for the reduction in the load carrying ability of the rod. This procedure was repeated for four different initial axial load, as detailed in figure 6.14. The figure also reveals that the higher the magnitude of the initially applied axial load, the greater is the rate of increase of the axial strain with the shear strain. It is worth noting that for the above mentioned type of biaxial loading, the axial strain rate was maintained arbitrarily at $6.8 \times 10^{-3} \text{ s}^{-1}$. Here a higher axial strain rate is maintained so

that the specimen can relax (when yielding begins) at a faster rate to keep the initial load constant

6.4 3 DETERMINATION OF YIELD POINTS DUE TO COMBINED LOADING

For the four types of biaxial loadings, just described, it was possible to determine the magnitudes of the combined stresses when the material yielded due to combined loading. During the present study only the first and the third cases were considered. The experimental results of the first case, shown in figure 6 5 for the steel and in figure 6 7 for the copper, are replotted in terms of the axial and shear stresses and are depicted in figures 6 15 and 6 16 respectively. Similarly the experimental results of the third case, shown in figures 6 10 and 6 12 for the steel and copper, are replotted and depicted in figures 6 17 and 6 18 respectively. Here the shear stress, from the corresponding torque reading, was calculated according to the procedure described by Nadai [9] as detailed in appendix E (section E 3).

The solid lines, (except the line "ab" which is the Mises yield locus based on the proof stress) shown in figures 6 15 and 6 17, depict the Mises yield loci based on the post-yield flow stress of the steel investigated. These figures reveal that most of the experimental points of the combined loading fall within the domains contained by these yield loci (i e , based on post-yield flow stress). However, few points remain outside these domains which may be due to the fact that von Mises yield criteria alone is not the governing factor of the material response within the plastic region, as it is well known that the behaviour of the material is strongly dependent on the strain path in the plastic region. Furthermore, it is seen from both figures that most of the experimental points overshoot the yield loci based on the initial yield stress (i e , proof stress), which is because of the strain-hardening of the materials. It is worth mentioning that during the uniaxial tensile and pure torsion tests the yield load and the yield torque of the steel investigated were defined at 0.05% offset and at the proportional limit point respectively. Figures 6 16 and 6 18 show the similar comparison between the

experimental results for the copper and the von Mises yield criteria, which reveal identical trend like those for the steel

To calculate the combined stress (i.e., equivalent stress) of the material when yielding started, the following procedure was adopted. As shown in figure 6.15, the initially applied shear stress of the material remains constant until the axial stress reaches a certain magnitude when plastic yielding commences. Thus the axial stresses, which correspond to the initiation of the decrease of the shear stresses, were determined from that figure. These axial stresses, thus obtained, and the initial values of the shear stresses were normalised and plotted in figure 6.19(a) for the steel. Similar procedures were followed for the other cases. Figure 6.19(b) shows the similar plot for the copper. In these figures, the upper solid line represents von Mises' criteria, whereas the lower one is that of Tresca's. The von Mises' and Tresca's curves were drawn according to the equations E.4 and E.5 of appendix E. It is worth noting that here the normalised shear stress is defined as $\underline{\tau} = \tau/\tau_y$, where τ_y is the yield stress in shear according to the von Mises' criteria. However, from figures 6.19(a) and 6.19(b) it is observed that though some of the points for copper have good agreement with the Tresca's criteria, but majority inclines towards Mises' ellipse, specially for the steel investigated. Thus it can be concluded that the results confirm the general opinion that the best yield criteria for metals is that of Mises and the loss of initially applied torque or load sustaining ability will be governed by this criteria.

From the above discussion and the results presented in the previous section, where the bars were subjected to four different types of biaxial loadings, it can be concluded that the torsional or the tensile stress carrying capability of a pre-torqued or a pre-loaded specimen starts to reduce (with the increasing load or torque) when the plastic deformation begins due to plastic yielding of the material.

6.5 MECHANICS GOVERNING THE RESPONSE UNDER COMBINED LOADING

As seen from the results of the first type of tests that for a pre-torqued specimen subjected to subsequently applied axial load whilst maintaining the angle of twist constant, the rod's capability to sustain the initially applied torque is reduced with the increase in the axial load. Such decrease in the torque carrying capability is easily recorded by means of the torque transducer. Previous investigators used strain gauges attached to the body of the rod to record such reductions even though the angle of twist was apparently kept constant. Question is thus raised as to the mechanics of deformation in the body of the rod between the two fixed ends which would cause the strain gauge readings to be reduced to indicate a fall in the torque.

Similarly, the mechanics of deformation in the body of the rod between the two fixed ends initially subjected to an axial load and then holding the axial displacement constant, subjected to gradually increasing torque, needs to be understood to understand the strain gauge readings showing fall in the axial load. A series of experiments were therefore carried out to enhance better understanding of this response.

To this end all the following tests were carried out using steel specimens made from the second lot of the steel, i.e., steel-2. The uniaxial tensile and the pure torsion tests for this steel are shown in figure F 3 and F 4 of appendix F and the mechanical properties are given in table F 1 of the same appendix.

Tests With Uniform Diameter Specimen

A number of biaxial tests were carried out with shear strain gauges attached at three different locations, at the top, middle and bottom, of uniform diameter specimens. Details of the specimen are shown in figure 5 8(a) of chapter five and positions of the strain gauges 1, 2 and 3 are shown in figure 5 8(b). Four steel specimens were used during this particular type of

loading Each specimen was subjected to an initial torque which was nearly equal to the yield torque of the specimen Then the rod was subjected to a gradually increasing axial load, and hence axial strain, whilst the angle of twist was kept constant The variation in the initially applied torque measured by the torque load cell, together with the variation in the three strain gauge readings, were recorded simultaneously and shown in figures 6 20(a), 6 20(b), 6 20(c) and 6 20(d) for specimens 1, 2, 3 and 4 respectively The figures reveal that all three strain gauges, attached to each specimen, gave different torque readings with the decrease of the torque as recorded by the torque transducer Some gauges showing increase and some showing decrease in the torque even when the angle of twist was kept constant Thus it can be concluded from the above that, when the plastic deformation begins, the measurement of the torque reduction using a strain gauge is dependent on its (gauge) location on the specimen To have a clear understanding as to the mechanics of such response, tests were conducted on reduced section specimens in order to simulate the preferential location for plastic deformation and unloading at all other locations

Tests With Reduced Section

Two biaxial loading tests, one similar to the first type of loading and the other to the third type, were conducted with the fitted strain gauges on the specimens During the tests the design of the specimen was modified as detailed in figure 5 8(c) of chapter five The reduced diameter section, shown in the figure, is provided to help initiate the localised plastic deformation, when yielding starts due to combined loading In the first test, three pairs of shear strain gauges were attached to a steel specimen and were positioned in section-a, section-b and section-c respectively Details of the strain gauges' positions are shown in figure 5 8(d) Then the bar was subjected to an initial torque of 30Nm, which was nearly equal to 75% of its yield torque Next, keeping the corresponding angle of twist constant, the axial load was gradually increased by extending the specimen quasi-statically Here, the variation in the initially applied torque as given by the torque transducer, along with the variation in three strain gauges' readings, were monitored simultaneously and presented in figure 6 21(a) It is

worth mentioning that the resulting shear strains obtained from strain gauges 1, 2 and 3, due to the initially applied torque, are 1196, 3702 and 1111 $\mu\epsilon$ respectively

Figure 6 21(a) reveals that initially the torque, together with the shear strains, remains constant with the increase of the axial strain, as dictated by the elastic theory. As the axial strain is further increased, the material begins to yield and the torque starts to decrease. Furthermore, from the figure it is also observed that when the initially applied torque begins to decrease due to the yielding of the material, the shear strain recorded by the gauge 2 increases very rapidly with the increase of the axial strain, while the strains recorded by both the gauges 1 and 3 decrease very slowly and almost at a constant rate.

The results just described above demonstrate the followings. When the specimen is yielded due to the combined loading, the yielding starts at the narrow zone, where the gauge 2 is attached. So that with the increase of the axial load, and hence the axial strain, the torque sustaining ability of section-b decreases drastically. But as both section-a and section-c of the specimen still remain elastic, the decrease in the torque sustaining ability in section-b causes section-a to rotate in the reverse direction (i.e., opposite to the direction of initial torque application) and section-c in the same direction for the elastic recovery of the specimen and for this reason the shear strain developed in section-b is very high. Thus it can be concluded from the above discussion that, though the overall angle of twist of the specimen was kept constant after applying a certain initial torque, the shear strain increases very rapidly at the confined zone where the localised yielding takes place, and hence the plastic deformation commences. As such strain gauges attached in this zone would indicate an increase in torque whereas strain gauges attached outside this zone would indicate a decrease in torque. Therefore, to rely on the strain gauge readings alone, when a uniform cross-section rod is tested, the results may be suspect as the location of the strain gauge may influence the results and cause erroneous observations. Thus, it appears that a uniform cross-section rod would preferentially yield at certain location(s) causing more localised twist (i.e., increase in the

strain gauge reading) and causing anti-twist at other locations (i.e., decrease in the strain gauge reading), which has been found true during the biaxial tests with the uniform diameter specimens. Furthermore, from these particular type of tests, i.e., tests with the uniform diameter specimens, it is observed that in case of specimens 1, 2 and 3 (as shown in figures 6.20(a), 6.20(b) and 6.20(c) respectively) yielding has started at the top ends of the specimen, where shear strain increases rapidly with the decrease of torque measured by the torque transducer. However, this particular behaviour of the specimens, i.e., yielding preferentially taking place at the top ends (except specimen 4), needs further study.

In the second test, a similar steel specimen was used where three pairs of axial strain gauges were attached and positioned in section-a, section-b and section-c respectively. The bar was then subjected to 24.5 kN initial load, which is approximately equal to 75% of the yield load. After that, holding the corresponding axial displacement constant, a torque was gradually applied to the specimen quasi-statically. The reduction in the initially applied load and strain gauges' readings were recorded and are plotted against shear strain as shown in figure 6.21(b). The figure reveals similar test results like those of the first type of test. It is seen from the figure that until the material is yielded due to the combined loading, the initial load as well as all the axial strains remain constant. However, when the material begins to yield, the axial strain measured by gauge 2 starts increasing and increases very rapidly, while the strains recorded by both the gauges 1 and 3 decrease very slowly and almost at a constant rate. This happens due to the similar reason as mentioned in the previous case. Thus it can be concluded from the second test results that, although the axial displacement of the specimen was held constant after applying a certain initial load, the axial strain increases very rapidly at the confined zone where the localised yielding, and hence the plastic deformation commences.

Furthermore, the findings of the above two mentioned tests illustrate the followings. When a bar is subjected to an initial torque or axial load and then, to a gradually increasing load or torque, keeping the corresponding angle of twist or axial displacement constant respectively,

measurement of reduction in the initially applied torque or axial load sustaining capability of the rod using strain gauges will be erroneous and unreliable if they are attached to the zones where the plastic deformation begins

6.6 SUCCESSIVELY APPLIED ALTERNATING TORQUE AND TENSION

In order to investigate further the aspect of the reduction in sustainability of the subsequently applied axial load or torque to a rod, initially subjected to a torque or axial load respectively, the subsequently applied load/torque was alternated in succession and the results are reported in this section. During this particular type of biaxial loading both the torque and the axial load were successively applied. The materials used during these tests were, the second lot of steel, i.e., steel-2, and the same copper.

Torque Applied First

With this particular type of biaxial loading it was possible to observe the effect of the successively applied axial load or torque on the initially applied torque or axial load of the material investigated. In this type of loading, the bar was first subjected to a known initial torque, within the elastic limit of the material and then, holding the corresponding angle of twist constant, the axial load was gradually increased until the specimen yielded due to the combined loading. Subsequently, small increments of torque and axial load were applied successively beyond the combined yield point, holding the axial displacement or the angle of twist constant, as appropriate, in an alternate manner. This procedure was repeated for three different initial torques.

For the steel, figures 6.22(a), 6.22(b) and 6.22(c) show the variation in the normalised torque and axial load with time for different initial torque, T equal to about 0.98, 0.75 and 0.5 respectively. During this particular type of loading, the axial load was successively applied in such a way that, when the yielding started, the percentage of reduction in the initially applied

torque was within 10-20% and during the subsequent application of the torque, it was gradually increased nearly upto its initial value

The figures reveal that, when the material is yielded due to the combined loading, at first the initially applied torque starts to decrease with the axial load. Then, subsequently when the torque is increased, holding the axial displacement constant, the axial load begins to decrease immediately. Thus it is seen from the figures that with the successive application of the axial load and the torque, (when yielding starts) the increment in the axial load results reduction in the torque and the increment in the torque results reduction in the axial load. Hence it can be concluded that the effect of the axial load or the torque, whichever is applied subsequently, is dominant on the specimen investigated. This happens due to the fact that according to the von Mises yield criteria the total stress in a material is equal to that corresponding to the uniaxial yield stress in pure tension and is constant, provided there is no strain-hardening of the material. So that for the above mentioned type of loading, when the combined stress due to the biaxial loading exceeds a critical value, the material can no longer carry that excess energy. As a result, when the material yields, any increment in the axial load, and hence any increment in the normal stress, causes instantaneous reduction in the torque, and hence in the shear stress, to satisfy the yield criteria. Furthermore, it is also observed from figures 6.22(a), 6.22(b) and 6.22(c) that subsequently when the axial load is gradually increased, the material soon regains its axial load carrying capability irrespective of the level of the initially applied torque.

Figure 6.22(a) shows that when the normalised axial load increases from zero to about 0.63, i.e., from point **a** to **b** as shown in the figure, the initially applied torque decreases from T equal to about 0.98 to 0.84, i.e., from **m** to **n**, which causes nearly 14.2% reduction in the initially applied torque. Then subsequently when the torque is increased from T equal to 0.84 to nearly to its initial value, i.e., from **n** to **o**, the normalised axial load decreases from 0.63 to about 0.57, thus results only 9.5% reduction in the axial load. Again the increase of the

normalised axial load from 0.57 to about 0.9, i.e., from **c** to **d**, causes nearly the same amount of drop in the torque. When the torque is again increased by nearly the same amount, from point **p** to **q**, the normalised axial load drops from 0.9 to about 0.83, i.e., from **d** to **e**, thus causes only 7.7% reduction in the axial load which is less than the previous case, for the same amount of torque increment. Similarly it is seen from the figure that the increase of nearly the same amount of torque from point **r** to **s**, results only about 4% reduction in the axial load. The test results of figures 6.22(b) and 6.22(c) show the similar trend like that of figure 6.22(a), when the yielding begins due to combined loading.

From the above it is clear that, the subsequently applied torque (in an alternate manner) results only very small reduction in the axial load, compared to the total amount of load applied. Thus it can be concluded that, for this particular type of biaxial loading where the torque and the axial load are applied successively and when the torque is applied initially, the influence of the axial load, (which in the present case is applied as a second load) is much dominant on the specimen investigated than that of the initially applied torque. Furthermore, it is also observed from figures 6.22(a)-6.22(c) that, the more the axial load is increased towards the yield, and hence towards the ultimate load of the material, the less the percentage of reduction in the axial load for the same amount of torque increment and, also the less amount of axial load is required to result in same drop in the torque.

Figures 6.23(a), 6.23(b) and 6.23(c) show the similar biaxial loading behaviour of the copper, for different initial torque, T equal to about 1.0, 0.75 and 0.50 respectively. These figures reveal the similar trend like those of the steel material.

Axial Load Applied First

In this type of loading, the bar was initially subjected to different levels of known axial load, within the elastic range of the material and then, keeping the corresponding axial displacement constant, a torque was applied and gradually increased quasi-statically until the material

yielded due to the combined loading. Subsequently, small increments of the torque and the axial load were successively applied beyond the combined yield point, holding the axial displacement or the angle of twist constant in an alternate manner. This procedure was repeated for four different initial axial loads.

For the above mentioned type of loading, the typical test results for the steel are shown in figures 6.24(a), 6.24(b), 6.24(c) and 6.24(d) for different initially applied axial loads, F being equal to about 1.0, 0.75, 0.5 and 0.25 respectively. During the tests, the torque was applied alternatively in such a way that, whenever yielding started, the percentage of reductions in the initially applied axial load were within 10-20%. However, subsequently when the axial load was applied, it was gradually increased nearly up to its initial value. The figures show that, when yielding begins, the initially applied axial load starts to decrease as the torque increases. Then, when the axial load is subsequently increased, keeping the corresponding angle of twist constant, the torque starts to decrease immediately.

Thus, from the figures it is seen that during the successive application of the torque and the axial load, (when the yielding begins) the increment in the subsequently applied torque results in immediate reduction in the axial load and similarly, the increment in the subsequently applied axial load results in instantaneous reduction in the torque. Hence it can be concluded that the effect of the axial load or torque, whichever is applied subsequently, is dominant on the specimen investigated. This happens due to the fact which has already been explained in the previous case. Moreover, it is also observed from figures 6.24(a)-6.24(d) that, when the torque is subsequently increased, the material soon regains its torque carrying capability irrespective of the level of the initially applied load.

From figure 6.24(a) it is seen that when the normalised torque increases from zero to about 1.35, i.e., from point **a** to **b** as shown in the figure, the initially applied axial load decreases from F equal to 1.0 to about 0.8, i.e., from point **m** to **n**, which results in nearly 20% reduction.

in the initially applied axial load. Then subsequently when the axial load is increased from **F** equal to 0.8 to nearly to its initial value, i.e., from point **n** to **o**, the normalised torque decreases from 1.35 to about 1.07, thus causes nearly 20.7% reduction in the torque. Again the increase in the normalised torque from 1.07 to about 1.33, i.e., from **c** to **d**, results nearly the same amount of drop in the axial load. When the axial load is again increased nearly to its initial value, i.e., from point **p** to **q**, the normalised torque decreases by the same margin as before and results about 21% reduction in the torque. The test results of figures 6.24(b)-6.24(d) show the similar trend like that of figure 6.24(a), when yielding commences due to combined loading.

Thus from the above discussion it is clear that the subsequently applied axial load results only small reduction in the torque, compared to the total torque applied. So that for this particular type of biaxial loading where both the axial load and torque are successively applied and when the axial load is applied initially, it can be concluded that the influence of the torque, (which is applied here as a second parameter) is much dominant on the specimen investigated than that of the initially applied axial load. Furthermore, in the previous case it was seen that the more the axial load was increased towards the uniaxial yield load of the material, the less was the percentage of reduction in the axial load for the same amount of torque increment. But in the present case it is observed that even when the torque is applied further beyond the yield torque of the material, the percentage of reduction in the torque is nearly constant for the same amount of load increment. From figure 6.24(a) it is seen that when the normalised axial load is subsequently increased, either from point **n** to **o** or from **p** to **q** which causes nearly 25% increment in the load, the percentage of reduction in the torque is nearly constant, which is about $20.5\% \pm 0.5\%$. Similarly for the same percentage of increment in the torque results nearly a constant drop in the axial load.

Figures 6 25(a)-6 25(d) show the similar biaxial loading behaviour of the copper, for different initial axial load, F equal to about 1 0, 0 75, 0 50 and 0 25 respectively These figures reveal similar trends like those of the steel

6.7 VERIFICATION OF THEORETICAL PREDICTION

In this section two theoretical models described in chapter four have been used to compare the time history of the different quantities obtained during the biaxial loading programme, particularly when the solid rods were subjected to torsion followed by tension and, tension followed by torsion In the first case, the corresponding angle of twist was kept constant after applying different levels of initial torque and, in the second case, the corresponding axial displacement was held constant after applying different initial axial loads

TORSION FOLLOWED BY TENSION

The experimental results obtained during this particular type of loading, where the bar was initially subjected to a torque, and then, holding its corresponding angle of twist constant, the axial load was gradually increased quasi-statically, are shown in figures 6 5 and 6 6(a)-6 6(c) The test results from these figures, for different initial torques, are replotted in figure 6 26, where the experimental points have been plotted in terms of normalised axial strain and normalised torque

The comparison between the experimental and the theoretical results, obtained using Gaydon's theoretical model for the above mentioned type of loading, is shown in the same figure It is apparent from the figure that, when the initial torque T is equal to 1 0 and 0 75, the experimental torque variation points lie reasonably close to the theoretical results nearly upto the point $\underline{\epsilon} = 1 65$ However, the theoretical results shown by solid lines give an underestimate of the reduction in torque For the other two cases, i e , for the initial T equal to 0 5 and 0 25, as the reduction in the torque is very small, the experimental points match with the theoretical curves only upto $\underline{\epsilon} = 0 9$ Furthermore, all the experimental results stop decreasing

nearly after $\underline{\epsilon}=1.65$, because of the reason already mentioned earlier and beyond that there is poor agreement between the theoretical and the experimental results. It is also observed from figure 6.26 that the higher the values of the initially applied torque \mathbf{T} , the better the agreement between the experimental results and the theory.

It is worth mentioning that the nature of the path followed by the experimental points mainly depends on the magnitude of the yield stress, so that if the yield stress is changed, the experimental points will follow different paths. From the uniaxial tensile test of the steel, the yield load was defined at 0.05% offset whose corresponding yield strain was 3060 micro-strain, see figure 6.1. Now if the yield load is defined at 0.02% offset and at the proportional limit point, whose corresponding axial yield strains are about 2500 and 1900 micro-strain respectively, then the resulting experimental results become as shown in figures 6.27(a) and 6.27(b) respectively, where the solid lines show the theoretical results.

Figure 6.27(a) shows that, for the initial \mathbf{T} equal to 1.0 and 0.75, the experimental points have better agreement with the theoretical predictions up to the point $\underline{\epsilon}$ equal to 1.5 and 1.2 respectively. But beyond those points the torque decreases relatively slowly compared to the theoretical results. However from figure 6.27(b), the effect of strain-hardening of the material is evident and the experimental results show poor agreement with the theory, where the torque decreases relatively slowly at a decreasing rate as a result of the increase in the hardening rate of the material. The lack of agreement between the experimental and the theoretical results, shown in figures 6.27(a) and in 6.27(b), is due to the fact that Gaydon's theoretical model was developed for non-strain-hardening of the material. However, as the steel under investigation behaves approximately like an elastic-perfectly plastic material for 0.05% offset yield load, as shown in figure 6.3, it can be concluded from figure 6.26 that, for the present biaxial loading and the steel investigated, Gaydon's theoretical predictions are in fair agreement with the experimental results before they become flat, specially for the cases when the initial \mathbf{T} is equal to 1.0 and 0.75.

The comparison between the experimental results, for initial $T = 1.0$ and yield load at the proportional limit, and the theoretical predictions based on Brooks' model for different strain-hardening rate (n) is shown in figure 6.28. It is worth noting that here Gaydon's curve for the elastic-perfectly plastic material has well matched with Brooks' theoretical curve for $n = 50$. The figure reveals that initially the experimental curve agrees well with the theoretical one for the strain hardening parameter $n = 50$ and so does with the Gaydon's curve upto the point $\underline{\epsilon} = 0.95$. After that, it diverges away from $n = 50$ curve and shows fairly good agreement with $n = 8$ curve upto the point $\underline{\epsilon}$ equal to about 1.75. Thus from figure 6.28 it is evident that, even though strain-hardening of the material is considered, there exists some disagreement between the experimental and the theoretical curves. This lack of agreement may be attributed to the discrepancy in the material behaviour due to the non isentropic hardening of the material, as Brooks's theoretical model was developed considering isentropic hardening of the material, or due to the inappropriateness of the model.

For similar type of biaxial loading, figure 6.29(a) shows the comparison between the experimental and the theoretical results for copper for different initial torques. Here the theoretical curves are plotted based on Gaydon's model. The figure reveals the similar trend like those of the steel. The experimental results shown in figure 6.29(a) were obtained on the basis of yield strain measured at 0.02% offset. However if the yield load of the copper is defined at the proportional limit, whose corresponding axial strain is about 1800 micro-strain, see figure F.1 of appendix F, the resulting experimental curves with the same theoretical plots are shown in figure 6.29(b). It appears from this figure that the experimental points show better agreement with the theory before the torque stops to decrease. Moreover if the experimental results for copper, shown in figure 6.29(b), are compared with those for steel, shown in figure 6.27(b), where in both cases the yield strain was defined at the proportional limit, it is observed that the rate of decrease of the initially applied torque with the increase of the axial strain is much faster in case for copper than that for steel. This is due to the fact that the copper has strain-hardened less than the steel specimen, as seen from figure 6.3. Thus, it

can be concluded that, for this particular type of biaxial loading where the bar is subjected to torsion followed by tension, Gaydon's theory agrees well with the experimental results of the material which behaves more closely like an elastic-perfectly plastic material

However, in the case of copper, as the theoretical curves obtained by Gaydon's model always give an over-estimate of the experimental results, even when the yield strain was defined at the proportional limit, it was felt not necessary to compare these results with those based on the Brooks' model

TENSION FOLLOWED BY TORSION

The experimental results for steel, shown in figures 6 11(a)-6 11(d), where the bar was initially subjected to an axial load, and then, a torque was gradually increased keeping the corresponding axial displacement constant, are combined together and plotted in figure 6 30 for different initial loads. The solid lines shown in the figure present the theoretical results based on Gaydon's model. The figure reveals that the experimental results agree well with the theoretical results up to a certain value of γ , which is different for different initial axial loads. After that the axial load decreases relatively slowly as a result of increase in the hardening rate of the material. However, unlike the previous case, where the strain-hardening of the material during the application of the axial load ceases when the axial strain reaches a certain value, in the present case the material strain-hardens continuously because of continuous increase in the twist and hence, in the shear strain, the experimental points deviate continuously compared to the theoretical results with the shear strain.

The comparison between the experimental and the theoretical results, based on Gaydon's model, under similar loading condition of the copper is depicted in figure 6 31. The figure shows the similar results like those for steel. Thus, for this particular type of biaxial loading where the bar was subjected to tension followed by torsion, it can be concluded that, though the copper specimens behave more closely like an elastic-perfectly plastic material (as seen

from figure 6.3), Gaydon's model provides poor agreement with the experimental results of both materials

The comparison of the experimental results for both steel and copper, when the initial axial load F is approximately equal to 1.0, with Brooks's theoretical model, for different strain-hardening rate, is shown in figure 6.32. The figure shows that the results for neither the steel nor the copper have close match with any of these theoretical curves. These lack of agreement between the experimental and the theoretical curves may be attributed to the discrepancy in the material behaviour due to the non-isentropic hardening of the material, as Brooks's theoretical model was developed considering isentropic hardening, or due to the inappropriateness of the model.

6.8 TESTS WITH THIN-WALLED SPECIMEN

In order to establish the extent to which the reduction in the sustainability of the initially applied torque or load due to a subsequently applied load or torque respectively is increased when the loaded member is subjected to approximately uniform shear and axial stresses across the cross-section, a test programme was undertaken with thin-walled tubular specimens instead of solid rod specimens.

Thin-walled steel tubes, as detailed in chapter five, were subjected to combined torque and tension to compare their results with those of the solid rod. Details of the uniaxial tensile and pure torsion tests of the tube are given in figures F.5 and F.6 of appendix F respectively. The mechanical properties are given in table F.1 of the same appendix. In the first test the tube was subjected to an initial torque, nearly equal to its yield torque, and then holding its corresponding angle of twist constant, the axial load was gradually increased quasi-statically. The reduction in the capability to sustain normalised torque with the subsequently applied normalised axial stress (hence strain) for the thin-walled tube, along with the solid steel and

copper rods, are depicted in figure 6.33. For all three cases the yield load and yield torque were defined at the proportional limit.

The figure reveals that, in the case of thin tube, the rate of decrease of the torque is much faster than those of the copper and steel rods, as was expected, with the increase in the axial strain. It is observed from the figure that when the normalised axial strain is increased to 2.0, the percentage of reductions of the torque, in case of the steel, copper and thin-walled tube, are about 34%, 53% and 77% respectively. Thus it is seen that in the case of the thin-walled tube the amount of the residual torque left within the specimen, after the torque curve becomes flat, is much less than those of the solid bars. However, in the case of the thin-tube, the torque did not decrease to less than 82% of the total torque because of the following reasons. For the present case, the ratio of the inside diameter of the tube to the wall thickness was 6. But from published literature [77] it is evident that for $D_{in}/t = 6.0$ the error involved in using the thin-wall theory is about 15%. Furthermore, the thin-walled tube strain-hardened, as shown in figure F.5 of appendix F. Thus, because of comparatively larger value of D_{in}/t , some residual torque is left within the material. It can be concluded that for a thin-walled tube with very large D_{in}/t ratio, the sustainability of the initially applied torque will be reduced to almost nil due to the subsequent application of the axial load.

In the second test the tube was first subjected to an initial axial load, nearly equal to its yield load, and then keeping its axial displacement constant, the torque was gradually increased quasi-statically. Figure 6.34 shows the reduction in the sustainability of the normalised load with the increase in the subsequently applied normalised shear strain. The experimental results for both solid steel and copper rods under similar condition are also depicted in the same figure. The yield load and the yield torque were considered at the proportional limit for all three cases.

The figure reveals that, in the case of the thin-walled tube, the axial load decreases very rapidly with the shear strain compared to that of the solid bars, as was expected. From the figure it is seen that when the normalised shear strain reaches a magnitude equal to 5.0, the percentage reductions of the axial load, in case of the solid steel, solid copper and thin-tube, are about 48%, 58% and 82% respectively. It is worth noting that as the tube strain-hardened during the tests, so the axial load decreases until the normalised shear strain reaches to about 6.4.

6.9 STUDY OF SUBSEQUENT YIELD LOCUS

Although the determination of the subsequent yield locus was not the primary concern of the current work, the resulting subsequent yield locus obtained during the particular biaxial loading, where both the torque and tension were successively applied are reported here. The experimental results for steel specimens obtained during these tests have already been presented in figures 6.22(a)-6.22(c) for the cases where the torque was applied initially, and in figures 6.24(a)-6.24(d) where the axial load was applied initially. However, because of the complexity in the paths followed during these biaxial loadings, it was not possible to calculate the shear stresses from its corresponding torque reading. Therefore all the resulting subsequent yield loci obtained during the tests are presented in terms of torque-load trajectories, instead of stress trajectories.

Figure 6.35(a) shows the variation of the initially applied torque with the axial load, where the first, second and third curves represent the replot of figures 6.22(a), 6.22(b) and 6.22(c) respectively. However, in figure 6.35(a) the test results are plotted further beyond the results shown in figures 6.22(a)-6.22(c). Figure 6.35(a) reveals that, during the successive application of axial load and torque, the load-torque trajectories always move in a zig-zag way and follow different loading paths until the axial load reaches a critical value. Furthermore, it is seen that when the axial load reaches a particular value, each load-torque

trajectory begins to move on the same loading path, i.e., nearly on a single line, which is different for different cases 1, 2 and 3, as shown in figure 6 35(a)

The above mentioned results demonstrate the following. When the axial load is increased successively during this particular type of biaxial loading, the material under investigation strain-hardens and the axial load gradually moves towards the ultimate load of the material. And hence, once the axial load reaches that value, each load-torque trajectory starts tracking the same loading path, as no excess axial load can be carried by the material. Thus by adding these loading paths, when they move nearly on a single line, it is possible to obtain the positive quadrant of the subsequent yield locus of the material, which is the ultimate yield locus obtainable for its particular strength. However during the successive application of the axial load and the torque, each zig-zag path followed by the torque-load trajectories represent an individual subsequent yield locus. Figure 6 35(b) represents the similar torque-load trajectories of copper under similar loading condition which have been replotted from figures 6 23(a)-6 23(c). Figure 6 35(b) shows the similar trend like that for steel.

The replot of figures 6 24(a)-6 24(c), in terms of torque and axial load, is shown in figure 6 35(c). The curves 1, 2 and 3 represent the conditions when the initially applied axial load were about 100%, 75% and 50% of the yield load. Figure 6 35(c) reveals that initially each torque-load trajectory follows different path due to the successively applied torque and axial load. But as the subsequently applied torque reaches a specific value, which is different for different loading curves, each torque-load trajectory starts to move on loading paths belonging to a single locus. The above facts demonstrate the following. Due to strain-hardening, when the subsequently applied torque reaches nearly equal to its maximum sustainable torque of the material, each torque-load trajectory begins to track the same loading path, as no surplus torque may be carried by the material. Thus by adding all these loading paths, (when they move nearly on a single line) the positive quadrant of the subsequent yield locus can be obtained, which is the ultimate yield locus before the specimen

breaks Figure 6 35(d) shows similar torque-load trajectories for the same loading behaviour of the copper which have been replotted from figures 6 25(a)-6 25(c) Figure 6 35(d) shows the similar trend like that for steel

To obtain almost the entire positive quadrant of the ultimate yield locus, a single steel specimen was first subjected to an initial torque of 30% of the yield torque and then to successively applied load and torque until the torque-load trajectory nearly started to move on a single line Then the specimen was subjected to a torque gradually increasing upto the maximum available torque of the specimen The test results were normalised as normalised torque T/T_h and normalised axial load F/F_h , where T_h is the yield torque and F_h is the yield load of a fully strain hardened material, and are depicted in figure 6 36 The figure shows almost the entire positive quadrant of the ultimate yield locus The same experimental results have been replotted in the same figure (i e , in figure 6 36) considering the normalised torque as T/T_{pl} , where T_{pl} is the value of the fully plastic torque of a fully strain-hardened material The solid line shown in the figure represents the von Mises yield locus based on the yield stress of a fully strain-hardened material The figure reveals that even when the experimental results were plotted as T/T_{pl} , (i e , when assuming that the rod has become fully plastic in torsion) the experimental points remain outside the yield locus which may be due to the following From the literature [77] it is known that the fully plastic torque of a non-strain hardening solid rod is 33% greater than that of the maximum elastic torque In the present case as the material strain-hardened, so the magnitude of the fully plastic torque of the specimen investigated may be much higher than 33% of the maximum elastic torque, which depends on the extent of strain hardening of the material Similarly obtained positive quadrant of the ultimate yield locus for copper is depicted in figure 6 37 which shows similar trend like that for steel

Figure 6 38 shows almost the entire positive quadrant of the ultimate yield locus for the other type of loading where the specimen was first subjected to an initial load, about 25% of the

yield load, and then, to successively applied torque and load until the torque-load trajectory nearly started to move on a single line. Then the specimen was subjected to a gradually increasing yield load. Figure 6.39 shows similar results for a copper specimen. Both the figures show similar trends like those of 6.36 and 6.37. The comparison between the various yield loci thus obtained for two different loading paths are shown in figures 6.40(a) and 6.40(b) for steel and, in 6.41(a) and 6.41(b) for copper. The experimental torques, plotted in figures 6.40(a) and 6.41(a), were normalised as T/T_h , whereas those of in figures 6.40(b) and 6.41(b) as T/T_{pl} . The experimental axial loads, plotted in all these figures, were normalised as F/F_h . The figures show that the corresponding ultimate yield loci obtained by two different loading paths match well with each other. Hence from these figures it can be concluded that yield loci thus obtained are the ultimate yield loci after which material can no longer sustain any further increase in the load or torque.

Though it was not possible to calculate the magnitudes of the shear stresses because of the reason mentioned earlier, and hence not possible to plot figures 6.36-6.41(b) in terms of axial and shear stresses, the general conclusions that may be drawn from figures 6.40(b) and 6.41(b) are as follows. The ultimate yield loci for both materials are expanded and seem to follow non-proportional isotropic hardening rule. However as there was no reverse loading during the test, no comment can be made regarding the Bauschinger effect of the yield locus.

It may be further concluded from the above that a rod made of a fully strain-hardened material and subjected initially to the yield torque, and then holding the angle of twist constant, may be subjected to an axial load upto the yield load. This would be achieved due to so called "off-loading" or effective reduction in the torque sustaining capability. The same would be true for the case when the axial yield load is applied first.

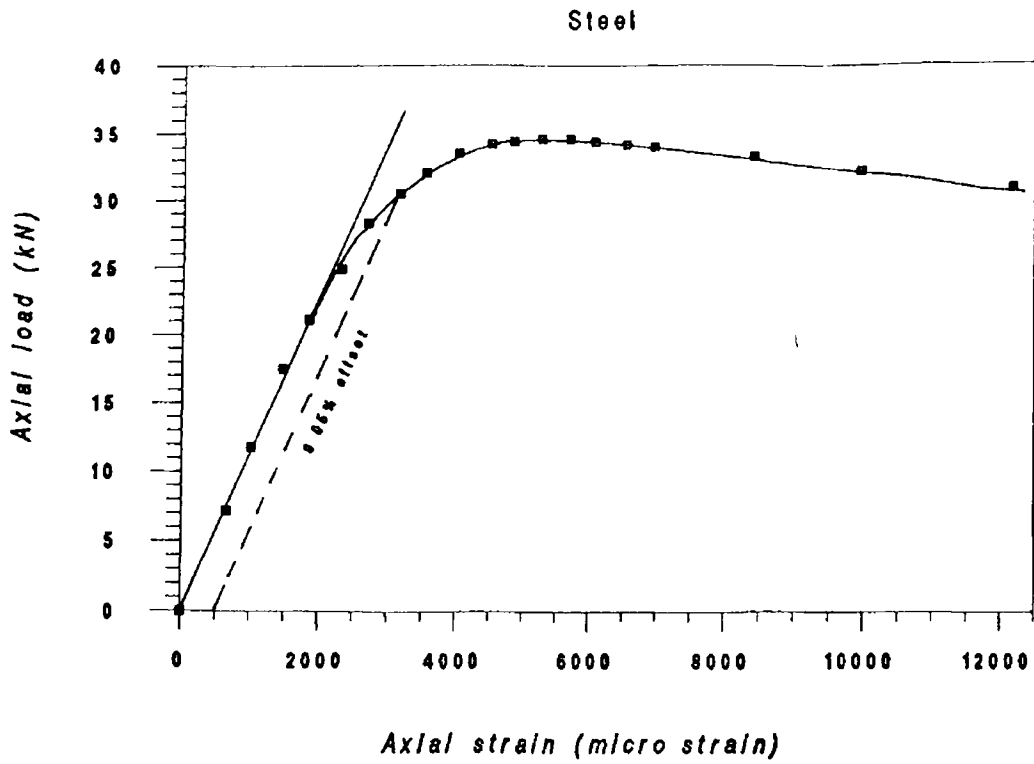


Figure 6.1 Uniaxial tensile load versus axial strain curve (for steel)

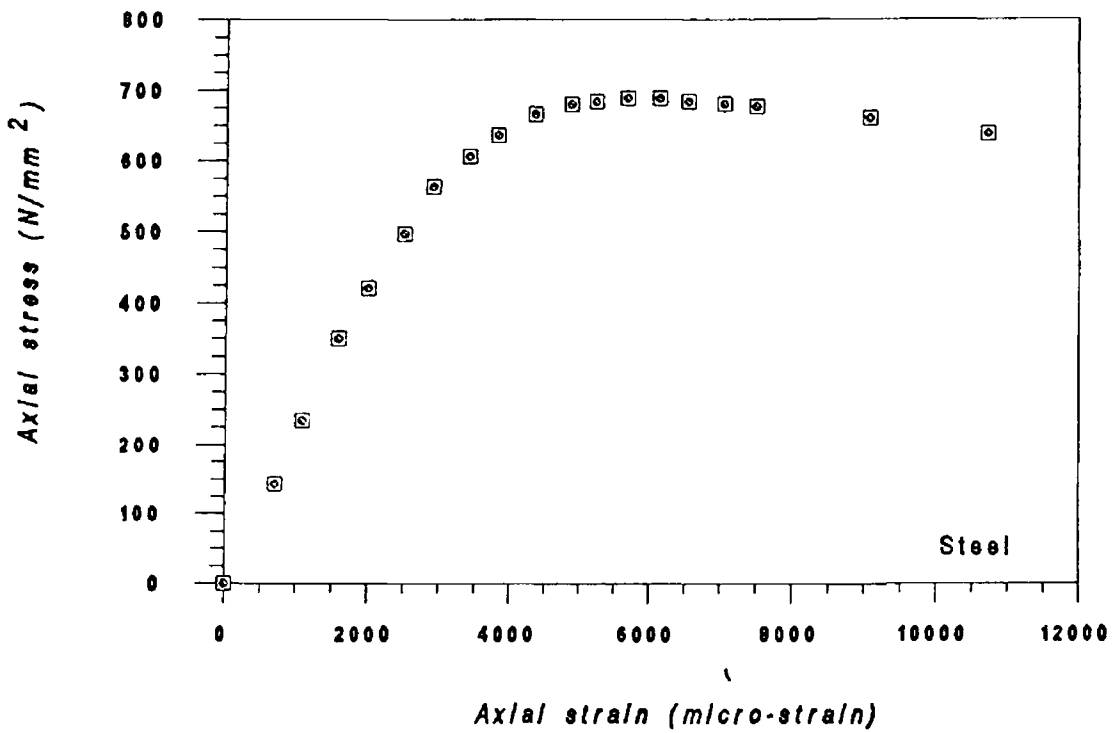


Figure 6.2 Axial stress versus axial strain curve

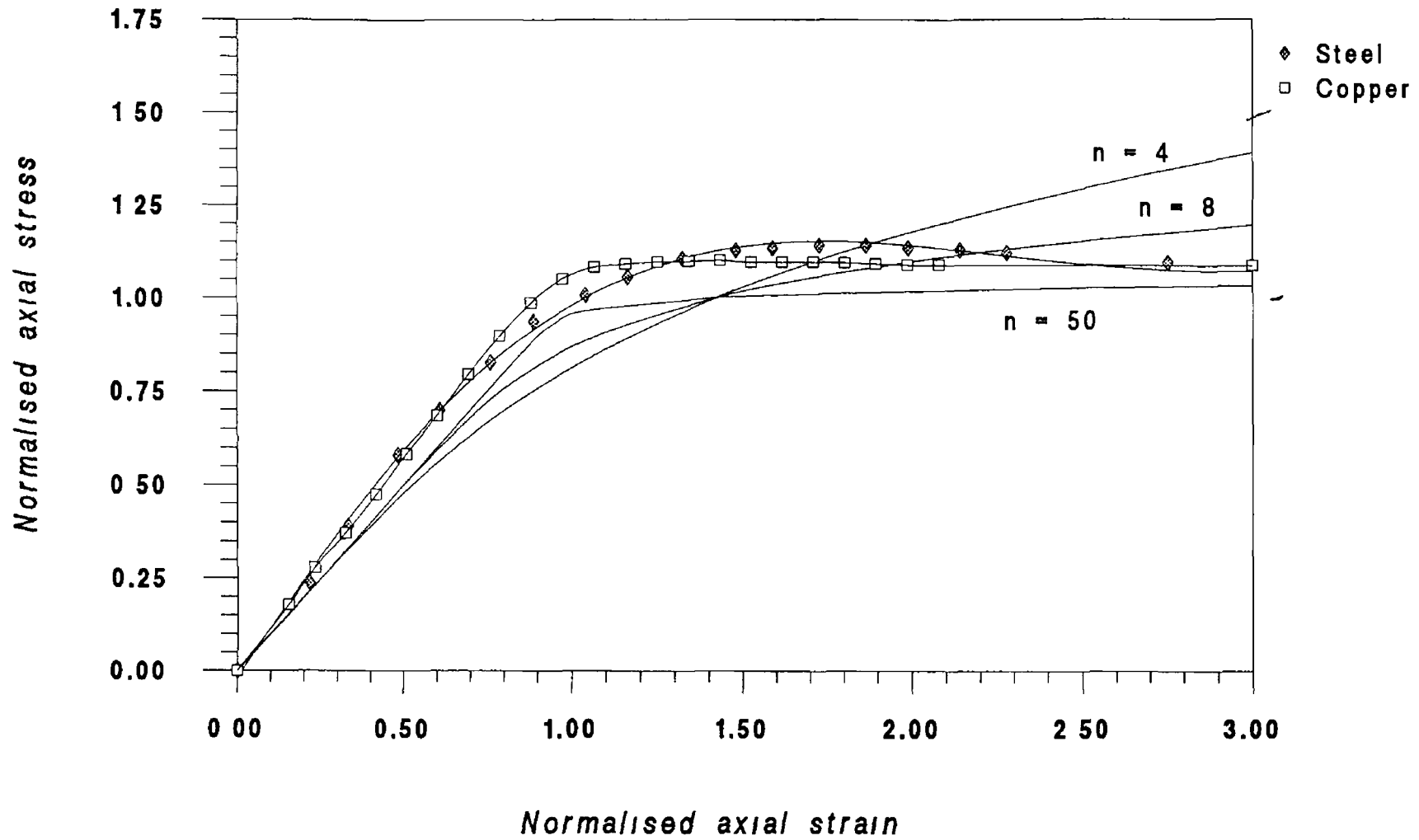


Figure 6.3 Normalised axial stress versus normalised axial strain curve

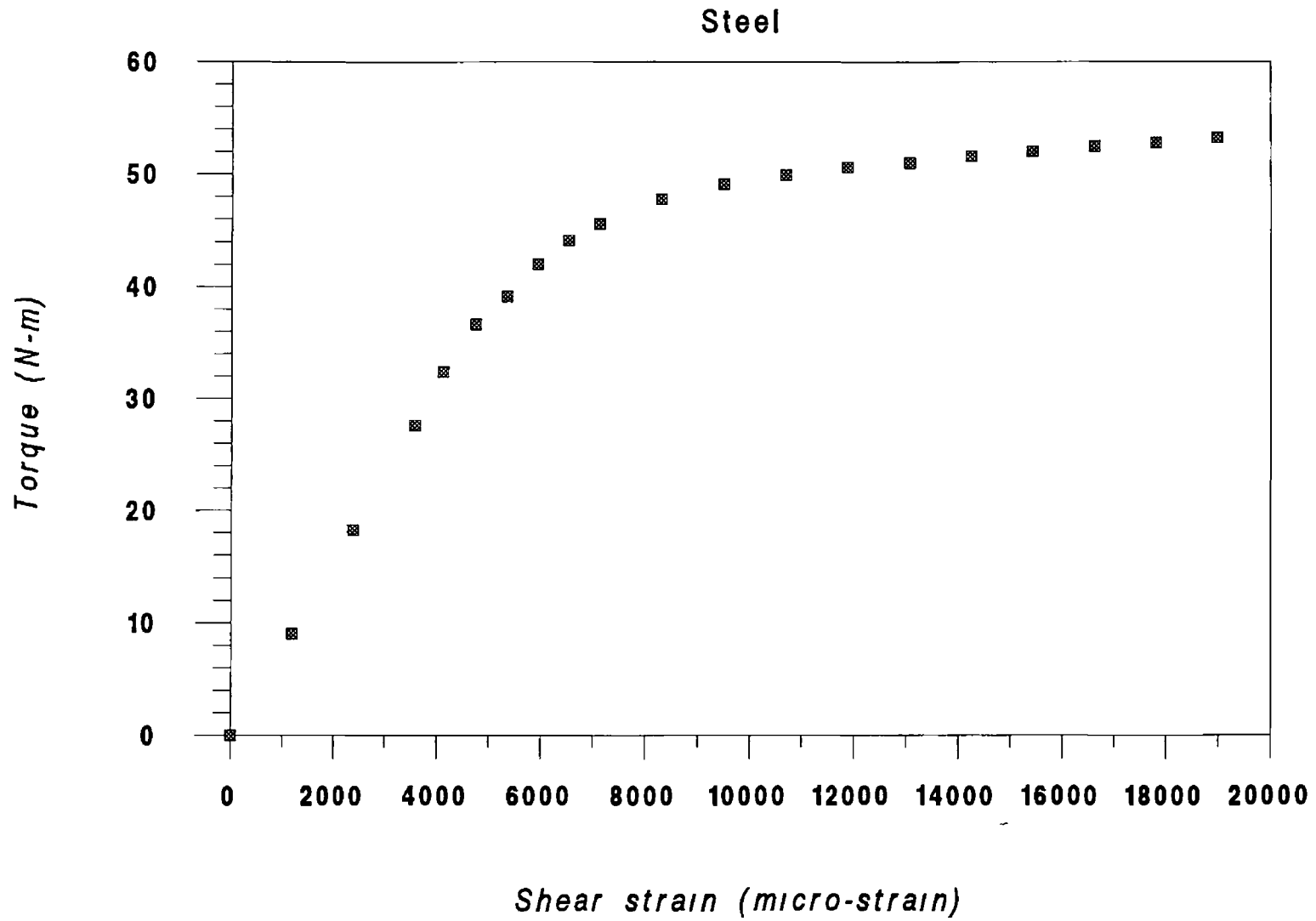


Figure 6-4 Torque versus shear strain curve

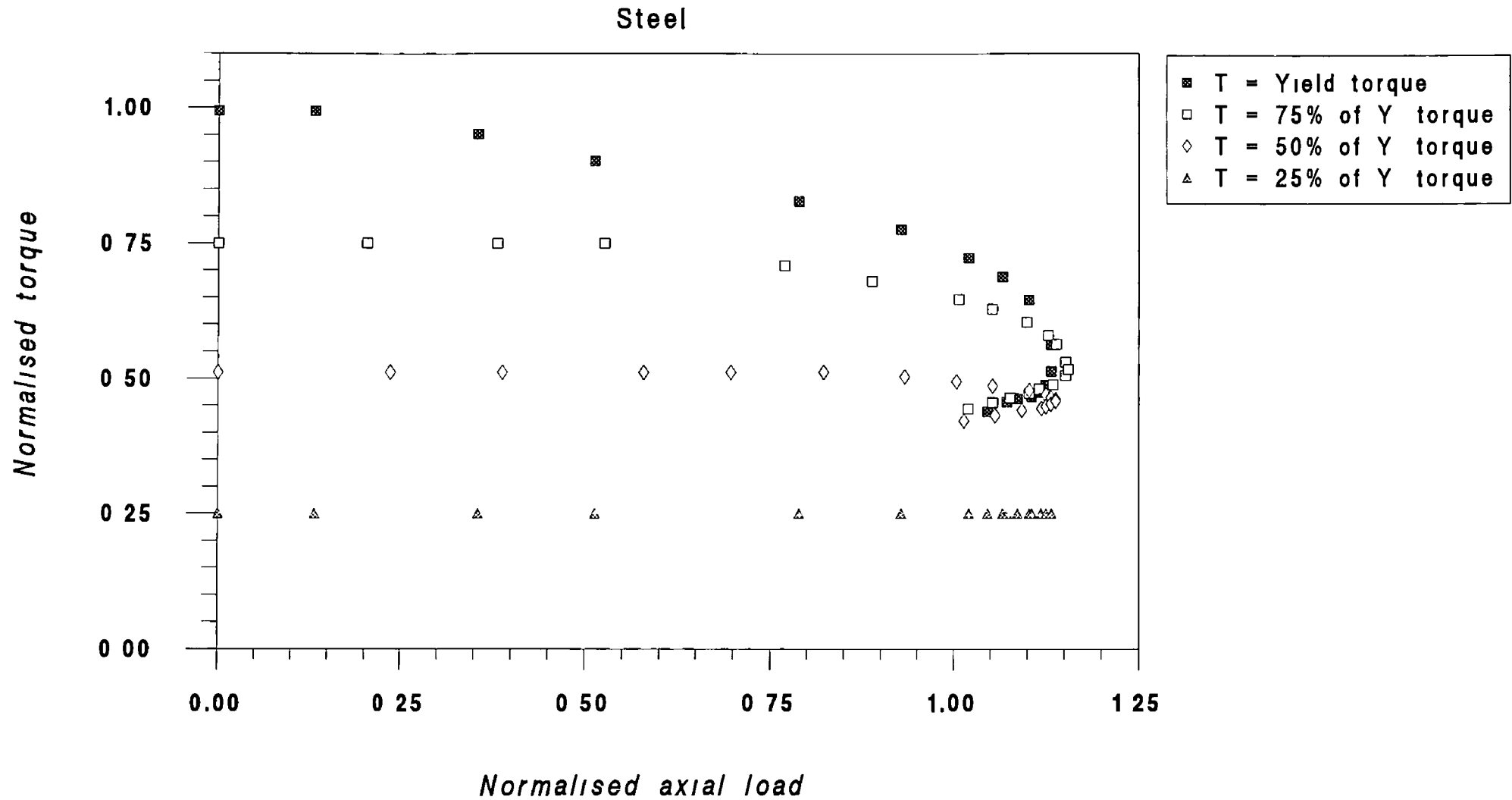


Figure 6.5 Normalised torque versus normalised axial load curve (angle of twist constant)

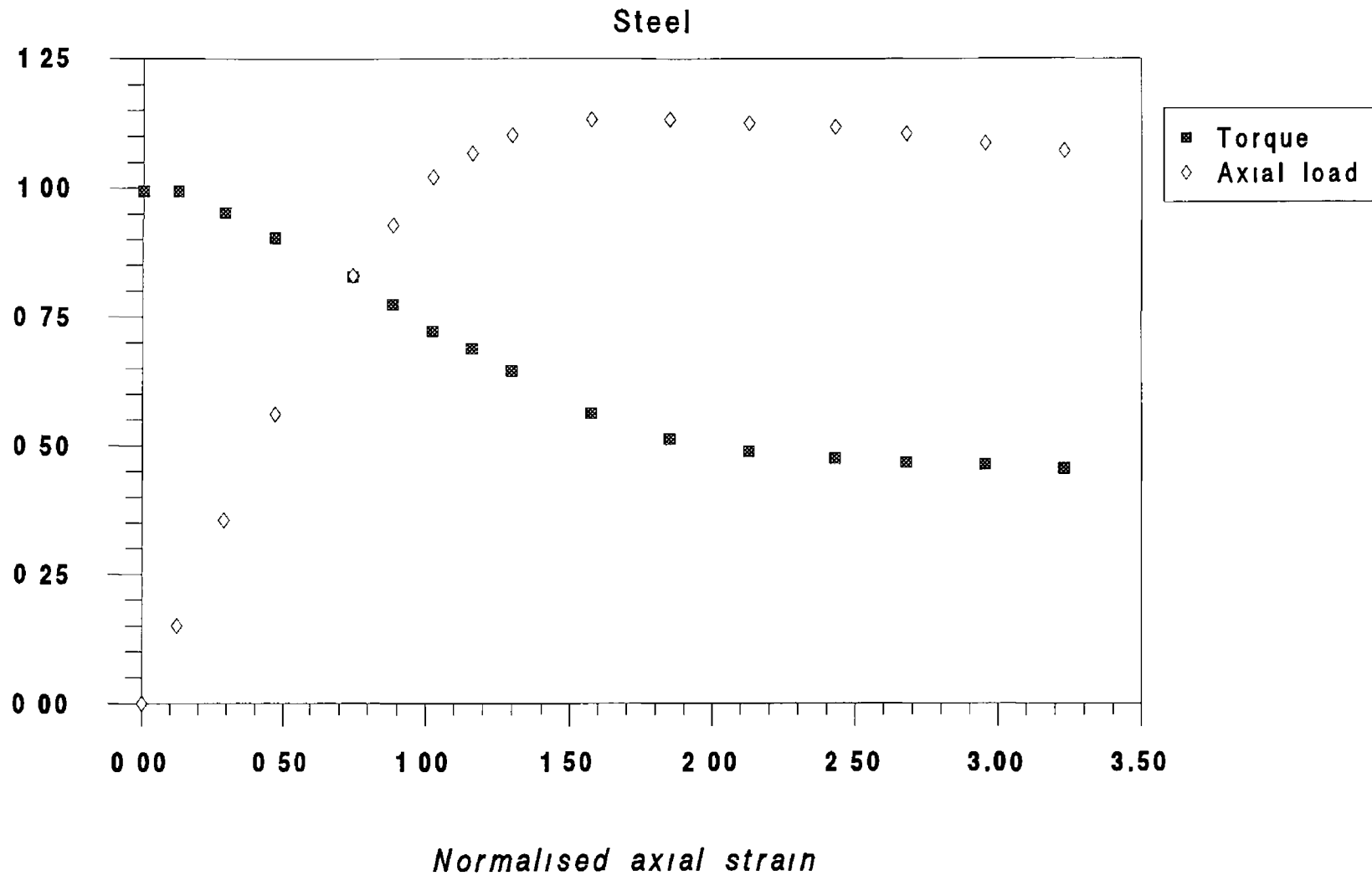


Figure 6.6(a) Normalised axial strain versus normalised torque and load curves
($T = \text{yield torque}$)

Steel

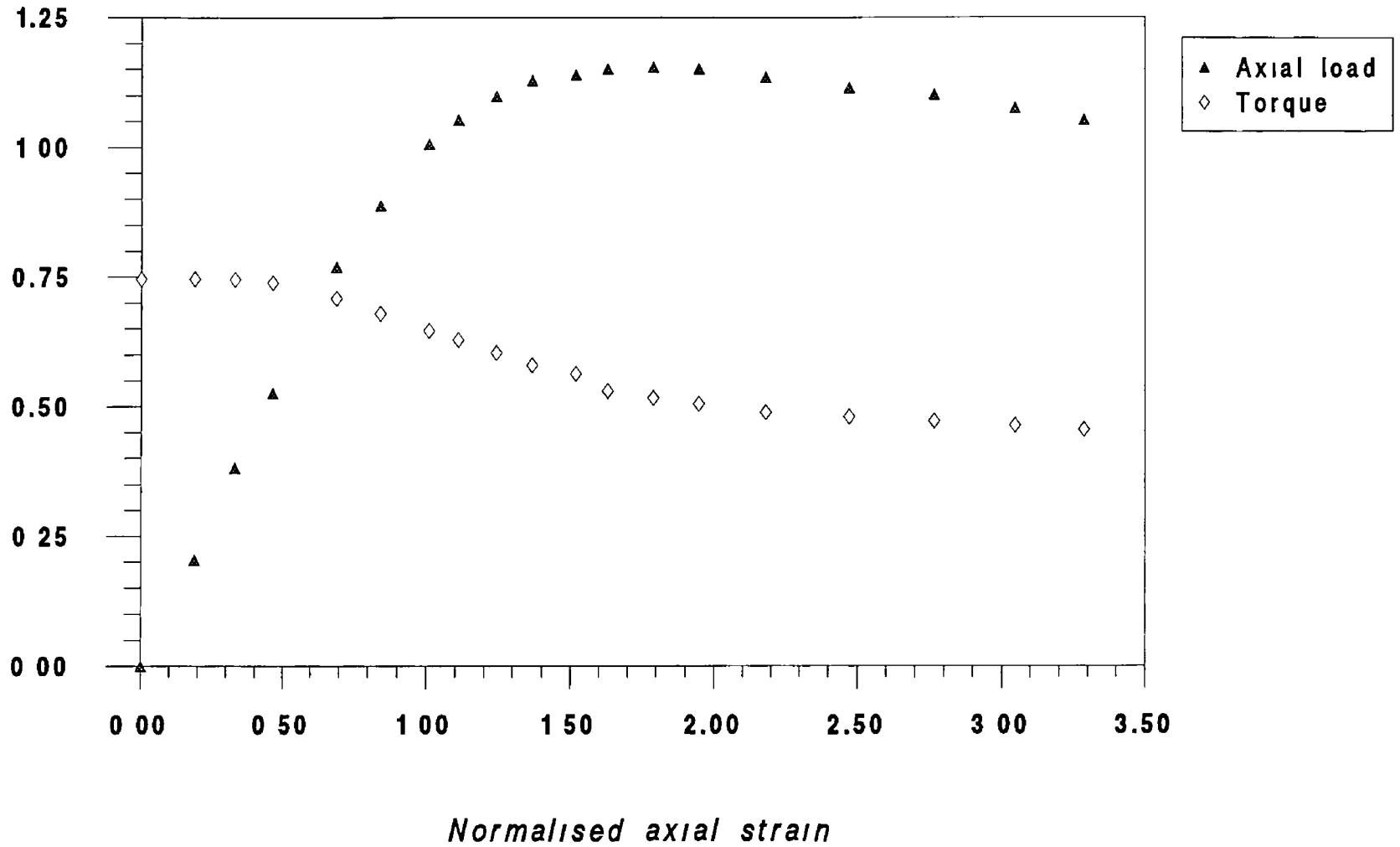


Figure 6.6(b) Normalised axial strain versus normalised torque and load (T = 75% of yield torque)

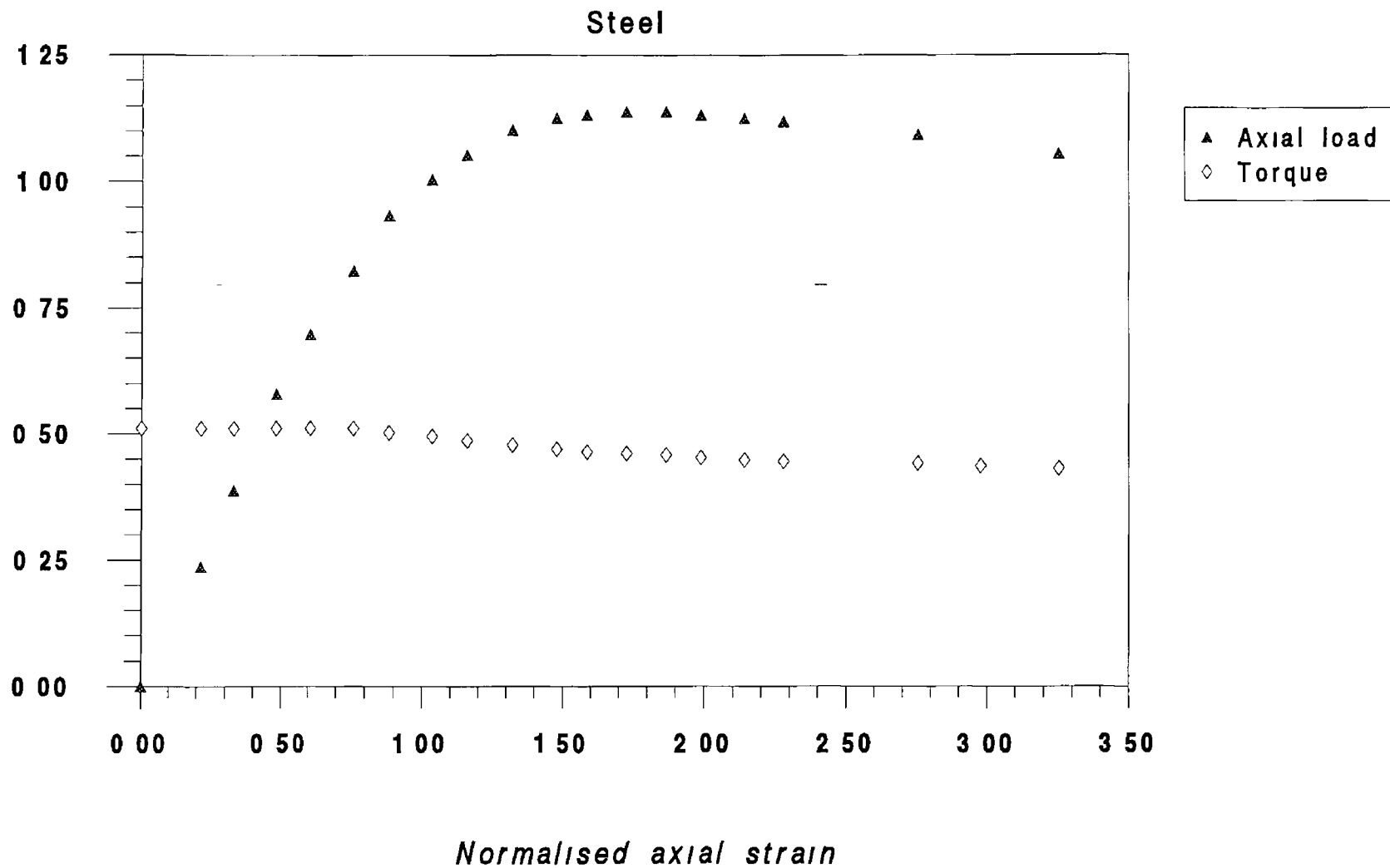


Figure 6.6(c) Normalised axial strain versus normalised torque and load
($T = 50\%$ of yield torque)

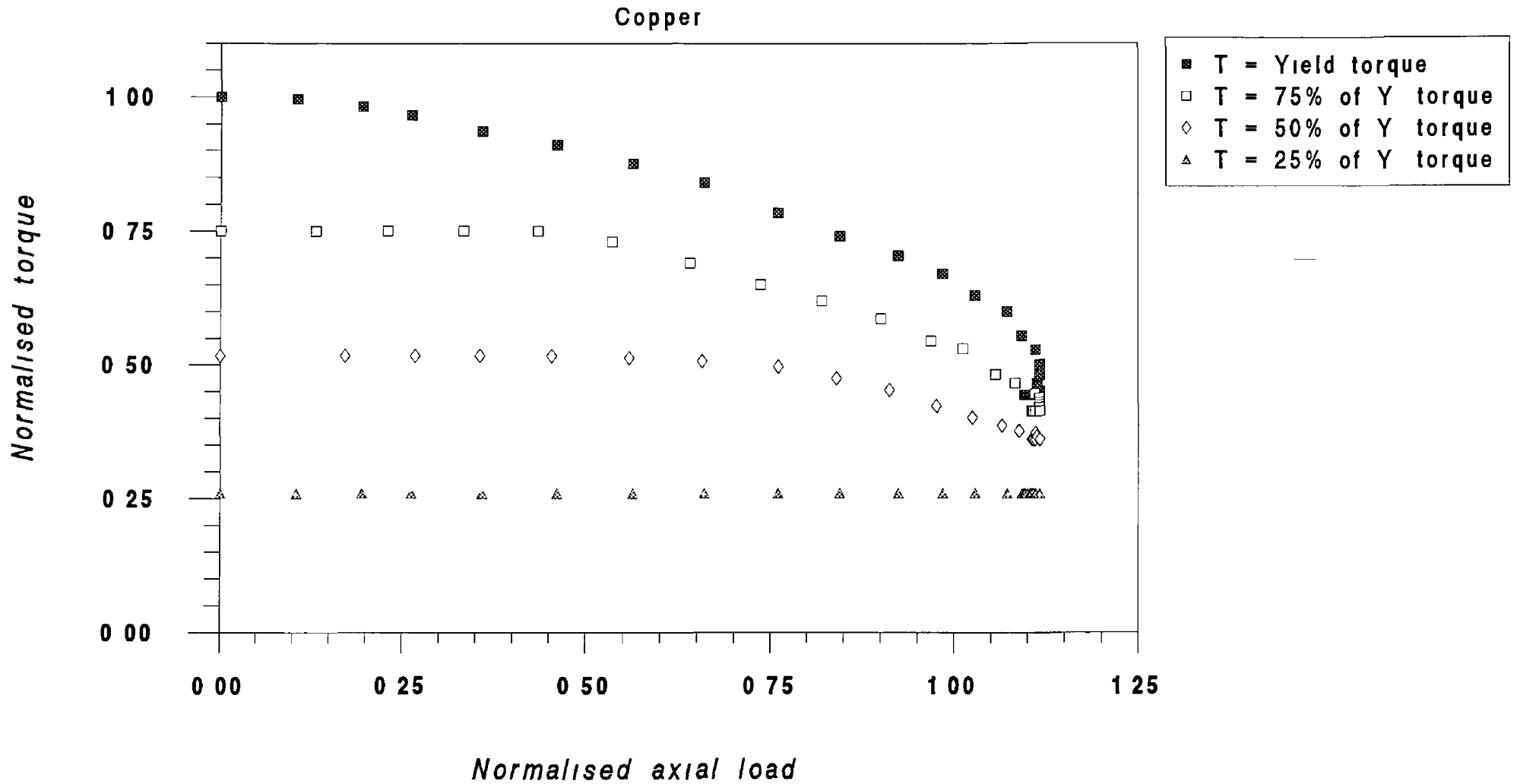


Figure 6.7 Normalised torque versus normalised axial load curve
(angle of twist constant)

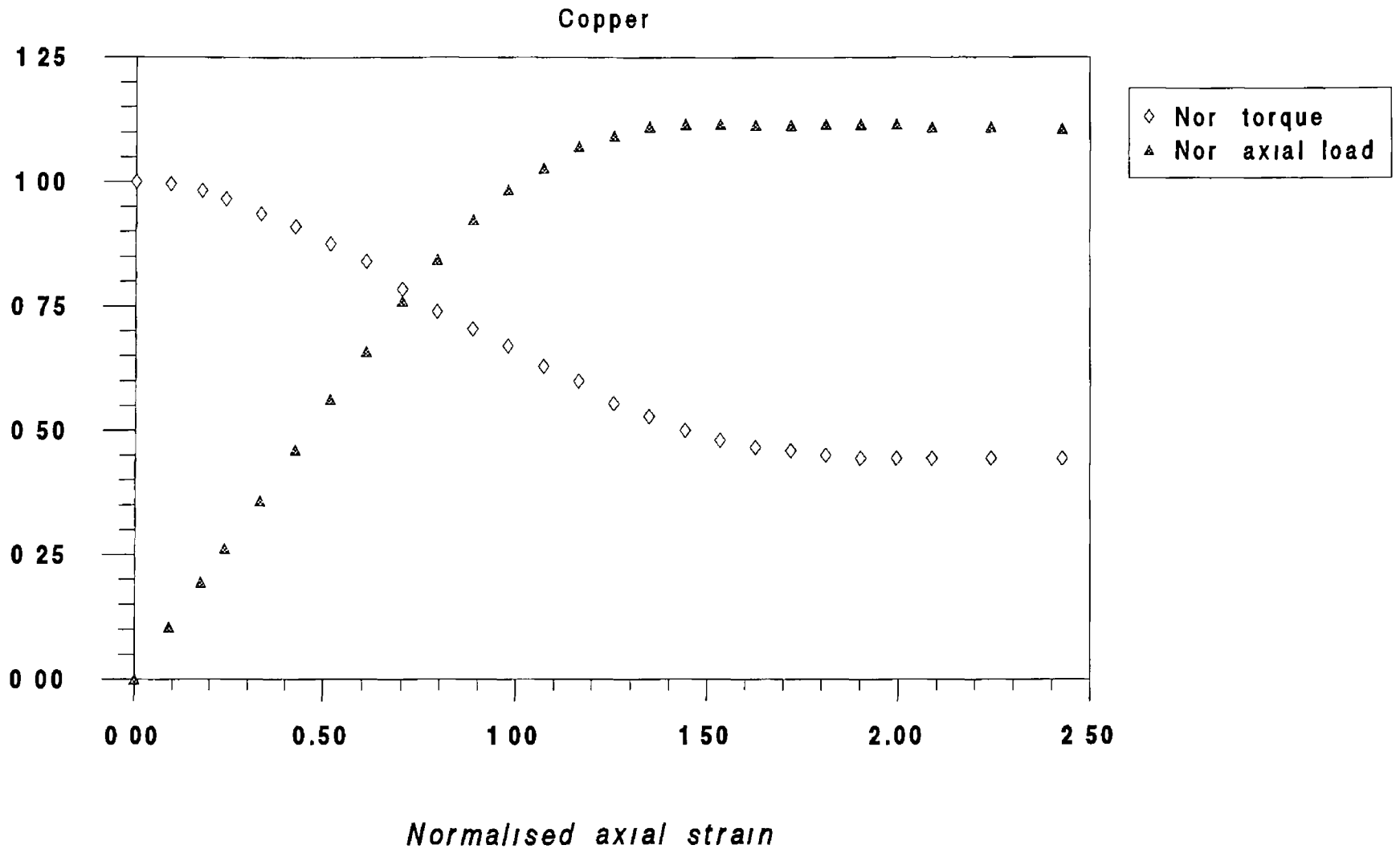


Figure 6.8(a) Normalised axial strain versus normalised torque and load curve
($T = \text{yield torque}$)

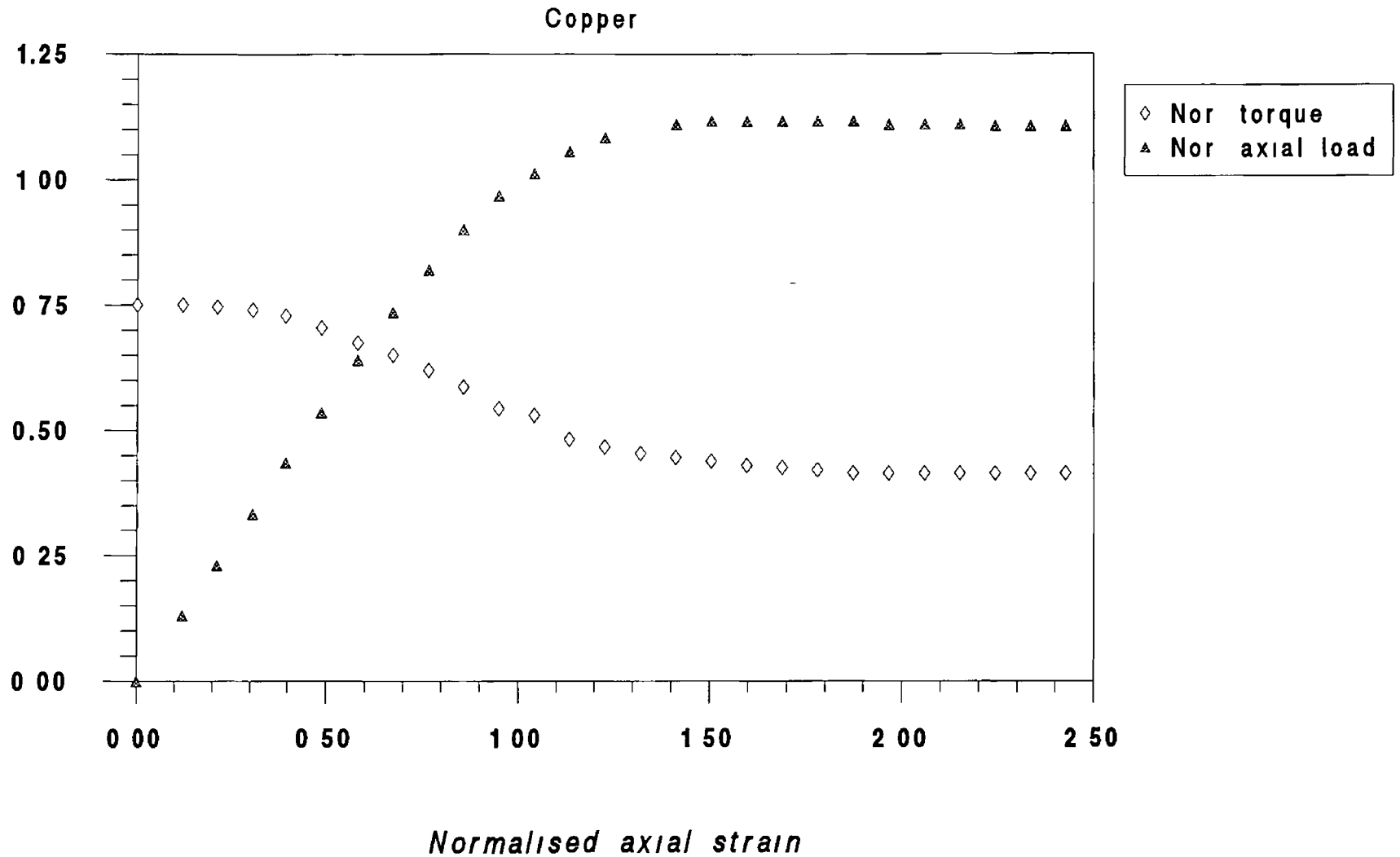


Figure 6.8(b) Normalised axial strain versus normalised torque and load curve
($T = 75\%$ of yield torque)

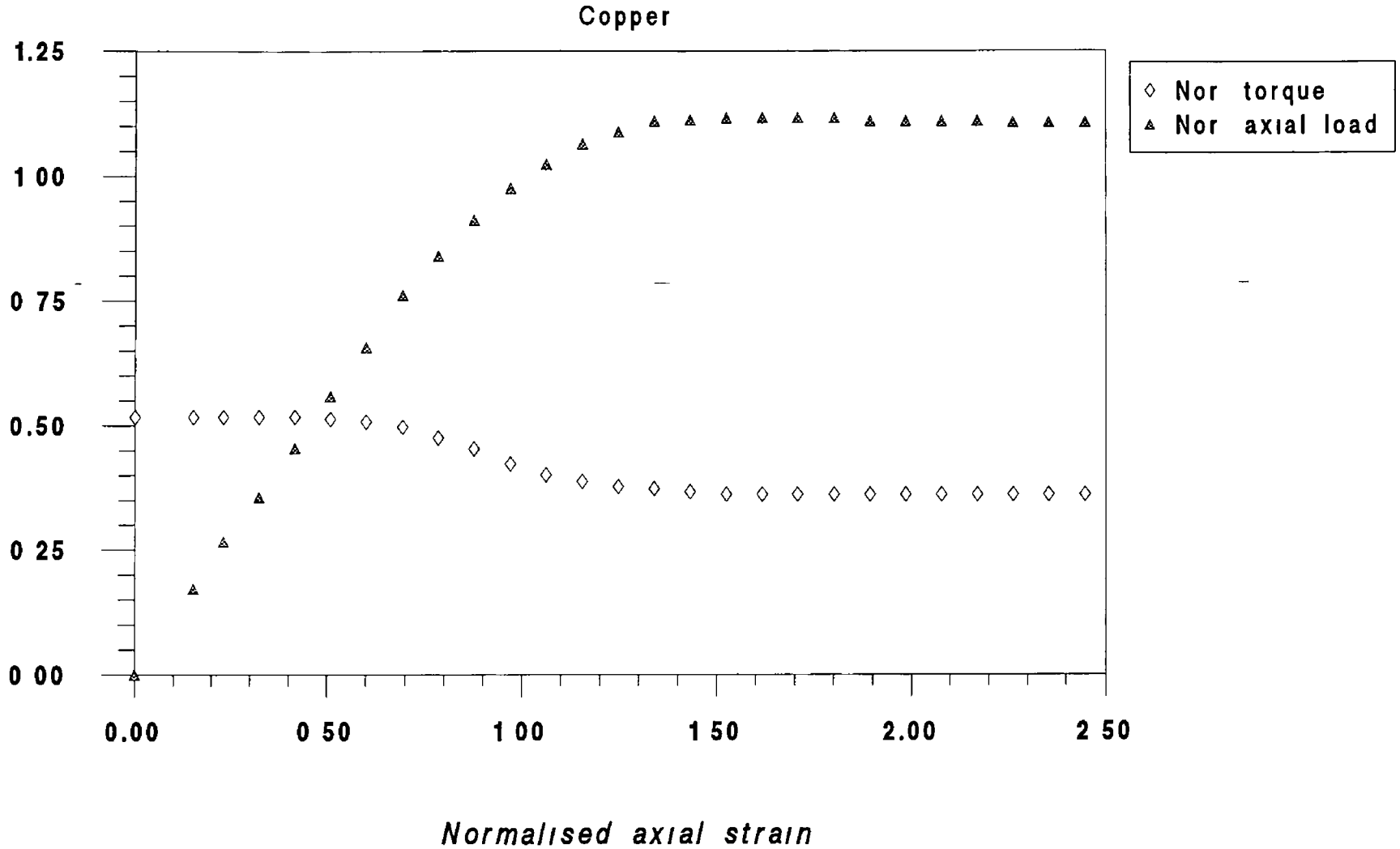


Figure 6.8(c) Normalised axial strain versus normalised torque and load (T = 50% of yield torque)

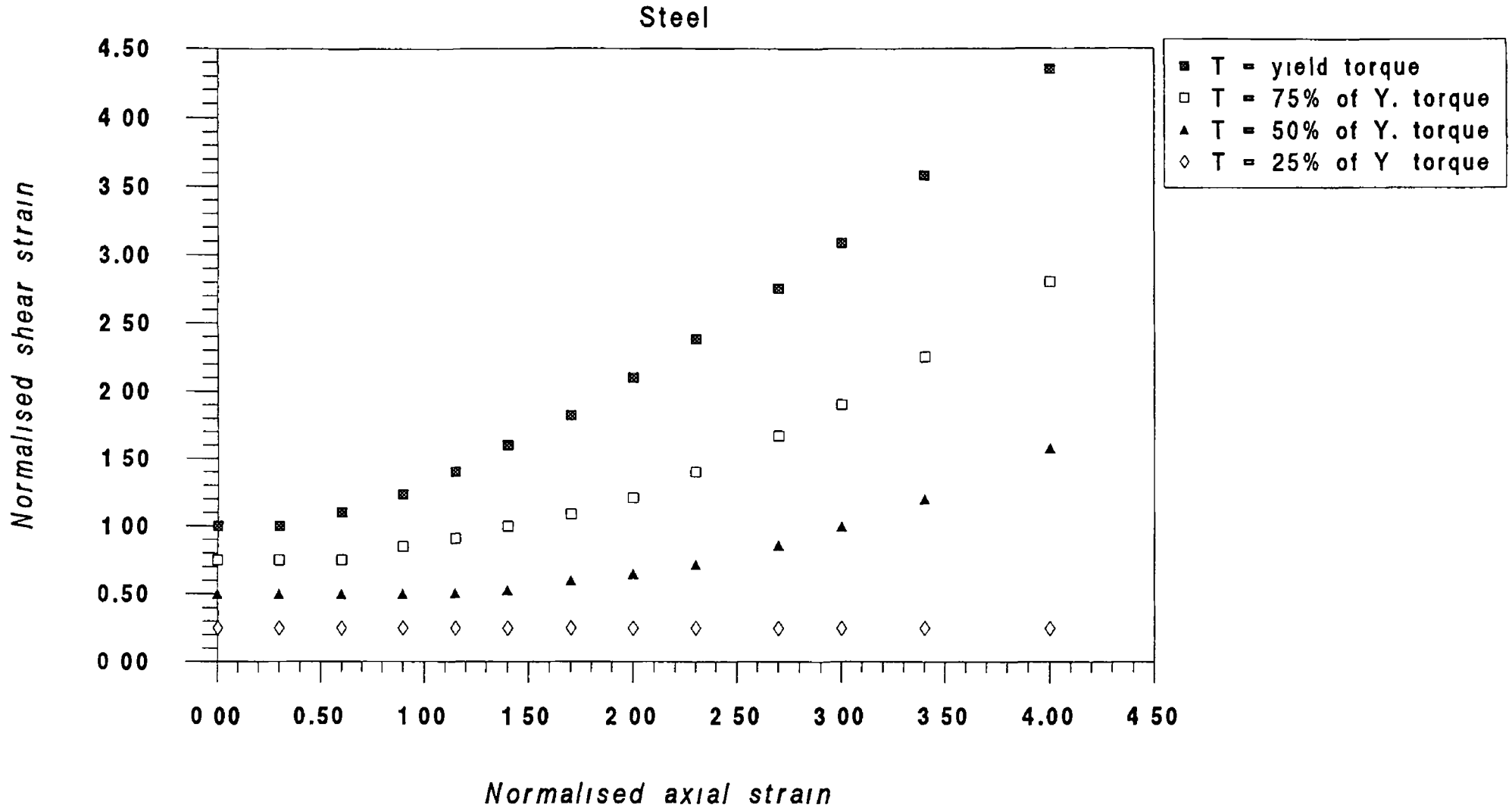


Figure 6.9 Normalised axial strain versus normalised shear strain
(torque maintained constant)

Steel

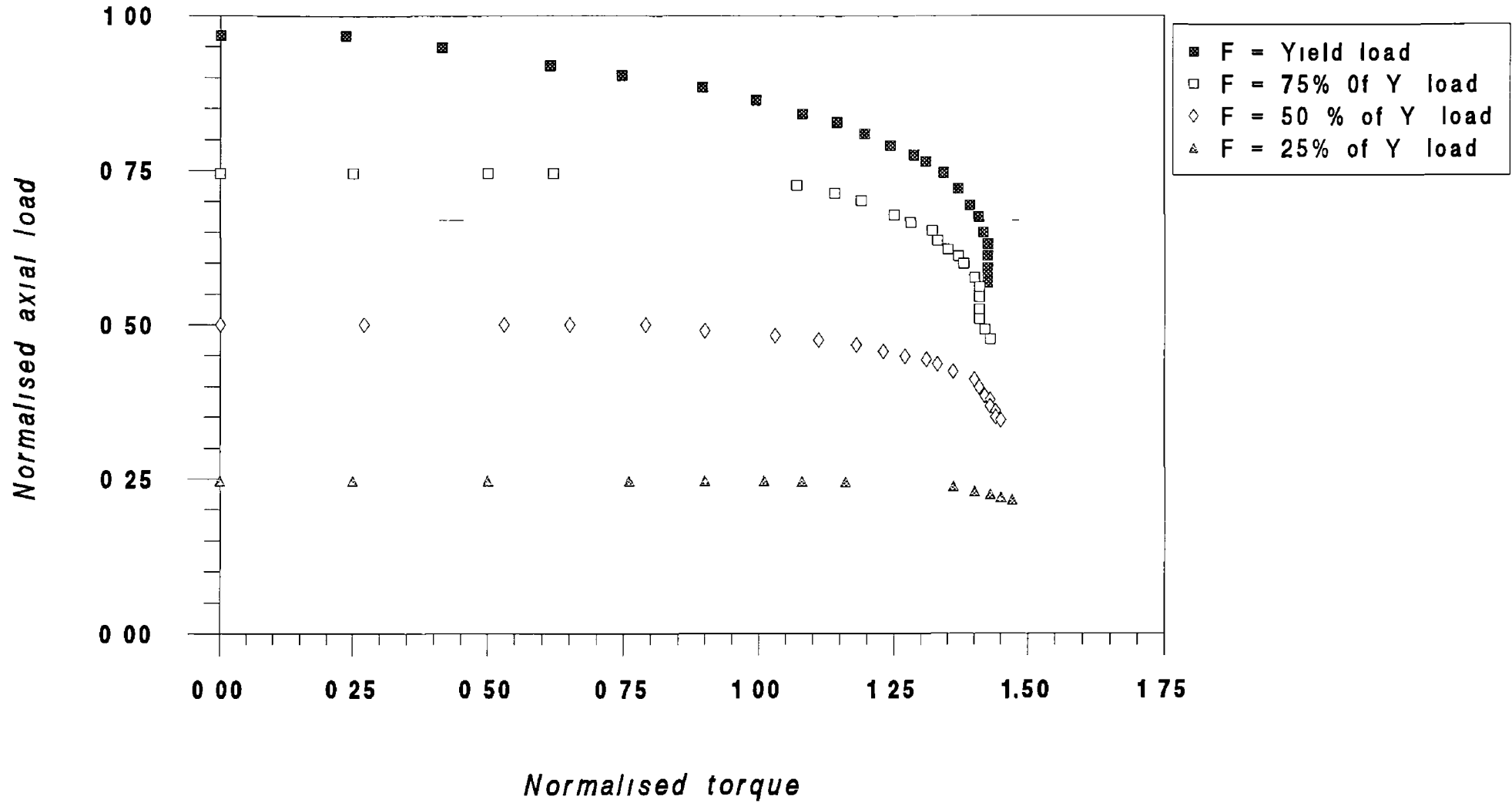


Figure 6.10 Normalised axial load versus normalised torque curve (axial displacement constant)

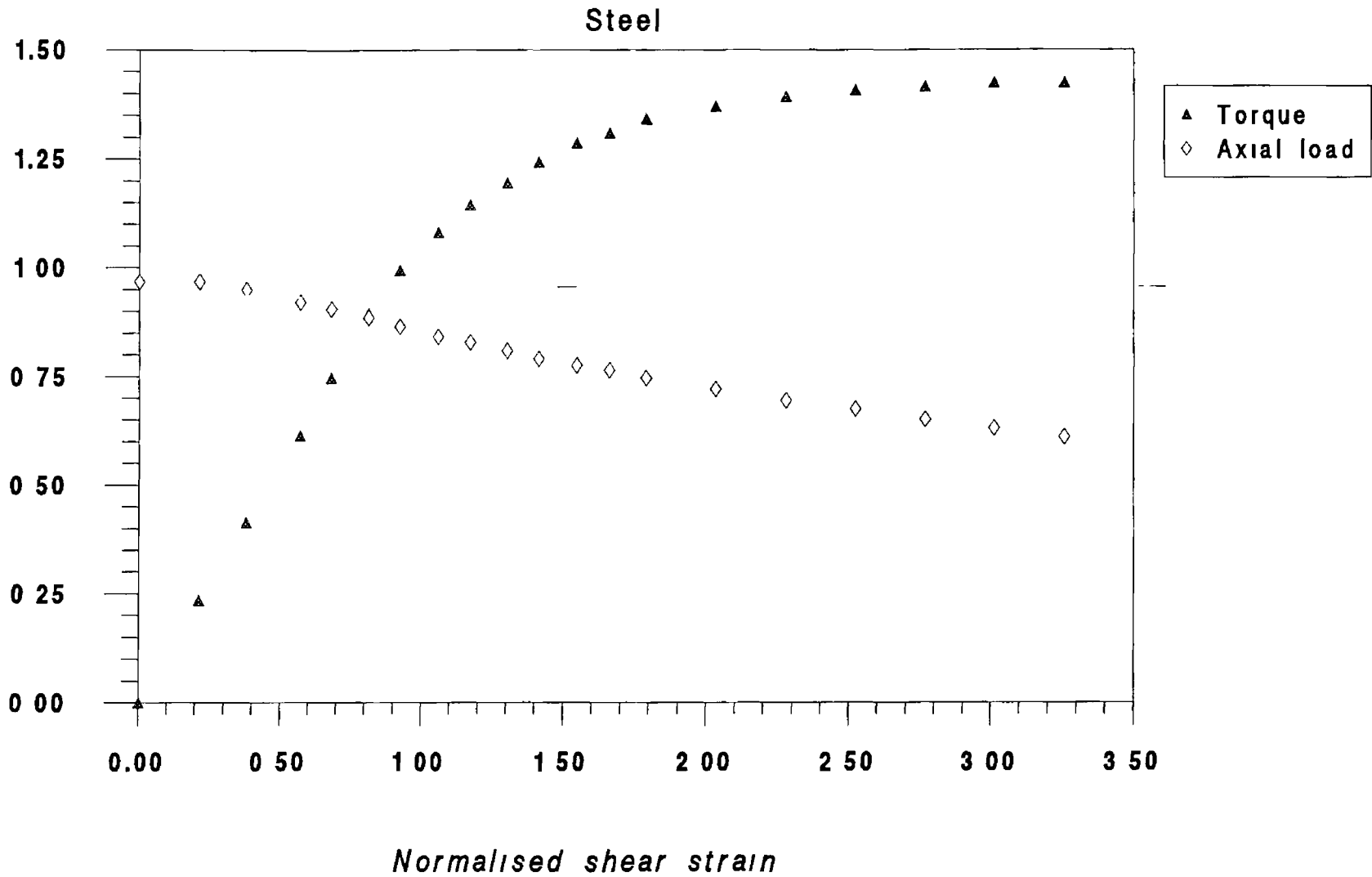


Figure 6.11(a) Normalised shear strain versus normalised axial load and torque curves
($F = \text{yield load}$)

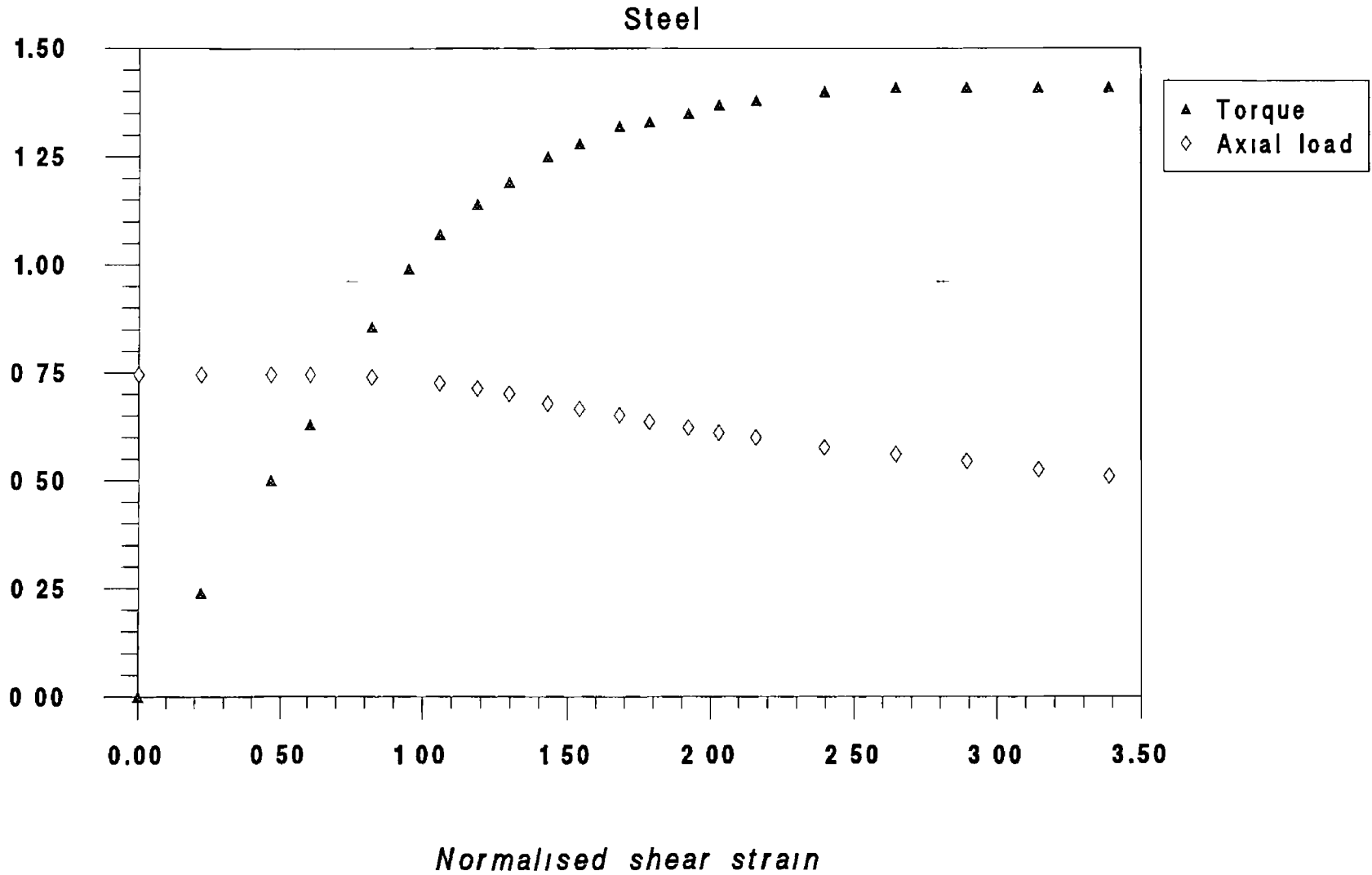


Figure 6.11(b) Normalised shear strain versus normalised axial load and torque curves
($F = 75\%$ of yield load)

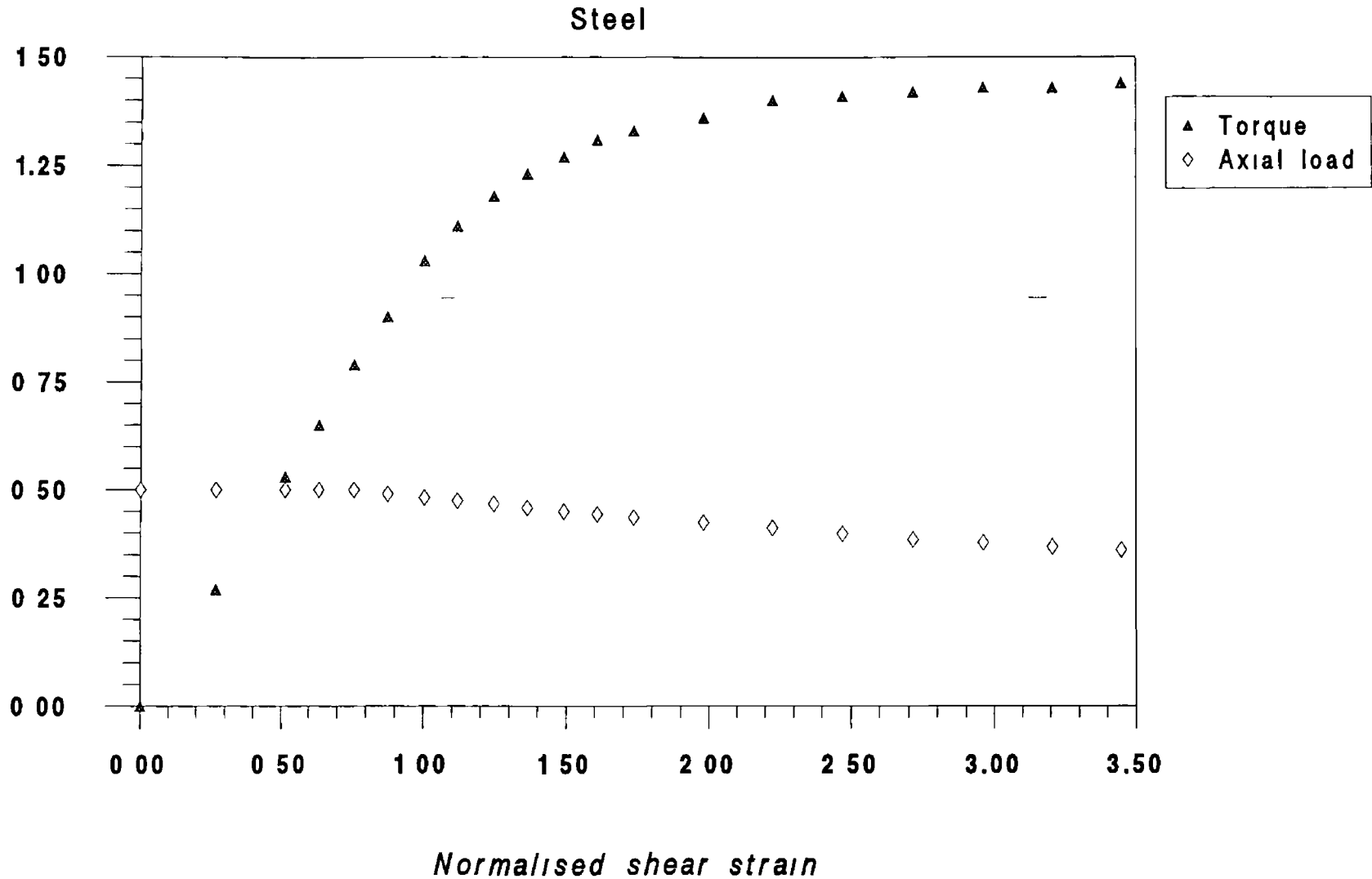


Figure 6.11(c) Normalised shear strain versus normalised axial load and torque curves
($F = 50\%$ of yield load)

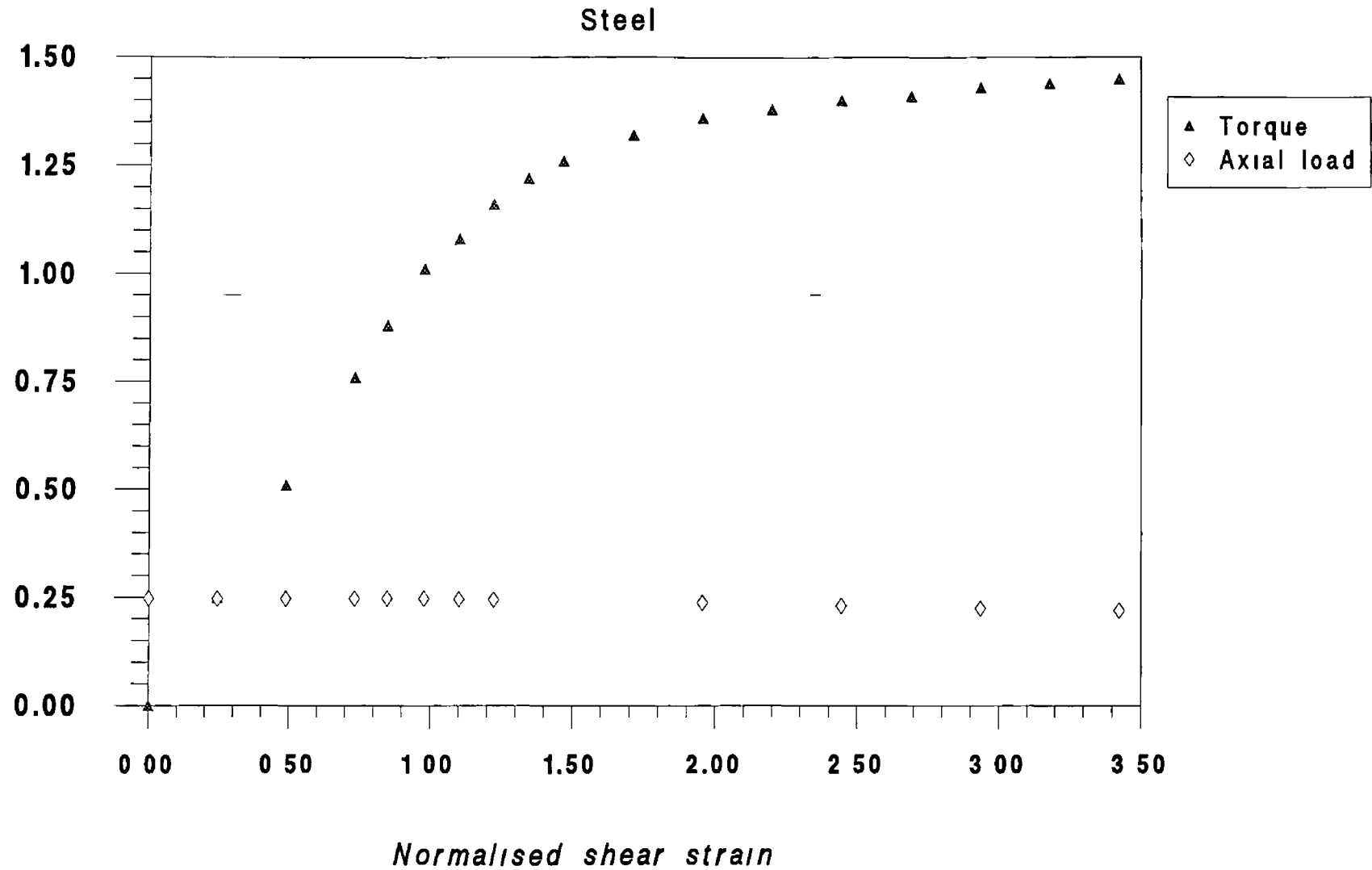


Figure 6 11(d) Normalised shear strain versus normalised axial load and torque curves
($F = 25\%$ of yield load)

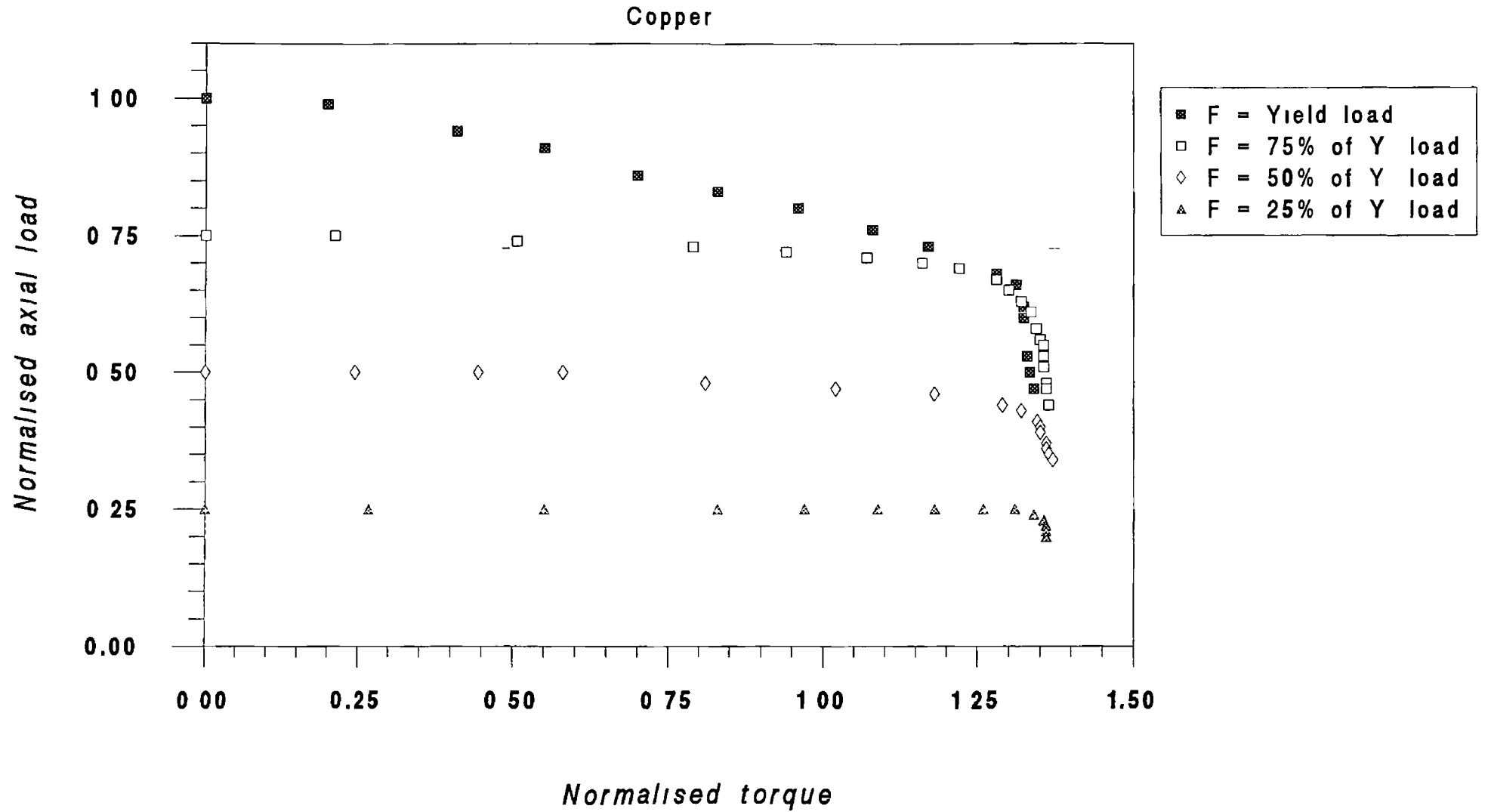


Figure 6.12 Normalised axial load versus normalised torque curve (axial displacement constant)

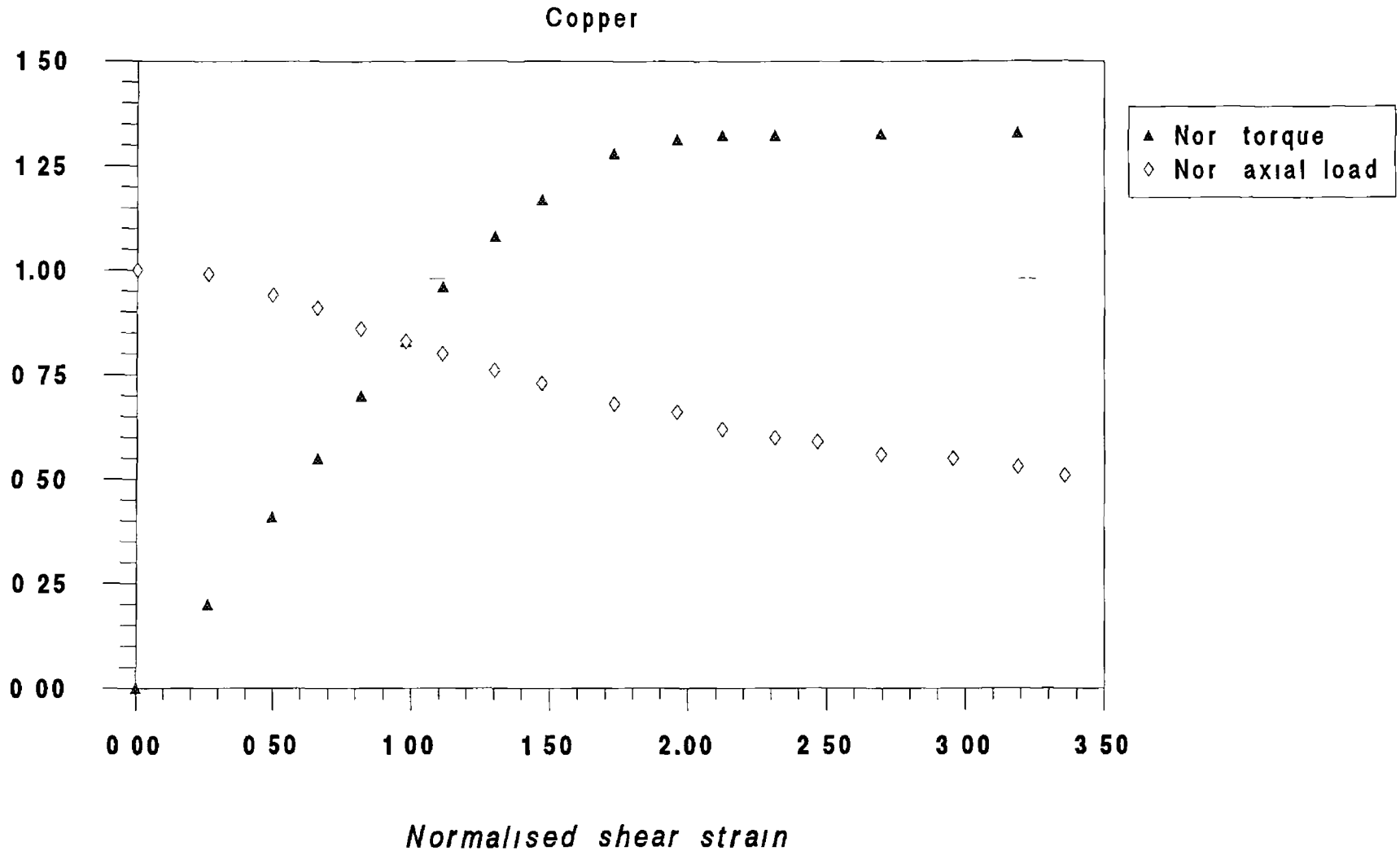
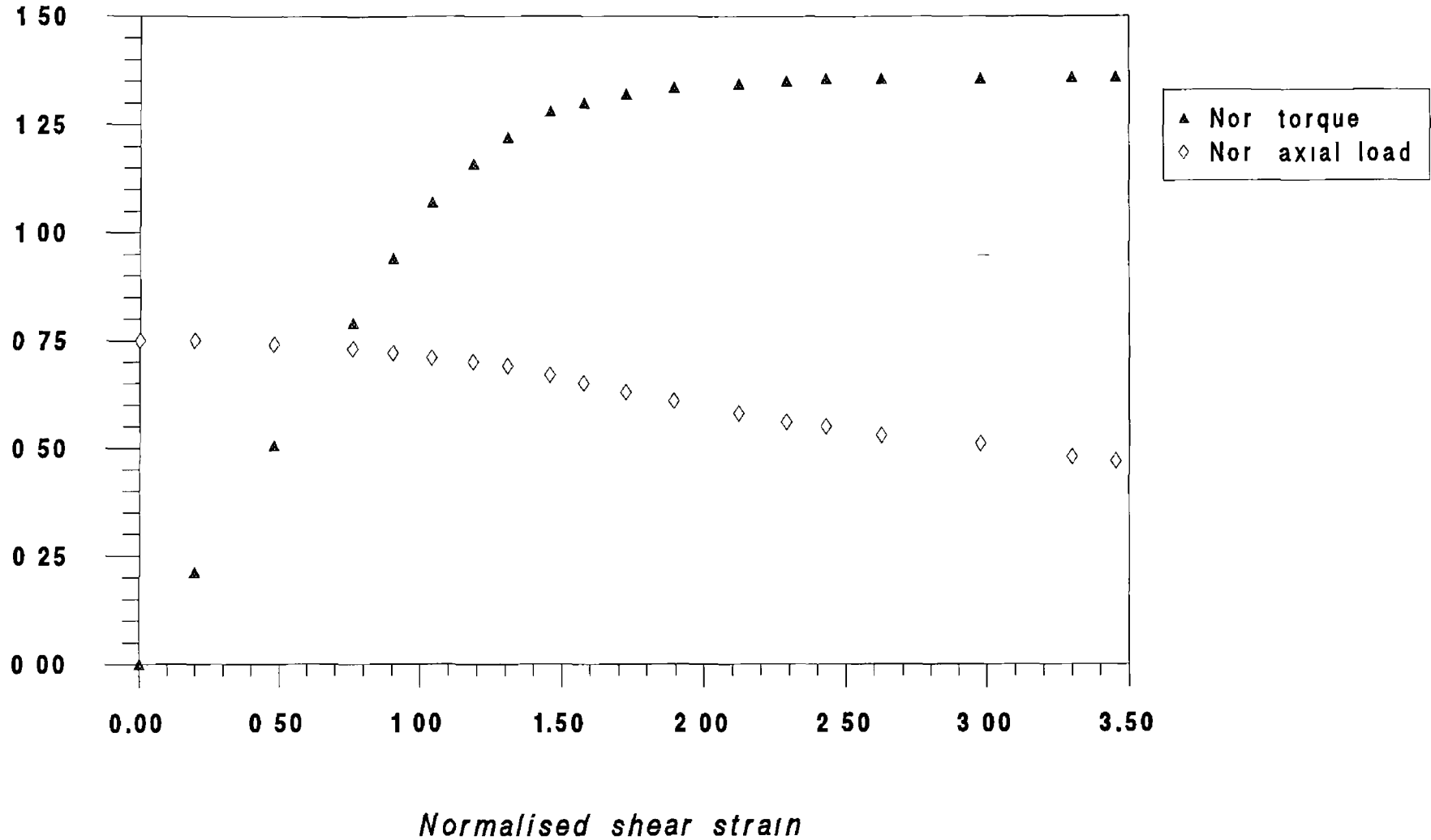


Figure 6 13(a) Normalised shear strain versus normalised axial load and torque curve
($F = \text{Yield load}$)

Copper



216

Figure 6.13(b) Normalised shear strain versus normalised axial load and torque curve (F = 75% of yield load)

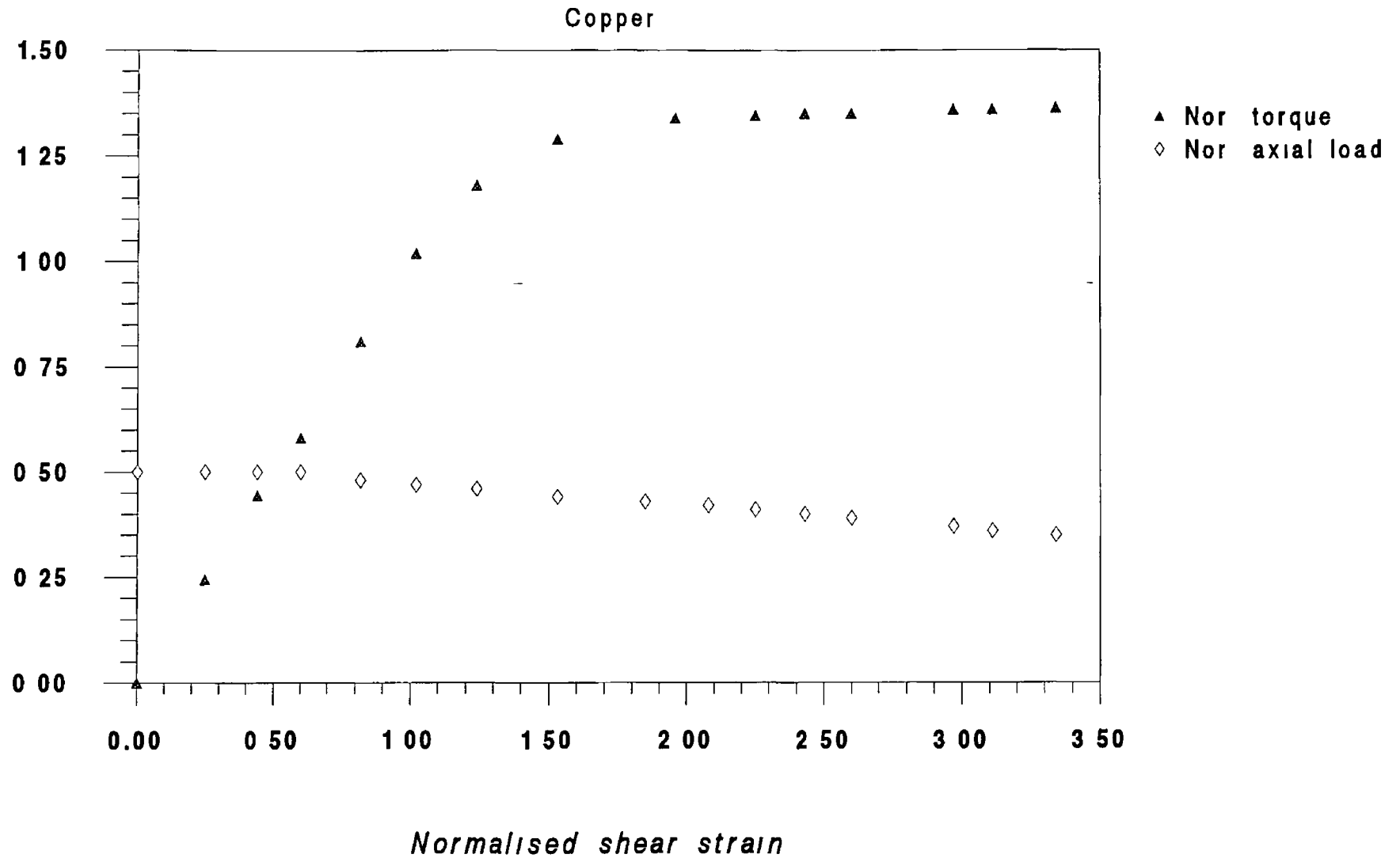


Figure 6.13(c) Normalised shear strain versus normalised axial load and torque curve
($F = 50\%$ of yield load)

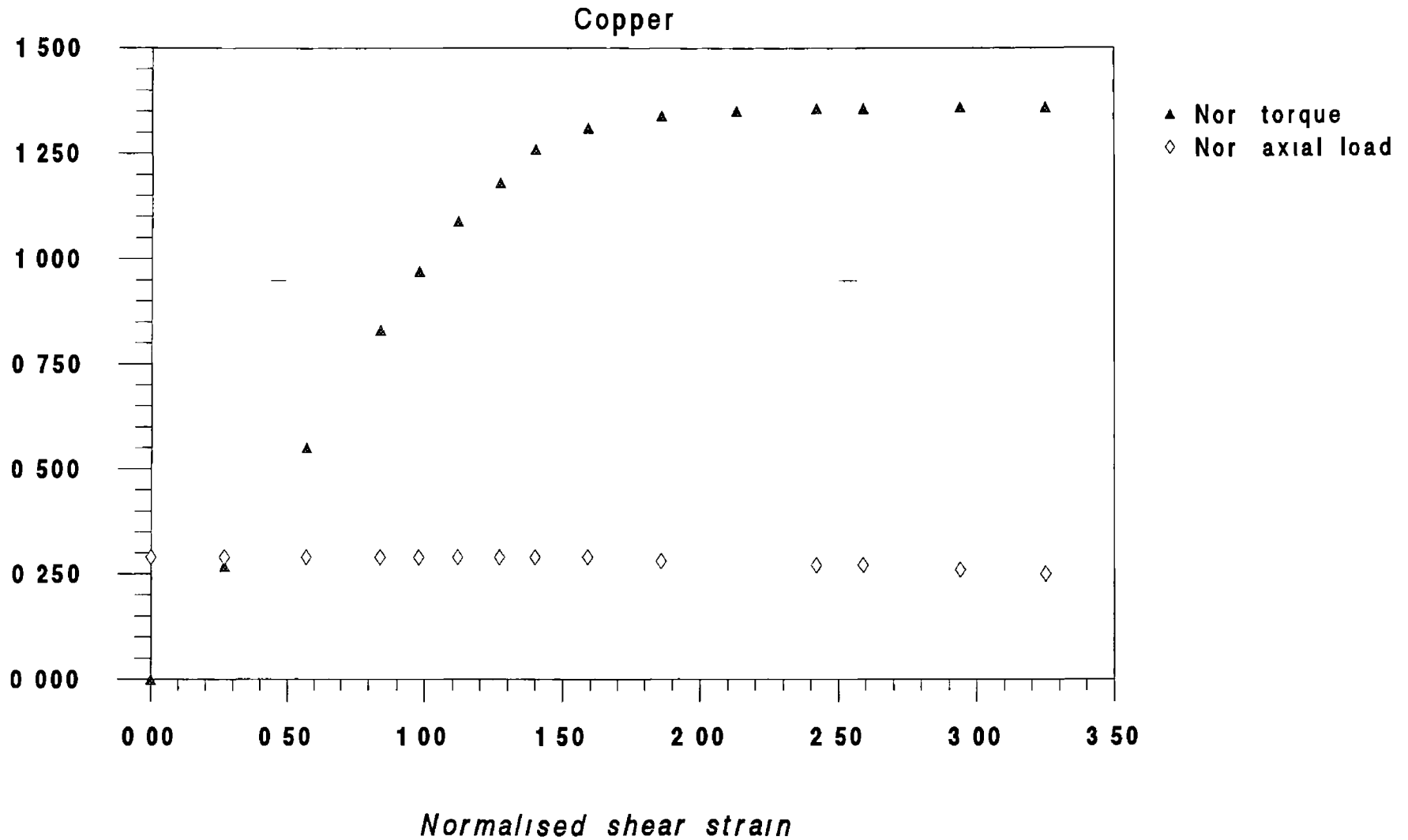


Figure 6.13(d) Normalised shear strain versus normalised axial load and torque curve
($F = 25\%$ of yield load)

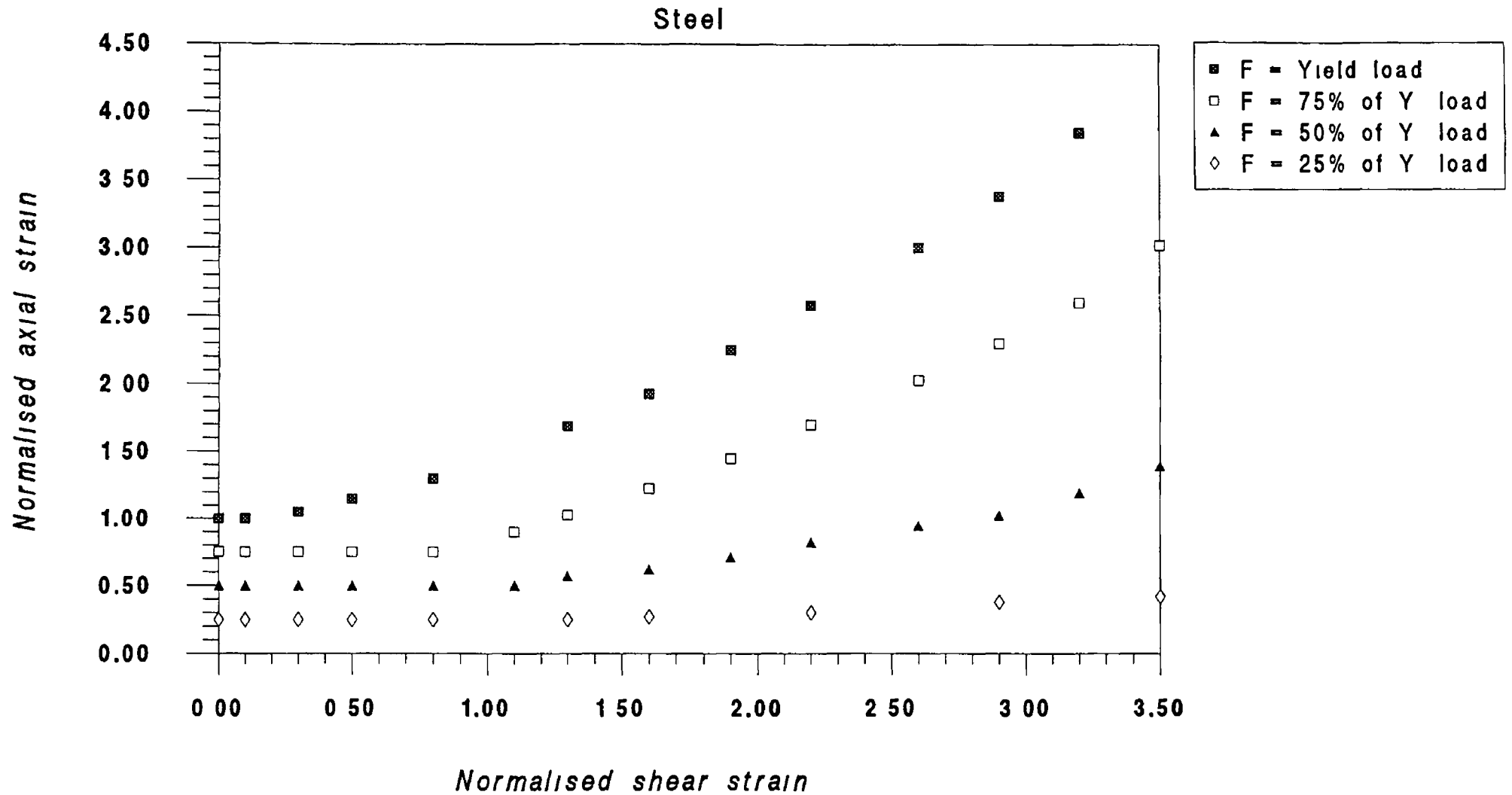


Figure 6.14 Normalised axial strain versus normalised shear strain curve (force maintained constant)

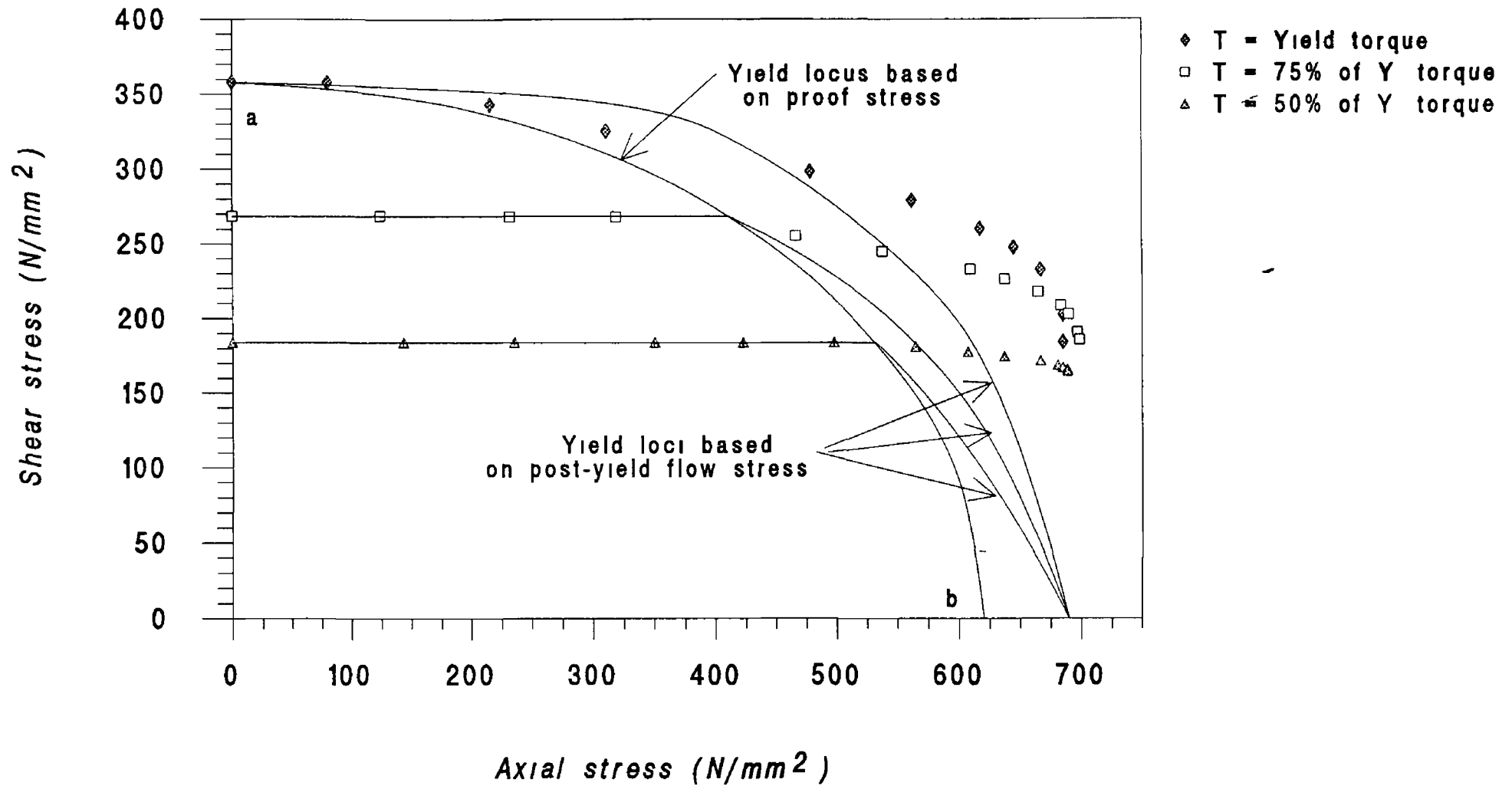


Figure 6.15 Determination of yield points due to combined loading (angle of twist constant)

Copper

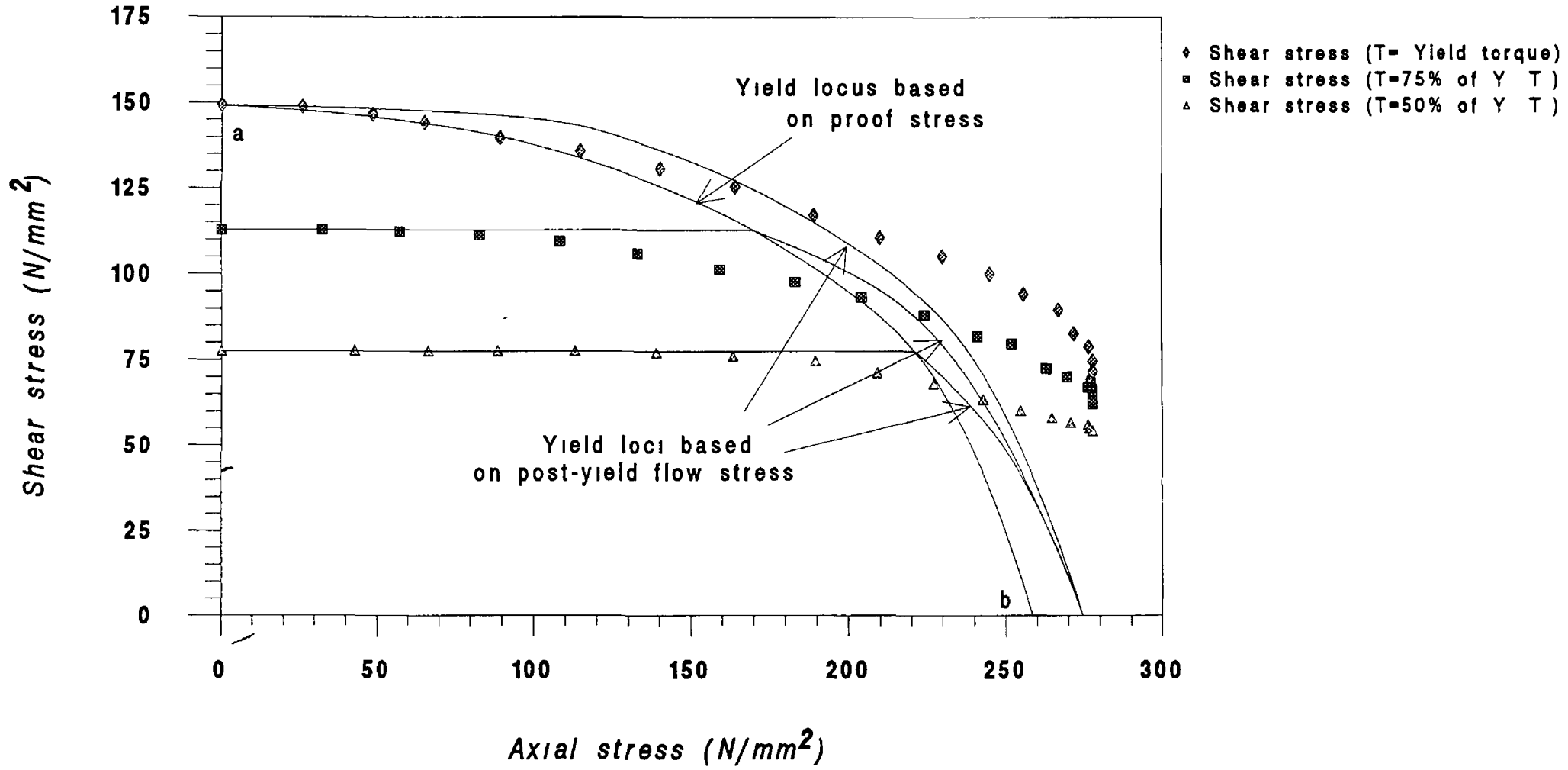


Figure 6 16 Determination of yield points due to combined loading (angle of twist constant)

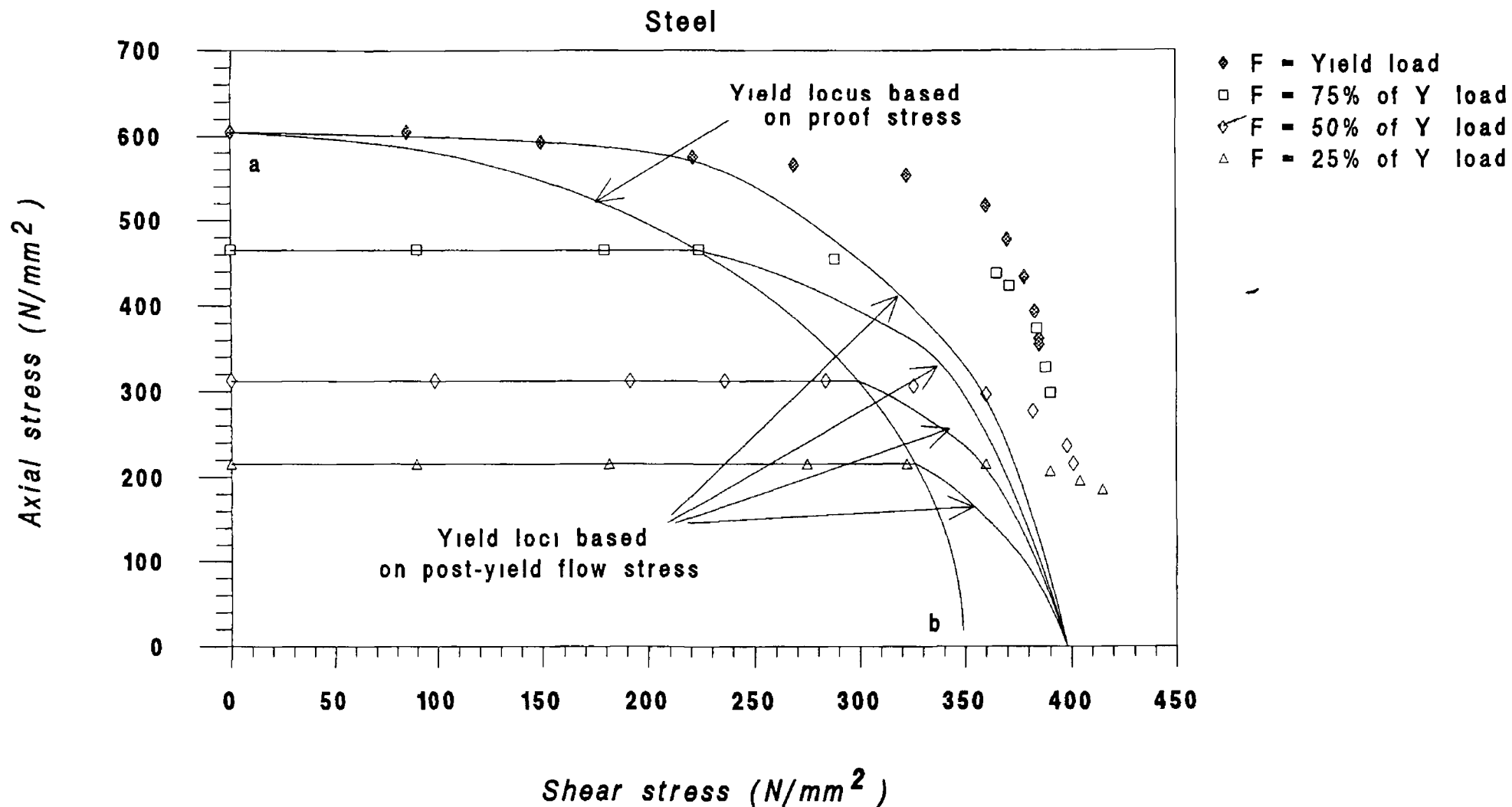


Figure 6.17 Determination of yield points due to combined loading (axial displacement constant)

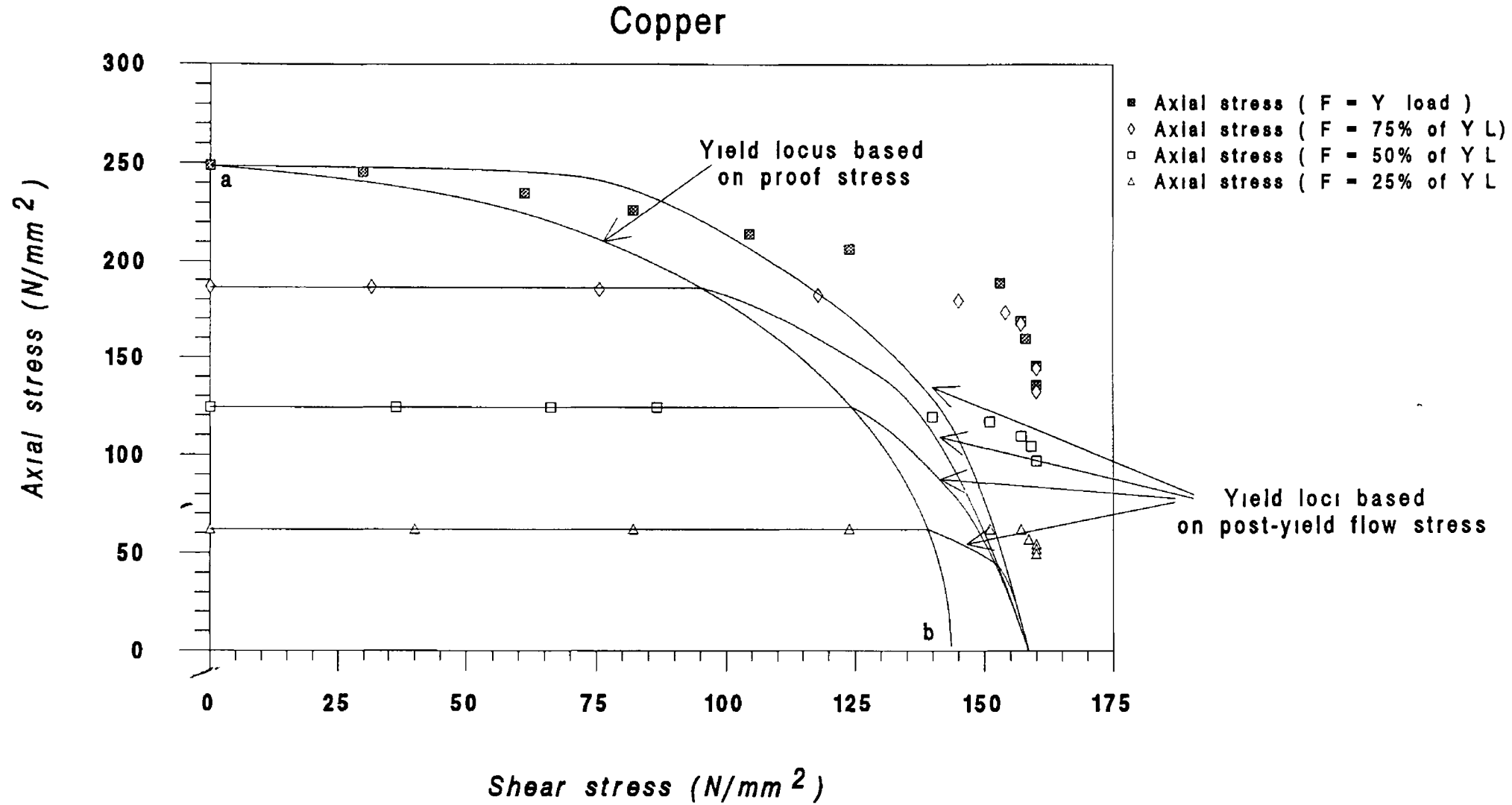


Figure 6.18 Determination of yield points due to combined loading (axial displacement constant)

Steel

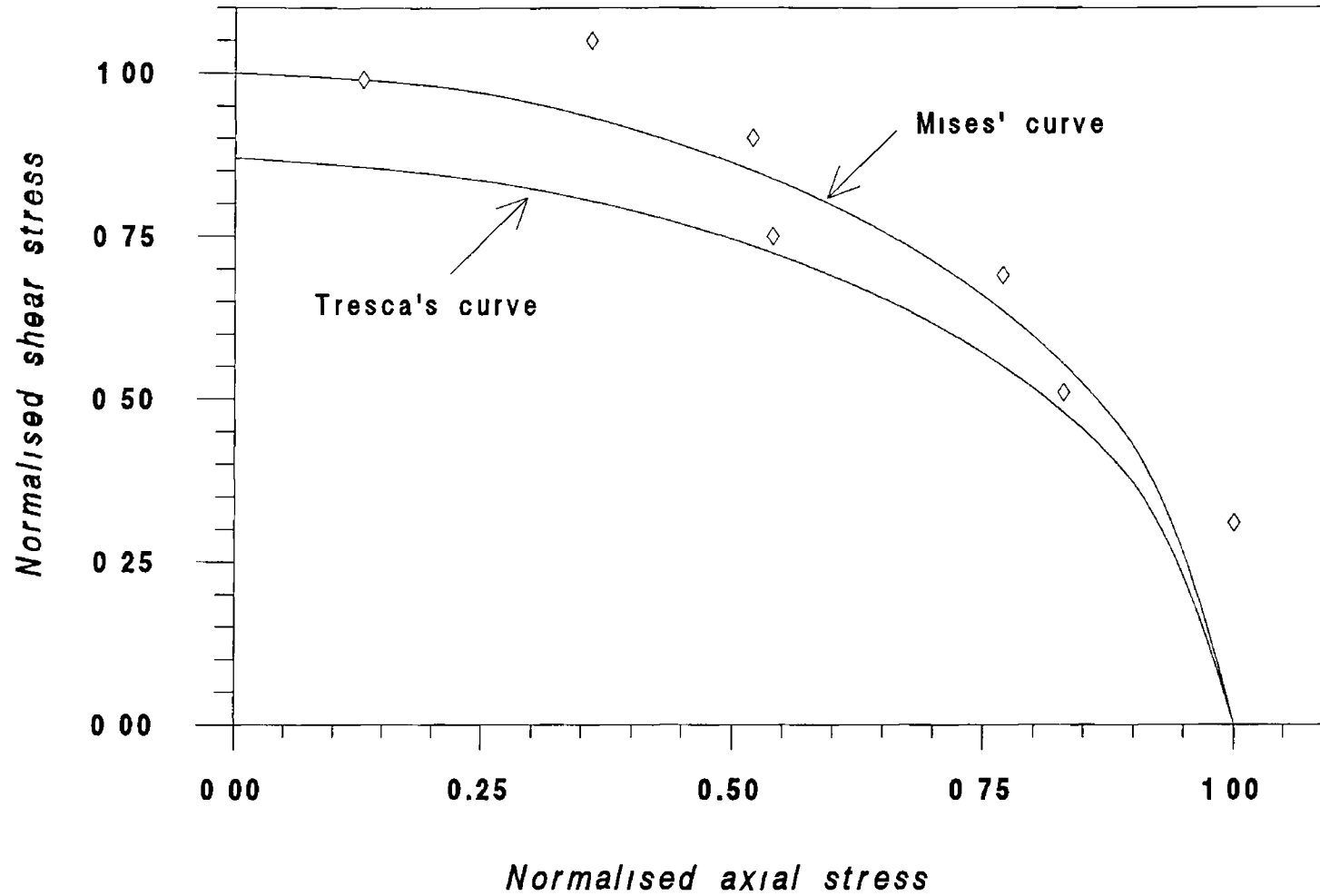


Figure 6 19(a) Comparison of experimentally obtained yield stresses with those of Mises' and Tresca's

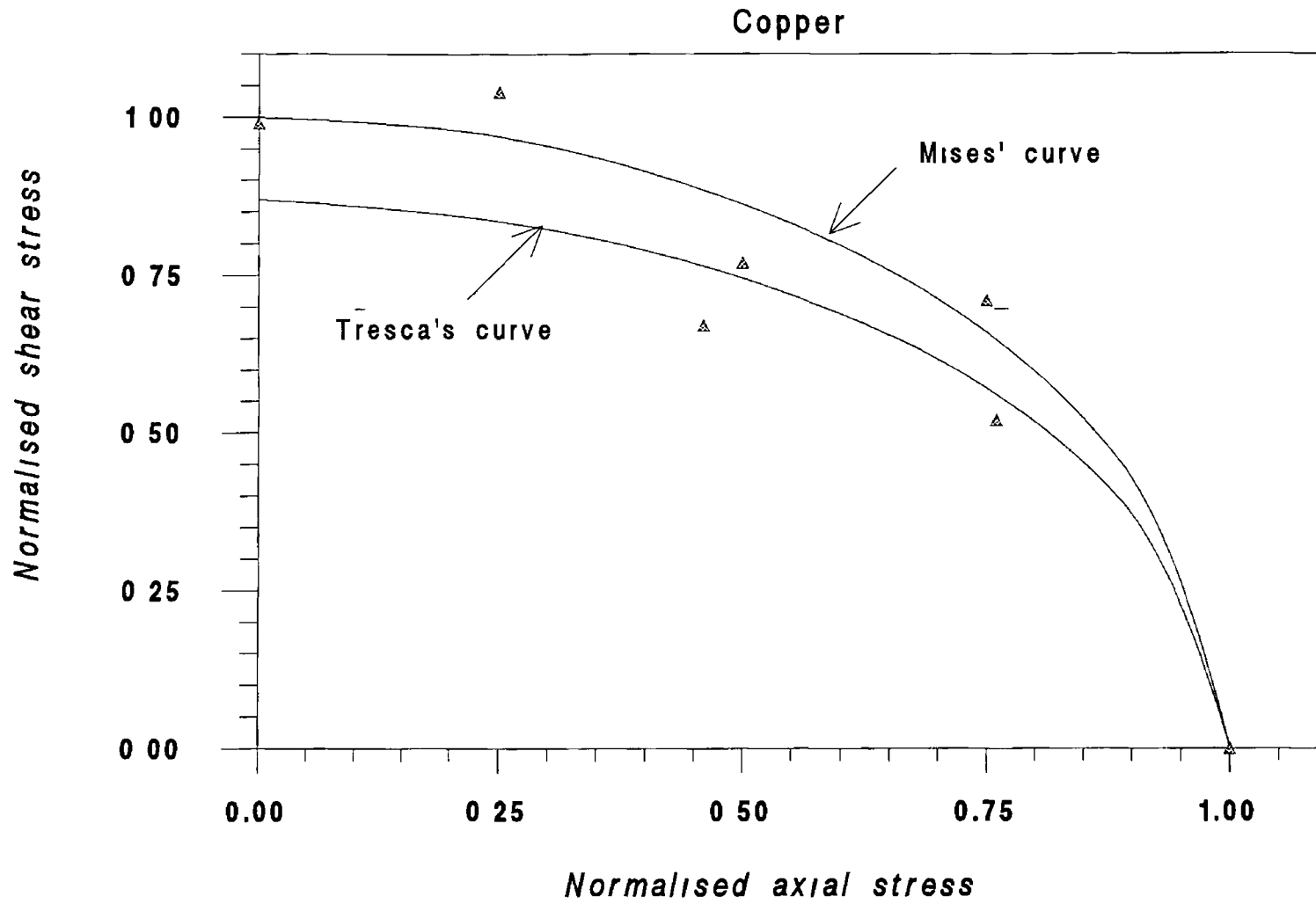


Figure 6.19(b) Comparison of experimentally obtained yield stresses with those of Mises' and Tresca's

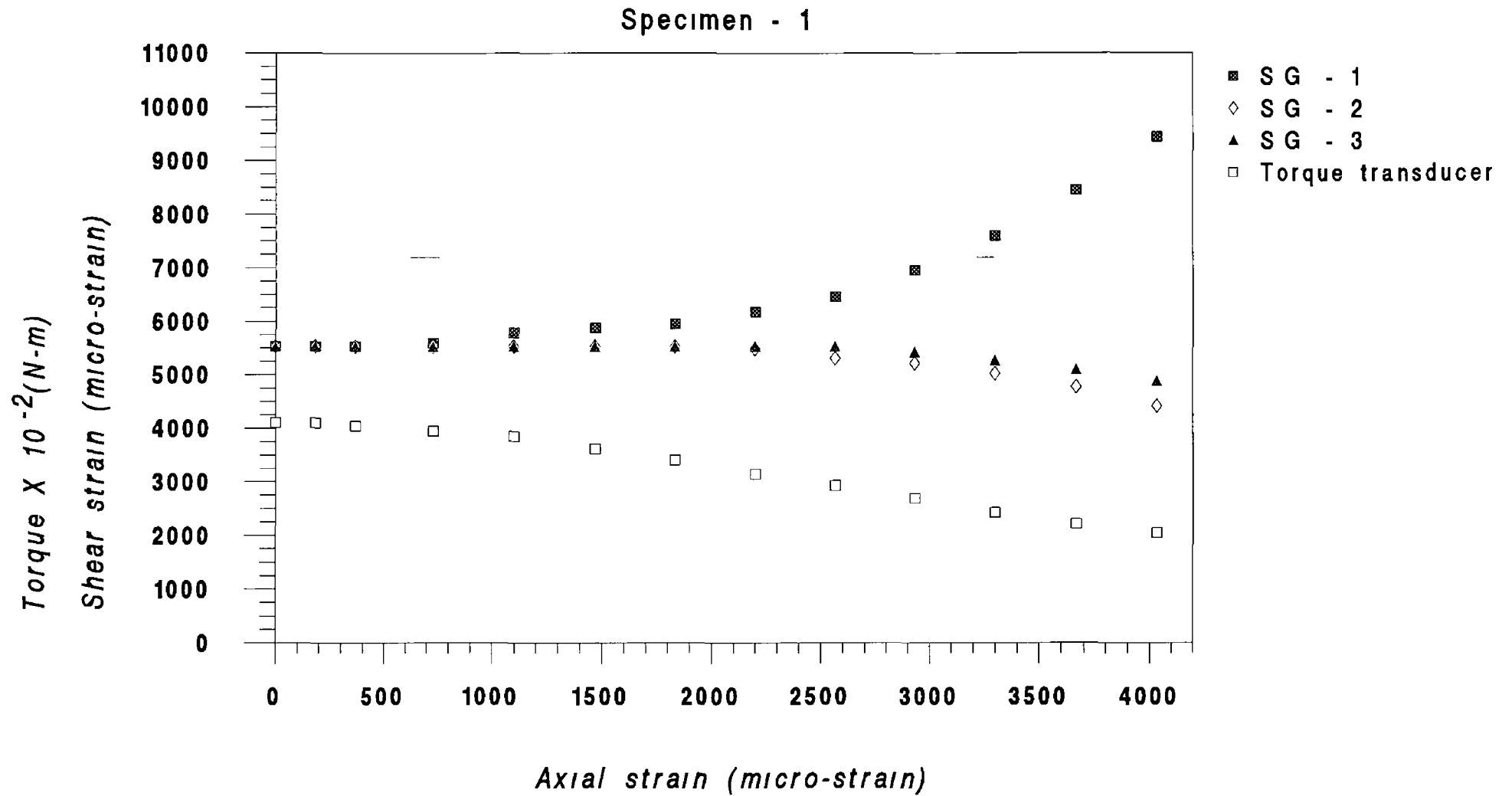


Figure 6 20(a) Variations of the torque and shear strain gauges' readings with axial strain (uniform diameter specimen)

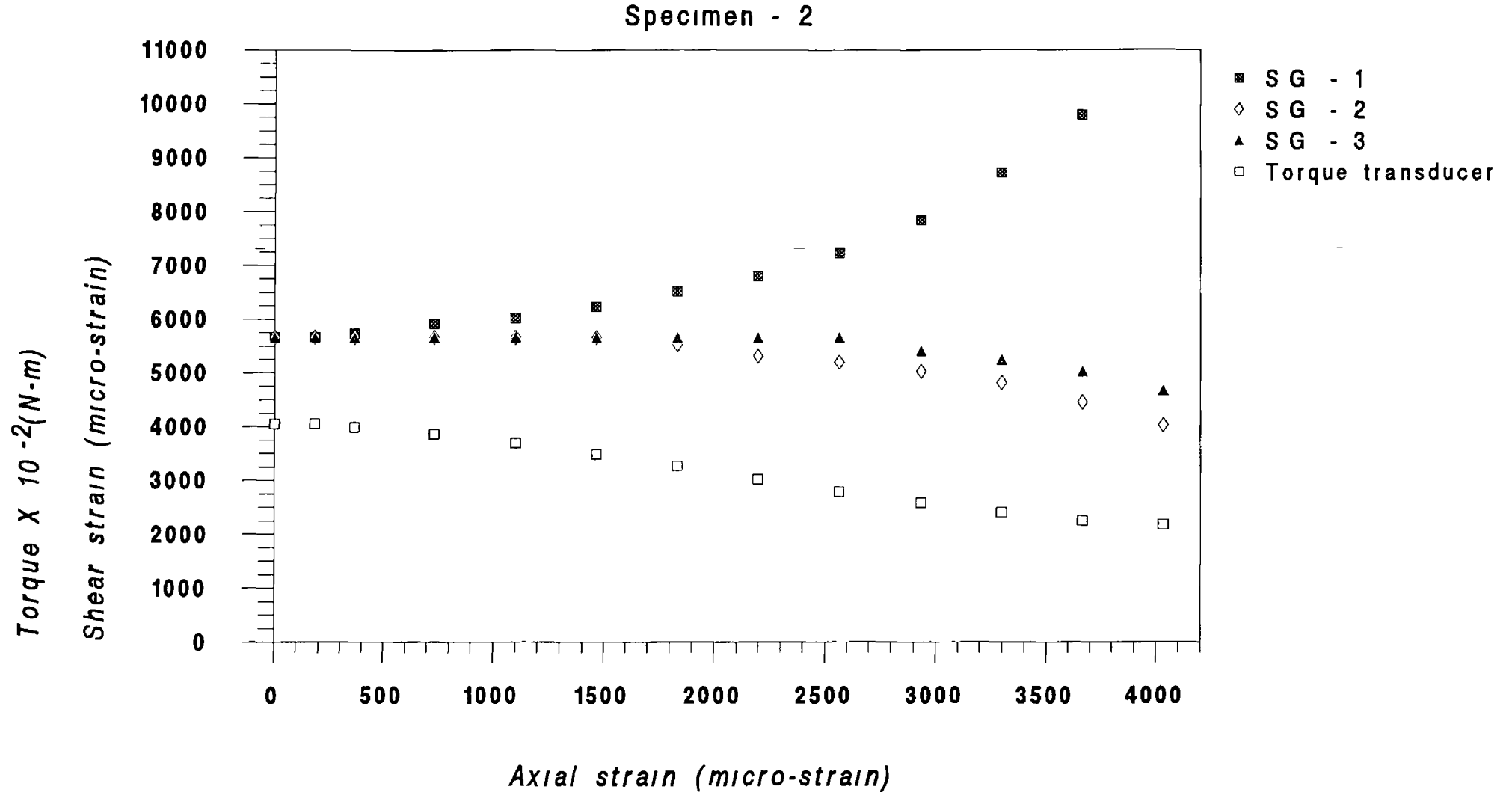


Figure 6.20(b) Variations of torque and shear strain gauges' readings with axial strain (uniform diameter specimen)

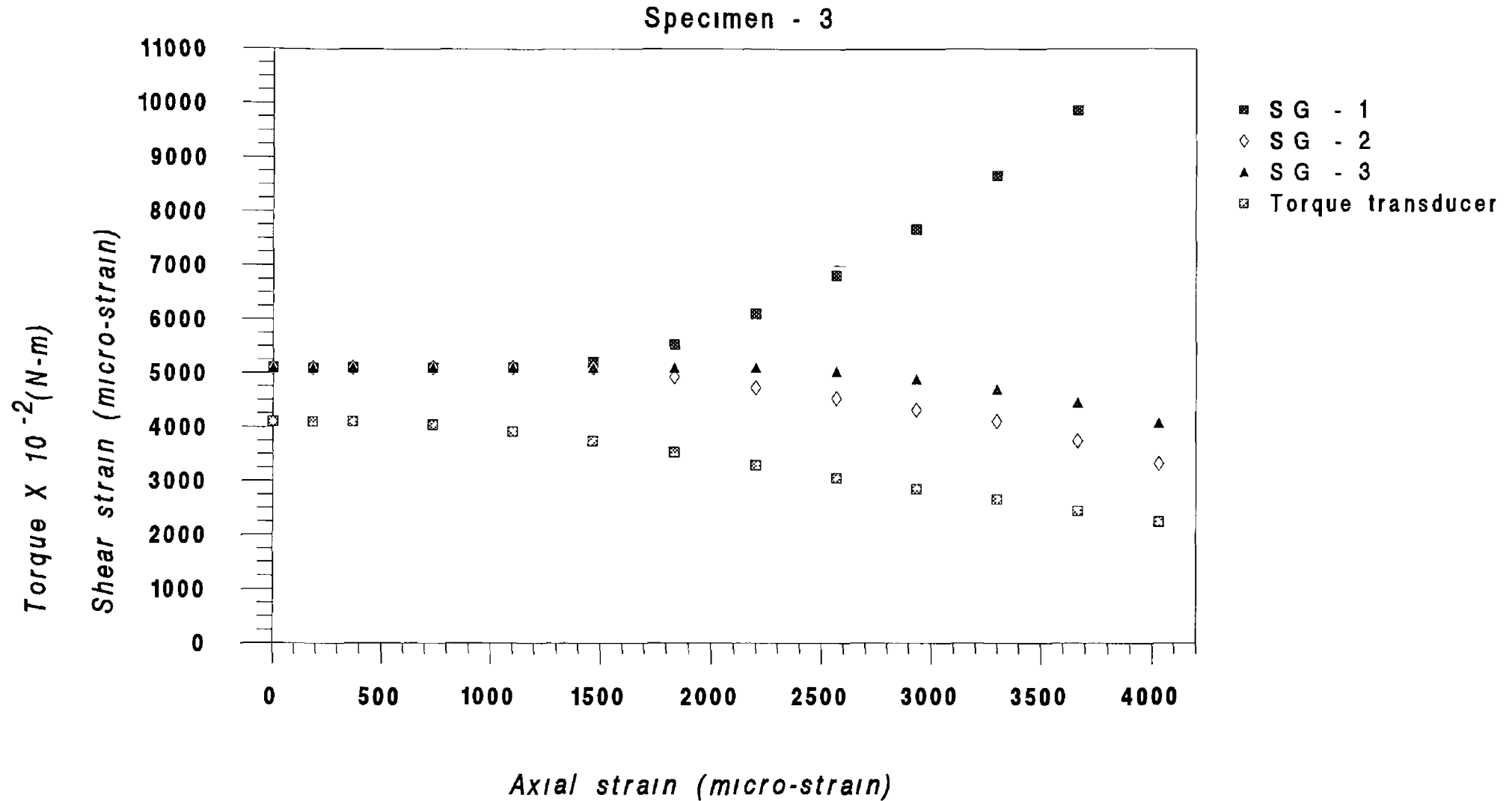


Figure 6.20(c) Variations of torque and shear strain gauges' readings with axial strain (uniform diameter specimen)

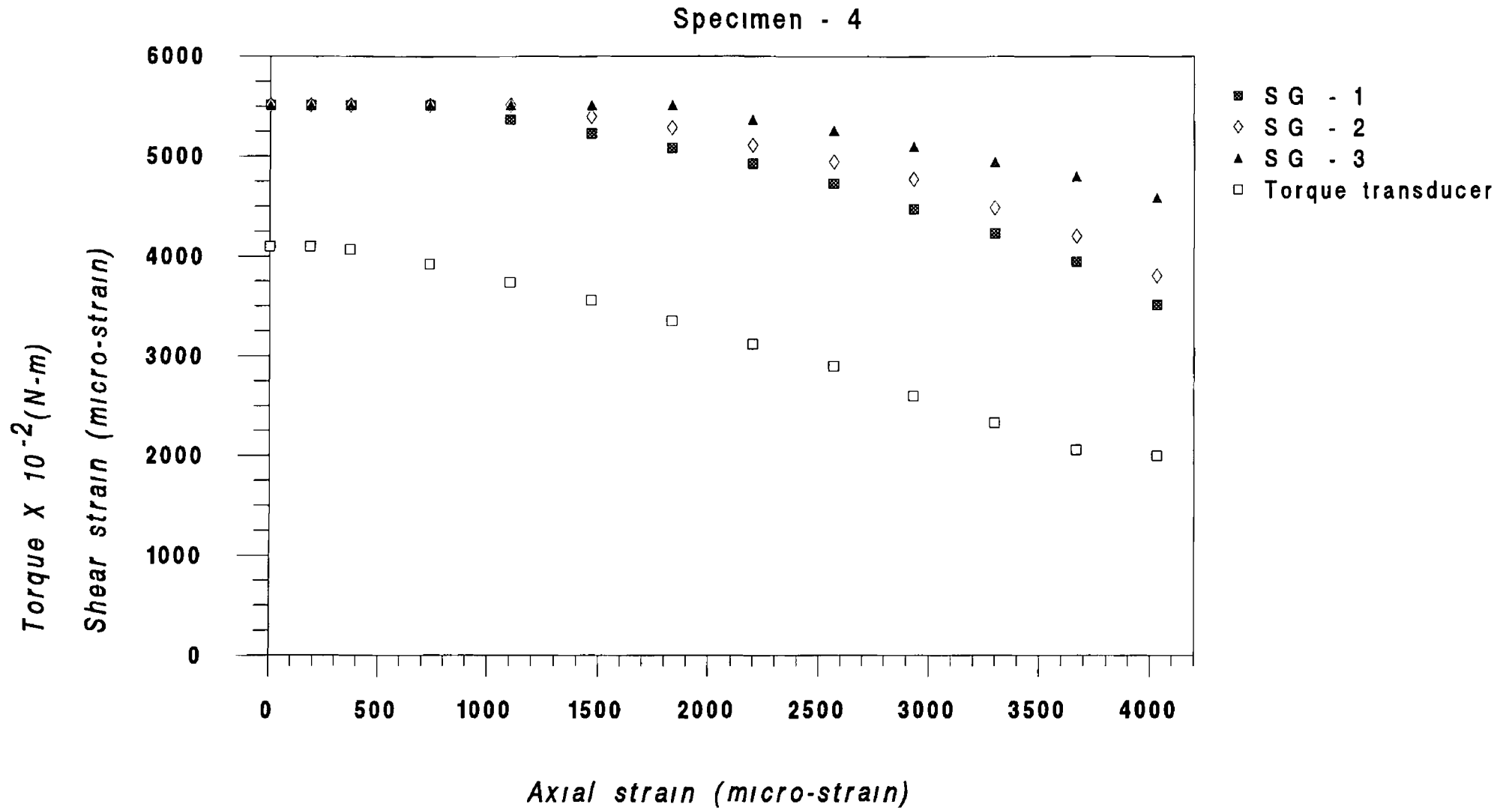


Figure 6.20(d) Variations of torque and shear strain gauges' readings with axial strain (uniform diameter specimen)

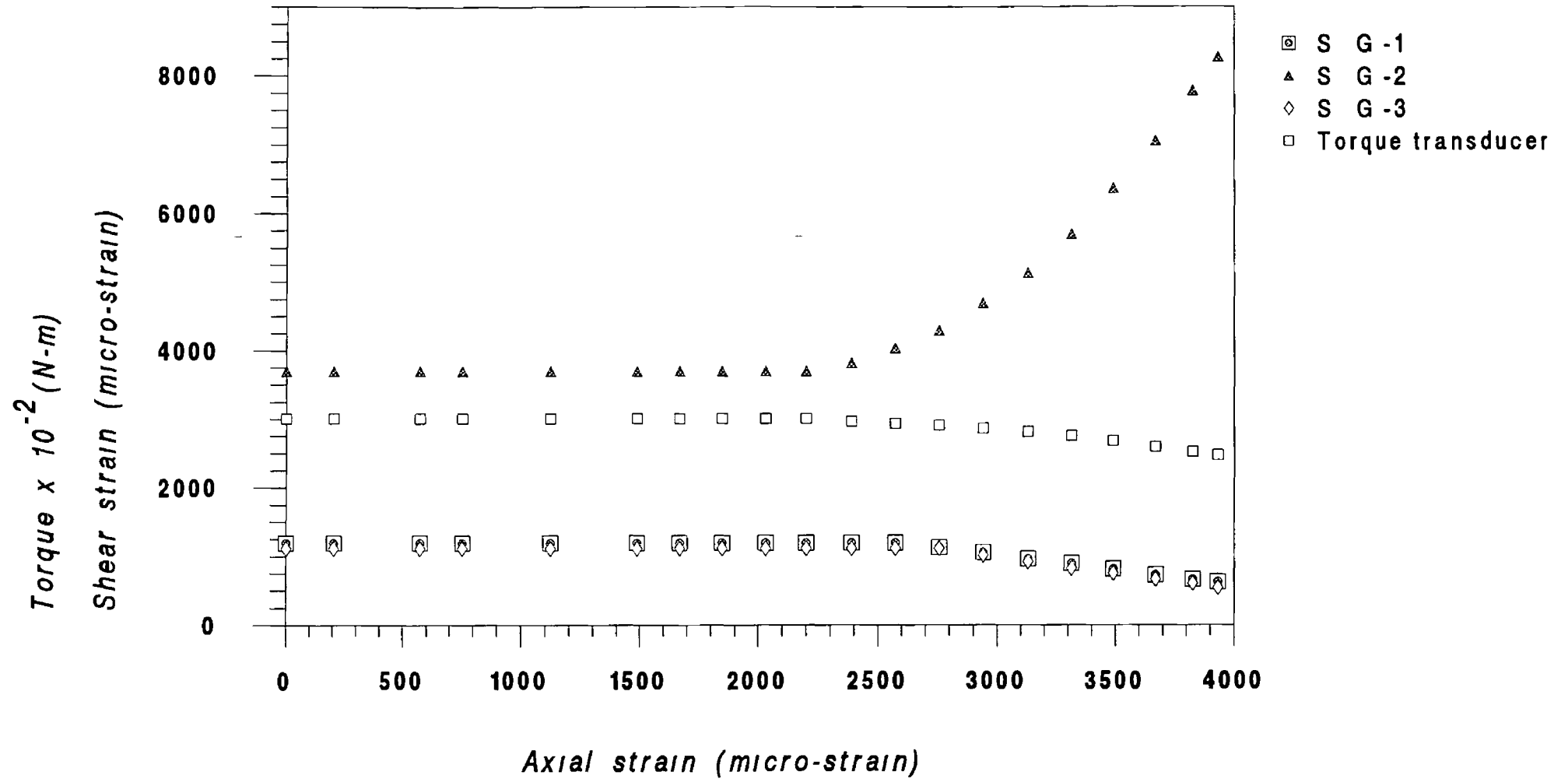


Figure 6.21(a) Variations of torque and strain gauges' readings with the axial strain (reduced section specimen)

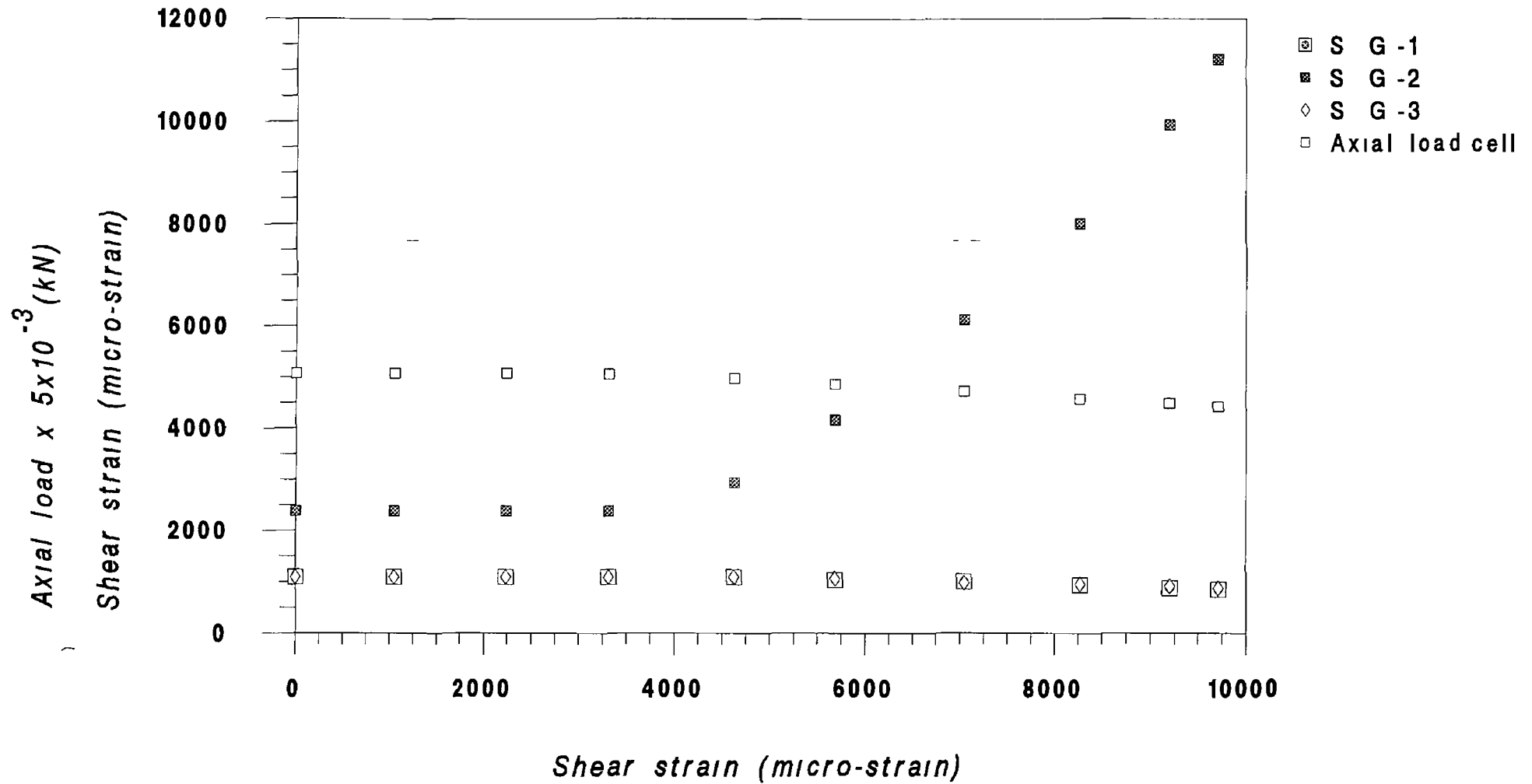


Figure 6.21(b) Variations of axial load and strain gauges' readings with the shear strain (reduced section specimen)

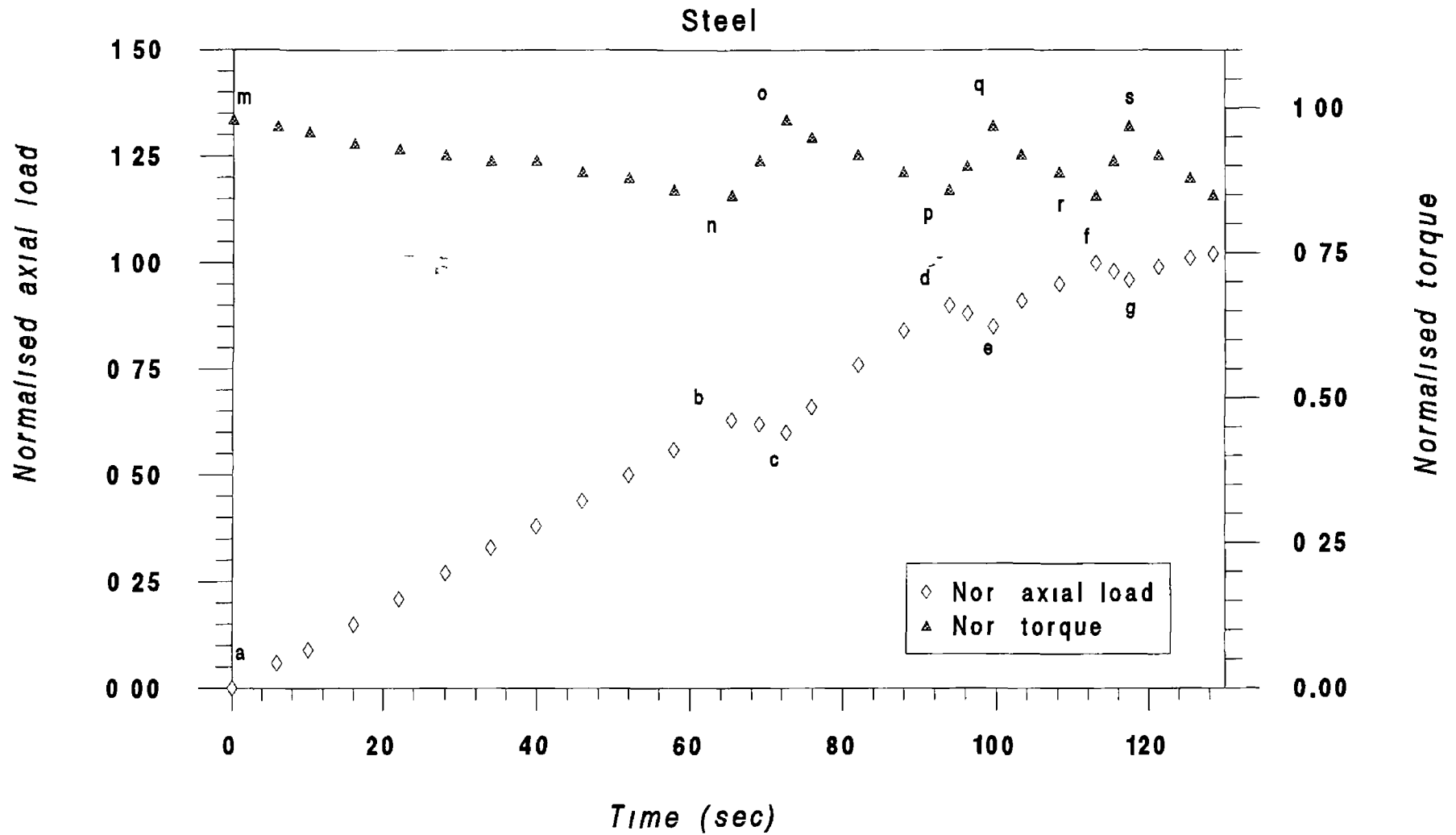


Figure 6.22(a) Variations of normalised torque and axial load with time
(initial $T = 98\%$ of yield torque)

Steel

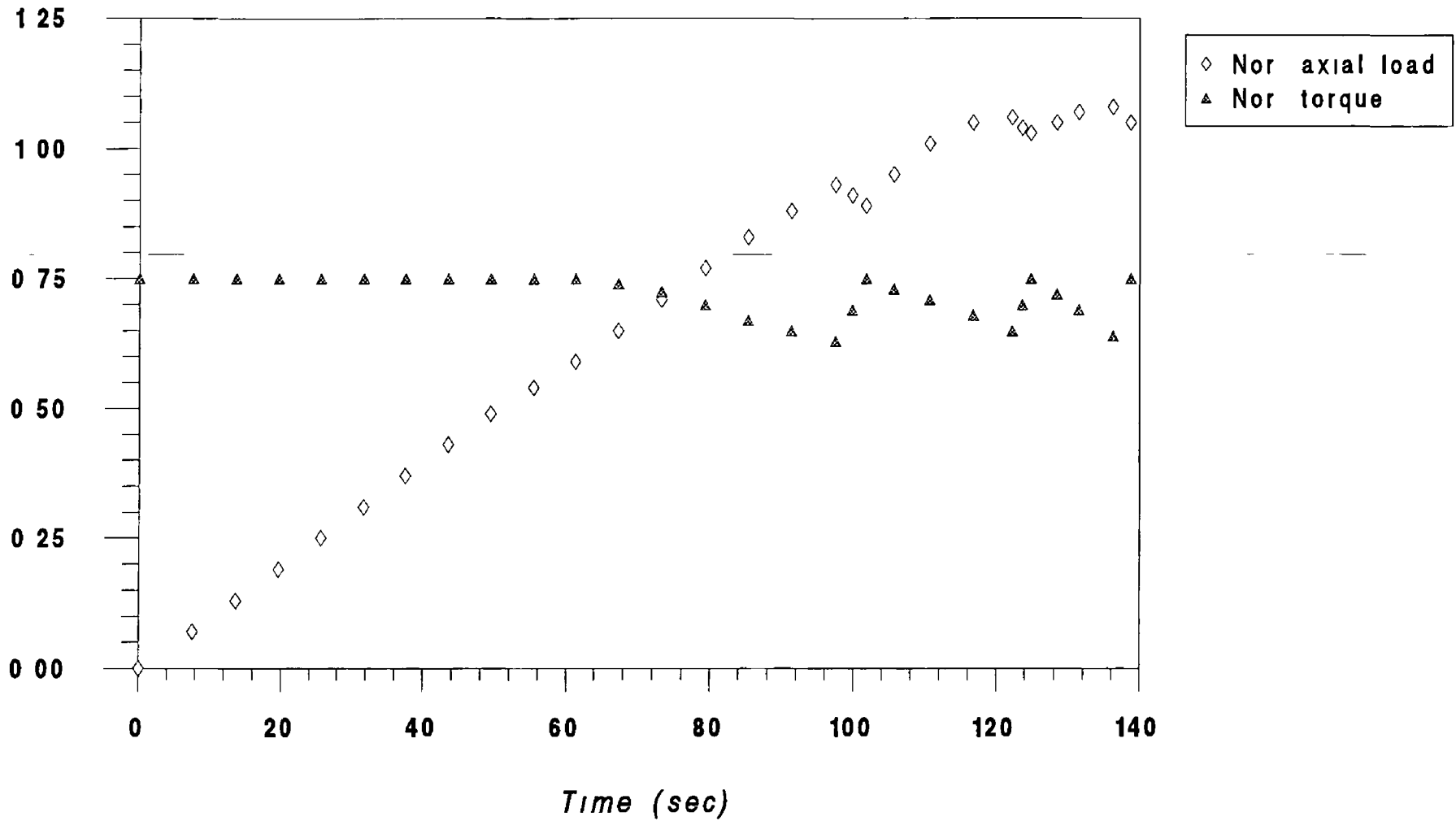


Figure 6.22(b) Variations of normalised torque and axial load with time (initial $T = 75\%$ of yield torque)

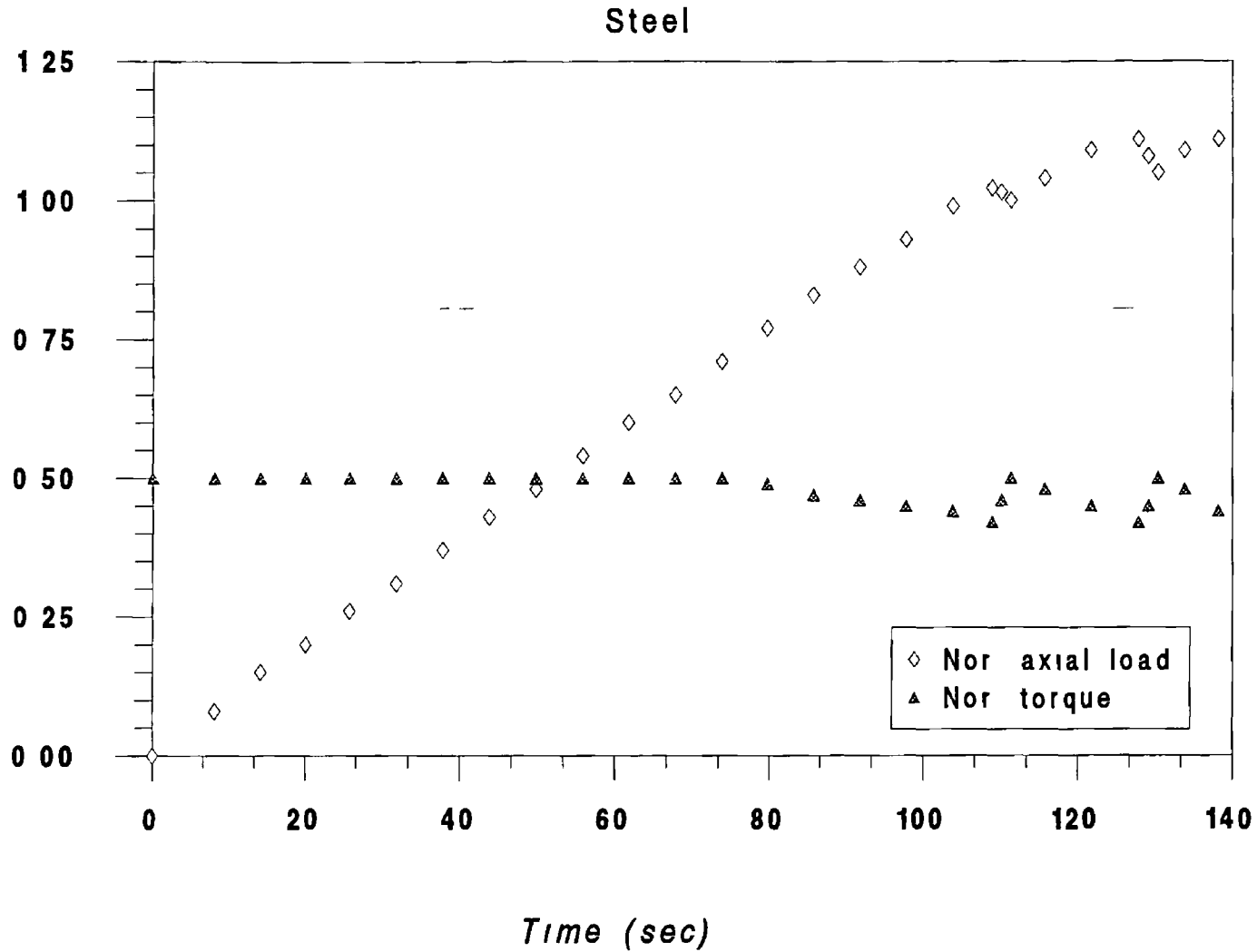


Figure 6.22(c) Variations of normalised torque and axial load with time
(initial $T = 50\%$ of yield torque)

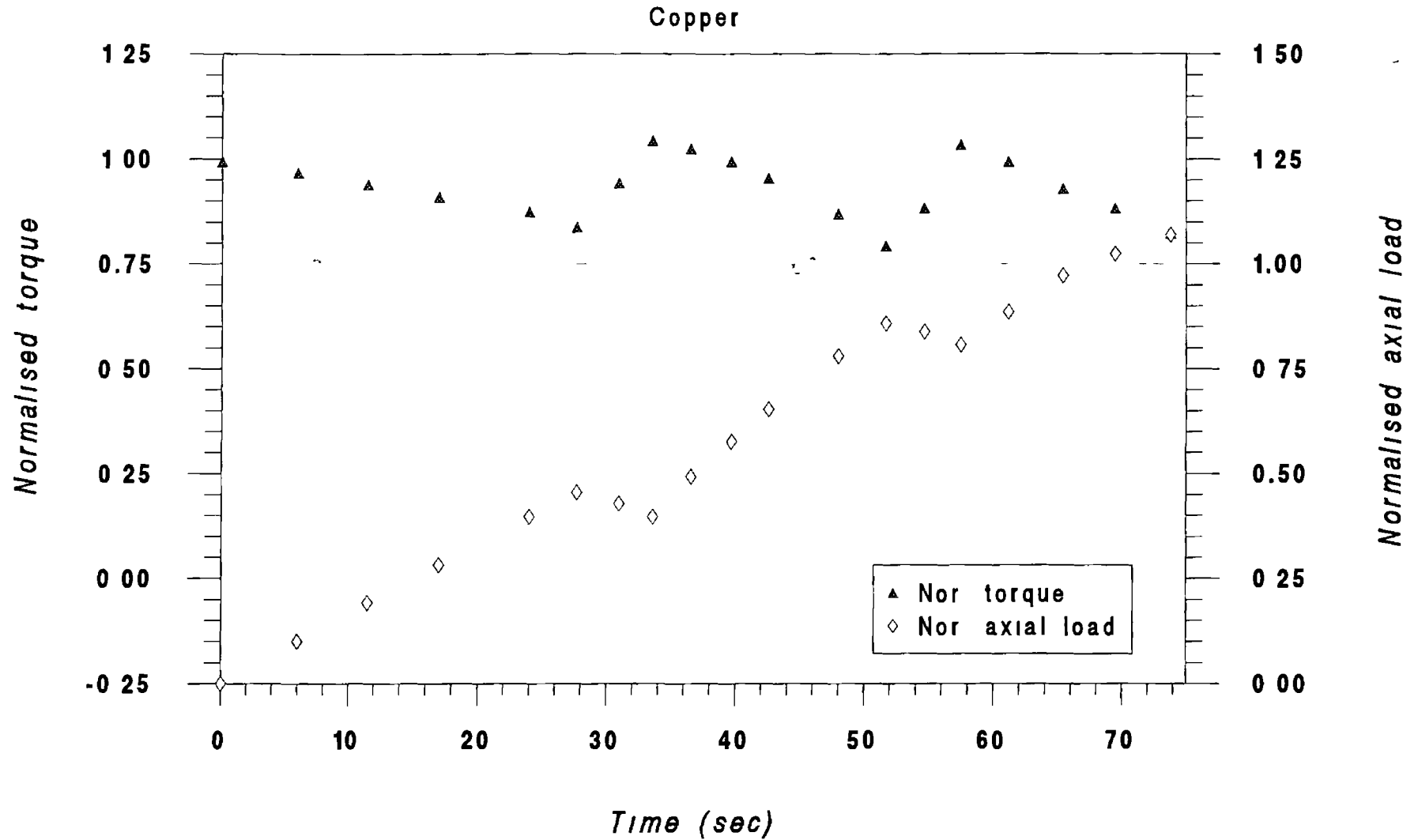


Figure 6.23(a) Variations of normalised torque and axial load with time (initial $T =$ yield torque)

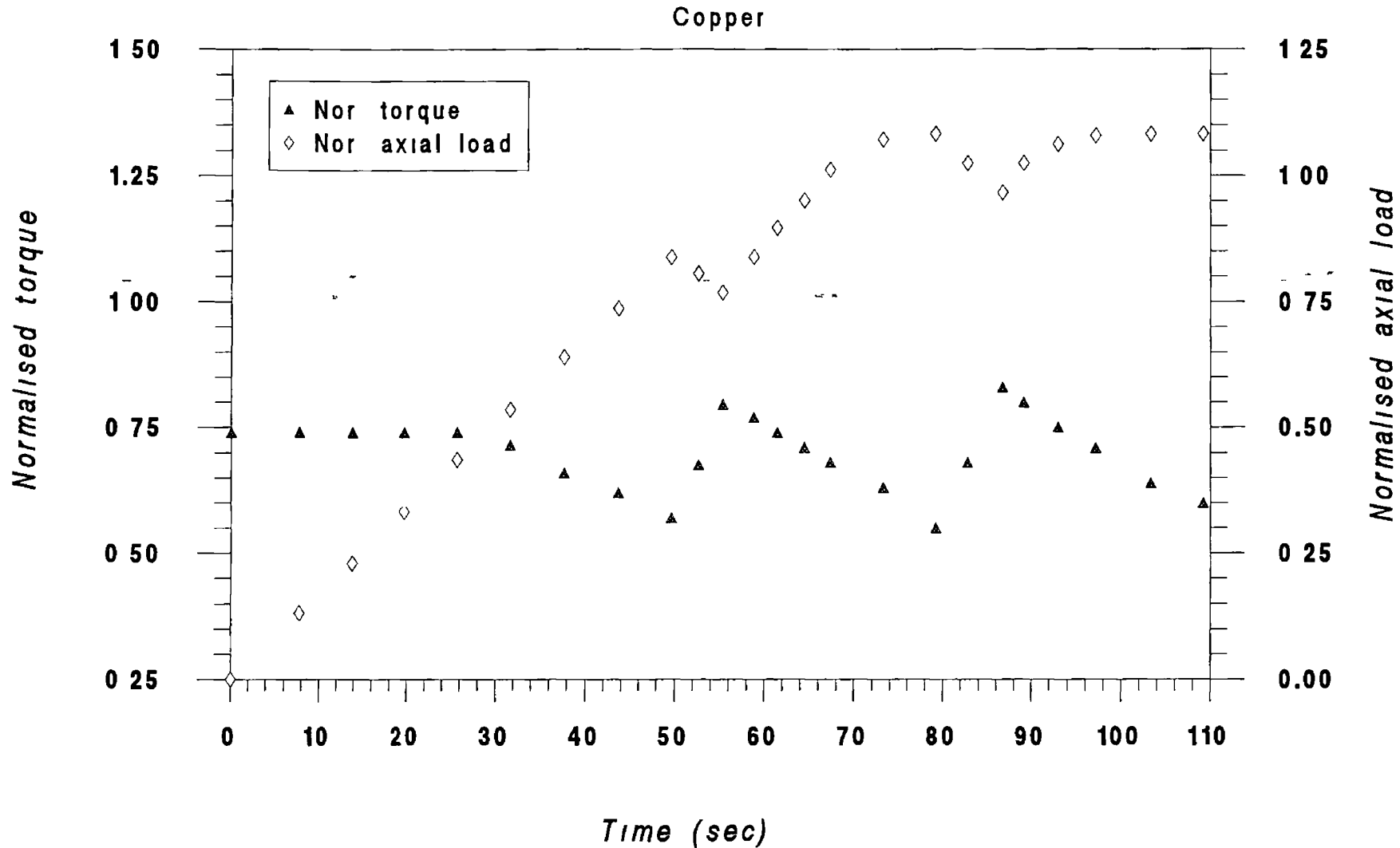


Figure 6.23(b) Variations of normalised torque and axial load with time
(initial $T = 75\%$ of yield torque)

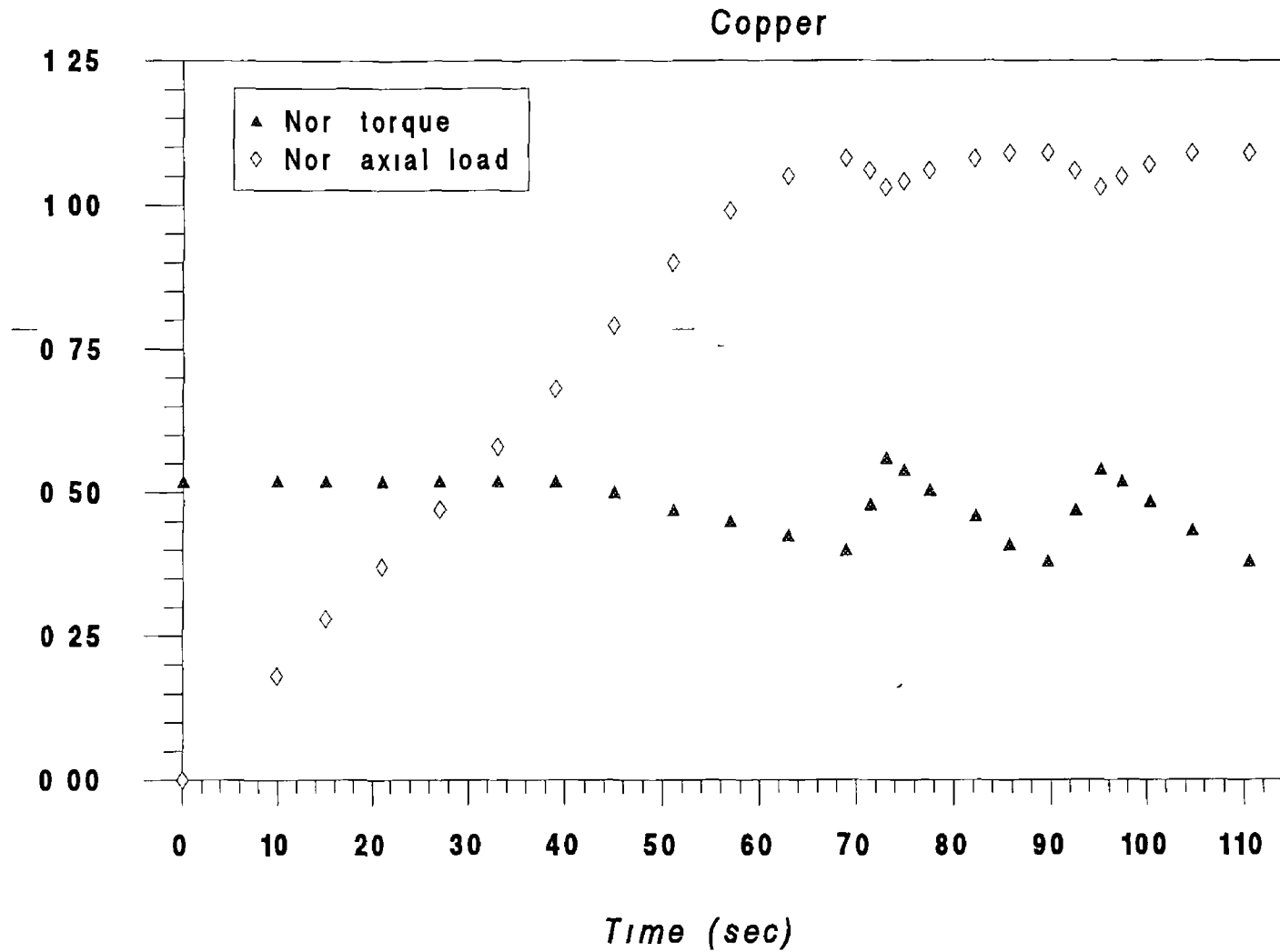


Figure 6.23(c) Variations of normalised torque and axial load with time
(initial $T = 50\%$ of yield torque)

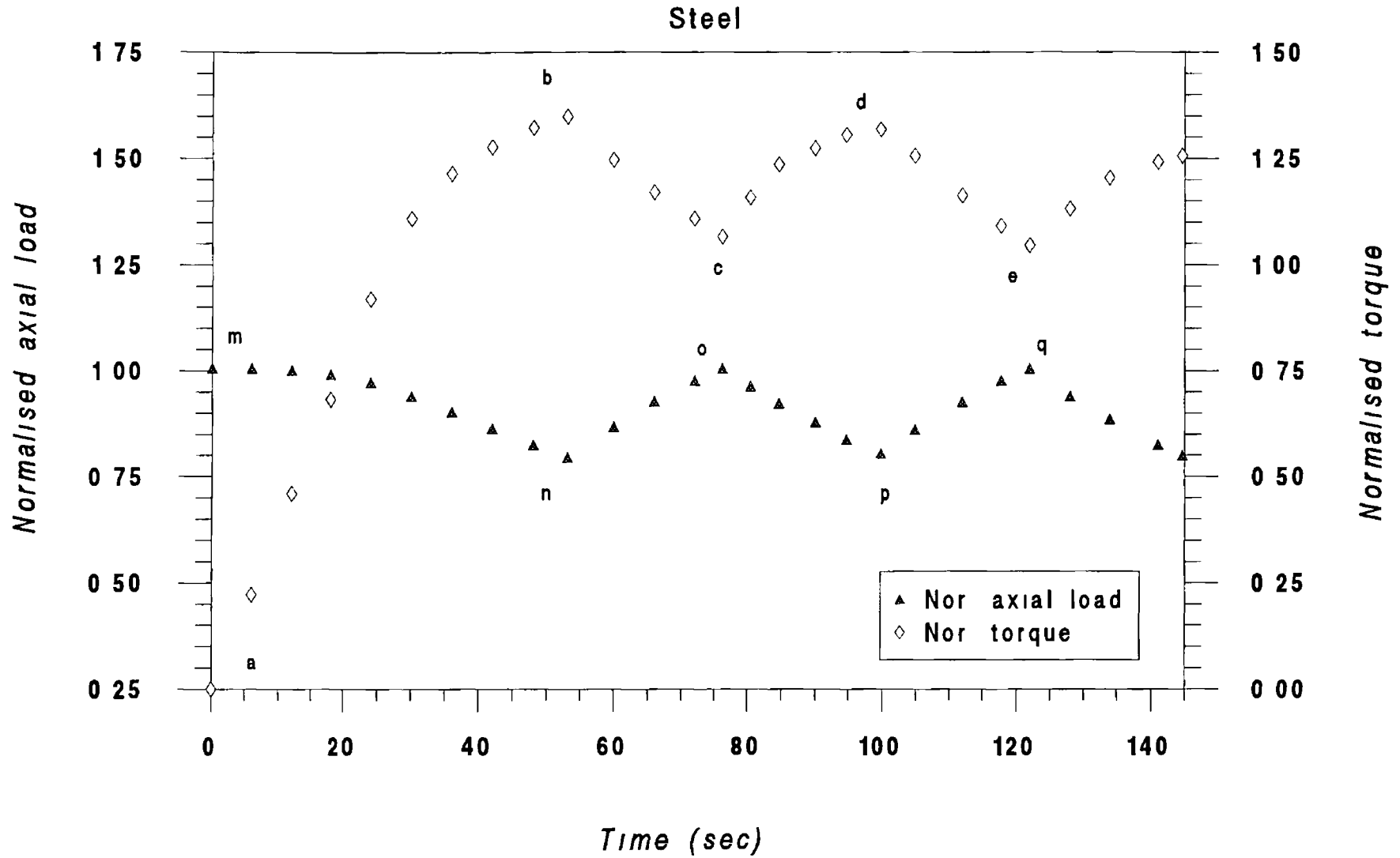


Figure 6.24(a) Variations of normalised axial load and torque with time (initial $F = \text{yield load}$)

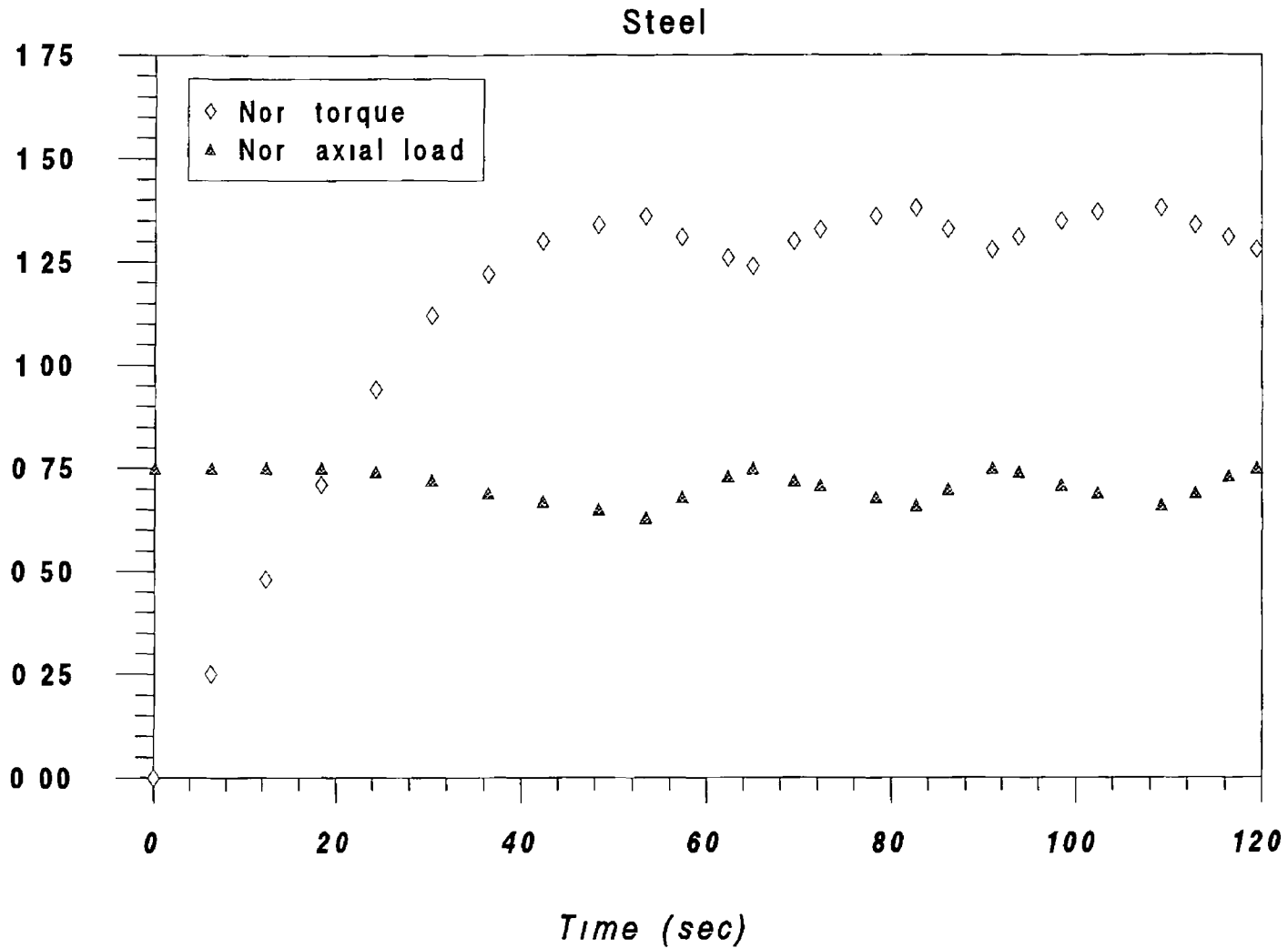
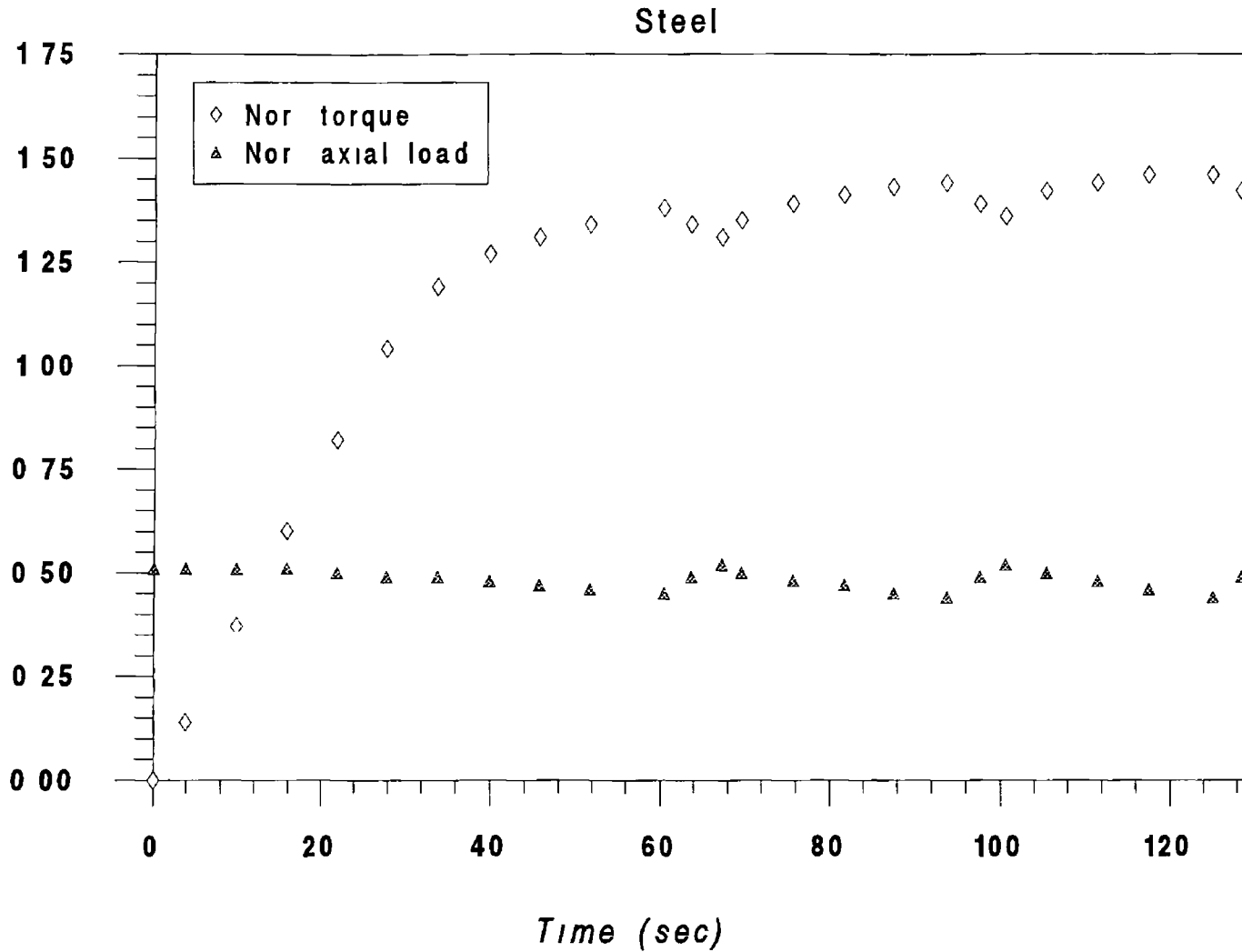


Figure 6 24(b) Variations of normalised axial load and torque with time
(initial $F = 75\%$ of yield load)



*Figure 6 24(c) Variations of normalised axial load and torque with time
(initial $F = 50\%$ of yield load)*

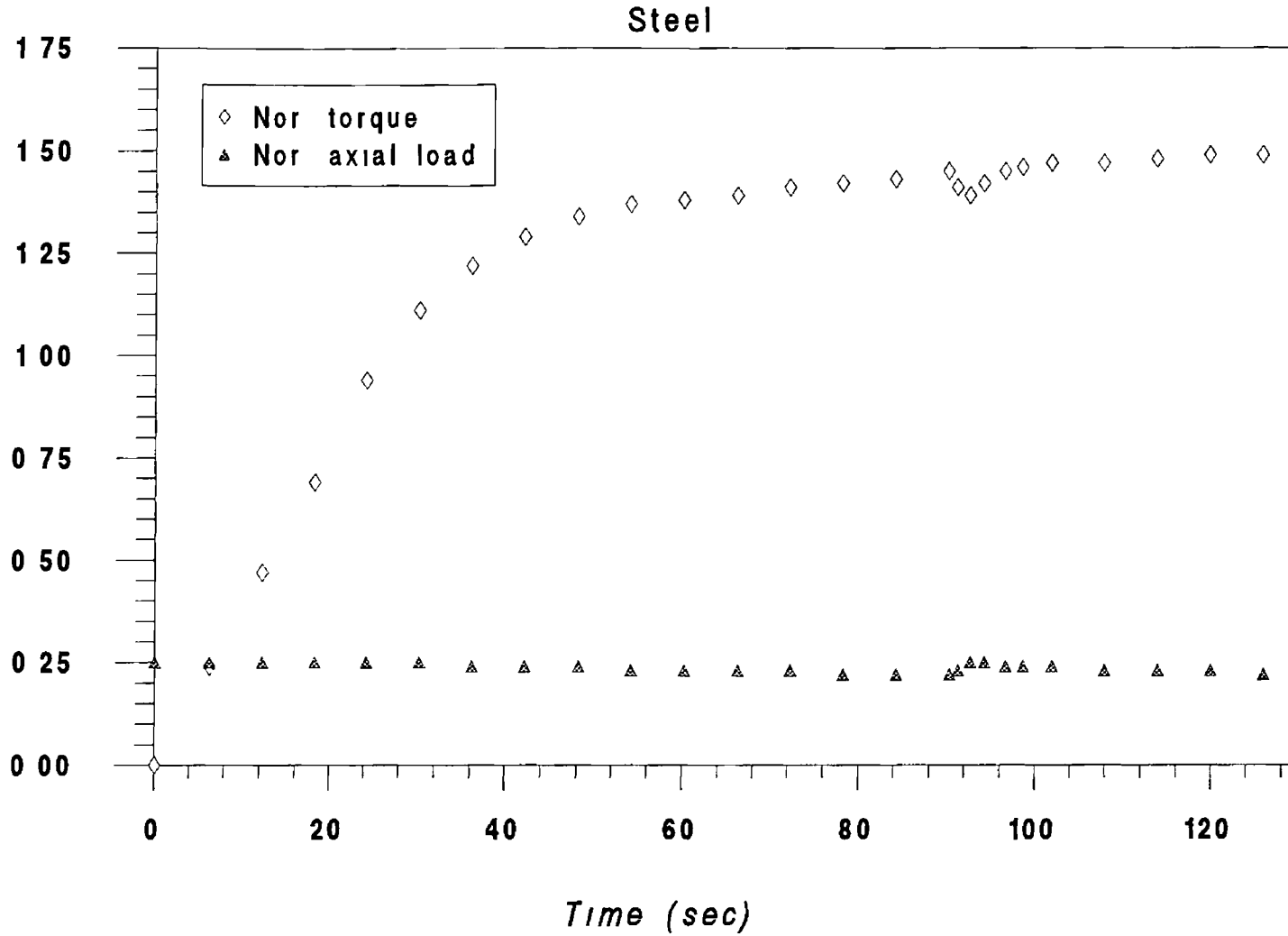


Figure 6 24(d) Variations of normalised axial load and torque with time
(initial $F = 25\%$ of yield load)

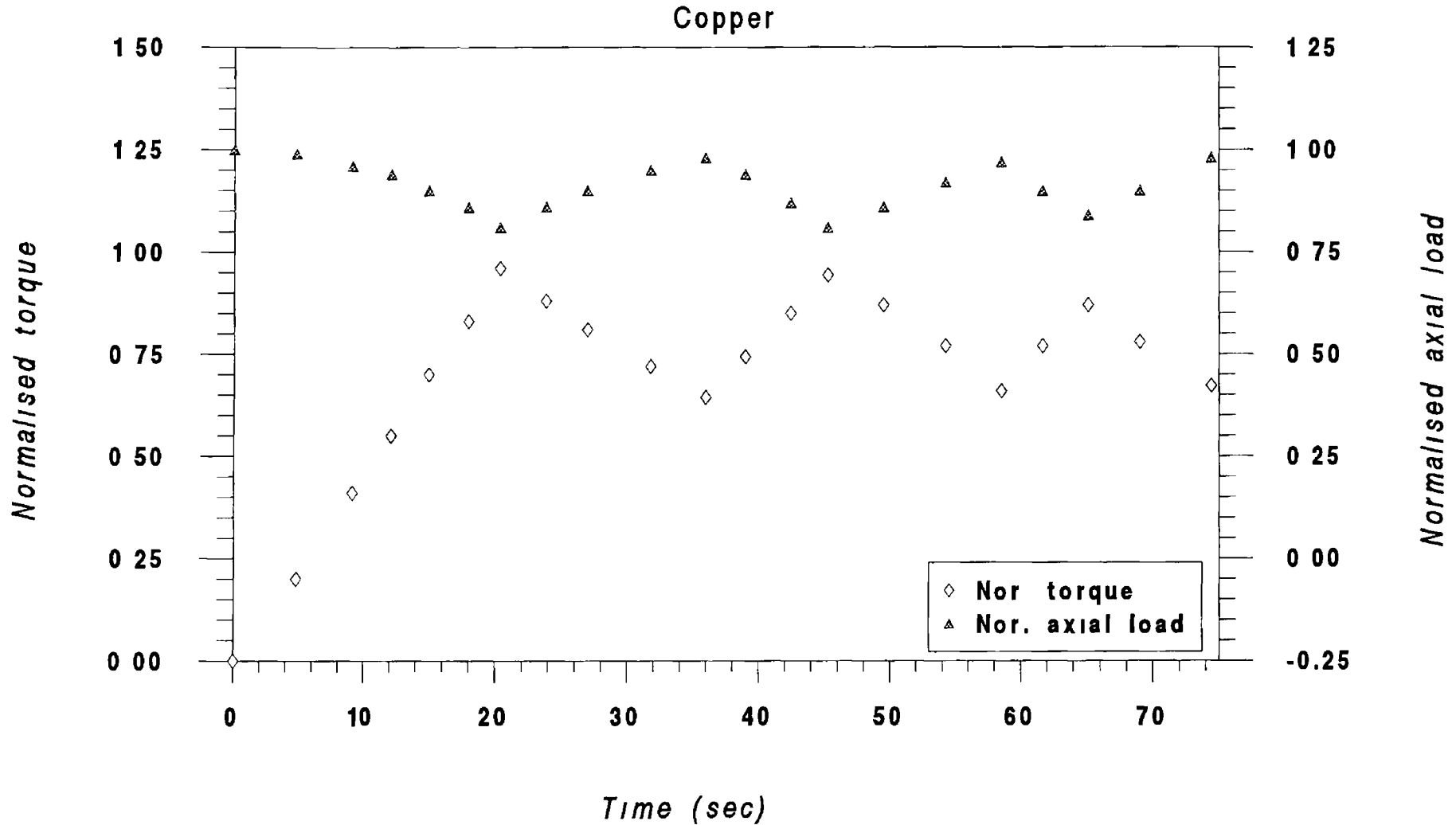


Figure 6 25(a) Variations of normalised axial load and torque with time (initial F = yield load)

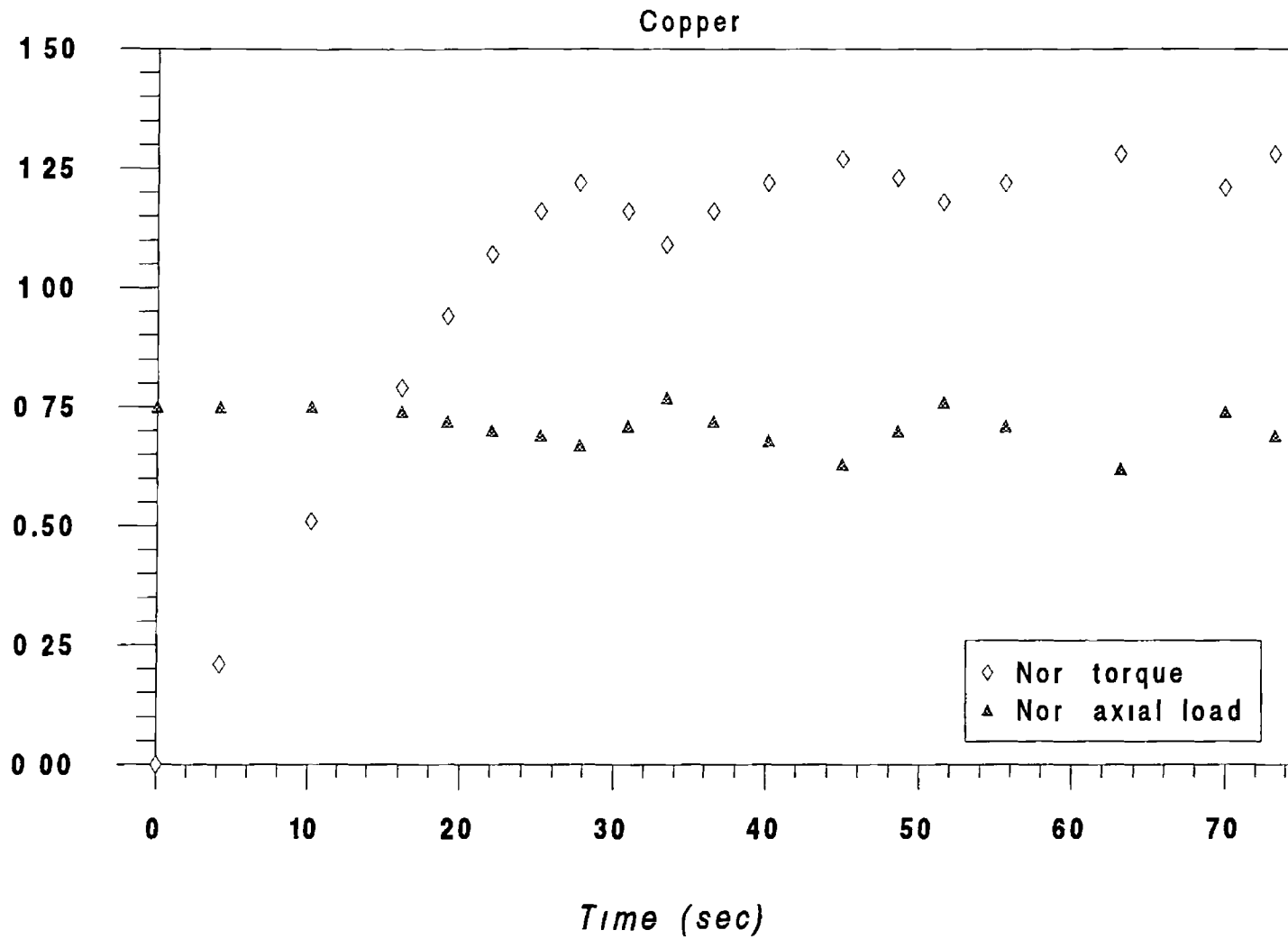


Figure 6 25(b) Variations of normalised axial load and torque with time
(initial $F = 75\%$ of yield load)

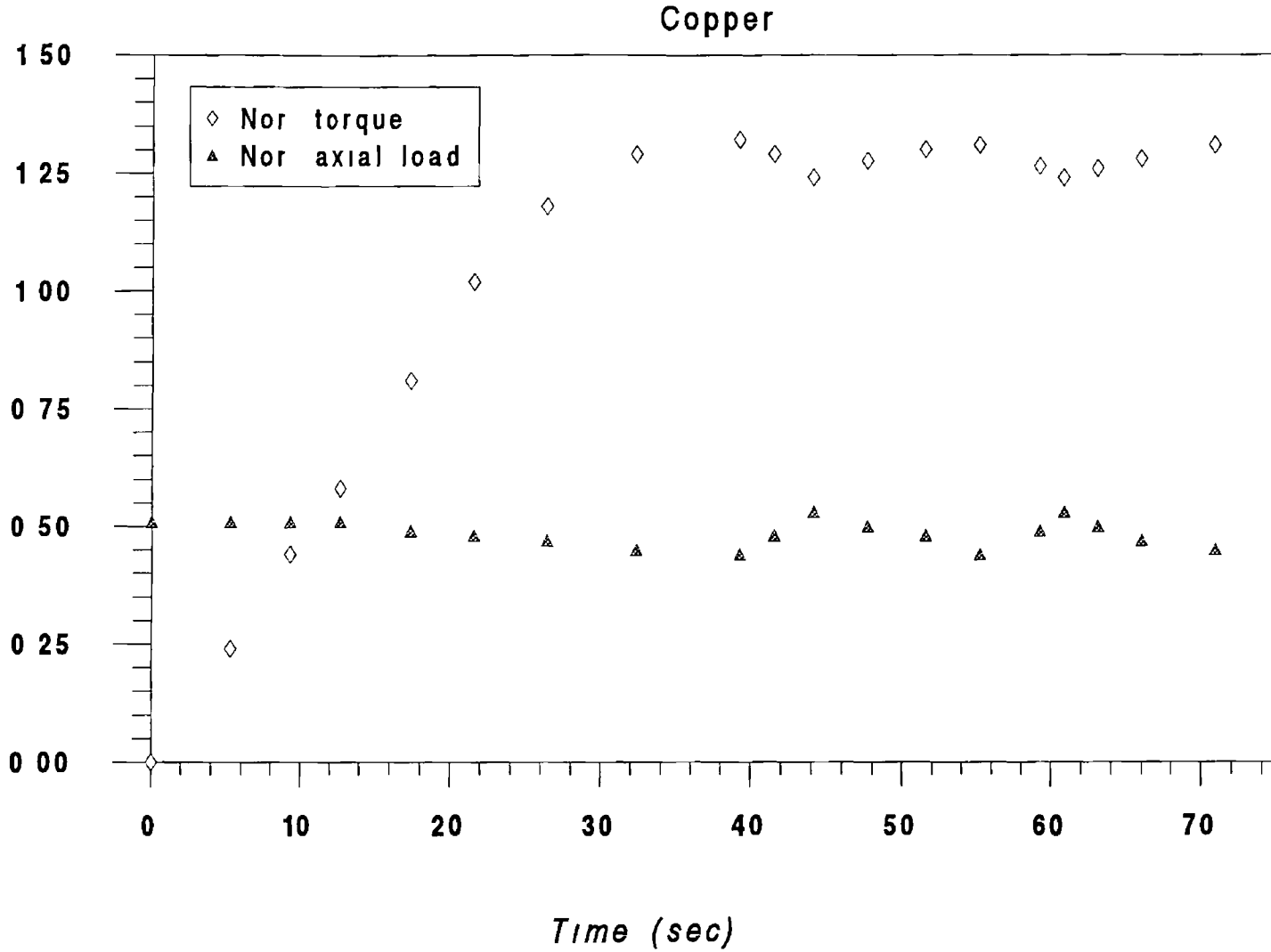
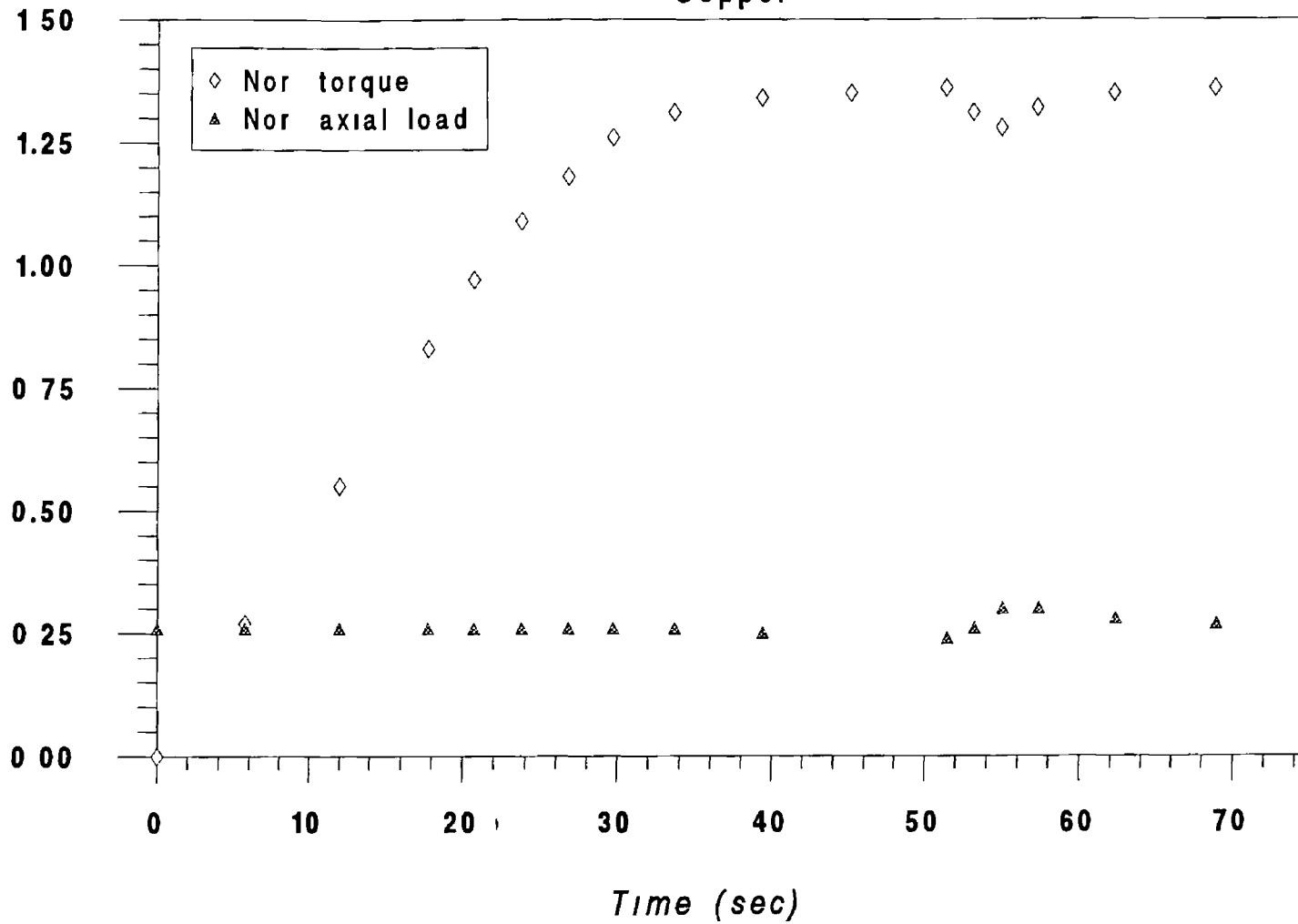


Figure 6.25(c) Variations of normalised axial load and torque with time (initial F = 50% of yield load)

Copper



245

Figure 6.25(d) Variations of normalised axial load and torque with time (initial F = 25% of yield load)

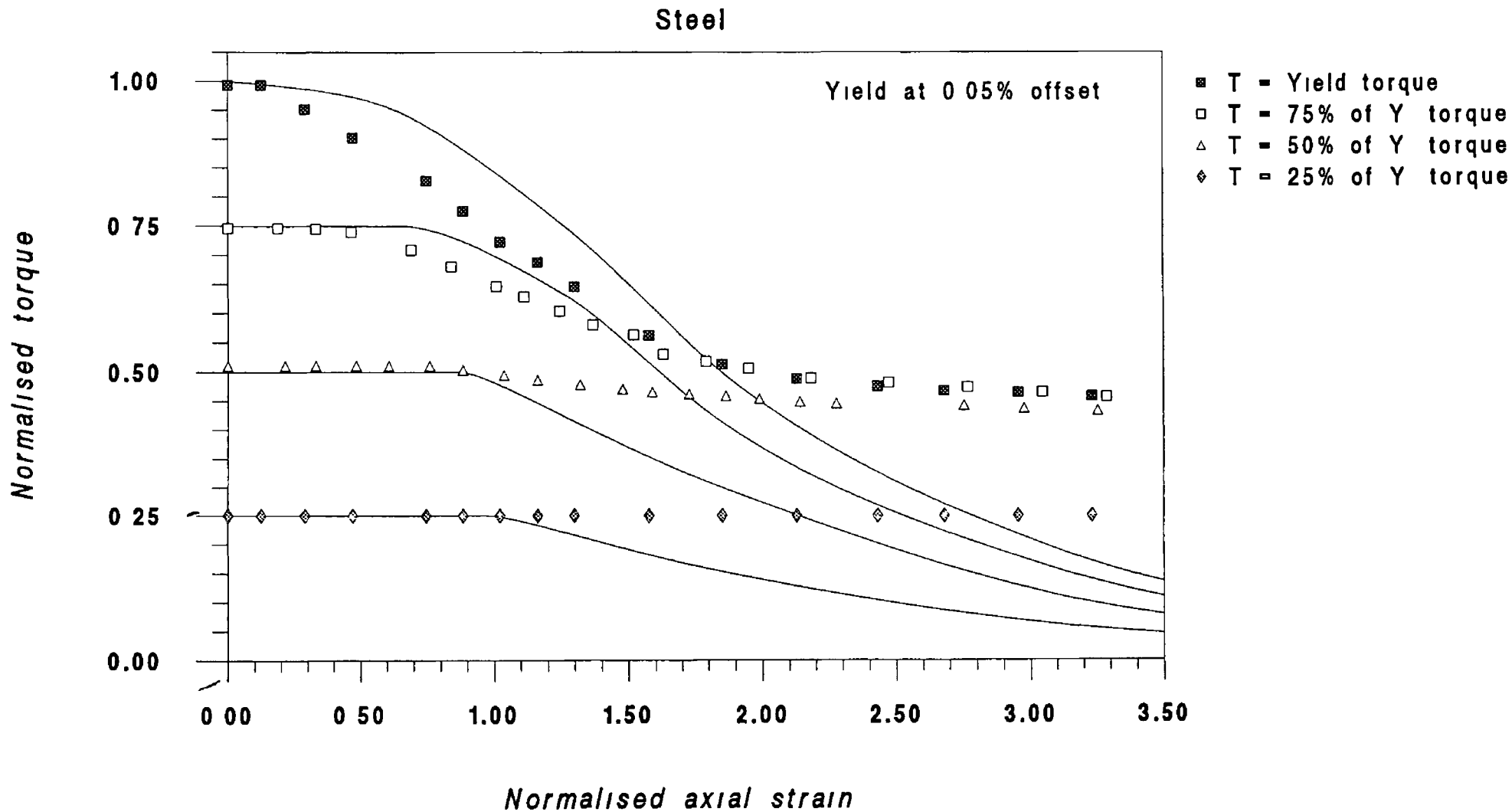


Figure 6.26 Comparison of experimental results with Gaydon's theoretical model (twist constant)

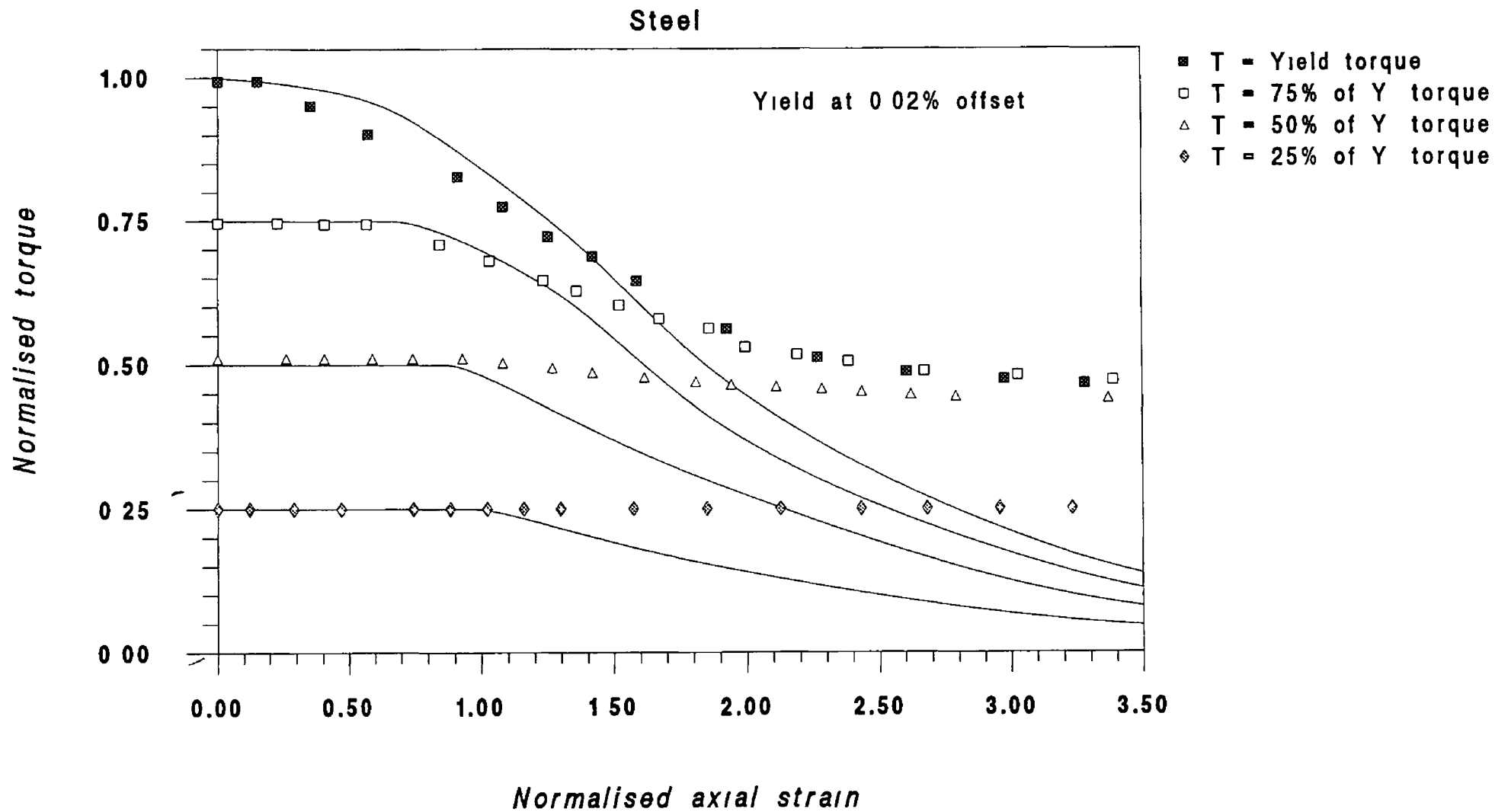


Figure 6 27(a) Comparison of experimental results with Gaydon's theoretical model (twist constant)

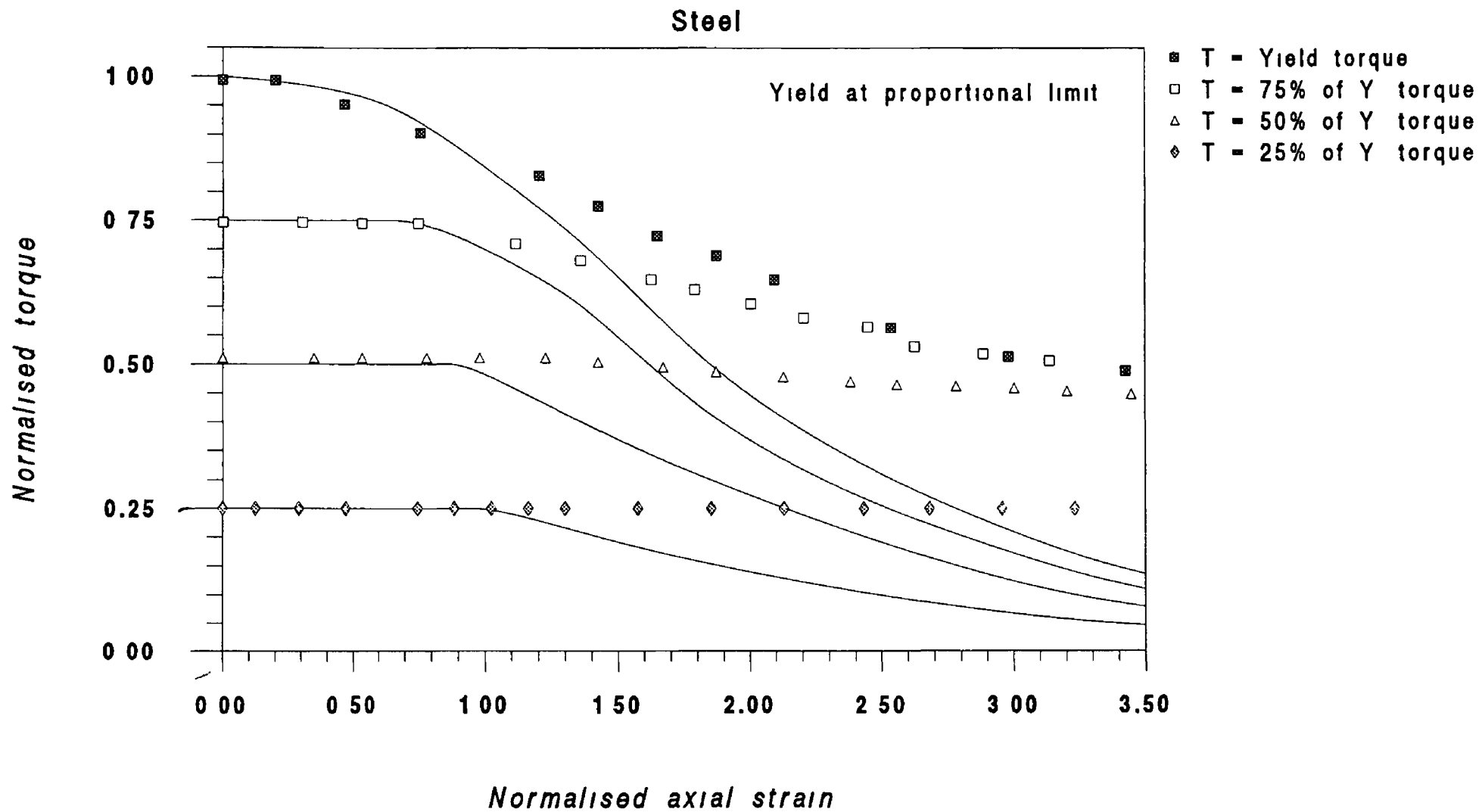


Figure 6.27(b) Comparison of experimental results with Gaydon's theoretical model (twist constant)

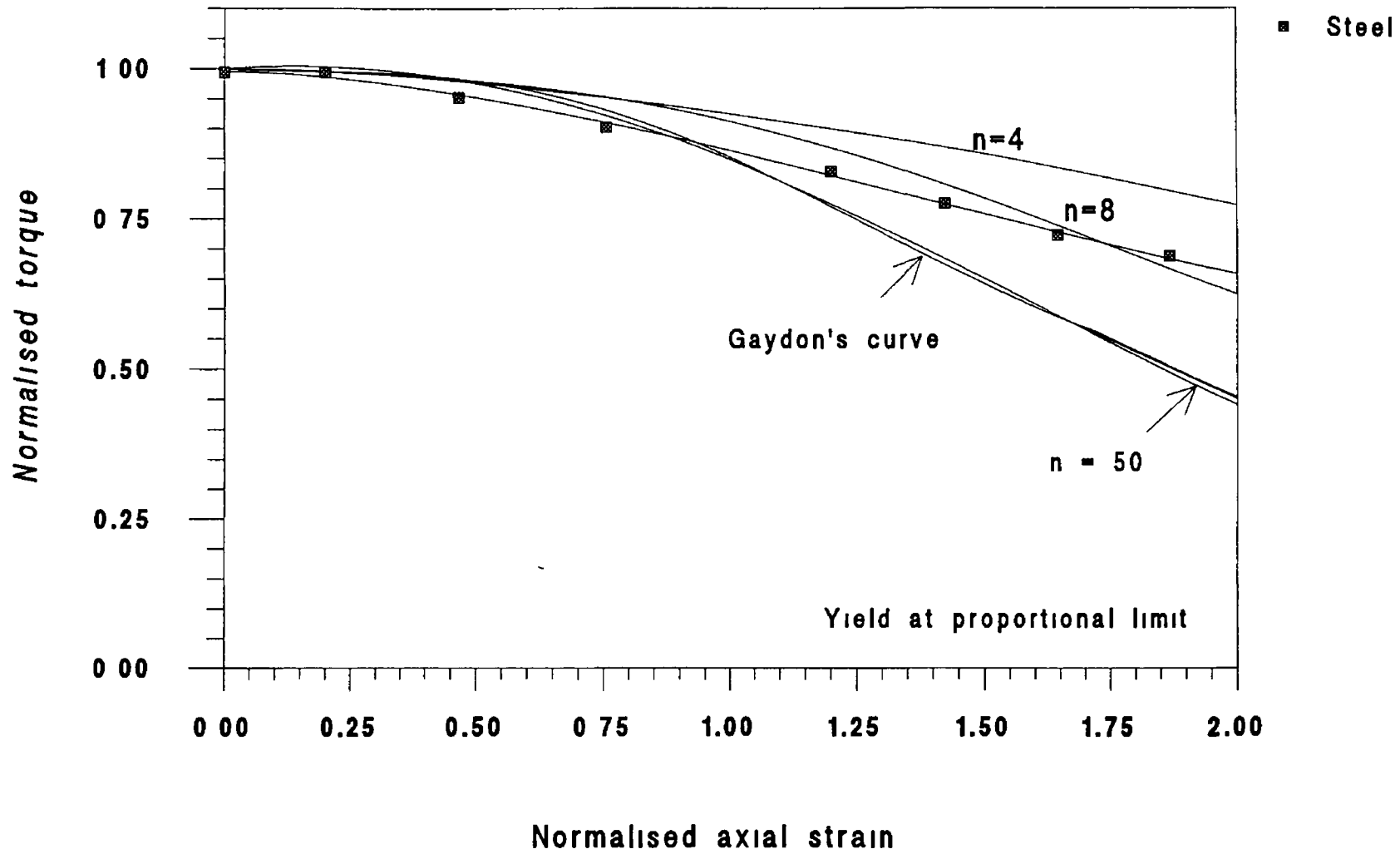


Figure 6.28 Comparison of experimental result with Brooks' model (angle of twist constant)

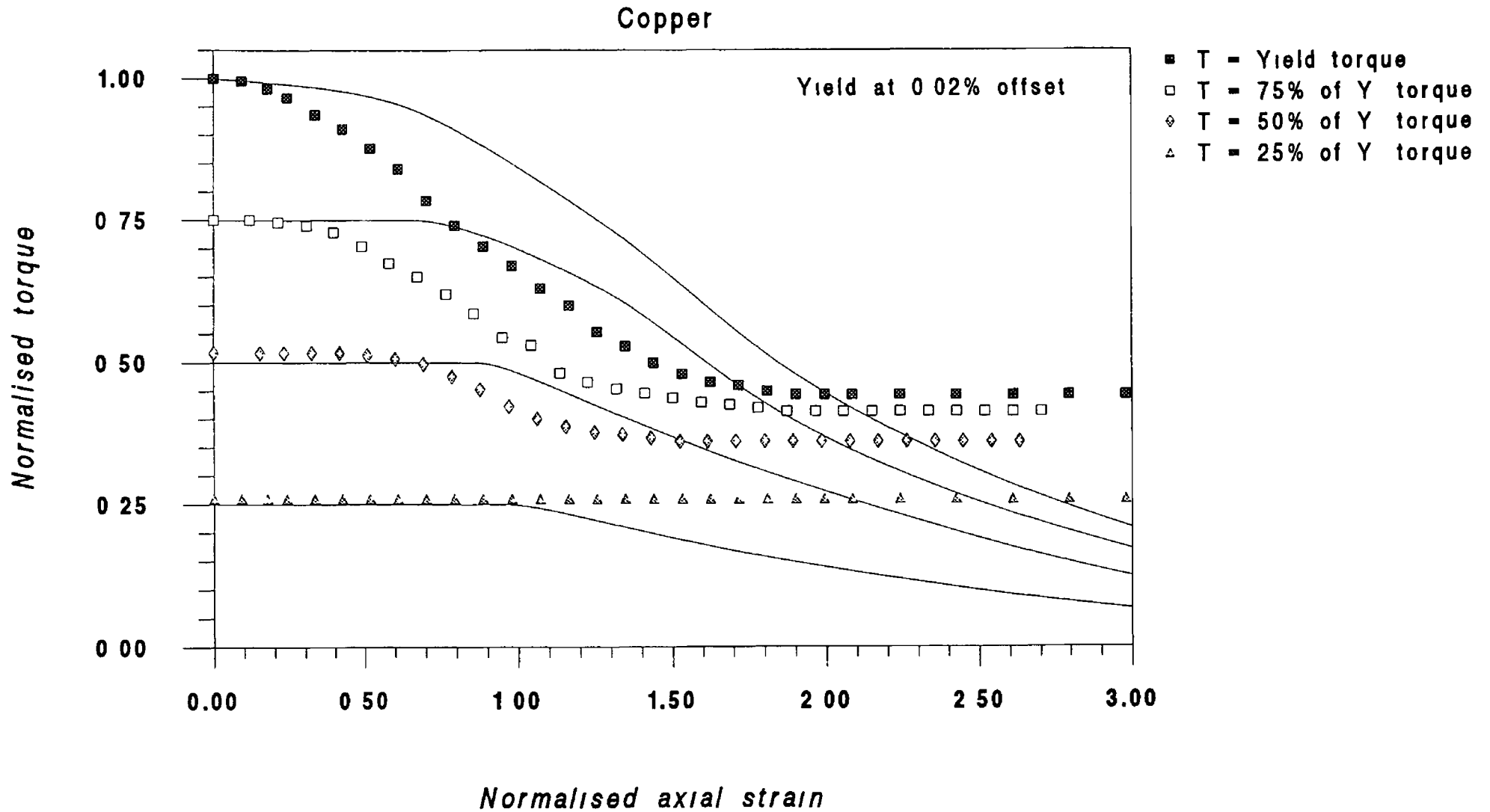


Figure 6.29(a) Comparison of experimental results with Gaydon's theoretical model (twist constant)

Copper

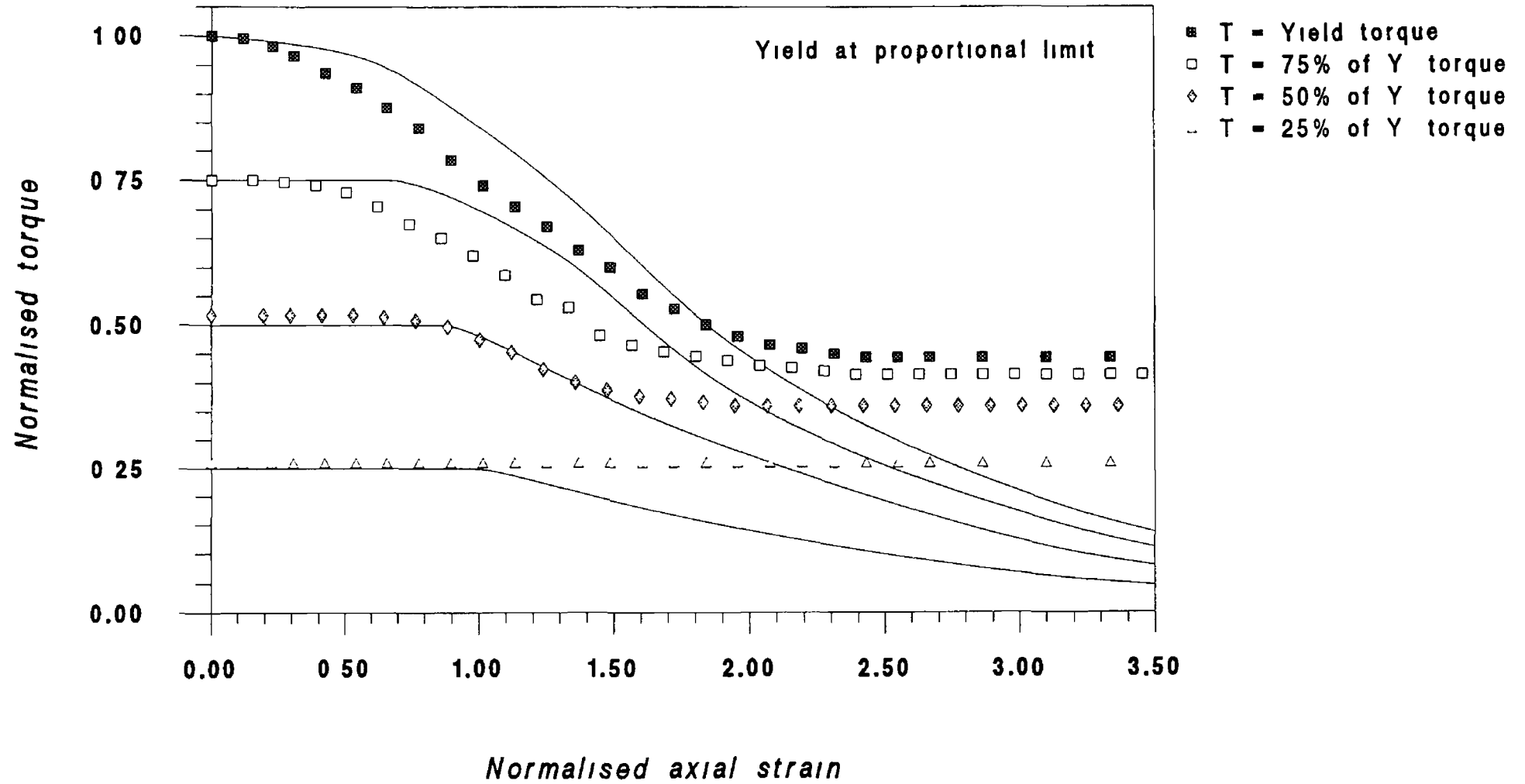


Figure 6.29(b) Comparison of experimental results with Gaydon's theoretical model (twist constant)

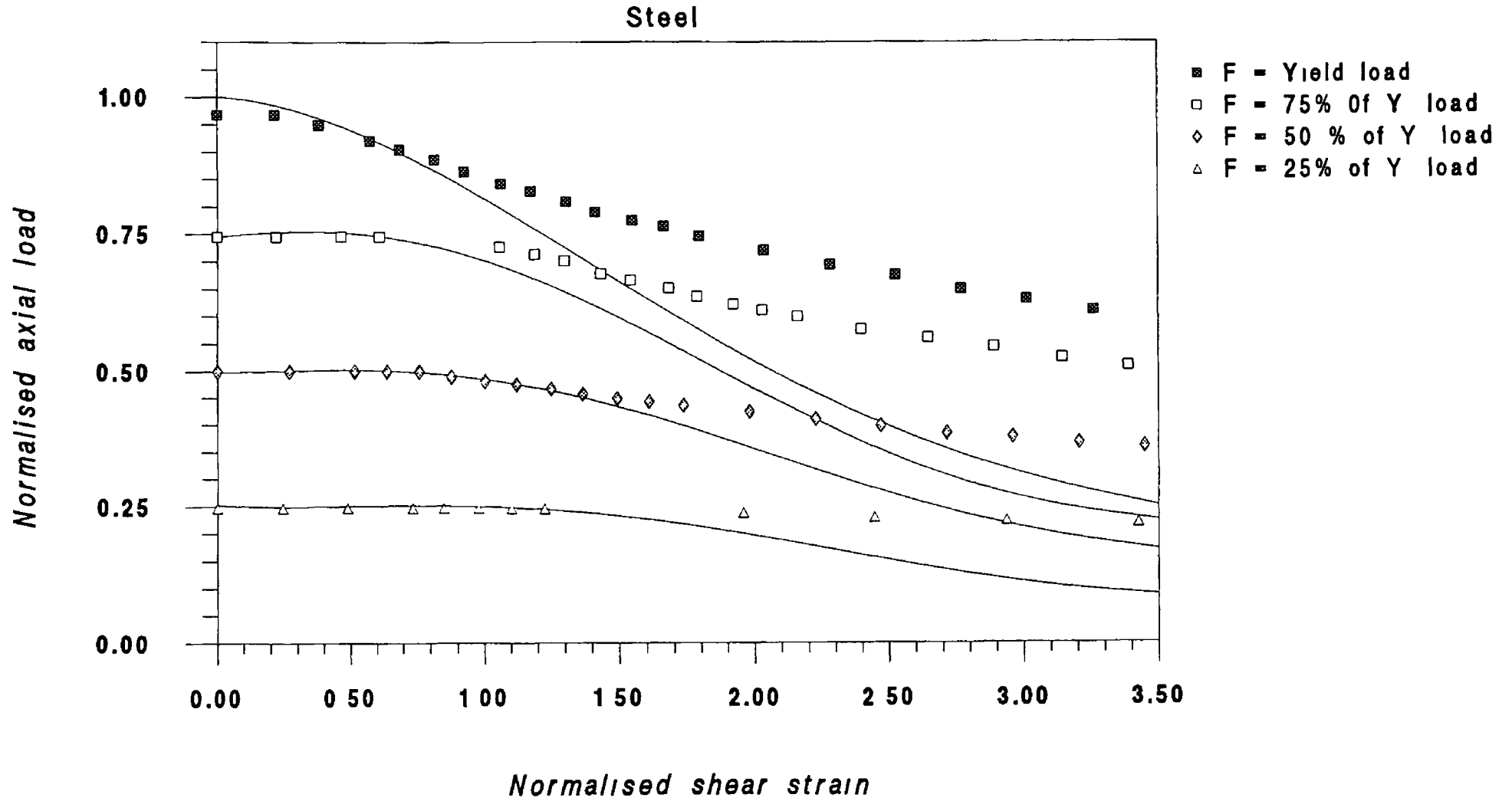


Figure 6.30 Comparison of experimental results with Gaydon's theoretical model (axial displacement constant)

Copper

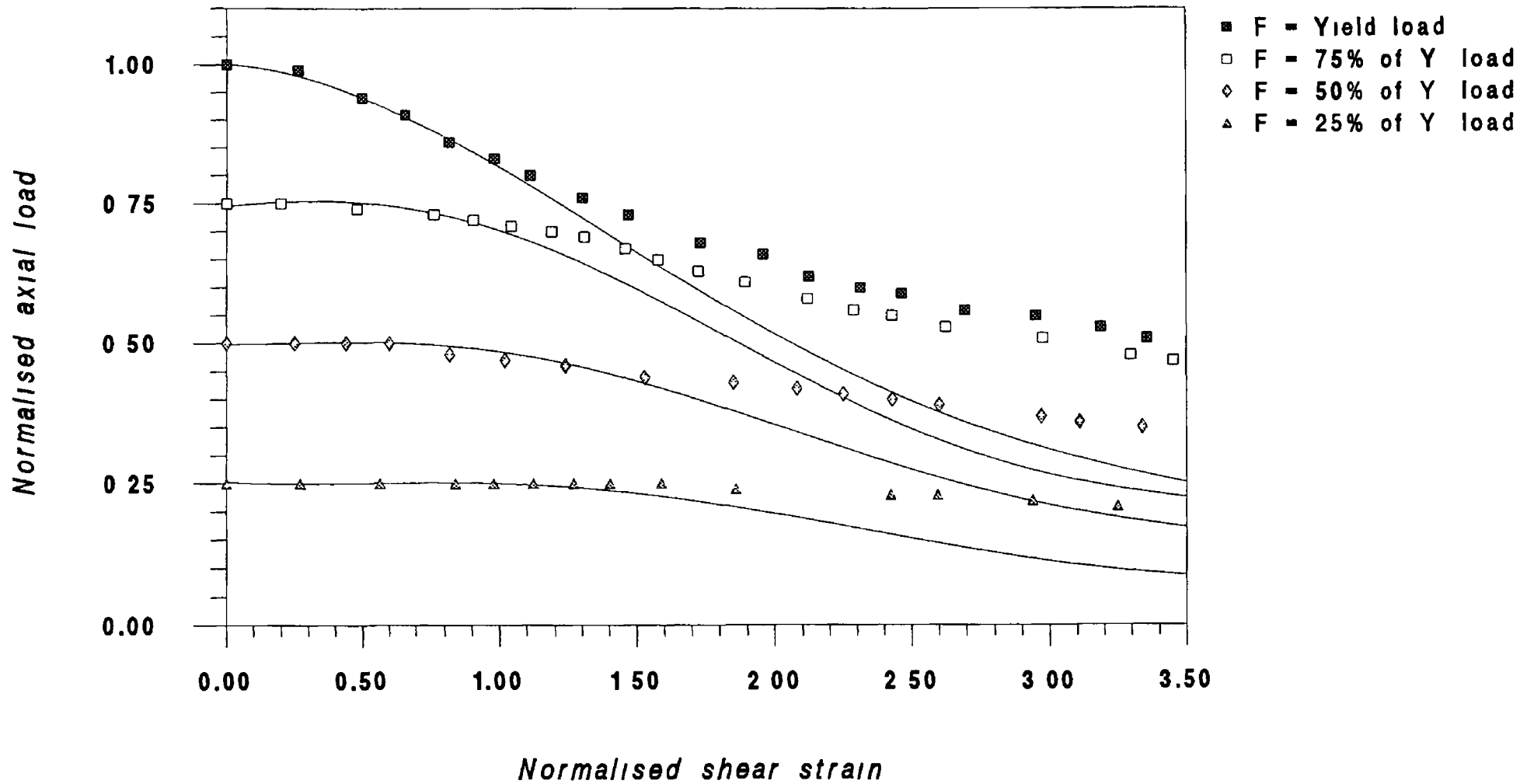


Figure 6.31 Comparison of experimental results with Gaydon's theoretical model (axial displacement constant)

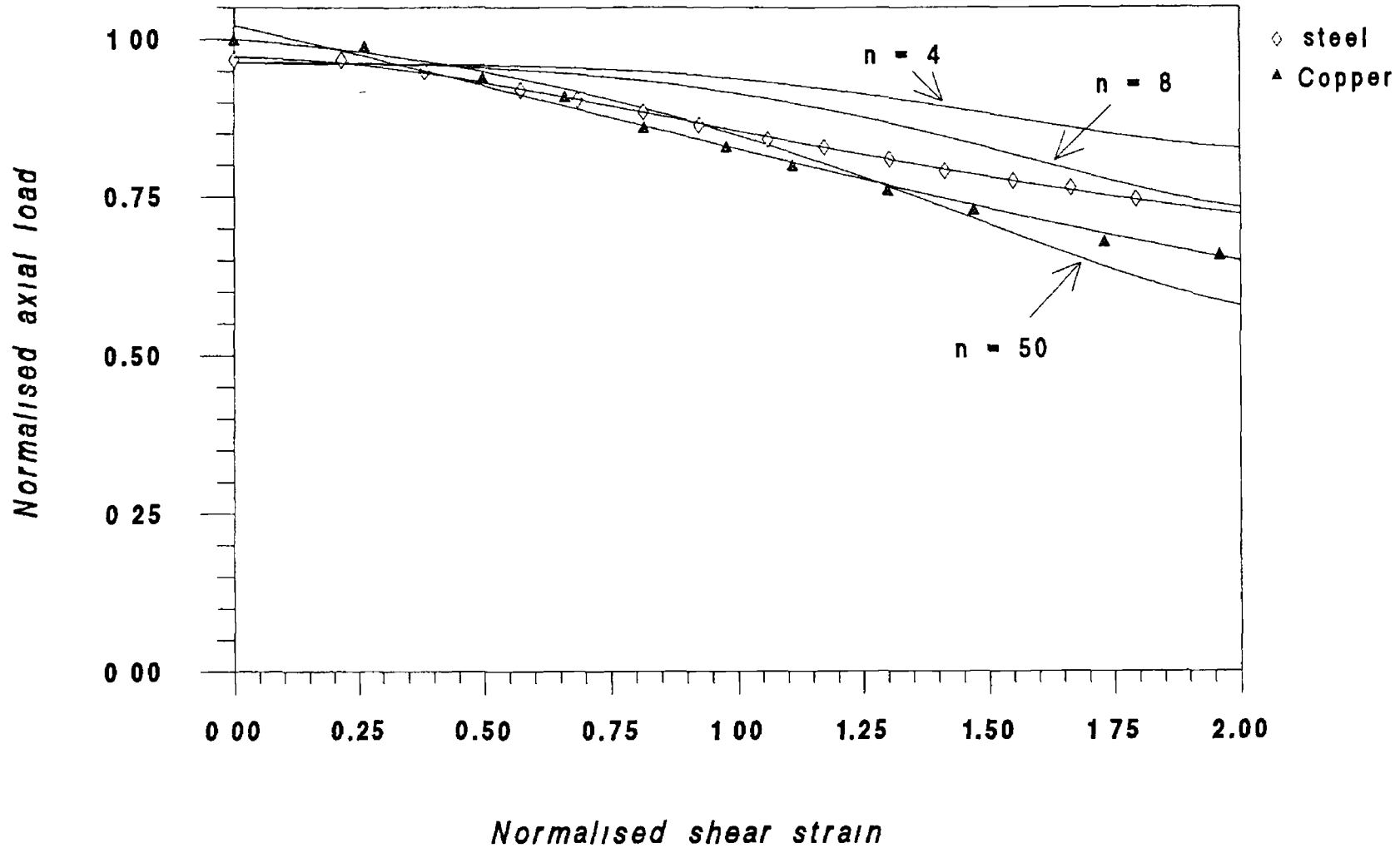


Figure 6.32 Comparison of experimental results with Brooks' theoretical model (axial displacement constant)

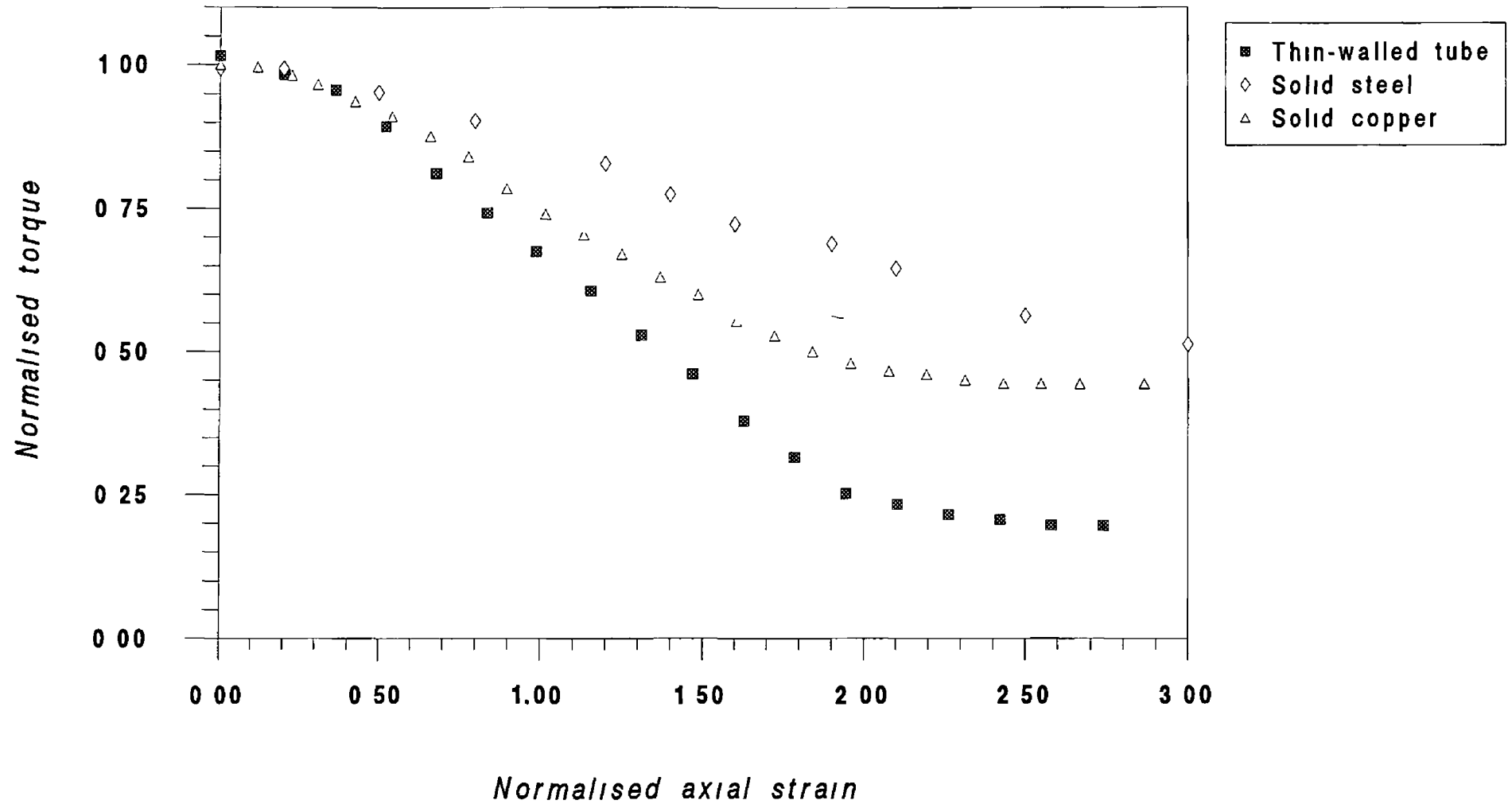


Figure 6.33 Comparison of thin-walled tube's results with those of solid steel and copper (angle of twist constant)

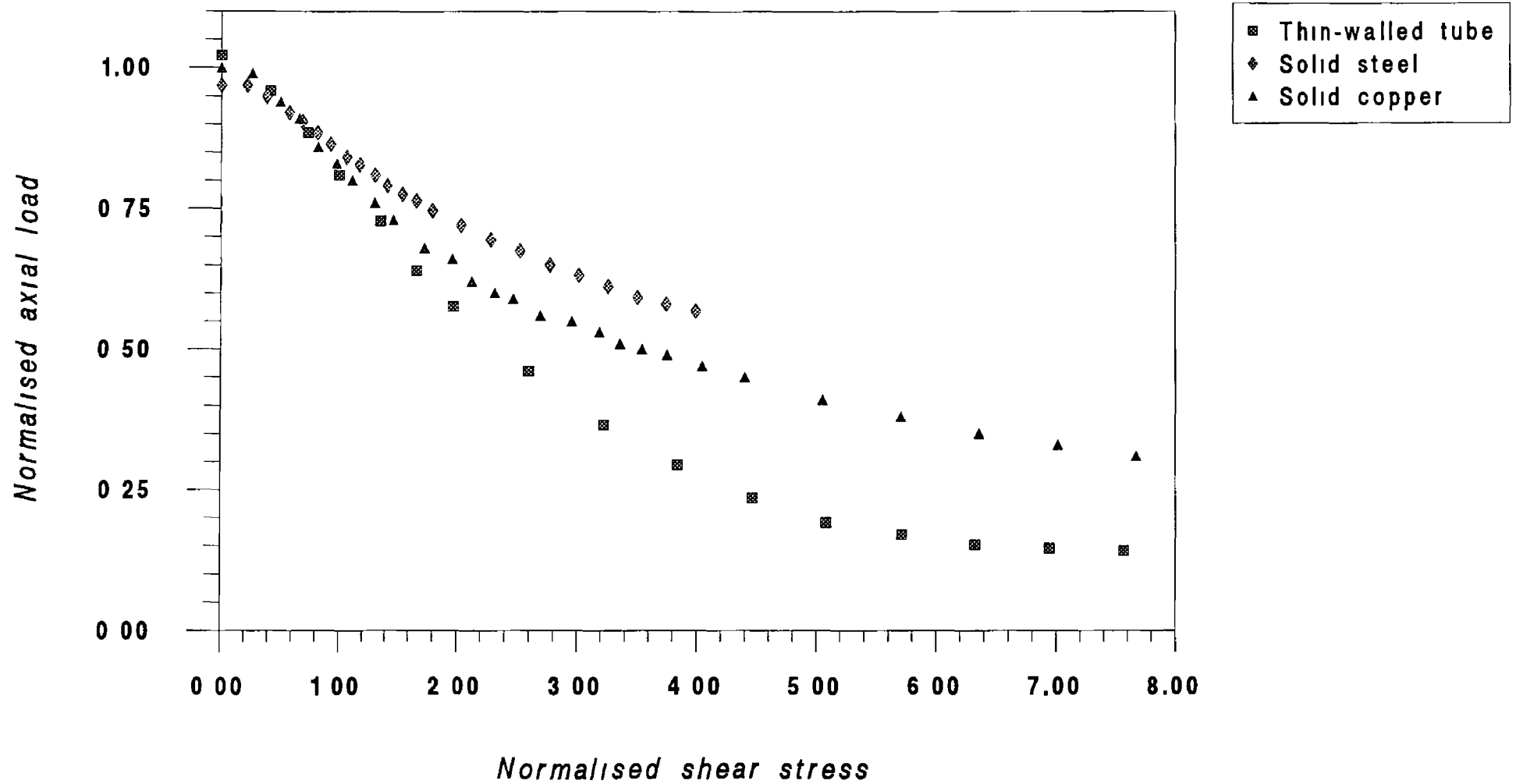


Figure 6.34 Comparison of thin-walled tube's results with those of solid steel and copper (axial displacement constant)

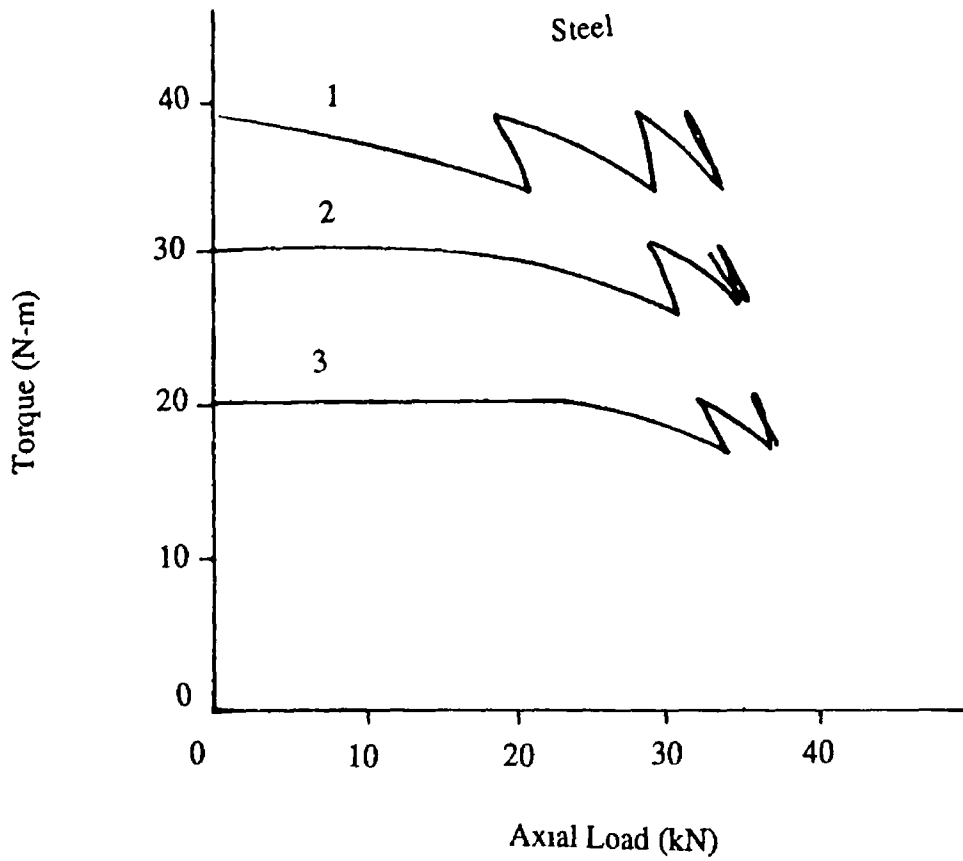


Figure 6 35(a) Variation of the applied torque with the axial load (torque applied first)

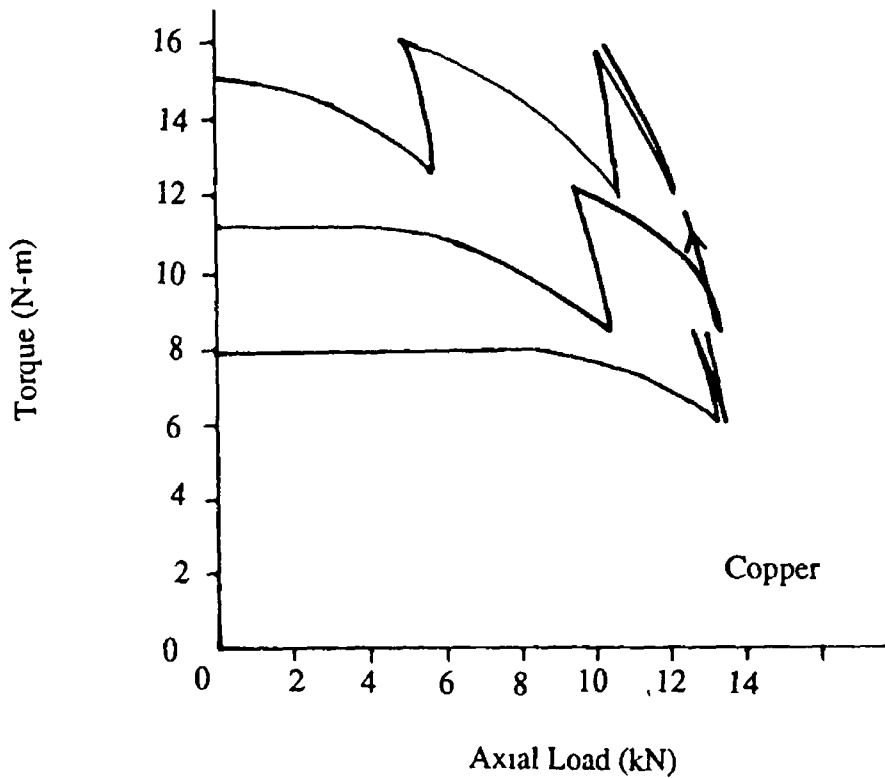


Figure 6 35(b) Variation of the applied torque with the axial load (torque applied first)

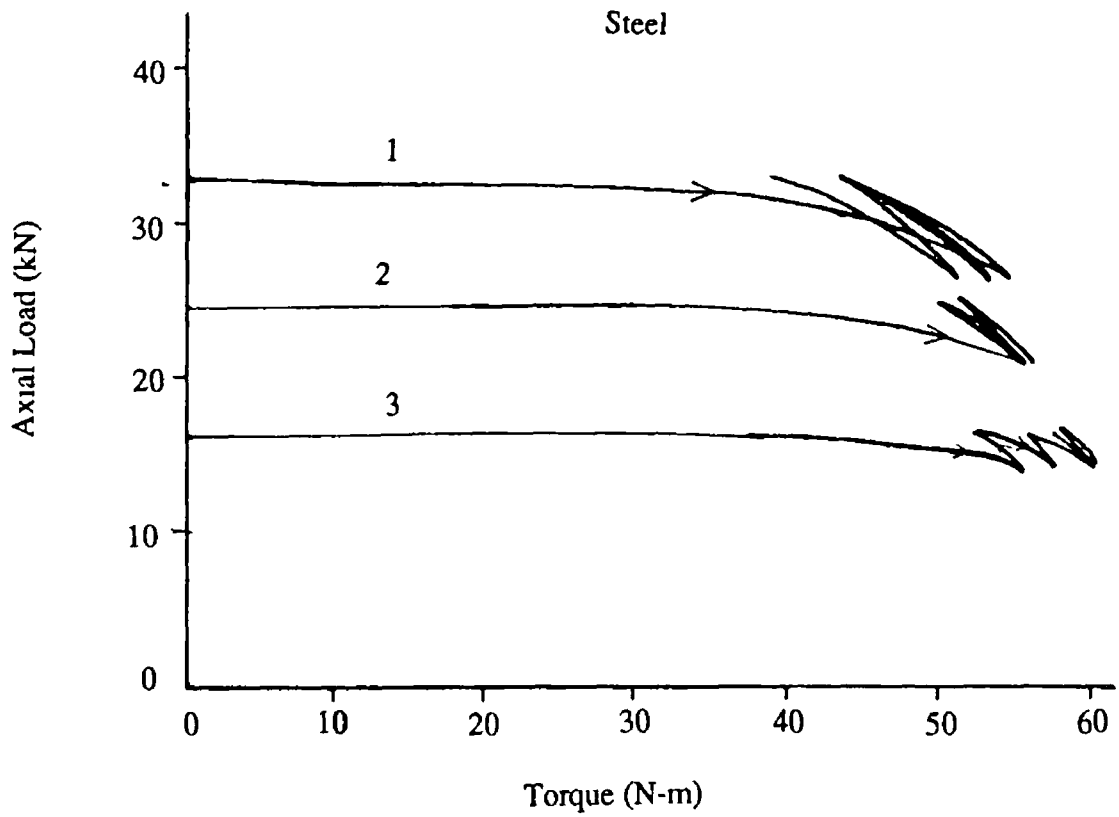


Figure 6 35(c) Variation of the applied axial load with the torque (load applied first)

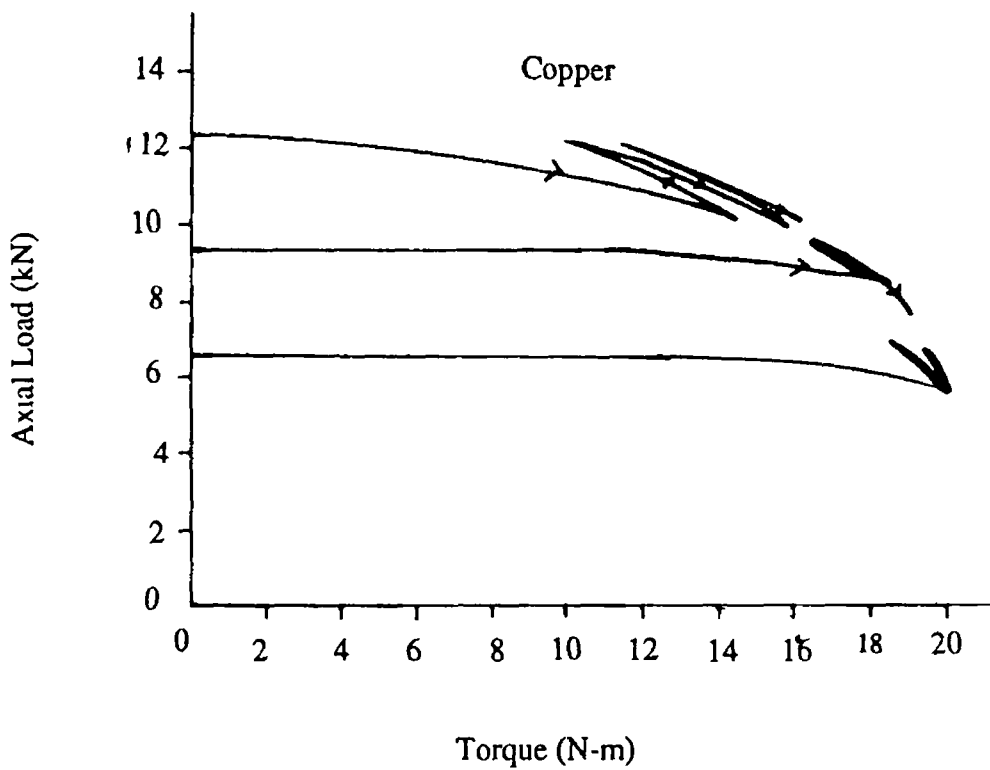


Figure 6 35(d) Variation of the applied axial load with the torque (load applied first)

Steel

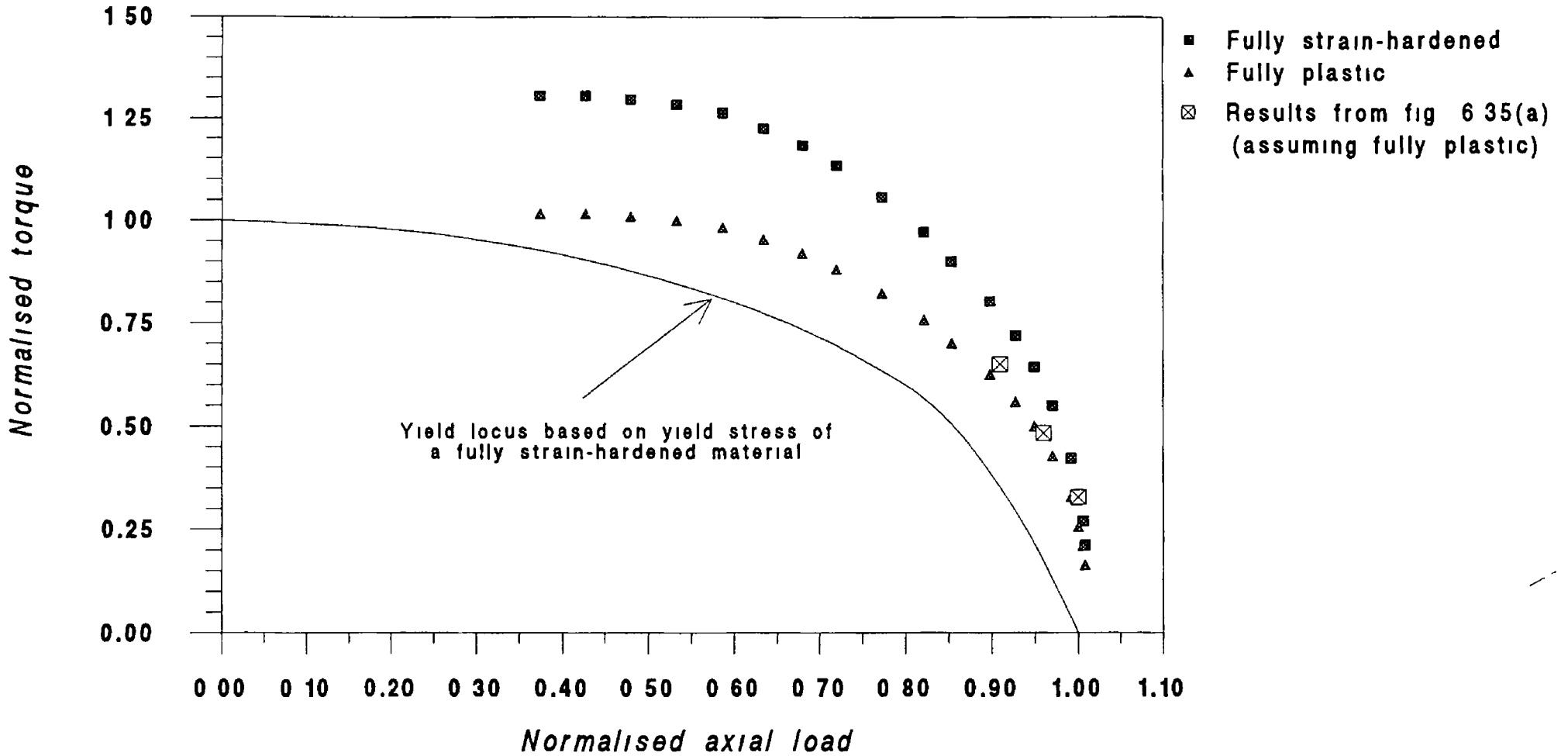


Figure 6.36 Subsequent ultimate yield locus (torque applied first)

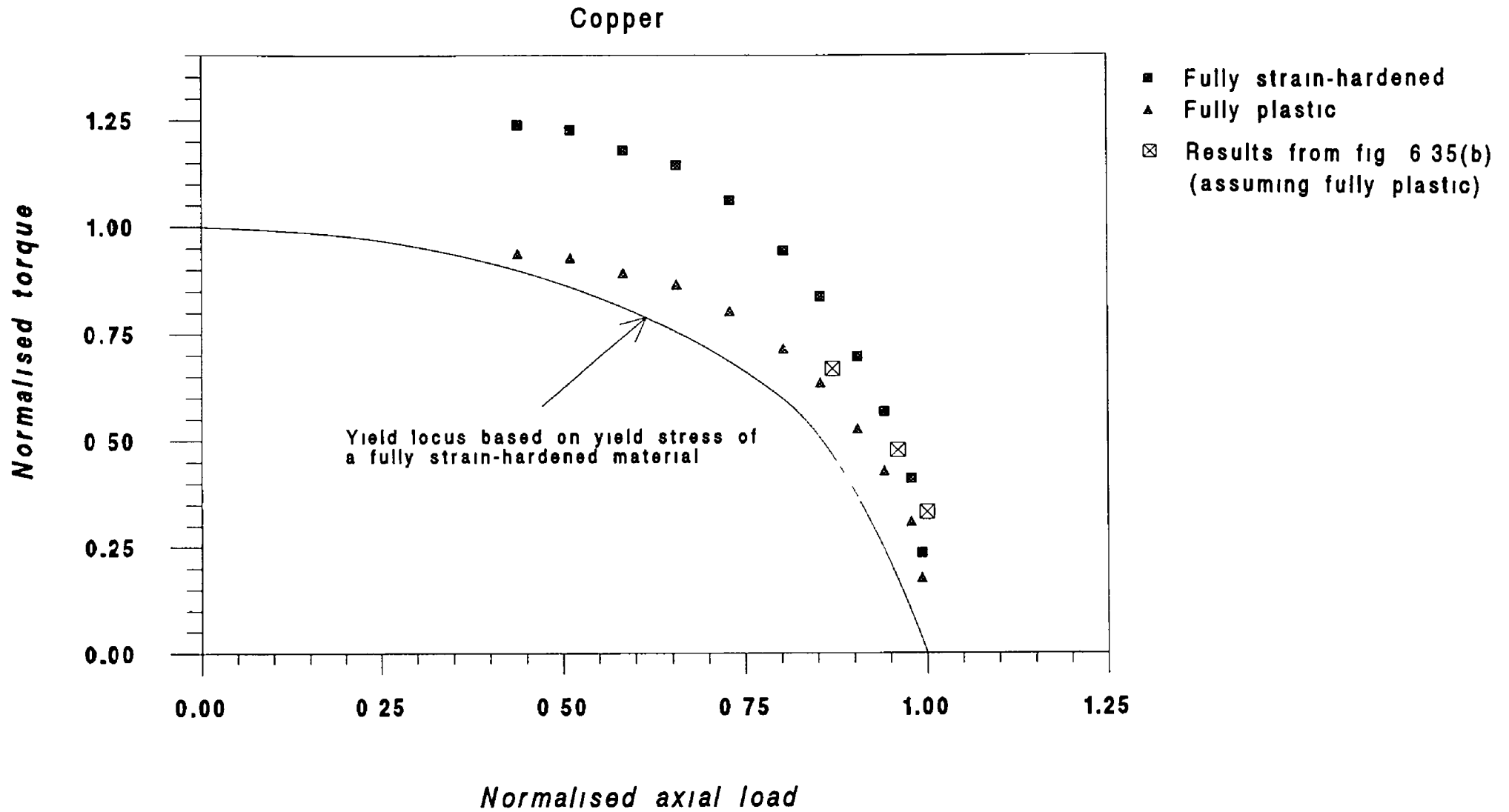


Figure 6.37 Subsequent ultimate yield locus (torque applied first)

Steel

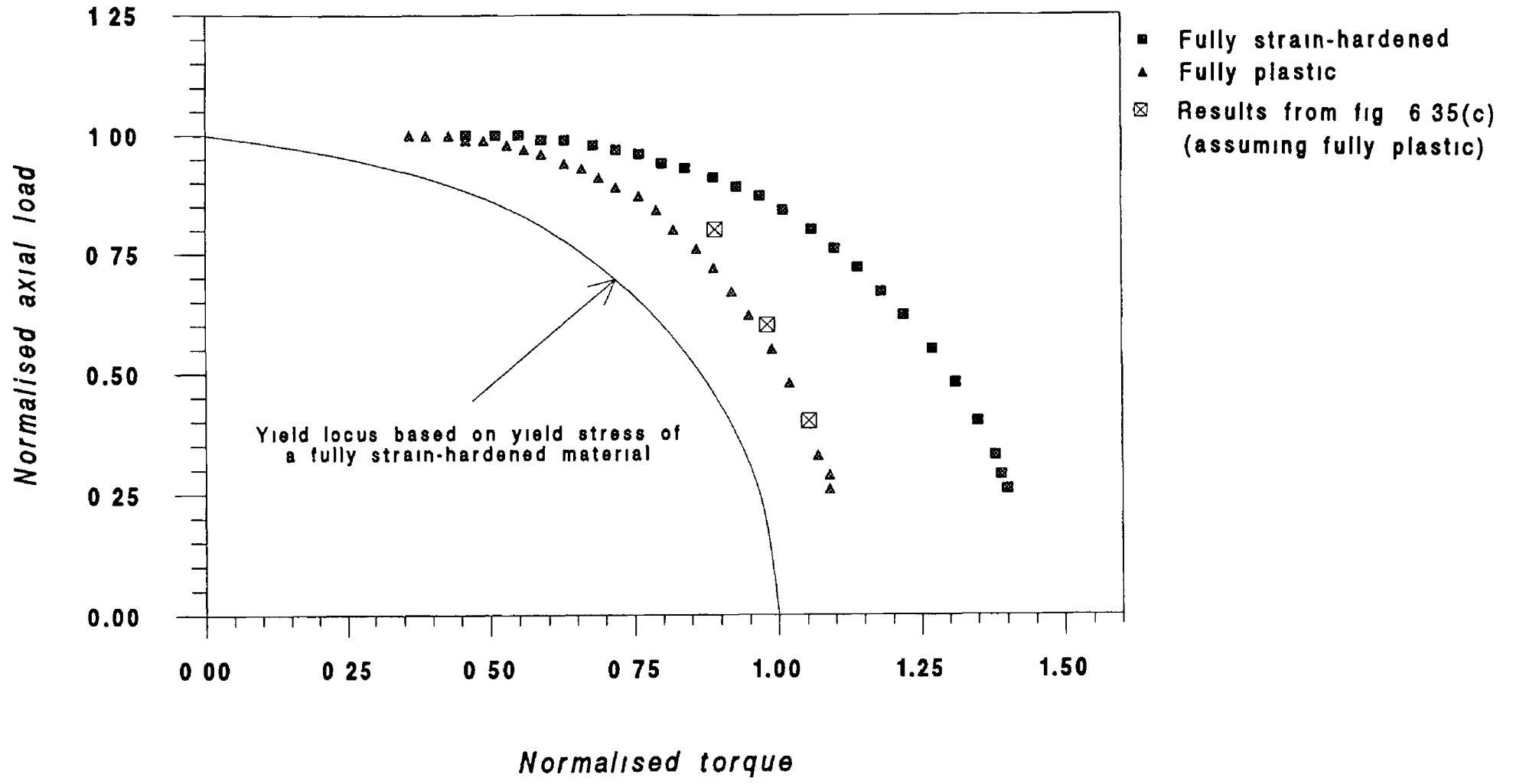


Figure 6.38 Subsequent ultimate yield locus (axial load applied first)

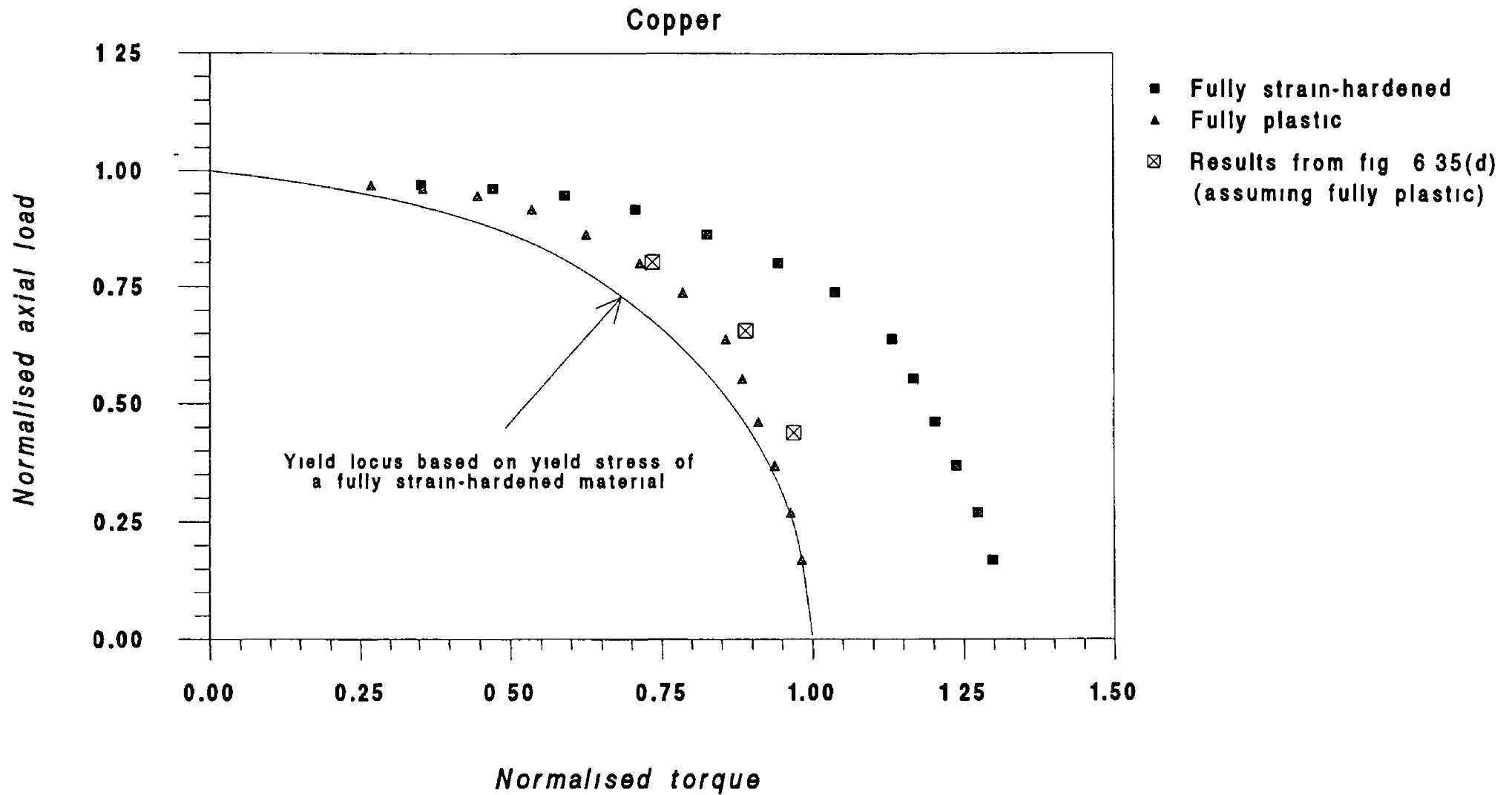


Figure 6.39 Subsequent ultimate yield locus (axial load applied first)

Steel

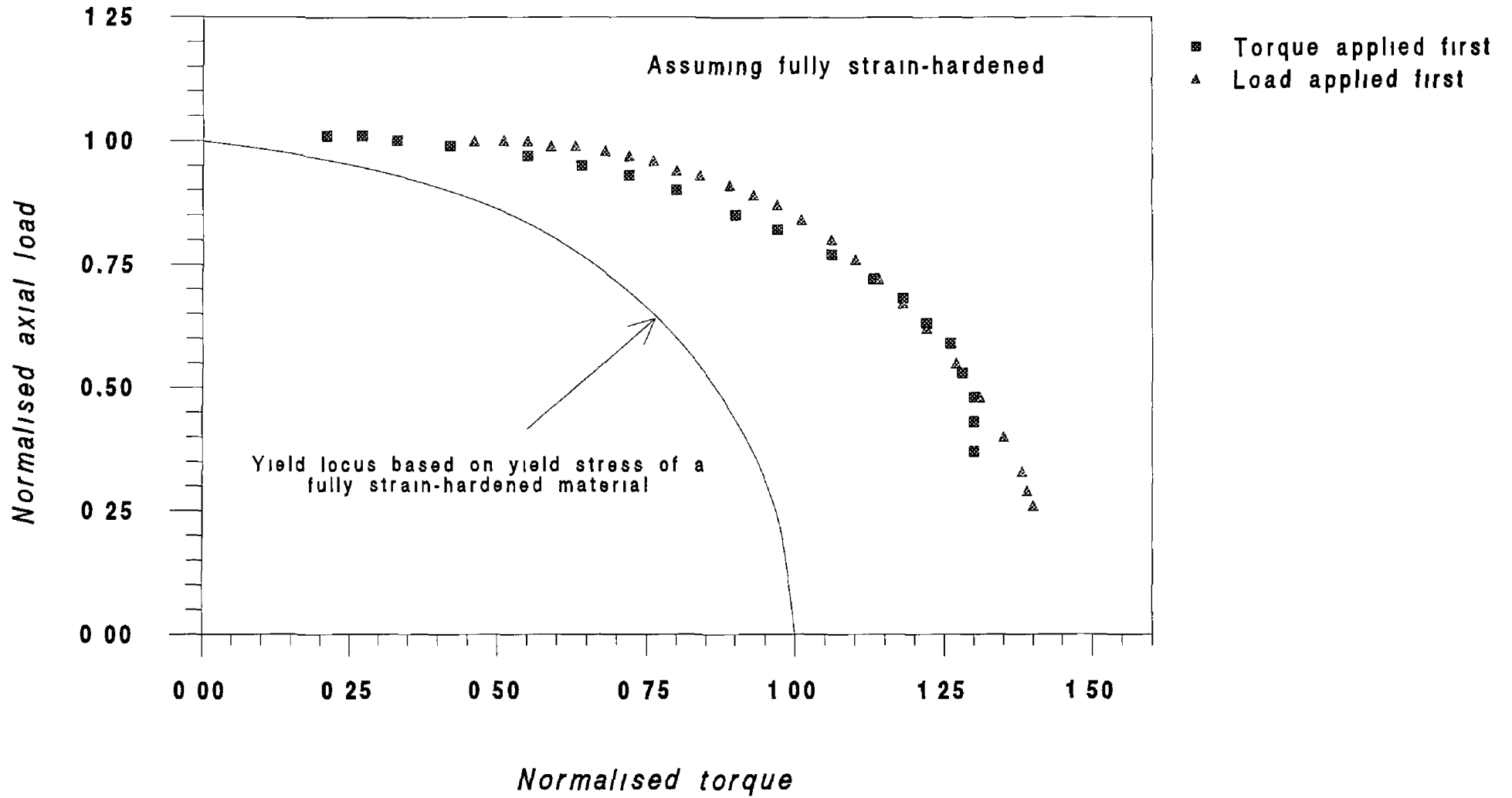


Figure 6.40(a) Comparison of subsequent ultimate yield loci for two different loading paths

Steel

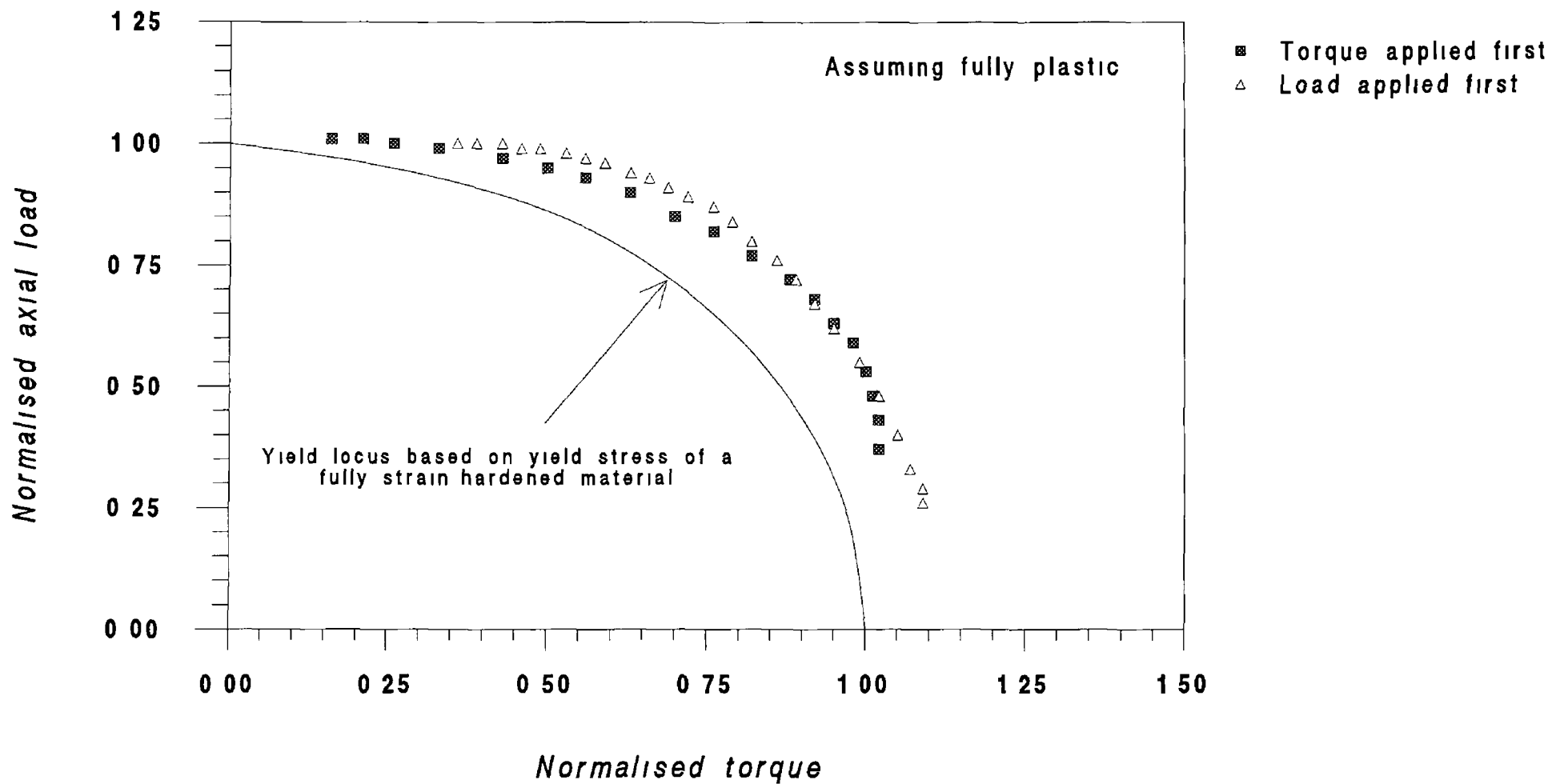


Figure 6.40(b) Comparison of subsequent ultimate yield loci for two different loading paths

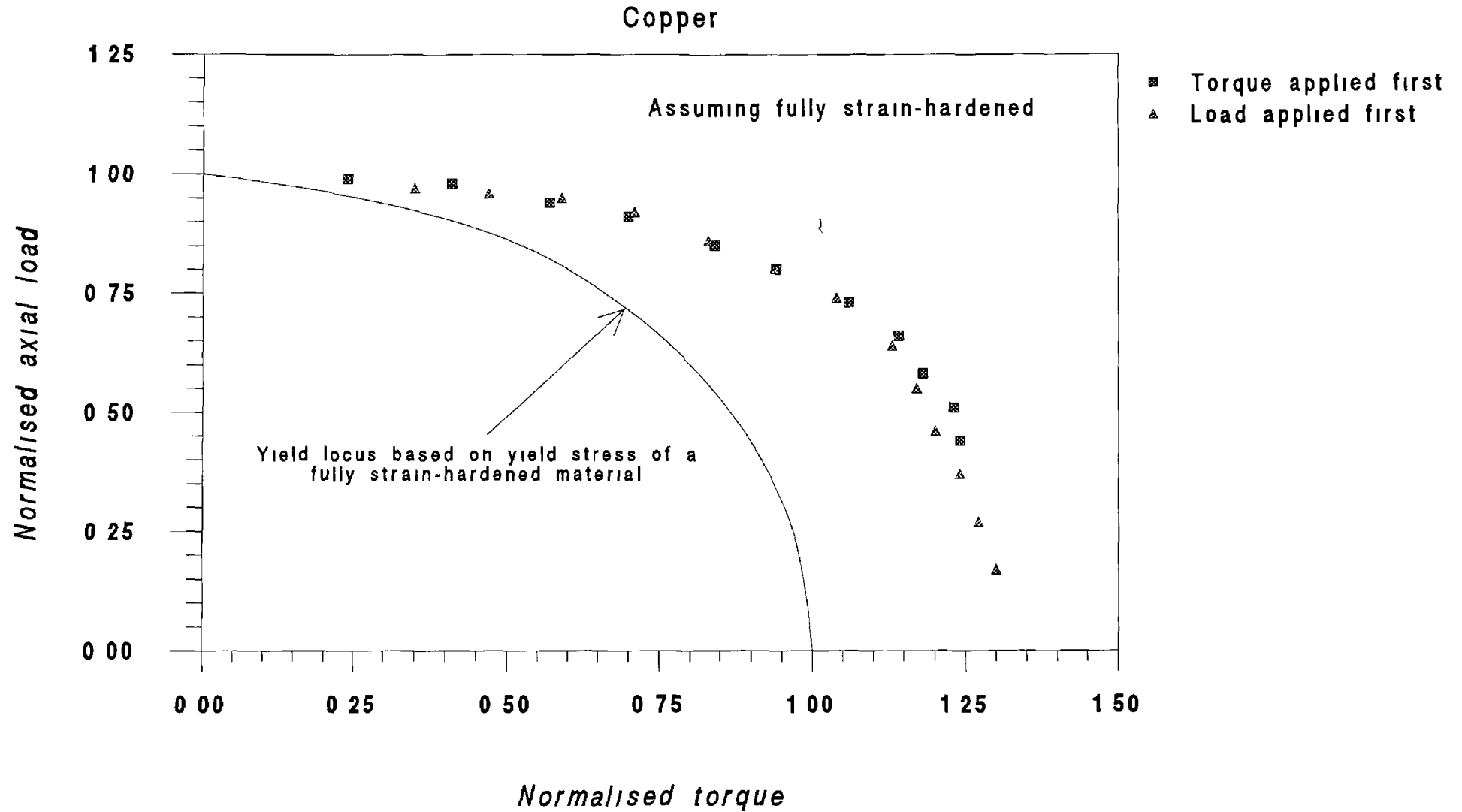


Figure 6.41(a) Comparison of subsequent ultimate yield loci for two different loading paths

Copper

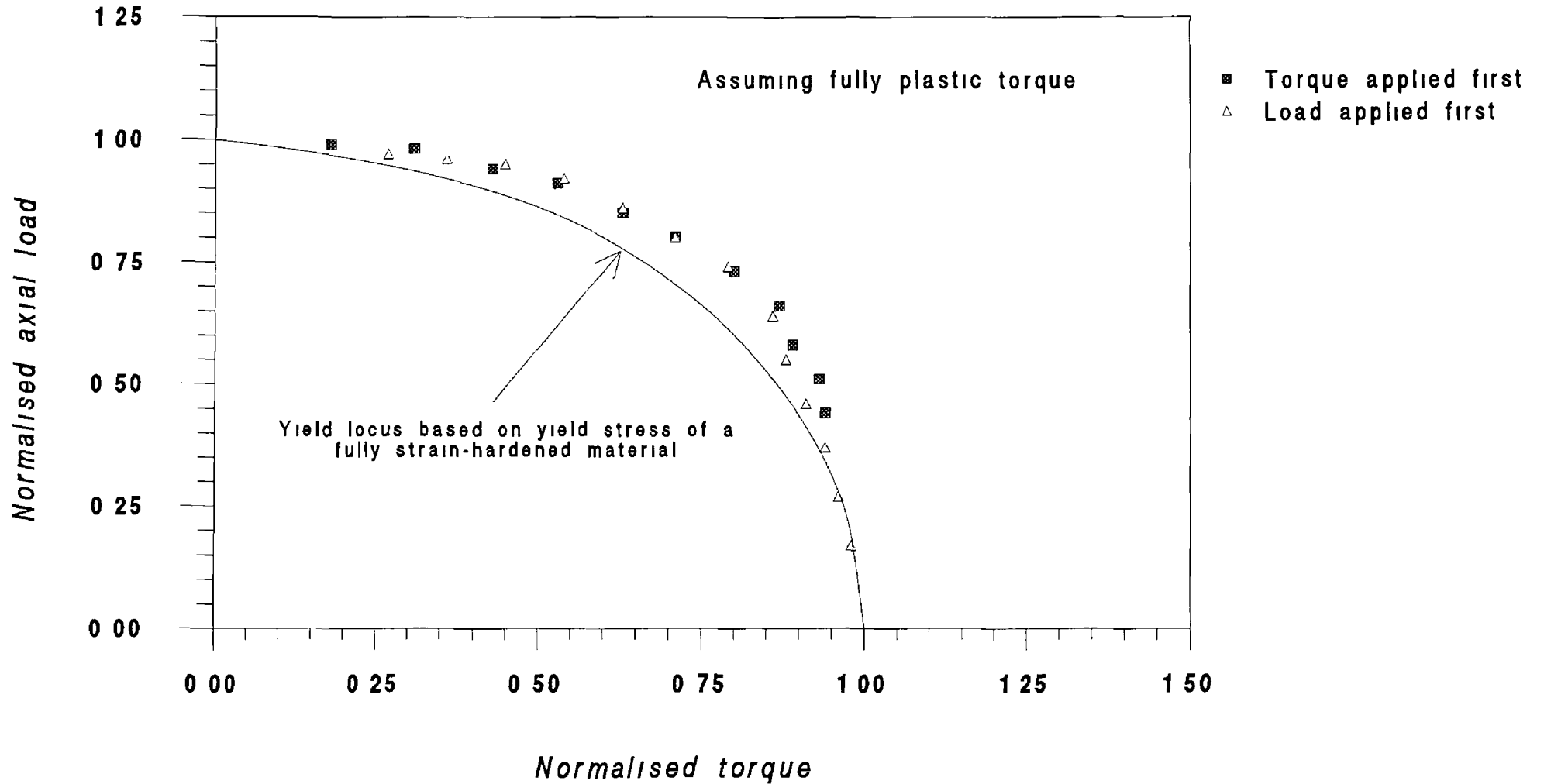


Figure 6.41(b) Comparison of subsequent ultimate yield loci for two different loading paths

CHAPTER SEVEN

CONCLUSIONS

7.1 INTRODUCTION

This chapter provides a brief summary of the conclusions of the present thesis. It is divided into three main sections: the first gives the summary of the general conclusions obtained during the experimental investigation, the second provides the gist of this thesis contribution and the third recommends suggestions for the future work.

7.2 GENERAL CONCLUSIONS

The conclusions resulting from the current experimental investigation are summarised below under the appropriate headings.

Torsion Followed By Tension - Angle of Twist Constant

- (i) In the first case, where the rod was initially subjected to a torque and then, keeping the angle of twist constant, to a gradually increasing axial load, the increase in the axial load resulted in a decrease in the initially applied torque according to the yield criteria.
- (ii) The initially applied torque started to decrease with the axial load only when the combined stress of the material reached approximately the uniaxial yield stress of the material.
- (iii) The increase in the axial load and hence the increase in the corresponding normal stress developed faster than the decrease in the torque and the corresponding shear stress.
- (iv) With a gradually increasing axial load, the rod behaved as if its torque carrying ability was drastically reduced without in any way affecting its axial load carrying ability.

(v) During this biaxial loading, though the material yielded due to the combined loading well before the applied axial load caused yielding on its own, all the axial load curves followed elastic path

(vi) The higher the magnitude of the initially applied torque, the greater is the rate of decrease of the torque with the increasing axial load

Torsion Followed By Tension - Torque Maintained Constant

(i) When the rod was initially subjected to a torque and then, maintaining the torque constant, to a gradually increasing load (and hence to a gradually increasing axial strain), the shear strain started to increase rapidly only when the rod yielded due to the combined loading

(ii) The higher the values of the initially applied torque, the higher is the rate of increase of the shear strain with the increasing axial strain

Tension Followed By Torsion - Axial Displacement Constant

(i) In the third case, where the axial load was applied first, increase in the torque resulted in decrease in the initially applied load according to the yield criteria

(ii) The initially applied load started to decrease with the torque only when the combined stress of the material reached approximately the uniaxial yield stress

(iii) The increase in the torque and hence the increase in the corresponding shear stress developed faster than the decrease in the axial load and the corresponding normal stress

(iv) With a gradually increasing torque, the rod behaved as if its axial load carrying ability was drastically reduced without in any way affecting its torque carrying ability

(v) During this particular loading, though the material yielded due to the combined loading well before the applied torque caused yielding on its own, all the torque curves followed elastic path

(vi) The higher the magnitudes of the initially applied load, the greater is the rate of decrease of these loads with the torque

(vii) The percentage reduction in the initially applied load due to the applied torque was much lower than the percentage of reduction in the initially applied torque due to applied load (as was observed in the first case) under similar biaxial loading conditions

Tension Followed By Torsion - Axial Load Maintained Constant

(i) In the fourth case, where the rod was subjected to an initial load and then, maintaining the load constant, to a gradually increasing torque (hence to a gradually increasing shear strain), the axial strain started to increase rapidly only when the rod yielded due to the combined loading

(ii) The higher the values of the initially applied load, the greater is the rate of increase of the axial strain with the shear strain

Combined Loading With The Reduced Section Specimen

(i) Test results with the reduced section specimen showed that, even though the angle of twist of the specimen was held constant after applying an initial torque, the shear strain increases very rapidly (with the axial strain) at the confined zone where the localised yielding, and hence the plastic deformation begins. The shear strain decreases at any other locations (unloading) thus suggesting that plastic deformation in a uniform cross-section specimen takes place at a certain preferred location with unloading taking place elsewhere

(ii) In the second test it has been observed that even though the axial displacement of the specimen was kept constant after applying an initial load, the axial strain increases very rapidly (with the shear strain) at the confined zone where the localised yielding and hence the plastic deformation begins. The axial strain decreases at any other locations, hence, confirming that plastic deformation takes place in a uniform cross-section specimen within a localised region with unloading taking place elsewhere

Successively Applied Torque And Tension - Torque Applied First

- (i) When the rod was initially subjected to an initial torque and then to successively applied load and torque, keeping the axial displacement or the angle of twist constant respectively in an alternate manner, the rod soon regains its axial load carrying capability irrespective of the level of the initially applied torque
- (ii) With the successive application of the axial load and the torque, and when the material yielded due to the combined loading, the increment in the axial load results reduction in the torque and the increment in the torque results reduction in the axial load, i.e., the effect of the axial load or the torque whichever was applied subsequently, was dominant on the specimen investigated
- (iii) For the same type of loading as mentioned in (i), the influence of the axial load was much stronger on the specimen investigated than that of the initially applied torque; as in this case the subsequently applied torque resulted only in small reduction in the axial load compared to the total amount of load applied
- (iv) The more the axial load was subsequently increased towards the yield and hence, towards the ultimate load of the material, the less the percentage of reduction in the axial load for the same amount of torque increment and also, the less amount of axial load was required to cause the same drop in the torque

Successively Applied Torque And Tension - Load Applied First

- (i) When the rod was initially subjected to an initial load and then to successively applied torque and load, keeping the angle of twist or axial displacement constant in an alternate manner, the rod soon regains its torque carrying capability irrespective of the initially applied load
- (ii) The influence of the torque (which was applied as a second parameter) was much stronger on the specimen investigated than that of the initially applied load, as the subsequently applied axial load resulted only small reduction in the torque compared to the total torque applied

Comparison Between The Experimental And The Theoretical Results

- (i) For the biaxial loading, where the rod was initially subjected to a torque and then, keeping the angle of twist constant, to a gradually increasing axial strain, Gaydon's theoretical predictions agree well with the experimental torque variation curves of the material which behaves more closely like an elastic-perfectly plastic material. In the present case, the theory has better agreement with the test results of the as received copper specimens than those of the steel.
- (ii) For the case, where the rod was initially subjected to an axial load and then, holding the axial displacement constant, to a gradually increasing shear strain, Gaydon's theoretical results provide poor agreement with the experimental load variation curves of the material which behaves closely like an elastic-perfectly plastic material.
- (iii) There exists some disagreement between the experimental and the theoretical curves, based on Brooks' model and for both the above mentioned types of loadings, which may be attributed to the discrepancy in the material behaviour due to non-isentropic hardening of the material, as Brooks' model was developed considering isentropic hardening of the material, or inappropriateness of the model.

Thin-Walled Tube tests

- (i) When the thin-walled tube was subjected to an initial torque and then to an increasing axial load, keeping the angle of twist constant, the rate of decrease in the initially applied torque was much faster than those of the solid rods.
- (ii) Similarly, when the tube was subjected to an initial load and then to a gradually increasing torque, holding the axial displacement constant, the rate of decrease in the initially applied load was much faster than those of the solid rods.

Study of Subsequent Yield locus

- (i) During the successive application of the torque and the axial load, keeping the corresponding angle of twist or axial displacement constant in an alternate manner, the

torque-load trajectories always moved in a zig-zag way until the material reached its ultimate subsequent yield locus

(ii) Almost the entire positive quadrant of the ultimate subsequent yield loci were obtained from the single run of a solid steel and a copper specimens

7.3 CONTRIBUTION OF THIS THESIS

The contribution of the current thesis is evident in three main areas as follows

DESIGN OF A NOVEL BIAXIAL TORQUE-TENSION MACHINE

(i) An instrumented mechanical torque-tension machine was designed, built and commissioned to enable the application of biaxial loading under controlled conditions

(ii) An analytical model was developed to determine the stiffness of the machine

THEORETICAL INVESTIGATION

(i) Numerical solutions were developed along the lines of Gaydon [18] to compare the elasto-plastic response of solid rods when they were subjected to torsion followed by tension, keeping the angle of twist constant, and tension followed by torsion, keeping the axial displacement constant. For similar biaxial loading paths, the experimental results were also compared with Brook' [20] analytical model

EXPERIMENTAL INVESTIGATION

(i) When the rod is initially subjected to a torque and then, keeping the angle of twist constant, to a gradually increasing axial load, the rod behaves as if its torque carrying ability becomes drastically reduced without in any way affecting its load carrying ability. Similarly, when the rod is initially subjected to an axial load and then, keeping the axial displacement constant, to a gradually increasing torque, the rod behaves as if its load carrying ability becomes drastically reduced without in any way affecting its torque carrying ability. Such

reductions in the load or torque capacity appear to be governed by the material plastic yield criterion

(ii) The torsional or the tensile stress of a pre-torqued or a pre-loaded specimen starts to unload (with the increasing load or torque) when the plastic deformation begins due to plastic yielding of the material. Thus these stresses are unloaded due to the relaxation of the material stresses in plastic form

(iii) When the rod is subjected to an initial torque or axial load and then, to a gradually increasing load or torque, keeping the corresponding angle of twist or axial displacement constant, measurement of the reduction in the initially applied torque or axial load using strain gauges will be entirely erroneous if they are attached to the zones where the plastic deformation begins first.

(iv) During the biaxial loading, where both the torque and the axial load are applied successively, the effect of the axial load or the torque whichever is applied subsequently, is dominant on the specimen investigated

(v) When the rod is initially subjected to an initial torque and then to a successively applied load and torque, keeping the axial displacement or the angle of twist constant in an alternate manner, the rod soon regains its axial load carrying capability irrespective of the level of the initially applied torque. Similarly, when the rod is initially subjected to an initial load and then to a successively applied torque and load, keeping the angle of twist or axial displacement constant in an alternate manner, the rod soon regains its torque carrying capability irrespective of the level of the initially applied load

(vi) Gaydon's theoretical model for the first type of loading, where the rod is subjected to an initial torque and then, keeping the angle of twist constant, to a gradually increasing axial strain, provides fair agreement with the experimental results, whereas his theoretical prediction for the third type of loading, where the rod is subjected to an initial load, gives poor agreement with the experimental results

(vii) During the successive application of the torque and the axial load, the state stress of the material reaches a yield locus after which it can no longer absorb any excess energy, and this yield locus may be called as the ultimate yield locus of the material

7.4 RECOMMENDATION FOR FUTURE WORK

(i) To control the torque-tension machine by means of a digital link from a computer and hence to monitor various data using an appropriate data acquisition card or a computer program

(ii) To develop numerical solutions of Brooks' [20] analytical model for both proportional and non-proportional loading using finite difference algorithms

(iii) To provide a more precise theoretical model by which the torsional and the tensile stresses are unloaded

(iv) The same non-proportional loading tests, as has been carried out in the present study, can be conducted after annealing the material and at various strain rates

(v) The proportional loading tests, which prevails in case of actual bolt tightening, under different controlled conditions can be carried out and can be compared with Brooks' analytical model

(vi) To observe the micro-structure of the fractured specimens, particularly which are subjected to successively applied torsion and tension loadings

References

- 1 Gardiner, W A , "Torque-tension relationships- what they are, why they are important", SME technical paper, No - AD75-771, 1975
- 2 Chapman, I, Newnhan, J, and Wallace, "The tightening of bolts to yield and their performance under load", J Vibration, Acoustics, Stress, and Reliability in Design, Vol - 108, 1986
- 3 Finkelston, R J and Wallace, P W , "Advances in high-performance mechanical fastening", SAE technical paper, No - 800451, 1980
- 4 Junker, G H and Wallace, P W , "The bolted joints Economy of design through improved analysis and assemble methods", Proc Inst Mech Engrs , Vol -198B, No - 14, 1984
- 5 Duff, B and Monaghan J , "Behaviour of fasteners tightened to yield", Proc IMC-1, Trinity College Dublin, 1984
- 6 Boys, J T and Wallace, P W , "Design and performance of an automatic control system for fastener tightening", Proc Instn Mech Engrs , Vol - 191, No - 38/77, I Mech E 1977
- 7 Monaghan, J M and Duff, B , "The influence of friction on the stress distribution within yield tightened fasteners", Proc IMC-2, University of Ulster, 1985
- 8 Newnham, J, Curley, L , and Boos, H P , " The response to external loads of bolted joint tightened to yield", VDI BERICHTE NR 766, 1989
- 9 Nadai, A , "Theory of flow and fracture of solids", Book, McGraw-Hill Book Company, Inc , Vol - 1, Second edition, 1950
- 10 Lode, W , "Versuche ueber den Einfluss der mittleren Hauptspannung auf das Fliesen der Metalle Eisen Kupfer und Nickel", Z Physik , 36, 1926, pp 913-939
- 11 Hill, R , "The mathematical theory of plasticity", Book, Oxford University Press, London, 1950

- 12 Hohenemser, K , Proc 3rd Int Cong App Mech , Stockholm, 2, 1930
- 13 Taylor, G I and Quinney, H , "The Plastic Deformation of Metals", Phil Trans Roy Soc , London, A230, 1931, pp 323-362
- 14 Morrison, J L M and Shepherd, W M , "An experimental investigation of plastic stress-strain relations", Proc Instn Mech Engrs , 163, 1950
- 15 Siebel, M P L , "The combined bending and twisting of thin cylinders in the plastic range", J of Mechanics and physics of solids, Vol 1, 1953, pp 189-206
- 16 Hill, R and Siebel, M P L , "On the plastic distortion of solid bars by combined bending and twisting", J of Mechanics and physics of solids, Vol 1, 1953, pp 207-214
- 17 Prager, W and Hodge, P G , "Theory of perfectly plastic solids", Book, Wiley, New York, 1951
- 18 Gaydon, F, A , "On the combined torsion and tension of a partly plastic circular cylinder", Quart J Mech and Applied Math , Vol 5, 1952, pp 29-41
- 19 Sved, G and Brooks D S , "Elasto-plastic behaviour of a round bar subjected to axial force and torque", Acta Techn Hung , Vol 50, 1965
- 20 Brooks, D S , "The elasto-plastic behaviour of a circular bar loaded by axial force and torque in the strain hardening range", Int J Mech Sci , Pergamon Press, Vol 11, 1969, pp 75-85
- 21 Naghdi, P M and Roeley, J C , "An experimental study of biaxial stress-strain relations in plasticity", J of the Mechanics and Physics of Solids, Vol 3, 1954, pp 63-80
- 22 Meguid, S A and Campbell, J D , "Elastic-plastic tension-torsion in a circular bar of rate-sensitive material", J of applied math (Trans of the ASME , Ser E), Vol 46(2), 1977, pp 311
- 23 Meguid, S A , "Plastic flow of mild steel (En8) at different strain rates under abruptly changing deformation paths", J Mech Phys Solids, Vol 29, No 5/6, 1981, pp 375-395

- 24 Meguid, S A , Klair, M S and Malvern, L E , "Theoretical and experimental results of the plastic and strain-hardening behaviour of En8 at a controlled rate", *Int J Mech Sci* , Vol 26, No 11/12, 1984, pp 607-616
- 25 McMeeking, R M , "The finite strain tension-torsion test of a thin-walled tube of elastic-plastic material", *Int J Solids structures*, Vol 18, No 3, 1982, pp 199-204
- 26 Narayanawamy, O S , Samanta, S K and Ghosh, A K , "Plastic deformation and springback of rectangular bars subjected to combined torsion and tension", *J Mech Phys Solids*, Vol 30, No 6, 1982, pp 427-445
- 27 Jiang, W , "The elastic-plastic response of thin-walled tubes under combined axial and torsional loads part I-monotonic loading", *Journal of Pressure Vessel Technology (Transactions of the ASME)*, Vol 115, August 1993, pp-283-290
- 28 Jiang, W , "The elastic-plastic response of thin-walled tubes under combined axial and torsional loads part II-variable loading", *J Pressure Vessel Techn (Transactions of the ASME)*, Vol 115, August 1993, pp-291-296
- 29 Jiang, W and Wu, K , "Thin-walled tubes subjected to combined internal pressure and axial load", *AIAA Journal*, Vol 31, No 2, February 1993, pp 377-387
- 30 Naghdi, P M , Essenburg, F and Koff, W , "Experimental study of initial and subsequent yield surface in plasticity", *J Appl Mech* , Vol 201, No 25, 1958, pp 201-209
- 31 McComb, H G Jr , "Some experiments concerning subsequent yield surface in plasticity", *NASA TN D-396*, 1960
- 32 Ivey, H J , "Plastic stress-strain relations and yield surfaces for aluminum alloys", *J Mech Eng Sci* , Vol 3, No 1, 1961, pp 15-31
- 33 Mair, W M and Pugh, H L D , "Effect of prestrain on yield surfaces in copper", *J Mech Engng Sci* , 6, 1964
- 34 Phillips, A , Tang, J L and Ricciuti, M , "Some new observations on yield surfaces", *Acta Mech* , 20, 1974, pp 23-29

- 35 Phillips, A and Weng, G J , "An analytical study of an experimentally verified hardening law", *Trans ASME, J Appl Mech* , Vol 42, 1975, pp 375-378
- 36 Phillips, A , Liu, C S and Justusson, J W , "An experimental investigation of yield surface at elevated temperature", *Acta Mech* , **14**, 1972, pp 119-146
- 37 Phillips, A and Tang, J L , "The effect of loading path on the yield surface at elevated temperature", *International Journal of Solids and Structures*", **8**, 1972, pp 463-474
- 38 Phillips, A and Kasper, R , "On the foundation of thermo-plasticity - an experimental investigation", *J Appl Mech* , Vol 40, 1973, pp 891-896
- 39 Tang, J L , "The effect of loading path on the yield surface at elevated temperatures", Ph D Thesis, Yale University, 1970
- 40 Bertsch, P K and Findley, W N , "An experimental study of subsequent yield surfaces- corners, normality, Bauschinger effect and allied effects", *Proc 4th U S Nat Cong Appl Mech* , 1962, pp 893-907
- 41 Marjanovic, R and Szczepinski, W , "On the effect of biaxial cyclic loading on the yield surface of M-63 brass", *Acta Mech* , **23**, 1975, pp 65-74
- 42 Shiratori, E , Ikegami, K and Kaneko, K , "Subsequent yield surface determined in consideration of Bauschinger effect", *Foundation of plasticity*, Ed Sawozuk, A , Noordhoff, 1973, pp 477-490
- 43 Shiratori, E , Ikegami, K and Kaneko, K , "Subsequent yield surface after proportional preloading of the Tresca-type material", *Bulletin of the JSME*, Vol 29, 1976, pp 1122-1128
- 44 Shiratori, E , Ikegami, K , Yoshida, F , Kaneko, K and Koike, S , "The subsequent yield surface after preloading under combined axial load and torsion", *Bulletin of the JSME*, Vol 19, 1976, pp 877-883
- 45 Moreton, D N , Moffat, D G and Parkinson, D B , "The yield surface behaviour of pressure vessel steels", *Journal of Strain Analysis*, Vol 16, No 2, 1981, pp 127-136

- 46 Rees, D W A and Mathur, S B , "Biaxial plastic flow and creep in anisotropic aluminium and steel", Non linear problems in stress analysis, Book, Edited by Stanley, E , Applied science publisher Ltd , ISBN-0-85334-780-8, 1978
- 47 Rees, D W A , "Yield surface motion and anisotropic hardening", Applied solid mechanics-1, Book, Edited by Tooth, A S and Spence, J , Elsevier applied science publishers, ISBN-0-85334-415-9, 1986
- 48 Rees, D W A , "Anisotropic hardening theory and the Bauschinger effect", J Strain Analysis, Vol 16, No 2, 1981, pp 85-95
- 49 Rees, D W A , "A theory of non-linear anisotropic hardening", Proc Instn Mech Engrs ", Vol 197(C), 1983, pp 31-41
- 50 Yeh, W C , "Investigation of deformation induced anisotropic strain hardening of metals", Ph D Thesis, University of Iowa, 1988
- 51 Han, C W and Yeh W C , "On the experimental determination of yield surfaces and some results of annealed 304 stainless steel", International Journal of Plasticity, Vol 7, 1991, pp 803-826
- 52 Meguid, S A , Malvern, L E and Campbell, J D , "Plastic flow of mild steel under proportional and non-proportional straining at a controlled rate", Journal of Engineering Materials and Technology, Vol 101, July 1979, pp 248-253
- 53 Duff, B P , "Tightening fasteners to yield and their performance under load", M Sc Thesis, Trinity College Dublin, 1985
- 54 Graves, F E , "Nuts and Bolts", Scientific America, June 1984, pp 108-115
- 55 Mackenzie, R , "Screw Threads Design, Selection and Specification", The Industrial Press, New York, 1961, pp 1-8
- 56 Ross, R B , "Metallic materials specification hand book", 3rd edition, 1980, pp 339
- 57 Alexander, E M , "Design and strength of screw threads", Trans of technical conference on metric mechanical fasteners, March 1975

- 58 Landt R C , "Criterion for evaluating bolt head design", Journal of engineering for industry, Nov 1976, pp 1179-1182
- 59 Bickford, J H , "An introduction to the design and behaviour of bolted joints", Marcel Dekker Inc , New York and Basel, 1981, pp 20-134
- 60 Junker, G H , "New criteria for self-loosening of fasteners under vibration", SAE paper no 690055, 1969, pp 314-335
- 61 Goodier, J N and Sweeney, R J , "Loosening by vibration of threaded fastenings", Mechanical Engineering, Dec 1945, pp 798-802
- 62 Sauer, J A , Lemmon, D C and Lynn, E K , "Bolts how to prevent their loosening", Machine Design, August 1950, pp 133-139
- 63 Sorel, M , Aubert, J and Brand, A , "Ultrasonic measurement of the tension due to tightening of bolted joints", 6th International Conference on NDE in the Nuclear Industry, Zurich Switzerland ASM metals park OH, USA, 1983
- 64 Becker, B R *et al*, "Measuring the accuracy and precision of a torque system that tightens bolts to yield", ASME paper 92-WA/DE-2, Published by ASME, New York, USA, 1992
- 65 Yamashita, H , Makimae, T , Yoshizu, K and Nakatani, S , "Development of plastic region tightening cylinder head bolts for new diesel engine", SAE technical paper, No 851641, 1985
- 66 Maruyama, K and Nakagawa, M , "Proposal of new torque control method and new design system in bolted joint", Bull Res Lab Precis Mach Electron , Tokyo Instron, Tokyo Inst Technol , Vol 55, March 1985, pp 25-29
- 67 Hagiwara, M , Ohashi, N and Yoshimoto, I , "Characteristics of bolted joints in plastic region tightening", Bull Japan Soc of Prec Engg , Vol 20, No 4, Dec 1986, pp 287-290
- 68 Nakagome, M , Kobayashi, N , Onodera, O and Mizuno, M , "Influence of clamping force and clamped parts on fatigue strength of bolts", Bull Japan Soc of Prec Engg , Vol 20, No 3, Sept 1986, pp 153-158

- 69 Nakagome, M , Isahaya, K and Mizuno, M , "Influence of clamping force and pre-clamping force on fatigue strength of rolled-bolt", Bull Japan Soc of Prec Engg , Vol 21, No 1, Mar 1987, pp 16-20
- 70 Monaghan, J M , "The influence of lubrication on the design of yield tightened joints", Journal of Strain Analysis, Vol 26, No 2, 1991, pp 123-132
- 71 Hariri, B T , "Establishment of design criteria for tightening bolted joints", M Eng Thesis, Dublin City University, Dec 1990
- 72 Tsuji, H and Maruyama, K , "Behaviour of bolted joints tightened in plastic region - Estimation of yield point load at threaded portion", Journal of the Japan Soc of Precs Eng , Vol 57(9), 1991, pp 1627-1632
- 73 Tsuji, H and Maruyama, K , "Behaviour of bolted joints tightened in plastic region - Equivalent diameter of threaded portion to estimate yield clamping force", Jnl of the Japan Soc of Precs Eng , Vol 58(7), 1992, pp 1227-1231
- 74 Tsuji, H and Maruyama, K , "Behaviour of bolted joints tightened in plastic region - Analysis based on rigid-plastic model", Journal of the Japan Soc of Precs Eng , Vol 59(4), 1993, pp 589-594
- 75 Wilhelm, J , "Torque-tension testing", Compressed Dir , Vol 75, No 8, 1070, pp 20
- 76 Mendelson, A , "Plasticity Theory and Application", Book, The Macmillan Company, New York, 1968, Library of Congress catatog card no 68-12718
- 77 Hearn, E J , "Mechanics of materials", Book, Pergamon Press Ltd , UK, 1985, ISBN-0-08-030529-6
- 78 Ford, H , "Advanced mechanics of materials", Book, Longmans Green and Co Ltd , UK, 1963
- 79 Tegart, W J M , "Elements of mechanical metallurgy", Macmillan, New York, 1967
- 80 Chakrabarty, J , "Theory of plasticity", Book, McGraw-Hill Book Company, 1987, ISBN- 0-07-010392-5

- 81 Lubliner, J , "Plasticity theory", Book, Macmillan Publishing Company, New York, 1990, ISBN- 0-02-372161-8
- 82 Johnson, W and Mellor, P B , "Engineering plasticity", Ellis Horwood Limited, 1983, ISBN- 0-85312-346-2
- 83 Lubahn, J D and Felgar, R P , "Plasticity and creep of metals", John Wiley & Sons, New York, 1961
- 84 Hoffman, O and Sachs, G , "Introduction to the theory of plasticity for engineers", McGraw-Hill Book Company, 1953
- 85 Kaliszky, S and Elsevier, "Plasticity Theory and engineering applications", Sept 1989, ISBN-0-444-98891-2
- 86 Kachanov, L M , "Foundations of the theory of plasticity", North Holland Publishing Company, 1971
- 87 Malvern, L E , "Introduction to the mechanics of continuous medium", Englewood Cliff, N J Prentice-Hall, 1969
- 88 Benham, P P and Warnock, F V , "Mechanics of solids and structures", Book, Pitman Publishing Ltd , 1979, ISBN 0-273-36191-0
- 89 Polakowski, N H and Ripling, E J , "Strength and structure of engineering materials", Book, Prentice-Hall Inc , 1966
- 90 Timoshenko, S and Young, D H , "Elements of strengths of materials", Book, D Van Nostrand Company, New York, 1968
- 91 Davis, H E , Troxell, G E and Wiskocil, C T , "The testing and inspection of engineering materials", Book, McGraw-Hill Book Company, Inc , Second edition, 1955
- 91 Alexander, J M , "Strength of materials", Book, Ellis Horwood Ltd , Vol - 1, 1981, ISBN - 0-85312-290-3

- 92 Faries, V M , "Design of machine elements", Book, The Macmillan Company, New York, 1965
- 93 Rothbart, H A , "Mechanical Engineering Essential Reference Guide", McGraw-Hill Book Company, 1988, ISBN - 0-07-054024-1
- 94 Shigley, J E and Mischke, C R , "Standard Handbook of Machine Design", McGraw-Hill Book Company, 1986, ISBN - 0-07-056892-8
- 95 ASM Handbook, Mechanical testing, Vol 8, 1992, ISBN - 0-87170-007-7 (v 1)
- 96 Rothbart, H A , "Mechanical Design and Systems Handbook", McGraw-Hill Book Company, 1985, ISBN- 0-07-054020-9

APPENDIX

APPENDIX - A

Detailed drawings of various components of the torque-tension machine

This section contains a number of drawings of different components of the torque-tension machine. The detailed description of these figures are given in chapter three. Figures have started from the next page.

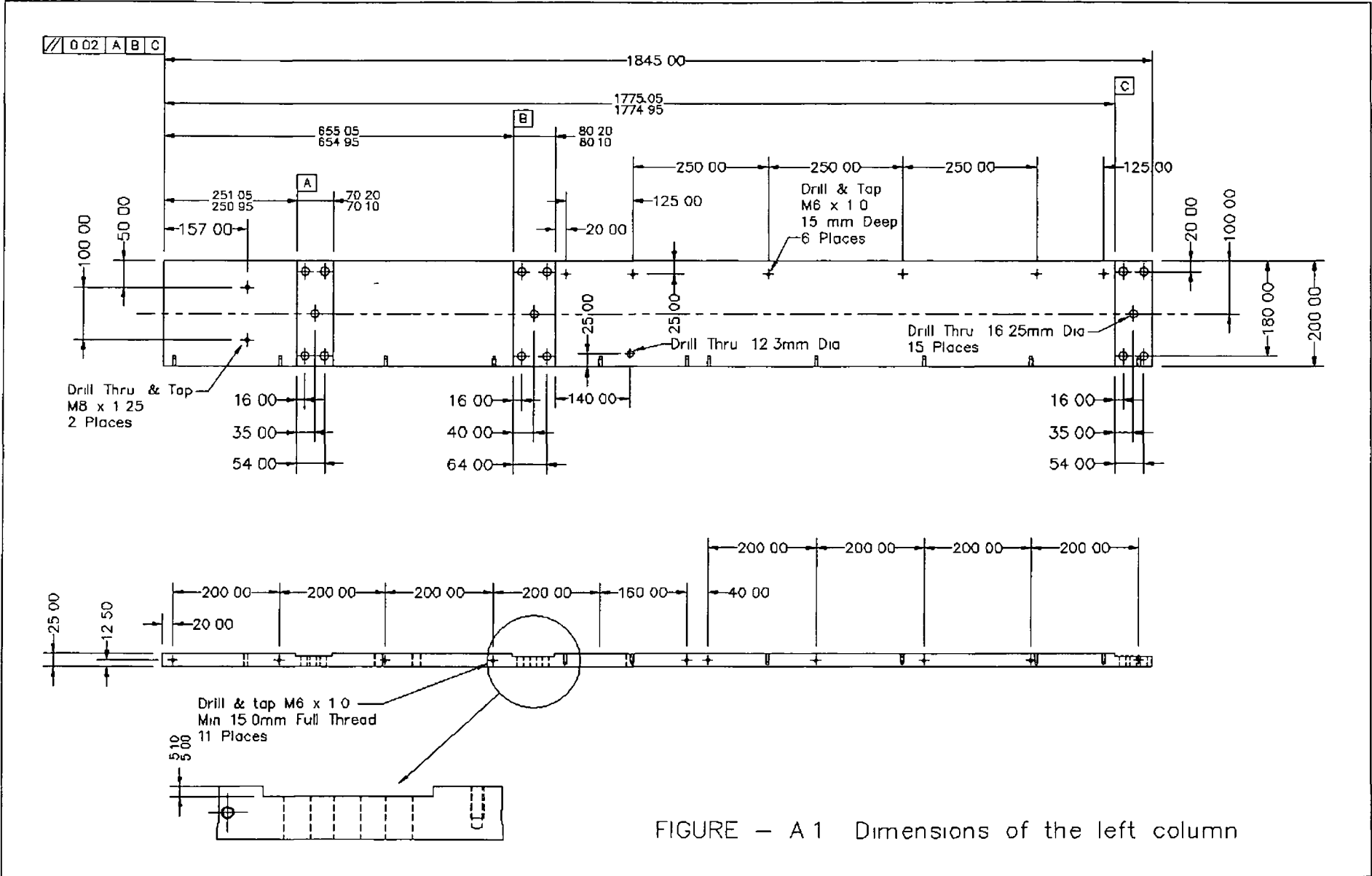
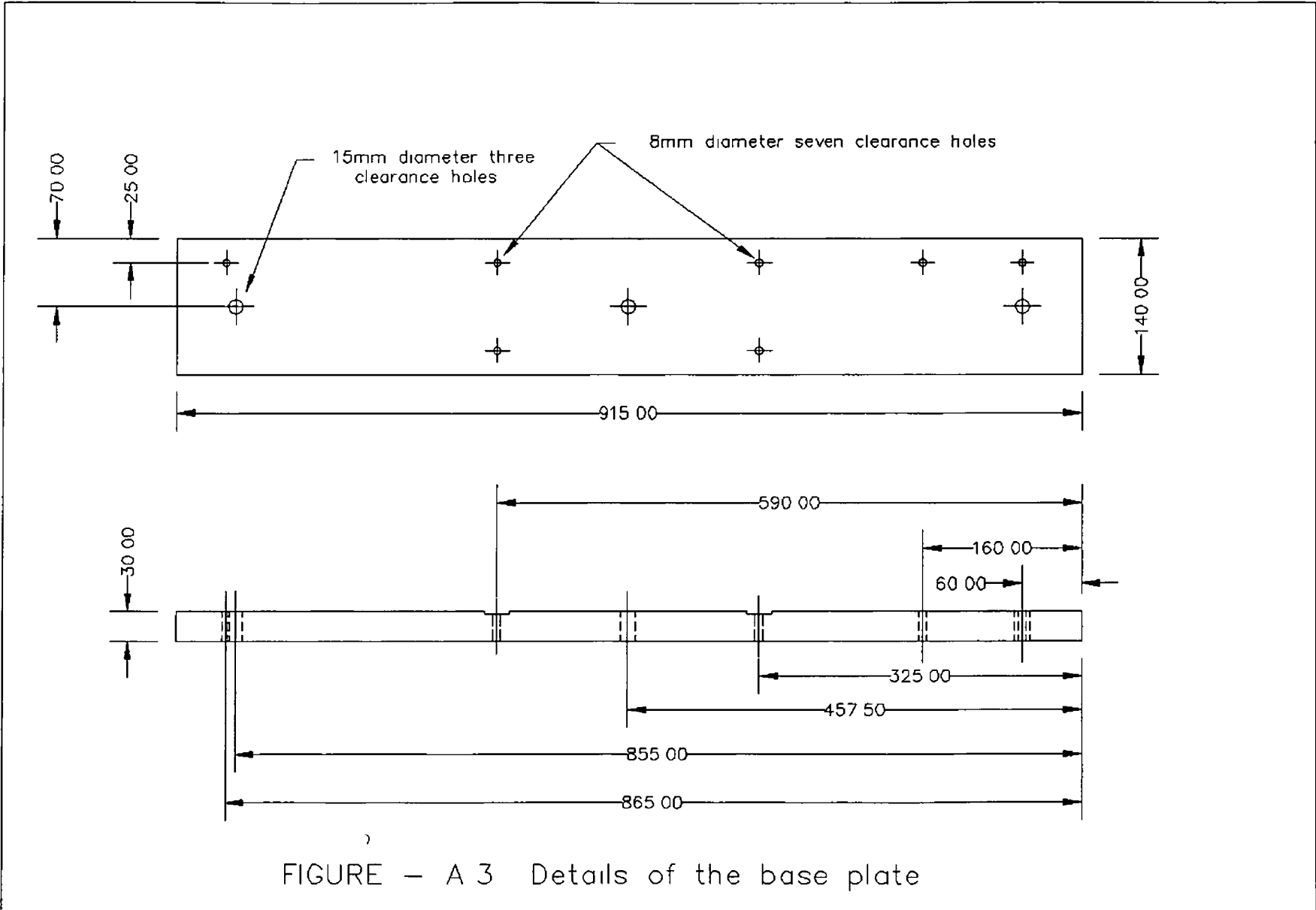


FIGURE - A1 Dimensions of the left column



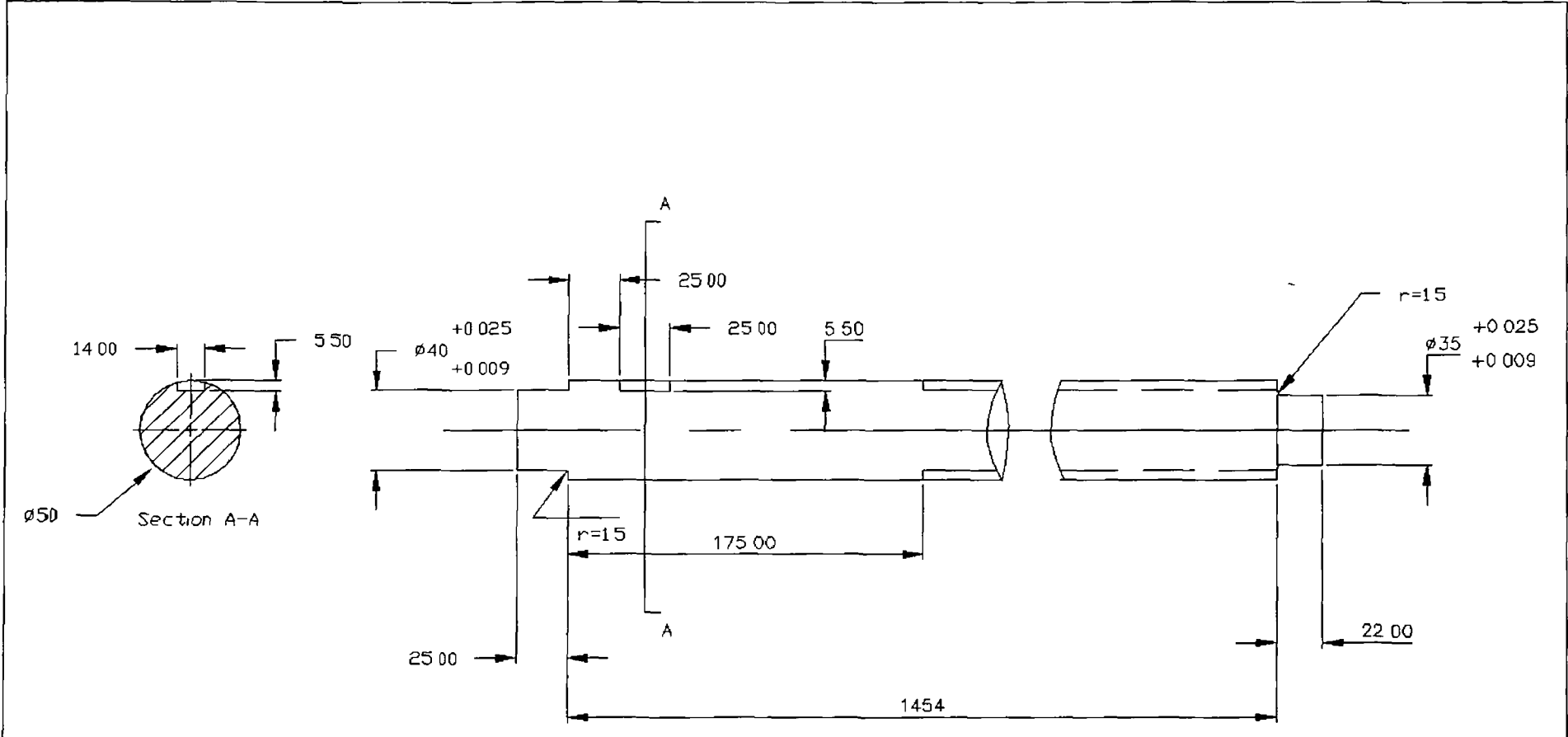


FIGURE - A 4 Position of the keyway in the left ballscrew

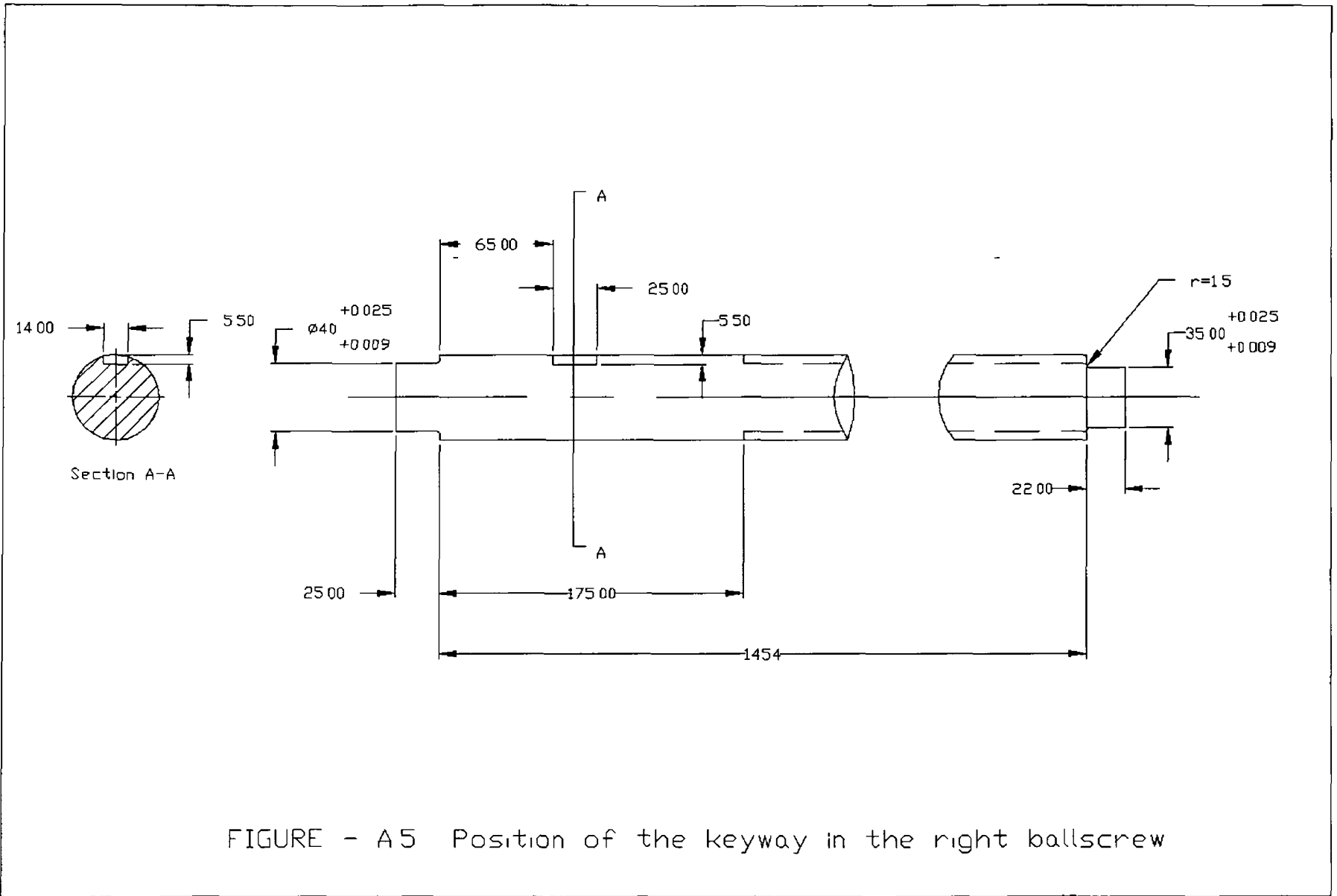


FIGURE - A5 Position of the keyway in the right ballscrew



Drill & Tap
M16 x 2.0
Min 30 full thread
2 places

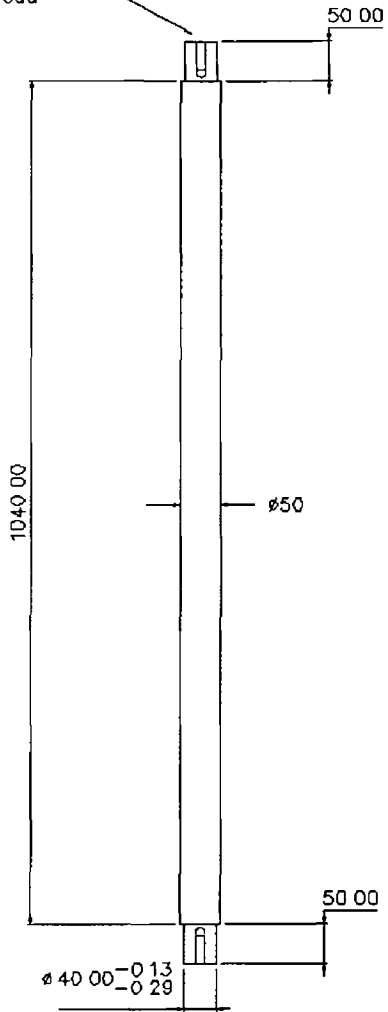
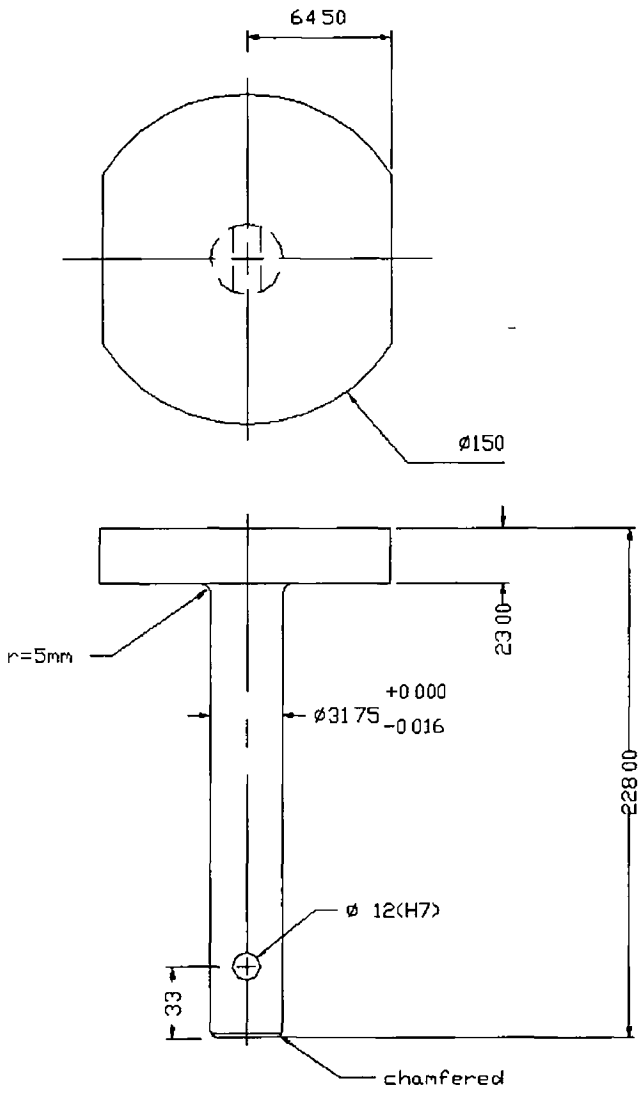


FIGURE - A 6 Dimensions of the guide rod

FIGURE -



- A7 Geometry of the stepped shaft

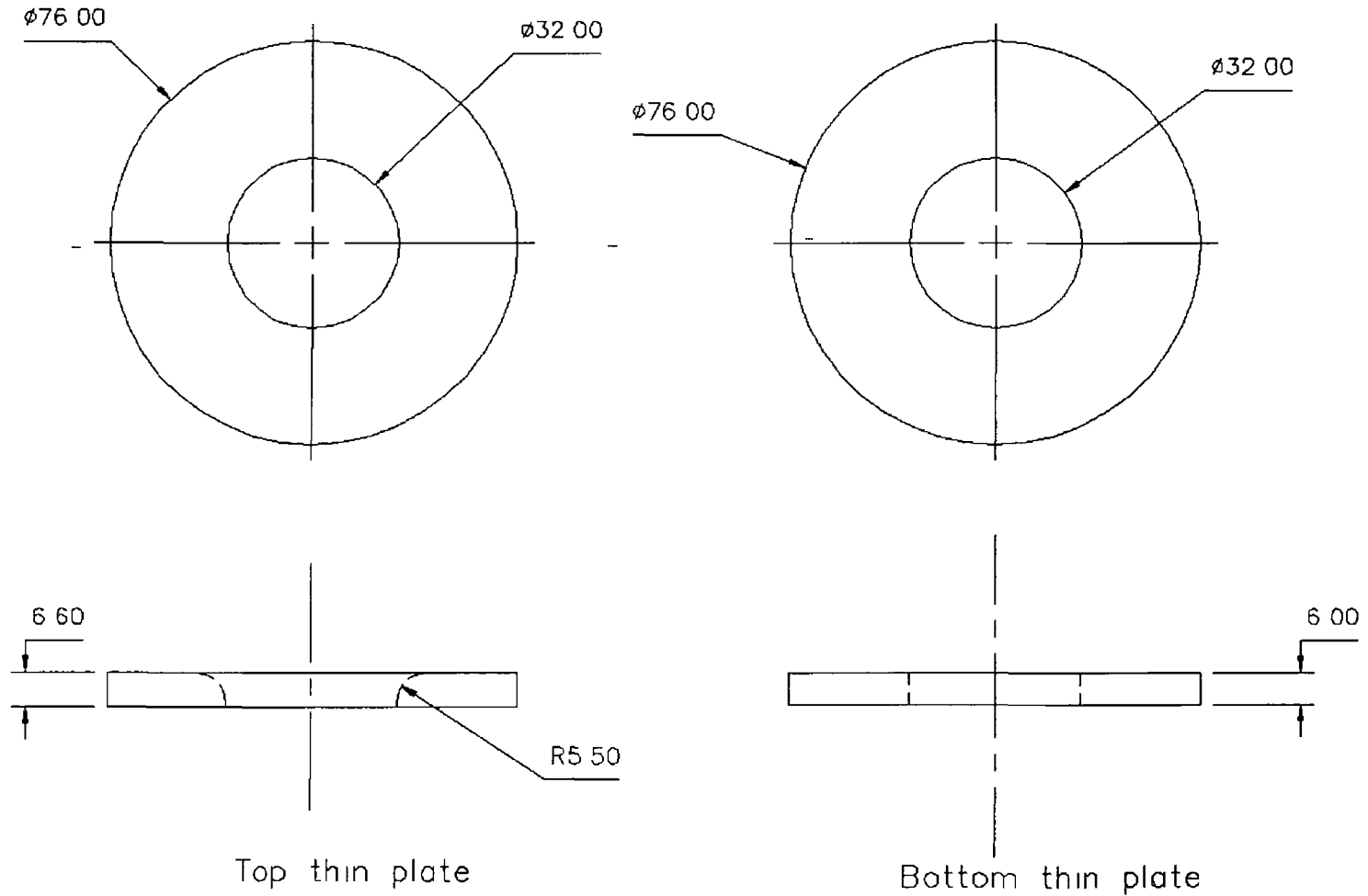


FIGURE - A 8 Details of the thin plates

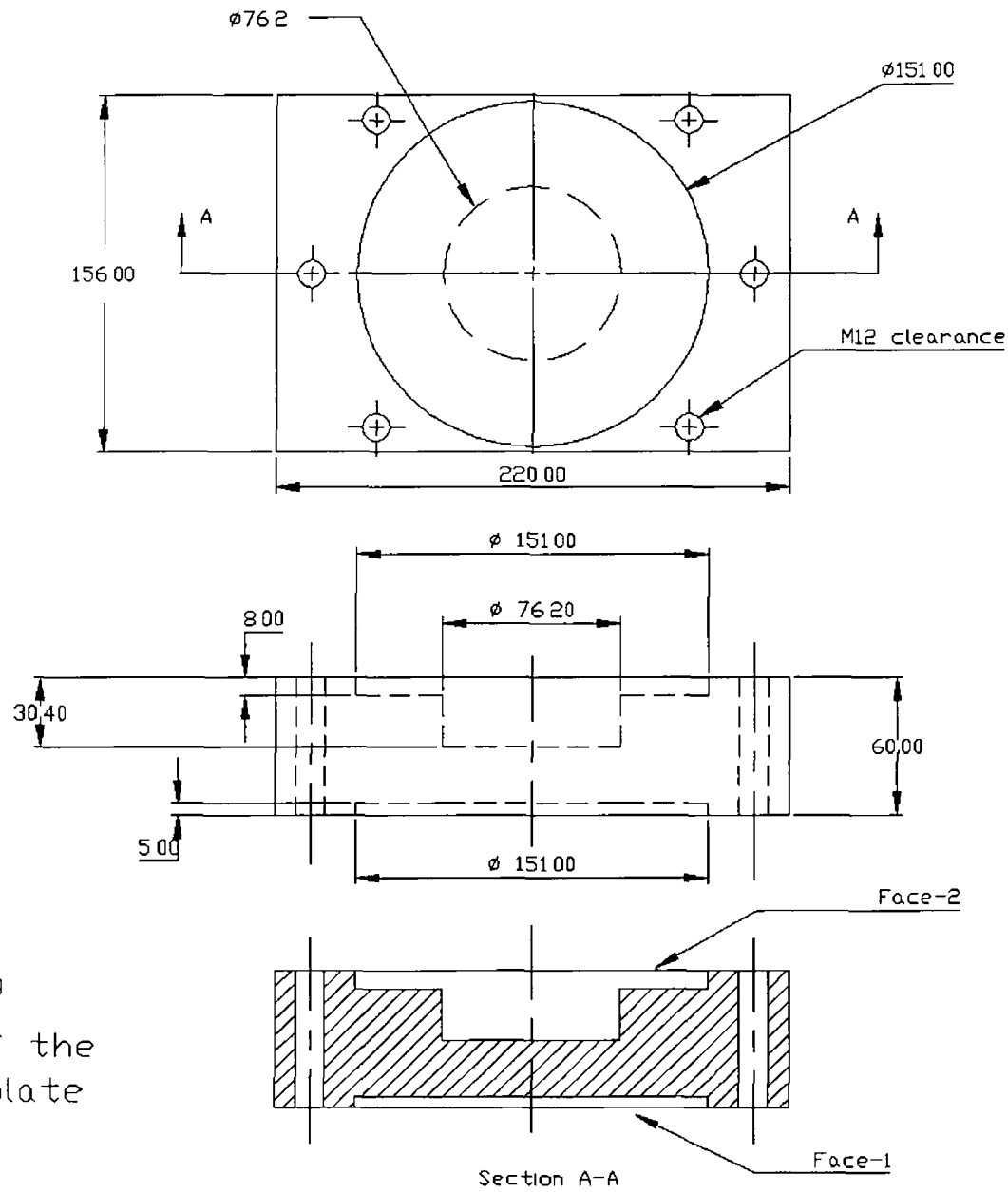
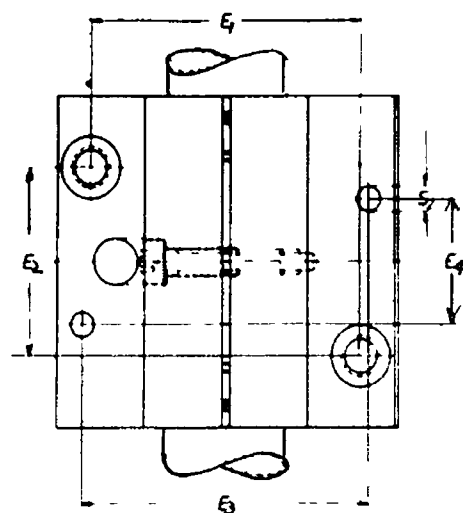
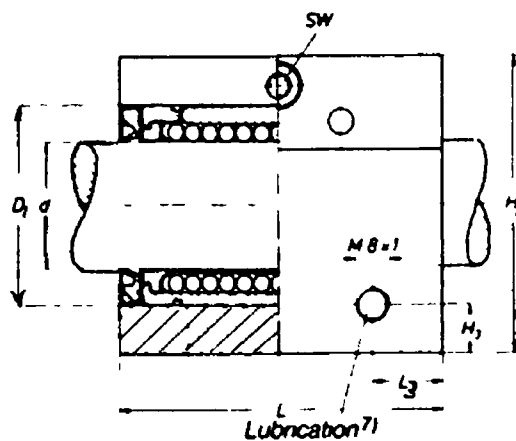
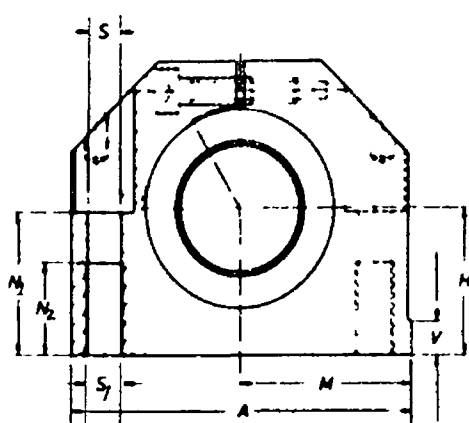


FIGURE - A9
Geometry of the
top cover plate



All dimensions are in mm

$D_1 = 75$	$S = 13.5$
$H = 50$	$S_1 = M16$
$H_1 = 10$	$S_2 = 10$
$M = 66$	$N_1 = 49$
$A = 132$	$N_2 = 34$
$L = 113$	$H_3 = 12.5$
$E_1 = 108 \pm 0.20$	$L_3 = 22$
$E_2 = 50 \pm 0.20$	$V = 12$
$E_3 = 108$	$SW = 8$
$E_4 = 42$	

Static load capacity = 7.1 kN

Dynamic load capacity = 8.6 kN

FIGURE - A 10 Details of the linear ball bearing

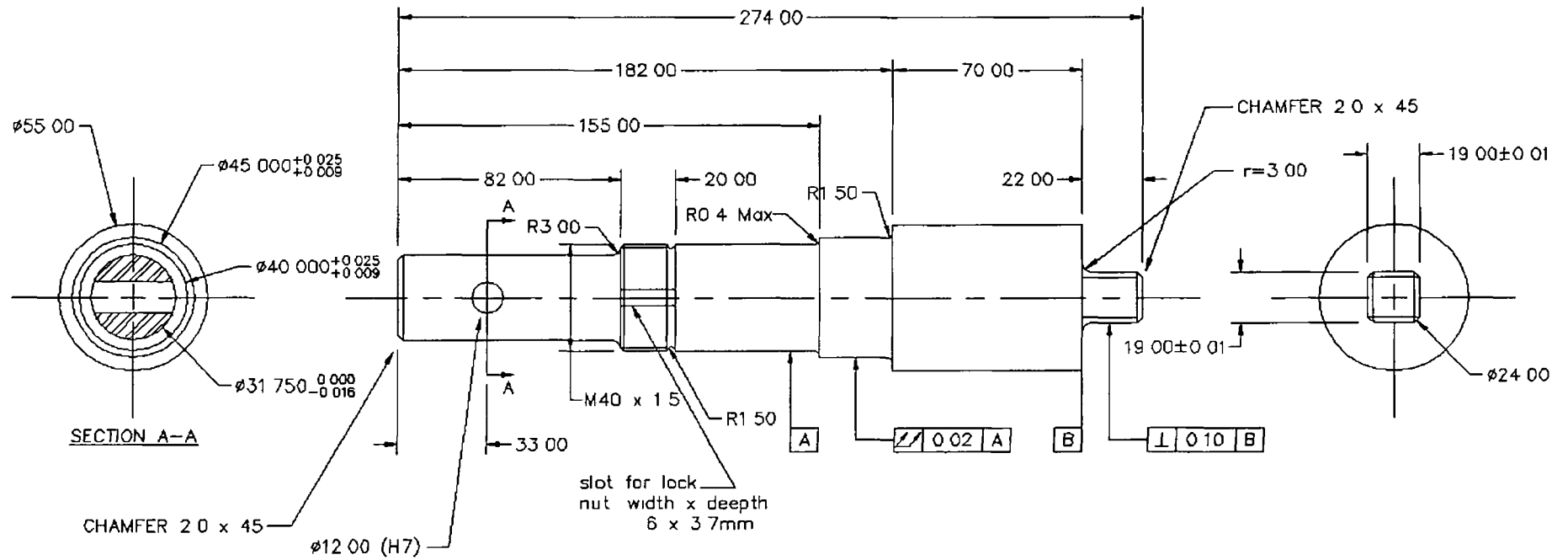


FIGURE - A 11 Details of the torque-tension shaft

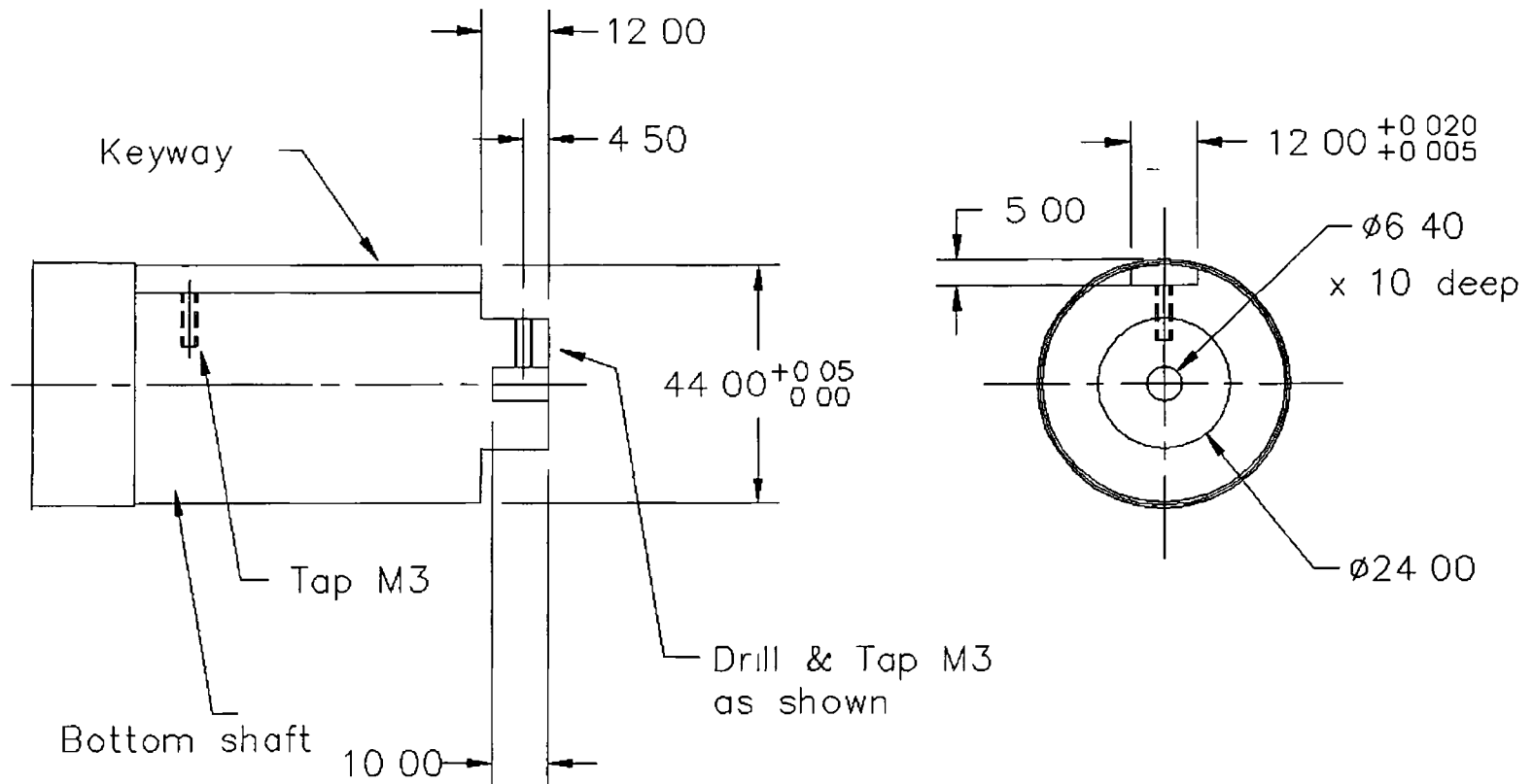


FIGURE – A13 Details of the bottom face of the torsion shaft

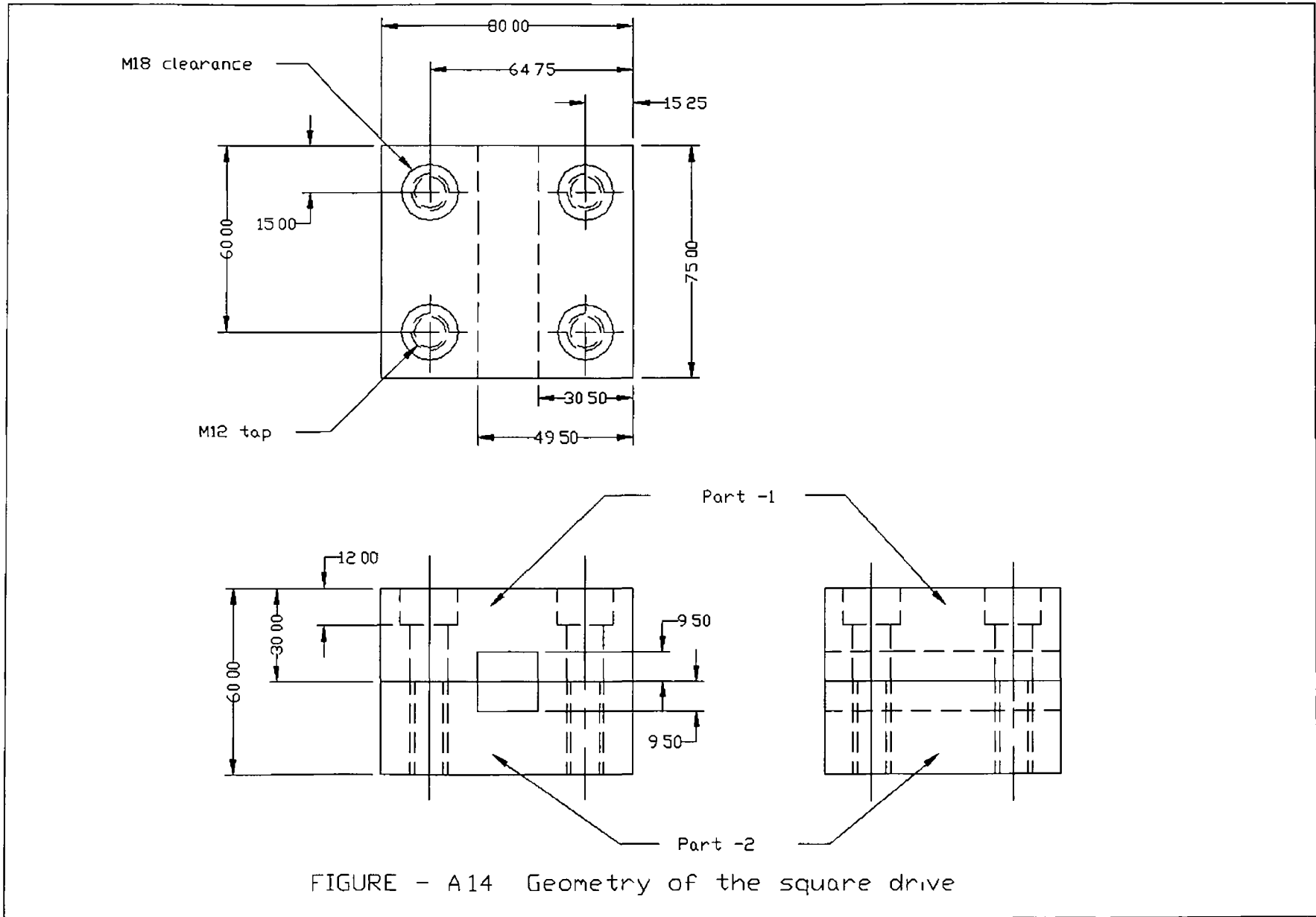


FIGURE - A14 Geometry of the square drive

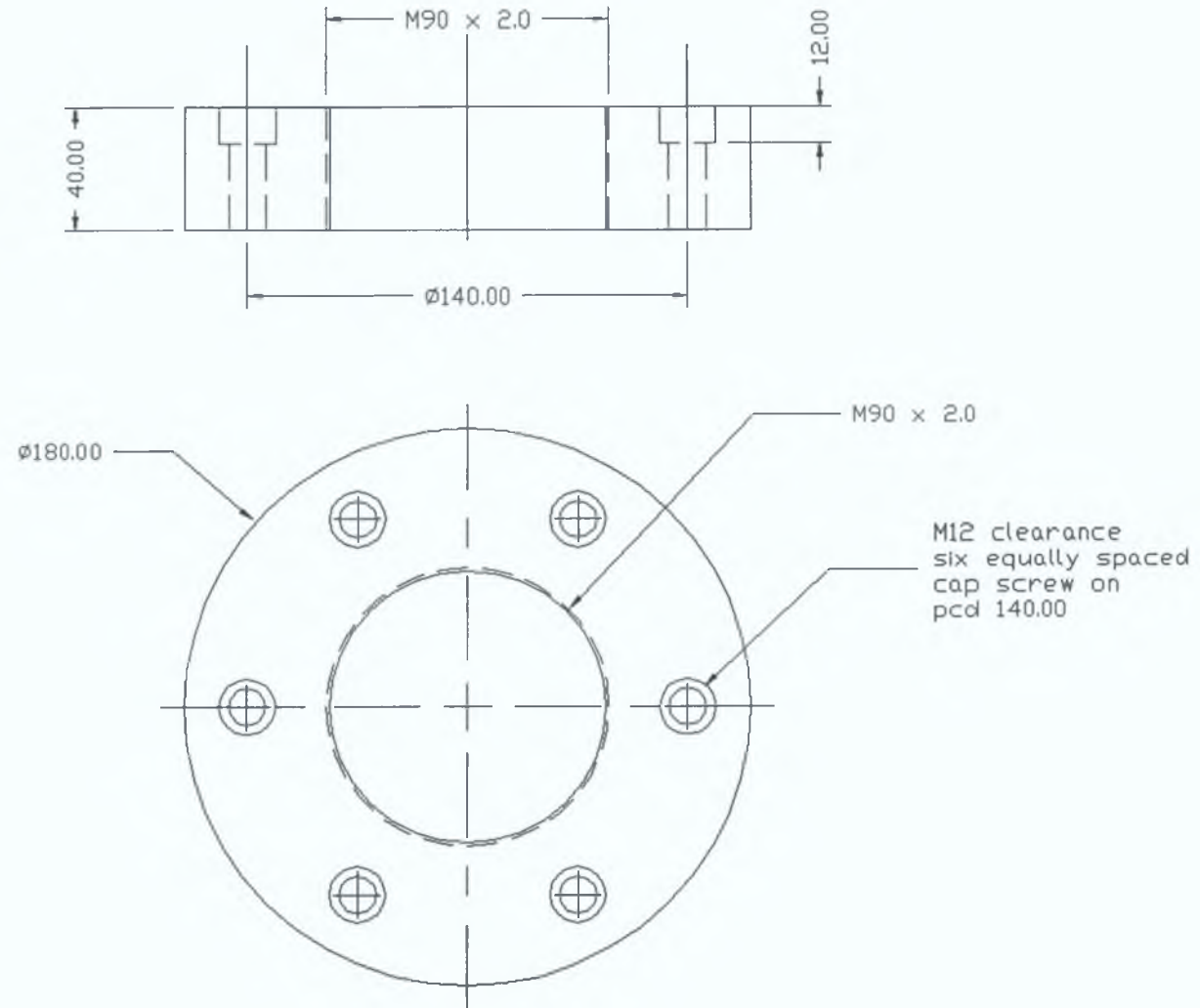


FIGURE - A.15 Geometry of the adjuster

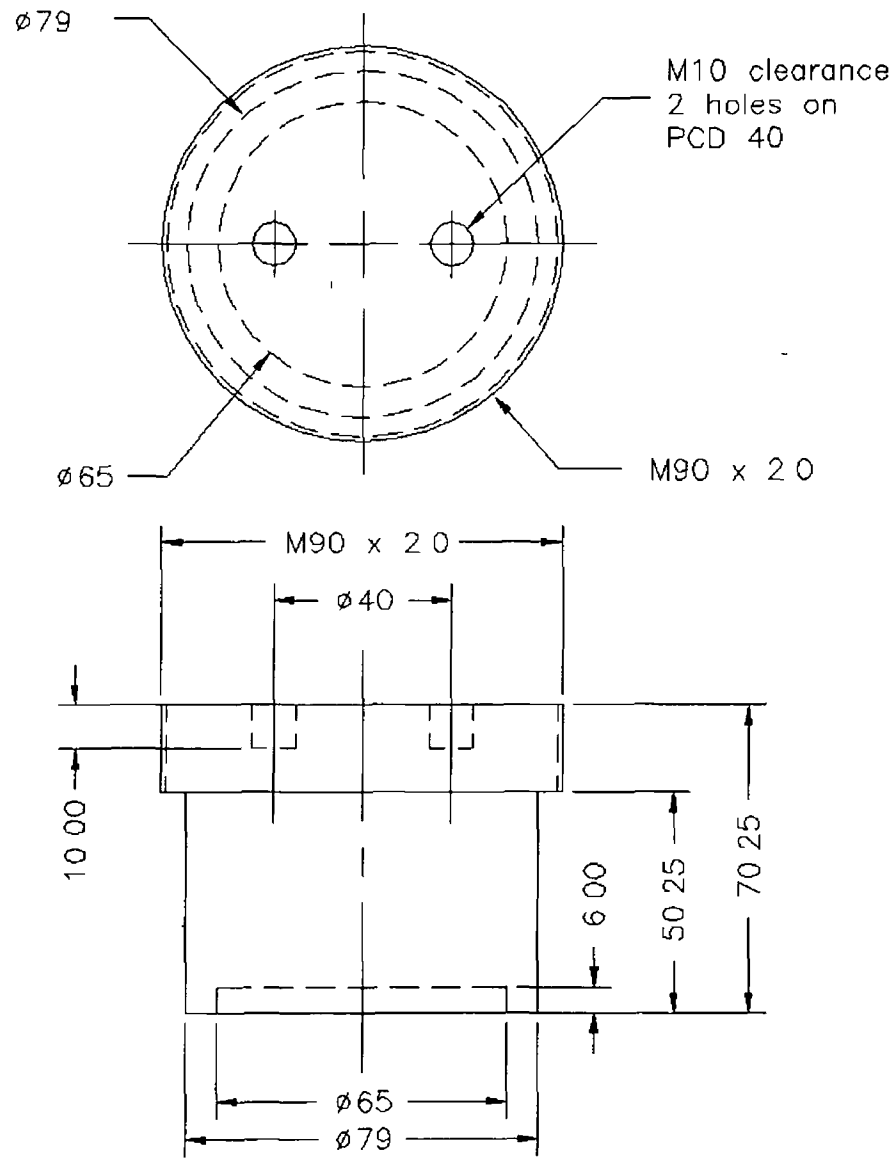


FIGURE - A 16 Geometry of the nut-1

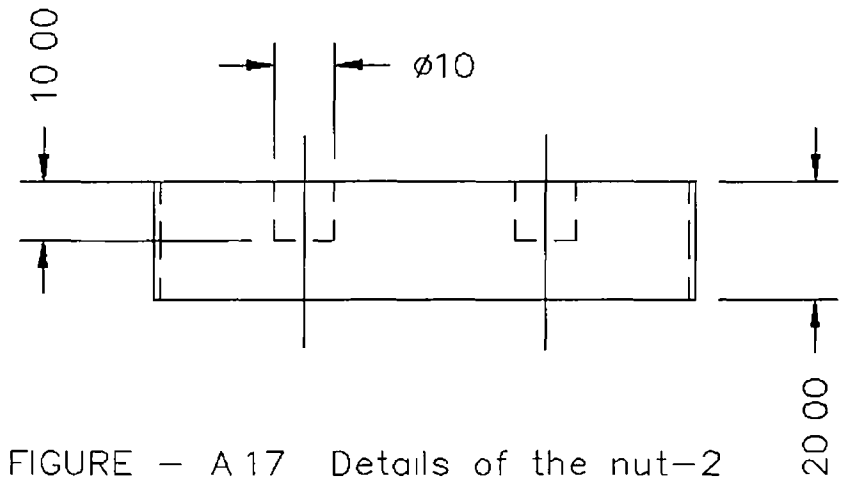
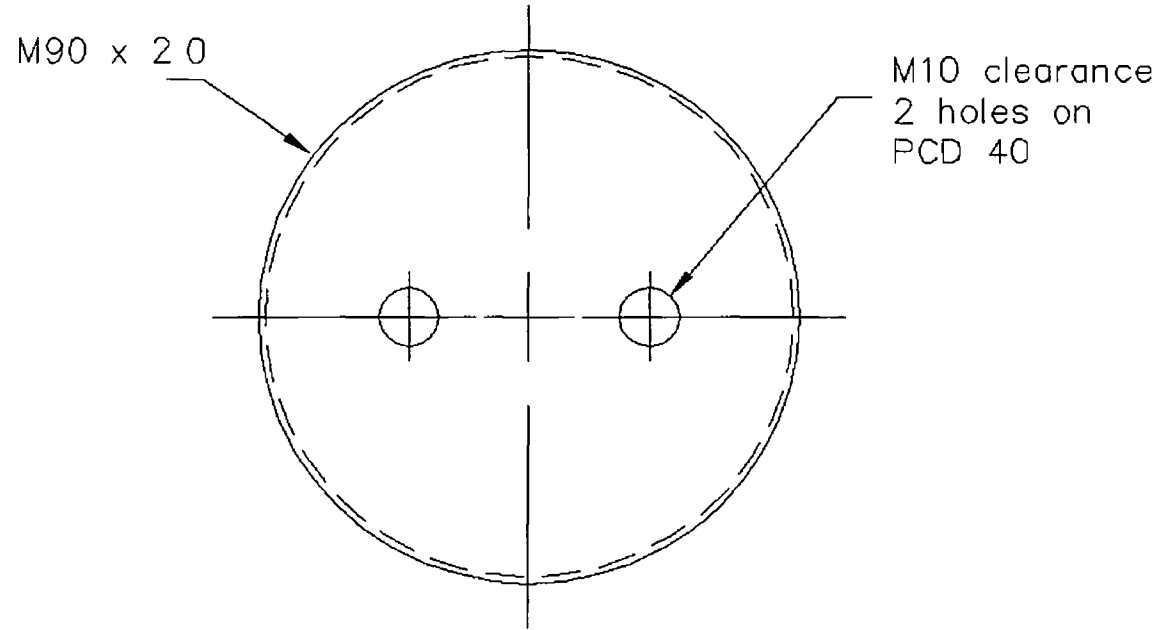


FIGURE - A 17 Details of the nut-2

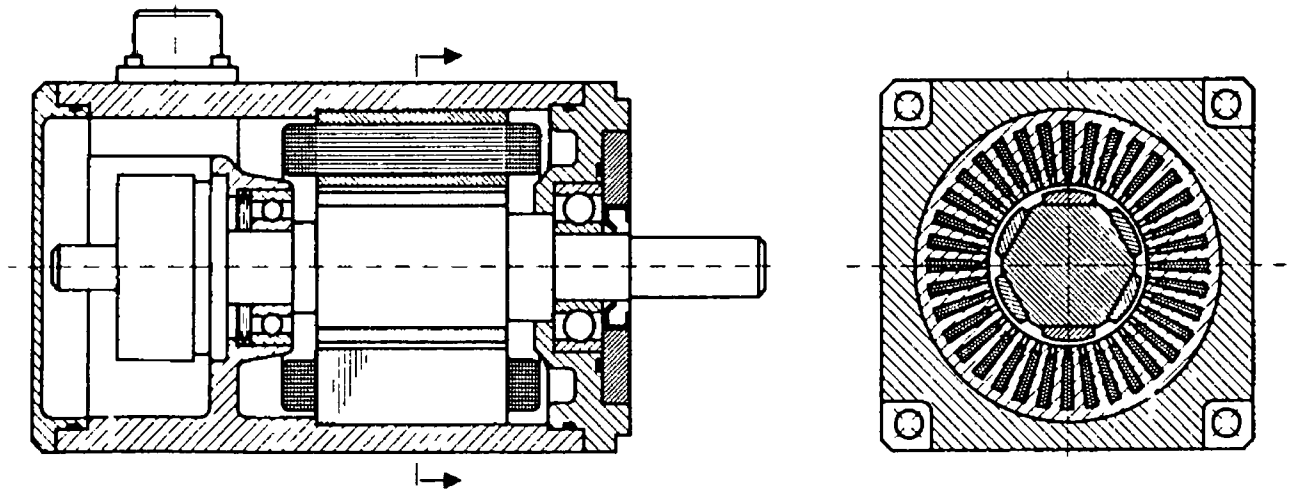


Figure - A 18 Schematic diagram of a Moog brushless servomotor

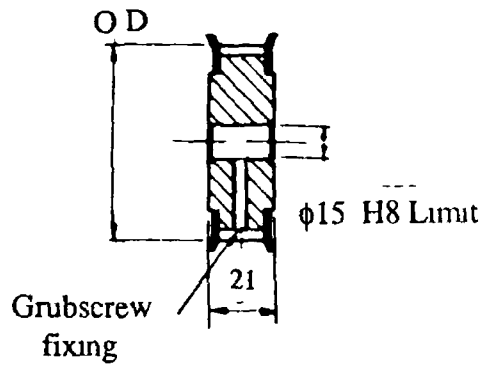


FIGURE - A 19 Dimensions of the timing pulley

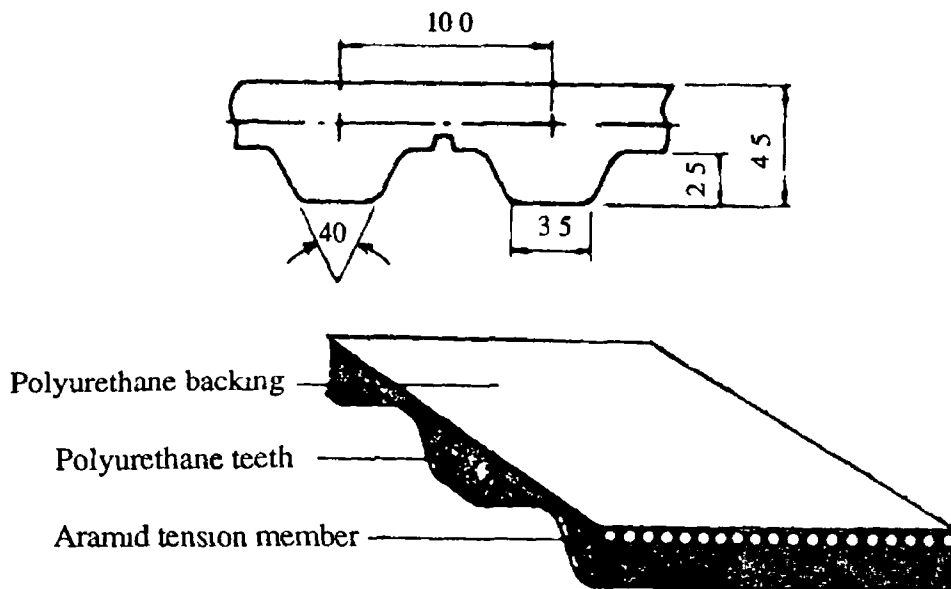


FIGURE - A 20 Details of the timing belt

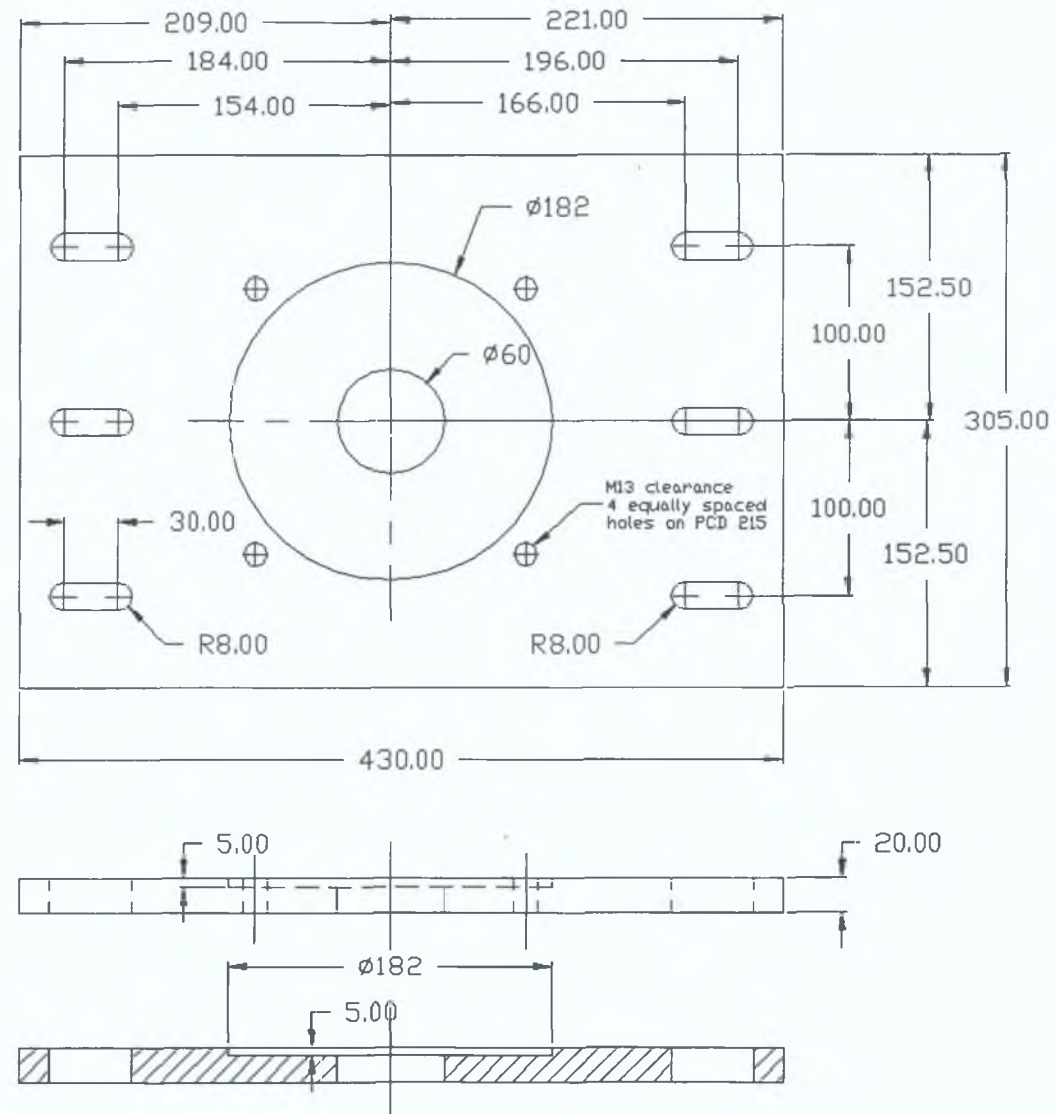


FIGURE - A.21 Geometry of the base plate-1

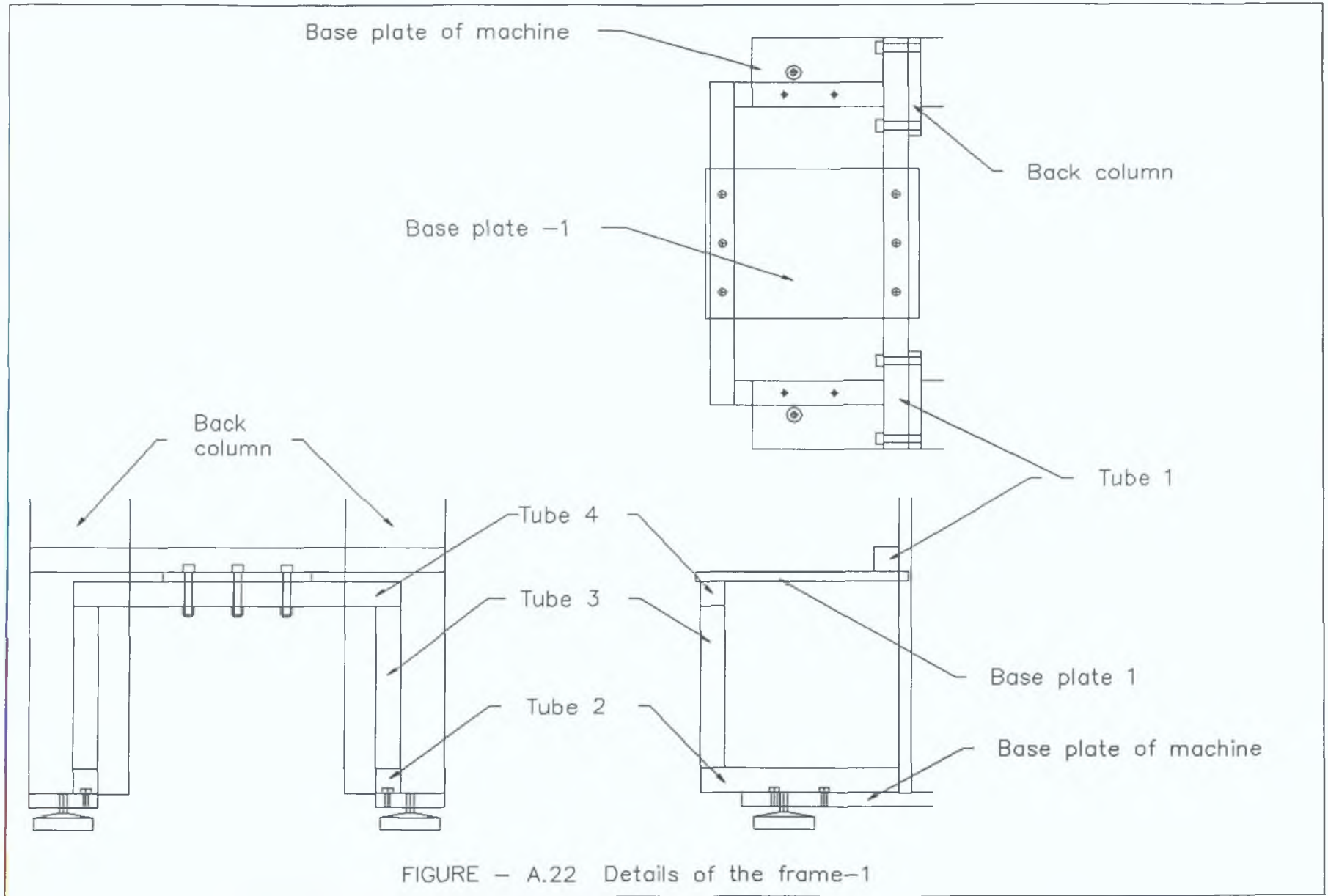


FIGURE - A.22 Details of the frame-1

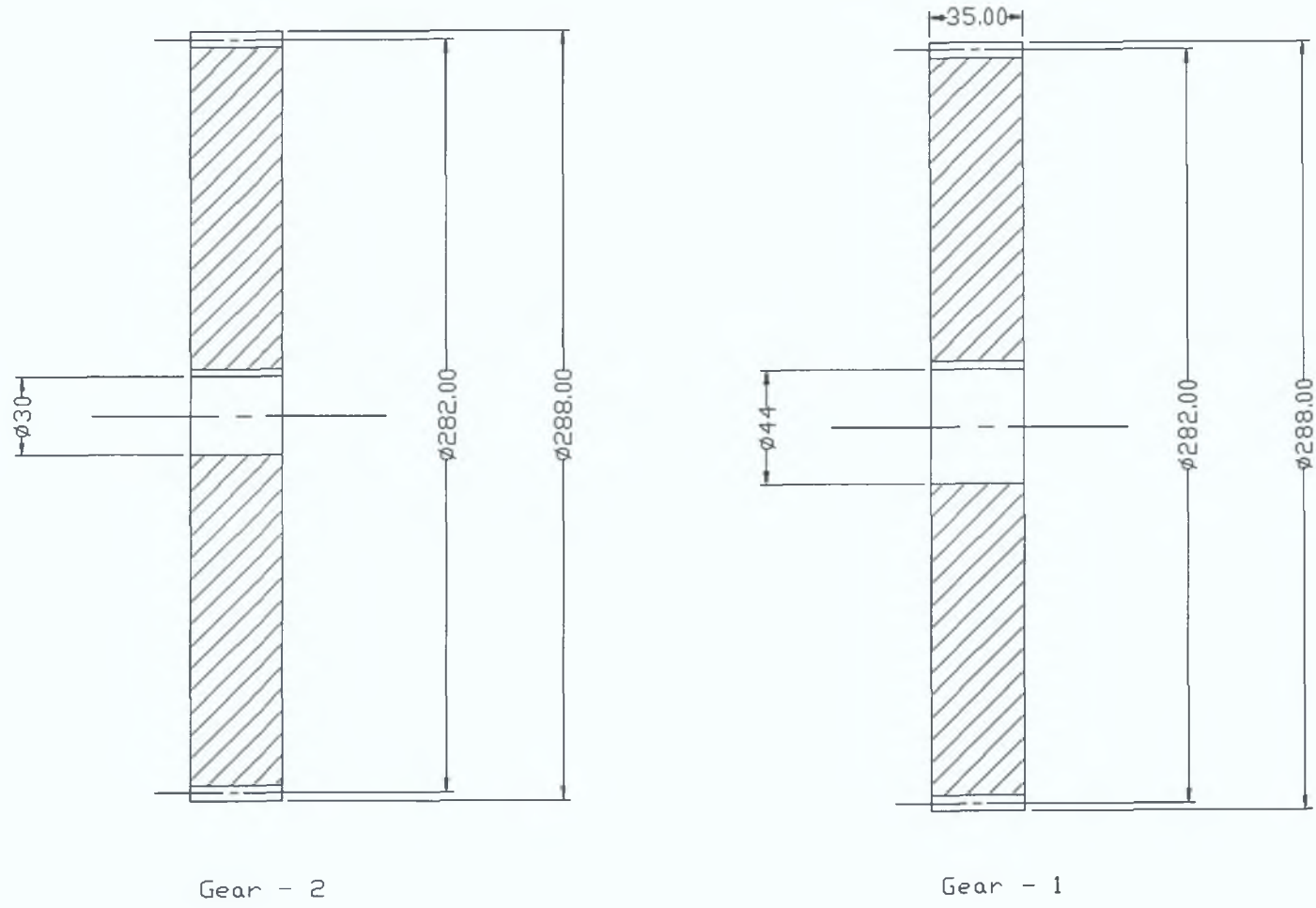


FIGURE - A.23 Details of the spur gears

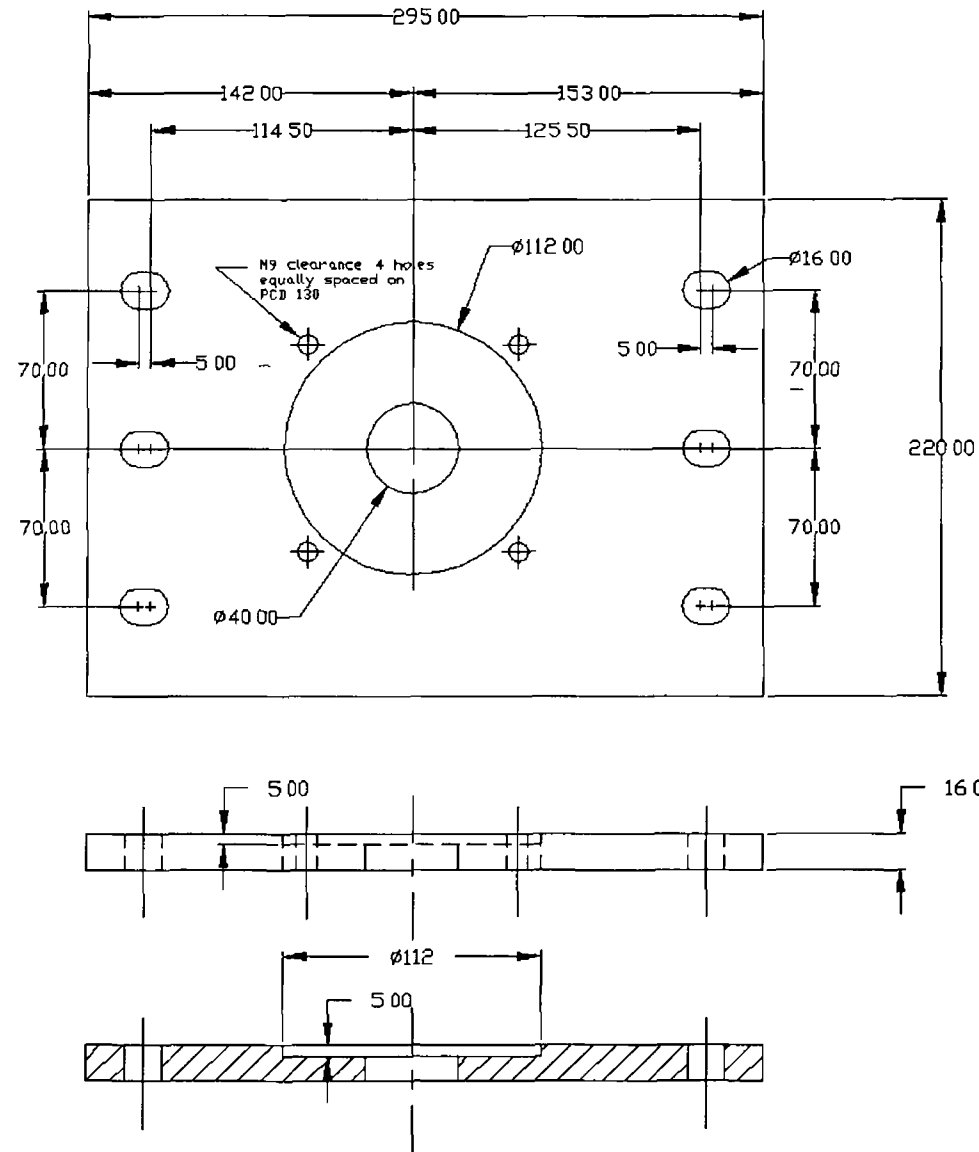
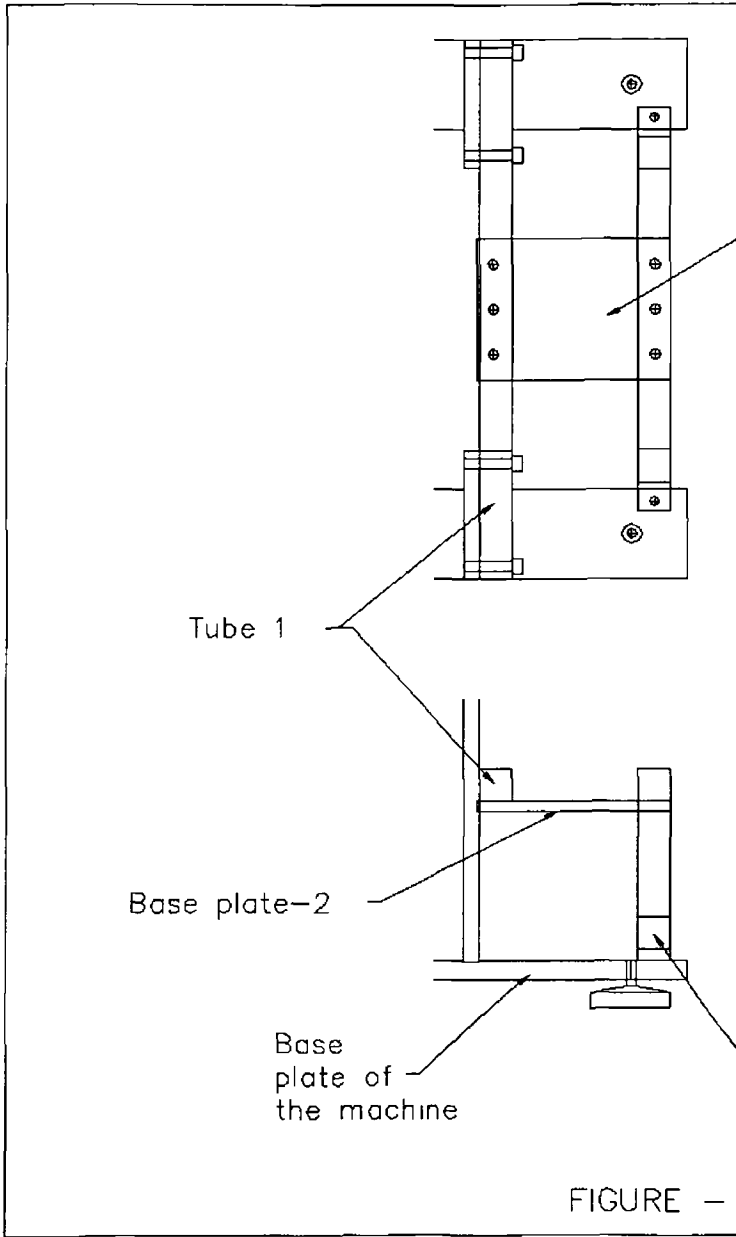
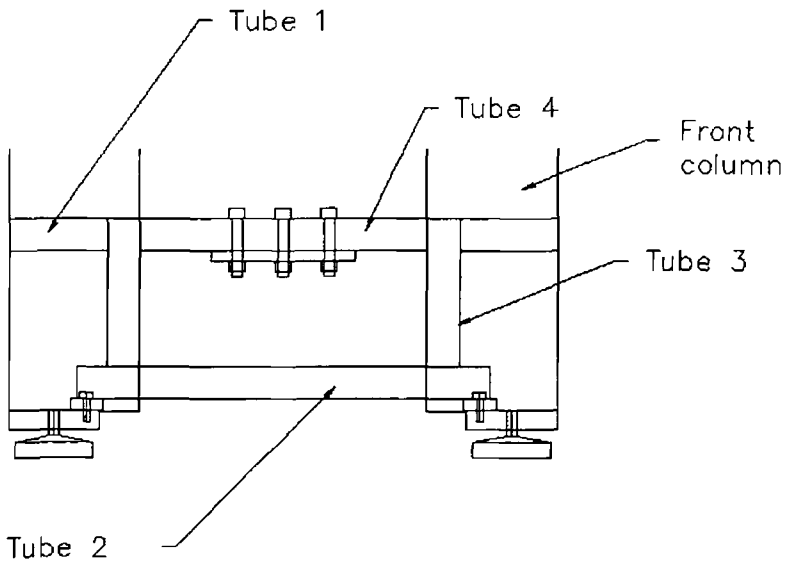


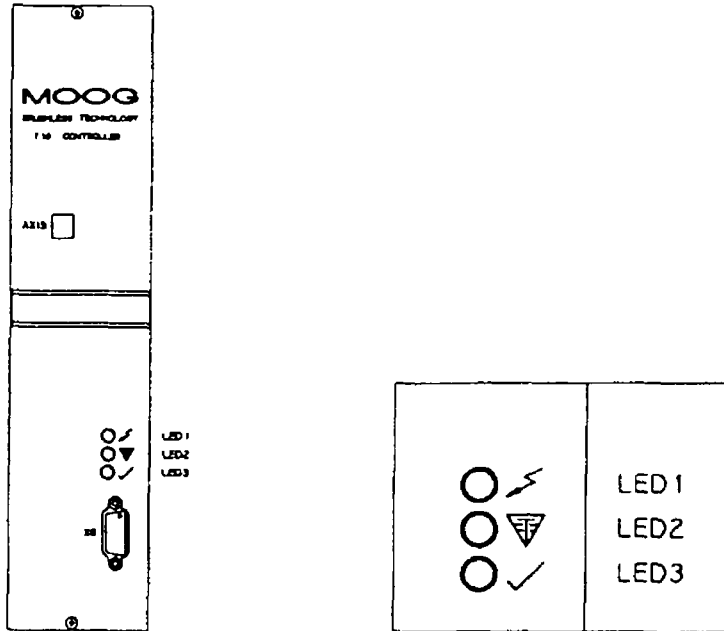
FIGURE - A24 Geometry of the base plate-2



Base plate-2



A 25 Details of the frame-2

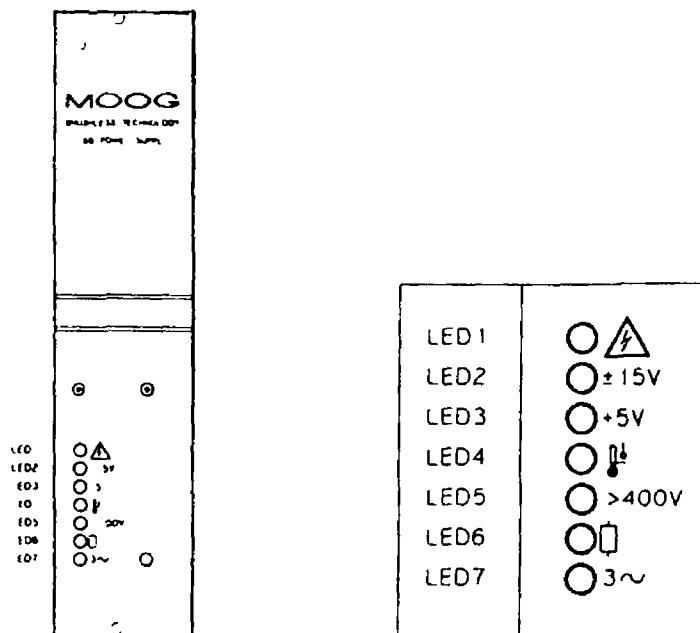


Controller T161 Status LEDs

Status LEDs

- LED 1** Fault (red)
Detailed fault description can be enquired via interface X6 (See section 3.3.7f) if a fault is active the fault LED signal is latched. Also relay *Axis OK* (X115/Pin 1/2) opens. Enabling the system again resets the fault LED if the fault is not active anymore.
- LED 2** Torque Limit active (yellow)
As long as torque limit is active *Thermal Limit* relay (X115/Pin 15/16) opens.
- LED 3** Enable (green)
Enabling of the system is only allowed after relay *Power supply OK* (X5/Pin 5/6) has closed. Otherwise surge current limiting function is not fully in access and power supply could be damaged.

FIGURE - A 26 Front connections of the controller



Power supply 160 status LEDs

Status LEDs

- LED 1 DC Bus voltage O K (green)
- LED 2 +/- 15VDC O K (green)
- LED 3 +5VDC O K (green)
- LED 4 Overtemperature Power supply (red)
- LED 5 DC Bus voltage >400VDC (red)
- LED 6 Bleed resistor active (yellow)
- LED 7 Loss of phase (red)

FIGURE - A 27 Front connections of the power supply unit

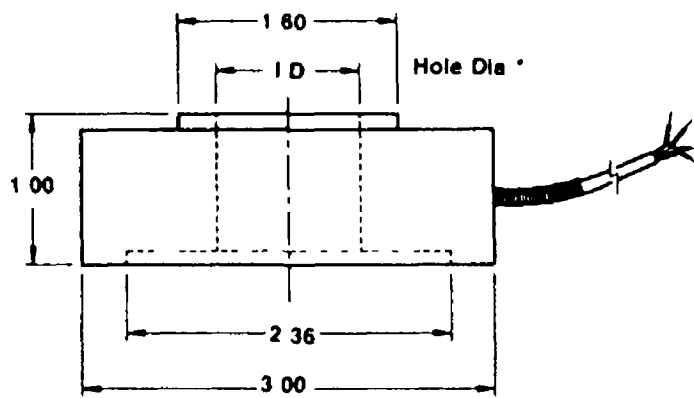


FIGURE - A 28 Details of the axial load cell

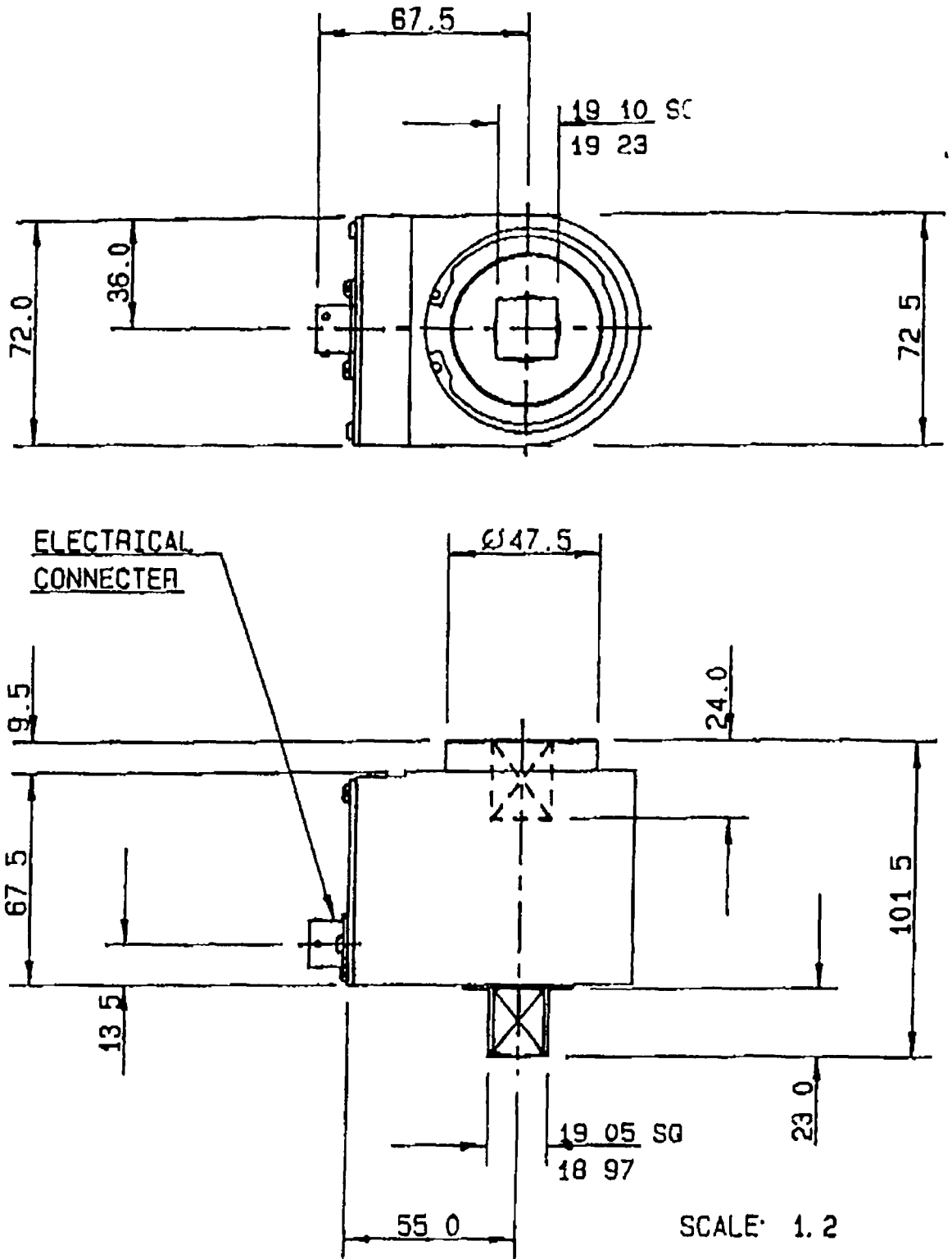
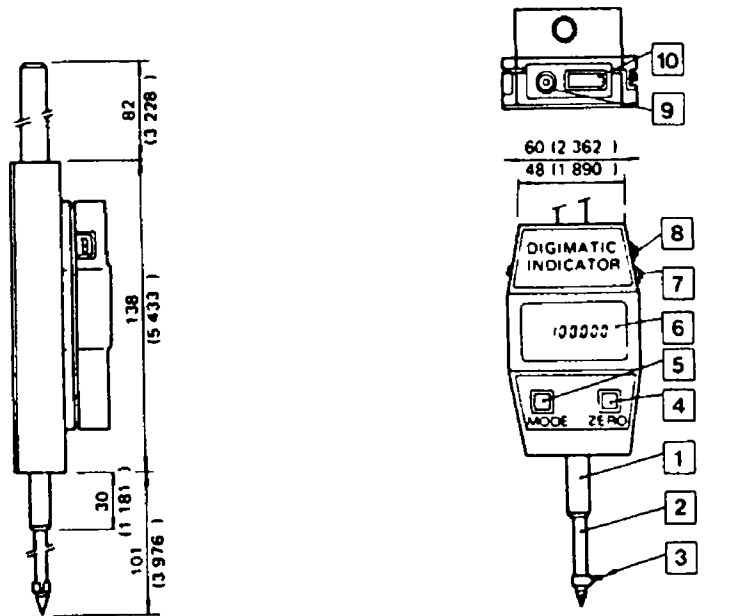


FIGURE - A 29 Details of the torque load cell



- | | |
|--|-------------------------------------|
| 1 9.52mm | 7 Direction selector |
| 2 Hardened stainless steel spindle | 8 Inch/mm selector |
| 3 Lifting lever | 9 Power supply jack |
| 4 Zero reset button | 10 Output (models with output only) |
| 5 Mode change button (models with output only) | 11 Power On/Off |
| 6 Blue/green fluorescent numbers | 12 Lifting cable mount |

FIGURE - A 30 Details of the L V D T

APPENDIX - B

The additional features and the list of the backpanel connections of the controllers

The additional features of both the controllers are summarised below

- i) **Current controller** optimises the motor dynamic performance by forcing the motor current to follow the 3-phase current demand signal from the electronic commutation
- ii) **DC/DC converter** provides all power requirements for the control electronics directly from the high voltage DC-Bus. No external power supply connection required
- iii) **Protection logic** monitors the system's critical functions and safely shuts down the system in case of error. All fault conditions are signalled on the front panel
- iv) **Pulse Width Modulation** modulates the power transistor conduction times to achieve variable phase voltage at the motor from a fixed voltage DC-Bus with maximum efficiency
- v) **Resolver Signal Converter** converts the analogue resolver signals to digital position information and also provides a high quality analogue velocity signal
- vi) **Encoder Simulation** processes the digital absolute rotor position information to provide an incremental encoder type signal
- vii) **Thermal Protection** directly monitors the motor winding temperature and the controller heat-sink temperature and limits the peak torque available so as to prevent thermal overload. The direct temperature monitoring and method of processing used ensures optimal torque availability from the system for all ambient temperatures and dynamic loading conditions
- viii) **Torque Limit** limits the available system peak torque according to the user's specification or in response to the thermal protection system
- ix) **Velocity Controller** compares the desired speed (command signal) with the actual speed of the motor and gives accurate speed tracking over a wide bandwidth

The backplane connections of the power supply and the controller units are given below

a) 160 Power Supply Connections

a1) Power Supply Connector X3

Type	Phoenix GSMKDS3 (angled screw terminal)		
Wire cross sectional area	max. 3mm ²		
Pin 1	PE	Protective Earth	Input/Output Reference
Pin 2	L1	Mains Input, Phase 1 230Vrms AC 50/60Hz	Input Ref PE (X3/1)
Pin 3	L2	Mains Input, Phase 2 230Vrms AC 50/60Hz	Input Ref PE (X3/1)
Pin 4	L3	Mains Input, Phase 3 230Vrms AC 50/60Hz	Input Ref PE (X3/1)
Pin 5	PE	Protective Earth	Input/Output Reference

a2) External Bleed Resistor Connector X4

Type	Phoenix GSMKDS3 (angled screw terminal)		
Wire cross sectional area	max. 3mm ²		
Pin 1	ReGen1	External Bleed Resistor	Output Ref ReGen2
Pin 2	ReGen2	External Bleed Resistor	Output Reference
Pin 3	PE	Protective Earth	Input/Output Reference
Pin 4	NC	Not Connected	

a3) Low Voltage Power and Status Connector X5

Type	Phoenix SMKDS 15 (angled screw terminal)		
Wire cross sectional area	max. 1.5mm ²		
Pin 1	24V B+	24V Brake Supply Plus	Input Ref 24V B- (X5/2)
Pin 2	24V B-	24V Brake Supply Ground	Input Reference
Pin 3	24V E+	24V External Supply Plus (Optional)	Input Ref 24V E (X5/4)
Pin 4	24V E-	24V External Supply Ground (Optional)	Input Reference
Pin 5	PSRly1	Power Supply OK Relay Pin 1	Output Ref PSRly2 (X5/6)
Pin 6	PSRly2	Power Supply OK Relay Pin 2	Output Reference
Pin 7	PE	Protective Earth	Input/Output Reference
Pin 8	+5V	5V Power Supply Output	Output Ref DGND (X5/12)
Pin 9	+15V	15V Power Supply Output	Output Ref AGND (X5/11)
Pin 10	-15V	15V Power Supply Output	Output Ref AGND (X5/11)
Pin 11	AGND	Analog Ground	Input/Output Reference
Pin 12	DGND	Digital Ground	Input/Output Reference
Pin 13	SRRly1	System Ready Relay Pin 1 (Optional)	Output Ref SRRly2 (X5/14)
Pin 14	SRRly2	System Ready Relay Pin 2 (Optional)	Output Reference
Pin 15	ComAm	Common Automatic Mode Input (Optional)	Input Ref 24V External Supply Ground

Type	Phoenix GSMKDS3 (angled screw terminal)		
Wire cross sectional area	max. 3mm ²		
Pin 1	DC+	High Power DC Bus Plus	Output Ref DC (X7/2)
Pin 2	DC-	High Power DC Bus Minus	Output Reference
Pin 3	PE	Protective Earth	Input/Output Reference

b) T161 Controller Connections

Controller II (µ - A - F)

51)	Power Connector X114	Phoenix GS4MKDS3 (angled screw terminal)		
	Type	max. 3mm		
	Wire cross sectional area			
	Pin 1 Brake+	Motor Brake Connection Plus (Optional)		Input Ref Brake (X114/2)
	Pin 2 Brake	Motor Brake Connection Minus (Optional)		Input Reference
	Pin 3 PE	Protective Earth		Input/Output Reference
	Pin 4 PE	Protective Earth		Input/Output Reference
	Pin 5 Motor_W	Motor Power Lead Phase W		Output Ref PE (X114/4)
	Pin 6 Motor_V	Motor Power Lead Phase V		Output Ref PE (X114/4)
	Pin 7 Motor_U	Motor Power Lead Phase U		Output Ref PE (X114/4)
	Motor connector pinout			
	Motor	pinout (brake+ B+ and brake- B-)		
	D312	Pin 5 B+ Pin 6 B- Pin 1 W Pin 4 V Pin 2 U		
	D313 (without brake)	Pin 1 W Pin 3 V Pin 2 U		
	D313 (with brake)	Pin 5 B+ Pin 6 B- Pin 1 W Pin 4 V Pin 2 U		
	D314	Pin 5 B+ Pin 6 B- Pin 1 W Pin 3 V Pin 2 U		
	D315L10 D315L20	Pin 5 B+ Pin 6 B- Pin 1 W Pin 3 V Pin 2 U		
	D315L30 D315L50	Pin 5 B+ Pin 6 B- Pin 1 W Pin 4 V Pin 2 U		
52)	I/O Connector X115	Phoenix SMKDS15 (angled screw terminal)		
	Type	max. 1.5mm ²		
	Wire cross sectional area			
	Pin 1 SysRdy1	System Ready Relay Axis 1 Pin 1		Output Ref SysRdy2 (X115/1)
	Pin 2 SysRdy2	System Ready Relay Axis 1 Pin 2		Output Reference
	Pin 3 PrAnaOut	Programmable Analog Output (+/- 10V)		
	Pin 4 +DC	Default Actual Velocity Monitor		Output Ref AGND (X115/5)
	Pin 5 AGND	Equivalent DC Motor Current Monitor (+/- 0V)		Output Ref AGND (X115/5)
	Pin 6 CW Lim	Analog Ground		Input/Output Reference
	Pin 7 CCW Lim	Clockwise Limit Switch Input		Input Ref ExtIO_GND (X115/14)
	Pin 8 PE	Counter Clockwise Limit Switch Input		Input Ref ExtIO_GND (X115/14)
	Pin 9 AutoMod	Protective Earth		Input/Output
	Pin 10 Enable	Automatic Mode Input		Input Ref ExtIO_GND (X115/14)
	Pin 11 PE	Axis Enable Input		Input Ref ExtIO_GND (X115/14)
	Pin 12 TorMod	Protective Earth		Input Output
	Pin 13 ExtIO_V+	Torque Mode Input		Input Ref ExtIO_GND (X115/14)
	Pin 14 ExtIO_GND	External I/O Supply Voltage Input		Input
	Pin 15 ThrmRly1	External I/O Supply Voltage Ground		Input
	Pin 16 ThrmRly2	Input Reference for X115 Pin 6 7 9 10 12		Output Ref ThrmRly2 (X115/16)
	Pin 17 CuLim1	Thermal Limit Relay Output Pin 1		Output Reference
	Pin 18 CuLim2	Thermal Limit Relay Output Pin 2		Input Ref CuLim2 (X115/18)
	Pin 19 Com+	Analog Current Limit Input Plus (0 - 10V)		Input Reference
	Pin 20 Com-	Analog Current Limit Input Minus		Input Ref Com (X115/20)
		Command Input Plus (+/- 10V)		Input Reference
		Command Input Minus		
53)	Resolver Connector X116	9 pin Sub D Connector female		Motor connector pinout
	Type			
	Pin 1 S3	Resolver Feedback SIN	Input Reference	Pin 2
	Pin 2 Thrm1	Motor Thermistor Pin 1	Input Ref DGND (X116/5)	Pin 5
	Pin 3 S2	Resolver Feedback COS	Input Reference	Pin 3
	Pin 4 R1	Resolver Supply	Output Ref R (X116/6)	Pin 7
	Pin 5 DGND	Motor Thermistor Reference	Input Reference	Pin 6
	Pin 6 S1	Resolver Feedback SIN+	Input Ref S (X116/1)	Pin 1
	Pin 7 PE	Protective Earth (Shield)	Input/Output Reference	
	Pin 8 S4	Resolver Feedback COS+	Input Ref S (X116/3)	Pin 4
	Pin 9 R2	Resolver Supply Reference	Input Reference	Pin 8

Encoder Simulation Connector X117		9 pin Sub-D Connector male	
Type			
Pin 1	GNDExtES	External Encoder Simulation Supply	Input/Output
Pin 2	M	Negated Marker Pulse	Output Reference for M (X117/6) Differential output
Pin 3	B	Negated Channel B	Output Reference for B (X117/7) Differential output
Pin 4	A	Negated Channel A	Output Reference for A (X117/8) Differential output
Pin 5	+VEExtES	External Encoder Simulation Supply	Input Ref GNDExtES (X117/1)
Pin 6	M	Marker Pulse	Output Ref GNDExtES for Differential output Ref M (X117/2)
Pin 7	B	Channel B	Output Ref GNDExtES for Differential output Ref B (X117/3)
Pin 8	A	Channel A	Output Ref GNDExtES for Differential output Ref A (X117/8)
Pin 9	PE	Protective Earth	Input/Output

c) Commissioning interface connector X6

Interface connector RS232		9 pin sub-D connector female	
Type			
Location			
Pin 1	N/C	Not Connected	
Pin 2	RxD	Read Data Input	Input Ref DGND (X6/5)
Pin 3	TxD	Transfer Data Output	Output Ref DGND (X6/5)
Pin 4	N/C	Not Connected	
Pin 5	DGND	Digital Ground	Input/Output Reference
Pin 6	PE	Protective Earth	Input/Output
Pin 7	N/C	Not Connected	
Pin 8	N/C	Not Connected	
Pin 9	5V	5V Output Supply Voltage	Output Ref DGND (X6/5)

Interface protocol	Baudrate	9600
	Startbits	1
	Databits	7
	Paritybit	ignored
	Stopbits	2

Interface connector RS485		9 pin sub D connector male	
Type			
Location			
Pin 1		Digital Serial Input/Output (Option)	
Pin 2		Digital Serial Input/Output (Option)	
Pin 3	RS485+	RS485 Bus Interface Plus	Input/Output
Pin 4	RS485-	RS485 Bus Interface Minus	Input/Output
Pin 5	PE	Protective Earth	Input/Output
Pin 6	PE	Protective Earth	Input/Output
Pin 7	N/C	Not Connected	
Pin 8	N/C	Not Connected	
Pin 9	N/C	Not Connected	

APPENDIX - C

Summary of the commands available in the built-in software of the terminal

The handheld terminal, type 64-PTR-25, which has a built in software (EPROMS) package, was used for the initial set-up of the controllers. It was supplied by "DTL". The summary of the commands available in this software are given below

		PARAMETER INPUT/OUTPUT
SL		Set/list all parameters
L	-	To list system configuration
SL	V	Set/list Motor Maximum Speed in [RPM] at 10V input command
SL	P	Set/list Proportional Gain in [Nm/(rad/s)]
SL	I	Set/list Integral Gain in [s]
SL	J	Set/list Observer Inertia in [kg m ²]
SL	W	Set/list Compensator Filter corner frequency in [Hz]
SL	Z	Set/list Filter Damping (no dimension)
SL	A	Set/list Acceleration Limit in [rad/s ²]
L	M	List motor parameters
L	D	List Multidrop Axis Number
SL	TA	Set/list Peak Torque in [Nm] in Automatic Mode
SL	TM	Set/list Peak Torque in [Nm] in Manual Mode
SL	LA	Set/list Speed Limit in [RPM] in Automatic Mode
SL	LM	Set/list Speed Limit in [RPM] in Manual Mode
SL	E	Limit Switch Braking Deceleration

		GAIN ADJUST MODES
=		Set Controller in Proportional Gain Tuning Mode
	U	increase P gain 5%
	D	decrease P gain 5%
	L	shows P gain
	S	sets P gain
	Z	set P gain to zero
	E	exit Tuning Mode
		Set Controller to Integral Gain Tuning Mode
	U	increase I Gain 5% (decrease I Time Constant 5%)
	D	decrease I Gain 5% (increase I Time Constant 5%)
	L	shows I gain
	S	sets I gain
	Z	set I gain to zero (set I Time Constant to Infinite 4s)
	E	exit Tuning Mode
J		Set Controller to Observer Gain Tuning Mode
	U	increase Observer Inertia
	D	decrease Observer Inertia
	L	shows J
	S	sets J
	Z	set Observer Inertia to zero
	E	exit Observer Inertia

		SPECIAL COMMANDS
D		Drive Initialization
C		For permanently saving the parameters in the EEPROM
Control T		Up/Down Load of the system parameters
Control X		Allows a Warm Start of the System
Alt S		Select Multidrop Axis (only in RS 485 Mode present)

		HELP
H		Help
.		Increases Help Level
.		Decreases Help Level

		ENQUIRE ABOUT CONDITIONS
7M	Motor temperature in [C]	
7B	Power Bridge Temperature in [C]	
7P	Motor shaft position in degrees 0 to 360	
7V	Average speed	
7L	Limit settings	
7F	Faults	
7S	Present Controller Status	

		OPTIONAL COMMANDS
OC	Set Filter type	
	1 Torque Mode	
	2 Velocity Mode	
OE	Only when using Encoder Simulation card (EF Card)	
	L Number of Lines	
	A Zero Pulse Angle	
	O Turn off Encoder Simulation	
OI	Input Offset	
OZ	Automatic Offset Adjust	
OA	Enable/disable Input Reference Filter	
OL	Enable/Disable Limit Switches	
OR	Enable/Disable Compensator Reference Source	
	1 Analog Reference (Default)	
	2 Function Generator	
OG	Function Generator Set up	
	N Set Function Generator Speed Amplitude and Offset in [rpm]	
	T Set Function Generator Torque Amplitude and Offset in [Nm]	
	P Set Function Generator Period in [s] and Duty Cycle in [%]	
OF	Programmable Analog Output (Front Panel Options)	
	1 dP/dt (Actual velocity)	
	2 Filtered dP/dt	
	3 IDC (Current monitor equal to a DC motor)	
	4 Observer Estimated Velocity	
	5 Observer Position Error	
OM	Enable/Disable Manual Mode	
OD	Enable/Disable Thermal Protection Software	
OT	IT Limit setting (Only used with motors MOOG INC 30X XXX)	
OO	Observer Velocity on/off	

		MOTOR MODE COMMANDS
M1	Enable Motor	
M0	Disable Motor	
M1T	Torque Mode	
M1V	Velocity Mode	
M1B	Brake relay Option	

APPENDIX - D

Plot of axial stress versus axial strain curve and calculation of the numerical values of torque using Gaydon's model

D 1 Normalised Axial Stress-Strain Curve

If a bar is initially twisted to an extent that makes it just plastic at $r = a$, then $Ga\theta_0 = Y/\sqrt{3}$ and $\epsilon_0 = 0$. Substituting in Eq 4.6 of chapter four, the stress distribution in the plastic region can be written as

$$\frac{\sigma}{Y} = \tanh\left(\frac{3G}{Y}\epsilon - \sqrt{1 - \frac{r^2}{a^2}} + \tanh^{-1}\sqrt{1 - \frac{r^2}{a^2}}\right) \quad (D 1)$$

Plot of equation D 1 in terms of σ/Y and $3G\epsilon/Y$, for initial $Ga\theta_0 = Y/\sqrt{3}$ at $r = a$ (i.e., when initial shear stress is equal to yield shear at $r = a$), is shown in figure D 1

D 2 Calculation of Numerical Value of Torque

Suppose the bar is initially twisted to an extent that makes it just plastic at $r = a$, i.e., $P = 1.0$. It is required to calculate the numerical value of torque when $\xi = 0.5$. As in the present case, yielding starts even when $\xi = 0$, so when ξ is increased to 0.5, elastic-plastic boundary also moves inward by the same amount, i.e., $\eta = 0.5$ (according to the assumption made in section 4.3.3 of chapter four). Thus the torque within the plastic region can be calculated by integrating equation 4.13 over the range $\xi = 0.5$ to 1.0. The torque within the elastic region can be calculated for $\xi = 0$ to 0.5 using the elastic equation. Thus total torque,

$$T = T_e + T_p$$

or
$$\frac{T}{T_y} = \left(\frac{T}{T_y}\right)_e + \left(\frac{T}{T_y}\right)_p$$

or
$$\frac{T}{T_y} = \left(\frac{\tau_1}{\tau_y}\right)\eta^3 + 4 \int_{\xi=\eta}^{1.0} \xi^2 \left(\frac{\tau_2}{\tau_y}\right) d\xi \quad (D 2)$$

where τ_1 is the maximum elastic shear stress at the layer $\xi = \eta$, which is a constant, and τ_2 is the shear stress within the plastic region which varies along ξ . Integration of the equation was performed using Simpson's rule for the increment of $\Delta\xi = 0.1$. Thus for $\eta = 0.5$, the values of shear stresses, within the plastic region, at different layers ξ is given in table D 1

TABLE - D 1 The values of the axial and shear stresses when $\eta = 0.5$

ξ	σ/Y from Eq 4.11	τ/τ_y from Eq 4.7
0.5	0.740	0.672
0.6	0.663	0.748
0.7	0.592	0.805
0.8	0.532	0.846
0.9	0.486	0.873
1.0	0.462	0.886

So the value of the plastic torque from the second part of Eq D 2 is equal to 0.867, whereas that of for the elastic portion is 0.084. Thus the total torque is 0.951.

Similarly, to find the total torque T at $\underline{\epsilon} = 1.0$, when $P = 0.5$, Eq 4.13 was integrated over the entire cross-section of the bar, because when $\underline{\epsilon}$ is increased to 1.0 the entire bar becomes plastic.

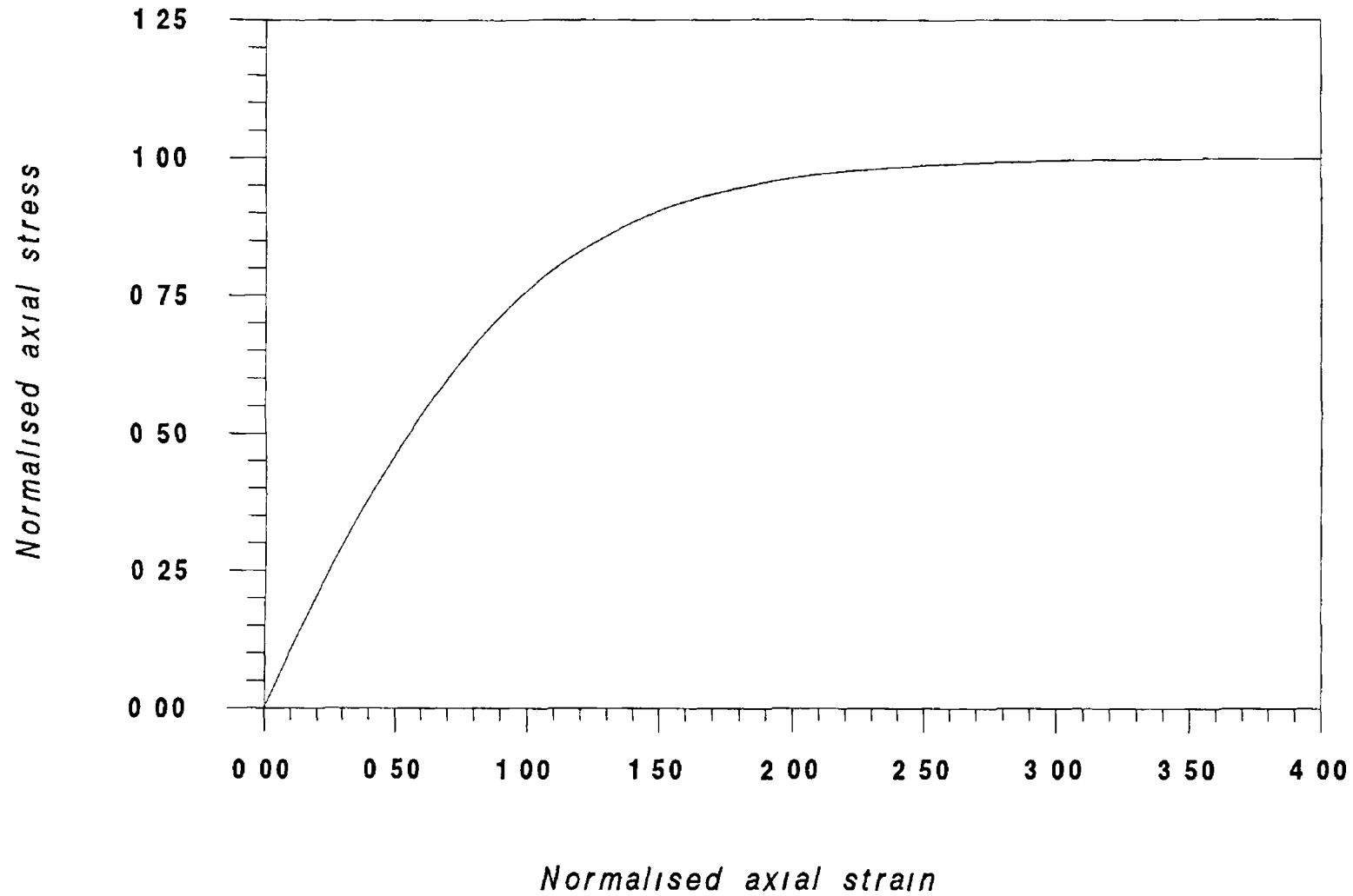


Figure D.1 Plot of normalised axial stress versus normalised axial strain curve from equation 4-6(a) of chapter four.

APPENDIX - E

ELASTIC-PLASTIC STRESS-STRAIN RELATIONS

E.1 THE ELASTIC STRESS-STRAIN RELATIONS

The complete stress-strain relations describe the elastic and plastic deformation of a material. In the following section the basic stress-strain relations in the elastic range are described where the effects of time and temperature are not considered. It is assumed that the material is isotropic and the Bauschinger effect is negligible. It should be noted that the shearing strains, γ_{xy} , γ_{yz} , γ_{zx} are the shear components of the strain tensor and therefore have values equal to half the corresponding values of engineering shear strain. If an element of material is subjected to a three-dimensional stress field, as shown in figure E 1, then for an isotropic material, the elastic stress-strain relations are usually written in the form (temperature effect are not considered)

$$\begin{aligned}E\varepsilon_x &= \sigma_x - \nu(\sigma_y + \sigma_z) \\E\varepsilon_y &= \sigma_y - \nu(\sigma_z + \sigma_x) \\E\varepsilon_z &= \sigma_z - \nu(\sigma_x + \sigma_y) \\2G\gamma_{xy} &= \tau_{xy} \\2G\gamma_{yz} &= \tau_{yz} \\2G\gamma_{zx} &= \tau_{zx}\end{aligned}\tag{E 1}$$

where E is the Young's modulus, ν Poisson's ratio and G the modulus of rigidity. If σ_m is the hydrostatic stress and ε_m the corresponding volumetric strain, then the above mentioned equations may be written in terms of hydrostatic and deviatoric components

$$\begin{aligned}\varepsilon_x &= \frac{1}{2G}(\sigma_x - \sigma_m) + \frac{(1-2\nu)}{E}\sigma_m \\ \varepsilon_y &= \frac{1}{2G}(\sigma_y - \sigma_m) + \frac{(1-2\nu)}{E}\sigma_m\end{aligned}\tag{E 2}$$

$$\varepsilon_z = \frac{1}{2G}(\sigma_z - \sigma_m) + \frac{(1-2\nu)}{E}\sigma_m$$

$$\gamma_{xy} = \frac{\tau_{xy}}{2G}$$

$$\gamma_{yz} = \frac{\tau_{yz}}{2G}$$

$$\gamma_{zx} = \frac{\tau_{zx}}{2G}$$

where $3\sigma_m = \sigma_x + \sigma_y + \sigma_z$. The terms $(\sigma_x - \sigma_m)$, $(\sigma_y - \sigma_m)$ and $(\sigma_z - \sigma_m)$ are reduced or deviatoric components and are generally written in the form σ_x . The complete elastic stress-strain relations may therefore be written, when using an obvious double suffix notation, as

$$\varepsilon_{ij} = \frac{\sigma_{ij}}{2G} + \frac{(1-2\nu)}{E}\delta_{ij}\sigma_m$$

$$\sigma_m = \frac{1}{3}\sigma_{ii} \quad (E 3)$$

The delta symbol, δ_{ij} , is equal to unity when $i = j$ and to zero when $i \neq j$

E.2 THEORIES OF YIELDING

A number of theoretical criteria for yielding [77], have been proposed over the years each seeking to obtain adequate correlation between estimated component life and that actually achieved under service load conditions for both brittle and ductile material applications. The five main theories are

- i) Maximum principal stress theory. This theory is accredited to Rankine. It gives good predictions for brittle materials.
- ii) Maximum shear stress theory. This theory is most frequently accredited to Guest and Tresca. This theory is suitable for ductile materials.
- iii) Maximum principal strain theory. This theory is accredited to Saint-Venant. It fits experimental data on brittle materials better than those on ductile materials.

iv) Total strain energy theory This theory was proposed by Beltrami and also attributed to Haigh. It gives fairly good results for ductile materials but is seldom used in preference to the theory below.

v) Shear or distortion strain energy theory This theory has received considerable verification in practice and is widely regarded as the most reliable basis for design, particularly when dealing with ductile materials. It is often referred to as the von Mises or Maxwell or Hencky criteria as this theory was independently established by them. It is also sometimes referred to as the "distortion energy" or "octahedral shear stress theory".

The strain energy of a stressed component can be divided into volumetric strain energy and shear strain energy components, the former being associated with volume change and no distortion, the latter producing distortion of the stressed elements. This theory states that failure occurs when the maximum shear strain energy components in the complex stress system is equal to that at the yield point in the tensile test,

$$\text{i.e.} \quad \frac{1}{12G} [(\sigma_1 - \sigma_2)^2 + (\sigma_2 - \sigma_3)^2 + (\sigma_3 - \sigma_1)^2] = \frac{Y^2}{6G}$$

$$\text{or} \quad \sigma_1^2 + \sigma_2^2 + \sigma_3^2 - (\sigma_1\sigma_2 + \sigma_2\sigma_3 + \sigma_3\sigma_1) = Y^2$$

where, Y represents the yield stress in tension and all the stresses in the left portion of the equation are expressed in principal stresses. For biaxial case it becomes

$$\sigma_1^2 - \sigma_1\sigma_2 + \sigma_2^2 = Y^2$$

For two dimensional normal and shear stresses it becomes

$$\sigma_x^2 + \sigma_y^2 - \sigma_x\sigma_y + 3\tau_{xy}^2 = Y^2$$

If an element is subjected to tensile load and torque, i.e., when $\sigma_y = 0$, the above equation reduces to

$$Y = \sqrt{\sigma_x^2 + 3\tau_{xy}^2} \quad (\text{E 4})$$

In the above theories it has been assumed that the properties of the material in tension and compression are similar. Similarly for the same type of loading Tresca's criteria provides the following relation

$$Y = \sqrt{\sigma_x^2 + 4\tau_{xy}^2} \quad (\text{E } 5)$$

E.3 PLASTIC STRESS-STRAIN RELATIONS

DISTINCTION BETWEEN ELASTIC AND PLASTIC STRESS-STRAIN RELATIONS

When a metal is deformed under continuously increasing stress, it is first strained elastically, the relationship between stress and strain under combined stress being expressed by the familiar equations of the theory of elasticity. With increasing stress, the material yields and permanent plastic flow occurs. The total strain under load is then a combination of an elastic and a plastic component. With release of stress the elastic component disappears and the material is left with the permanent plastic strain. Unless previous working has been severe the microscopic elastic behaviour of a metal can only slightly be affected by distortions of lattice. During unloading, elastic recovery is limited by the plastic yielding of favourably oriented grains [11].

In the elastic range the strains are uniquely determined by the stresses, i.e., for a given set of stresses one can compute the strains directly using Hooke's law without any regard as to how this stress state was attained whereas in the plastic range the strains are in general not uniquely determined by the stresses but depend on the whole history of loading or how the stress state was reached [76]. Plastic stress strain relations are considered to be governed by the "incremental" or "flow" type of theory, as opposed to the "total" or "instant" type of theory which is sufficient to describe the elastic stress strain [78].

If a circular steel specimen is strained in uniaxial tension beyond the initial yield to some point C as shown in figure E 2, where CDE defines the subsequent yield curve, then the plastic strains are

$$\begin{aligned}\epsilon_x^p &= \epsilon^p \\ \epsilon_y^p &= \epsilon_z^p = -\frac{1}{2} \epsilon^p \\ \epsilon_{xy}^p &= \epsilon_{yz}^p = \epsilon_{zx}^p = 0\end{aligned}$$

If the specimen is now unloaded to the point B and then a shear stress is applied increasing from B to D on the new yield locus, the plastic strains will still be as given above. Now if the specimen is first stressed in shear to the point E on the new yield locus and then, by any other path inside EDC, such as EGD, is stressed to the point D, the plastic strains would be

$$\epsilon_{xy}^p = \gamma^p \quad \text{and} \quad \epsilon_x^p = \epsilon_y^p = \epsilon_z^p = \epsilon_{xz}^p = \epsilon_{yz}^p = 0$$

which is obviously completely unrelated to the previous strain state. Thus even though the same stress state at D exists for both loading paths, and therefore the elastic strain states are the same, the plastic strain states are different. Because of the above mentioned dependence of the plastic strains on the loading path, the differentials or increments of plastic strain throughout the loading history is computed and then the total strain is obtained by integration or summation.

THE ASSUMPTIONS IN PLASTICITY THEORY

As outlined by Ford [78], following assumptions are made regarding the behaviour of plastic solids in the theory

- (a) It is assumed that the material is isotropic and remains so throughout the deformation.
 - (b) Plasticity theory assumes that the onset of plastic yield takes place sharply, either from zero strain (rigid plastic material) or from an elastic strain (elastic-plastic material).
- Because of the complex nature of the stress-strain curve, it has become customary to idealise this curve in various ways. Different idealised stress-strain curves assumed in the plastic

theories are shown in figure E 3 The stress-strain curves of actual materials diverge more or less from these curves

(c) In plasticity theory it is assumed that the yield stress is independent of the direction of straining, i e , there is no Bauschinger effect and the current yield stress depends only upon the total strain up to the point considered

(d) The period of time for which the load is applied can be ignored as long as the rate of straining is not considered to effect the yield stress characteristics

(e) The plastic stress-strain relations are used only when all of the material has reached to yield Localised yielding or gradual transition from elastic to plastic behaviour may lead to plastic theory being adopted while most of the material remains elastic

(f) The laws of plasticity are such that the strains occurring at any point are related to the current stresses at that point Logarithmic or natural strain are considered in the plasticity theory The logarithmic and conventional strains are almost equal for small strains (i e , of elastic order) but diverge for large strains

ELASTIC-PLASTIC TORSION

As outlined by Ford [78] when a gradually increasing torque T is applied to a circular shaft of uniform diameter D , the strain is entirely elastic until the shear stress at the outer surface reaches the yield stress in shear The shear stress and strain vary linearly with radius in the elastic regime so that, as the outermost fibres take on a permanent set, the rest of the cross-section will still be elastic As the torque continues to increase more and more of the cross-section becomes plastic, the elastic-plastic interface being a concentric circle of decreasing diameter

The elastic stress distribution across the prismatic bar of circular cross section is expressed by

$$\tau_{z\theta} = \frac{Gr\theta}{L} \quad (\text{E } 6)$$

and the value of the maximum shear stress is given by

$$\tau_{z\theta\max} = \frac{Ga\theta}{L} \quad (\text{E } 7)$$

The stress distributions for a non-strain-hardening and a strain-hardening material are shown schematically in figure E 4. The total torque transmitted by a non-strain-hardening bar, according to the Tergart [79] is given by

$$T = \int_{r=0}^{r=c} \tau_{z\theta} 2\pi r^2 dr + \int_{r=c}^{r=a} \tau_y 2\pi r^2 dr \quad (\text{E } 8)$$

The first term on the right side of the above equation is the torque transmitted by the elastic core, where the shear stress varies linearly with r . The second term is the torque transmitted by the plastic annulus, where the shear stress is constant and independent of r . The elastic-plastic boundary occurs at $r = c$. Integration of equation E 8 provides

$$T = \frac{\pi c^4 G \theta}{2L} + \frac{2\pi a^3 \tau_y}{3} - \frac{2\pi c^3 \tau_y}{3} \quad (\text{E } 9)$$

Compatibility at the elastic-plastic boundary requires that

$$\tau_y = \frac{G\theta c}{L} \quad (\text{E } 10)$$

Combining equation E 9 and E 10 and rearranging gives

$$T = \frac{2\pi a^3 \tau_y}{3} \left\{ 1 - \frac{1}{4} \left(\frac{c}{a} \right)^3 \right\} \quad (\text{E } 11)$$

Thus when the entire section becomes plastic $c = 0$, and the above equation is converted to

$$T_p = \frac{2\pi a^3 \tau_y}{3} \quad (\text{E } 11a)$$

where T_p is the torque required to make the bar fully plastic. In the elastic-plastic and fully plastic regimes, the shear stress at the surface of the bar is τ_y . The shear strain at the surface of the bar is $\gamma = a\theta/L$ for all regimes

For a strain-hardening material, the torque according to Nadai [9] is given by

$$T = \int_0^a \tau 2\pi r^2 dr$$

where the subscripts on the shear stress are dropped. Changing the variable from r to γ gives

$$T = \int_0^{\gamma_a} \frac{\tau 2\pi\gamma^2 d\gamma}{\theta_1^3} \quad (\text{E 12})$$

where θ_1 is the twist per unit length. In general, the shear stress versus shear strain curve can be written as $\tau = f(\gamma)$. Thus Eq. E 12 gives

$$T = \int_0^{\gamma_a} \frac{2\pi f(\gamma)\gamma^2 d\gamma}{\theta_1^3}$$

Differentiating the above equation with respect to θ_1 gives

$$d(T\theta_1^3) = 2\pi f(\gamma_a)\gamma_a^2 d\gamma_a \quad (\text{E 12a})$$

At the specimen surface $\tau_a = f(\gamma_a)$ and $\gamma_a = a\theta_1$. Thus substituting these values into Eq. E 12a

$$d(T\theta_1^3) = 2\pi\tau_a a^3 \theta_1^2 d\theta_1$$

or

$$\frac{d(T\theta_1^3)}{d\theta_1} = 2\pi\tau_a \theta_1^2 a^3$$

Expanding the above equation gives

$$\frac{dT}{d\theta} \theta_1^3 + 3T\theta_1^2 = 2\pi\tau_a a^3 \theta_1^2$$

or

$$\tau_a = \frac{1}{2\pi a^3} \left[3T + \theta_1 \frac{dT}{d\theta_1} \right] \quad (\text{E 13})$$

The first term on the right side of Eq. E 13 is the torque due to the maximum yield shear stress of τ_a in a fully plastic non-strain-hardening material, whereas the second term is a correction for strain hardening. These terms can be readily derived from the torque-twist curve shown in figure E 5, where

$$\frac{dT}{d\theta_1} = \frac{BC}{CD}$$

$$\theta_1 = CD$$

$$\theta_1 \frac{dT}{d\theta_1} = BC$$

so that
$$\tau_a = \frac{1}{2\pi a^3} \{3BA + BC\} \quad (E 14)$$

The shear strain at the surface is given by $\gamma_a = a\theta_1$. Thus, the shear stress versus shear strain curve can be deduced by drawing tangents to the torque versus the angle of twist per unit length curve

THE LÉVY-MISES AND PRANDTL-REUSS EQUATIONS

The general three-dimensional equations relating the increments of total strain to the stress deviations were given independently by Lévy and von Mises. These equations are

$$\frac{d\epsilon_x}{\sigma_x} = \frac{d\epsilon_y}{\sigma_y} = \frac{d\epsilon_z}{\sigma_z} = \frac{d\gamma_{yz}}{\tau_{yz}} = \frac{d\gamma_{zx}}{\tau_{zx}} = \frac{d\gamma_{xy}}{\tau_{xy}} = d\lambda \quad (E 15)$$

The proportionality factor is written as $d\lambda$ to indicate that incremental strains are being related to finite stresses. $d\lambda$ is an instantaneous non-negative constant of proportionality which may vary throughout a straining programme. In these equations the total strain increments are assumed to be equal to the plastic strain increments, the elastic strains being ignored. These equations can be applied to problems of large plastic flow and cannot be used in the elastic-plastic range.

The generalised equations to include both elastic and plastic components of strain are due to Prandtl and Reuss, and known as Prandtl-Reuss equations. Reuss assumed that the plastic strain increment at any instant of loading is proportional to the instantaneous stress deviation and the shear stresses, i.e.,

$$\frac{d\epsilon_x^p}{\sigma_x} = \frac{d\epsilon_y^p}{\sigma_y} = \frac{d\epsilon_z^p}{\sigma_z} = \frac{d\gamma_{yz}^p}{\tau_{yz}} = \frac{d\gamma_{zx}^p}{\tau_{zx}} = \frac{d\gamma_{xy}^p}{\tau_{xy}} = d\lambda \quad (E 16)$$

or
$$d\epsilon_{ij}^p = \sigma_{ij}' d\lambda \quad (E 17)$$

The total strain increment is the sum of the elastic and plastic strain increment. Thus,

$$d\epsilon_{ij} = d\epsilon_{ij}^p + d\epsilon_{ij}^e$$

So from equations E 3 and E 17

$$d\epsilon_{ij} = \sigma_{ij}d\lambda + \frac{d\sigma_{ij}}{2G} + \frac{(1-2\nu)}{E}\delta_{ij}d\sigma_m \quad (E 18)$$

Since plastic straining causes no changes of plastic volume, the condition of incompressibility, in terms of the principal or normal strains can be written as

$$d\epsilon_1^p + d\epsilon_2^p + d\epsilon_3^p = d\epsilon_x^p + d\epsilon_y^p + d\epsilon_z^p = 0 \quad (E 19)$$

If the principal stress directions are considered, equation E 16 gives,

$$\frac{d\epsilon_1^p - d\epsilon_2^p}{\sigma_1 - \sigma_2} = \frac{d\epsilon_2^p - d\epsilon_3^p}{\sigma_2 - \sigma_3} = \frac{d\sigma_3^p - d\sigma_1^p}{\sigma_3 - \sigma_1} = d\lambda$$

With the help of Eq E 19, equation E 16 can be rewritten in terms of the actual stresses as

$$d\epsilon_x^p = \frac{2}{3}d\lambda[\sigma_x - \frac{1}{2}(\sigma_y + \sigma_z)]$$

$$d\epsilon_y^p = \frac{2}{3}d\lambda[\sigma_y - \frac{1}{2}(\sigma_z + \sigma_x)]$$

$$d\epsilon_z^p = \frac{2}{3}d\lambda[\sigma_z - \frac{1}{2}(\sigma_x + \sigma_y)]$$

$$d\gamma_{xy}^p = d\lambda\tau_{xy}$$

$$d\gamma_{yz}^p = d\lambda\tau_{yz}$$

$$d\gamma_{zx}^p = d\lambda\tau_{zx}$$

Thus equation E 18 consists of three equations of the type

$$d\epsilon_x = \frac{2}{3}d\lambda[\sigma_x - \frac{1}{2}(\sigma_y + \sigma_z)] + [d\sigma_x - \nu(d\sigma_y + d\sigma_z)]/E \quad (E 20)$$

and three of the type

$$d\gamma_{xy} = \tau_{xy}d\lambda + d\tau_{xy}/2G \quad (E 21)$$

Finally, it is seen from equation E 18 that the volumetric and deviatoric strain increments can be separated for the total strain increment Thus Eq E 18 may be rewritten

$$d\epsilon_{ij} = \sigma_{ij}d\lambda + d\sigma_{ij}/2G \quad (E 22)$$

$$d\epsilon_{ii} = \frac{1-2\nu}{E}d\sigma_{ii} \quad (E 23)$$

However, Hill [11] has shown that for a material which strain hardens isotropically, $d\lambda$ of Eq E 22 can be replaced by $3d\bar{\sigma}/2\bar{\sigma}H$, where $\bar{\sigma}$ is the equivalent stress and H slope of equivalent stress equivalent strain curve Thus Eq E 22 becomes

$$d\epsilon_{ij} = 3\sigma_{ij}d\bar{\sigma}/2\bar{\sigma}H + d\sigma_{ij}/2G \quad (E 24)$$

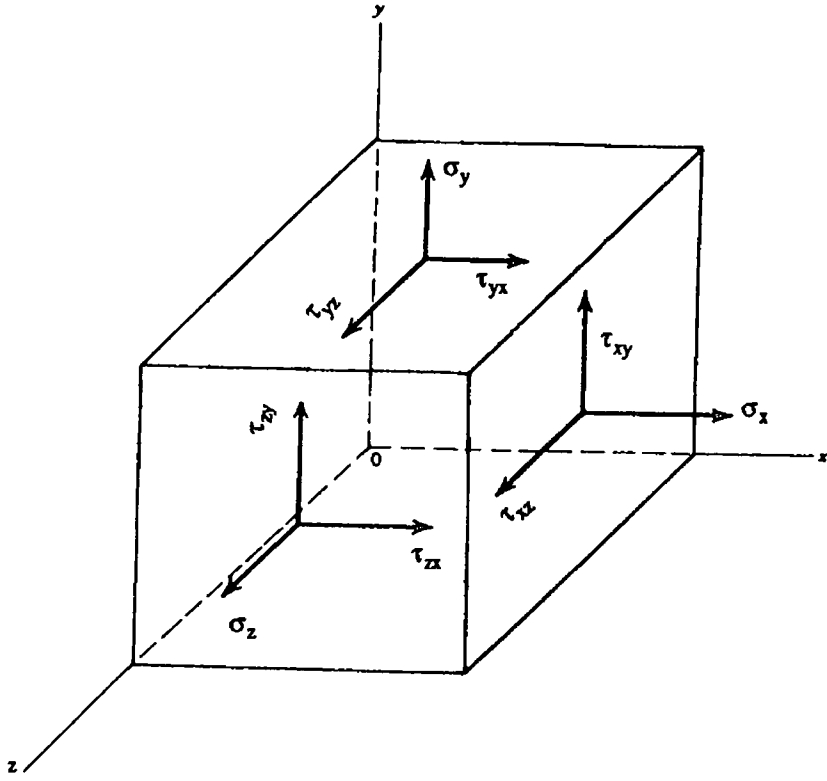


Fig E 1 Stress components at a point in loaded body

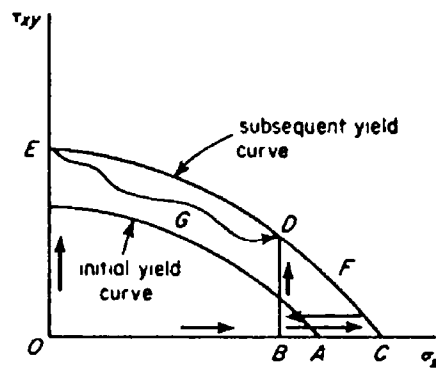


Fig E 2 Effect of loading path on plastic strains

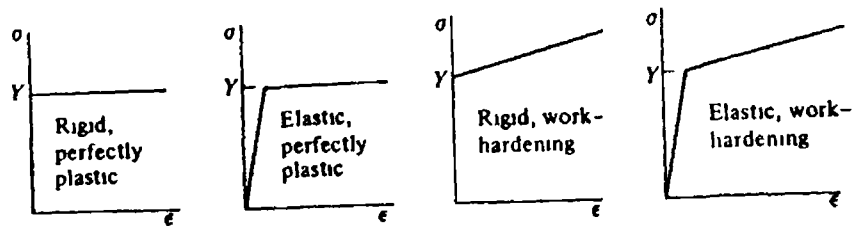


Fig E 3 Idealized stress-strain curves

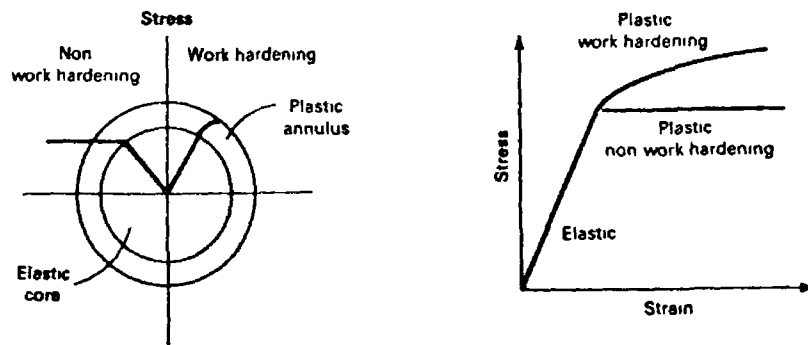


Fig E 4 Stress distributions for a non-strain-hardening and a strain-hardening material

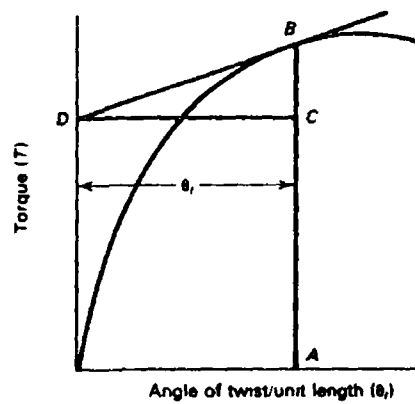


Fig E 5 Torque versus angle of twist/unit length curve

APPENDIX - F

Characteristic curves of different materials investigated

This section contains the uniaxial tensile and pure torsional test results of different materials investigated during the actual biaxial loading programme. The mechanical properties of these materials are given in table F 1. The uniaxial yield load of the copper was measured at 0.025% offset, whereas those of the steel-2 and thin-walled tube at zero offset (i.e., at the proportional limit). The yield torque of all these materials were measured at the proportional limit.

Table - F 1 Mechanical properties of the steel-2 and thin-walled tube

Materials	Modulus of Elasticity (GPa)	Modulus of Rigidity (GPa)	Tensile Yield Load (kN)	Yield Torque (Nm)	Tensile Yield Stress (MPa)	Shear Yield Stress (MPa)
Steel (lot-2)	205	83	32.8	40.5	652.7	402.95
Thin-walled tube	216	71	4.7	6.6	249.3	132.4

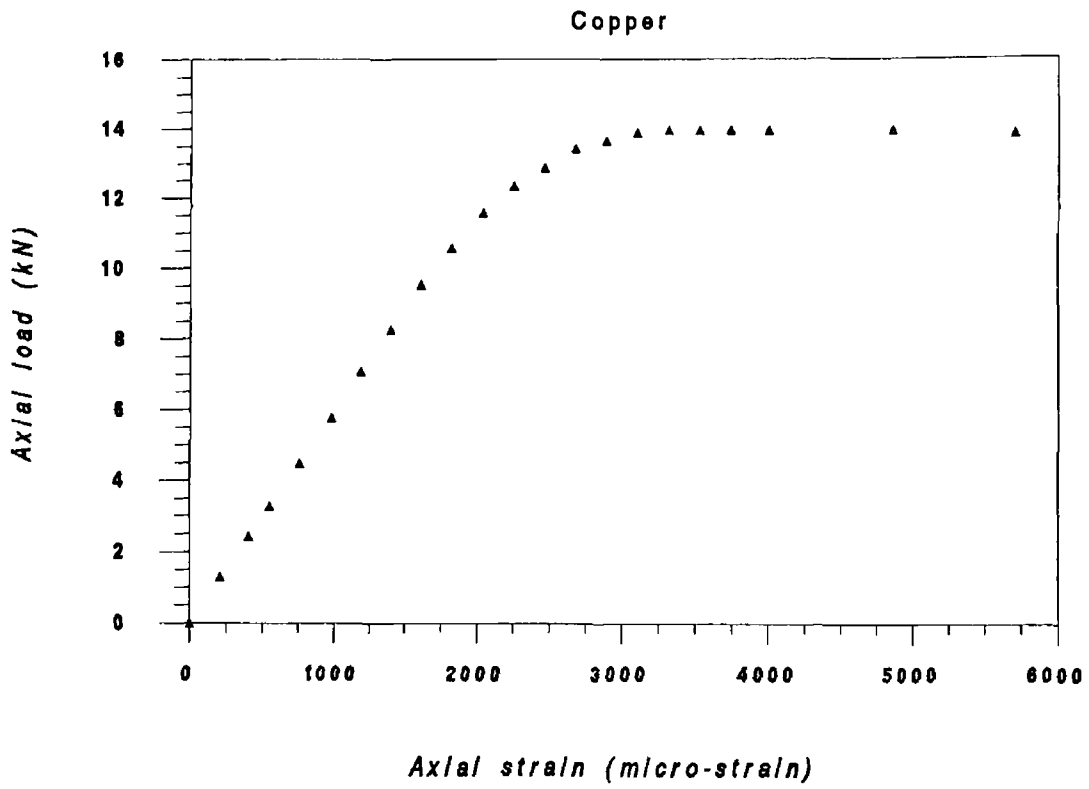


Figure F 1 The uniaxial tensile load versus the axial strain curve of the copper

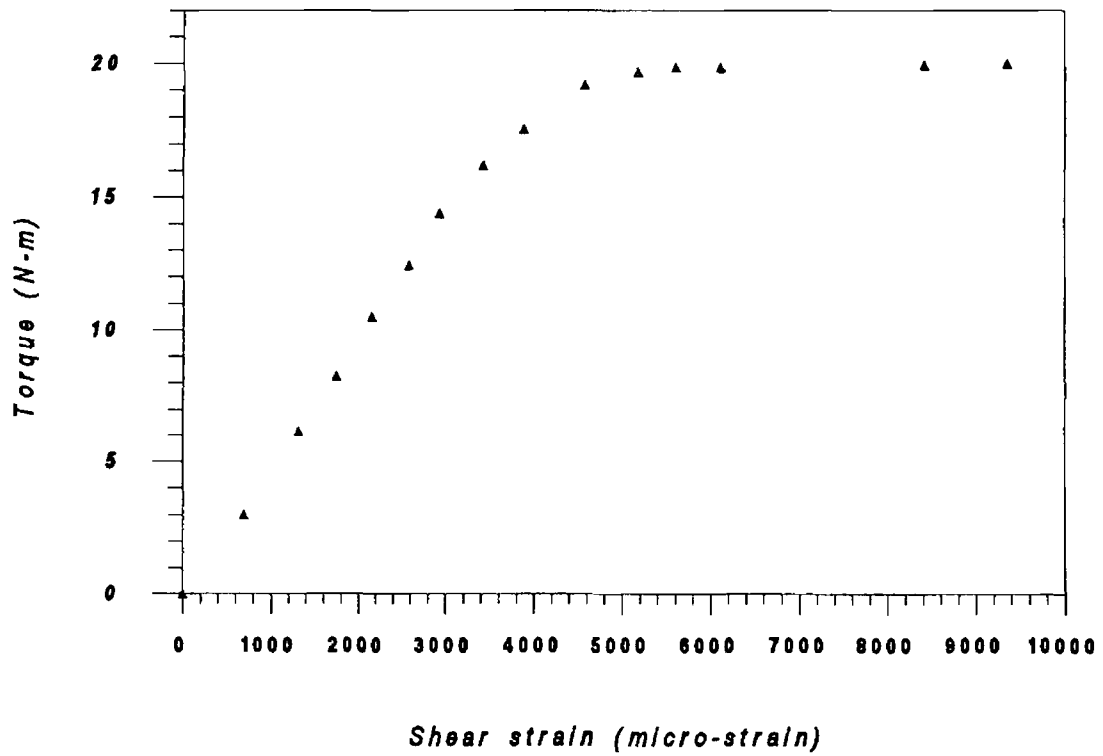


Figure F.2 The torque versus the shear strain curve of the copper

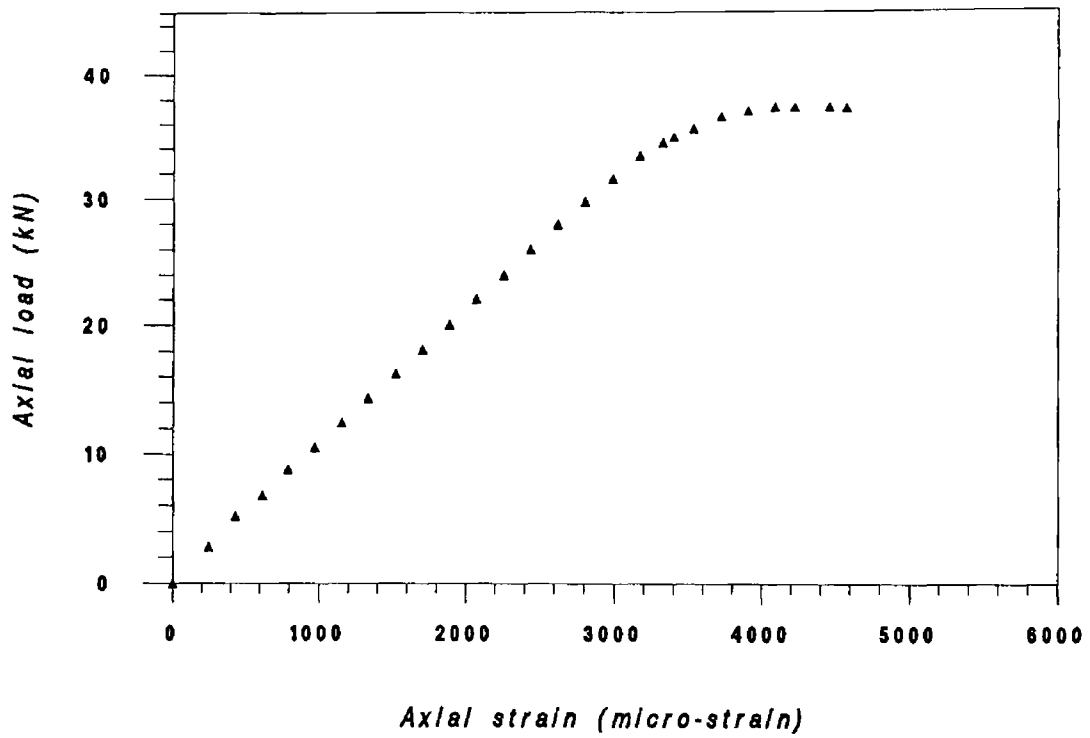


Figure - F 3 The uniaxial tensile load versus the axial strain curve of the steel-2

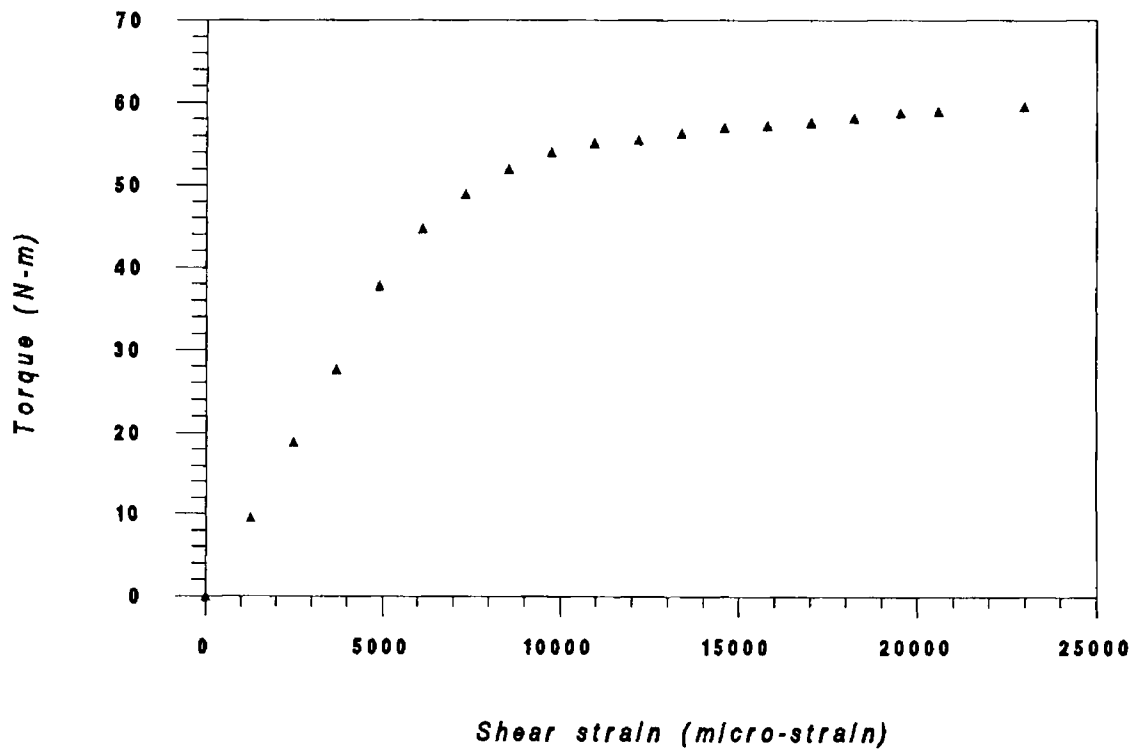


Figure F 4 The torque versus the shear strain curve of the steel-2

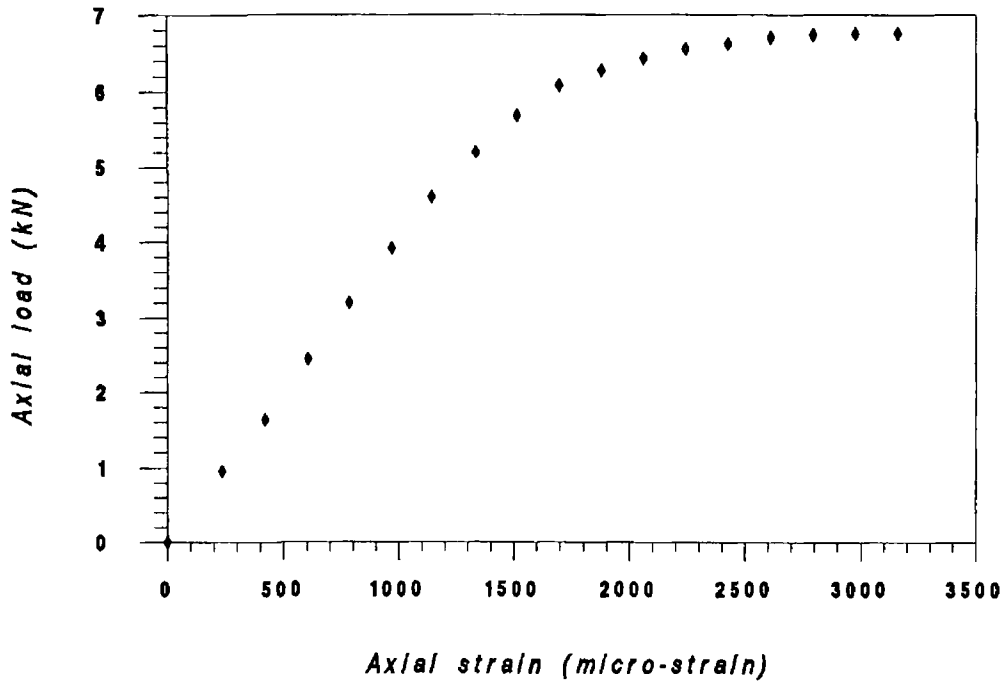


Figure F 5 The uniaxial tensile load versus the axial strain curve of the thin-walled tube

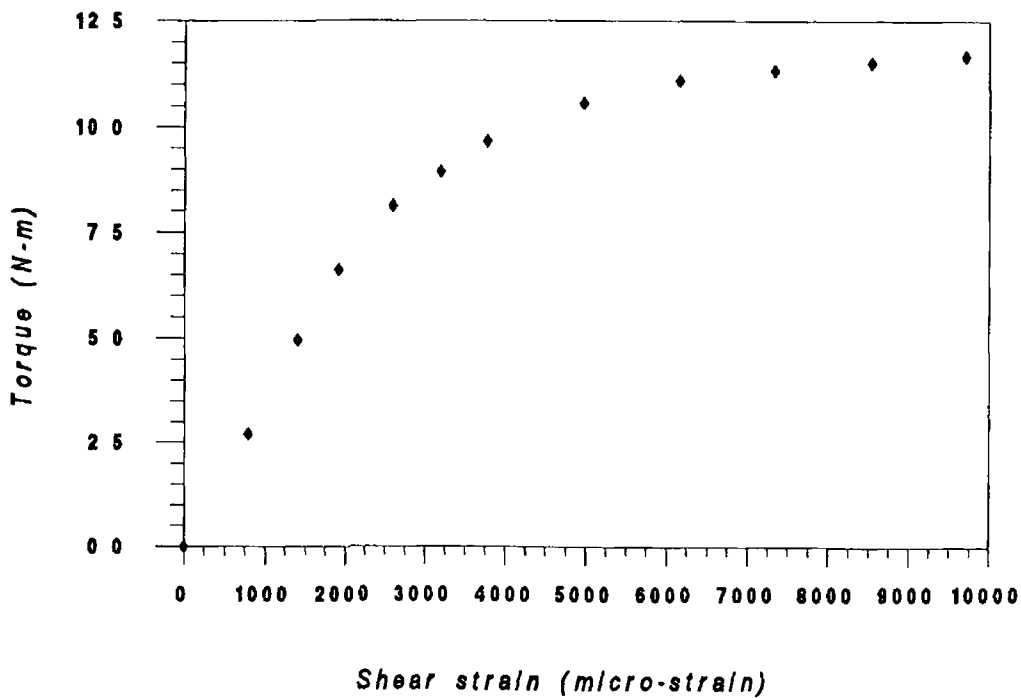


Figure F 6 The torque versus the shear strain curve of the thin-walled tube